

Best Available Copy

AD 646610

AFWL-TR-65-116

AFWL-TR  
65-116

**ENGINEERING CLASSIFICATION  
AND INDEX PROPERTIES  
FOR INTACT ROCK**

D. U. Deere  
R. P. Miller

University of Illinois  
Urbana, Illinois  
Contract AF 29(601)-6319



TECHNICAL REPORT NO. AFWL-TR-65-116

December 1966

**AIR FORCE WEAPONS LABORATORY**  
Research and Technology Division  
Air Force Systems Command  
Kirtland Air Force Base  
New Mexico

ARCHIVE COPY

RECEIVED  
FEB 13 1967  
C

20040702015

AFWL-TR-65-116

Research and Technology Division  
AIR FORCE WEAPONS LABORATORY  
Air Force Systems Command  
Kirtland Air Force Base  
New Mexico

When U. S. Government drawings, specifications, or other data are used for any purpose other than a definitely related Government procurement operation, the Government thereby incurs no responsibility nor any obligation whatsoever, and the fact that the Government may have formulated, furnished, or in any way supplied the said drawings, specifications, or other data, is not to be regarded by implication or otherwise, as in any manner licensing the holder or any other person or corporation, or conveying any rights or permission to manufacture, use, or sell any patented invention that may in any way be related thereto.

This report is made available for study with the understanding that proprietary interests in and relating thereto will not be impaired. In case of apparent conflict or any other questions between the Government's rights and those of others, notify the Judge Advocate, Air Force Systems Command, Andrews Air Force Base, Washington, D. C. 20331.

Distribution of this document is unlimited.

SECTION FOR		
1	WHITE SECTION	<input checked="" type="checkbox"/>
	BUFF SECTION	<input type="checkbox"/>
INDUCED IFICATION <i>rev statement</i>		
<i>g m doc</i>		
DISTRIBUTION/AVAILABILITY CODES		
ST.	AVAIL.	and/or SPECIAL
1		

21050704006

BLANK PAGE

ENGINEERING CLASSIFICATION AND INDEX  
PROPERTIES FOR INTACT ROCK

D. U. Deere  
R. P. Miller

University of Illinois  
Urbana, Illinois  
Contract AF29(601)-6319

TECHNICAL REPORT NO. AFWL-TR-65-116

Distribution of this document  
is unlimited.

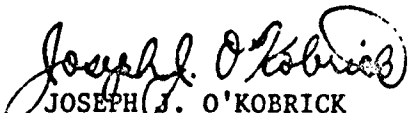
FOREWORD

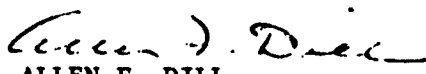
This report was prepared by the Department of Civil Engineering at the University of Illinois, Urbana, Illinois under Contract AF29(601)-6319. The research was performed under Program Element 6.16.46.01.D, Project 5710, Sub-task 13.144, and was funded by the Defense Atomic Support Agency (DASA).


Inclusive dates of research were 1 February 1964 through 1 April 1966. The report was submitted 6 October 1966 by the AFWL Project Officer, Captain Joseph J. O'Kobrick (WLDC). Captain Thomas E. O'Brien was the former Project Officer for the Air Force.

Dr. Don U. Deere, Professor of Civil Engineering and of Geology, was the project supervisor. R. P. Miller, Research Associate in Civil Engineering was immediately responsible for all phases of the test program and preparation of the written report. E. J. Cording, Research Assistant in Civil Engineering, assisted in development of special equipment and testing techniques. J. T. Wilband, Teaching Assistant in Geology, performed the petrographic analysis. J. H. Coulson, Graduate Fellow in Civil Engineering, assisted in specimen preparation and testing, and prepared the computer programs for data reduction and statistical analysis. The drawings were prepared by E. E. Boatz. Acknowledgment is extended to the Corps of Engineers, Walla Walla District, and the U. S. Bureau of Reclamation, Denver, who furnished core samples; and also to the numerous rock quarries, most of whom furnished block samples without charge.

This report has been reviewed and is approved.

  
JOSEPH J. O'KOBRIK  
Captain, USAF  
Project Officer

  
ALLEN F. DILL  
CDR, CEC, USNR  
Chief, Civil Engineering Branch

  
GEORGE C. DARBY, JR.  
Colonel, USAF  
Chief, Development Division

## ABSTRACT

Physical and elastic properties of NX-size rock core from 27 localities were investigated in order to develop an engineering classification system for intact rock, and also to develop index properties related to important physical and engineering characteristics. Thirteen rock types are represented. Laboratory tests were conducted on these rocks as follows: unit weight, Shore scleroscope hardness, Schmidt hammer hardness, abrasion hardness, absorption, sonic-velocity stress-strain under cyclic loading to 5,000 psi, uniaxial stress-strain to failure, and point-load tensile strength. A total of 257 specimens with L/D ratios of 2:1 were tested. Statistical studies were conducted with the IBM 7094 computer to determine correlation and regression relationships for selected pairs of variables. A system of engineering classification is proposed in which rocks are classified on the basis of their strength and modulus properties either obtained directly from laboratory tests, or approximately from index properties recommended herein. Application of the proposed engineering classification system to data obtained by others is shown by individual charts for each of several different rock types. Five charts are presented for estimating the strength or modulus properties for intact rock from the numerical indices obtained by either the Schmidt hammer, the Shore scleroscope, or the sonic pulse velocity, all used in conjunction with the unit weight of the rock.

This page intentionally left blank.

## CONTENTS

SECTION	PAGE
1. INTRODUCTION	1
1. Nature of the Problem	1
2. Objectives of Investigation	2
3. Scope of Study	3
2. EXISTING SYSTEMS OF ROCK CLASSIFICATION	5
1. General	5
2. Geological Classification	5
3. Classification by Physical Character of Rock Materials	7
4. Classification by In-Situ Character of Rock Mass	11
3. HARDNESS OF ROCKS	15
1. General	15
2. Types of Hardness and Their Methods of Measurement	16
3. Toughness and Resilience	20
4. Hardness and Other Physical Properties	25
5. Hardness and Drilling	30
4. EXPERIMENTAL STUDIES	33
1. General	33
2. Description of Rocks	33
3. Preparation of Test Specimens	38
4. Laboratory Tests	46
5. Test Results	67
5. DISCUSSION AND INTERPRETATION OF EXPERIMENTAL DATA	84
1. General	84
2. Statistical Procedures	84
3. Physical Properties	87
4. Elastic Properties	90
5. Relationships Among Various Physical Properties	99
6. Relationships Among Physical and Elastic Properties	108
7. Comparison of Static and Dynamic Properties	122



SECTION	PAGE
<b>6. ENGINEERING CLASSIFICATION AND INDEX PROPERTIES FOR INTACT ROCK</b>	<b>136</b>
1. General	136
2. Proposed Engineering Classification	136
3. Index Properties	160
4. Unit Weight as an Index of Strength and Deformation	161
5. Schmidt Hardness as an Index of Strength and Deformation	162
6. Shore Hardness as an Index of Strength and Deformation	171
7. Sonic Velocity as an Index of Deformation	180
<b>7. SUMMARY AND CONCLUSIONS</b>	<b>185</b>
1. Summary	185
2. Conclusions	186
3. Suggestions for Further Research	189
<b>APPENDIX A. PETROGRAPHIC DESCRIPTIONS AND THIN-SECTION PHOTOMICROGRAPHS</b>	<b>191</b>
<b>APPENDIX B. TYPICAL TEST RESULTS</b>	<b>219</b>
<b>APPENDIX C. STATISTICAL METHODS OF ANALYSIS</b>	<b>276</b>
<b>BIBLIOGRAPHY</b>	<b>291</b>
<b>DISTRIBUTION</b>	<b>301</b>

## LIST OF TABLES

Table No.		Page
2.1	SCALE OF ROCK HARDNESS	9
2.2	CLASSIFICATION OF ROCKS FOR ROCK MECHANICS	11
3.1	MOHS HARDNESS SCALE AND CRYSTAL STRUCTURE	17
4.1	LIST OF ROCK TYPES	34
4.2	SUMMARY OF AVERAGE PHYSICAL PROPERTIES FOR ROCK	71
4.3	SUMMARY OF AVERAGE ELASTIC PROPERTIES FOR ROCK	75
5.1	NUMBER OF TESTS AND COEFFICIENTS OF VARIATION FOR MEASURED ROCK PROPERTIES	86
5.2	EFFECT OF OVEN-DRYING ON THE DILATATIONAL WAVE VELOCITY FOR ROCKS	99
5.3	PERCENT BY WHICH DYNAMIC PROPERTIES ARE GREATER THAN STATIC PROPERTIES FOR ROCKS	132
6.1	ENGINEERING CLASSIFICATION FOR INTACT ROCK	137

## LIST OF FIGURES

Figure No.		Page
3.1	RELATIONSHIP BETWEEN RELATIVE VALUES OF IMPACT TOUGHNESS AND WEAR RESISTANCE FOR ROCK	22
3.2	RELATIONSHIP BETWEEN SHORE HARDNESS AND ABRASION HARDNESS FOR ROCK	23
3.3	MODULI OF RESILIENCE OF SOME TYPICAL ROCKS TESTED BY U. S. BUREAU OF MINES	24
3.4	RELATIONSHIP BETWEEN ABRASION HARDNESS AND ULTIMATE COMPRESSIVE STRENGTH FOR ROCK IN UNIAXIAL COMPRESSION	26
3.5	RELATIONSHIP BETWEEN SHORE HARDNESS AND ULTIMATE COMPRESSIVE STRENGTH FOR ROCK IN UNIAXIAL COMPRESSION	28
3.6	RELATIONSHIP BETWEEN SHORE HARDNESS AND ULTIMATE COMPRESSIVE STRENGTH FOR ROCK IN UNIAXIAL COMPRESSION	29
4.1	DRILL PRESS	39
4.2	BLOCK SAMPLE CLAMPED IN POSITION FOR CORE DRILLING	41
4.3	DIAMOND ROCK SAW	43
4.4	CORE SPECIMEN CLAMPED IN SAW CARRIAGE	44
4.5	LAPPING MACHINE	45
4.6	CORE SPECIMEN, CYLINDRICAL CORE HOLDER, CONDITIONING RING, AND PRESSURE PLATE	45
4.7	SHORE SCLEROSCOPE	48
4.8	LONGITUDINAL SECTION OF THE TYPE L SCHMIDT TEST HAMMER	50
4.9	SCHMIDT TEST HAMMER BESIDE SPECIMEN CRADLE BLOCK AND BASE PLATE	51
4.10	ABRASION APPARATUS	53
4.11	SCHEMATIC INTERCONNECTION DIAGRAM FOR SONIC PULSE VELOCITY MEASURING EQUIPMENT	56
4.12	TYPICAL SONIC PULSE WAVE-FORM DISPLAYS	58
4.13	EQUIPMENT FOR MEASURING SONIC PULSE VELOCITY AND STATIC STRESS-STRAIN DURING CYCLIC LOADING	60
4.14	CORE SPECIMEN IN POSITION FOR MEASURING SONIC PULSE VELOCITY, STRESS AND STRAIN UNDER UNIAXIAL LOAD	61
4.15	STRAIN READ-OUT	62
4.16	COMPRESSION TEST MACHINE	64
4.17	CORE SPECIMEN IN POSITION FOR COMPRESSION TEST TO FAILURE	65

Figure No.		Page
4.18	TYPICAL COMPRESSIVE FAILURES	66
4.19	SCHEMATIC DIAGRAM FOR POINT-LOAD TENSILE TEST	68
4.20	POINT-LOAD TENSILE TEST EQUIPMENT	69
4.21	CORE SPECIMEN IN POSITION FOR POINT-LOAD TENSILE TEST	70
5.1	REPRESENTATIVE STRESS-STRAIN CURVE FOR ROCK IN UNIAXIAL COMPRESSION	91
5.2	TYPICAL STRESS-STRAIN CURVES FOR ROCK IN UNIAXIAL COMPRESSION TO FAILURE	94
5.3	RELATIONSHIP BETWEEN AVERAGE VALUES OF DRY UNIT WEIGHT AND ULTIMATE COMPRESSIVE STRENGTH FOR ROCK IN UNIAXIAL COMPRESSION	100
5.4	RELATIONSHIP BETWEEN AVERAGE VALUES OF SHORE HARDNESS AND ULTIMATE COMPRESSIVE STRENGTH FOR ROCK IN UNIAXIAL COMPRESSION	102
5.5	RELATIONSHIP BETWEEN AVERAGE VALUES OF SCHMIDT HARDNESS AND ULTIMATE COMPRESSIVE STRENGTH FOR ROCK IN UNIAXIAL COMPRESSION	103
5.6	RELATIONSHIP BETWEEN AVERAGE VALUES OF ABRASION HARDNESS AND ULTIMATE COMPRESSIVE STRENGTH FOR ROCK IN UNIAXIAL COMPRESSION	104
5.7	RELATIONSHIP BETWEEN ABSORPTION AND AVERAGE VALUES OF ULTIMATE COMPRESSIVE STRENGTH FOR ROCK IN UNIAXIAL COMPRESSION	106
5.8	RELATIONSHIP BETWEEN AVERAGE VALUES OF POINT-LOAD TENSILE STRENGTH AND ULTIMATE COMPRESSIVE STRENGTH FOR ROCK IN UNIAXIAL COMPRESSION	107
5.9	RELATIONSHIP BETWEEN AVERAGE VALUES OF SHORE HARDNESS AND ABRASION HARDNESS FOR ROCK	109
5.10	RELATIONSHIP BETWEEN AVERAGE VALUES OF DRY UNIT WEIGHT AND TANGENT MODULUS OF DEFORMATION AT STRESS LEVEL OF ONE-HALF ULTIMATE STRENGTH FOR ROCK IN UNIAXIAL COMPRESSION	110
5.11	RELATIONSHIP BETWEEN AVERAGE VALUES OF ULTIMATE COMPRESSIVE STRENGTH AND INITIAL MODULUS OF DEFORMATION FOR ROCK IN UNIAXIAL COMPRESSION	111
5.12	RELATIONSHIP BETWEEN AVERAGE VALUES OF ULTIMATE COMPRESSIVE STRENGTH AND TANGENT MODULUS OF DEFORMATION AT STRESS LEVEL OF ONE-HALF ULTIMATE STRENGTH FOR ROCK IN UNIAXIAL COMPRESSION	112
5.13	RELATIONSHIP BETWEEN AVERAGE VALUES OF SHORE HARDNESS AND TANGENT MODULUS OF DEFORMATION AT STRESS LEVEL OF ONE-HALF ULTIMATE STRENGTH FOR ROCK IN UNIAXIAL COMPRESSION	114

Figure No.		Page
5.14	RELATIONSHIP BETWEEN AVERAGE VALUES OF SCHMIDT HARDNESS AND TANGENT MODULUS OF DEFORMATION AT STRESS LEVEL OF ONE-HALF ULTIMATE STRENGTH FOR ROCK IN UNIAXIAL COMPRESSION	115
5.15	RELATIONSHIP BETWEEN ABSORPTION AND AVERAGE VALUES OF TANGENT MODULUS OF DEFORMATION AT STRESS LEVEL OF ONE-HALF ULTIMATE STRENGTH FOR ROCK IN UNIAXIAL COMPRESSION	116
5.16	RELATIONSHIP BETWEEN AVERAGE VALUES OF DRY UNIT WEIGHT AND DILATATIONAL WAVE VELOCITY FOR ROCK UNDER UNIAXIAL COMPRESSIVE STRESS OF 5,000 psi	118
5.17	RELATIONSHIP BETWEEN AVERAGE VALUES OF INITIAL MODULUS OF DEFORMATION AND DILATATIONAL WAVE VELOCITY FOR ROCK UNDER UNIAXIAL COMPRESSIVE STRESS OF 100-150 psi	119
5.18	RELATIONSHIP BETWEEN AVERAGE VALUES OF TANGENT MODULUS OF DEFORMATION AT STRESS LEVEL OF ONE-HALF ULTIMATE STRENGTH AND DILATATIONAL WAVE VELOCITY FOR ROCK UNDER UNIAXIAL COMPRESSIVE STRESS OF 5,000 psi	120
5.19	VELOCITY-MODULUS VECTORS FOR ROCK UNDER INCREASING UNIAXIAL COMPRESSIVE STRESS	121
5.20	SONIC STRESS WAVE SUPERIMPOSED UPON A STATICALLY APPLIED STRESS	125
5.21	THEORETICAL CURVE RELATING CONSTRAINED MODULUS OF DEFORMATION AND YOUNG'S MODULUS OF ELASTICITY FOR DIFFERENT VALUES OF POISSON'S RATIO	126
5.22	RELATIONSHIP BETWEEN AVERAGE VALUES OF INITIAL AND CONSTRAINED MODULI OF DEFORMATION FOR ROCK UNDER UNIAXIAL COMPRESSIVE STRESS OF 100-150 psi	127
5.23	RELATIONSHIP BETWEEN AVERAGE VALUES OF TANGENT MODULUS AT STRESS LEVEL OF ONE-HALF ULTIMATE STRENGTH AND CONSTRAINED MODULUS OF DEFORMATION FOR ROCK UNDER UNIAXIAL COMPRESSIVE STRESS OF 5,000 psi	128
5.24	RELATIONSHIP BETWEEN AVERAGE VALUES OF CONSTRAINED MODULI OF DEFORMATION COMPUTED FROM STATIC AND DYNAMIC MEASUREMENTS FOR ROCK UNDER UNIAXIAL COMPRESSIVE STRESS OF 100-150 psi	130
5.25	RELATIONSHIP BETWEEN AVERAGE VALUES OF CONSTRAINED MODULI OF DEFORMATION COMPUTED FROM STATIC AND DYNAMIC MEASUREMENTS FOR ROCK UNDER UNIAXIAL COMPRESSIVE STRESS UP TO 5,000 psi	131
5.26	RELATIONSHIP BETWEEN AVERAGE VALUES OF DILATATIONAL WAVE VELOCITY COMPUTED FROM STATIC AND DYNAMIC MEASUREMENTS FOR ROCK UNDER UNIAXIAL COMPRESSIVE STRESS OF 100-150 psi	133

Figure No.		Page
5.27	RELATIONSHIP BETWEEN AVERAGE VALUES OF DILATATIONAL WAVE VELOCITY COMPUTED FROM STATIC AND DYNAMIC MEASUREMENTS FOR ROCK UNDER UNIAXIAL COMPRESSIVE STRESS UP TO 5,000 psi	134
6.1	ENGINEERING CLASSIFICATION FOR INTACT ROCK - AVERAGE VALUES FOR 13 ROCK TYPES (28 Locations)	139
6.2	ENGINEERING CLASSIFICATION FOR INTACT ROCK - INDIVIDUAL TEST RESULTS (124 Specimens, 13 Rock Types)	142
6.3	ENGINEERING CLASSIFICATION FOR INTACT ROCK - EFFECT OF ANGLE OF BEDDING AND FOLIATION	143
6.4	ENGINEERING CLASSIFICATION FOR INTACT ROCK - SUMMARY PLOT IGNEOUS ROCK (176 Specimens, 75% of Points)	144
6.5	ENGINEERING CLASSIFICATION FOR INTACT ROCK - DIABASE (26 Specimens, 8 Locations, Various Sources)	145
6.6	ENGINEERING CLASSIFICATION FOR INTACT ROCK - GRANITE FAMILY (80 Specimens, 16 Locations, Various Sources)	146
6.7	ENGINEERING CLASSIFICATION FOR INTACT ROCK - BASALT AND OTHER FLOW ROCKS (70 Specimens, 20 Locations, Various Sources)	147
6.8	ENGINEERING CLASSIFICATION FOR INTACT ROCK - SUMMARY PLOT SEDIMENTARY ROCKS (193 Specimens, 75% of Points)	149
6.9	ENGINEERING CLASSIFICATION FOR INTACT ROCK - LIMESTONE AND DOLOMITE (77 Specimens, 22 Locations, Various Sources)	150
6.10	ENGINEERING CLASSIFICATION FOR INTACT ROCK - SANDSTONE (82 Specimens, 18 Locations, Various Sources)	151
6.11	ENGINEERING CLASSIFICATION FOR INTACT ROCK - HARD SHALE (34 Specimens, 14 Locations, Various Sources)	152
6.12	ENGINEERING CLASSIFICATION FOR INTACT ROCK - POROUS TUFF (44 Specimens, 2 Locations, Various Sources)	154
6.13	ENGINEERING CLASSIFICATION FOR INTACT ROCK - SUMMARY PLOT METAMORPHIC ROCKS (167 Specimens, 75% of Points)	155
6.14	ENGINEERING CLASSIFICATION FOR INTACT ROCK - QUARTZITE (41 Specimens, 11 Locations, Various Sources)	156

Figure No.		Page
6.15	ENGINEERING CLASSIFICATION FOR INTACT ROCK - GNEISS (43 Specimens, 14 Locations, Various Sources)	157
6.16	ENGINEERING CLASSIFICATION FOR INTACT ROCK - MARBLE (22 Specimens, 7 Locations)	158
6.17	ENGINEERING CLASSIFICATION FOR INTACT ROCK - SCHIST (61 Specimens, 11 Locations, Various Sources)	159
6.18	RELATIONSHIP BETWEEN AVERAGE VALUES OF $\gamma_a \cdot R$ AND ULTIMATE COMPRESSIVE STRENGTH FOR ROCK IN UNIAXIAL COMPRESSION	163
6.19	RELATIONSHIP BETWEEN AVERAGE VALUES OF $\gamma_a \cdot R$ AND ULTIMATE COMPRESSIVE STRENGTH FOR ROCK IN UNIAXIAL COMPRESSION (SEMI-LOG PLOT)	165
6.20	ROCK STRENGTH CHART BASED ON SCHMIDT HARDNESS	167
6.21	RELATIONSHIP BETWEEN AVERAGE VALUES OF $\gamma_a \cdot R$ AND TANGENT MODULUS OF DEFORMATION AT STRESS LEVEL OF ONE-HALF ULTIMATE STRENGTH FOR ROCK IN UNIAXIAL COMPRESSION	168
6.22	RELATIONSHIP BETWEEN AVERAGE VALUES OF $\gamma_a^2 \cdot R$ AND TANGENT MODULUS OF DEFORMATION AT STRESS LEVEL OF ONE-HALF ULTIMATE STRENGTH FOR ROCK IN UNIAXIAL COMPRESSION	169
6.23	ROCK MODULUS CHART BASED ON SCHMIDT HARDNESS	170
6.24	RELATIONSHIP BETWEEN AVERAGE VALUES OF SHORE HARDNESS AND SCHMIDT HARDNESS FOR ROCK	172
6.25	RELATIONSHIP BETWEEN AVERAGE VALUES OF $\gamma_a \cdot S_h$ AND ULTIMATE COMPRESSIVE STRENGTH FOR ROCK IN UNIAXIAL COMPRESSION	174
6.26	RELATIONSHIP BETWEEN AVERAGE VALUES OF $\gamma_a \cdot S_h$ AND ULTIMATE COMPRESSIVE STRENGTH FOR ROCK IN UNIAXIAL COMPRESSION (SEMI-LOG PLOT)	175
6.27	ROCK STRENGTH CHART BASED ON SHORE HARDNESS	176
6.28	RELATIONSHIP BETWEEN AVERAGE VALUES OF $\gamma_a \cdot S_h$ AND TANGENT MODULUS OF DEFORMATION AT STRESS LEVEL OF ONE-HALF ULTIMATE STRENGTH FOR ROCK IN UNIAXIAL COMPRESSION	177
6.29	RELATIONSHIP BETWEEN AVERAGE VALUES OF $\gamma_a^2 \cdot S_h$ AND TANGENT MODULUS OF DEFORMATION AT STRESS LEVEL OF ONE-HALF ULTIMATE STRENGTH FOR ROCK IN UNIAXIAL COMPRESSION	178
6.30	ROCK MODULUS CHART BASED ON SHORE HARDNESS	179

Figure No.		Page
6.31	RELATIONSHIP BETWEEN AVERAGE VALUES OF $\gamma_a \cdot V_p$ AND TANGENT MODULUS OF DEFORMATION AT STRESS LEVEL OF ONE-HALF ULTIMATE STRENGTH FOR ROCK IN UNIAXIAL COMPRESSION	181
6.32	RELATIONSHIP BETWEEN AVERAGE VALUES OF $\gamma_a \cdot V_p$ AND TANGENT MODULUS OF DEFORMATION AT STRESS LEVEL OF ONE-HALF ULTIMATE STRENGTH FOR ROCK IN UNIAXIAL COMPRESSION (SEMI-LOG PLOT)	182
6.33	ROCK MODULUS CHART BASED ON DILATATIONAL WAVE VELOCITY	184
B.1A- B.28A	STRESS-STRAIN BEHAVIOR AND SONIC PULSE VELOCITY FOR ROCK IN UNIAXIAL COMPRESSION	220-274
B.1B- B.28R	STRESS-STRAIN CURVE AND POISSON'S RATIO FOR ROCK IN UNIAXIAL COMPRESSION TO FAILURE	221-275
C.1	CHARACTERISTICS OF NORMAL DISTRIBUTION	281
C.2	RELATIONSHIP BETWEEN VARIABLES X AND Y	281
C.3	EFFECT OF SAMPLING VARIATION ON REGRESSION ESTIMATES OF POPULATION MEANS	289



## PRINCIPAL SYMBOLS

$a$	= Y-intercept of regression line
$A_h$	= abrasion hardness
$b$	= slope of regression line, or coefficient of regression
BLH	= Baldwin-Lima-Hamilton
CL	= confidence limits
$D$	= diameter of core specimen
$D_i$	= deviation, error or residual
$e$	= 2.71828, the base of natural logarithms
$E$	= Young's modulus of elasticity
$E_d$	= Young's modulus of elasticity determined dynamically
$E_i$	= initial tangent modulus of deformation
$E_s$	= secant modulus of deformation
$E_t$	= tangent modulus of deformation
$F$	= total failure load
$g$	= acceleration of gravity
$G$	= modulus of rigidity (or shear modulus)
$K$	= bulk modulus of elasticity
$L$	= length of core specimen
$L/D$	= length/diameter ratio of specimen
$M_c$	= constrained modulus of deformation
$M_r$	= modulus of resilience
$M_t$	= modulus of toughness
$n$	= number in group or sample
$P_1$	= weight of oven-dry specimen
$P_2$	= weight of saturated specimen
$r$	= coefficient of correlation
$r^2$	= coefficient of determination
$R$	= Schmidt hammer hardness
$s$	= sample standard deviation
$s^2$	= sample variance
$s_{y.x}$	= sample standard deviation from regression, or standard error of estimate (Y on X)
$s_{\bar{x}}$	= standard deviation of the means, or standard error

$S_h$	= Shore scleroscope hardness
$t$	= "Student's" t-distribution
$T$	= point-load tensile strength
USBM	= U. S. Bureau of Mines
USBR	= U. S. Bureau of Reclamation
$V\%$	= coefficient of variation
$V_p$	= sonic pulse velocity or dilatational wave velocity in an unbounded medium (P-wave)
$V_s$	= distortional or shear wave velocity (S-wave)
$\bar{x}$	= sample mean of $X$
$X$	= independent variable (abscissa)
$\bar{y}$	= sample mean of $Y$
$Y$	= dependent variable (ordinate)
$Y_{est.}$	= value of $Y$ estimated from regression
$Z$	= standard normal distribution
$\alpha$	= level of significance
$\gamma$	= unit weight
$\gamma_a$	= unit weight (air-dry)
$d\sigma/d\epsilon$	= tangent modulus
$\epsilon$	= strain
$\epsilon_f$	= strain at failure
$\tan \theta$	= slope of linear stress-strain curve
$\mu$	= mean of population
$\nu$	= Poisson's ratio
$\pi$	= 3.14159
$\phi$	= angle of internal friction
$\rho$	= mass density ( $\frac{Z}{g}$ )
$\sigma_a(y)$	= yield stress
$\sigma_a(ult.)$	= uniaxial compressive strength (ultimate)
$\sigma/\epsilon$	= secant modulus
$\sigma$	= stress (in engineering mechanics)
$\sigma$	= standard deviation of population (in statistics)
$\Sigma$	= summation

This page intentionally left blank.

## SECTION 1

### INTRODUCTION

#### 1. NATURE OF THE PROBLEM

Traditionally, civil and military engineers have been involved with the mechanics of rock behavior on projects in rock such as deep foundations of dams, buildings, and bridges; deep rock cuts for highway, railway, and canal construction; and rock tunnels for power supply or vehicular use. Mining engineers also have been keenly interested in the behavior of the rock surrounding their operations for extraction of materials from beneath the earth's surface. In recent years, the scope of projects concerned with rock engineering has broadened extensively with the advent of underground power plants, missile launch and control facilities, and other types of military protective construction. These latter projects involve dynamic or shock loading at high intensities of pressure as well as the normal static loading.

Many early projects were successfully completed by applying procedures and rule-of-thumb techniques gained from experience; however, this is not possible with the current array of projects. If the engineering behavior of rock under superimposed stresses is to be rationally predicted, knowledge concerning the geological discontinuities of the rock mass, physical properties of the geological materials, and principles of mechanics, should be utilized.

Physical discontinuities are present in all rock masses in the form of planes or surfaces separating intact blocks of rock. Geologically, these discontinuities are recognized as joints, faults, bedding planes, or cleavage planes. The strength and deformation characteristics of a rock mass are both influenced by:

- i) the physical properties of the intact blocks of rock, and
- ii) the number and nature of the discontinuities bounding the individual blocks.

The problem is, therefore, two-fold. In order to develop, ultimately, a meaningful system for evaluating in-place rock behavior at a potential construction site, it is logical to investigate, initially, the properties of the intact rock materials. Because of the discontinuous nature of a rock mass, appropriate reduction factors should then be determined for application to the "upper limits" defined by the intact rock.

The present investigation is not concerned with the behavior and classification of the in-situ rock mass with its inherent discontinuities. Rather, it is limited to the first phase of the problem -- the physical properties of the intact rock. Intact rock is defined herein as a polycrystalline solid, consisting of a natural aggregate of minerals, the properties of which depend upon:

- i) the physical properties of the constituents, and
- ii) the type of bonding of these constituents to one another.

Rock cores obtained in exploratory drilling are normally the first physical evidences from which the engineer may get an indication of the nature of the subsurface rock. The cores contain the intact rock materials and also show evidence of some of the discontinuities. Consequently, proper classification of these cores is an important step toward an understanding of the behavior to be expected, both during and after construction. Unfortunately, the qualitative descriptions presently used (e.g., on boring logs, in design, and in construction specifications for rock engineering projects) permit too broad an interpretation for universal engineering usage.

The identification and classification of the products of nature constitute an artificial procedure, because these materials are infinitely varied and do not lend themselves to separation into distinct categories (Peck, Hanson, and Thornburn, 1953). As a result, various arbitrary systems of classification have been developed, each with a particular purpose or application to a specific locale. As attempts are made to refine any of these systems, the system inevitably becomes more complicated and ultimately more cumbersome, so as to defeat the purpose for which it was intended. To avoid this difficulty, it is desirable to make use of relatively simple systems of classification with small numbers of categories. Detailed information concerning any given rock (or soil) can be summarized by stating numerical results, known as index properties, of certain physical classification tests. If the classification tests are properly chosen, rock (or soil) materials having similar index properties, regardless of their geologic origin, are likely to exhibit similar engineering behavior (Peck, Hanson and Thornburn, 1953).

The importance and usefulness of index properties for soil have already been well established in the field of soil mechanics and foundation engineering. The desirability of similar procedures for rock is repeatedly demonstrated in rock engineering problems. In order for an index property to be useful, it must have the following three general characteristics, whether it is used to describe soil, rock, or other engineering materials (Pomeroy, 1957; Deere, 1963a):

- i) It must be an index of a material property which is used by an engineer in solving a design problem.
- ii) The test to determine the property must be simple, inexpensive, and rapidly performed.
- iii) The test results must be reproducible, within certain limits, by different operators in different locations using standardized equipment and procedures.

## 2. OBJECTIVES OF INVESTIGATION

The objective of this research was to develop an engineering classification system for intact rock, which has as its basis index properties that are related to important physical properties of the rock. An experimental investigation was conducted in order to determine the physical and elastic properties of intact core specimens, representative of rock types most commonly encountered in civil engineering projects in the United States. Relationships among these various properties were studied, and the most significant correlations were used in developing the desired indices.

Because of its widespread application in metals, and the promise it has shown for other investigators in rock, hardness in its various forms was of primary interest for possible use as an index property. The properties of toughness, resilience, strength, and elasticity, are all involved to some degree in hardness tests. The latter two, strength and elasticity (or deformability), are the material properties which are of primary concern in the majority of civil engineering projects. Therefore, both the index tests and the classification system are directed toward a relationship with these properties.

### 3. SCOPE OF STUDY

In the following section, a review of existing systems of rock classification is presented. These consist of: (1) the most common, geological classifications, (2) systems which give consideration to classification on the basis of the physical properties of the rock substance, and (3) in situ classifications.

Section Three deals with the concepts of hardness and their application to rocks. The three basic types of hardness and their methods of measurement are presented, along with some of the relationships previously found between hardness and other properties. The relationship of rock hardness to drilling is also discussed.

In Section Four, a description of the 28 rock groups studied in this investigation is given. The following 13 different geological rock types are included: basalt, diabase, dolomite, gneiss, granite, limestone, marble, quartzite, rock salt, sandstone, schist, siltstone, and tuff. A detailed explanation of sample preparation is presented, in addition to a description of all tests performed. NX-size, intact core specimens, with L/D ratios of 2:1, were subjected to the following laboratory tests: unit weight, Shore (scleroscope) hardness, Schmidt hammer hardness, abrasion hardness, absorption, sonic velocity stress-strain under cyclic loading, stress-strain to failure, and point-load tensile strength. A summary of all test data is given in tabular form at the end of Section Four.

The test results are discussed and interpreted in Section Five. Data plots are presented of those properties which show the most significant degree of correlation with other properties, or are of general interest. Least-square regression lines are shown on each plot, together with the functional relationship, standard error of estimate, and correlation coefficient. A comparison of static and dynamic properties of rock, as observed in this investigation, is also discussed.

Section Six presents the correlations from which the index properties are defined, and proposes a system for the engineering classification of rock. This system is used to provide qualitative descriptions in terms of compressive strength and Young's modulus for intact specimens of rock. Classification is determined from numerical data obtained from index property tests, as described herein, or from actual laboratory measurements of strength and modulus. Estimates of the general range of strength and

modulus values for various rock types can also be obtained from the charts in Section Six.

In the last section, the summary and conclusions are presented. Future research which appears warranted as a result of this investigation is also suggested.

## SECTION 2

### EXISTING SYSTEMS OF ROCK CLASSIFICATION

#### 1. GENERAL

One of the primary purposes for rock classification in subsurface engineering and construction projects is to provide an effective means of communication among the engineering geologist, laboratory and design engineers, field engineer, and contractor. The records of underground explorations shown on contract drawings furnish the basic data for contractors' bids, and during performance of the work form the basis from which all changed conditions must be evaluated. The responsibility for presenting an accurate description of the materials to be encountered rests with the design engineer and the engineering geologist. It is desirable that the characteristics of the rock which will influence the construction methods be clearly conveyed to the contractor.

For the engineer, the appropriate classification of both the rock materials and rock mass would greatly assist in making the initial appraisal of the project, and in pointing to the areas where additional engineering information must be obtained for use in arriving at the final solution to the problem (Coates, 1964). Because of the important role of experience, especially in subsurface engineering projects, the individual experiences of all engineers should be summarized into a body of knowledge that can be readily assimilated; otherwise their value is lost to the profession. Proper classification of rocks (and other subsurface materials) into groups, within each of which the significant engineering properties are somewhat similar, is thus an important step in connection with any foundation project (Peck, Hanson, and Thornburn, 1953).

This section is concerned with a description of some of the systems which have been developed for rock classification. Geological systems are, in general, most widely used. Other systems have been developed for particular purposes, but are often limited in their application. Some systems are concerned with the properties of the rock material only, while others are more concerned with the continuity, size, and arrangement of the intact rock blocks (or slabs) within the rock mass. Still others give consideration to both of these characteristics.

The following part of this section deals with geological classification. The next part is concerned with systems which given consideration to description and classification on the basis of the physical properties of the rock substance. The last part discusses rock classification systems which are primarily concerned with the in-situ character of the rock mass.

#### 2. GEOLOGICAL CLASSIFICATION

In its broadest geological sense, a rock is any naturally-formed aggregate or mass of mineral matter, whether or not coherent, constituting an essential and appreciable part of the earth's crust (AGI Glossary, 1962).



To the layman and the engineer (and, in truth, to most geologists), the term "rock" refers to any hard, solid matter derived from the earth (Stokes and Varnes, 1955).

A single scheme for classifying rocks that is both complete and practical is presently not available. Rocks are classified chemically, petrographically, or genetically, depending on the purpose of the classification. Each basis has its own merits but none can fully combine the advantages of all (Huang, 1962). A primary division of rocks into three groups according to their genesis or mode of origin is almost universal in usage. Igneous rocks are the primary rocks formed by cooling of molten magmas, or by recrystallization of older rocks under heat and pressure great enough to render them fluid. If magmas cool beneath the surface, they form intrusive rocks; magmas reaching the surface form extrusive rocks. Sedimentary rocks are the products of deposition of plant and animal remains (organic), and of materials formed by chemical decomposition (chemical), and of physical disintegration of igneous, sedimentary, or metamorphic rocks (clastic). Metamorphic rocks are those produced by internal processes of heat, pressure, or permeation by other substances, acting on preexisting rocks of any kind. Metamorphic rocks are usually referred to as foliated or nonfoliated.

Petrographically, the most important properties utilized for identification and classification are texture, structure, and mineralogical composition. Although there is no general agreement as to which physical features of rocks shall be included as textures, and which are to be regarded as structures, the term, fabric, is used to include data from both categories. Spock (1953) refers to texture as the size and shape of rock constituents, together with variation in these properties. Structure covers the distribution and grouping of minerals and also the immediate effects of their arrangement, such as foliation and bedding. Mineral composition is the fundamental basis in geological classification of rocks, because the actual units (minerals) of which rocks consist are used (Huang, 1962).

Chemical classification is primarily useful for comparison of rocks on the basis of chemical data in which each oxide is presented as a weight percent. However, it is impossible to determine the character of a rock from a chemical analysis alone, since rocks of closely related composition may differ in origin, as well as in texture and mineralogy (Spock, 1953).

Detailed geological classifications are readily available in various texts dealing with rocks (Grout, 1940; Spock, 1953; Huang, 1962). Travis (1955) presents in compact form the generally accepted conventions for naming rocks on the basis of mineralogy and texture. Mielenz (1961) gives a mineralogic and textural classification of igneous rocks only.

Unfortunately, the above geological grouping and classification procedures give little or no information concerning the engineering capabilities of the rock. For example, some limestones have compressive strengths of 6,000 psi, whereas others have strengths of 36,000 psi. Or for example, the term "granite" may mean a hard, coherent rock. However, it is known

that granite can be extremely variable from location to location, depending upon the various weathering conditions to which it has been subjected. In some tropical climates, granites are weathered to such a degree that they can be excavated by hand with an ordinary shovel. Sandstones, also, may fall under classifications such as "poorly cemented sandstone" to "partially cemented sand" for the same rock, depending upon the background and experience of the geologist assigning the classification. If the former of the two classifications were used in the contract documents, the contractor would be prepared for excavation by blasting--and probably no bracing. If the latter classification were used, the contractor would normally be prepared for excavation with mechanical power equipment and extensive bracing. The cost and procedures for either case are entirely different. These and other examples clearly illustrate the limitations of a strictly geological classification.

### 3. CLASSIFICATION BY PHYSICAL CHARACTER OF ROCK MATERIALS

Some of the earlier ground classification methods used in mining are given by Harley (1926); he states that the factor that most influences all underground operations is the physical nature of the "ground" with which the mine operator has to deal. In the past, operations in mining were initiated by using trial and error methods; many believed that the conditions underground made this method of approach inherently necessary. Most general for local usage were such terms as hard, medium, soft, easy-breaking, et cetera. Other schemes, based upon rock names, were unsatisfactory because they did not consider the wide range of mineralogical composition, texture, weathering, and alterations occurring in each rock type.

Harley (1926) proposed a scheme of classification which considered the following physical characteristics:

- i) unit weight,
- ii) degree of hardness,
- iii) degree of toughness, and
- iv) occurrence of slips (or joints) in the rock.

This scheme was based upon the ft.-lbs. of energy required for drilling one cubic inch of rock, which was correlated to a grinding resistance obtained by a small grinding machine. The hardest rock in the drill test was assigned a grinding resistance factor of 1.0 and a classification of A+; the softest rock was classified as D+, and the grinding resistance factor was some decimal part of 1.0. There is no evidence that Harley's proposed scheme gained popular usage.

Head (1951) proposed a classification of geological rock formations based entirely upon the relative efficiency with which the formations could be drilled with a small rolling-cutter type of test bit. The micro-bit was about 2 inches in diameter, and consisted of two rolling cutters (approximately 1-inch diameter) mounted on opposite ends at a slight angle to the axis of the shaft. The test bit was designed to facilitate the replacement of the cutters after each drillability test. The Drillability Classification Number (DCN) was obtained by mounting the micro-bit in a lathe and measuring

the time interval, in seconds, required to drill 1/16-inch depth into a sample of each formation. Rotational speed was 110 rpm at a constant bit thrust of 417 pounds. By using the average result of at least two tests, the relative drillability was established for 15 rock formations commonly encountered in drilling. The DCN ranged from 1.9 for Wilcox sandstone to 555.7 for Hosston quartzite.

To determine whether or not this classification was consistent with results obtained from actual bits, drilling these same formations under field conditions, Head examined the performance of seven different types of bits used in these formations in the field. He found that the rates of penetration of the field bits fell in the same order as the rates of penetration of the test bit (the DCN is inversely proportional to the corresponding rate of penetration of the test bit). On the basis of these tests, Head concluded that any rolling-cutter type of bit should drill all formations for which a Drillability Classification Number has been established, in the same succession as the test bit, if chipping action occurs.

Hughes Tool Company, Houston, Texas, has developed an empirical, drillability classification chart on the basis of micro-bit data from samples of the same rock formations on which full-size bits have been run (Rollow, 1963). The estimated drilling rate of a new bit (in the field) is obtained by entering the chart, using micro-bit drilling rate and weight on the bit in pounds per inch of diameter. The micro-bit is 1 1/4 inches in diameter and is of slightly different design than the one used by Head (1951). The bit is placed in a small, radial drill press under 200 lbs load at 55 rpm; air is used to remove cuttings. Each test consists of drilling 3/32 inch, with drilling time recorded for each 1/32 inch drilled. The average drilling rate and cutter wear are calculated from the drilling tests.

The laboratory micro-bit test provides a basis for predicting rock drillability from small samples. In oil-field work, where cores have been checked with the micro-bit, the results have been accurate within 10%. The results have been somewhat more erratic in the blast-hole industry, but still usable. As Rollow points out, the micro-bit test is obviously valid only to the extent that the micro-specimen is representative of the whole. Also, the test procedure is reported to ignore several factors which affect bit life. The major limitation of this test for universal rock classification appears to be its specialized relation to particular types of equipment and procedures for specific rock formations.

A scale of hardness applicable to rock material was given by the Panama Canal Company (1947). This scale was slightly modified and used for classification of rock during construction of the Balboa Bridge (1959). The system is simple and is based upon the relative ease or difficulty with which intact rock can be broken. Although qualitative in nature, it uses terms familiar to all, providing a gradation from rock that can be broken in the hand to rock that can only be chipped with heavy blows of the hammer. This classification scale is shown in Table 2.1.

The U. S. Army Corps of Engineers (1961) present a "Guide for Classification and Description of Rocks with Emphasis on Their Engineering Properties," which is essentially qualitative in nature. The basic classification

TABLE 2.1

SCALE OF ROCK HARDNESS

After Panama Canal Company (1959)

RH-1	<u>Soft</u>	Slightly harder than very-hard overburden, rock-like character but crumbles or breaks easily by hand. (Some clay-shales and uncemented sandstones and agglomerates.)
RH-1	<u>Medium Soft</u>	Cannot be crumbled between fingers, but can be easily picked with light blows of the geology hammer. (Some shales and slightly-cemented sandstones and agglomerates.)
RH-2	<u>Medium Hard</u>	Can be picked with moderate blows of geology hammer. Can be cut with knife.
RH-3	<u>Hard</u>	Cannot be picked with geology hammer, but can be chipped with moderate blows of the hammer.
RH-4	<u>Very Hard</u>	Chips can be broken off only with heavy blows of the geology hammer.

includes a symbol and a name for each of 24 rock types encountered on Corps of Engineers projects. The physical properties of the rock are designated on the boring logs, either by word descriptions or by using the appropriate key number or numbers shown on the guide for the applicable physical properties. There are 46 descriptive key terms which may be selected as characterizing the following properties: bedding, lithology, hardness and degree of cementation, texture, structure, degree of weathering, solution and void conditions, swelling, and slaking. Of the nine properties listed, only three are not directly concerned with material properties, i.e., bedding, lithology, and structure. These three are characteristics of the rock mass.

A simple, quantitative procedure which can be correlated with in-situ and laboratory test results of the strength and compressibility of rock is described by Hamrol (1961). In this procedure, the index of alteration (a measure of the short-term water absorption of rock samples) is determined for a large number of samples over an entire site and, by using the established correlations, the foundation area can be mapped in terms of a particular engineering property (Rocha, 1964). This technique appears to be applicable primarily in differentiating zones of weathered and altered rock.

Deere (1963b) gives emphasis to those geological features which can be observed in rock cores, and which appear to be significant in rock engineering. The significant features include those which have a direct bearing on the homogeneity of the rock mass with respect to (1) variations in hardness, and (2) physical discontinuities. In the routine logging of rock cores, it has been the custom to check the hardness by nothing more than a knife blade or geology pick. Since it is not the slight differences in degree of hardness from one rock to another that is important, but rather the large variations, a relative term for hardness may be satisfactory. In order to obtain a more meaningful numerical hardness value, Deere (1963b) suggests the use of a small version of the Schmidt concrete test hammer. This procedure was recently reported by Knill and Jones (1965) for granite cores from a dam in England. Although the impact numbers were not shown to be directly related to any engineering property, they clearly reflect the decrease in the effects of weathering in the rock with depth.

From an engineering point of view, Deere (1963b), also suggests that a textural classification system eventually may prove to be of greater value than the normal, mineralogical one. He has proposed that most rocks can be fitted into one of the following three textural groups: interlocking, cemented, laminated-foliated. Here, texture refers to the manner in which the constituent grains are arranged and bound together (the petrographer's fabric), rather than reference to grain size.

Coates (1964) reviews the uses to be made of rock mechanics in engineering work, and lists five characteristics or properties which he considers to be most important for engineering applications. On the basis of the five characteristics, he proposes a classification system which recognizes that the rock substance (or material) has certain properties that can be identified, but that the condition of the rock substance in-situ is also of great importance. The three characteristics which deal with the properties of the intact rock material are listed as follows:

- i) The uniaxial compressive strength is the property which immediately indicates whether the rock substance is weak enough, with respect to the application, to be a source of trouble in itself.
- ii) The pre-failure information characteristics of the rock substance indicate whether creep of some nature could be expected in the material itself, at stress levels less than those required to produce failure.
- iii) The failure characteristics of the rock substance, i.e., brittle, or plastic, should influence the safety factor that is used in design, as well as precautions to be taken during construction.

The classification system proposed by Coates is given in Table 2.2. It will be noted that his system is based on both the material properties (Items 1-3) and the in-situ geological discontinuities (Items 4 and 5).

TABLE 2.2

CLASSIFICATION OF ROCKS FOR ROCK MECHANICS

After Coates (1964)

1. Uniaxial compression strength of the rock substance
  - a. Weak (less than 5,000 psi)
  - b. Strong (between 5,000 psi and 25,000 psi)
  - c. Very Strong (greater than 25,000 psi)
2. Pre-failure deformation of rock substance
  - a. Elastic
  - b. Viscous (at stress of 50% of uniaxial compressive strength the strain rate is greater than 2 microstrain per hour)
3. Failure characteristics of the rock substance
  - a. Brittle
  - b. Plastic (more than 25% of the total strain before failure is permanent)
4. Gross homogeneity
  - a. Massive
  - b. Layered (i.e., generally including sedimentary and schistose, as well as any other, layering effects which would produce parallel lines of weakness)
5. Continuity of the rock substance in the formation
  - a. Solid (joint spacing greater than 6 ft.)
  - b. Blocky (joint spacing between 3 in. and 6 ft.)
  - c. Broken (in fragments that would pass through a 3-in. sieve)

4. CLASSIFICATION BY IN-SITU CHARACTER OF ROCK MASS

In the process of assessing the engineering behavior of rock, the engineering geologist and the foundation engineer are faced with the major problem of translating the significant geological observations into engineering terms. The information normally required by the engineer includes data on the strength, compressibility, and permeability characteristics of the foundation rock. In addition, the existing state of stress, the ground-water conditions, and chemical stability of the rock may also be required. Of these characteristics, the first three and the last are properties of both the rock material and the in-situ rock mass. The existing state of stress and ground-water conditions deal only with in-situ characteristics.

A classification system to be used for determining the appropriate kind and amount of support for tunnels in rock was proposed by Terzaghi (1946). In this system, rocks are placed in the following groups in

decreasing order of competency: intact, stratified, moderately jointed, blocky and seamy, crushed, squeezing, and swelling. A similar classification is given by Talobre (1957), except he has six categories, apparently omitting moderately jointed rock. Neither system is particularly concerned with the properties of the rock material. On the other hand, the description of the rock mass is fairly informative from a qualitative standpoint.

The U. S. Bureau of Mines (1962) report that "the type of rock, its physical and geological characteristics, and the stress field before mining, determine, in general, the size and shape of underground openings that can be used and the amount of artificial support that must be installed." A classification system for underground openings in rock is given, in which in-situ rock is divided into two main divisions as follows:

- a. Competent rock -- rock that will sustain an opening without artificial support.
  - (1) massive-elastic (homogeneous and isotropic)
  - (2) bedded-elastic (homogeneous, isotropic beds with thickness less than the span of the opening and little cohesion between beds)
  - (3) massive-plastic (rocks which flow under low stress)
- b. Incompetent rock -- rock which requires artificial support to sustain an opening.

As stated in the USBM report, the system is only for competent rocks, which limits its application to other than the specific purpose intended. Its use would also be limited to engineers with considerable experience because of its qualitative, rather than quantitative basis. It provides no numerical definition or other means for determining whether or not a rock is competent, or to what degree.

A rock classification chart based on joint spacing and weathering has been developed by the Austrian school of rock mechanics (John, 1962). This chart relates two of the important factors governing the bulk strength of a rock mass. These factors are the spacing of the geological joints, and the degree of decomposition (weathering) and resulting compressive strength of the rock material. The rock material is divided into four descriptive classifications as follows:

- |          |   |                                      |
|----------|---|--------------------------------------|
| Type I   | - | Sound                                |
| Type II  | - | Moderately sound, somewhat weathered |
| Type III | - | Weak, decomposed, and weathered      |
| Type IV  | - | Completely decomposed                |

Numerical limits for rock strength are assigned to each of the above categories. A chart of this type will be useful for classification if the description of the rock composition can be made quantitative and reproducible for all rock types (irrespective of the project site), and can be related to the engineering properties of the rock.

Estimation of the degree of jointing (or soundness) in a rock mass may be obtained by use of seismic tests (Onodera, 1963). A laboratory seismic (sonic pulse velocity) test performed on an intact rock specimen is unaffected

by the discontinuities present in the field. The field seismic wave, on the other hand, will be affected by the discontinuities in the rock mass through which it travels; the greater the degree of jointing, the lower will be the seismic velocity. The ratio of the field seismic modulus (a square function of the seismic velocity) to the laboratory seismic modulus can, therefore, be used to estimate the degree of jointing. For an unjointed rock mass, the ratio is assumed to be unity, i.e., the field velocity is the same as the laboratory velocity (assuming no sampling disturbance and identical moisture conditions). For a jointed rock mass, the ratio will be less than unity.

Onodera (1963) presents a classification which correlates the degree of jointing and weathering with the seismic or "soundness" ratio. This procedure includes both the properties of the rock material as well as the discontinuities which affect the mass behavior. Descriptive geological diagnostics are also given by Onodera in which the rock is graded from excellent to bad, and assigned corresponding alphabetical symbols from A to E, respectively. He also suggests that a similar concept may be applied to rock samples from a given site in which an "ideal" specimen is assigned the ideal modulus as determined from a laboratory, sonic velocity test. Other specimens with lower modulus values are downgraded accordingly.

A Rock Quality Designation based on rock hardness and fracture frequency, as determined from rock core examination, has been developed in an attempt to generalize the average, in-situ rock quality (Deere, 1964). In this method, the length of sound, relatively unfractured core per length of core-hole is determined, by considering only core which has a certain minimum hardness, and which is longer than 4 inches. The rock is then rated in designations of Excellent, Good, Fair, Poor, in descending order of rock quality, based upon the percentage of sound core obtained from the boring. A rock which is soft or weathered, a closely jointed rock, or a rock from which the core recovery is low, would fall into the Poor to Fair category. A quantitative method for evaluating rock hardness is desirable in order for this scheme to be reliably used by inexperienced personnel.

Because of the complex relationships which exist between various rock types at a dam-site in the Sudan, four separate grades of rock condition were utilized by Knill and Jones (1965) as follows:

- Grade I : Fresh rock
- Grade II : Slightly weathered rock
- Grade III : Highly or moderately weathered rock
- Grade IV : Completely weathered rock

They report that by this means it was possible to group together rocks of different types which have similar engineering properties. Slopes cut in Grade IV rock disintegrate under wet conditions to angles between 25° and 30°. This rock can be excavated mechanically and, generally, can be dug manually. Grade III rock was usually excavated by blasting; slopes up to 10 meters high were stable, apart from minor spalling. Rock in both Grades I and II was excavated by blasting and, in general, the sounder rock required less explosive than that needed to excavate a similar volume of Grade II and III rock. The four grades of this system are similar to the types proposed by John (1962). For exploratory purposes, the method for assigning a rock to



any particular grade, above, appears to be one based upon experience, thus restricting its universal applicability.

The difficulties to be encountered in obtaining a universal engineering classification system for rock cannot be over-emphasized. Geological classification systems, while providing a basis for naming and describing rocks, contain little information or relationship with the rock properties important to their mechanical behavior. The specific purpose for which a classification system is developed obviously plays an important role in determining whether the emphasis is placed on the material properties of the rock substance or the continuity of the substance in the rock mass. It is important that the process of analysis of a particular problem be made from the point of view of the proposed service of the rock. However, the basic data from which the engineering evaluations are to be made should be an inherent property of the rock (both material and mass), and should be determined from standardized procedures. The same rock should have the same classification regardless of how it is being used (Coates, 1964). For each type of information, a systematic collection of the data, correlated with engineering experience through a consistent system of classification, can lead to improved methods for predicting rock behavior.

It is clearly seen that a universally acceptable engineering classification system for rock should indicate both the properties of the rock material and also the in-situ characteristics of the rock mass. Because the rock-mass characteristics involve both the material properties and the geological discontinuities, a meaningful system for in-situ classification is not likely to be developed without also evaluating the behavior of the rock substance. Thus, the investigation described herein is limited to the first phase of the problem -- the physical properties of the intact rock. This study is not concerned with the behavior and classification of the in-situ rock mass with its inherent discontinuities.

The next section deals with one of the more important physical characteristics of the intact rock material. The concepts of hardness and their application to rocks are presented. The three basic types of hardness (i.e., abrasion, indentation, and rebound) and their methods of measurement are discussed, along with some of the relationships previously observed between hardness and other properties.

## SECTION 3

### HARDNESS OF ROCKS

#### 1. GENERAL

For the past 65 years or more, engineers and metallurgists have been making hardness measurements of metals as a means for assessing their general mechanical properties. Because of the apparent connection between hardness and other properties, simple hardness measurements on the surface serve as an indication of the bulk properties of the material. This application has been extremely valuable in metallurgy; its usefulness for rock materials also shows considerable promise.

Hardness is one of the most investigated properties of materials, and yet it is also one of the most complex to understand. As has been pointed out by many investigators (Obert et al. 1946), hardness is an elusive property; the concept of hardness does not lend itself to exact definition in terms of the customary physical units. A numerical value of hardness is as much a function of the kind of test used as it is a material property.

The term hardness, when used as a technological property of materials, is primarily associated with the surface (Richards, 1961). Mineralogists were among the first to be concerned with hardness because of its close association with the resistance of precious stones to surface scratching and abrasion. The hardness of a mineral is defined by Dana (1932) as "the resistance which a smooth surface offers to abrasion." This connotation was carried over to metals with the development of alloys that could be hardened for high abrasion resistance. If the material is uniform in composition and structure, the surface constitutes a layer only a few atoms thick and loses much of its importance. Thus, in the usual means of measuring hardness, any such thin-surface layer is penetrated and the hardness of the bulk of the material is measured.

In general, hardness implies the resistance to deformation. Richards (1961) defines technological hardness as "the resistance of a material to permanent deformation of its surface." When metals are deformed or indented the deformation is predominantly outside the elastic range and often involves considerable plastic or permanent deformation. However, in dynamic hardness measurements, the elastic properties may be as important as the plastic properties. In all types of hardness, the properties of toughness, resilience, strength, and elasticity are involved to some degree.

Rock hardness is considered to consist of the resistance of rock to the displacement of surface particles by a tangential abrasive force, as well as its resistance to a normal, penetrating force, whether static or dynamic. Rock hardness depends on substantially the same factors as toughness. Toughness is governed by the efficiency of the matrix in binding together the grains or minerals comprising the bulk of the rock. In addition, rock toughness is a function of the grain strength or mineral toughness. The

toughest rocks comprise those having strong minerals embedded in a strong matrix or cement (Shepherd, 1951). Both hardness and toughness depend on the type of binding forces between atoms, ions, or molecules and increase, like strength, with the magnitude of these forces. Both properties are also closely related to the yield strength of the material (Jastrzebski, 1959).

## 2. TYPES OF HARDNESS AND THEIR METHODS OF MEASUREMENT

No other tests on materials approach in numbers the tests made under the name of "hardness tests" as the criteria whereby materials may be classified or selected for special purposes (Williams, 1942). Hardness measurements usually fall into three main categories: abrasion or scratch hardness, indentation hardness, and rebound or dynamic hardness. For laboratory study of rocks, some form of abrasion hardness and the scleroscope rebound hardness have been investigated to the greatest extent.

### a. Abrasion hardness

#### (1) Mohs' scale

Since 1824, Mohs' scale of hardness, although only relative in nature, has been accepted universally as the method of measuring mineral, and therefore, rock hardness. By use of Mohs' scale, the relative hardness of a mineral can be determined. This scale consists of a group of minerals having increasing hardness values from 1 to 10. Each mineral can be scratched by those that follow it, and will scratch the preceding ones in the scale. Minerals 1 and 2 can be scratched by the fingernail; those 3 to 5 by the point of a knife, 6 cannot be marked by a knife but can by a steel file. Number 7 can scratch glass, 8 scratches the file, while 9 is only scratched by the diamond, which is assigned the highest hardness number of 10.

Tabor (1954) showed that the Mohs' hardness scale gives scratch hardness values which correspond to fairly well-defined indentation hardness values. Each increment on the Mohs' scale corresponds to a 60% increase in indentation hardness, excluding diamond, which is anomalous. This regularity in behavior suggests that Mohs did not simply choose "ten common minerals arranged in order of increasing hardness," but experimented until he had satisfied himself that he had obtained "equality of intervals."

Table 3.1 lists the minerals representing the ten steps of the scale, together with their crystal structure (Zwicker, 1954).

#### (2) Rock hardness based on mineral composition

Mohs' scale is obviously applicable only to minerals having homogeneity. Each rock consists of several minerals; scratch tests based on this scale are useless for determining the hardness values of heterogeneous bodies. Shepherd (1950) cites a method for measurement of composite rock hardness, based on mineral hardness as obtained by the Mohs' scale.

TABLE 3.1  
**MOHS' HARDNESS SCALE AND CRYSTAL STRUCTURE**  
 After Zwikker (1954)

Mohs' Hardness Number, $H_M$	Mineral	Formula	Crystal Structure
1	Talc	$3Mg0.4SiO_2 \cdot H_2O$	Layer
2	Gypsum	$CaSO_4 \cdot 2H_2O$	Layer
3	Calcite	$CaCO_3$	Layer
4	Fluorite	$CaF_2$	Ionic
5	Apatite	$CaF_2 \cdot 3Ca_3P_2O_8$	Ionic
6	Feldspar	$K_2O \cdot Al_2O_3 \cdot 6SiO_2$	Mixed ionic-covalent
7	Quartz	$SiO_2$	Mixed ionic-covalent
8	Topaz	$(AlF)_2SiO_4$	Mixed ionic-covalent
9	Corundum	$Al_2O_3$	Covalent
10	Diamond	C	Covalent

This is done by multiplying the percentage of each mineral in a rock by the Mohs' mineral hardness and dividing by 100 as follows:

$$H = \frac{S \times M}{100} \quad (3.1)$$

in which H = hardness of the rock  
 S = percentage of mineral present  
 M = Mohs' number for the mineral

Thus, in a rock containing 74% quartz (7), 6% feldspar (6), and 20% mica (3), the rock hardness would be 6.14. There are obvious disadvantages attached to this method as a difficulty lies in obtaining a true estimation of the mineral content, and errors in measuring hard-mineral content may seriously affect the final results. Moreover, the type and strength of the mineral bonds, which are very important in determining aggregate hardness, are not considered in the procedure.

### (3) Dorry abrasion test

A standard test for determining rock hardness, which was developed by the Office of Public Roads and Rural Engineering, U. S. Department of

Agriculture, is the Dorry test (Jackson, 1916). The Dorry hardness test is performed on a cylindrical sample of rock, 25 mm. in diameter, which is held against a revolving, cast-steel disk under a pressure of 250 gms. per sq. cm. (total load 1,250 gms.). Standard crushed quartz, sized between 30- and 40-mesh screens, is fed upon the revolving disk. Each end of the specimen is worn away in inverse ratio to its hardness. The loss in weight, obtained by averaging both ends after 1,000 revolutions of the disk, is an index of the hardness of the specimen. In order to compare the results with other abrasion tests, the hardness coefficient is calculated by subtracting one-third of the loss in weight from the constant, 20. Hardness values from this test compare remarkably well with those obtained on the basis of mineral composition (Gyss and Davis, 1927).

#### (4) Deval abrasion test

This apparatus consists of one or more hollow, cast-iron cylindrical buckets, 20 cm. in diameter, and 34 cm. long. These closed buckets are mounted together in a frame which supports them at an angle of 30 degrees to a horizontal axis of rotation. The test sample usually consists of about 50 pieces of broken rock weighing 5 kg. After revolving the cylinders 10,000 times at 30 rpm, the amount of material finer than 1/16 in. is obtained and expressed as a percentage of the original weight of the sample. The French coefficient of wear is likewise used in reporting results and is calculated by dividing the number 40 by the percentage of wear. The standard method of test for abrasion of rock by the Deval machine is given by ASTM Designation: D 2-33.

#### (5) Other abrasion tests

(a) Burbank (1955) describes a device for determining the relative abrasiveness of rocks, minerals, and ores. It consists of a steel, single-paddle impactor turning on a shaft at 632 rpm. The paddle strikes a column of rock particles (4 lbs. per test) falling away from an outer, slowly revolving, 13-inch-diameter drum. The loss in weight of the paddle, during controlled test conditions, represents the abrasive action of the rock.

(b) A tentative method of test for abrasion resistance of concrete is given by ASTM Designation: C 418-64T. This test consists of subjecting the concrete to the impingement of air-driven, silica sand.

(c) Tentative methods of test for resistance to abrasion of small- and large-size aggregates by use of the Los Angeles Machine are given by ASTM Designations: C 131-64T and C 535-64T, respectively.

(d) A tentative method of test for relative resistance to wear of unglazed ceramic tile by the Taber Abraser is given by ASTM Designation: C 501-62T.

(e) A standard method of test for resistance of transparent plastics to surface abrasion is given in ASTM Designation: D 1044-56. This involves the measurement of the optical effects produced on transparent plastics by the Taber Abraser.

(f) A standard method of test for plastic materials to withstand mechanical abrasive action such as rubbing, scraping or erosion, is given in ASTM Designation: D 1242-56.

(g) A tentative test method for Bierbaum scratch hardness of plastic materials is given in ASTM Designation: D 1526-58T. A known weight is applied directly above an accurately-ground, diamond point, mounted on the end of a leaf spring. The specimen is moved laterally causing the point to cut a groove in the surface. The index of hardness is calculated from the weight applied and the measured width of the groove.

b. Indentation hardness

Since about 1900, a wide variety of penetrator sizes and loading devices have been used for the static indentation hardness of metals, in which the depth, area, or diameter, of an impression under a known load is measured. Summaries of these and comparisons of several of the standard tests are given by Devries (1911), Lea (1936), Williams (1942), and Tabor (1951). Essentially, three penetrator shapes are used in all of these tests; indenters are either spherical, conical, or pyramidal. Spherical indenters are used in the Brinell and Rockwell tests; conical indenters are used in the Rockwell and Ludwik tests; and pyramidal indenters are used in the Knoop and Vickers tests. Loading varies from as little as 7 kg. in the Vickers test (Brace, 1960) to as much as 3,000 kg. in the Brinell test (Tabor, 1951). A description of the standard method of test for Brinell hardness of metallic materials is given by ASTM Designation: E 10-65. Standard methods of test for Rockwell hardness and Rockwell superficial hardness of metallic materials are given by ASTM Designation: E 18-65. The standard method of test for diamond pyramid hardness of metallic materials is given by ASTM Designation: E 92-65.

More recently, indentation hardness tests have been performed on minerals and rock materials. Knoop, Peters, and Emerson (1939) determined the Knoop hardness numbers for the standard minerals of Mohs' scale. The hardness ratio of diamond and quartz on this basis is 8:1 rather than 10:7 as given by Mohs' scale. King and Tabor (1954) compared hardness with compressive strength of halite. Brace (1960) reports indentation tests on polycrystalline, monomineralic, isotropic samples of four rock types using a Vickers indenter, with loads from 7 to 75 kg. Kraatz (1964) performed Rockwell hardness tests on samples of 24 different rocks from the present study.

Another type of indentation tester is the durometer. This is described in the standard method of test for indentation hardness of plastics, ASTM Designation: D 1706-61.

c. Rebound or dynamic hardness

Dynamic hardness of a material may be defined, by analogy with static hardness, as the resistance to local indentation when the indentation is produced by a rapidly moving indenter. In most practical methods, the indenter is allowed to fall under gravity onto the surface. It rebounds to a certain height and leaves an indentation in the surface.

A review of the literature on rebound-hardness testing of materials, indicates that several methods have been developed and put to various applications. Greaves (1909) describes the Shore scleroscope, in which the relative

height of rebound of a diamond-tipped hammer falling freely on a horizontal, plane surface, is a measure of the hardness of the material. Griffith (1937) and Obert et al. (1946) used the scleroscope in obtaining hardness values in their studies on the physical properties of rock. Wolansky (1949) reports use of the scleroscope in Germany in an attempt to obtain reliable and comparable values for the hardness of rock, particularly with respect to drillability and workability. Shepherd (1950) used the Shore scleroscope for rock-hardness measurements in studying physical properties and drillability of rock. Wuerker (1953), in plotting data from the U. S. Bureau of Mines for a group of more than 100 rocks, gives three equations for describing the relation of compressive strength to Shore hardness. He further suggests that since the scleroscope test is fast and inexpensive, it could be useful for determining strength and other physical data, outside of the testing laboratory. Kapadia (1951) correlated scleroscope hardness with elastic and strength characteristics of a limited number of rock types. Gilbert (1954) determined the scleroscope hardness of single crystals of Mohs' scale minerals and found an approximate, linear relationship, in the range of two to seven, inclusive. Harvey (1963) describes a specially-designed instrument for determining the relative impact resistance of limestones and dolomites of various textures. He concluded that the resistance to impact for these rocks is controlled by the porosity and size of crystals composing the rock.

### 3. TOUGHNESS AND RESILIENCE

Because of the apparent connection between hardness, toughness, resilience, strength, and elasticity, it is appropriate to discuss briefly the properties of toughness and resilience.

#### a. Toughness

Toughness primarily reflects the ability of a material to absorb energy during plastic deformation. In a static test, this energy is measured by the area under the stress-strain curve, which represents the work required to fracture the test specimen. The specific property, modulus of toughness, is the maximum amount of energy a unit volume of the material can absorb without fracture; it is expressed in inch-pounds per cubic inch. The modulus of toughness,  $M_t$ , can be estimated, for materials that indicate a parabolic-shaped stress-strain curve, i.e., cast iron, concrete, et cetera, by multiplying two-thirds of the ultimate strength,  $\sigma_a(\text{ult.})$ , by the strain at failure,  $\epsilon_f$ , as follows:

$$M_t = \frac{2}{3} \sigma_a (\text{ult.}) \times \epsilon_f \quad (3.2)$$

It can be seen that materials of high toughness must have high strength and high ductility. Brittle materials usually have low toughness since they show only small plastic deformation before fracture (Jastrzebski, 1959).

A simple method for measuring the impact toughness of rock is embodied in the Page impact machine. The impact test is made on carefully prepared cylinders of intact rock, 25 mm. high by 25 mm. in diameter. A weight of 2 kg. is permitted to fall vertically between parallel guides, upon a spherical-ended plunger weighing 1 kg., which rests in contact with the specimen. The height of the first blow is 1 cm. and each successive

blow thereafter is increased in height by 1 cm. The height in centimeters of the blow at failure is recorded as the toughness of the material. The standard method of test for toughness of rock by this method is given in ASTM Designation: D 3-18. Obert et al. (1946) used this procedure, with slight modification, in standardizing tests of mine rock.

From data obtained by the U. S. Department of Agriculture with the Page impact machine, Gyss and Davis (1927) have compiled a table comparing relative values of toughness with relative wear (i.e., relative resistance to wear). These data are plotted in Figure 3.1. The property of rock toughness is also seen to be related to rebound hardness. This is indicated by the relationship in Figure 3.2 between abrasion and Shore hardness, since both Figures 3.1 and 3.2 have a measure of abrasion hardness plotted as the ordinate.

#### b. Resilience

"The capacity of a material to absorb energy in the elastic range is designated as its resilience" (Jastrzebski, 1959). The modulus of resilience is equal to the area under the elastic portion of the stress-strain curve and is defined as the strain energy absorbed per unit volume when the material is stressed to its proportional limit. The two properties, strength (here yield strength) and elasticity, which seem to influence resistance to compression most, both occur in the following formula for modulus of resilience:

$$M_r = \frac{\sigma_a(y)^2}{2E} \quad (3.3)$$

in which  $M_r$  is the modulus of resilience in inch-pounds per cubic inch, and  $\sigma_a(y)$  is the yield strength. This equation indicates that for a high modulus of resilience the material should have high yield strength and low elastic modulus.

The term resilience should not be confused with modulus of resilience. Within the proportional limit, the resilience is equal to the external work put into a material during deformation. Thus the total resilience of a material is the product of its volume and the modulus of resilience (Eshbach, 1952). A low resilience is desirable for good damping, and high resilience for low internal heat generation (Richards, 1961).

The moduli of resilience in compression, of some typical rocks tested by the U. S. Bureau of Mines (Windes, 1949), are represented graphically in Figure 3.3. The sample of concrete of conventional mix is shown for purpose of comparison. The values of the moduli of resilience of the various specimens in the plot are:

<u>Rock</u>	<u><math>M_r</math> (in-lb/in<sup>3</sup>)</u>
Jaspilite	448.0
Hematite ore	134.0
Amphibolite	124.5
Marble	66.3
Sandstone	62.5
Concrete	5.0



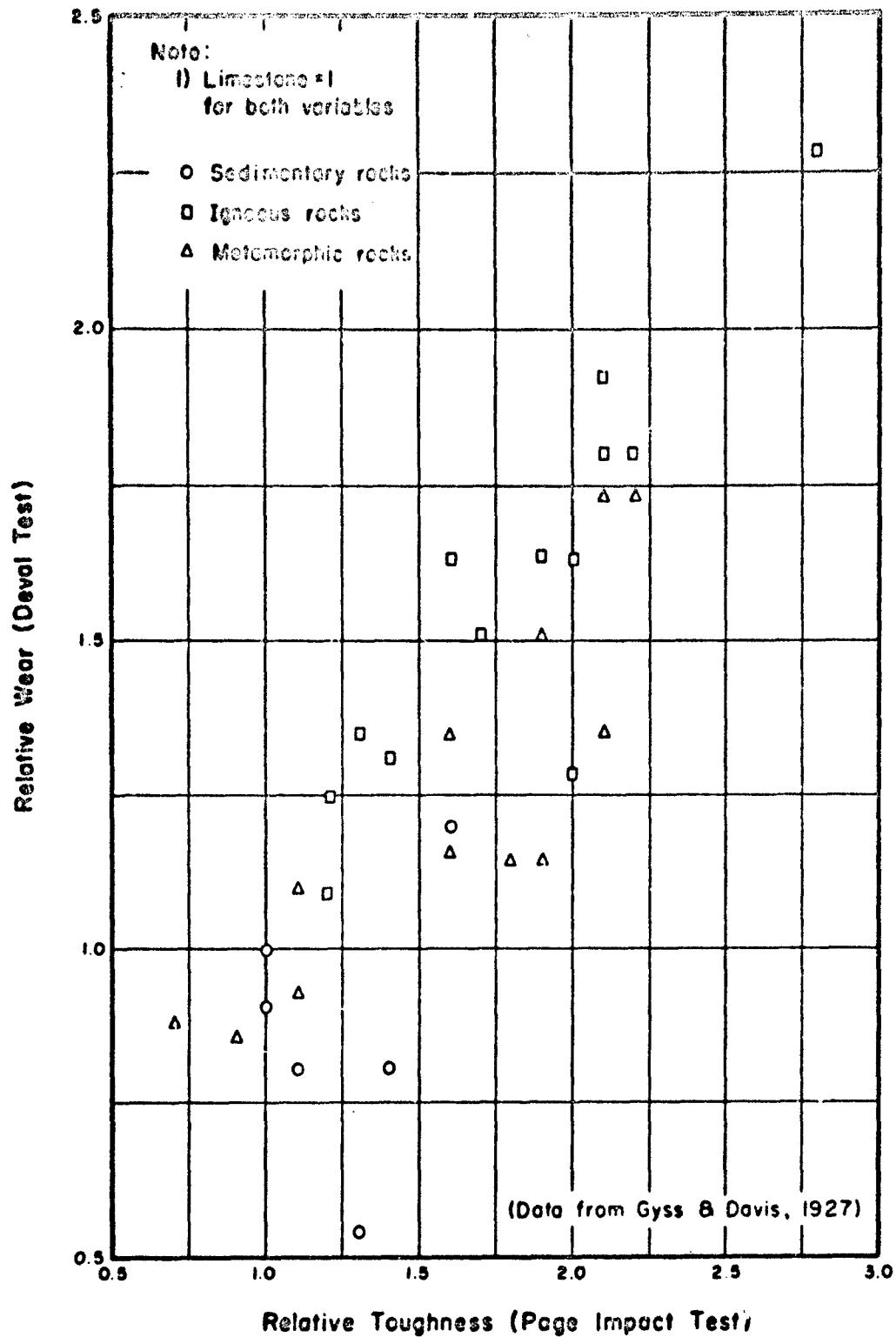


FIGURE 3.1 RELATIONSHIP BETWEEN RELATIVE VALUES OF IMPACT TOUGHNESS AND WEAR RESISTANCE FOR ROCK

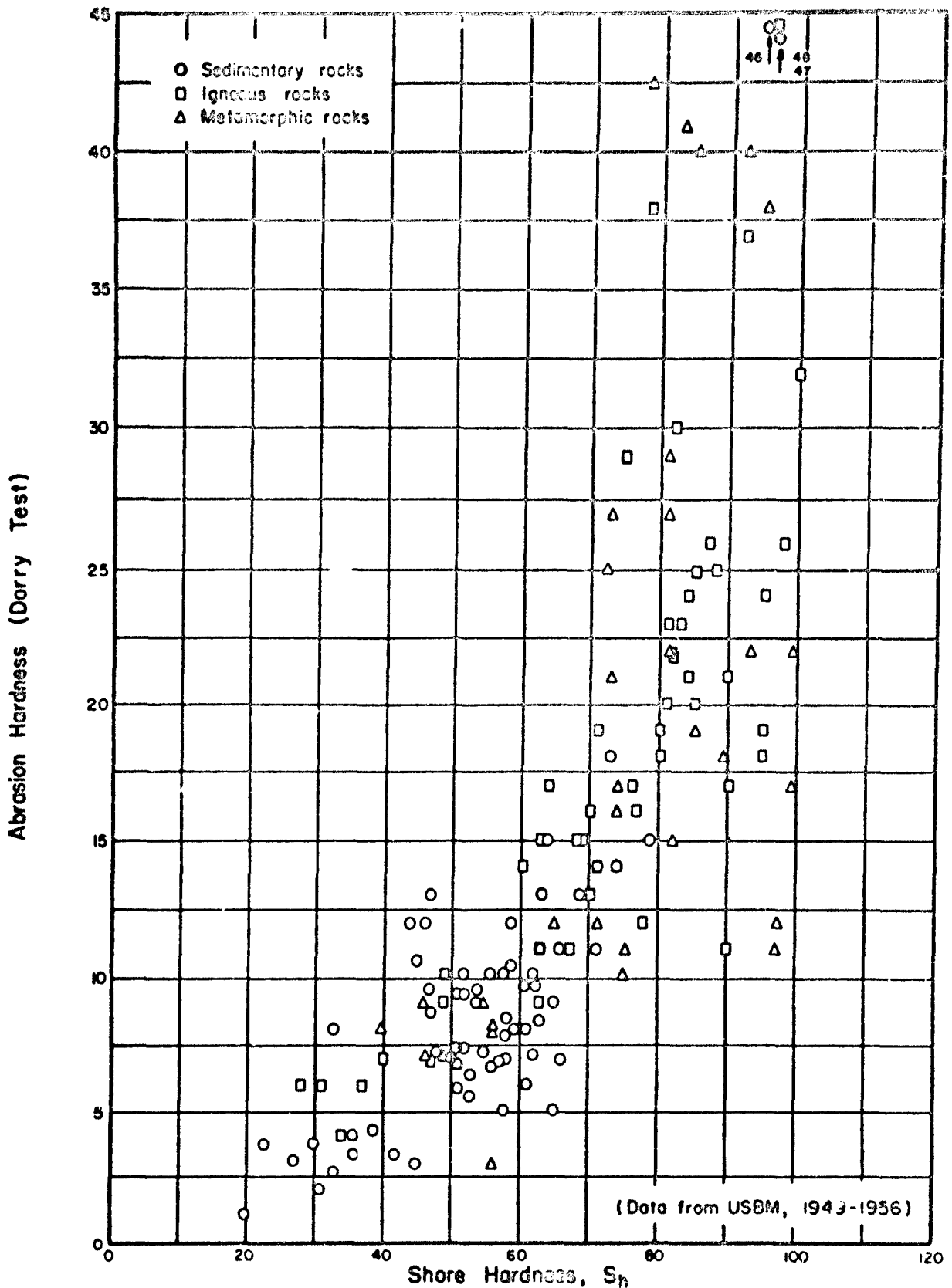


FIGURE 3.2 RELATIONSHIP BETWEEN SHORE HARDNESS AND ABRASION HARDNESS FOR ROCK

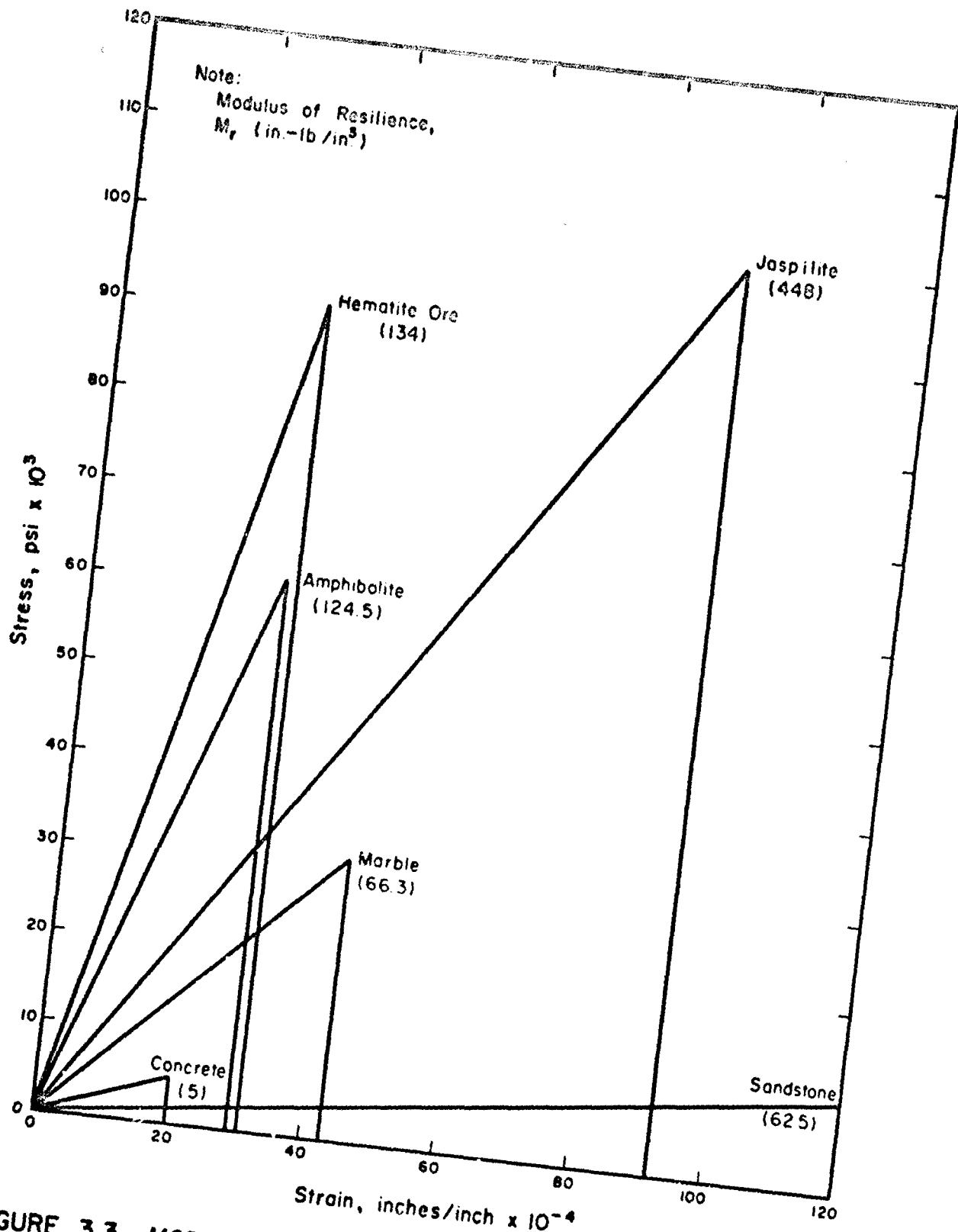


FIGURE 3.3 MODULI OF RESILIENCE OF SOME TYPICAL ROCKS  
TESTED BY U.S. BUREAU OF MINES (After  
Wuerker, 1953)

The concept of strain-energy expressed by  $M_r$ , which is equal to the area under each of the stress-strain diagrams herein, shows clearly the influence of the two variables, strength and elasticity, on the failure of these particular rocks. Although the marble and the sandstone have about the same modulus of resilience, it is evident from the generalized stress-strain diagrams in Figure 3.3 that the former sustains a much higher load and a smaller deformation. The overall energy in either case is theoretically about the same. It should be noted that only in exceptional cases (in the static determination of the modulus of elasticity of rocks) are straight-line relations between stress and strain obtained (Wuerker, 1953).

#### 4. HARDNESS AND OTHER PHYSICAL PROPERTIES

Because of the highly complex state of stress around an indentation, there is no way of relating hardness measurements to each other, or to other mechanical properties on the basis of theory. However, in view of their similarities, different types of hardness numbers can be related to each other empirically for any given material. Qualitatively, we might also expect some sort of correlation between hardness and other properties involving about the same amount of deformation (Richards, 1961).

##### a. Relationship between abrasion hardness and compressive strength

Data obtained by the U. S. Bureau of Mines (1949-1956) are plotted in Figure 3.4, and indicate a reasonably consistent proportionality between abrasion hardness and compressive strength. This plot is remarkably similar in shape to Figure 3.2. It can be concluded from these plots that compressive strength and Shore (scleroscope) hardness may be linearly related.

##### b. Relationship between indentation hardness, compressive strength, and modulus of deformation

Brace (1960) compared the indentation hardness and compressive strength of limestone, marble, anhydrite, and artificial rock salt. He used a  $136^\circ$  Vickers pyramidal indenter which produces an approximately hemispherical, deformed zone beneath the surface indentation. By means of model analysis and elastic theory, approximate stress and strain fields were determined for the deformed zone, from which average values of stress difference, confining pressure, and strain were determined. These three quantities agreed fairly well with a point on a stress-strain curve obtained from a confined compression test of a cylinder of the same material. Brace concluded that, for nearly all incompressible isotropic materials, strength is about one-third of the hardness ( $\text{kg}/\text{mm}^2$ ); and that for rocks, this strength is the stress difference which can be supported at a confining pressure of about one-sixth of the hardness.

Kraatz (1964) performed Rockwell tests using a major load of 150 kg. and a 1/2-inch diameter steel-ball indenter. He found an approximately linear relationship between compressive strength and Rockwell number for rocks having strengths of less than 12,500 psi. Similarly, a linear relationship was indicated for tangent modulus values below  $6 \times 10^6$  psi. Above these limits, the Rockwell number remains essentially constant irrespective

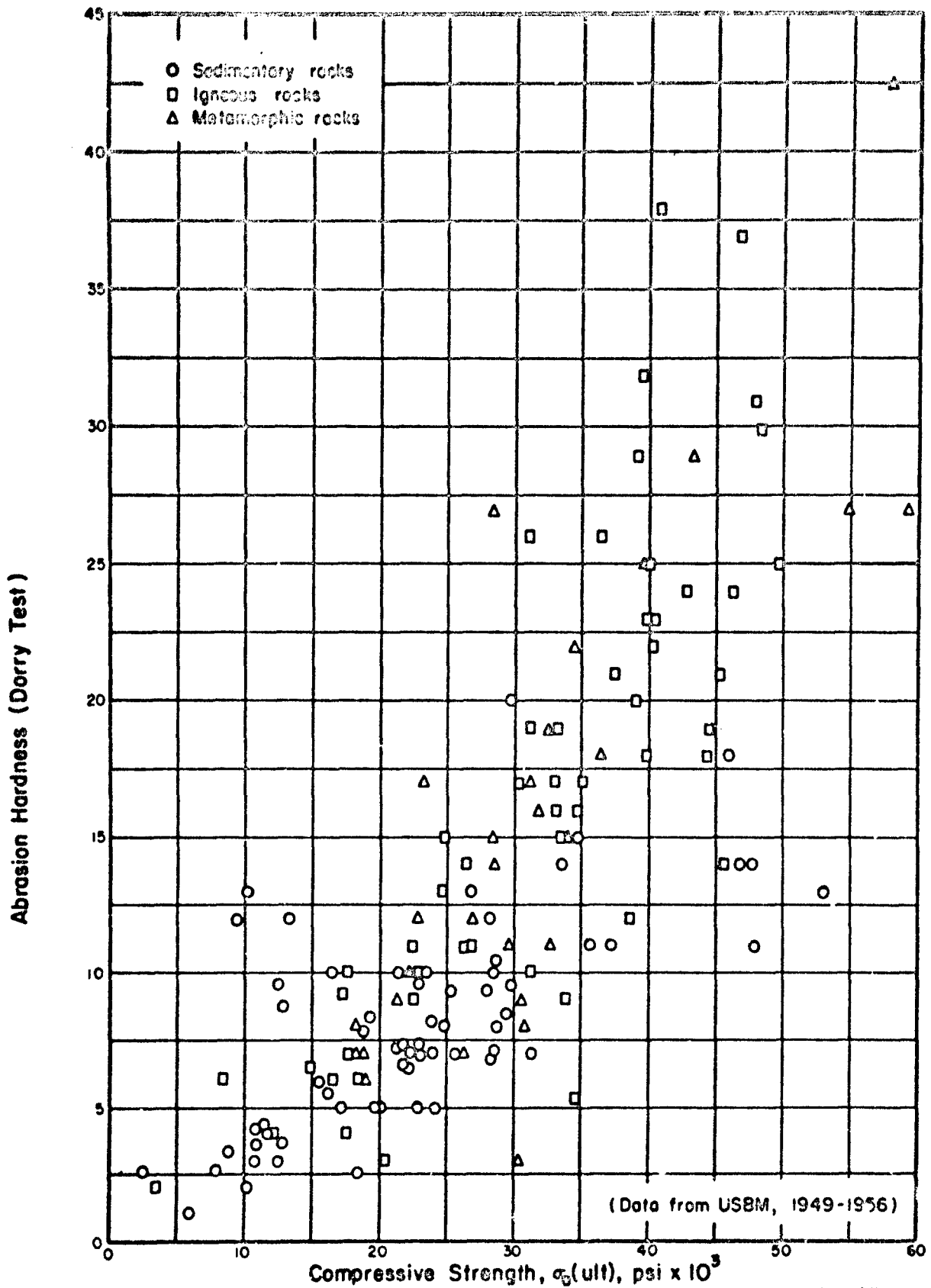


FIGURE 3.4 RELATIONSHIP BETWEEN ABRASION HARDNESS AND ULTIMATE COMPRESSIVE STRENGTH FOR ROCK IN UNIAxIAL COMPRESSION

of increased strength and modulus. Kraatz concluded that the effective range of the Rockwell equipment was exceeded above these limits.

c. Relationship between rebound hardness and compressive strength

Griffith (1937) obtained data on the physical properties of approximately 100 typical American rocks, and formulated much of these data analytically into simple working formulas. In correlating the uniaxial compressive strength data with rebound hardness, as determined by the Shore scleroscope, Griffith suggested the following relation:

$$S_c = 300 H (1 \pm \frac{1}{10}) \quad (3.4)$$

in which  $S_c$  = compressive strength in psi  
 $H$  = scleroscope hardness in scleroscope units

The data obtained by Griffith are replotted in Figure 3.5. Griffith's suggested "average" line is shown, although different symbols have been used for the two parameters as follows:

$$\sigma_a \text{ (ult.)} = 300 S_h \quad (3.5)$$

in which  $\sigma_a$  (ult) = compressive strength in psi  
 $S_h$  = Shore (scleroscope) hardness in scleroscope units

The same variables have been plotted from a group of nearly 250 rock specimens, tested by the U. S. Bureau of Mines (1949-1956). Wuerker made the same plot in 1953 for the first 100 of this group. Figure 3.6 indicates that the average relation between compressive strength and Shore hardness is described by the equation:

$$\sigma_a \text{ (ult.)} = 400 S_h \quad (3.6)$$

Griffith's formula forms a lower limiting range for these rocks, while the upper range, as suggested by Wuerker (1953), is formed by the line:

$$\sigma_a \text{ (ult.)} = 500 S_h \quad (3.7)$$

Many of the very high strength rocks tested by the U. S. Bureau of Mines lie above this, and suggest (as Wuerker did) that a parabola would probably fit the plotted values better than a straight line.

The L/D ratios of the USBM specimens were 1:1. If we assume that Griffith's specimens were 2:1, and apply the correction recommended by ASTM Designation: C 170-50 for relating the compressive strengths of specimens of different L/D ratio's, the average line for the Griffith data is:

$$\sigma_a \text{ (ult.)} = 340 S_h \quad (3.8)$$

This is in somewhat better agreement with the USBM data for the lower Shore values; however, equation (3.6) provides the better average relationship for all values.

The Shore (scleroscope) hardness test is rapidly performed, inexpensive, and nondestructive. These data suggest the desirability of attempting to establish the general application of this test, or one of similar nature,

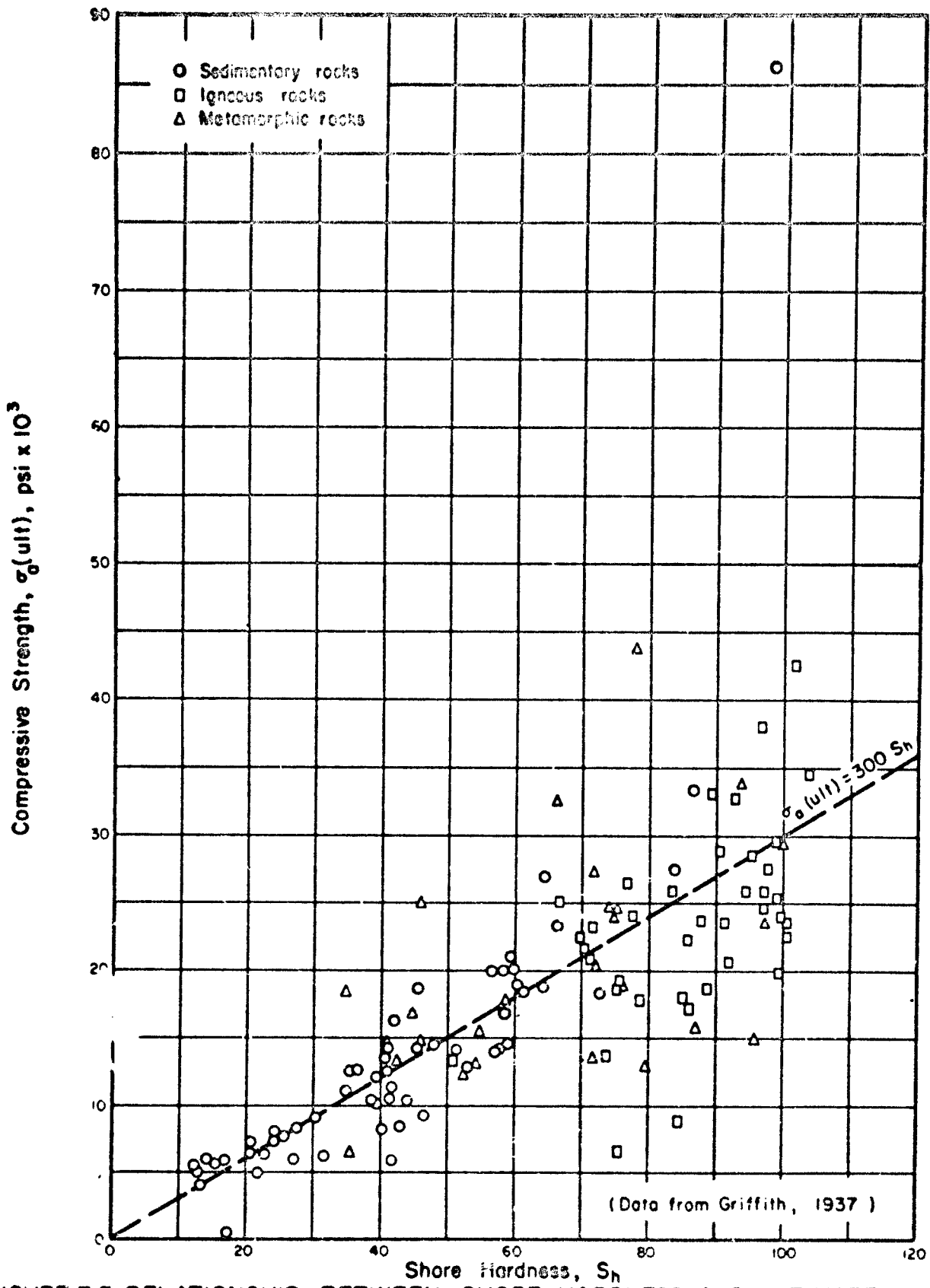


FIGURE 3.5 RELATIONSHIP BETWEEN SHORE HARDNESS AND ULTIMATE COMPRESSIVE STRENGTH FOR ROCK IN UNIAxIAL COMPRESSION

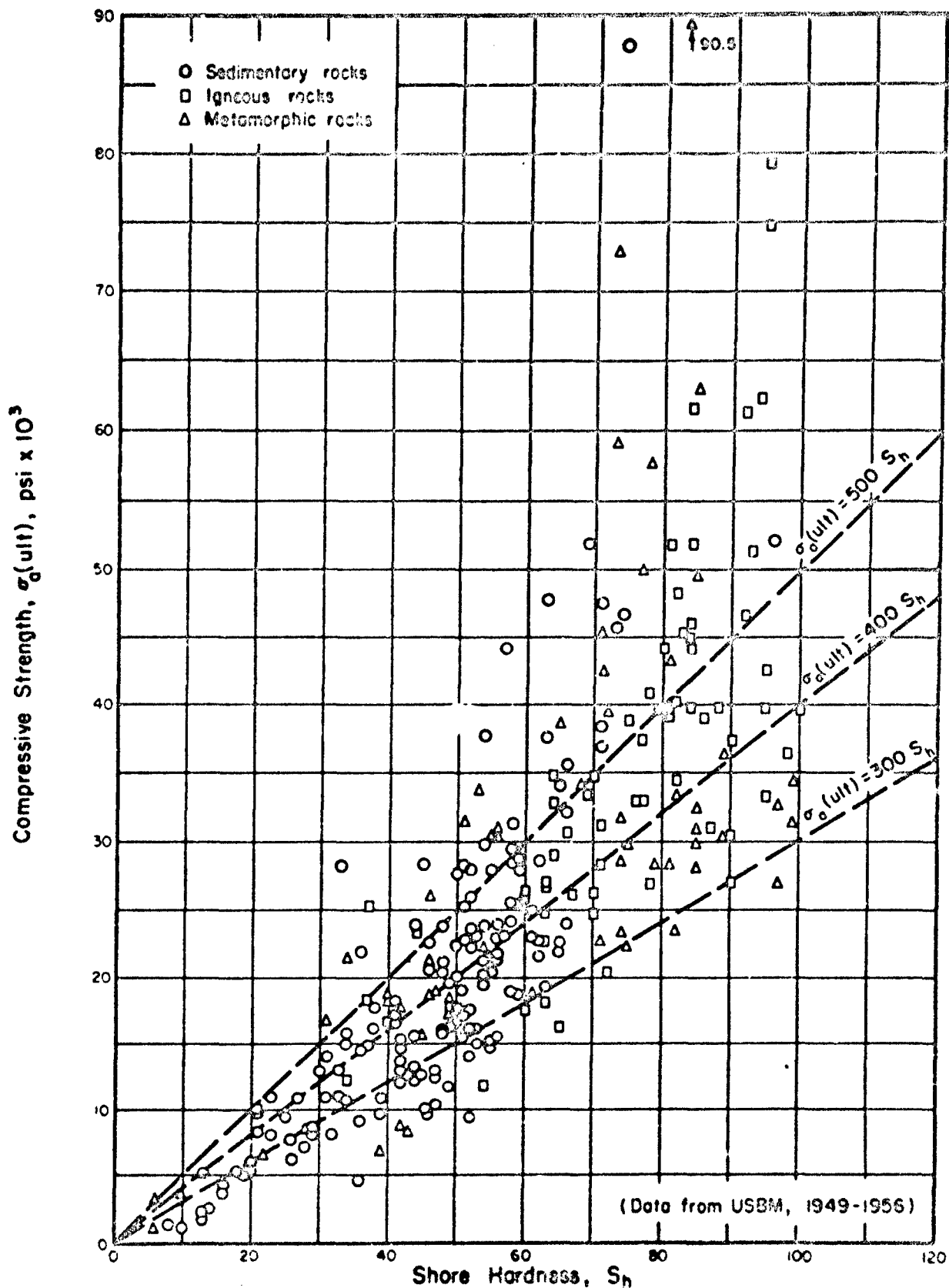


FIGURE 3.6 RELATIONSHIP BETWEEN SHORE HARDNESS AND ULTIMATE COMPRESSIVE STRENGTH FOR ROCK IN UNIAxIAL COMPRESSION



for estimating other physical properties of rock. The significant relationships might then be used as a basis for an engineering classification for intact rock specimens.

## 5. HARDNESS AND DRILLING

Economic and efficient breaking of rock is governed to a very great extent by the successful application of rock drills, whether they consist of the percussive or rotary type. Because of the many variables involved, this subject has been somewhat difficult to interpret by fixed rules governing the amount of energy that must be used to drill any particular rock stratum. So-called "hard rocks" have been drilled easily compared with softer rocks because of their more brittle and chipping characteristics. For example, a hard igneous or metamorphic rock may be drilled more efficiently than a compact limestone (Shepherd, 1950).

The word hardness as used in the drilling industry, has a variety of meanings which depend upon the type of drilling method employed. The term, "hard rock", is generally used to describe a geological formation which for any reason is difficult to drill. In diamond drilling, hardness is interpreted as resistance to abrasion. In percussion drilling, the term implies resistance to impact or indentation; while in rotary drilling, hardness is considered as analogous to compressive strength. Although these may be conflicting variables for different types of rock, the term hardness is applied indiscriminately by the industry for the resistance of rock to penetration by any type of drilling technique (Mather, 1951).

The volume of blast- and bore-hole drilling done in the mining, oil, and construction industries is exceedingly great. Hence, the problem of increasing drilling efficiency takes on a great deal of significance. Drilling efficiency depends on the mechanical properties of rocks, the drilling tools, and the men who do the drilling (Protodyakonov, 1963). Extensive research has been conducted by manufacturers of various drilling rigs, drill steel, bits and other equipment, in order to determine the most suitable types for drilling in certain strata. However, until the last 15 years or so, very little research has been concerned with the more fundamental aspects of drilling and the influence of the physical characteristics of rock on the vague property "drillability."

Some of the studies which have dealt with this problem have been concerned with the basic processes by which energy is transmitted through the system into the rock during percussive drilling (Hartman, 1959; Fairhurst, 1961a). Others discuss the mechanism and fundamentals of rock failure under impact and percussion (Pennington, 1954; Singh and Hartman, 1961); and the mechanics of rock penetration and fragmentation with both percussive and rotary drilling systems (Fairhurst and Lacabanne, 1957; Cheatham, 1958; Appl and Gatley, 1961). Correlation of physical property tests with force-displacement data was used by Reichmuth (1963) as the basis of a new theory concerning the sequences of failures produced by penetration of a wedge into brittle materials.

Some investigators have felt that although a knowledge of the physical properties is helpful, in general, physical properties are not a reliable guide to drillability. Rollow (1963) suggested that the best way to measure formation drillability, with respect to rolling cutters, is to "drill with rolling cutters." He describes a laboratory test, whereby drillability can be predicted on the basis of drilling small samples with a 1 1/4-inch diameter micro-bit. By drilling rock-formation samples with this micro-bit, and measuring drilling rate and tooth wear, estimates can be made of large bit performance. First use of the micro-bit was reported by Scott (1946) to assist in correlating the drillability of rock with the crushing strength. Head (1951) used a micro-bit in establishing a drillability classification for 15 geological formations.

Mather (1951) indicates that the principal cause of confusion in the literature dealing with rock drilling can be attributed to varying definitions of the hardness factor of rock and cutting media. Although none of the above referenced research was directly concerned with a study of hardness properties as such, use of the micro-bit actually involves all three types of hardness, i.e., abrasion, indentation, and dynamic or impact.

Other investigators have felt that hardness is closely connected to drillability and have made attempts to discover this relationship, with varying degrees of success. Protodyakonov (1963) states that it is essential to know the hardness, plasticity (deformability), and abrasivity, in order to characterize the mechanical properties of rocks in drilling. For determining the strength of rocks, he describes a pounding technique for breaking up rock in which an empirical strength coefficient is obtained. He estimates deformation from Shore hardness tests, by use of equation (5.6) herein. Hardness and abrasivity are evaluated by means of a specially-devised drilling apparatus. (Protodyakonov does not make a clear distinction between his various uses of the word, hardness.) Head (1951) conducted limited tests using a Knoop indenter, in order to determine the relationship between the drillability of seven different geological formations and the hardness of specimens from these formations. He concluded that no consistent relationship exists between the hardness and drillability of the tested formations, but, rather, that drillability is more related to the manner in which the hard crystals are bound together.

Rebound hardness tests have also been investigated to determine their application as an index of drillability. Wolansky (1949) made use of the scleroscope in Germany for obtaining reliable and comparable values for the hardness of rocks, particularly with respect to drillability and workability. An interesting comparison between results obtained by the use of various makes of scleroscope was made and it was concluded that the Shore instrument gives the most reliable results. It was further concluded that the scleroscope can be useful for indicating drillability, if comparative values are emphasized, rather than absolute numbers. Shepherd (1950, 1951) performed original research on the drillability of rocks, in order to compare the resistance to penetration and to correlate the results with the physical properties. He discusses the use and limitations of hardness tests when applied to drilling, and concludes that scleroscope readings, unless correctly analyzed, give no useful guide to rock drillability.

The next section describes the laboratory studies which were performed in order to obtain specific values for comparison of physical properties of selected rock types under controlled conditions. Among the numerous tests conducted were two types of rebound hardness measurements, and a new (but as yet unperfected) method for measuring abrasion hardness. Indentation hardness tests for the majority of rocks from this study were performed by Kraatz (1964); therefore these tests were not repeated in the present study.

## SECTION 4

### EXPERIMENTAL STUDIES

#### 1. GENERAL

The compressive strengths, elastic properties, sonic velocities, various types of hardness measurements, and other physical properties, were determined for rocks from 27 localities. Thirteen geologically distinct rock types are represented. Selection of the rocks was primarily limited to the common types most likely to be encountered in civil engineering projects within the United States. Other rocks -- marbles, rock salt, tuff, and Solenhofen limestone -- were selected because of their research interest, either in the laboratory or in the field.

All tests reported herein were performed on intact, cylindrical rock specimens, macroscopically homogeneous and free from fractures, joints, and seams. The specimens were prepared from diamond-drill cores from field projects, or from core drilled in the laboratory from rough, quarry blocks. All cores were standard NX-size, having a nominal diameter of 2 1/8 inches and, for the most part, oriented at right angles to the bedding planes. The cores were cut approximately to length with a diamond cut-off saw, and then the ends were lapped. All test specimens had a standard length to diameter ratio of 2:1. A total of 257 specimens were prepared and tested in this investigation.

#### 2. DESCRIPTION OF ROCKS

A list of the rock types and the number of specimens of each type are given in Table 4.1. These are listed in numerical order by group numbers which were assigned and maintained for identification throughout the program. The group number is somewhat arbitrary, but consists of assigning consecutive integers to each geologic rock type listed alphabetically (basalt, diabase, etc.). Rocks from different locations, but of the same type, are given a second number following a decimal point in the group number. Thus, for example, the Berea sandstone is numbered 10.1 and the Navajo sandstone is 10.3. The town or city nearest to the project site or quarry from which the rock was obtained is also given in Table 4.1.

Petrographic analyses were conducted on thin sections oriented at right angles to the axis of a representative core specimen from each group. The thin sections were ground to 30 microns ( $\pm 5$  microns tolerance) and covered with 22 x 40 mm. glass cover-plates. The thin sections were examined with a Zeiss petrographic microscope. A mechanical point counter was used to determine the mineral percentages of most of the rocks, except for some of the essentially monomineralic sedimentary and metamorphic varieties. The spacing of the counter, and the number of counts per section were varied at the discretion of the operator, depending upon the grain size, so that the best statistical averages were obtained.

TABLE 4.1  
LIST OF ROCK TYPES

<u>Group No.</u>	<u>Rock Type (Name)</u>	<u>Location</u>	<u>No. Specimens</u>
1.1	Basalt (Lower Granite)	Pullman, Washington	12
1.2	Basalt (Little Goose)	Walla Walla, Washington	6
1.3	Basalt (John Day)	Arlington, Oregon	6
2.1	Diabase (Palisades)	West Nyack, New York	12
2.2	Diabase (Coggins)	Culpeper, Virginia	6
2.3	Diabase (French Creek)	St. Peters, Pennsylvania	6
3.1	Dolomite (Onyota)	Kasota, Minnesota	12
3.2	Dolomite (Lockport)	Niagara Falls, New York	6
3.3	Dolomite (Bonne Terre)	Bonne Terre, Missouri	6
4.1	Gneiss (Dworshak)	Orofino, Idaho	12
5.1	Granite (Pikes Peak)	Colorado Springs, Colorado	6
5.2	Granite (Pikes Peak)	Colorado Springs, Colorado	6
5.3	Granite (Barre)	Barre, Vermont	12
6.1	Limestone (Bedford)	Bedford, Indiana	12
6.2	Limestone (Ozark Tavernelle)	Carthage, Missouri	12
6.3	Limestone (Solenhofen)	Solenhofen, Bavaria	6
7.1	Marble (Taconic White)	West Rutland, Vermont	12
7.2	Marble (Cherokee)	Tate, Georgia	6
7.5	Marble (Imperial Danby)	West Rutland, Vermont	13
8.1	Quartzite (Baraboo)	Baraboo, Wisconsin	7
9.1	Rock Salt (Diamond Crystal)	Jefferson Island, Louisiana	6
10.1	Sandstone (Derea)	Amherst, Ohio	12
10.2	Sandstone (Crab Orchard)	Crossville, Tennessee	9
10.3	Sandstone (Navajo)	Glen Canyon, Arizona	12
11.1	Schist (Luther Falls) ⊥	Unknown Origin	12
11.2	Schist (Luther Falls)	Unknown Origin	6
13.1	Siltstone (Hackensack)	Hackensack, New Jersey	12
14.1	Tuff (NTS-E Tunnel)	Mercury, Nevada	12
<b>Total</b>			<b>257</b>

Photomicrographs of the thin sections were filmed on a Zeiss 'Ultra-phot 11" camera-microscope using Polaroid 4 x 5 sheets (type 55 positive/negative). The petrographic descriptions and photomicrographs are presented in Appendix A.

A brief description of a typical core specimen, from each of the 20 rock samples studied in this investigation, is given in the following paragraphs:

- 1.1 Basalt (Lower Granite), Pullman, Washington  
Dark gray, massive, compact to vesicular basalt; interlocking, crystalline texture. Core samples from dam-site on the Snake River.
- 1.2 Basalt (Little Goose), Walla Walla, Washington  
Very dark gray, massive, compact to vesicular basalt; interlocking, crystalline texture. Core samples from dam-site on the Snake River.
- 1.3 Basalt (John Day), Arlington, Oregon  
Very dark gray to black, massive, compact to vesicular basalt; interlocking, crystalline texture. Some flows of this rock are very highly vesicular; however, the specimens selected for testing contained few or no vesicles. Core samples from dam-site on the Columbia River.
- 2.1 Diabase (Palisades), West Nyack, New York  
Black with lighter gray, speckled appearance, medium-grained, dense, massive diabase; tightly-interlocking, crystalline texture. Block sample from New York Trap Rock Corporation quarry, located in sill intrusion in Newark Group of Late Triassic age.
- 2.2 Diabase (Coggins), Culpeper, Virginia  
Dark gray with lighter gray, speckled appearance, medium-grained, dense, massive diabase; tightly-interlocking, crystalline texture. Block sample from Coggins Granite Industries quarry in Allegheny Mountains near Culpeper.
- 2.3 Diabase (French Creek), St. Peters, Pennsylvania  
Dark gray to black with lighter gray, speckled appearance, medium-grained, dense, massive diabase; tightly-interlocking, crystalline texture. Block sample from French Creek Granite Company, Inc.
- 3.1 Dolomite (Oneota), Kasota, Minnesota  
Buff, fine-grained, massive, porous dolomite; slightly mottled appearance from small, irregular, white veins of calcite; predominantly granular, interlocking texture. Block sample from The Babcock Company.
- 3.2 Dolomite (Lockport), Niagara Falls, New York  
Gray to dark gray, very fine-grained, slightly porous, massive dolomite, containing small infrequent blebs of anhydrite;

texture intermediate between cemented-granular and interlocking crystalline. Block sample from Niagara Stone Division, McLain Industries, Inc.

- 3.3 Dolomite (Bonne Terre), Bonne Terre, Missouri  
Yellowish buff, extra fine-grained, compact dolomite, containing numerous, narrow to very fine calcite-filled fracture veins that are well-healed; interlocking, crystalline texture. Block sample from Valley Dolomite Corporation.
- 4.1 Gneiss (Dworshak), Orofino, Idaho  
Black and white, fine- to medium-grained granodiorite gneiss, with foliation making an angle of 45° with the axis of the core. Somewhat interlocking, foliated, crystalline texture. Core samples from dam-site located in the Orofino series on the North Fork Clearwater River.
- 5.1 Granite (Pikes Peak), Colorado Springs, Colorado  
Predominantly pink with small, irregular, dark patches of biotite mica, coarse-grained, weathered granite; interlocking, crystalline texture. Core samples from NORAD project, Cheyenne Mountain.
- 5.2 Granite (Pikes Peak), Colorado Springs, Colorado  
Gray and pink, fine- to medium-grained, fresh, dense granite; tightly-interlocking, crystalline texture. Core samples from NORAD project, Cheyenne Mountain.
- 5.3 Granite (Barre), Barre, Vermont  
Uniform gray, black, and white, medium-grained, fresh, dense granite; interlocking, crystalline texture. Block samples from Rock of Ages Corporation.
- 6.1 Limestone (Bedford), Bedford, Indiana  
Very light grayish buff, slightly porous, oolitic bioclastic limestone; cemented texture of rounded fossil shells. Block sample from Indiana Limestone Company, Inc.
- 6.2 Limestone (Ozark Tavernelle), Carthage, Missouri  
Light uniform gray, fine-grained, compact limestone, containing numerous fossil shell fragments; cemented, crystalline texture. Block sample from Carthage Marble Corporation.
- 6.3 Limestone (Solenhofen), Solenhofen, Bavaria  
Light grayish buff, extremely fine-grained, massive, lithographic limestone, containing lighter, thin, uniformly distributed "bedding" streaks. Tight, interlocking, crystalline texture. Block samples from U. S. Geological Survey necessitated coring parallel to bedding because of size and shape.
- 7.1 Marble (Canaan White), West Rutland, Vermont  
Very fine white, uniform, fine-grained, massive, saccharoidal marble; tightly-interlocking, crystalline texture. Block sample from Vermont Marble Company.

- 7.2 Marble (Cherokee), Tate, Georgia  
Light grayish white, medium- to coarse-grained, massive marble; tightly-interlocking, crystalline texture. Block sample from the Georgia Marble Company.
- 7.5 Marble (Imperial Danby), West Rutland, Vermont  
Off-white, medium-grained, massive marble, containing infrequent patches of dark impurities; tightly-interlocking, crystalline texture. Block sample from Vermont Marble Company.
- 8.1 Quartzite (Baraboo), Baraboo, Wisconsin  
Pinkish gray to purple, fine-grained, brittle, semi-vitreous, massive Pre-Cambrian quartzite, containing numerous undulatory bedding surfaces; tightly-interlocking, crystalline texture. Block sample from Baraboo Quartzite Company, Inc.
- 9.1 Rock Salt (Diamond Crystal), Jefferson Island, Louisiana  
Grayish white, translucent, very coarse-grained, massive rock salt; interlocking texture. Block sample from Diamond Crystal Salt Company.
- 10.1 Sandstone (Berea), Amherst, Ohio  
Light gray, fine-grained, massive, slightly porous sandstone, containing very fine, light orange, uniformly to randomly distributed flecks; cemented to partially-interlocking texture of subangular to rounded quartz grains. Block sample from Cleveland Quarries Company.
- 10.2 Sandstone (Crab Orchard), Crossville, Tennessee  
Light reddish brown, very fine-grained, compact quartzose sandstone; tightly-interlocking texture. Core axis parallel to bedding planes. Block samples from Luther Falls Stone Company, Urbana, Illinois, and Crab Orchard Stone Company, Inc.
- 10.3 Sandstone (Navajo), Glen Canyon, Arizona  
Orange-red to brown, porous, fine- to medium-grained, friable sandstone; loose hematite-cemented texture of subrounded quartz grains. Core samples from dam-site on the Colorado River.
- 11.1 Schist (Luther Falls)  $\perp$ , Unknown origin  
Light to dark gray quartz-mica-schist. Extreme crenulations visible on sides of core specimens, which were cored perpendicular to the foliation. Numerous garnets visible throughout. Interlocking, crystalline quartz texture, interspersed with micaceous foliation planes. Block sample from Luther Falls Stone Company, Urbana, Illinois. Exact origin is unknown; however, this schist resembles the Manhattan schist in essentially all respects.
- 11.2 Schist (Luther Falls)  $\parallel$ , Unknown origin  
Description as above except axis of each core parallels foliation planes.



13.1 Siltstone (Hackensack), Hackensack, New Jersey  
Dark reddish brown, massive, compact, clayey siltstone; some more sandy and some more shaly phases; clay- and hematite-rich, cemented texture. Core samples from frozen-in-ground gas storage facility in Hackensack Meadows, located in Newark Series of Triassic age.

14.1 Tuff (NHS-E Tunnel), Mercury, Nevada  
Very light pink, porous tuff, containing uniformly-distributed, white, dark gray, and a few random, brown, lithic fragments; cemented texture and a very low-density rock. Block sample from Nevada Test Site.

### 3. PREPARATION OF TEST SPECIMENS

Rock samples were obtained either as NX-size cores from the field, or as block quarry samples which were then core-drilled in the laboratory. In both cases, the samples were in an air-dried state. The standard NX-size core, as accepted by the Diamond Core Drill Manufacturers Association, has a diameter of 2.155 inches  $\pm$  .005 inch. The field cores received for this study were in most instances slightly below these limits; the smallest diameter being 2.070 inches. Laboratory cores were almost uniformly 2.160 inches in diameter; the largest size cores were 2.165 inches.

Block samples were in nearly all cases quarry-sawed, having dimensions on the order of 1-foot square and approximately 5 to 7 inches in thickness. Samples which were irregular or larger than this were cut to the desired dimensions by means of a 30-inch-diameter, water-cooled, diamond-abrasive, cut-off wheel.

#### a. Laboratory core drilling

Coring of the block samples was accomplished by a large, modified shop drill press, fitted with a special diamond-core bit. The drill press, which is illustrated in Figure 4.1, was manufactured by The Fosdick M. T. Co., Cincinnati, Ohio. It is equipped with a 24-inch-square table with edge drains, and has a 2 1/2-inch-diameter spindle with 6 inches travel for any one run. Both the head and the table may be raised and lowered as desired for maximum flexibility in sample size. The throat dimension is 12 inches. The drill is powered with a 1-horsepower, 3-phase, 60-cycle, 220-volt, 1730-rpm, Allis-Chalmers induction motor. Drill speeds can be varied when required as follows: 225, 370, 480, 800, 1085, and 1800 rpm.

The drill press is fitted with a large, water-coolant swivel (#33 Jacobs taper on spindle) and high-pressure hoses for supplying large volumes of water directly from the domestic, water-supply line. Recirculation of the coolant is possible by means of an electric pump from the drill-press sump; however, this did not prove to be satisfactory because the volume and pressure were too low. An 8-inch-diameter aluminum pulley is mounted on the hand-feed wheel by means of which a cable and a weight system provide constant load on the drill bit, as desired.

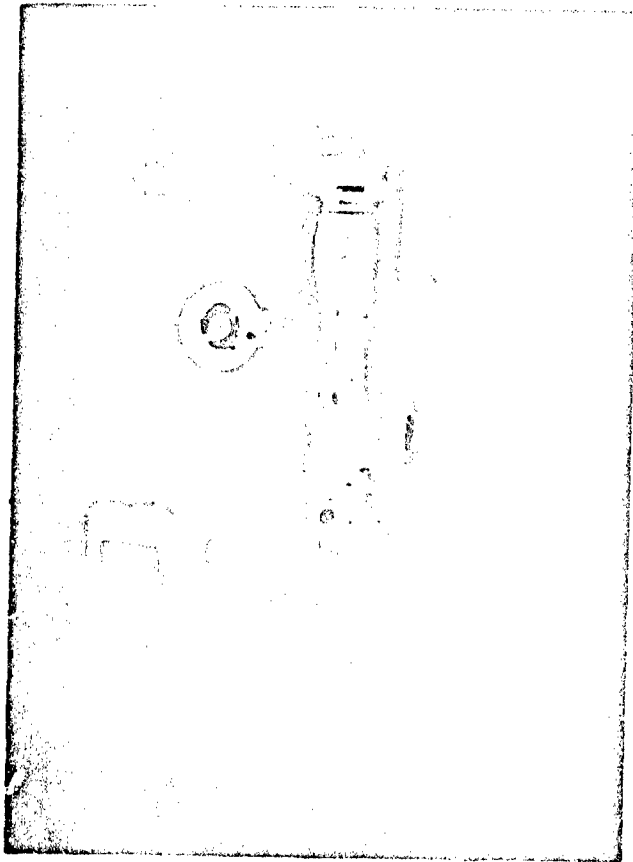


**FIGURE 4.1 DRILL PRESS**

For successful core drilling, it is imperative that the block sample be securely clamped in place. A clamp arrangement which was found to be entirely satisfactory is illustrated in Figures 4.1 and 4.2. This consists of two 10- to 12-inch steel "hairpin" clamps, bolted to the slotted table-top with two 12-inch long bolts. Each clamp is supported at one end by a 2 x 4 wood block; the opposite end holds down the sample. In order to help align the block sample and provide rotational resistance, steel angles are placed on two sides of the block and bolted to the table-top as well.

The drill bit used for all laboratory-drilled core was manufactured by Anton Smit & Co., Inc., New York. This is a core-matic "glass" drill (so named because of its designed use for cutting holes in plate glass). An annular, diamond-impregnated ring extends  $3/16$  inch below the bottom of the hollow, steel-tube, drill body. Because the thickness of this annular cutting ring is approximately  $1/16$  inch, a minimum amount of power and drilling pressure is required. Difficulty was experienced, initially, during drilling of soft limestone and marble specimens with this bit. Circumferential ridges were obtained all the way down the sample, even though constant loading was applied through all ranges of drilling speed. The ridges were found to be caused by irregular, weld-metal surfaces on the inside root of the annular diamond cutting ring. This was remedied by first coring several specimens of quartz-bearing rocks (granite or quartzite) in order to "clean up" the inside surface of the bit. Later, the manufacturer was careful to correct each bit before shipment. The drill-bit size, used throughout the investigation, was 8 inches in length and  $2.155 (\pm .005)$  inches inside diameter.

The most satisfactory drilling speed was generally found to be 225 rpm (the slowest available), particularly for the softer rocks such as the Bedford limestone. The denser diabases appeared to drill a little more efficiently at 370 rpm, although no method to evaluate this was established. With a reasonably new bit and a weight of 45 pounds on the pulley cable, a 6-inch long specimen of limestone generally required 6 to 8 minutes for drilling. The same size specimen of diabase, with 75 to 100 pounds weight, required 15 to 25 minutes. A specimen of Barre granite required 20 to 45 minutes with the same weight. The most difficult specimens to drill were those from the Baraboo quartzite. With a maximum of 135 to 150 pounds weight, these specimens required approximately 30 minutes to 1 hour to drill with a new, sharp bit. The fifth or sixth consecutive specimen with the same bit required up to 2 hours.

Water was used as a coolant for drilling all rocks except one. Compressed air was fed into the coolant swivel for drilling rock salt. This proved to be relatively satisfactory, although the bit heated considerably (too hot to touch). The operator was equipped with goggles and a respirator. A large, commercial vacuum-sweeper, intake nozzle was installed above the drill bit to minimize the dust during this operation. Because of the necessity for stopping intermittently to allow the bit to cool, approximately 30 to 45 minutes were required to drill each specimen of rock salt, 6 inches in length.

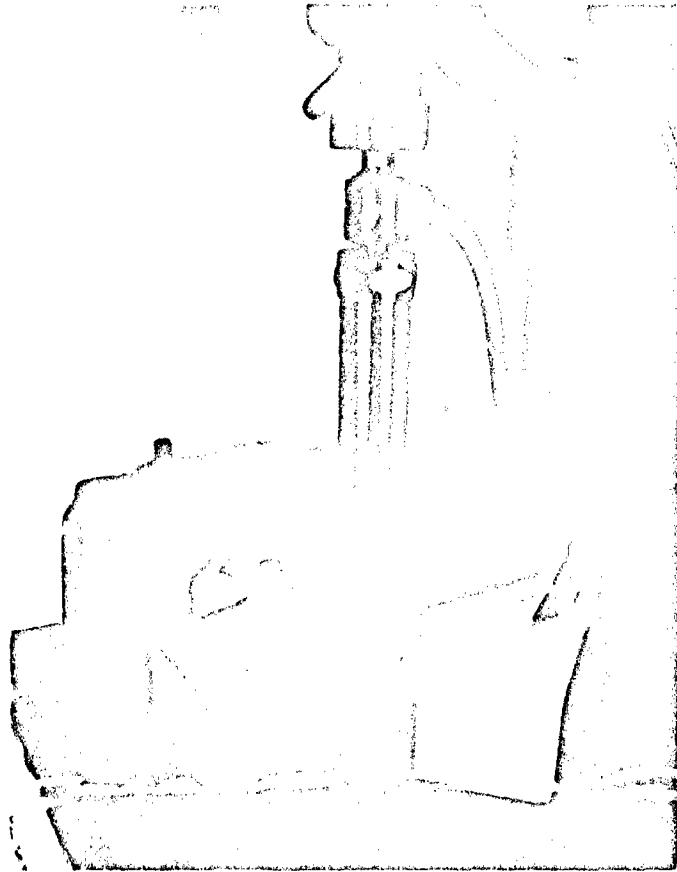


**FIGURE 4.2 BLOCK SAMPLE CLAMPED  
IN POSITION FOR CORE DRILLING**

### b. Sawing to length

All core samples were cut to a length of approximately 4.38 inches with a diamond saw blade. The saw, which is illustrated in Figure 4.3, is a Model J-3 Rock Slab Saw, manufactured by the Highland Park Manufacturing Co., South Pasadena, California. This saw has a 16-inch diameter, 750-rpm constant-speed, diamond blade, and is equipped with a 3-speed, power feed and automatic, cut-off switch. Power for the saw is provided by a 1/2-horsepower, heavy-duty, General Electric motor. The cutting solution and coolant for the blade consists of a mixture of soluble oil (20%) and water (80%). The coolant is placed in the saw box or tank to a depth sufficient to immerse the rim of the blade 3/8 inch.

In order to prevent (or at least minimize) the cutting solution from being absorbed by the sample during sawing, all samples were soaked in water for at least 15 minutes prior to this operation. Those samples which had just been drilled were effectively soaked under pressure. This procedure proved to be quite satisfactory for all rocks except the more porous, Navajo sandstone. A bar of hand soap was used to provide a temporary, relatively impermeable coating over these specimens. The soap was removed by soaking in water following completion of sawing. The rock salt specimens were cut "dry," after lowering the level of the coolant in the saw box below the bottom of the blade.

Just as in drilling, the specimen must be rigidly secured during sawing. This is effectively accomplished by the vise on the saw carriage, a close-up of which is shown in Figure 4.4. Rate of sawing can be adjusted, depending upon the abrasive or other hardness characteristics of the rock. The softer limestones and tuff are cut at the faster rate, which requires about 6 minutes for a single cut through an NX-size specimen. The quartz-bearing granites and quartzites are cut at the slowest rate, and require about 12 to 15 minutes per cut. The diabases, basalts, and harder sandstones are cut at the medium rate of about 10 minutes per cut. Use of these procedures provided smooth, right-angle cuts, relatively free of saw chatter marks.

### c. Lapping the ends

In order to obtain polished, flat surfaces, the ends of all specimens were lapped. A Lapmaster, Model 12 lapping machine, manufactured by the Crane Packing Company, Morton Grove, Illinois was used for this purpose. In the lapping process, a compound consisting of No. 1800 aluminum-oxide abrasive in an oil-based, lapping vehicle is sprayed onto the surface of a circular, serrated, rotating lap plate. One specimen is placed in each of three, close-fitting, aluminum, cylindrical core holders, which are slightly shorter than the finished specimen. The aluminum cylinders containing the specimens fit loosely inside the three conditioning rings, which rest directly on the rotating, serrated lap plate. A circumferential lip on the aluminum cylinders rests on the shoulders of the conditioning rings, thus holding the cylinders off the lap plate and allowing only the specimens and conditioning rings to be in contact with it. A felt pad is placed on top of each specimen, followed by a 4-pound pressure plate. After lapping one end, the specimen is turned over and the pad and plate again replaced for lapping the opposite end. The Lapmaster and various lapping accessories are illustrated in Figures 4.5 and 4.6.

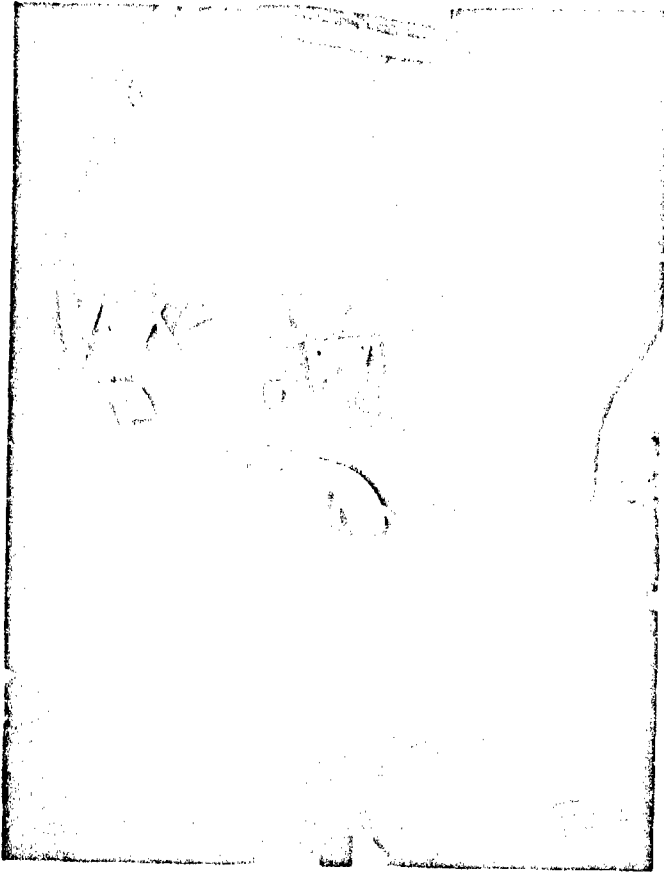


**FIGURE 4.3 DIAMOND ROCK SAW**

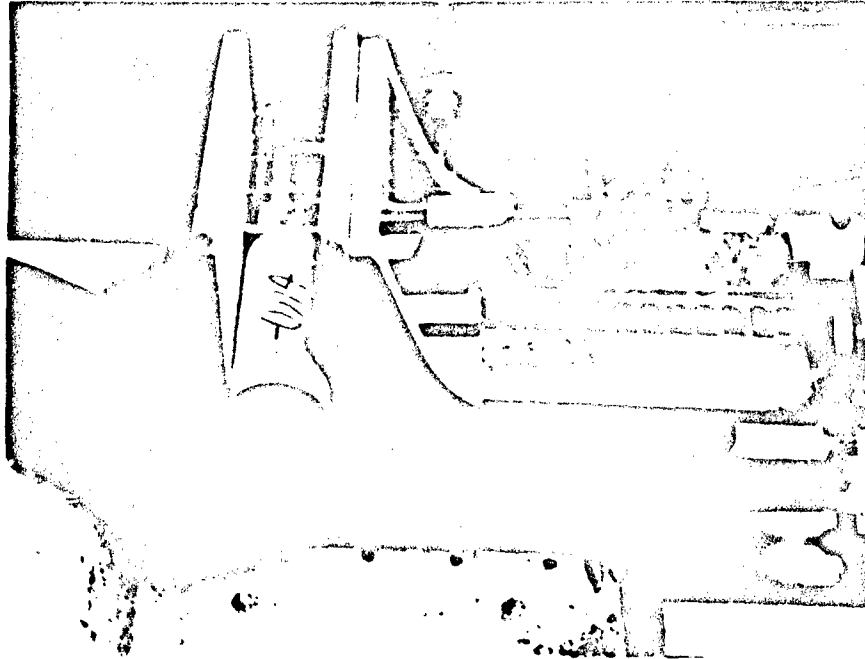


**FIGURE 4.4 CORE SPECIMEN CLAMPED IN  
SAW CARRIAGE**



**FIGURE 4.5 LAPPING MACHINE**

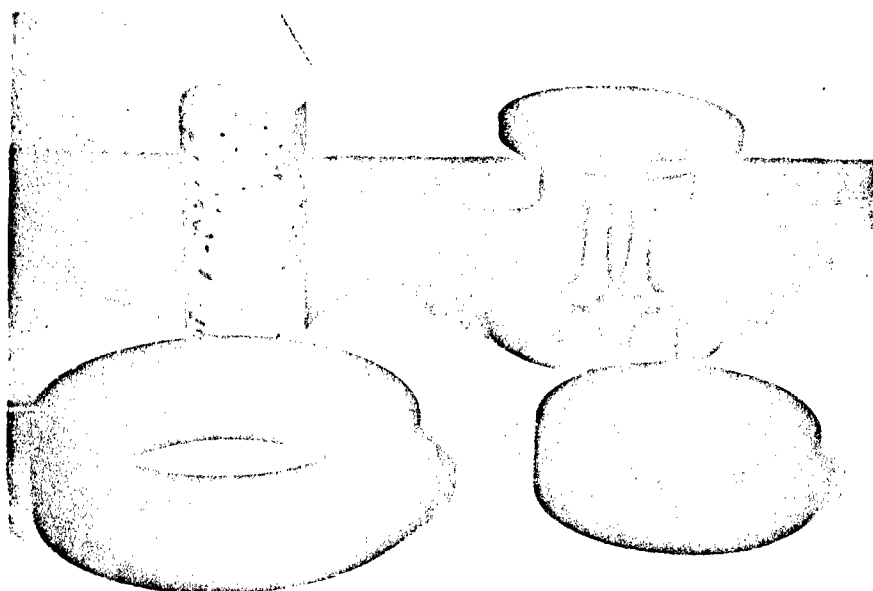


**FIGURE 4.6 CORE SPECIMEN, CYLINDRICAL CORE  
HOLDER, CONDITIONING RING, AND PRESSURE  
PLATE**



Prior to lapping, each specimen (except rock salt) was soaked in water at least 15 minutes to fill up accessible pore spaces, and reduce the amount of lapping vehicle that might enter the sample. In general, 20 to 30 minutes were required for lapping each end of a specimen for nine of the rock samples. The quartz-bearing granites and one diabase required 45 to 60 minutes. The Berea sandstone specimens were lapped from 60 to 90 minutes on each end. The softer dolomites, limestone, tuff, and one marble required approximately 5 to 10 minutes lapping time. Because of their friable nature, the Navajo sandstone specimens could not be lapped.

By use of the above procedures, flatness and parallelism of the test specimens were maintained predominantly within  $\pm 0.0015$  inch. After lapping, the specimen ends were rinsed in benzine solvent, then soaked for 30 minutes in a water solution containing Tide soap. This procedure, which was followed by oven-drying at 100°C. for 24 hours, was very effective in removing all foreign cutting oil, lapping vehicle, and moisture from the test specimens.

#### 4. LABORATORY TESTS

Following oven-drying, all specimens were allowed to remain open to the ambient conditions of the laboratory for at least 2 weeks before undergoing any tests. Because of the variety of porosities represented by the selected rock types, and the various moisture and pore fluid conditions to which the specimens were subjected during preparation, the drying procedures used were considered to be the most desirable for providing a uniform basis from which to begin the test program.

In recommending that testing of rock be accomplished in the 2-week, air-dry condition, conclusions reached by Obert et al. (1946) state that "oven-drying often produces pronounced and sometimes erratic changes in both the elastic constants and the specific damping capacity - - - more-over, this effect is often irreversible." However, the data from which these conclusions were drawn indicate that in going from an initial air-dry to oven-dry condition the following physical property changes were observed:

- i) Dynamic E and G decreased by less than 15%.
- ii) Uniaxial compressive strength increased, on an average, 6%.
- iii) Shore hardness showed no change for marble, granite and one sandstone. Another sandstone increased by 20%.
- iv) Specific damping capacity (ratio of energy dissipated per cycle vibration to the total vibrational energy) showed inconclusive results. There was a two- to three-fold increase in some cases and a 50% decrease in another.

On the other hand, in going from an initial, air-dry state through various moisture conditions to the saturated state, the following changes were observed:

- i) Dynamic E and G generally increased 19% to 35% for some rocks and decreased by the same or greater percentage for others.
- ii) Compressive strength decreased, on an average, 12%.
- iii) Shore hardness decreased 10%.
- iv) Specific damping capacity increased three- to ten-fold.

Colback and Wiid (1965) present data to show that the moisture content has a major influence on the compressive strength characteristics of some rocks. In tests on specimens of quartzitic shale and quartzitic sandstone, they found that the compressive strength under saturated conditions (submerged in water) is on the order of 50% of that under dry conditions (dried for specified time over  $\text{CaCl}_2$  or  $\text{P}_2\text{O}_5$ ).

It is therefore apparent that the potential errors and discrepancies resulting from "wet," variable, and unknown moisture conditions are likely to be much greater, and further from the air-dry state (as recommended by Obert et al., 1946), than the potential errors resulting from the initially oven-dry state as used herein.

a. Unit weight

All specimens were weighed on a Model K-4T Mettler, precision balance to the nearest 0.1 gram immediately following oven-drying, and then again after remaining 2 weeks in the ambient air of the laboratory. The latter values are reported and are used in all computations. During this period, the length and diameter were measured. Lengths were measured by means of an Ames dial comparator to the nearest 0.0001 inch. The average of five different readings, four at opposite points on the circumference and one on the center axis of the specimen, was recorded as the correct length. The diameter was taken as the average of three different measurements with a standard shop caliper, one in the middle and one near either end of the specimen.

b. Shore scleroscope hardness

The scleroscope hardness was determined for all specimens by means of a Model C-2 scleroscope, manufactured by the Shore Instrument & Mfg. Co., Jamaica, New York. The Shore scleroscope is a nondestructive, hardness-measuring device which indicates relative values of hardness by the height of rebound of a small diamond-pointed hammer dropped vertically onto the test surface, from a distance of approximately 10 inches. The hammer falls and rebounds within a close-bore glass tube. Air pressure, supplied by hand compression of a rubber bulb, operates a catch which releases the hammer. The bulb is connected by a rubber tube to a cylinder, containing a piston, at the top of the instrument. The vertical ascent of the hammer after a test is effected by squeezing the bulb, the hammer again being suspended by the catch at the top. The height of rebound is read from a scale of 0-140 divisions.

This instrument is illustrated in Figure 4.7, which shows the position of the specimen for taking readings along the sides. The scleroscope is supported on a cantilever, jointed-arm and may be freely moved to any position over the specimen. The instrument is lowered into contact with the test surface by means of the hand wheel on the left.

Two types of observations were made in this investigation:

- i) Twenty readings, spaced at approximately 0.2 inch were taken along each of four opposite sides of the specimen, making a total of 80 side readings per specimen.

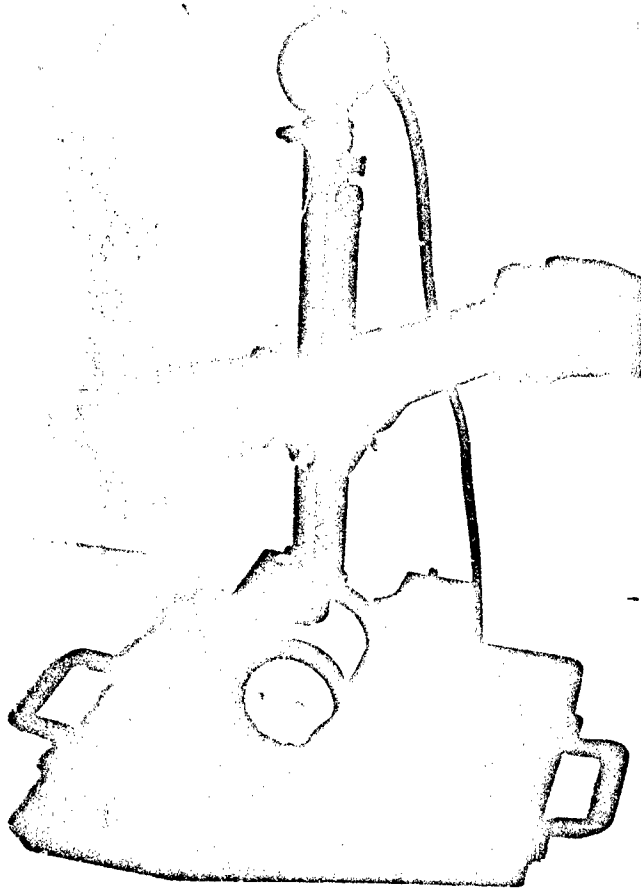


FIGURE 4.7 SHORE SCLEROSCOPE

- ii) Five readings, equally spaced on each of four separate diameters, were taken on each lapped-end surface of the specimen, making a total of 40 end readings per specimen.

The Shore hardness is taken to be the average value of the readings obtained by either method. Both values are reported in the test results. Before a series of tests on any day, the scleroscope was checked by taking a minimum of ten readings on a steel standard, supplied by the manufacturer.

#### b. Schmidt hardness

The Schmidt hardness was determined by means of a Type L Concrete Test Hammer, designed by E. Schmidt, Basel, Switzerland. This instrument has been developed for use in estimating the strength of concrete, and is particularly suitable for concrete already in place within a structure. Use of the Schmidt hammer for rock testing, as described herein, is relatively new, although several authors have recently reported of its application to rock for various purposes. Roxborough and Whittaker (1964-65) report the use of the Schmidt hammer for assessing variations in coal hardness along a mine face in relation to changes in mine-roof conditions. Knill and Jones (1965) used the Schmidt hammer for determining the relative hardness of granite cores, as noted in Section Two. Also Hucka (1965) suggests the use of the Schmidt hammer for rapidly determining the strength of rock, in-situ in a coal mine.

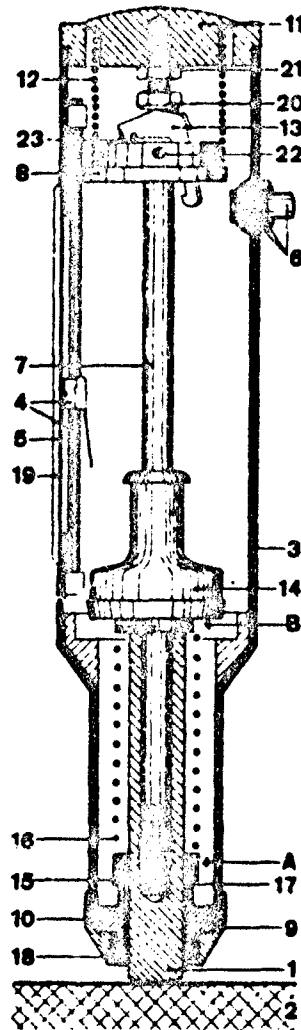
The Schmidt hammer is essentially a nondestructive, portable test device which expends a definite amount of stored energy from a spring, and indicates the degree of rebound of a hammer mass within the instrument, following impact. Initial tests were conducted with the Type N hammer, which has an impact energy of 1.63 ft.-lbs. These tests were unsatisfactory because all but the strongest specimens broke upon impact. The Type L hammer has an impact energy of 0.54 ft.-lbs., which is only 1/3 that of the Type N hammer. This was found to be extremely satisfactory as only occasional, weaker specimens, were broken during impact.

Because of the possibility of cracking, or other damage to the specimens during Schmidt hardness tests, representative specimens from each rock group were set aside for this test series. These specimens were all initially subjected to the nondestructive Shore hardness and sonic velocity tests, but were not used for determining compressive strength and static modulus properties.

A longitudinal section of the Schmidt Test Hammer is shown in Figure 4.8, in which the various component parts are indicated by number. Figure 4.9 shows a photograph of the hammer lying alongside the steel "cradle," which was developed for holding the specimens during testing. The cradle consists of three main parts:

- i) A steel block, weighing approximately 35 lbs., with a semi-cylindrical machined slot of the same radius as the rock specimen,
- ii) steel U-clamps for holding the specimen, if desired, and
- iii) a flat steel plate, also weighing 35 lbs., to which the block may be bolted, for use outside of the laboratory where a firm base is not available.

1. Impact plunger
2. Test specimen
3. Housing
4. Rider with guide rod
5. Scale
6. Pushbutton
7. Hammer guide bar
8. Disk
9. Cap
10. Two-part ring
11. Rear cover
12. Compression spring
13. Pawl
14. Hammer mass
15. Retaining spring
16. Impact spring
17. Guide sleeve
18. Felt washer
19. Plexiglass window
20. Trip screw
21. Lock nut
22. Pin
23. Pawl spring
- A. Front fixation of impact spring
- B. Rear end of impact spring engaged to hammer mass



Note:

(a) Plunger (1) in impacted position

(b) Impact energy = 0.075 mkg (0.542 ft-lb)

**FIGURE 4.8 LONGITUDINAL SECTION OF THE TYPE L SCHMIDT TEST HAMMER**

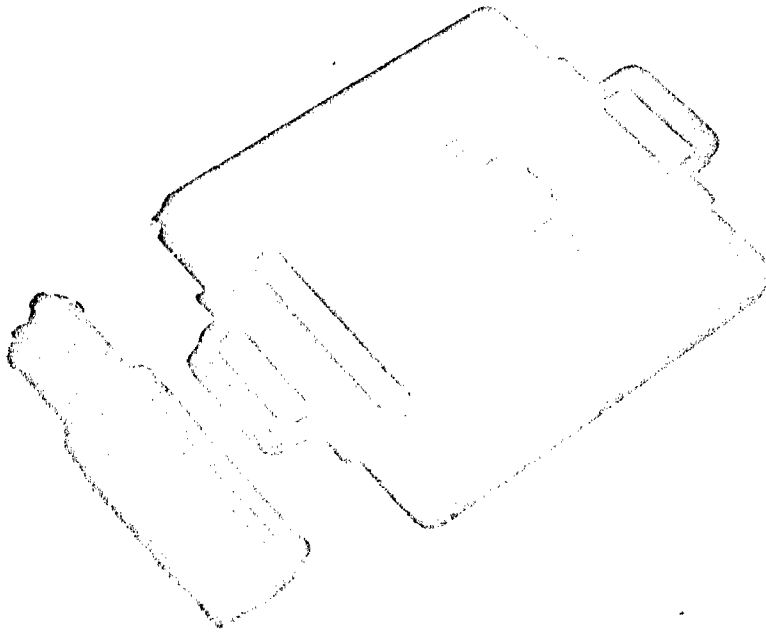


**FIGURE 4.9 SCHMIDT TEST HAMMER BESIDE  
SPECIMEN CRADLE BLOCK AND BASE PLATE**

Test observations are made by placing the specimen in the cradle (clamped or unclamped) and impacting the hammer at various points along the topmost side. The hammer is held vertically in both hands, and should be at right angles to the axis, and tangent to the surface of the specimen. The plunger is placed against the spot to be tested. The hammer is impacted by gradually depressing the plunger into the housing. After impact, the hammer mass rebounds by an amount related to the hardness of the rock. This is indicated on the scale by a sliding rider. The rider position gives the rebound value in percent of the total forward movement of the hammer mass. By simply removing the hammer from the spot tested, it is reset for a further test and at the same time the reading is cancelled.

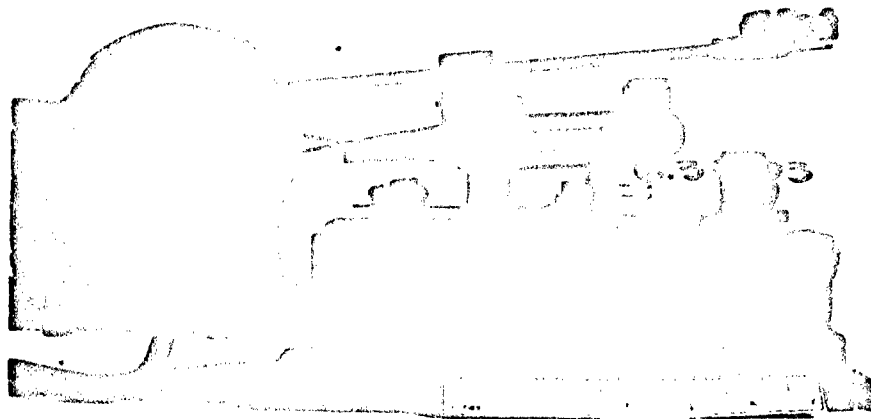
In this investigation, three separate readings were made at equal spacing along a line on the upper side of each test specimen. The specimen was then rotated 45° and three more readings taken. This procedure was repeated until a total of 24 readings for each specimen was obtained. The average of these readings, for all specimens of any given rock sample, is the Schmidt hardness. Any obviously erroneous readings (such as improper holding or slipping of the hammer) were disregarded and replaced by readings in an adjacent spot.

Schmidt hardness readings could not be obtained on core specimens of the Diamond Crystal rock salt, because they fractured during impact. Instead, the top of a block sample was marked into 1-inch squares and one reading was taken in each square. The average value of these readings is reported as the Schmidt hardness for rock salt used in this study. Preliminary tests on selected block samples of the other rock types proved this procedure to be valid. There was found to be no perceptible difference in Schmidt hardness values from block samples or from NX-size core, as long as the core or block remained intact. The problem of fracturing cores during impact was also encountered to a lesser degree in the Navajo sandstone, particularly in the more friable specimens and those containing bedding planes. In this case, additional core specimens were tested.

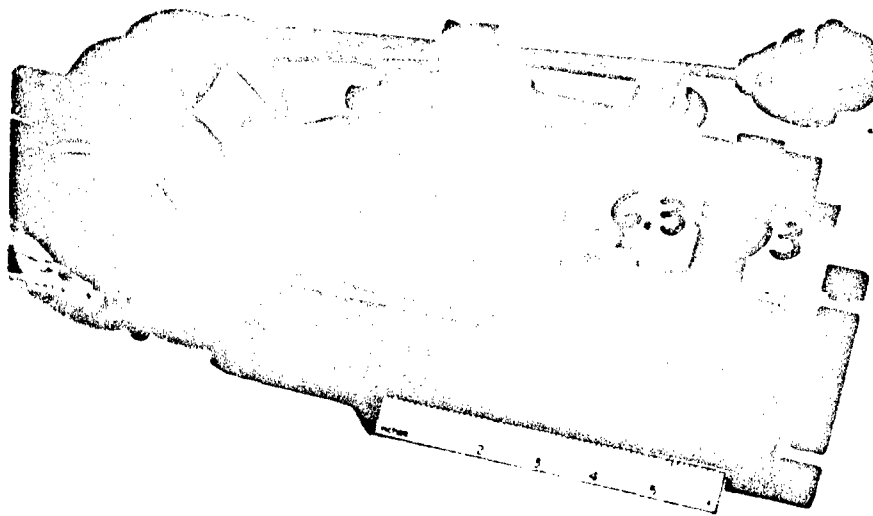
#### d. Abrasion hardness

A special device was developed to measure the abrasion resistance qualities of the various rock types studied in this investigation. This device was designed to be a mechanized, self-cleaning, "scratch" hardness tester. An attempt was made to provide some degree of control over the variables of force, abrasive, and time, while making this test, and to average out the various mineral hardnesses encountered within any particular rock specimen.

Two views of the abrasion apparatus are shown in Figure 4.10. As can be seen in these photographs, the steel cradle block utilized in the Shore and Schmidt hardness tests was used as a base for the apparatus, which is primarily constructed of aluminum. A 6-inch long, adjustable rod is mounted in a square pivot-block which is free to rotate on two pin-button bearings. The bearings are mounted in a U-shaped yoke which is screwed to the base plate. A steel axle-shaft is mounted horizontally in teflon bearings, at right angles to the outer end of the adjustable rod. At one end of the axle is a 7/8-inch diameter abrasion wheel, and at the other end is a pulley of the same diameter.



(a) Side View



(b) Three-Quarter View

FIGURE 4.10 ABRASION APPARATUS



The abrasion apparatus is powered by a 1/10-horsepower, 115-volt A.C., Foredom electric motor. It has a speed range up to 14,000 rpm, which is controlled by a foot rheostat. Power is supplied to the apparatus through two, 1/8-inch O-ring belts. In order to maintain fixed tension in the drive-belt system during cutting, two pulleys are mounted at the rotational axis of the pivot-block, necessitating the two-belt system. Normal force applied by the cutting wheel is varied by means of the extension arm and shot bucket mounted on the pivot-block. A Voder counter is installed adjacent to the cutting wheel, in order to measure the number of revolutions of the wheel during a test.

Each test was performed by clamping a specimen in the cradle block and mounting a new, thin, double-cutting, dental carborundum disc on the device. The disc rests directly upon the specimen surface, colinear with the radius and in a line paralleling the axis of the specimen. A short weight of 55 grams was used with an extension arm length of 4 inches and a distance of 3 inches between the cutter-axle and the pivot-point. The instrument was supplied with full power for a timed period of 3 seconds. No attempt was made to allow for frictional starting resistance, or inertia, at the end of the timed period. These two unknowns were assumed to balance out. Tests made at 5-second and 10-second periods proved this assumption to be reasonably correct, as no significant differences were noted in the abrasion resistances, when compared with the 3-second interval. The counter provided a means for quantitatively checking the relative amount of slippage in the belt-drive system during a test, and indicating the validity for comparison with the other test data.

In general, one test was performed on each of four opposite sides of a single test specimen from each group. A new carborundum disc was used for each test. The depth of each cut was measured with the Ames dial comparator, using a specially-built foot which was the exact size of the carborundum abrasion disc. Areas of the circle segments thus cut were computed and averaged to obtain a relative, abrasion-resistance number. Since the softer rocks had deeper cuts (thus higher numbers), the abrasion hardness is reported as the reciprocal of the computed area cut. Abrasion hardness values were not obtained for the Berea (10.1) or Navajo (10.3) sandstones, because their coarser grains blocked and clogged the cutting wheel, thus stopping the test.

#### e. Absorption

The absorption (or porosity) characteristics were obtained for one representative specimen from each rock type by using a vacuum-saturation process, similar to that suggested by the U.S. Bureau of Reclamation (1953). This process consists of:

- i) oven-drying the specimen for a period of 24 hours at 105°C.,
- ii) placing the specimen in a bell jar under a vacuum exceeding 20 inches of mercury for 24 hours,
- iii) immersing the specimen in water while continuing with vacuum for another 24 hours,
- iv) removing the vacuum and exposing the water containing the immersed specimen to the atmosphere for at least 48 hours.

This procedure eliminates air from the rock pores, and de-airs the water; atmospheric pressure then drives water into the rock, thus assuring saturation. Upon completion of the 5-day cycle, the specimen is removed from the water, surface dried, and then weighed to the nearest 0.1 gram. The absorption is computed by the following equation:

$$\text{Absorption (\%)} = \frac{P_2 - P_1}{P_1} \times 100 \quad (4.1)$$

In which  $P_2$  = weight of saturated specimen  
 $P_1$  = weight of oven-dry specimen

Absorption was not determined for Baraboo quartzite (8.1) and Diamond Crystal rock salt (9.1).

f. Sonic pulse velocity measurements (at seating load)

Standard pulse techniques were used for the determination of the sonic velocity for all rock specimens while subjected to a low, axial stress (seating load) of 100-150 psi. This technique involves the generation of a short-duration stress pulse of low amplitude at one end of a specimen, and accurately measuring the time taken for the arrival of the first recognizable energy-pulse at the opposite end. The velocity,  $V_p$ , which is the velocity of dilatational waves in an unbounded medium, or the bulk compressional velocity, is then computed by simply dividing the length of the specimen by the measured travel time.

The schematic diagram in Figure 4.11 illustrates the interconnection between the major components used for applying a pulse and measuring its travel time through a rock specimen, subjected to a uniaxial, static load. The two stainless-steel transducer cups, referred to as the "receiver" and "transmitter," are identical in construction and are, therefore, interchangeable. Each of the transducers contains a 1/8-inch thick, barium titanate crystal, which has a natural frequency of 200-300 kc/s. The crystal is cemented directly to the interior face of the transducer cup. Coupling with the test specimen is greatly improved with a thin coating of Dow-Corning high-vacuum grease, smeared between the face of the transducers and each end of the specimen.

A short-duration, high voltage (1,000 volts maximum) pulse is applied to the transmitting crystal from a high-gain, high-pass signal amplifier. This pulse generator causes the crystal to expand and contract rapidly, thus imparting stress pulses to one end of the sample. In this way, intermittent trains of ultrasonic waves are propagated through the rock specimen. The arrival of the pulses at the opposite end of the specimen, causes mechanical contraction of the receiver crystal, generating a voltage across the crystal faces. The induced electrical signals are amplified and displayed on the cathode-ray tube of a Tektronix Type 535A Oscilloscope, equipped with a Type B Plug-In Unit.

The oscilloscope display is formed by a repetitive sweep of the input wave-form across the oscilloscope screen. In order to examine the characteristics of the wave-form in detail, it is necessary for the repetitive wave-form to appear stationary on the screen. This type of display requires that

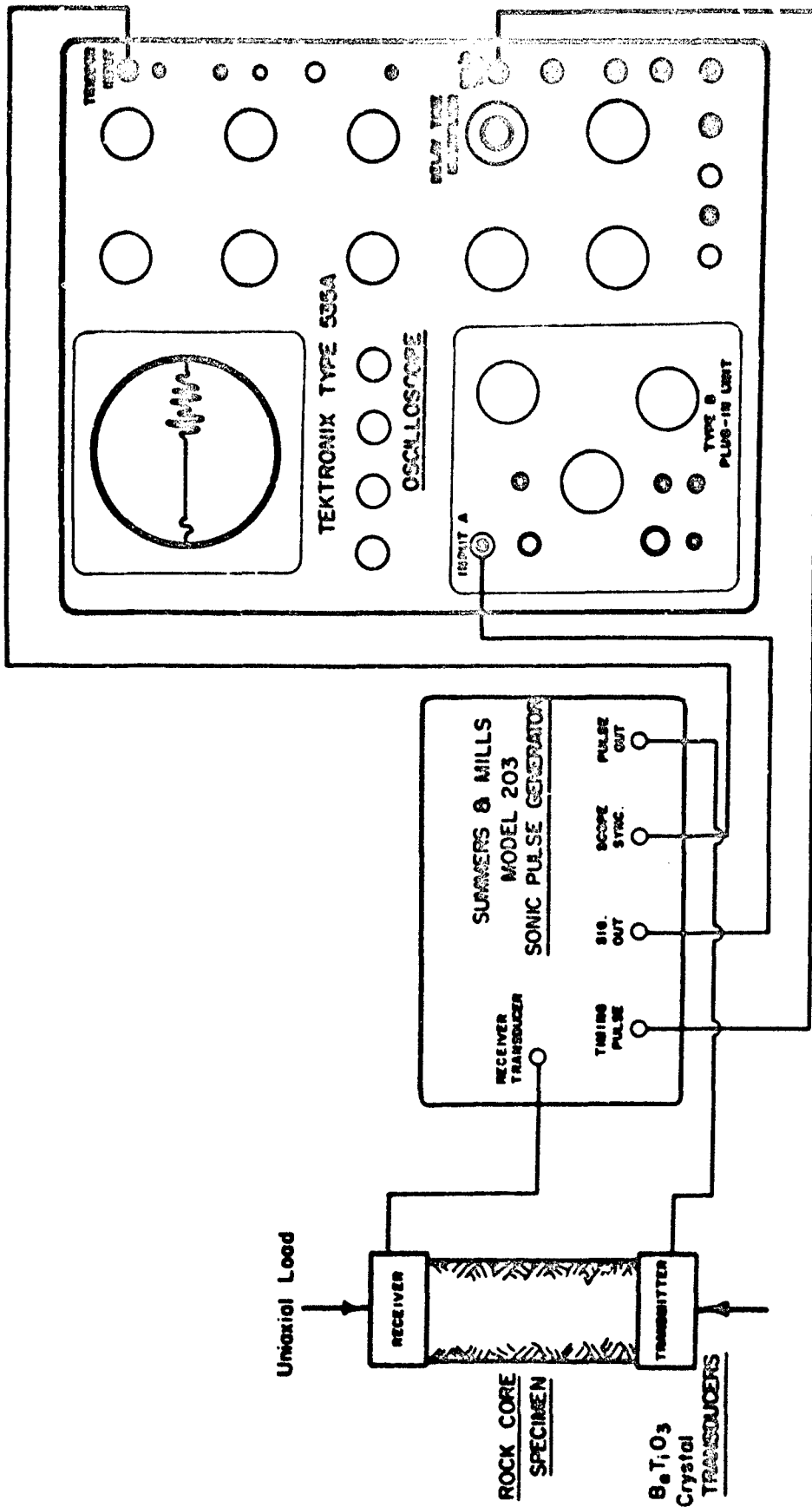


FIGURE 4.11 SCHEMATIC INTERCONNECTION DIAGRAM FOR SONIC PULSE VELOCITY MEASURING EQUIPMENT

the start of the sweep bear a definite, fixed-time relationship (hence, synchronized) with the appearance of the input wave-form. This is accomplished in the oscilloscope by triggering (starting) the sweep with the displayed wave-form.

The calibrated sweeps of the Type 535A Oscilloscope cause any horizontal distance on the screen to represent a definite, known interval of time. Because of this feature, the time lapse between two events displayed on the screen, i.e., the beginning and the "first arrival" of a sonic pulse at the opposite end of a specimen, may be accurately measured. Two methods are used for time measurement:

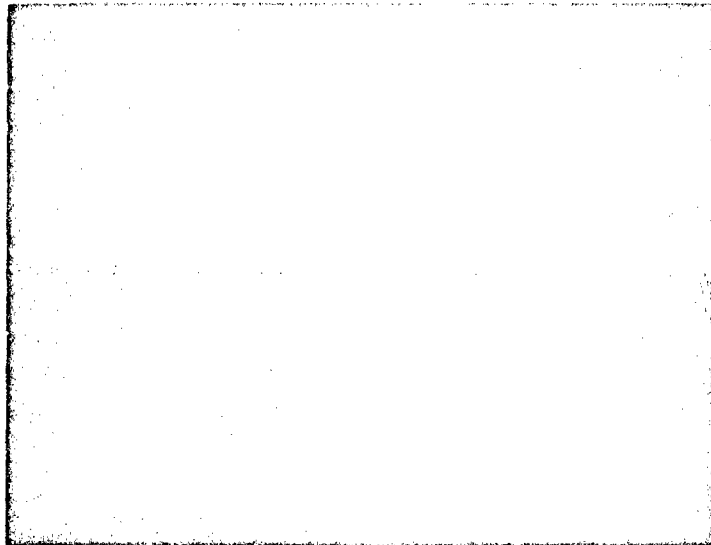
- i) Using the graticule on the screen, the horizontal distance between the two displayed events is measured directly. The distance measured in centimeters is multiplied by the appropriate time/centimeter control setting (which determines the horizontal spread of the displayed wave-form). Photographs of typical records obtained in this way are shown in Figure 4.12. The first arrival of the dilatational wave occurs at the first break (bend) in the horizontal portion of the displayed wave-form. Since we are interested in the first arrival only, the entire wave-form is not displayed.
- ii) Use of the delayed sweep feature of the oscilloscope provides a very high degree of accuracy. The delay-time multiplier control is rotated until the leading edge of the tracking pulse just merges with the first break in the horizontal line of the wave-form. The reading from the delay time control is then multiplied by the time/centimeter control setting.

Although both methods are used simultaneously as a check, each on the other, all time measurements were made in this investigation by the second method. This method eliminates parallax errors, and those resulting from visual determination of the location of the beginning of the sonic pulse, which are inherent in the first method (using the graticule only). Correction for instrument delay time must be made by subtracting this predetermined "constant" from the time readings obtained by either of the above procedures.

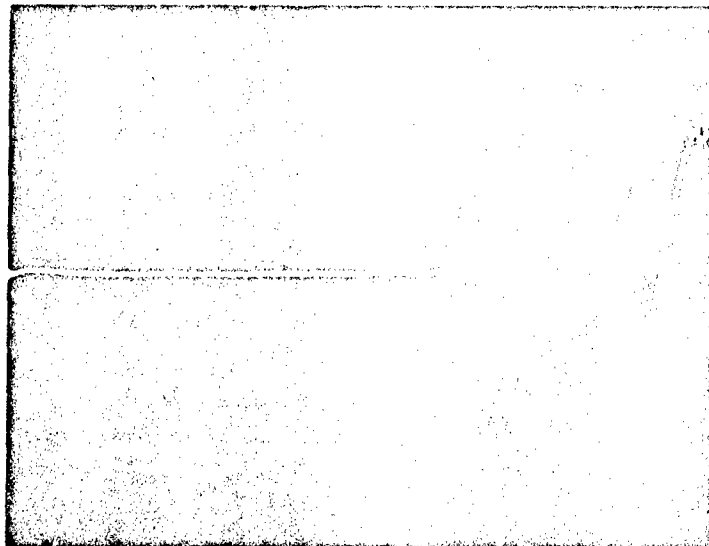
A uniaxial seating load is applied during this test by placing the core specimen, along with the transducer cups, between the loading heads of a hydraulic load press. The seating load is applied only to obtain better coupling of the transducers to the specimen. Load is measured with a standard steel-column, SR-4 type, Baldwin load cell. The strain indicator is set to a predetermined value of load, computed from the load-strain calibration of the load cell. A hydraulic hand pump is used to maintain the desired load.

g. Sonic pulse velocity and static stress-strain measurements (during cyclic loading)

Approximately half of the test specimens were individually subjected to simultaneous measurements of sonic pulse velocity, Poisson's ratio, and modulus of elasticity, at various axial stress levels during cyclic loading under static conditions. Sonic pulse techniques as previously described were



**(a) Berea sandstone under uniaxial compressive stress of 105 psi**



**(b) Berea sandstone under uniaxial compressive stress of 5,000 psi**

**FIGURE 4.12 TYPICAL SONIC PULSE WAVE-FORM DISPLAYS**

employed for measurement of the dilatational wave velocities. Application and measurement of uniaxial loads were accomplished by the procedures discussed in the preceding paragraph. Vertical and lateral strain measurements were obtained by use of resistance strain gages bonded directly to the specimen. Equipment for performing this test series is illustrated in Figure 4.13.

A specimen which has an L/D ratio of 2:1 may be considered to be under almost uniform vertical stress under the middle 5/6 of its height, during compression testing (Fairhurst, 1961b). In this test series, two Baldwin SR-4, Type A-1 strain gages, having a gage length of 13/16 inch are placed vertically on opposite sides at mid-height of the specimen. These are wired in series for vertical strain measurements. A second set of two gages are placed horizontally at mid-height on the opposite diameter to the vertical set, and are also wired in series for lateral strain measurements.

All four strain gages are securely bonded to the specimen by means of Eastman 910 cement, which is pressure-sensitive and sets up in approximately 30 seconds. This is a cyanoacrylate adhesive, which is manufactured by the Tennessee Eastman Company of Kingsport, Tennessee, a division of Eastman Kodak Company. The combination of rapid setting action, high bond strength, and ability to bond to dissimilar materials, all at ambient temperatures, make this cement an excellent bonding agent for this purpose. There is an extreme reactivity associated with cyanoacrylate, and any water, or water vapor is sufficiently basic to cause deterioration of the adhesive over a period of time (McCarthy, 1964).

The surface of the specimen is first cleaned with acetone, and the back of the gage is coated with a special catalyst. Following application of the cement to the specimen, the gage is mounted and moderate thumb pressure is applied through a sponge rubber pad, which is prevented from sticking by means of a small sheet of teflon. The gage is finally coated with a plastic water-proofing (in an organic solvent) to keep out moisture. Both the water-proofing and catalyst accelerator are produced by the Budd Company, for use in conjunction with the Eastman 910 cement for strain gage application.

A close-up view of the specimen, strain gages, sonic pulse transducers, and load cell within the hydraulic loading frame is shown in Figure 4.14. Measurement of strain in both sets of strain gages is accomplished with one SR-4 strain indicator, by means of a single-pole, double-throw switch. Strain read-out is illustrated by the photograph in Figure 4.15.

In this investigation, each specimen was subjected to two complete loading and unloading cycles up to 5,000 psi, except rock salt (9.1) and tuff (14.1). Because of their low strengths, these two latter groups were cycled to 1,500 psi only. Loading proceeded at a uniform rate by smooth, steady strokes of the hydraulic hand pump. Loading was stopped and maintained at constant values while sonic velocity and strain readings were made. These readings were obtained at zero axial stress and every 1,000-psi stress interval for both loading and unloading, following an initial seating load of 100-150 psi. Readings were taken at stress intervals of 250 psi for the rock salt and tuff samples. Efficient performance of these tests require the combined efforts of two operators. By use of the procedures described above, approximately 1 hour is required for performance of one complete test through two loading cycles.

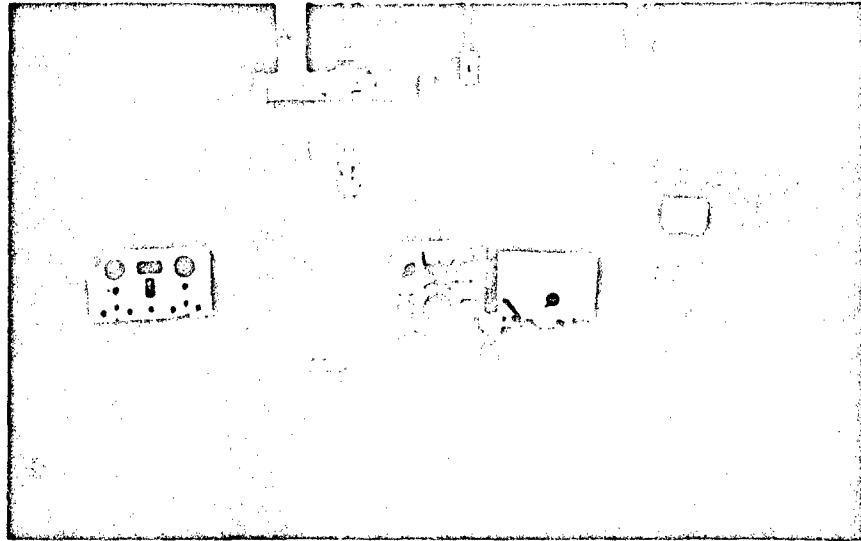


**FIGURE 4.13 EQUIPMENT FOR MEASURING SONIC PULSE VELOCITY AND STATIC STRESS-STRAIN DURING CYCLIC LOADING**



**FIGURE 4.14 CORE SPECIMEN IN POSITION FOR MEASURING SONIC PULSE VELOCITY, STRESS AND STRAIN UNDER UNIAXIAL LOAD**



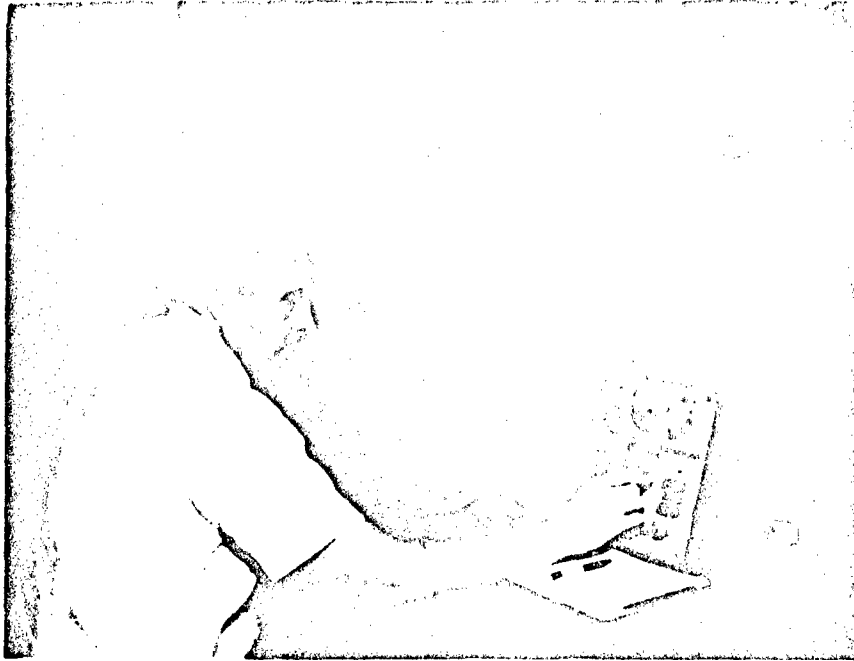


**FIGURE 4.15 STRAIN READ-OUT**

#### h. Compression tests to failure

All specimens which had been tested under cyclic loading conditions, described above, were also tested in static compression to failure. A 300-kip, universal, Riehle hydraulic testing machine was used for loading the specimens. This machine has six load ranges. The lowest range was used for balancing the machine and the ranges were progressively increased, as the specimen approached failure, in order to insure maximum accuracy in the axial load measurements. A photograph of the static compression test machine is shown in Figure 4.16.

Vertical and lateral strain measurements were obtained by means of the SR-4 resistance strain gages previously used in the cyclic loading tests. However, in order to maintain a continuous rate of load application, strain read-out was facilitated by two strain indicators, one for each set of gages, rather than by using the much slower, switching procedure as in the cyclic load tests. In order to provide a means for checking the vertical resistance strain gage readings, one dial indicator was placed between the loading platens of the compression machine, as close as possible to the test specimen. A close-up view of the specimen as instrumented and positioned in the test machine is shown in Figure 4.17.

All compression tests were conducted on uncapped specimens, as recommended by Obert et al. (1946). Care was exercised in centering the specimens in the testing machine and zero-load, strain readings were taken from the strain indicators. An initial load of 100-150 psi was then applied very slowly to permit adjustment of the spherical compression block. After application of the "seating" load, initial readings were taken on the mechanical dial indicator, which was graduated to 0.0001 inch per division. Loading proceeded continuously to failure, with all strain readings obtained simultaneously at predetermined load intervals based upon the estimated compressive strength of the specimen. Since loading was manually controlled, rate of loading was not the same for all rock types. In general, the average loading rate was 10 to 25 psi/sec for the low to medium strength specimens, 35 to 50 psi/sec for the medium to high strength specimens, and 60 to 70 psi/sec for the very high strength specimens. Essentially constant loading rates were maintained for specimens from any one particular sample. Typical compressive failures are shown in the photographs of Figure 4.18.

The compression tests constituted the third loading cycle for those specimens previously subjected to the cyclic loading tests. Selected additional specimens from each rock group were tested in compression to failure without strain readings. These were conducted at the same rates of loading as those specimens with strain measurements. Ultimate compressive strengths were computed by dividing the maximum load at failure by the average initial cross-sectional area of the specimen.

#### i. Point-load tensile tests

Measurement of point-load tensile strengths of representative specimens from each rock group was accomplished by methods described by Reichmuth (1963), and D'Andrea, Fischer, and Fogelson (1964). The point-load tensile strength is determined by applying compressive point-loads to the curved surface of a cylindrical core specimen, of which the axis is placed horizontally; the specimen is tested between the loading heads of a load press. The point

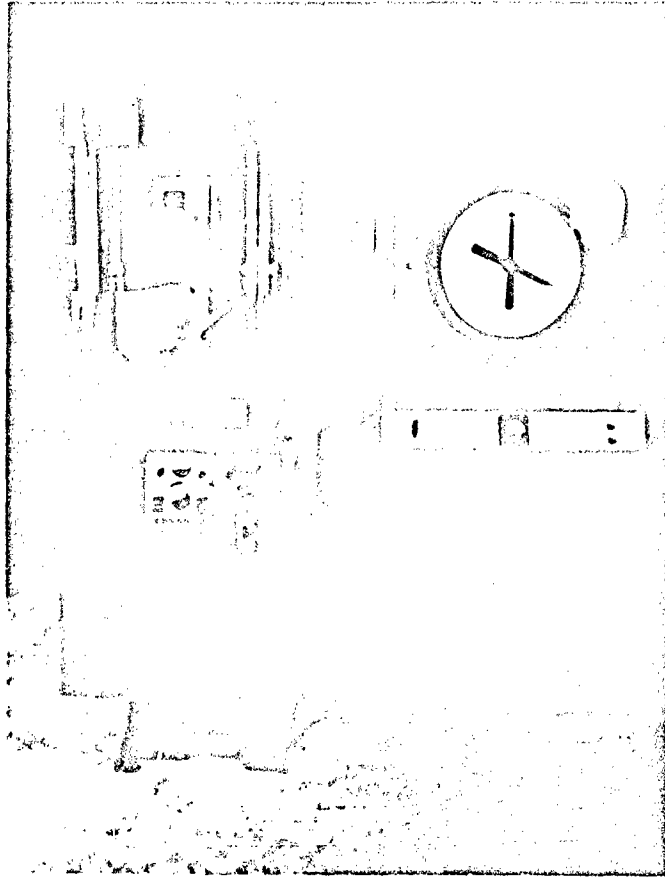


**FIGURE 4.16 COMPRESSION TEST MACHINE**

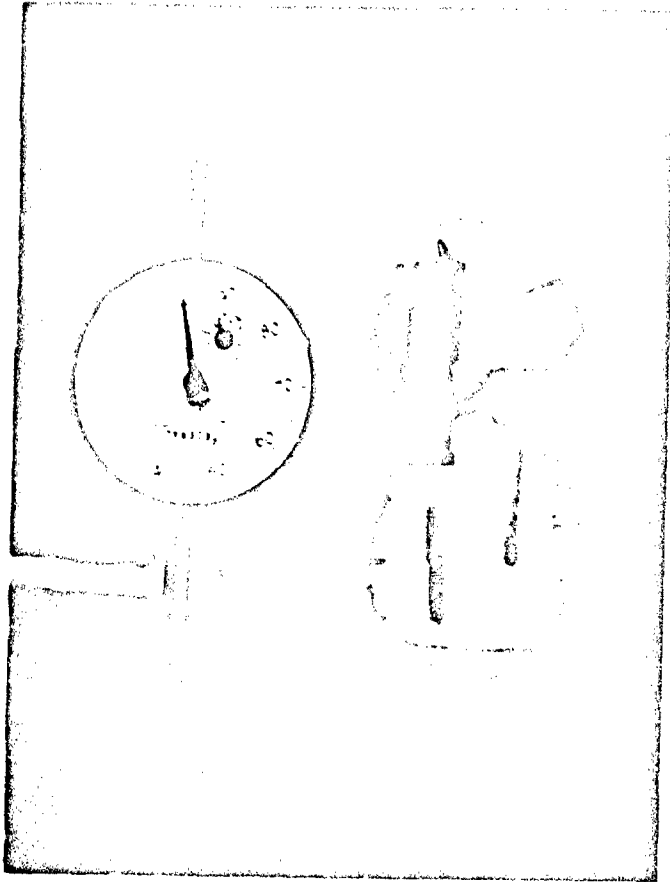
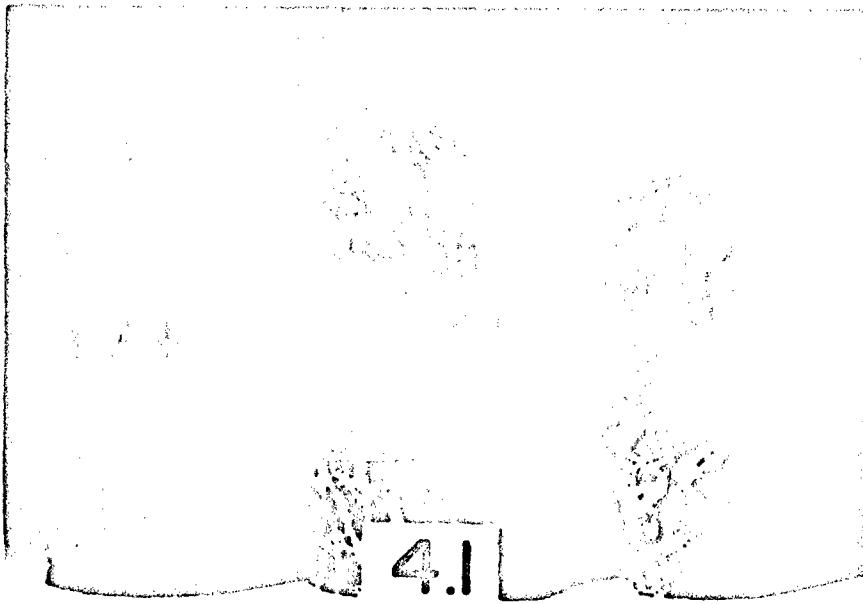
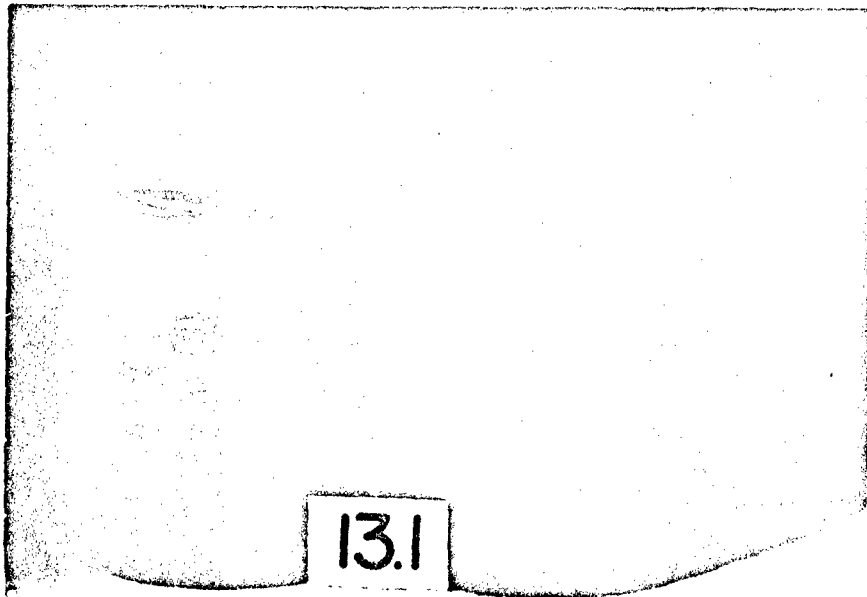


**FIGURE 4.17 CORE SPECIMEN IN POSITION  
FOR COMPRESSION TEST TO FAILURE**



**(a) Dworshak Gneiss**



**(b) Mackenzack Siltstone**

**FIGURE 4.10 TYPICAL COMPRESSIVE FAILURES**

loads are obtained by means of small-diameter, hardened steel rollers oriented at right angles to the axis of the specimen. This produces internal tensile stresses perpendicular to the loading axis. A schematic drawing in Figure 4.19 illustrates the general geometry of this test. Figures 4.20 and 4.21 are photographs of the actual apparatus used.

Test specimens for this series were identical in all respects with those used in other tests. They were selected from all groups prepared initially for this investigation. Hence, nondestructive test data had been obtained for each specimen. Special loading heads, equipped with 3/8-inch diameter, hardened steel rollers were fabricated and installed directly on the load cell and hydraulic-jack piston of the load press. The Baldwin load cell was raised an additional three inches with flat, steel bearing blocks. This reduced the amount of jack extension to a minimum, effectively providing maximum lateral support for the jack piston.

A Speed-O-Max, Type G, strip recorder was used for determining the maximum failure load. The recorder was adjusted for full-scale readings of 500, 1,000, and 2,000 micro-inches/inch (depending upon the estimated strength of the specimen) by means of a BLH Strain Indicator. Since the load-cell calibration was known to be 9.6 lbs/ $\mu$ -in/in, the total load could be accurately computed by multiplying the proportion of the full-scale reading reached at failure by 9.6.

Each specimen was loaded mid-way between the ends; the load was applied by smooth, even strokes with the hydraulic hand pump. The point load tensile strength,  $T$ , was computed from the following empirical expression given by Reichmuth (1963):

$$T = 0.96 \frac{F}{D^2} \quad (4.2)$$

in which  $F$  = total failure load in pounds  
 $D$  = core diameter in inches

Two tests in this series were conducted from each of 19 rock groups. One test was conducted for each of the other nine groups.

## 5. TEST RESULTS

The physical and elastic properties for 28 different rock samples studied in this investigation are summarized in Tables 4.2 and 4.3. Division of the data into two separate tables is primarily for convenience in presentation, because of the large number and kinds of variables involved. Both tables, though slightly different in organization, present the same type of information for each variable:

- i) the average value of each variable,
- ii) the number of tests from which the average was obtained, and
- iii) the coefficient of variation,  $V\%$ , for the variable.

All raw test data were put on standard keypunch cards and reduced by means of an IBM 7094 computer. Individual test results for each specimen were subjected to statistical analyses, as described in Appendix C, in order to obtain average values and dispersion characteristics for each property of each rock group.

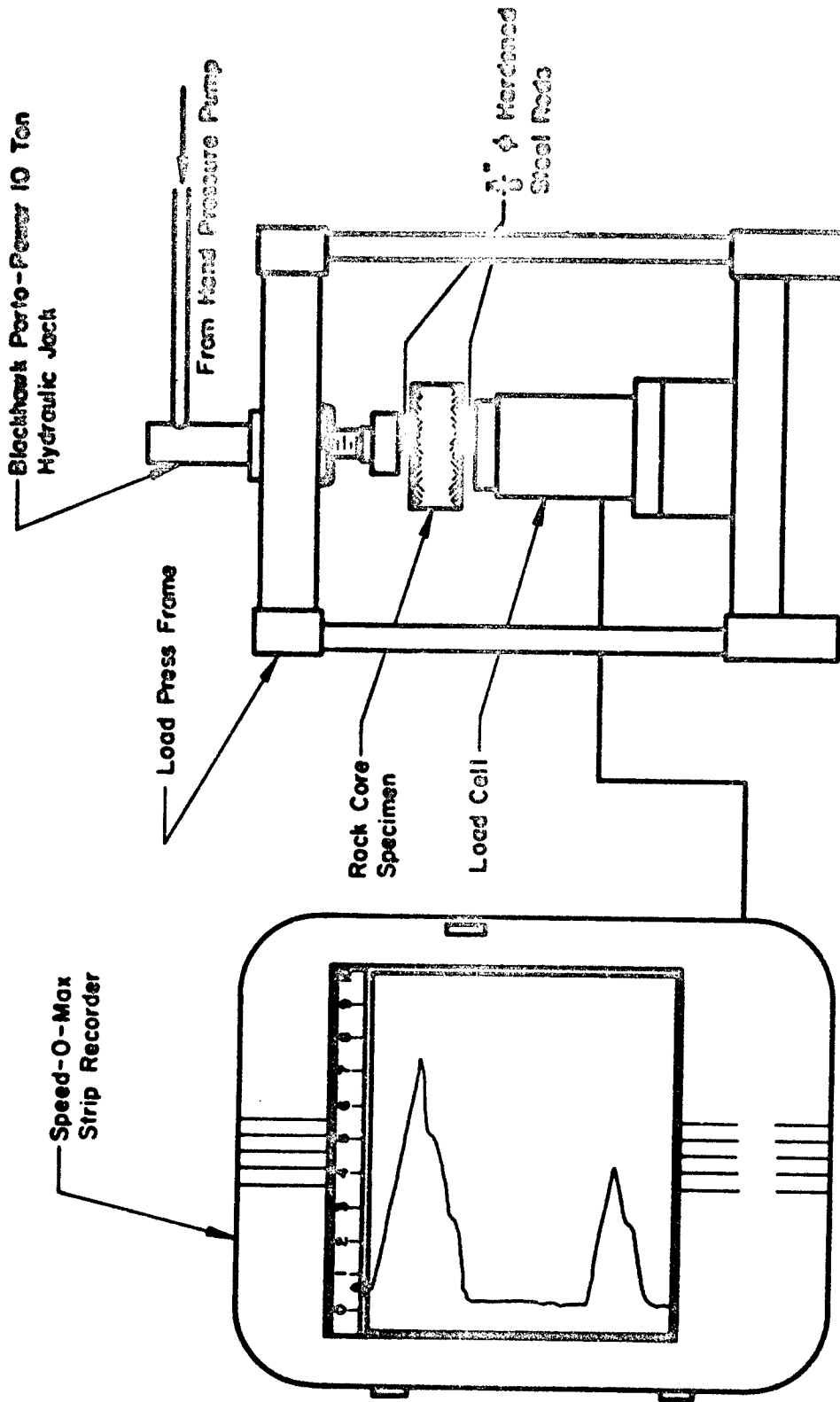
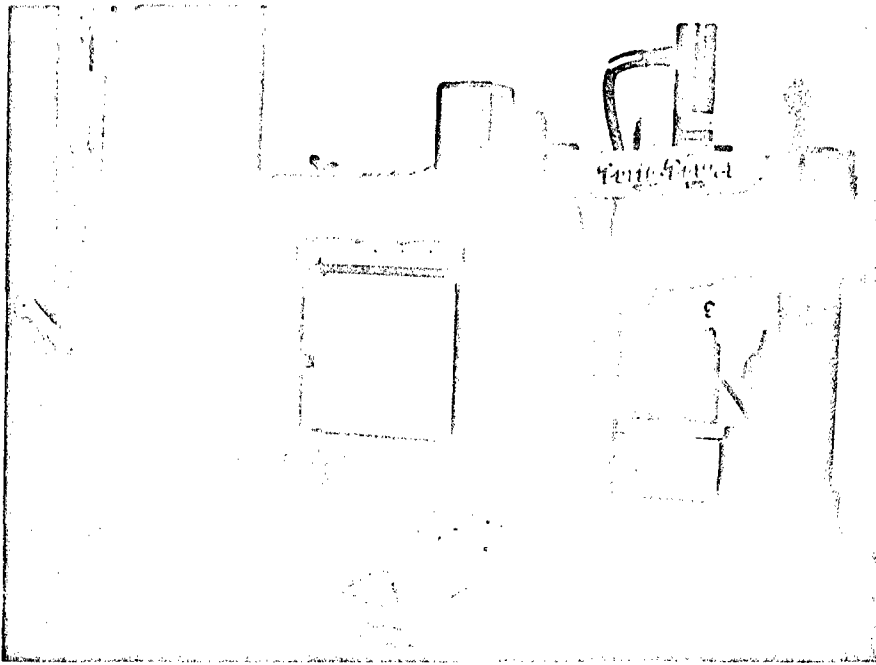
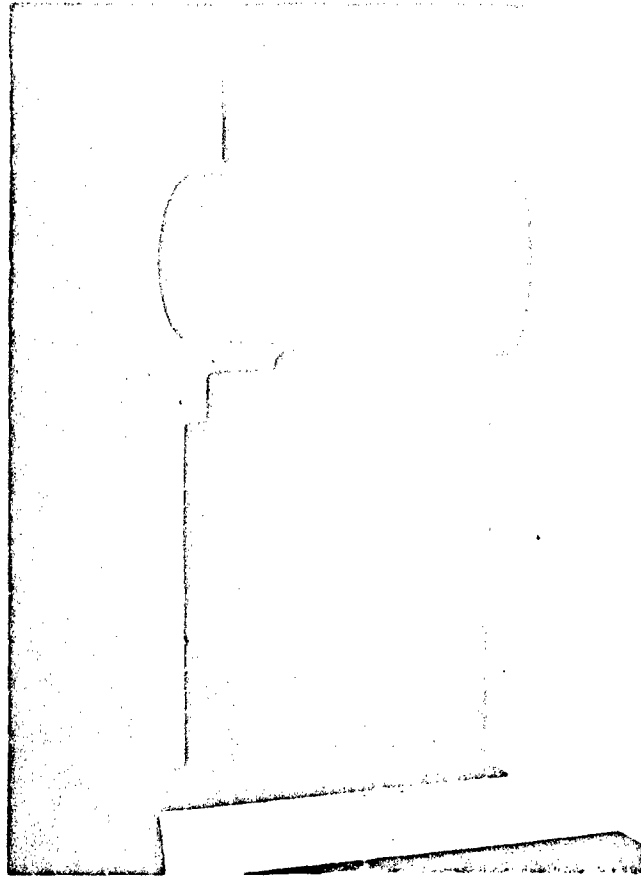


FIGURE 4.19 SCHEMATIC DIAGRAM FOR POINT-LOAD TENSILE TEST



**FIGURE 4.20 POINT-LOAD TENSILE TEST EQUIPMENT**





**FIGURE 4.21 CORE SPECIMEN IN POSITION  
FOR POINT-LOAD TENSILE TEST**

TABLE 4.2

SUMMARY OF AVERAGE PHYSICAL PROPERTIES FOR ROCK

Note:  
VZ = Coefficient of variation

Group No.	Rock Type and Location	No. Tests VZ	Unit Weight, $\gamma_u$		L/D	Compressive Strength		Shore Hardness, $S_s$		Schmidt Hardness, $H_s$		Absorption % of dry weight	Tensile Strength
			gms/cm <sup>3</sup>	lbs/ft <sup>3</sup>		$\sigma_c$ (ult) psi x 10 <sup>3</sup>	Load Rate psi/sec	SItons	Ends	All edges	W100 50%		
1.1	Basalt (Lower Granite) Pullman, Washington	No. Tests VZ	2.73	170.2	2.08	33.3	35	79	85	53	57	122	1.87
			12	12		8	8	480	480	144	72	4	
1.2	Basalt (Little Goose) Vella Vella, Washington	No. Tests VZ	2.82	175.8	2.12	43.0	60	70	87	54	58	175	1.61
			6	6		3	2	480	240	72	36	4	
1.3	Basalt (John Day) Arlington, Oregon	No. Tests VZ	2.87	179.1	2.03	51.5	65	82	91	55	58	224	2.10
			6	6		3	2	480	240	72	36	8	
2.1	Diorite (Palisades) West Nyack, New York	No. Tests VZ	2.92	182.5	2.01	35.0	52	85	89	57	59	239	1.65
			12	12		6	8	800	400	144	72	0	
2.2	Diorite (Coggins) Catsper, Virginia	No. Tests VZ	3.04	189.5	2.03	11.3	11.3	6.4	5.3	4.3	2.0	10.0	2.0
			6	6		5.5	5.3	6.0	3.4	8.0	1	1	
2.3	Diorite (French Creek) St. Peters, Pennsylvania	No. Tests VZ	3.06	190.8	2.03	43.6	59	85	93	56	58	249	1.77
			6	6		3	3	480	240	72	36	4	
3.1	Gabbro (Oneco) Oneco, Minnesota	No. Tests VZ	2.45	153.0	1.89	12.6	24	31	35	39	43	22	.64
			12	12		8	8	480	480	144	72	4	
					5.3	5.3	25.0	20.1	11.5	6.9	25.1	6.5	

TABLE 4.2 - Continued

SUMMARY OF AVERAGE PHYSICAL PROPERTIES FOR ROCK

Note:

V% = Coefficient of variation

Group No.	Rock Type and Location	No. Tests V%	Unit Weight, $\gamma$		L/D	Compressive Strength		Shore Hardness, $S_n$		Schmidt Hardness, R		Abrasion Loss, $\frac{1}{Area}$ (in <sup>2</sup> )	Absorption % of dry weight	Tensile Strength, $\frac{P_{Tens}}{A_{Tens}}$ (psi x 10 <sup>3</sup> )				
			gm/cm <sup>3</sup>	lbs/ft <sup>3</sup>		$\sigma_c$ (ult) psi x 10 <sup>3</sup>	Load Rate psi/sec	Sides	Ends	All Rdgs.	Nish 50%							
3.2	Dolomite (Lockport) Niagara Falls, New York	No. Tests V%	2.58	161.2	2.03	26	45	40	47	51	46	25	4.16	.64				
			6	6		3	480								240	72	4	2
				.9		5.6	23.7								27.6	16.5	23.5	11.7
3.3	Dolomite (Bonne Terre) Bonne Terre, Missouri	No. Tests V%	2.64	164.5	2.03	40	51	40	47	51	46	42	3.11	.73				
			6	6		3	480								240	72	4	1
				.7		17.3	11.9								8.8	9.3	11.4	6.5
4.1	Gneiss (Dwarshak) Drofino, Idaho	No. Tests V%	2.79	174.5	2.11	36	89	36	69	89	45	117	.24	1.00				
			12	12		8	480								480	144	4	2
				.6		6.8	9.1								6.8	8.1	5.5	4.6
5.1	Granite (Pikes Peak) Colorado Springs, Colorado	No. Tests V%	2.67	166.8	2.02	23	80	23	60	80	42	148	.50	.57				
			6	6		3	480								240	72	5	2
				.6		7.8	25.4								15.0	8.7	16.1	5.4
5.2	Granite (Pikes Peak) Colorado Springs, Colorado	No. Tests V%	2.64	164.6	2.02	61	101	61	86	101	55	203	.10	1.73				
			6	6		3	480								240	72	4	1
				.1		3.4	8.4								4.9	6.9	16.3	5.5
5.3	Granite (Barre) Barre, Vermont	No. Tests V%	2.64	165.2	2.04	38	98	38	93	98	51	199	.24	1.55				
			12	12		8	960								480	144	4	2
				.1		.8	4.2								4.4	5.7	20.0	3.5
6.1	Limestone (Bedford) Bedford, Indiana	No. Tests V%	2.21	137.7	2.01	14	20	14	18	20	31	16	8.14	.23				
			12	12		8	480								480	144	9	2
				.3		4.2	18.1								14.6	7.6	11.4	3.9

TABLE 4.2 - Continued  
SUMMARY OF AVERAGE PHYSICAL PROPERTIES FOR ROCK

Note:  
V% = Coefficient of variation

Group No.	Rock Type and Location	No. Tests V%	Unit Weight, $\gamma_g$		L/D	Compressive Strength		Shore Hardness, S		Schmidt Hardness, R		Absorption % of dry weight	Tensile Strength Point Load psi x 10 <sup>3</sup>	
			gm/cm <sup>3</sup>	lbs/ft <sup>3</sup>		$\sigma_c$ (ult) psi x 10 <sup>3</sup>	Load Rate psi/sec	Sides	Ends	All Edges	High 50%			Abrasion Hardness $\frac{1}{\text{Area (in}^2\text{)}}$
6.2	Limestone (Ozark Taverneville) Carthage, Missouri	No. Tests V%	2.65	165.6	1.99	14.2	37	47	50	47	49	.59	.57	
			12	12		8	8	960	144	72	4			2
				.1		3.1	3.1	5.0	4.4	3.6	1.6			23.4
6.3	Limestone (Solenhofen) Solenhofen, Bavaria	No. Tests V%	2.62	163.6	2.03	35.5	46	61	64	51	54	1.34	.53	
			6	6		3	3	430	240	72	5			1
				.2		3.8	3.8	2.6	2.4	7.9	3.5			11.2
7.1	Marble (Taconic White) West Rutland, Vermont	No. Tests V%	2.71	169.0	2.01	9.0	17	36	36	29	31	.21	.17	
			12	12		8	7	880	480	144	4			1
				.0		3.0	3.0	5.2	4.8	9.5	5.0			21.7
7.2	Marble (Cherokee) Tate, Georgia	No. Tests V%	2.71	169.1	2.03	9.7	16	38	43	34	36	.11	.26	
			6	6		3	3	480	240	72	4			2
				.0		1.2	1.2	8.0	6.6	8.2	5.2			5.2
7.5	Marble (Imperial Benby) West Rutland, Vermont	No. Tests V%	2.71	169.3	2.02	9.4	12	32	37	33	40	.13	.32	
			13	13		6	4	240	520	72	4			2
				.2		5.5	5.5	10.3	10.0	6.2	4.8			18.7
8.1	Quartzite (Baraboo) Baraboo, Wisconsin	No. Tests V%	2.62	161.0	2.02	45.5	40	104	114	56	59	---	1.60	
			7	7		3	3	450	240	95	4			2
				.4		5.4	5.4	3.2	2.6	6.6	3.9			20.3
9.1	Rock Salt (Diamond Crystal) Jefferson Island, Louisiana	No. Tests V%	2.16	135.0	2.01	3.1	4	12	12	20	23	---	.12	
			6	6		5	5	480	240	144	4			2
				.0		7.4	7.4	5.8	5.1	18.2	12.7			19.1

TABLE 4.2 - Concluded  
SUMMARY OF AVERAGE PHYSICAL PROPERTIES FOR ROCK

Notes:  
V% = Coefficient of variation

Group No.	Rock Type and Location	No. Tests V%	Unit Weight, $\gamma_u$		L/D	Compressive Strength		Shore Hardness, $S_h$		Schmidt Hardness, $S_c$		Absorption	Tensile Strength	
			gms/cm <sup>3</sup>	lbs/ft <sup>3</sup>		$\sigma_c$ (ult) psi x 10 <sup>3</sup>	Load Rate psi/sec	Sides	Ends	All Adj.	HI 50%			Area (in <sup>2</sup> )
10.1	Sandstone (Berea) Amherst, Ohio	No. Tests V%	2.18 12	136.2 12	2.01 12	10.7 6 3.0	20 6	33 480 7.8	42 480 9.0	39 144 8.6	42 72 4.2	--- --- ---	6.27 1 16.8	.17 2 16.8
10.2	Sandstone (Grab Orchard) Crossville, Tennessee	No. Tests V%	2.53 9	157.9 9	2.02 9	31.1 6 5.9	40 6	83 980 5.0	85 480 3.6	44 144 11.8	47 72 6.6	177 8 12.4	1.03 1 ---	1.13 2 9.3
10.3	Sandstone (Navajo) Glen Canyon, Arizona	No. Tests V%	2.02 12	125.8 12	2.07 12	6.3 6 19.4	16 6	24 960 19.2	23 480 25.1	26 108 26.3	30 54 13.3	--- ---	11.03 1 ---	.19 1 ---
11.1	Schist (Luther Falls) I Unknown Origin	No. Tests V%	2.81 12	175.8 12	2.01 12	6.0 6 11.5	13 6	40 960 32.9	47 480 26.5	33 144 17.4	37 72 11.7	204 4 21.1	.5 1 ---	.03 2 49.3
11.2	Schist (Luther Falls) II Unknown Origin	No. Tests V%	2.82 6	176.1 6	2.04 6	12.0 3 24.7	20 3	38 480 27.0	49 240 28.1	26 72 14.6	29 36 7.2	125 4 23.8	.33 1 ---	.78 1 ---
13.1	Siltstone (Hackensack) Hackensack, New Jersey	No. Tests V%	2.59 12	162.0 12	2.04 12	17.8 7 6.4	23 6	47 480 15.9	58 480 16.6	44 120 8.4	47 60 5.9	35 4 21.5	.63 1 ---	.43 4 7.7
14.1	Tuff (ETS-E Tunnel) Mercury, Nevada	No. Tests V%	1.61 12	100.7 12	2.01 12	3.5 7 15.9	6 7	24 960 34.0	26 480 35.2	38 144 9.3	40 72 5.8	19 1 ---	24.2 1 ---	.21 2 31.1

TABLE 4.3

SUMMARY OF AVERAGE ELASTIC PROPERTIES FOR ROCK

Note:

- $E_t$  = Tangent modulus (static)
- $\nu$  = Poisson's ratio
- $V_p$  = Dilatational wave velocity
- $E_c$  (dynamic) =  $\rho V_p^2$
- $E_c$  (static) =  $E_t \left[ \frac{1-\nu}{(1+\nu)(1-2\nu)} \right]$

Group No.	Rock Type and Location	Axial Stress psi	Elastic Properties (First Loading Cycle)						Stable Elastic Properties (Loading to Failure)			
			Static			Dynamic			Stress Level % $\sigma_c$ (ult)	$E_t$	$\nu$	No. Tests
$E_t$ psi x 10 <sup>6</sup>	$\nu$	$M_c$ psi x 10 <sup>6</sup>	No. Tests	$V_p$ fps	$N_c$ psi x 10 <sup>6</sup>	No. Tests	Initial	psi x 10 <sup>6</sup>				
1.1	Basalt (Lower Granite) Pullman, Washington	100	11.00	.28	12.1	6	17,280	11.0	12	12.60	.45	6
		1,000	27.3	56.3	9.6	6	3.2	11.1	6	63.2	66.4	6
		5,000	8.67	.20	10.9	6	17,360	11.3	6	8.60	.24	6
1.2	Basalt (Little Goose) Walla Walla, Washington	110	12.03	.21	13.9	3	19,050	13.8	6	11.22	.26	3
		700-1,000	16.8	45.2	12.5	3	.6	13.9	3	21.4	26.4	3
		5,000	10.73	.23	12.8	3	19,135	14.0	3	10.55	.24	3
1.3	Basalt (John Day) Arlington, Oregon	110	15.57	.16	16.9	3	19,645	14.9	6	11.42	.22	3
		700-1,000	36.8	24.7	14.6	3	2.4	15.0	3	23.8	126	3
		5,000	11.97	.25	14.4	3	19,695	15.1	3	11.61	.26	3
2.1	Diorite (Palisades) West Nyack, New York	120	13.50	.30	18.0	6	20,155	16.0	12	14.19	.31	6
		1,000	12.2	40.1	14.6	6	.4	16.0	6	23.6	69.7	6
		5,000	11.57	.23	13.4	6	20,210	16.3	6	12.39	.24	6
			3.4	3.4	3.4	.6	20,360	16.3	6	2.8	10.9	6
			3.4	3.4	3.4	.4				11.03	.28	6
										3.0	10.0	6

TABLE 4.3 - Continued

SUMMARY OF AVERAGE ELASTIC PROPERTIES FOR ROCK

Note:

$E_t$  = Tangent modulus (static)

$\nu$  = Poisson's ratio

$V_p$  = Dilatational wave velocity

$M_c$  (dynamic) =  $\frac{V_p^2}{(1-\nu)}$

$M_c$  (static) =  $\frac{E_t}{(1-\nu)}$

Group No.	Rock Type and Location	Elastic Properties (First Loading Cycle)										Static Elastic Properties (Loading to Failure)				
		Static					Dynamic					Stress Level % $\sigma_{N(ult)}$	$E_t$ psi $\times 10^6$	$\nu$	No. Tests	
		Axial Stress Psi	$E_t$ psi $\times 10^6$	$\nu$	$M_c$ psi $\times 10^6$	No. Tests	$V_p$ fps	$M_c$ psi $\times 10^6$	No. Tests	Stress Level % $\sigma_{N(ult)}$	$E_t$ psi $\times 10^6$					$\nu$
2.2	Diabase (Coggins) Culpoper, Virginia	120	11.67	.10	12.1	3	17,555	12.6	6	Initial	9.52	.15	3			
		1,000	30.1	100	8.9	3	1.4	12.6	3	10	8.4	105	1			
		5,000	8.65	.11	8.4	3	17,605	14.9	3	50	9.09	.12	3			
2.3	Diabase (French Creek) St. Peters, Pennsylvania	120	15.22	.13	16.3	3	18,480	14.0	6	Initial	11.47	.15	3			
		1,000	57.0	56.7	11.6	3	.5	14.1	3	10	23.2	143	3			
		5,000	10.86	.16	10.2	3	19,540	16.0	3	50	10.24	.12	3			
3.1	Dolomite (Oneota) Kasota, Minnesota	115	6.90	.22	6.5	6	16,305	8.8	12	Initial	5.68	.19	6			
		1,000	36.5	56.8	7.0	6	1.8	9.1	6	10	12.4	27.2	6			
		5,000	6.29	.20	8.6	6	16,615	9.6	6	50	6.18	.23	6			
3.2	Dolomite (Lockport) Niagara Falls, New York	115	2.84	.14	3.0	3	14,335	7.2	6	Initial	2.90	.05	3			
		1,000	10.6	18.2	2.5	3	6.6	9.6	3	10	38.7	71.3	3			
		5,000	2.48	.08	13.1	3	16,565	12.0	3	50	3.87	.17	3			
			21.3	42.9		2.2				21.2	44.8					
			6.65	.36		18,515				7.40	.74					
			13.7	19.7		1.5				12.9	33.9					

TABLE 4.3 - Continued

SUMMARY OF AVERAGE ELASTIC PROPERTIES FOR ROCK

Note:

- $E_t$  = Tangent modulus (static)
- $\nu$  = Poisson's ratio
- $V_p$  = Dilatational wave velocity
- $M_c$  (dynamic) =  $\frac{pV_p^2}{1-\nu}$
- $M_c$  (static) =  $E_t \left[ \frac{1-\nu}{(1+\nu)(1-2\nu)} \right]$

Group No.	Rock Type and Location	Axial Stress Psi	Elastic Properties (First Loading Cycle)						Static Elastic Properties (Loading to Failure)				
			Static			Dynamic			Stress Level % $\sigma_c$ (ult)	$E_t$ psi $\times 10^6$	$\nu$	No. Tests	
			$E_t$ psi $\times 10^6$	$\nu$	$M_c$ psi $\times 10^6$	No. Tests	$V_p$ fps	$M_c$ psi $\times 10^6$					No. Tests
3.3	Belamite (Bonne Terre) Bonne Terre, Missouri	115	9.82	.16	10.5	3	18,510	12.2	6	Initial	9.46	.29	3
		1,000	12.0	12.0	9.1	3	19,050	12.9	3	10	26.9	59.1	3
		5,000	4.5	8.8	16.4	3	19,965	14.2	3	50	4.8	31.1	3
4.1	Gneiss (Dwarsbak) Grafino, Idaho	130	4.05	-.05	4.2	6	12,340	5.7	12	Initial	3.82	.05	6
		1,000	16.1	.270	3.4	6	13,035	6.4	6	10	21.5	53.8	6
		5,000	5.15	.18	5.6	6	15,350	8.9	6	50	11.8	29.1	6
5.1	Granite (Pikes Peak) Colorado Springs, Colorado	100	2.71	.02	2.7	3	13,115	6.2	6	Initial	1.83	.03	3
		1,000	25.0	.173	2.4	3	14,745	7.8	3	10	45.1	133	3
		5,000	4.04	.25	4.9	3	16,730	10.0	3	50	2.89	11	3
5.2	Granite (Pikes Peak) Colorado Springs, Colorado	100	8.41	.18	10.1	3	17,465	10.8	6	Initial	8.72	.20	3
		1,000	3.45	.14	8.8	3	17,825	11.4	3	10	23.4	129	3
		5,000	9.18	.21	10.4	3	18,980	12.8	3	50	8.93	18	3
			5.4	16.6		2.8				6.1	32.3		
			5.4	16.6		2.8				10.24	10.24		
			5.4	16.6		2.8				2.5	2.5		



**TABLE 4.3 - Continued**  
**SUMMARY OF AVERAGE ELASTIC PROPERTIES FOR ROCK**

**Notes:**  
 $E_c$  = Young's modulus (static)  
 $\nu$  = Poisson's ratio  
 $V_p$  = Dilatational wave velocity  
 $P_c(\text{dynamic}) = P_c^2$   
 $K_c(\text{static}) = E_c / (1 - \nu_c^2)$

Group No.	Rock Type and Location	Elastic Properties (First Loading Cycle)										Static Elastic Properties (Loading to Failure)				
		Static					Dynamic					Stress Level (psi)	No. Tests	$E_c$ (psi x 10 <sup>6</sup> )	$\nu$	No. Tests
		Axial Stress (psi)	$E_c$ (psi x 10 <sup>6</sup> )	$\nu$	$K_c$ (psi x 10 <sup>6</sup> )	No. Tests	$V_p$ (fps)	$K_c$ (psi x 10 <sup>6</sup> )	No. Tests	Stress Level (psi)						
3.3	Granite (Barre) Barre, Vermont	120	6.28	.15	7.1	6	14,505	7.6	12	Initial	5.93	.00	6			
		1,000	24.1	77.4	5.7	6	1.3	14,845	7.8	6	12.1	.02	6			
		5,000	5.67	.05	29.9	6	1.3	16,600	9.8	6	2.6	12.7	.50	6		
6.1	Limestone (Bedford) Bedford, Indiana	130	3.93	.15	4.6	6	12,825	4.9	12	Initial	4.53	.20	6			
		1,000	5.8	59.5	3.8	6	1.5	13,365	5.3	6	43.9	33.5	.10	6		
		5,000	3.58	.16	10.0	6	1.1	13,825	7.1	6	3.9	9.6	.29	6		
6.2	Limestone (Ozark Taverneille) Carthage, Missouri	115	7.19	.25	9.9	6	15,675	9.0	12	Initial	5.93	-.05	6			
		1,000	21.3	57.6	7.0	6	2.9	16,355	9.5	6	24.5	270	.21	6		
		5,000	6.48	.16	9.2	6	1.6	17,960	11.5	6	7.04	9.9	.20	6		
6.3	Limestone (Solnhofen) Solnhofen, Bavaria	115	9.26	.17	10.3	3	18,885	12.6	6	Initial	8.46	-.23	3			
		1,000	22.8	57.4	12.4	3	.5	18,820	12.6	3	14.9	78.9	.20	3		
		5,000	3.1	12.7	11.5	3	.4	18,960	12.7	3	3.1	5.4	.20	3		
			2.5	.6		.2				2.6	7.6					

TABLE 4.3 - Continued

SUMMARY OF AVERAGE ELASTIC PROPERTIES FOR ROCK

Note:

$E_t$  = Tangent modulus (static)

$\nu$  = Poisson's ratio

$V_p$  = Distortional wave velocity

$R_c$  (dynamic) =  $\frac{E_t V_p^2}{\rho}$

$R_c$  (static) =  $E_t \left[ \frac{1+\nu}{1-\nu} \right]$

Group No.	Rock Type and Location	Elastic Properties (First Loading Cycle)										Static Elastic Properties (Loading to Failure)			
		Static					Dynamic					Stress Level $\frac{1}{2} \sigma_c$ (ult)	$E_t$	$\nu$	No. Tests
		Axial Stress psi	$E_t$ psi x 10 <sup>6</sup>	$\nu$	$R_c$ psi x 10 <sup>6</sup>	No. Tests	$V_p$ fps	$R_c$ psi x 10 <sup>6</sup>	No. Tests	$V_p$ fps	$R_c$ psi x 10 <sup>6</sup>				
7.1	Marble (Taconic White) West Rutland, Vermont	115	0.63	-0.006	0.6	6	7,445	2.0	12	Initial	0.61	-0.03	6		
		1,000	13.4	.139	1.4	6	2.8	6.0	6	10	24.9	75.9	6		
		5,000	23.7	.197	13.5	6	1.7	10.1	6	50	17.3	23.6	6		
7.2	Marble (Cherokee) Tato, Georgia	115	2.33	.0305	2.4	3	11,440	4.8	6	Initial	1.76	.69	3		
		1,000	6.9	---	2.1	3	1.3	9.1	3	10	15.2	0	3		
		5,000	13.1	.214	9.2	3	15,775	13.0	3	50	3.70	.05	3		
7.5	Marble (Imperial Beahy) West Rutland, Vermont	115	6.85	.02	6.4	6	17,655	11.8	13	Initial	7.75	.20	6		
		1,000	11.6	.245	7.0	6	6.0	12.9	6	10	25.7	81.0	6		
		5,000	14.6	.159	12.8	6	10,765	15.1	6	50	6.75	.18	6		
8.1	Quartzite (Baraboo) Baraboo, Wisconsin	110	10.2	.11	11.1	4	19,270	11.8	7	Initial	9.04	.03	4		
		1,000	28.7	.118	11.3	4	6.8	12.1	3	10	10.1	.117	3		
		5,000	23.9	.066	11.6	4	18,485	12.5	3	50	11.01	.07	3		
			11.5	.05		7.0		3		19.5	35.3				
			11.0	.477		4.0		3		12.82	.11	3			
										3.3	25.0				

TABLE 4.3 - Continued

SUMMARY OF AVERAGE ELASTIC PROPERTIES FOR ROCK

Note:

$E_t$  = Tangent modulus (static)

$\nu$  = Poisson's ratio

$V_p$  = Dilatational wave velocity

$\rho_c(\text{dynamic}) = \rho \frac{V_p^2}{G}$

$\rho_c(\text{static}) = \rho \frac{E_t}{G(1-\nu)}$

Group No.	Rock Type and Location	Axial Stress psi	Elastic Properties (First Loading Cycle)						Static Elastic Properties (Loading to Failure)				
			Static			Dynamic			Stress Level % $\sigma_{ult}$	$E_t$ psi x 10 <sup>6</sup>	$\nu$	No. Tests	
			$E_t$ psi x 10 <sup>6</sup>	$\nu$	$\rho_c$ psi x 10 <sup>6</sup>	No. Tests	$V_p$ fps	$\rho_c$ psi x 10 <sup>6</sup>					No. Tests
9.1	Rock Salt (Diamond Crystal) Jefferson Island, Louisiana	110	2.97	.19	3.8	5	13,500	5.3	6	Initial	0.87	.19	5
		750	42.9	78.2	1.8	5	2.9	13,705	5.5	10	50.7	60.9	5
		1,500	1.08	.32	---	5	2.8	34.5	5.7	50	1.62	.35	5
10.1	Sandstone (Berea) Amberst, Ohio	105	0.95	.00	1.0	6	8,655	2.2	12	Initial	0.75	.01	6
		1,000	15.1	16.6	0.8	6	3.8	10,845	3.5	10	24.0	---	6
		5,000	0.82	.13	5.6	6	3.2	12,540	4.6	50	1.11	.14	6
10.2	Sandstone (Crab Orchard) Crossville, Tennessee	115	3.42	.06	3.5	3	11,290	4.3	9	Initial	3.37	.09	3
		1,000	19.9	12.3	2.5	3	2.2	12,110	5.0	10	1.4	125	3
		5,000	2.46	.04	3.6	3	.3	13,880	6.6	50	3.26	.63	3
10.3	Sandstone (Navajo) Glen Canyon, Arizona	110	1.37	.10	1.4	6	8,370	1.9	12	Initial	1.19	.12	6
		1,000	19.7	10.0	1.1	6	5.4	9,750	2.6	10	19.9	39.5	6
		5,000	1.09	.10	7.7	6	5.4	11,405	3.6	50	1.26	.21	6
			15.5	35.4	7.7	6	4.0	4.0	6	15.5	34.3	6	
			2.44	.61	25.0	6	2.22	2.22	6	2.22	.31	6	
			13.7	25.0	13.7	6	22.4	22.4	6	22.4	13.7	6	

TABLE 4.3 - Concluded  
SUMMARY OF AVERAGE ELASTIC PROPERTIES FOR ROCK

Note:

$E_t$  = Tangent modulus (static)

$\nu$  = Poisson's ratio

$V_p$  = Dilatational wave velocity

$P_c$  (dynamic) =  $\rho V_p^2$

$P_c$  (static) =  $E_t \left[ \frac{1-\nu}{(1+\nu)(1-2\nu)} \right]$

Group No.	Rock Type and Location	Elastic Properties (First Loading Cycle)						Static Elastic Properties (Loading to Failure)					
		Static			Dynamic			Stress Level % $\sigma_{25}$ (ult)	$E_t$ psi $\times 10^6$	$\nu$	No. Tests		
		Axial Stress psi	$E_t$ psi $\times 10^6$	$\nu$	$M_c$ psi $\times 10^6$	No. Tests	$V_p$ fps					$M_c$ psi $\times 10^6$	No. Tests
11.1	Schist (Luther Falls) ⊥ Unknown Origin	110	0.24	-.02	0.2	6	5,975	1.4	12	Initial	0.33	-.02	6
		1,000	39.4	53.7	0.7	6	18.8	4.0	6	10	49.6	58.5	6
		5,000	43.0	161	1.7	6	10,240	7.3	6	50	1.50	.03	6
11.2	Schist (Luther Falls)    Unknown Origin	110	10.9	-.11	11.4	3	18,620	13.2	6	Initial	8.20	-.04	3
		1,000	27.3	95.2	7.0	3	2.5	13.4	3	10	17.9	.173	3
		5,000	6.7	58.8	7.6	3	18,745	14.9	3	50	7.85	.05	3
13.1	Siltstone (Hackensack) Hackensack, New Jersey	135	4.37	.09	4.5	6	13,095	6.0	12	Initial	4.64	.12	6
		1,000	37.1	96.4	4.4	6	9.3	6.3	6	10	39.9	83.9	6
		5,000	30.6	40.3	4.1	6	13,460	6.9	6	50	4.17	.09	6
14.1	Tuff (MTS-E Tunnel) Mercury, Nevada	105	0.82	.09	0.8	5	7,380	1.2	12	Initial	0.76	-.13	5
		750	3.0	25.3	0.7	5	2.1	1.3	5	10	10.7	15.9	5
		1,500	15.7	21.5	0.8	5	7,810	1.4	5	50	0.75	.13	5
			18.8	32.6		1.1				0.73	-.21	5	

Table 4.2 summarizes those properties which may be considered more or less as single-valued, or "constants" for each rock type. In contrast, the properties in Table 4.3 have several values, depending upon the stress level involved. (Use of these terms is not rigorous, but is intended for purposes of general clarification.) Table 4.3 is divided into two sections:

i) Elastic Properties (First Loading Cycle)

This section contains both static and dynamic values for those properties computed from data obtained during the first loading cycle only of the two-cycle, sonic velocity stress-strain tests to 5,000 (and 1,500) psi, described in paragraph (g).

ii) Static Elastic Properties (Loading to Failure)

This section contains those properties computed from data obtained during the compression tests to failure (third loading cycle), described in paragraph (h).

All values reported for E and  $\nu$  are tangent values computed from a tangent to the corresponding curve at the reported stress levels. Secant values are not reported in these tables.

Appendix B contains graphical summaries of typical data obtained for one representative specimen from each of the 28 different rock samples. Two consecutive sheets, A and B, constitute the summary for each specimen. Information within the square box in the upper corner of each sheet identifies the rock type and specimen, and includes certain physical data for that particular specimen. The Shore hardness is given for the average values obtained from the lapped ends of the specimen. The sonic velocity,  $V_p$ , given in the data box on sheet B of each set, is the dilatational wave velocity at a seating load of 100 to 150 psi.

Sheet A of each graphical data set, summarizes the data obtained during the static cyclic loading tests to 5,000 (and 1,500) psi. Plot (a) shows the axial stress-strain behavior, during both loading cycles. Plot (b) shows the variation of Poisson's ratio with stress, as determined from the SR-4 strain gages, for the first loading cycle only. Both the tangent and secant values are shown thereon. Plot (c) shows the variation of the dilatational wave (sonic pulse) velocity with stress, during both loading cycles. Plot (d) shows the changes in the various moduli of deformation, during the first cycle of loading. The tangent and secant moduli values,  $E_t$  and  $E_s$ , respectively, are computed from the static stress-strain data given in plot (a). The constrained modulus values,  $M_c$ , are computed from the sonic pulse velocity data given in plot (c) by the equation:

$$M_c = \rho V_p^2 \quad (4.3)$$

in which  $\rho$  = mass density  
 $V_p$  = dilatational wave velocity in an unbounded medium

Sheet B of each graphical data set presents the data obtained during uniaxial compression to failure. Plot (a) shows the axial stress-strain behavior. Both the initial modulus value,  $E_1$ , and the tangent modulus,  $E_t$ ,

which was computed at a stress equal to one-half the ultimate compressive strength, are recorded thereon. Strain measurements determined from the SR-4 strain gages are shown to start from zero, although this test is actually the third loading cycle for the specimen. These tests were performed a minimum of 2 to 3 weeks after the cyclic load tests, during which time no attempt was made to measure strain rebound. Little or no permanent set was measured during the cyclic loading tests, however, except for the specimens of rock salt (9.1). Plot (b) shows the variation of Poisson's ratio during loading to failure, computed for both the tangent and secant values. The theoretical limit of Poisson's ratio is 0.5, and hence, no values are shown above this limit.

Relationships among various pertinent physical and elastic properties are presented graphically in Section Five. Significant correlations used in development of index-property designations, and consequent rock classification charts, are given in Section Six.

## SECTION 5

### DISCUSSION AND INTERPRETATION OF EXPERIMENTAL DATA

#### 1. GENERAL

In this section the experimental data are examined statistically and the correlations among the various rock properties are given. The difficulties encountered in measuring some of the properties and the bases for the interpretation of the test data are discussed. A summary is given of the procedure used in the present statistical correlations including a discussion of the necessary replication (sample size) for statistical inference.

#### 2. STATISTICAL PROCEDURES

##### a. Required sample size

When a treatment or test procedure occurs more than once in an experiment, it is said to be replicated. According to Steel and Torrie (1960), the functions of replication are:

- i) to provide an estimate of experimental error,
- ii) to improve the precision of an experiment by reducing the standard deviation of the sample mean for a particular property,
- iii) to increase the scope of inference of the experimental data by selection and appropriate use of a wide variation of test samples, and
- iv) to effect control of the error variance.

An estimate of experimental error is required for determination of significance and for confidence-interval estimation of a given set of test data. When there is no method of estimating experimental error, there is no way to determine whether observed differences indicate real differences or are due to inherent variation. In such cases, any inference must be based upon prior experience.

The degree of precision required is probably the most important factor affecting the number of replicates. Increased replication usually improves precision, decreasing the width of the confidence intervals and increasing the power of statistical tests.

Replication does not reduce error due to faulty technique or equipment. Neither does mere statistical significance give information as to the practical importance of a departure from the null hypothesis (i.e., a statistical hypothesis formulated for the sole purpose of rejecting or nullifying it). The magnitude of a real departure that is of practical significance can be judged only by one with technical knowledge of the subject; this magnitude, together with a measure of how desirable it is to detect it, serves to determine the required precision and, eventually, the necessary number of replicates (Steel and Torrie, 1960).

Rock test data, published by the U. S. Bureau of Mines (1949-1956), are reported to have a probability of 75 chances out of 100 or better of being within 20% of the population mean (i.e., the mean approached as more and more observations are made). For standardized physical property tests, the Bureau of Mines (Blair, 1955) recommends an optimum and minimum number of specimens for each test as listed below:

	No. of Specimens per test	
	<u>Optimum</u>	<u>Minimum</u>
(1) Compressive strength	10	5
(2) Shore hardness	10	5
(3) Sonic velocity (dynamic-elastic constants)	6	3
(4) Modulus of elasticity (static-elastic constants)	4	3

From the definition of limit of accuracy, it is possible to determine the sample size,  $n'$ , required to predict the population mean within a certain definite range for a certain degree of accuracy. Since limit of accuracy,

$$L = \frac{ts}{\sqrt{n'}}, \text{ then } \sqrt{n'} = \frac{ts}{L}, \text{ or the required sample size:}$$

$$n' = \left(\frac{ts}{L}\right)^2 \quad (5.1)$$

where  $s$  = sample standard deviation, and  
 $t$  = "Student's"  $t$ , for  $n-1$  degrees of freedom.

Thus the required sample size depends on the specified confidence interval and level of significance, which can be altered to fit various experimental conditions (Liu and Thornburn, 1965).

In the present investigation, the number of specimens or measurements performed to determine each property was not the same for each rock group because of the type of test involved and the number of specimens prepared for each group. A summary of the average (or usual) number of tests per group and the average coefficient of variation for each measured property is given in Table 5.1. In general, either 6 specimens or 12 specimens were prepared for each group. The number of tests from the 6-specimen groups is given on the left of the middle column of Table 5.1, and the number from the 12-specimen groups is on the right of the middle column of this table. For example, for compressive strength, 3-8, means that in general, there were three tests performed for the 6-specimen groups, and eight tests for the 12-specimen groups. The average coefficient of variation was computed as a weighted average on the basis of the number of tests and the corresponding coefficient for each group.

With two exceptions, the compressive strengths of the population means,  $\mu$ , of each rock group in the present investigation have a 95% probability of being within 25% of the sample means,  $\bar{x}$ . In other words, the number of tests performed for 26 of the 28 rock groups is greater than the number of tests required by equation (5.1) at the 5% level of significance and a limit of accuracy (confidence interval) equal to  $\pm 25\% \bar{x}$ . For the standard deviations obtained in this study, Group 3.3 requires nine tests for compressive strength



**TABLE 5.1**  
**NUMBER OF TESTS AND COEFFICIENTS OF**  
**VARIATION FOR MEASURED ROCK PROPERTIES**

<u>Property measured</u>	<u>No. Tests per group</u>	<u>Average Coefficient of variation, V %</u>
Unit weight	6-12	.5
Compressive strength	3-8	7.6
Shore hardness (sides)	480-960	12.7
Shore hardness (ends)	240-480	11.8
Schmidt hardness (all readings)	72-144	7.7
Schmidt hardness (high 50%)	36-72	4.7
Abrasion hardness	4	15.3
Tensile strength (point-load)	1-2	12.0
Initial tangent modulus (1st cycle)	3-6	22.4
Tangent modulus (at 50% $\sigma_a$ ult.)	3-6	11.3
Initial Poisson's ratio (1st cycle)	3-6	82.4
Poisson's ratio (at 50% $\sigma_a$ ult.)	3-6	19.5
Dilatational wave velocity (100-150 psi)	6-12	2.7
Dilatational wave velocity (5,000 psi)	3-6	1.9

and only three were performed. Group 11.2 requires 18 tests and only three were performed.

For the modulus of elasticity at 50% ultimate strength, three groups do not meet the above precision criteria. Group 3.2 requires five tests and three were performed; Group 9.1 requires 19 tests and only five were performed; and Group 13.1 requires eight tests and six were performed.

The unit weight, Shore hardness, Schmidt hardness, and sonic velocity are well within the above precision criteria. Indeed, with few exceptions the population means of these properties are within 10% of the sample means at the 5% level of significance as computed by equation (5.1).

**b. Correlation studies**

Statistical methods of analysis were used for obtaining the least-square regression line, the standard error of estimate, and the coefficient of correlation for each set of variables. The statistical methods are described in Appendix C and are similar to those employed by Judd and Huber (1961).

The average data given in Section Four for each rock property were put on standard keypunch cards for computer analysis. Correlation and regression programs written by the Statistical Service Unit of the University of Illinois and described in "SSUPAC, Manual of Computer Programs for Statistical Analysis," were used in this study. SSUPAC consists of a collection of IBM 700M computer programs stored permanently on the IBM 1301 Disk Storage File. Included in the collection are many common statistical procedures, a complete set of basic matrix operations, and other processes for the manipulation of data. In order to call a program from the disk into the core memory ready for use, it is necessary only for the user to supply a program-call card on which is punched the name of the program, followed by whatever specific program parameters and data cards are required.

The program output lists the means and standard deviations of all variables, and the simple-correlation coefficients between all pairs of variables. The simple linear-regression coefficients and coordinate-axes intercepts are also listed, from which the least-square regression lines and corresponding equations are obtained. By transformation of the variables into logarithmic and square functions and denoting each of these as another variable, nonlinear relationships, in many cases, were reduced to linear relationships and subjected to the same methods of analysis. The SSUPAC program is based on natural logarithms, rather than common logarithms. Hence, another transformation to the base 10 is required when using this program. In all, 74 variables were analyzed in this manner.

The covariance matrices and standard errors of estimate were obtained for selected pairs of variables by use of the SSUPAC Multiple Correlation Program. In this program, it is necessary to specify in advance which variable is to be independent, and which is to be dependent. Numerous other statistical matrices are included in the printed output of the program.

Each of the data plots presented in this section shows one "best-line" as determined by the method of least squares. The equation of this line is given on the face of the plot, along with the standard error of estimate,  $s_{y.x}$ , and the coefficient of correlation,  $r$ . The coefficients of correlation are all significant at the 1% level. In most cases the X-variable is taken to be independent and the Y-variable as dependent. Thus, the regression equations and standard errors of estimate are given for "Y on X". There are one or two exceptions in which "X on Y" is given, but these are readily apparent and shown as  $s_{x.y}$ .

### 3. PHYSICAL PROPERTIES

#### a. Unit weight

The unit weight was the simplest property to determine and also showed the least variation, equal to 0.5%. Unit weights ranged from the lower value of 101 pcf for tuff (14.1) to the upper value of 191 pcf for diabase (2.3). The average unit weight for all rock groups included in this study is 162.3 pcf.

## b. Compressive strength

The ultimate compressive strength of a test specimen is defined herein as the ratio of the maximum load at failure to the cross-sectional area of the specimen before the test. Failure was considered to have taken place when a sudden drop in applied load was observed and no further load could be supported. The majority of the compressive strength tests in this study can be classified as either "cone" or shear failures. The latter is sometimes termed "diagonal," in which a plane of shear is inclined to the axis of the specimen (Hardy, 1959). Except for specimens cored parallel to bedding or foliation (e.g., schist 11.2 and limestone 6.3), "splitting" or longitudinal failures rarely occurred. Even in the case of sandstone (10.2), cored parallel to bedding, cone failures were usually obtained. However, in numerous instances, i.e., for high-strength basalts and diabases, the failure surfaces intersected the ends of the specimen near the edges. This is an indication that the loading heads offered little or no end-confining restraint to the specimens. This was verified by placing a set of lateral SR-4 strain gages near the end of a specimen, as well as at mid-height. The lateral strains obtained from these two sets of gages were identical.

By measuring the slope angle between a horizontal plane and the shear plane, the angle of internal friction,  $\phi$ , can be approximated from the Mohr-Coulomb failure theory. For the high-strength rocks, the computed friction angle was found to be generally about  $50^\circ$ . The lowest values of  $20^\circ$ - $25^\circ$  were computed for the schist (11.1), cored perpendicular to foliation. Friction angles for intact rock have been reported to range from  $27^\circ$  to  $58^\circ$ , with average values of approximately  $48^\circ$  (Deere, 1963a). Theoretically, in order for the failure plane to be entirely located within the length of a specimen, having a friction angle of  $48^\circ$ , the L/D ratio should be 2.6. Thus for NX-size cores, the required length would be on the order of 5 1/2 inches, rather than approximately 4 3/8 inches as used in the present study.

The effect of rate of loading on the compressive strength was not a part of this study. According to Hardy (1959), there is no significant difference in ultimate compressive strength determined by tests on specimens of similar material using rates of loading of 100, 200, and 400 psi/sec. As reported by Wuerker (1959), the effect of rate of stress application on concretes was investigated by Watstein (1953). He found less than a 5% increase in strength when tested at 100 psi/sec as compared to 10 psi/sec. The increase was less than 10% even up to a stress rate of 1,000 psi/sec. (The same comparison and percentage increases were obtained for modulus of elasticity.) The average rates of loading used in the present study varied from a minimum of 4 psi/sec to a maximum of 66 psi/sec. Average rates for each rock group are given in Table 4.2.

An indication of the uniformity of testing procedures and homogeneity of the rock specimens is given by the coefficient of variation. A minimum variation of less than 1% was obtained for Barre granite (5.3), and a maximum value of 25% was obtained for the Luther Falls schist (11.2), the latter cored parallel to the planes of foliation. The average coefficient of variation was computed to be slightly less than 8% for the compressive strengths measured for all rocks in this investigation.

### c. Shore hardness

The nondestructive Shore hardness tests, for which a larger number of observations were obtained than for any other test, has an average coefficient of variation of 12-13%. The average coefficient of variation for the "as-scored" sides is not significantly different from that obtained for the lapped ends. In general, the end readings are somewhat higher than the sides; the magnitude of this difference varies from sample to sample. The number of side observations is double the number of those taken on the ends. Because of these factors, and the higher degree of correlation of the results of side observations with other properties, the side readings are used in the graphical relationships and discussions presented hereafter in this study.

### d. Schmidt hardness

Inasmuch as erroneous readings tend to low values (Sosman, 1927), it appeared to be desirable to eliminate automatically a portion of the observations obtained with the Schmidt hammer. Since the readings are taken uniformly over all the specimen surface, it was somewhat arbitrarily decided to select the high 50% of observations as being representative of the Schmidt hardness for any particular rock group. The average values for all readings, and also the high 50%, are both reported in the summary tables and show, somewhat surprisingly, very little difference. Average coefficients of variation are approximately 8% for all readings, and 5% for the high 50% of readings. Average values of Schmidt hardness, for rocks in this study, range from 23 through 59.

### e. Abrasion hardness

The abrasion hardness tests exhibited the largest variations of all the physical tests conducted. However, the average coefficient is on the order of 15% which should be acceptable by most experimental standards. Unfortunately, time did not permit the modification and perfection of the equipment for a large number, or extensive control, of the tests. Although the device performed satisfactorily for this series, prolonged use would require a more rugged design. The Veeder counter had to be replaced twice. The biggest problem was to obtain a means for a positive drive system, and at the same time, produce a constant load on the specimen. The present belt drive permits a constant load, but the critical balance between starting friction and vertical load sometimes causes belt slippage. This is particularly observed in poorly-cemented, granular rocks, such as the Berea (10.1) and Navajo (10.3) sandstones, in which the particles ultimately become lodged between the cut and the wheel, stopping rotation completely. The prototype apparatus consisted of a right-angle, dental handpiece, equipped with a cable-drive system. This soon proved to be unsatisfactory because the cable drive did not permit the application of a constant load on the cutter, and also the bevel gears in the dental handpiece were not constructed for such rugged applications. Therefore, the device was modified as described in Section Four. In general, the abrasion tests as conducted were surprisingly reproducible, and gave the overall impression that further tests on additional specimens of the same rock groups would produce essentially the same results.

#### f. Absorption

Absorption values ranged from .01% for the Palisades diabase (2.1) to a maximum of 24% for the NTS tuff (14.1). An average value of 3.2% was obtained for all rocks tested. However, this has no particular significance as the majority of rocks tested were relatively dense and nonporous.

#### g. Point-load tensile strength

The average coefficient of variation for the point-load tensile strength is computed to be 12%, as compared to 21% obtained by D'Andrea, Fischer and Fogelson (1964). However, the latter performed an average of 17 tests for each rock, and the results reported herein are obtained from two tests per rock group.

A series of preliminary tests was conducted on specimens of limestone (6.1), dolomite (3.1), and siltstone (13.1) in order to determine the effect of end (or edge) distance on the measured strength. Reichmuth (1963) indicates the use of a distance greater than  $D/2$  from the point load to the end of the core specimen. The preliminary tests showed quite conclusively that end distance can be a significant factor in the magnitude of the point-load tensile strengths. When the tensile strengths obtained for end distances of  $D$  were compared to those of  $D/2$ , they were found to be 15%, 33%, and 38% higher, respectively, for the limestone, dolomite, and siltstone. As a result, for the data reported in Table 4.2, only one test was performed on each specimen, in order to maintain an end distance equal to the specimen diameter,  $D$ .

The primary problem in performing this test is in maintaining alignment between the upper and lower, hardened-steel rods. These had to be realigned after each test. Even so, this is not a serious problem as the test is rapidly performed, requiring approximately 10 minutes per test, including set-up. In addition, because the ends require no preparation, the tests can be performed rapidly on field core.

### 4. ELASTIC PROPERTIES

#### a. Modulus of deformation

Use of the terms, Young's modulus, elastic modulus, compression modulus, and modulus of deformation is normally clearly understood (and in fact the terms are interchangeable) for those materials which have linear stress-strain curves. In such cases, Young's modulus,  $E$ , is simply the slope of the curve,  $\tan \theta$ ; and also the ratio of the stress,  $\sigma$ , to the strain,  $\epsilon$ . This is shown by the relationship on the right-hand side of Figure 5.1. Thus for linear stress-strain curves, the two methods for measuring  $E$  (tangent and total strain or secant method) give exactly the same results.

The shape of stress-strain curves for rock in compression is somewhat unusual among the common engineering materials, and may depart substantially from simple proportionality between  $\sigma$  and  $\epsilon$ . Young's modulus, or the modulus of deformation, is a function of the applied stress as well as of the material. Most crystalline rocks have stress-strain curves similar to that shown in

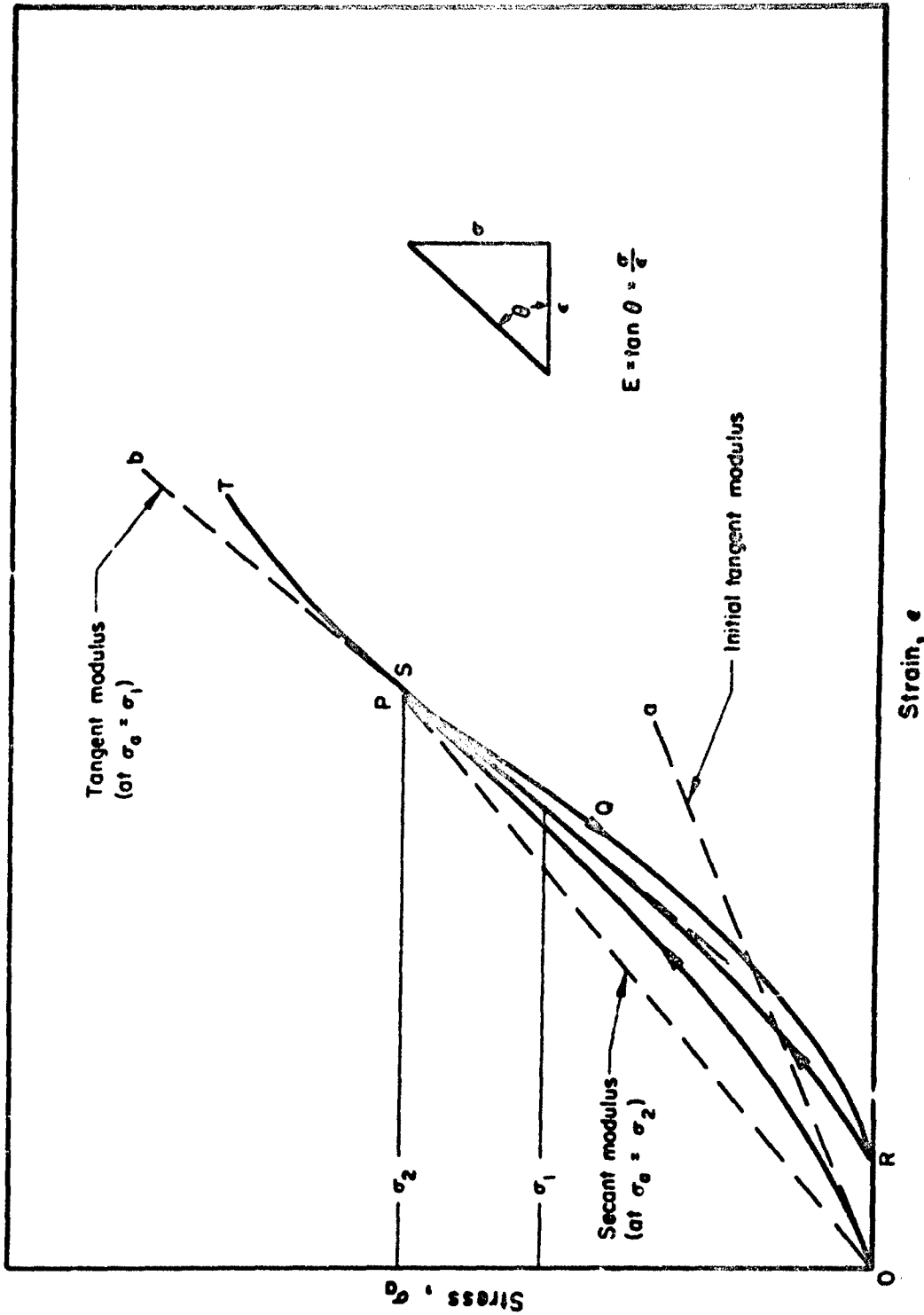


FIGURE 5.1 REPRESENTATIVE STRESS-STRAIN CURVE FOR ROCK IN UNIAxIAL COMPRESSION

Figure 5.1 (Krynine and Judd, 1957; Jaeger, 1962; Brace, 1963). This figure is typical of the sandstones investigated in the present study. At low stresses, the curve is strongly nonlinear and concave upward; Young's modulus increasing as the stress is increased. The initial tangent modulus is given by the slope of the stress-strain curve at the origin, shown by line *a*. Gradually, a stress is reached where the curve becomes approximately linear (i.e., between  $\sigma_1$  and  $\sigma_2$ ). In this region, the modulus of deformation is defined either as the tangent modulus,  $d\sigma/de$ , or the secant modulus,  $\sigma/c$ , which is given by the slope of the line *OP*. At this stress level, the secant has a lower value than the tangent modulus because it includes the initial "plastic" stress history of the curve.

In addition to nonlinear elastic behavior, most rocks exhibit an elastic hysteresis. However, unlike nonlinearity, according to Walsh (1965), hysteresis is restricted to uniaxial compression and does not seem to occur during hydrostatic compression. Under uniaxial stress, the slope of the stress-strain curve during unloading, *PQ* (Figure 5.1), is initially greater than the slope during loading for all values of stress. As the stress is decreased to zero, a residual strain *OR* is often observed. Sometimes the hysteresis loop closes at zero stress.

Reloading the rock specimen produces the curve *RS* which has a shape similar to *OP*, but is steeper. Further cycles of unloading and reloading to the same maximum stress produce loops similar to *PQRS*, but moving slightly to the right. These effects may be associated with transient creep (involving no permanent set) or anelasticity, a term used by Jaeger (1962). The rock can be loaded to failure at *T* during any desired loading cycle.

The nonlinear elastic behavior of rocks under uniaxial compression can be attributed to the presence of pores or minute cracks, which at low stresses are open (Ide, 1936; Jaeger, 1962; Walsh, 1965). As the stress is raised, cracks are closed and the rock becomes elastically stiffer, i.e., Young's modulus increases with stress. Since most cracks in rock are quite flat, nearly all are essentially closed by relatively small stresses. Above these stresses, no change in stiffness due to crack closure occurs and the stress-strain curve is linear. However, according to Walsh, Young's modulus in this portion of the stress-strain curve is still less than that for an equivalent, uncracked solid. This is because sliding of crack surfaces past each other may take place even after a crack has closed during the loading cycle.

The elastic hysteresis of crystalline rocks is explained by Walsh to be the effect of friction between crack surfaces. Because of friction, cracks which have undergone sliding during compression do not immediately slide in the opposite sense when the load is reduced, thus a clockwise loop is formed as the stress is raised, then reduced to zero. Therefore, Young's modulus for an uncracked solid can be found from the initial slope of the unloading curve for a specimen which has been stressed to the linear portion of the stress-strain curve. This is shown by *PQ* in Figure 5.1. Walsh states further that even this modulus obtained during initial unloading is not necessarily the value obtained for a "solid" sample, since the rock may contain cavities other than cracks which do not close under pressure.

Typical stress-strain relationships of the rocks used in this study are shown graphically in Appendix B. These curves show that the behavior under two

consecutive loading cycles is essentially as described above. Loading to failure during the third cycle occurs along the line represented by RST in Figure 5.1. However, since a minimum period of 2 weeks occurred between the second and third failure loading cycles, the residual strain  $\epsilon_R$  is assumed to be zero. Because of the small order of magnitude of  $\epsilon_R$ , observed in the present investigation, this is probably a valid assumption for all groups except rock salt (9.1).

Stress-strain curves for the 29 rock groups in this study are typified by the six types shown in Figure 5.2. In reality, these consist of four basic shapes, since Types III, IV and V are each modifications of the representative S-curve given in Figure 5.1. Type I is the classical, straight-line behavior of brittle materials (Jaeger, 1962). This is typical of the more explosive failures of the basalts, quartzite, one diabase, two dolomites, and the Solenhofen limestone. The softer limestones, siltstone, and tuff, exhibit a more concave-downward, stress-strain curve, as shown by Type II. These are generally somewhat linear in the early and central portions of the curve, gradually yielding "plastically" as failure is approached.

The Type-III curve is representative of ten rock groups. These include the sandstones, granites, two diabases, one dolomite, and the schist cored parallel to foliation. The three marbles and Dworshak gneiss are represented by the steeper Type-IV curve. Only the schist, cored perpendicular to foliation, has the long sweeping S-shaped curve of Type V.

Each of the Types III, IV and V is characterized by initial "plastic" crack closing, followed by a definite steeper linear portion. The upper part of the curves exhibits varying degrees of plastic yield as failure is approached. Obviously, the Type-III rocks have more explosive, brittle-type failures (similar to Type I) than either IV or V. The intensity, of course, is much greater in the high-strength rocks, because of the larger amount of energy involved. The Type-VI curve for rock salt has an initial small elastic straight-line portion, followed by a combination of plastic deformation and continuous creep.

As demonstrated in the foregoing discussions, stated values of elastic moduli may have very little usefulness for a given engineering project, unless the conditions under which they were obtained are specified. Further, meaningful relationships with other rock properties are impossible unless the stress level, and the method for computing the moduli values are known, i.e., initial, secant or tangent at a specified stress level. It may also be important to know whether they were determined from a first-loading curve, unloading, or reloading curve.

All of the curves shown in Figure 5.2 except the last exhibit a linear or straight-line portion in the central part of the curve. This was found to be consistently the case for 27 rock groups at a stress level equal to 50% of the ultimate failure strength in compression, regardless of the magnitude of the strength. For rock salt, the linear portion is in the range of 10% of the ultimate strength.

Elastic moduli are reported for several stress levels in the summary tables of Section Four. All of these are computed by the tangent method, i.e., the slope,  $d\sigma/d\epsilon$ , of the stress-strain curve at the particular stress level



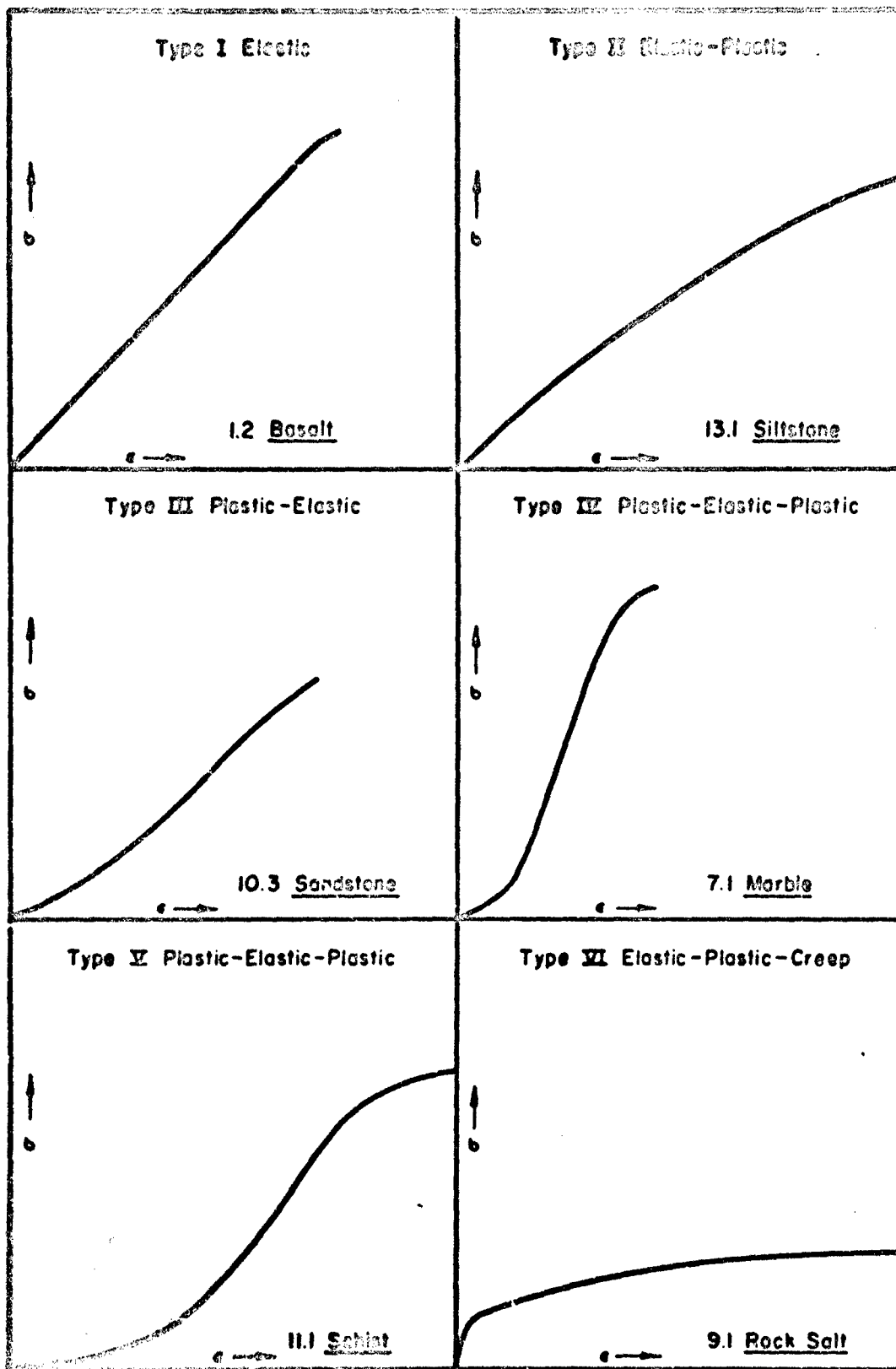


FIGURE 6.0 TYPICAL STRESS-STRAIN CURVES FOR ROCK IN UNIAxIAL COMPRESSION TO FAILURE

indicated. This reduces the influence of "stress history," or initial effects of large strain at lower stress levels, and deals only with that portion of the curve under study.

Two moduli of deformation are considered to be significant to the purposes of this investigation; they are used exclusively in all discussions and correlations that follow. These are the initial tangent modulus,  $E_i$ , for the first-loading cycle, and the tangent modulus,  $E_t$ , obtained at a stress equal to 50% of the ultimate compressive strength, during loading to failure. The initial modulus is represented by line a in Figure 5.1 and is given at the first stress increment, 100-150 psi, in Table 4.3. The tangent modulus at 50%  $\sigma_a$  (ult.) is represented by line b in Figure 5.1, and is a good approximation of the modulus of elasticity for the uncracked rock. Since the tangent modulus at 50% ultimate was measured during the third-loading cycle, at  $\sigma_a - \sigma_1$ , this line would normally be shifted slightly to the right. However, because of the elapsed time between the second and third cycles, CR was assumed to decrease to zero. This shifts the curve back to the left, in the vicinity of line b and the upper part of the first loading curve OP. It is clearly seen that the difference between any of these values is not likely to be significant. The tangent modulus at 50%  $\sigma_a$  (ult.) is given in Table 4.3 under the right-hand section entitled, "Static Elastic Properties (Loading to Failure)." The initial tangent modulus is also given for the third-loading cycle for comparison with the first cycle in the left-hand section of Table 4.3.

The coefficient of variation for  $E_i$  (1st cycle) is approximately 22%. This is roughly twice the variation computed for  $E_t$  at 50%  $\sigma_a$  (ult.), which is 11%. Such a relative variation is not surprising as the initial moduli are usually somewhat difficult to determine accurately because of problems associated with specimen seating and initial strain readings. According to Walsh (1965), Brace has minimized this error by extending the applied stress into the tension region.

The tangent modulus values at 50% ultimate strength, as computed from the dial-gage strain measurements, were consistently 25-35% lower than those obtained by the SR-4 gages. This difference may be explained qualitatively by the probable presence of more numerous micro-cracks near the ends of the specimen and, also, by additional seating imperfections which were not removed during application of the seating load. Both of these potential sources of variation are obviously included in the dial-gage readings, but would not be included in the SR-4 gage readings.

#### b. Poisson's ratio

The shortening of a specimen under axial compressive stress is usually accompanied by an increase in the cross-sectional area. The ratio of lateral unit deformation to linear unit deformation, within the elastic limit, is known as Poisson's ratio.

Theoretically, Poisson's ratio may have values ranging between -1 and 0.5. These minimum and maximum values are determined by the following equations:

$$G = \frac{E}{2(1+\nu)} \quad (5.2)$$

and 
$$K = \frac{2}{3} G \frac{1+\nu}{1-2\nu} \quad (5.3)$$

In which E = modulus of elasticity  
 G = modulus of rigidity (or shear modulus)  
 K = bulk modulus of elasticity  
 $\nu$  = Poisson's ratio

In equation 5.2, as the value of  $\nu$  approaches the value,  $\nu = -1$ , the value of G approaches infinity and becomes negative as  $\nu$  passes the value,  $\nu = -1$ . Hence, the minimum value of Poisson's ratio is  $\nu = -1$ . Similarly, in equation 5.3, the maximum value of Poisson's ratio is  $\nu = 1/2$ . At this value the bulk modulus, K, becomes infinite and, for  $\nu > 1/2$ , K is negative (Seely and Smith, 1959).

The nonlinearity of the stress-strain curves has an influence on Poisson's ratio similar to that which it has on the modulus of deformation. The numerous factors discussed in the previous section are therefore applicable to Poisson's ratio. Thus, Poisson's ratio, as given in Table 4.3, is the tangent to the curve relating lateral and linear unit deformation. It is defined by  $de_h/de_v$ , at the indicated levels of stress.

The average, initial value of Poisson's ratio for all rocks studied in this investigation, is 0.125. At a stress level of 50%  $\sigma_a$ (ult.), the average Poisson's ratio is 0.341. The average coefficient of variation for the initial value of Poisson's ratio is 82%. Unfortunately, this reflects one disadvantage of the coefficient of variation, in that it fails to be useful when the property mean is close to zero. The coefficient of variation for  $\nu$  at  $\sigma_a = 50\% \sigma_a$ (ult.) is 20%, which is considerably lower than the initial variation.

Negative values of Poisson's ratio were consistently observed for two marbles (7.1 and 7.2) and one schist (11.1) at low stress levels. Although such values are in agreement with theory, the physical concept of this phenomenon is not clearly understood. It should be noted here that other investigators have also observed negative values for Poisson's ratio (i.e., Windes, 1950; Blair, 1955; Wuerker, 1953). Perhaps other parameters are required for defining the elastic behavior of anisotropic materials, in addition to the "constants" given by elastic theory.

### c. Dilatational wave velocity

According to Rinehart et al. (1961) the propagation velocity,  $V_p$ , of dilatational stress waves in rocks depends on the following factors: the state of stress, stress level of the wave, water content, porosity, temperature, direction of propagation with respect to stratification of the rock, and texture. Some of these factors have previously been studied quite thoroughly; others, such as the stress intensity of the wave, have not been investigated as yet.

#### (1) State of stress

The influence of state of stress upon the propagation velocity of P-waves in rock is quite well known (Tocher, 1957; Wyllie, Gregory, and Gardner, 1958). Generally the velocity increases when pressure increases. It has been

shown in each of these references that P-wave velocities, measured in the same direction as the applied uniaxial pressure, appear to be equivalent to velocities obtained with the same specimen under uniform (hydrostatic) or triaxial compression of the same intensity. When the velocity was measured in a direction perpendicular to the stress in a uniaxial test, Tocher found values 10% lower than those measured parallel to the stress. The relative simplicity of the experimental apparatus and the technique required for uniaxial compression make the use of this test attractive for many purposes.

As described in Section Four, all sonic velocity tests in this investigation were conducted under uniaxial compression. The measured dilatational wave velocities,  $V_p$ , for the 28 rock groups at a seating load of 100-150 psi, vary from about 6,000 fps to a little more than 20,000 fps. Rinehart et al. (1961) state that for rocks with a well-defined texture the range of propagation velocity is relatively narrow, not exceeding 15%. They also state that for rock of the same type, but of a different origin, the velocities may range over a six-fold interval. Generally, rocks which are more dense and compact have higher velocities. Those which are less dense have lower velocities. In the present study, Solenhofen limestone (6.3) has a velocity 1 1/2 times that of Bedford limestone (6.1). Danby marble (7.5) has a velocity nearly 2 1/2 times the velocity of Taconic marble (7.1).

For most rocks, propagation velocities increase with an increase in stress. When the stress increases from 115 psi to 5,000 psi (340 bars), the P-wave velocity in Taconic marble increases 125% above the initial value (i.e., 2 1/4 times). On the other hand, for Danby marble,  $V_p$  increases only 13% for the same stress increase. The largest effect of stress increase is observed in the Luther Falls schist (11.1), for which  $V_p$  increases by 132%. The smallest effect of stress increase on the dilatational wave velocity is exhibited by the Solenhofen limestone, in which  $V_p$  increases by less than 1/4%.

Rinehart et al. (1961) report that propagation velocity in rocks generally increases 10 to 13% above the initial value, when ambient pressure increases from 1 to 500 bars. Only six rock groups in the present study fall within this range. The majority (13 groups) fall within the range of 2 to 10% increase in  $V_p$ . Four groups increase by less than 2%; three groups increase by 30 to 70%; and two, mentioned previously, by more than 100%.

The average coefficients of variation for the dilatational wave velocity measurements are smaller than for any other property except for unit weight. At a stress level of 100-150 psi,  $V\%$  is 2.7, and at 5,000 psi  $V\%$  is 1.9; the relative order being as expected.

The increase in  $V_p$  with increasing axial stress is concluded as being the result of the closing of micro-cracks. A transient stress pulse cannot be transmitted across narrow air gaps without very large loss in amplitude (U. S. Bureau of Reclamation, 1948). When there is no pressure on the rock, the open cracks impede the progress of the wave, which must then travel around the cracks. This transit time is greater than the transit time of a wave which could travel directly in an unfractured rock, or a rock in which pressure closes the cracks (Zisman, 1933; Rinehart et al., 1961). Wyllie, Gregory, and Gardner (1958) conclude that in order "to obtain simple and meaningful data from natural, consolidated rocks it is necessary to apply a large (differential)

pressure so that a terminal velocity is approached. Under these circumstances, the rock material may be considered perfectly homogeneous; at low pressures, the flaws and cracks in the matrix lower the measured velocity appreciably.<sup>ii</sup>

The figures in Appendix B show the effect of variation in stress on  $V_p$  for typical specimens of all rock groups in this study. It is noted that in general the velocities measured during unloading are higher than those measured during loading. Just as for the modulus of deformation,  $E$ , the reason for this hysteresis effect is probably due to friction between crack surfaces, which prevents sliding in the opposite sense (hence, crack opening) immediately after the load is reduced. The factors affecting the elastic parameters,  $E$  and  $\nu$ , should similarly influence  $V_p$ , as shown by the following equation:

$$V_p = \sqrt{\frac{E(1-\nu)}{\rho(1+\nu)(1-2\nu)}} \quad (5.4)$$

in which  $V_p$  = dilatational wave velocity in an unbounded medium  
 $E$  = Young's modulus  
 $\nu$  = Poisson's ratio  
 $\rho$  = mass density  $\left(\frac{Z}{g}\right)$

This equation assumes that the static and dynamic properties are interchangeable. The validity and implications of this assumption are discussed later in the chapter.

## (2) Water content and porosity

The influence of water content upon the dilatational wave velocity was not included in this investigation. As noted in Section Four, all rocks started from an initially oven-dry condition, then remained open to the ambient air of the laboratory for at least 2 weeks before testing. Gain in moisture content during this period was imperceptible. The influence of absorption or porosity upon  $V_p$  is discussed in a later part of this section.

## (3) Temperature

Rinehart et al. (1961) report that an increase in temperature generally causes a decrease in velocity of from 1 to 5% per 100°C. at atmospheric pressure. The decrease is attributed to unequal expansion of the crystals as the temperature rises, which may cause some internal cracking. Thus when cooling takes place, the crystals may be more loosely joined. At higher stresses, this effect disappears as would be expected. The effect of oven-drying on  $V_p$  was briefly studied on one specimen from each of 12 rock groups. These are listed in Table 5.2, and show the percent change in  $V_p$ , at 100-150 psi following oven-drying, compared to  $V_p$  prior to oven-drying. Except for Groups 3.2 and 7.2, the changes agree with the information given by Rinehart et al. The 21.6% decrease in  $V_p$  shown by 7.2 indicates that this effect might be related to the very large grain size of this marble and, corresponding, nonuniform expansion and contraction. Corrections to the velocities reported for this group at the lowest stress level may be justified. However, the 8.5% decrease shown by 3.2 is within acceptable limits.

## (4) Stratification

The velocity parallel to the layering and stratification in rocks is usually greater than the velocity perpendicular to the layers. The effects of

TABLE 5.2  
EFFECT OF JVEN-DRYING ON THE  
DILATATIONAL WAVE VELOCITY FOR ROCKS

<u>Group No.</u>	<u>Rock Type (name)</u>	<u>Percent Increase or Decrease</u>
1.2	Basalt (Little Goose)	+1
1.3	Basalt (John Day)	+1
2.2	Diabase (Coggins)	-2.2
2.3	Diabase (French Creek)	0
3.2	Dolomite (Lockport)	-8.5
3.3	Dolomite (Donne Terre)	- .25
5.3	Granite (Barre)	- .6
6.3	Limestone (Solenhofen)	+1
7.2	Marble (Cherokee)	-21.6
10.2	Sandstone (Crab Orchard)	- .25
10.3	Sandstone (Navajo)	-1
11.2	Schist (Luther Falls) II	0

anisotropy, which is characteristic of most rocks, were not a part of this investigation. However, a comparison of the Luther Falls schist specimens (11.1 and 11.2), which are from the same sample and oriented at right angles, illustrate this effect. The anisotropy factor is defined as the ratio of the velocity along layers or cleavages to the velocity perpendicular to them (Rinehart et al., 1961). For the Luther Falls schist this ratio is 3.1:1 at a stress level of 110 psi, and 1.4:1 at a stress of 5,000 psi. The influence of the level of stress is seen to be quite an important variable in this case. The maximum value reported by Rinehart is 1.36:1 for a mica-schist from Woodsville, Vermont.

## 5. RELATIONSHIPS AMONG VARIOUS PHYSICAL PROPERTIES

Simple linear-regression lines, relating the more significant physical properties, are shown graphically in Figures 5.3 through 5.9. Their significance and inclusion herein are based primarily upon their usefulness in the development of index properties for rock. In general, a relatively high degree of correlation, as indicated by the coefficient,  $r$ , is shown.

### a. Unit weight and compressive strength

Figure 5.3 shows the relationship between unit weight and compressive strength. This figure indicates that the more compact and denser rocks

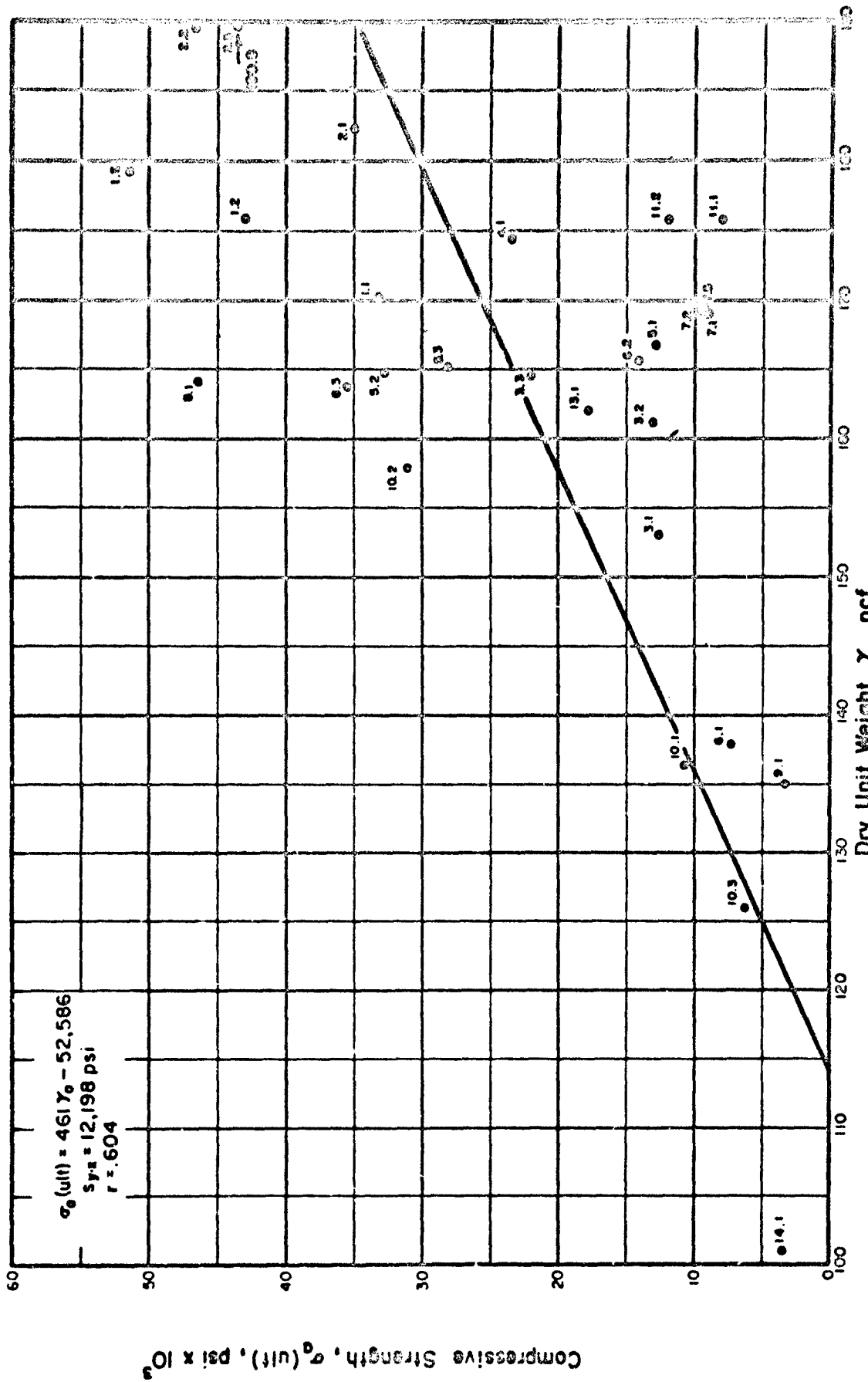


FIGURE 5.3 RELATIONSHIP BETWEEN AVERAGE VALUES OF DRY UNIT WEIGHT AND ULTIMATE COMPRESSIVE STRENGTH FOR ROCK IN UNIAXIAL COMPRESSION

generally have a higher strength than those of lower density, as would be expected. There is, however, considerable scatter from the least-squares line. In fact, above 160 pcf this relationship is not well-defined. The most notable exceptions to the suggested relationship are the marbles (7.1, 7.2, and 7.5), which are grouped closely together some distance below the line. The reason for this behavior is not completely understood although both the strength of the calcite grains and the nature of the bonding between grains are involved. The correlation coefficient,  $r = .604$  for these two variables, is essentially identical with that obtained by Judd and Huber (1961). They obtained,  $r = .59$ , for the apparent specific gravity and compressive strength from the USBM data. On the other hand, D'Andrea et al. (1964) obtained  $r = .761$ . The relationship between unit weight and compressive strength is discussed in greater detail in Section Six, in the development and formulation of index property designations.

b. Shore hardness and compressive strength

The relationship between Shore hardness and compressive strength in Figure 5.4 is comparable to the plots shown in Figures 3.5 and 3.6. However, the relationship  $\sigma_a(\text{ult.}) = 300 S_h$ , as suggested by Figure 3.5, diverges appreciably from the least-squares regression line, defined in Figure 5.4. The slope of the latter is closer to the "500  $S_h$ " line given in the USBM data in Figure 3.6. Because of the difference in L/D ratio, the reported strengths herein should be increased by approximately 12.5% when they are compared with the USBM data. Closer examination of these, as well as the referenced data, indicates that a curvilinear relationship between compressive strength and Shore hardness may be more appropriate.

The correlation coefficient reported by Judd and Huber (1961) between Shore hardness and compressive strength is  $r = .71$ . This is somewhat lower than for either the ends,  $r = .874$ , or the sides,  $r = .897$ , reported herein. The former data, however, include a greater variety of rock types, many of which would not generally be encountered in civil engineering projects. The relationship between Shore hardness and compressive strength is discussed in more detail in Section Six, in the development of index property designations.

c. Schmidt hardness and compressive strength

Figure 5.5 shows the arithmetic relationship between Schmidt hardness and compressive strength. Although the correlation, in which  $r = .880$ , appears to be quite "good," a curvilinear relationship is very strongly suggested by the individual data points. Below  $R = 40$ , the points tend to become asymptotic to the X-axis. Above  $R = 55$ , the points tend to become parallel with the Y-axis. The relationship between Schmidt hardness and compressive strength is discussed in greater detail in Section Six, in the development and formulation of index property designations.

d. Abrasion hardness and compressive strength

The relationship between abrasion hardness and compressive strength, shown in Figure 5.6, is remarkably similar to the USBM data, plotted in Figure 3.4, even though completely different methods were employed to measure the abrasion properties. If the strength values in Figure 5.6 were increased by



Compressive Strength,  $\sigma_c(\text{ult})$ , psi x  $10^3$

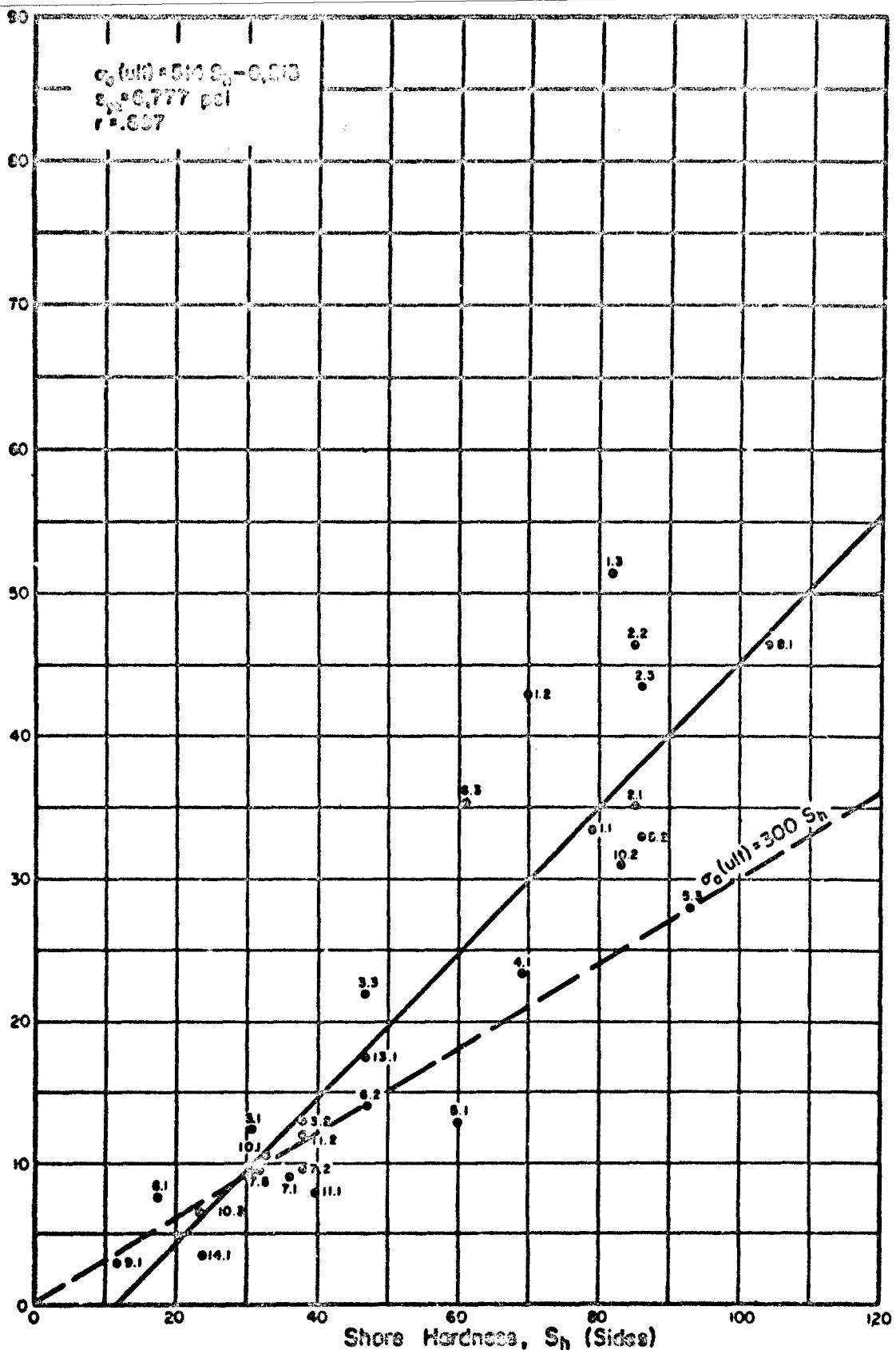


**FIGURE 5.4 RELATIONSHIP BETWEEN AVERAGE VALUES OF SHORE HARDNESS AND ULTIMATE COMPRESSIVE STRENGTH FOR ROCK IN UNIAXIAL COMPRESSION**

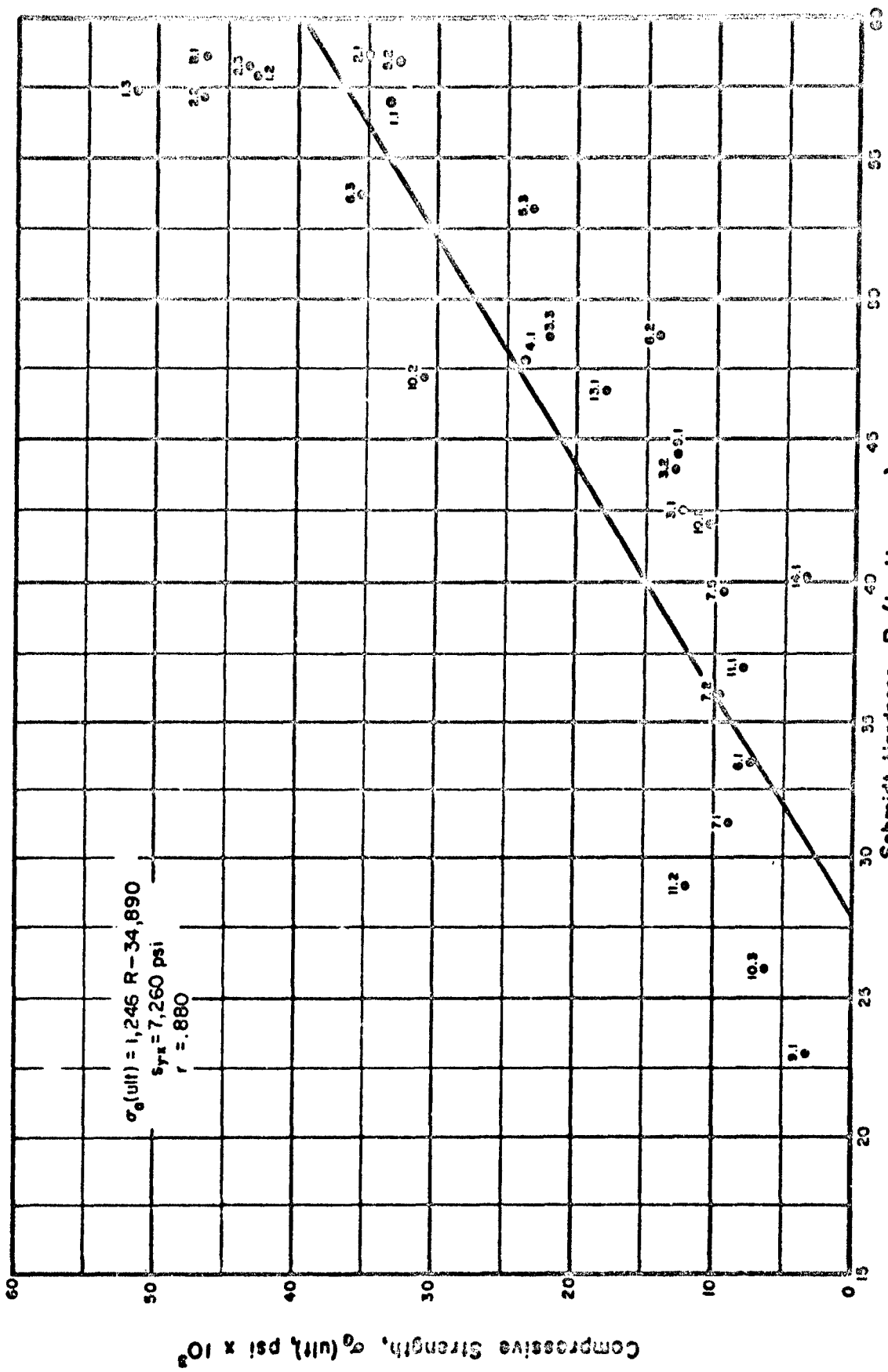
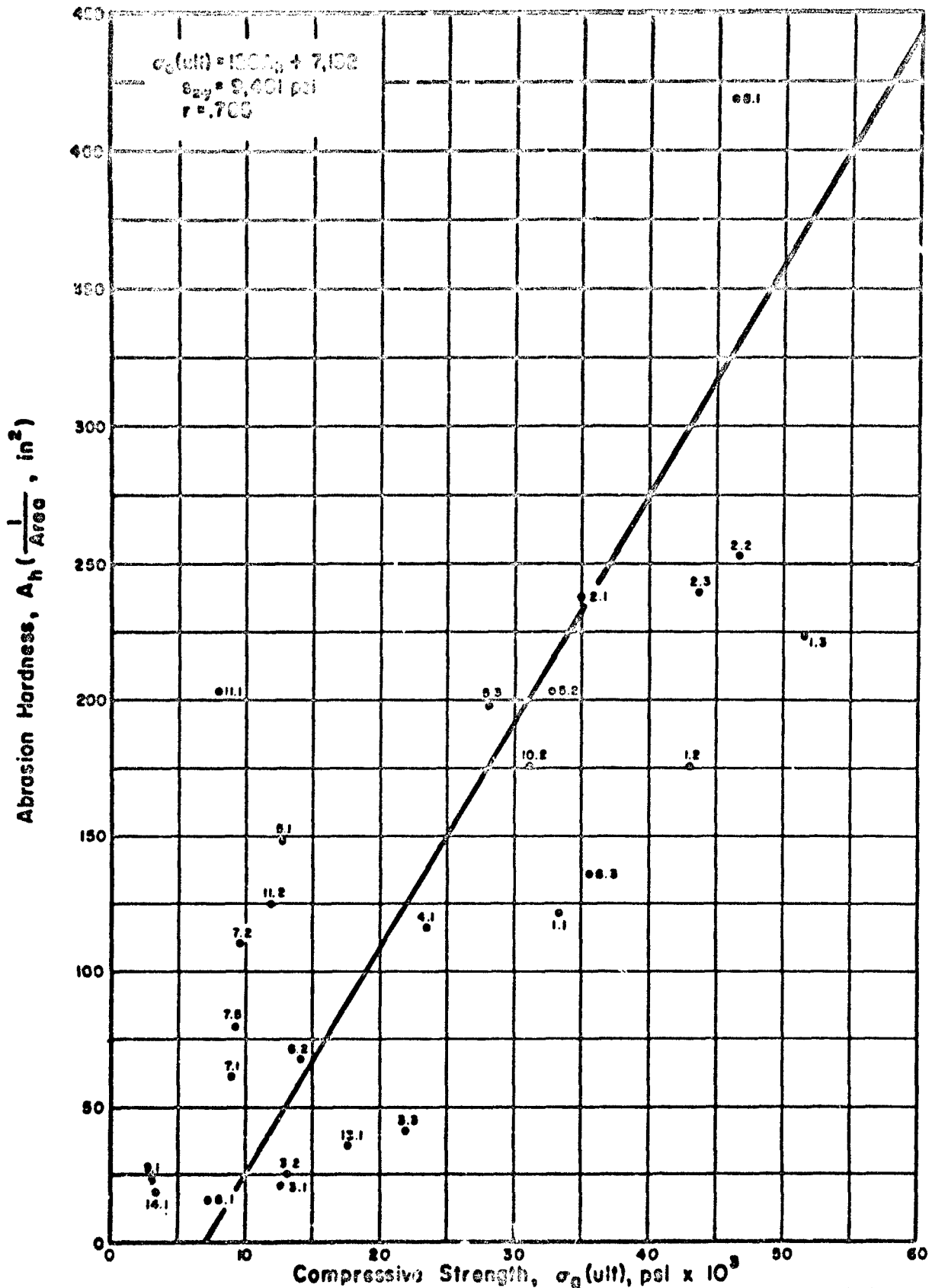


FIGURE 5.5 RELATIONSHIP BETWEEN AVERAGE VALUES OF SCHMIDT HARDNESS AND ULTIMATE COMPRESSIVE STRENGTH FOR ROCK IN UNIAXIAL COMPRESSION



**FIGURE 5.6 RELATIONSHIP BETWEEN AVERAGE VALUES OF ABRASION HARDNESS AND ULTIMATE COMPRESSIVE STRENGTH FOR ROCK IN UNIAXIAL COMPRESSION**

12.5% (because of the difference in L/D ratio), these two plots would be even more similar.

The trend indicated by the marbles (7.1, 7.2, and 7.5), schists (11.1 and 11.2), the one granite (5.1), (i.e., divergence from the regression line) may possibly be explained on the basis of their grain structure. Although their mineral constituents have average abrasion properties comparable to other rocks having higher strengths, the actual strength is governed by the bond (or lack of bond) between the individual grains. The coarser-grained marbles (7.5 and 7.2) depart from the relationship more than the fine-grained one (7.1). The Baraboo quartzite (8.1), which has a very high abrasion hardness, also falls below (to the left of) the least-squares regression line. This rock, although welded and made up of fine grains, typically contains numerous bedding planes and intermittent micro-cracks related to its geologic history, which lower the strength of the intact specimen.

#### e. Absorption and compressive strength

The regression line in Figure 5.7 indicates that the compressive strength for rock decreases with increasing absorption (or porosity). This would be the expected relation; however, the scatter of the data shows quite clearly that some rocks having low porosity may also have low strength. Over one-half of the rocks have absorption values of less than 1%. For the semi-logarithmic plot of Figure 5.7, the correlation coefficient  $r$  is  $-.429$  (the minus sign indicates inverse relation). When plotted arithmetically (not shown),  $r$  is  $-.496$ . This is closer to the value obtained by Judd and Huber (1961) in which  $r = -.48$ . (They do not record the minus sign, but their scatter-gram indicates this to be the case.)

Griffith (1937) suggests that the average compressive strength of silicate rocks can be reasonably predicted by the following formula:

$$\sigma_a(\text{ult.}) = \frac{80,000}{(A+4)} \quad (5.5)$$

in which  $A$  = sensible absorption of water by weight, expressed as a percentage  
 $\sigma_a(\text{ult.})$  = uniaxial compressive strength in psi.

This curve is shown in Figure 5.7, and is noted to be generally parallel to the least-squares line for absorption values greater than 1%. For lower values of absorption, the lines diverge. Griffith suggests that one reason for the scatter usually obtained in the region of low absorption (i.e., less than 1 to 4%) is that there are no very precise methods of measuring absorption near the zero limit. For example, a sensible (or measurable) absorption of 0.25% may actually be an insensible (or undetectable) absorption less than the parametric value 4%. Thus, rocks with high strengths, near  $A = 0$ , should be plotted in a region of insensible absorption ( $0 \leq A_i \leq 4\%$ ), instead of as functions of  $A$ . Griffith's explanation seems to be plausible but appears to leave room for personal bias, and/or judgment, for engineering application.

#### f. Point-load tensile strength and compressive strength

Simple regression between point-load tensile strength and uniaxial compressive strength, as shown in Figure 5.8, reveals a relatively high degree of correlation. Line A includes all data, in which  $r = .917$ . D'Andrea et al.

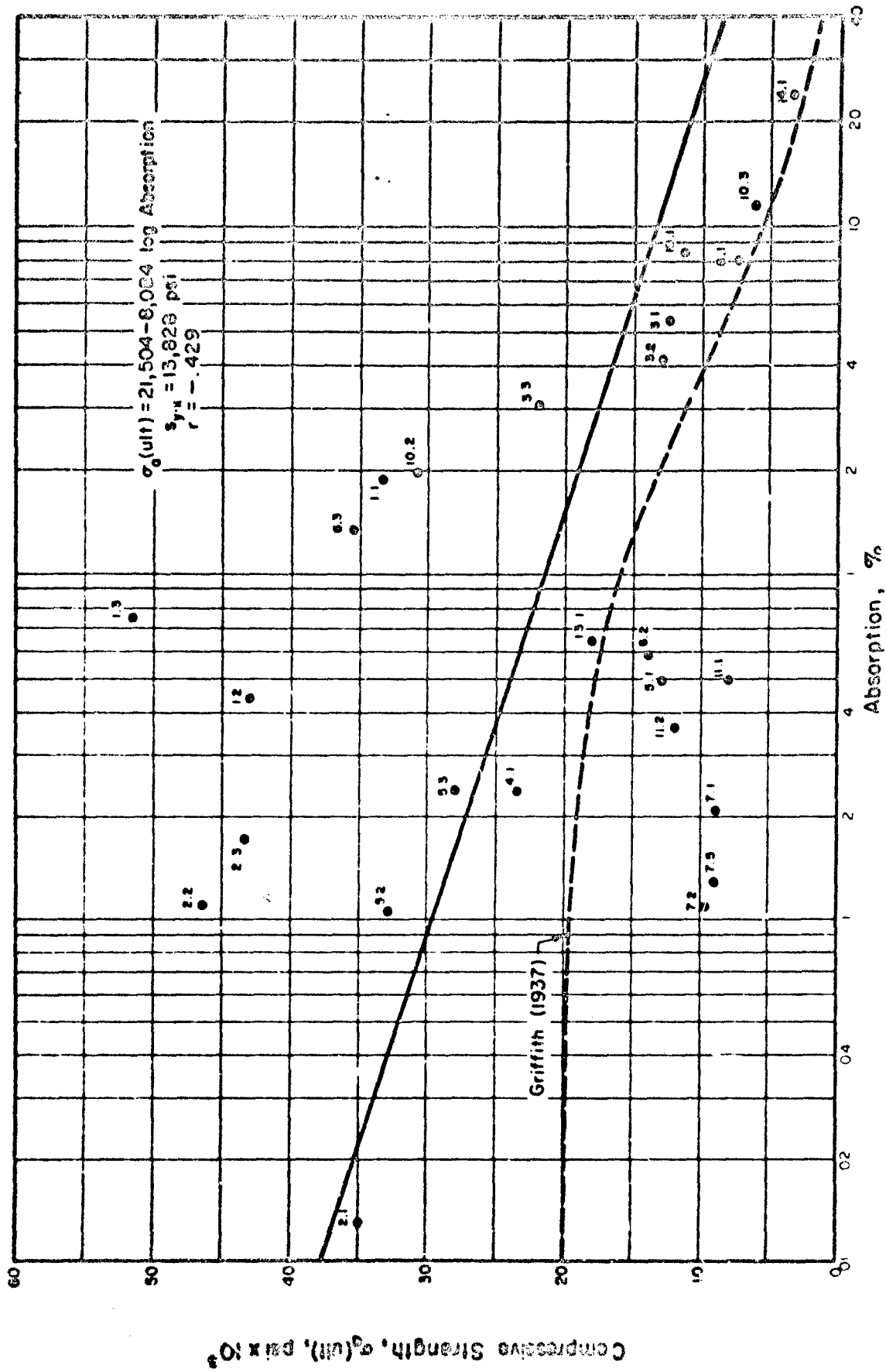


FIGURE 5.7 RELATIONSHIP BETWEEN ABSORPTION AND AVERAGE VALUES OF ULTIMATE COMPRESSIVE STRENGTH FOR ROCK IN UNIAXIAL COMPRESSION

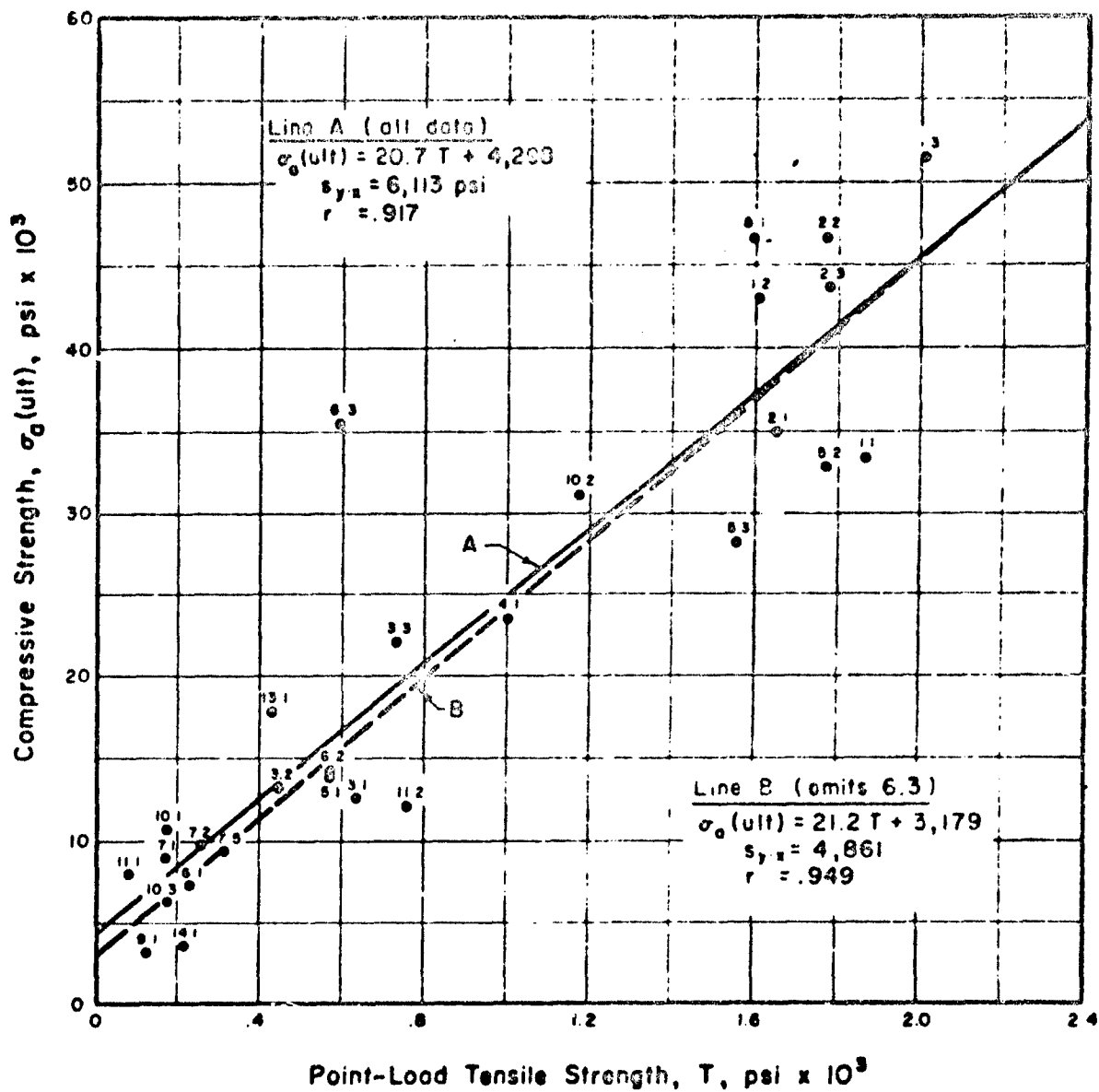


FIGURE 5.8 RELATIONSHIP BETWEEN AVERAGE VALUES OF POINT — LOAD TENSILE STRENGTH AND ULTIMATE COMPRESSIVE STRENGTH FOR ROCK IN UNIAXIAL COMPRESSION

(1964) report a better correlation, in which  $r = .947$  and  $s_{y,x} = 3,744$  psi. This is almost one-half the standard error of estimate shown by Line A. The reason for this is probably, in part, due to the method of least squares for "fitting" data. This method has the disadvantage of undesirable weighting being given to extreme values, because the differences from the mean are squared. For example, the Solenhofen limestone (6.3) has a high compressive strength, but is very brittle and has an unusually low tensile strength. If 6.3 is omitted from this relationship, Line B is given, in which  $r = .949$  and  $s_{y,x} = 4,861$  psi. These values are in considerably better agreement with those obtained by D'Andrea et al.

Data plots relating point-load tensile strength with either Shore hardness, abrasion hardness, or Schmidt hardness, produce a pattern similar to each of these variables when related to compressive strength. This should be expected, because of the relatively high degree of correlation between tensile and compressive strength given in Figure 5.8.

g. Shore hardness and abrasion hardness

Figure 5.9 is quite comparable to Figure 3.2, from USBM data, even though two different methods were used for determining abrasion hardness. Both sets of these data suggest a curvilinear relationship; however, this emphasis is stronger in Figure 3.2.

6. RELATIONSHIPS AMONG PHYSICAL AND ELASTIC PROPERTIES

Figures 5.10 through 5.19 contain plots of average data, which show the relationships among significant physical and elastic properties, and also among the elastic properties themselves. Simple linear-regression lines, along with their corresponding equations, coefficients of correlation, and standard errors of estimate are also shown, just as in the previous part.

a. Unit weight and tangent modulus of deformation

The relationship between unit weight and tangent modulus at 50% ultimate strength is shown in Figure 5.10. This relationship is more highly correlated ( $r = .784$ ) than the initial modulus and unit weight, for which  $r = .619$  (not shown). In both cases, however, the deformation moduli for intact rock specimens generally increase proportionally with the unit weight. Approximately one-half of the rock groups investigated fall within the range of 160-170 pcf. In this zone, the relation between unit weight and modulus is not so clearly defined. The relationship between unit weight and tangent modulus is discussed further in Section Six, in the development of index property designations.

b. Compressive strength and moduli of deformation

Figures 5.11 and 5.12 both show the relationship between compressive strength and the static moduli of deformation. Figure 5.11, on which are plotted the initial modulus values, shows a slightly greater standard error and lower correlation coefficient ( $r = .815$ ) than Figure 5.12 ( $r = .828$ ). Although neither regression line passes precisely through the origin, both

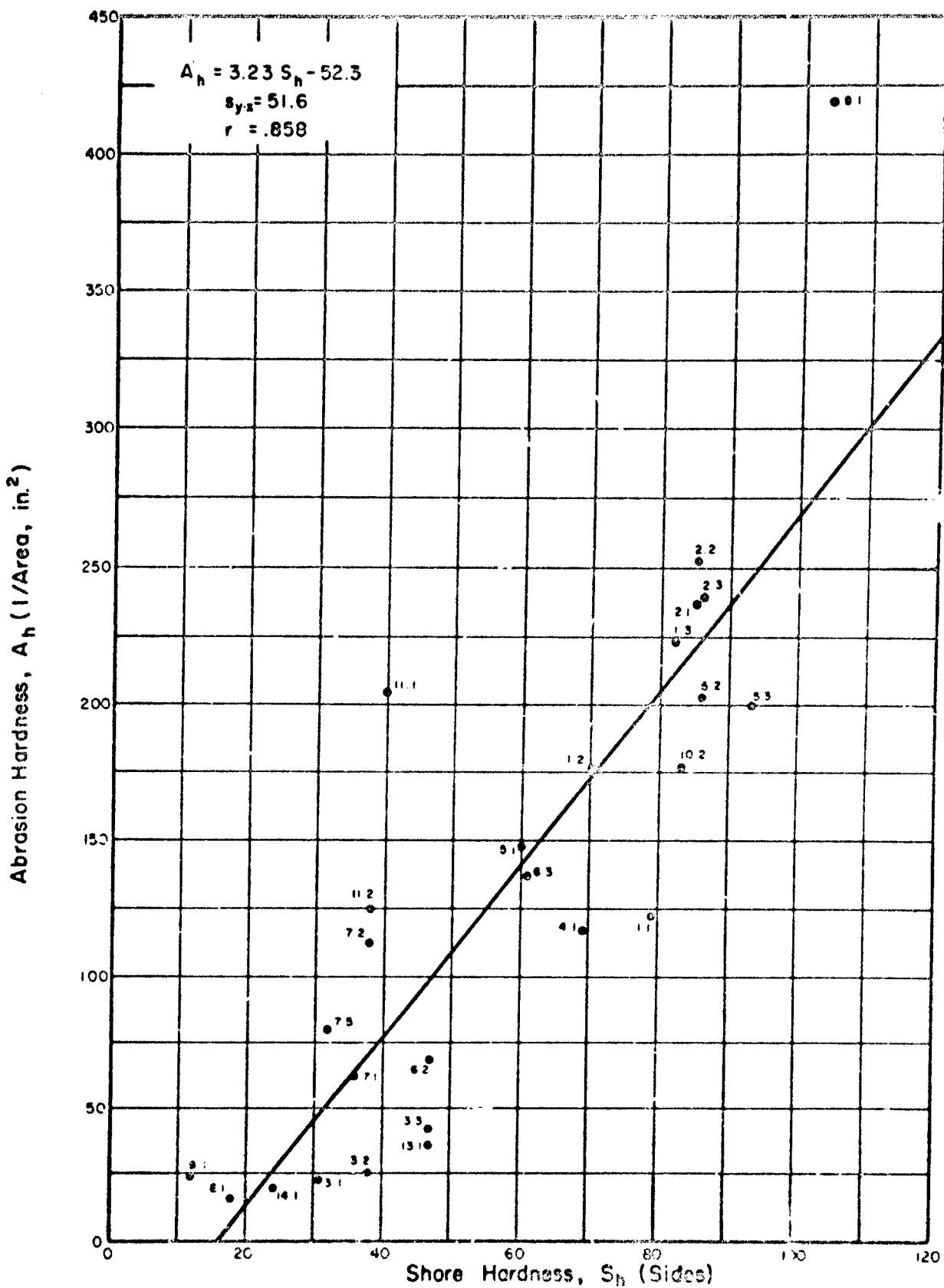
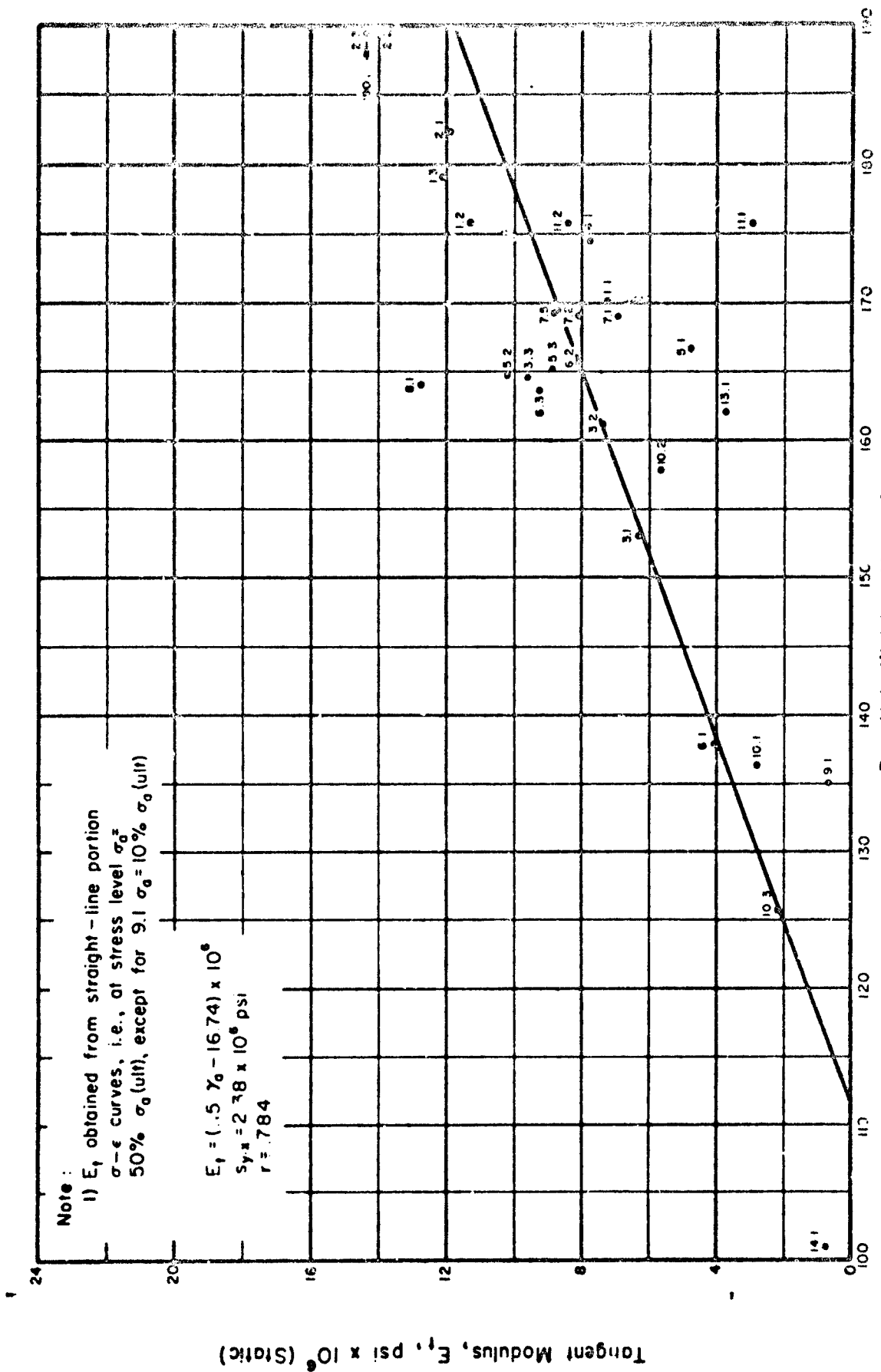


FIGURE 59 RELATIONSHIP BETWEEN AVERAGE VALUES OF SHORE HARDNESS AND ABRASION HARDNESS FOR ROCK





**FIGURE 5.10 RELATIONSHIP BETWEEN AVERAGE VALUES OF DRY UNIT WEIGHT AND TANGENT MODULUS OF DEFORMATION AT STRESS LEVEL OF ONE-HALF ULTIMATE STRENGTH FOR ROCK IN UNIAXIAL COMPRESSION**

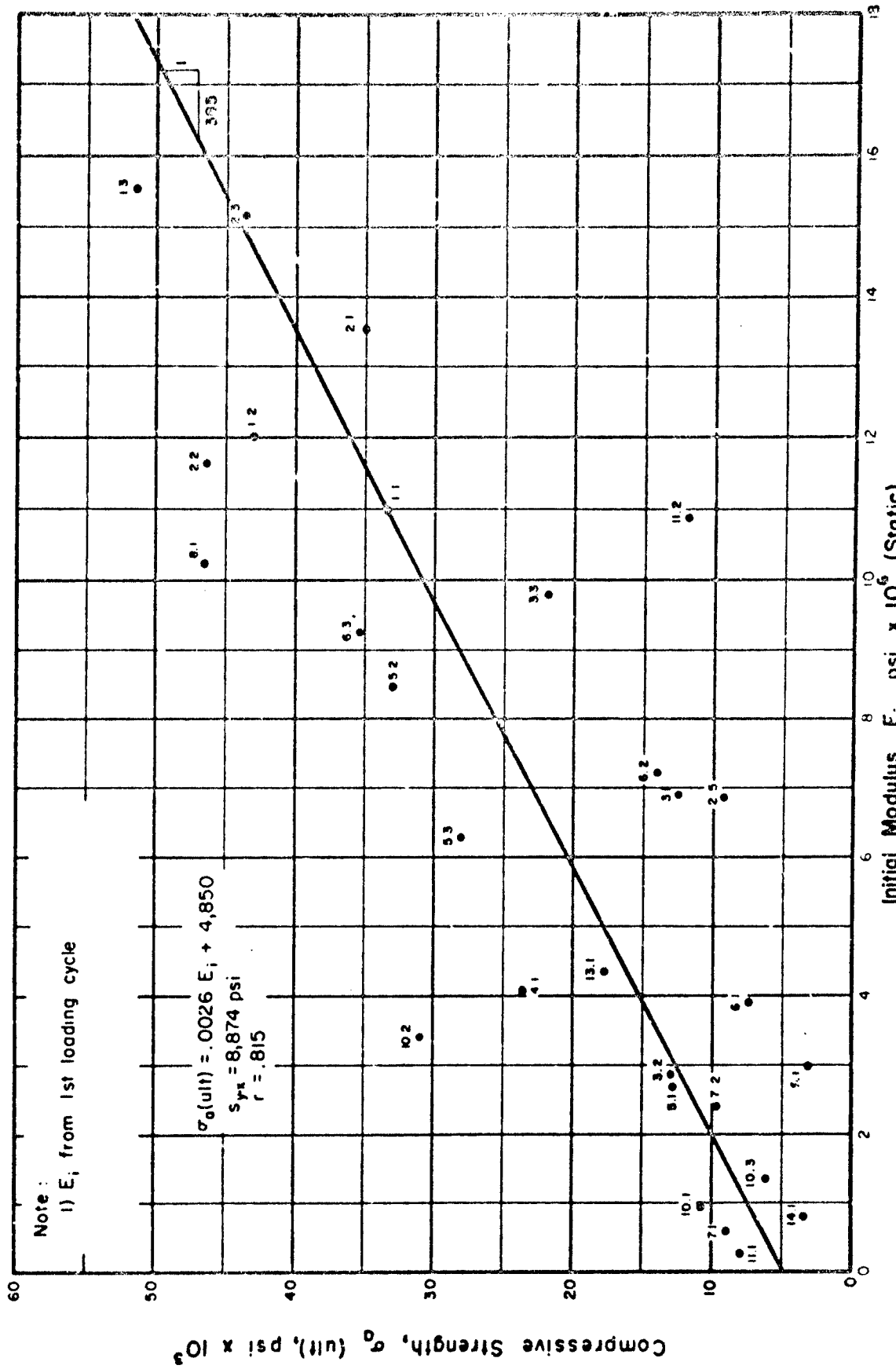


FIGURE 5.11 RELATIONSHIP BETWEEN AVERAGE VALUES OF ULTIMATE COMPRESSIVE STRENGTH AND INITIAL MODULUS OF DEFORMATION FOR ROCK IN UNIAXIAL COMPRESSION

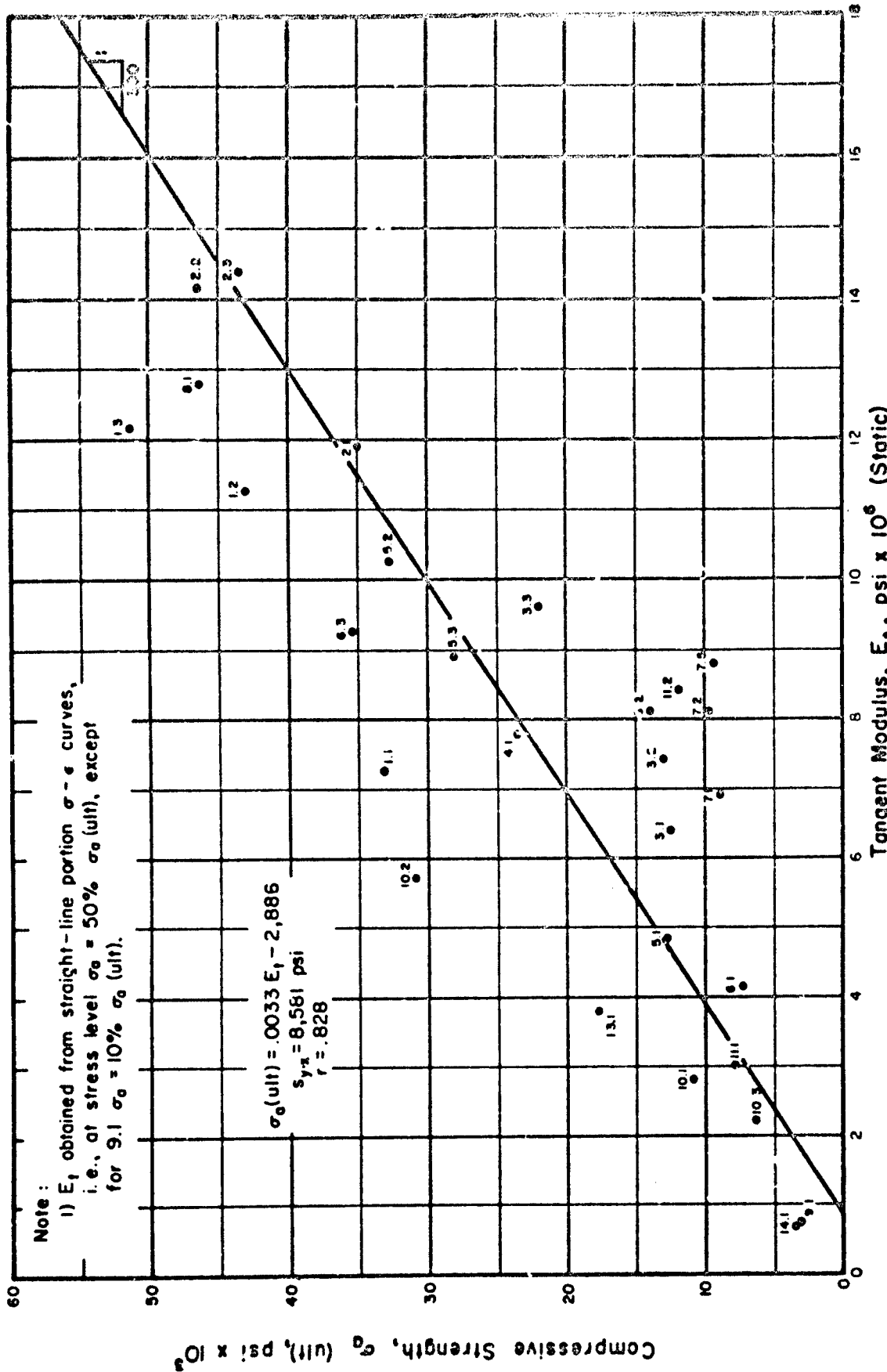


FIGURE 5.12 RELATIONSHIP BETWEEN AVERAGE VALUES OF ULTIMATE COMPRESSIVE STRENGTH AND TANGENT MODULUS OF DEFORMATION AT STRESS LEVEL OF ONE-HALF ULTIMATE STRENGTH FOR ROCK IN UNIAXIAL COMPRESSION.

are reasonably close. The ratio of the initial modulus to the compressive strength, as shown in Figure 5.11, is 385 to 1. The ratio of the tangent modulus (at 50% ultimate) to the compressive strength is shown as 300 to 1, in Figure 5.12. Both of these plots show a higher degree of correlation than that reported by either Judd and Huber (1961) or D'Andrea et al. (1964) for the dynamic modulus and compressive strength. For these,  $r = .68$  and  $.72$ , respectively. The relationship between compressive strength and the tangent modulus of deformation is utilized in the development of an engineering classification system for rock. This system is presented in Section Six.

c. Shore hardness and tangent modulus of deformation

Both methods of rebound hardness (Shore and Schmidt) employed in this study demonstrate a reasonable degree of correlation with the tangent modulus at 50% ultimate strength. Correlation with Shore hardness (which has the higher correlation coefficient of the two relationships) is shown in Figure 5.13. In general, the tangent modulus increases proportionally with Shore hardness. There is a noticeably distinct, vacant zone which parallels and includes the least-squares regression line below  $S_h = 70$ . Up to this value, the data are at a distance approximately equal to  $s_{y,x}$  from the regression line. This relation is also more or less typical of the initial modulus for all values of Shore hardness, but this plot is not included.

M. M. Protodyakonov (1963) suggests an empirical formula relating Shore hardness,  $S_h$ , with the modulus of longitudinal compression,  $E$ , in  $\text{kg/cm}^2$  as follows:

$$E = 1.07 \times 10^6 \frac{S_h}{154 - S_h} \text{ kg/cm}^2 \quad (5.6)$$

This equation is plotted in Figure 5.13, and appears to represent all the data as well as or better than the least squares line up to  $S_h = 60-70$ . Above this value, the line diverges considerably upward, away from both the data obtained herein and the resulting regression line. The data from which Protodyakonov derived this equation was not presented. Therefore, it is difficult to arrive at a reasonable explanation for the apparent differences.

d. Schmidt hardness and tangent modulus of deformation

Figure 5.14 shows the relationship of tangent modulus with Schmidt hardness. This plot resembles the plot relating unit weight and modulus (Figure 5.10), however, the correlation coefficient ( $r = .731$ ) is slightly less for this relation, but the data are more evenly distributed. Most notable scatter occurs in the zone between  $R = 28$  to  $40$ , in which schist (11.2) and tuff (14.1) show the greatest deviations. The relationship between initial modulus and Schmidt hardness (not shown), for which  $r = .705$ , has a similar pattern, but the scatter is more pronounced. The relationship between Schmidt hardness and tangent modulus is discussed in greater detail in Section Six, in the development and formulation of index property designations.

e. Absorption and tangent modulus of deformation

The semilogarithmic plot in Figure 5.15 shows the relationship between absorption and tangent modulus at one-half ultimate strength. An inverse relation is indicated, as expected, in which the modulus decreases as the

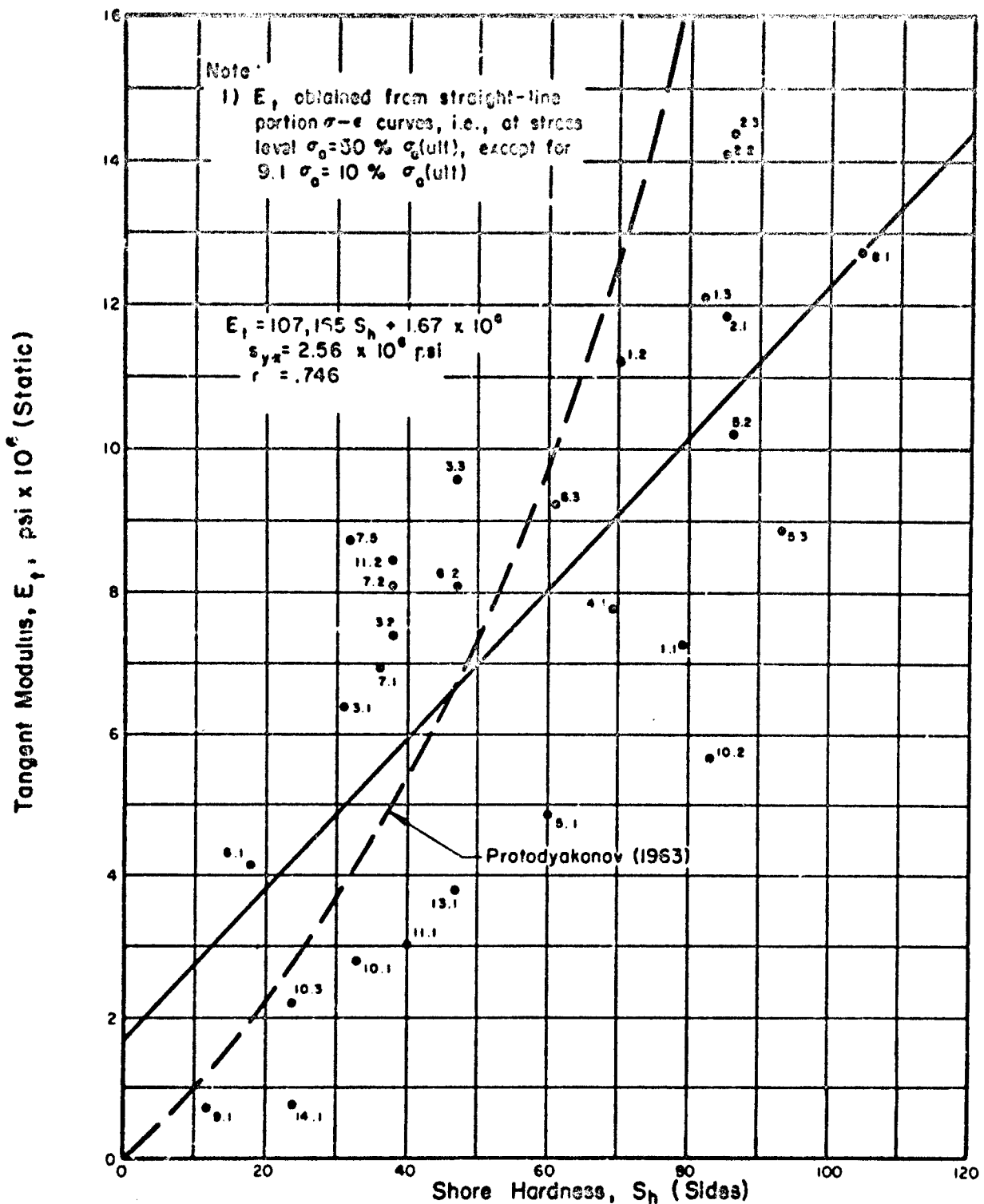


FIGURE 5.13 RELATIONSHIP BETWEEN AVERAGE VALUES OF SHORE HARDNESS AND TANGENT MODULUS OF DEFORMATION AT STRESS LEVEL OF ONE-HALF ULTIMATE STRENGTH FOR ROCK IN UNIAXIAL COMPRESSION

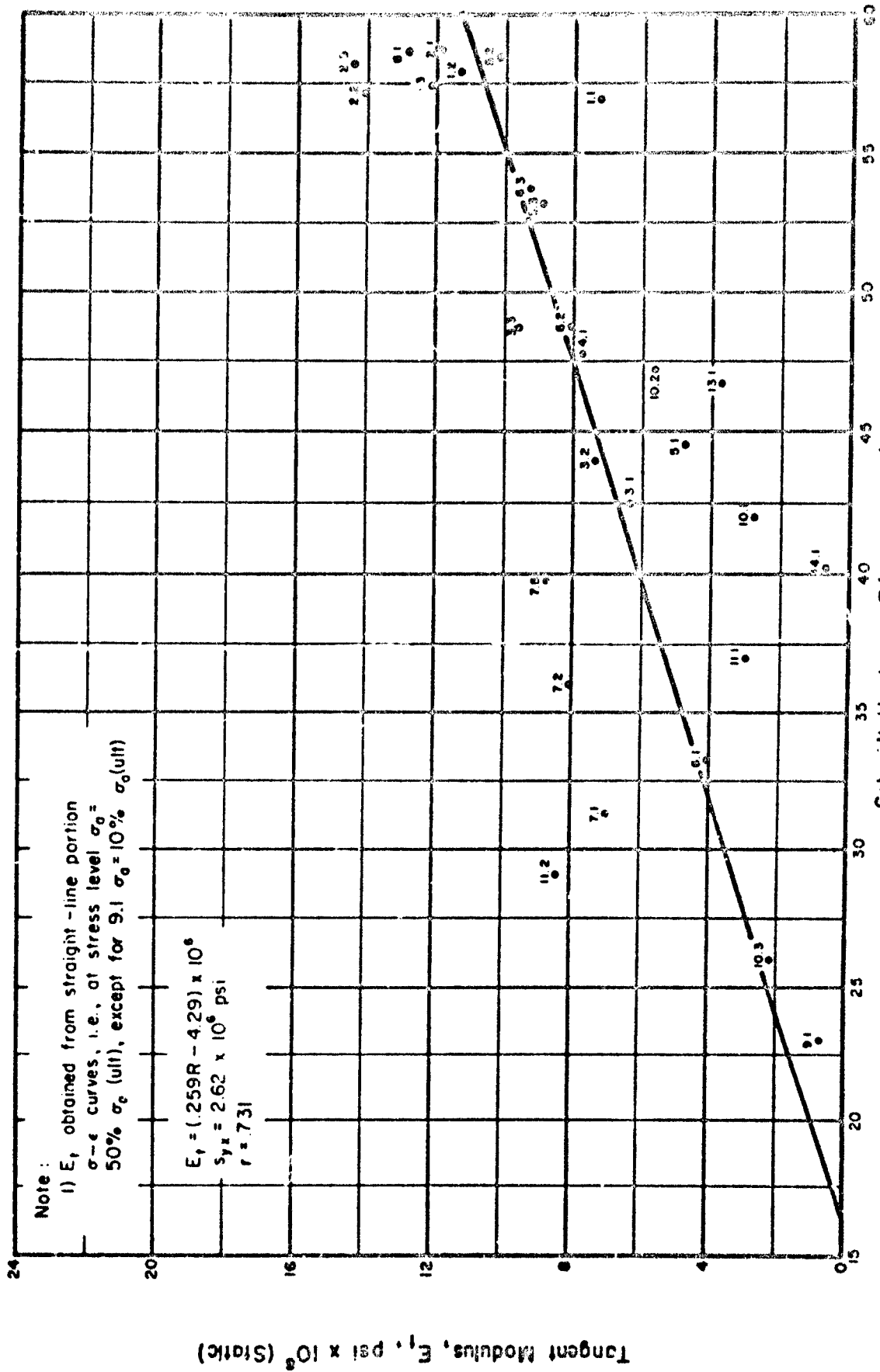


FIGURE 5.14 RELATIONSHIP BETWEEN AVERAGE VALUES OF SCHMIDT HARDNESS AND TANGENT MODULUS OF DEFORMATION AT STRESS LEVEL OF ONE-HALF ULTIMATE STRENGTH FOR ROCK IN UNIAXIAL COMPRESSION

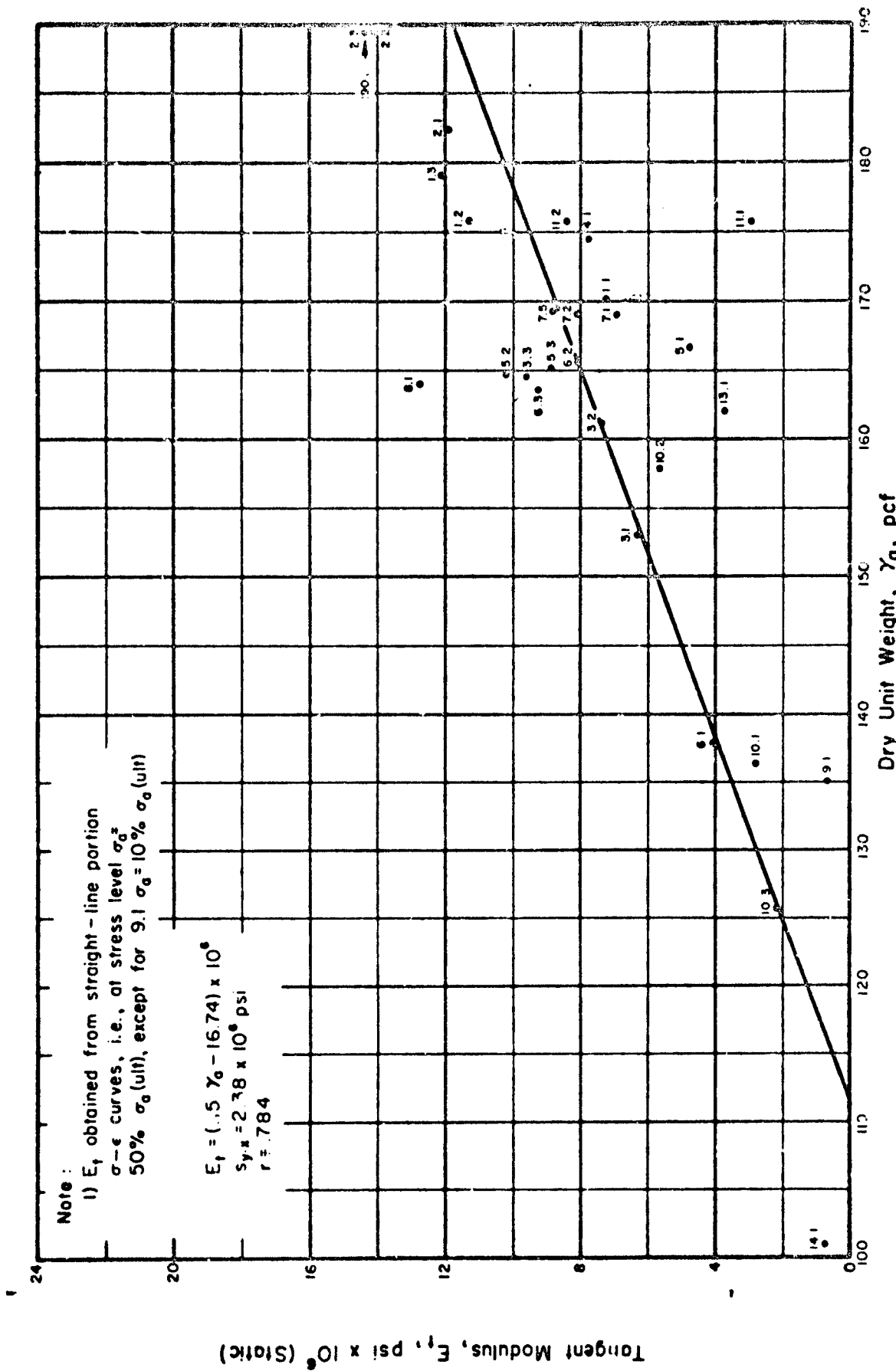


FIGURE 5.10 RELATIONSHIP BETWEEN AVERAGE VALUES OF DRY UNIT WEIGHT AND TANGENT MODULUS OF DEFORMATION AT STRESS LEVEL OF ONE-HALF ULTIMATE STRENGTH FOR ROCK IN UNIAXIAL COMPRESSION

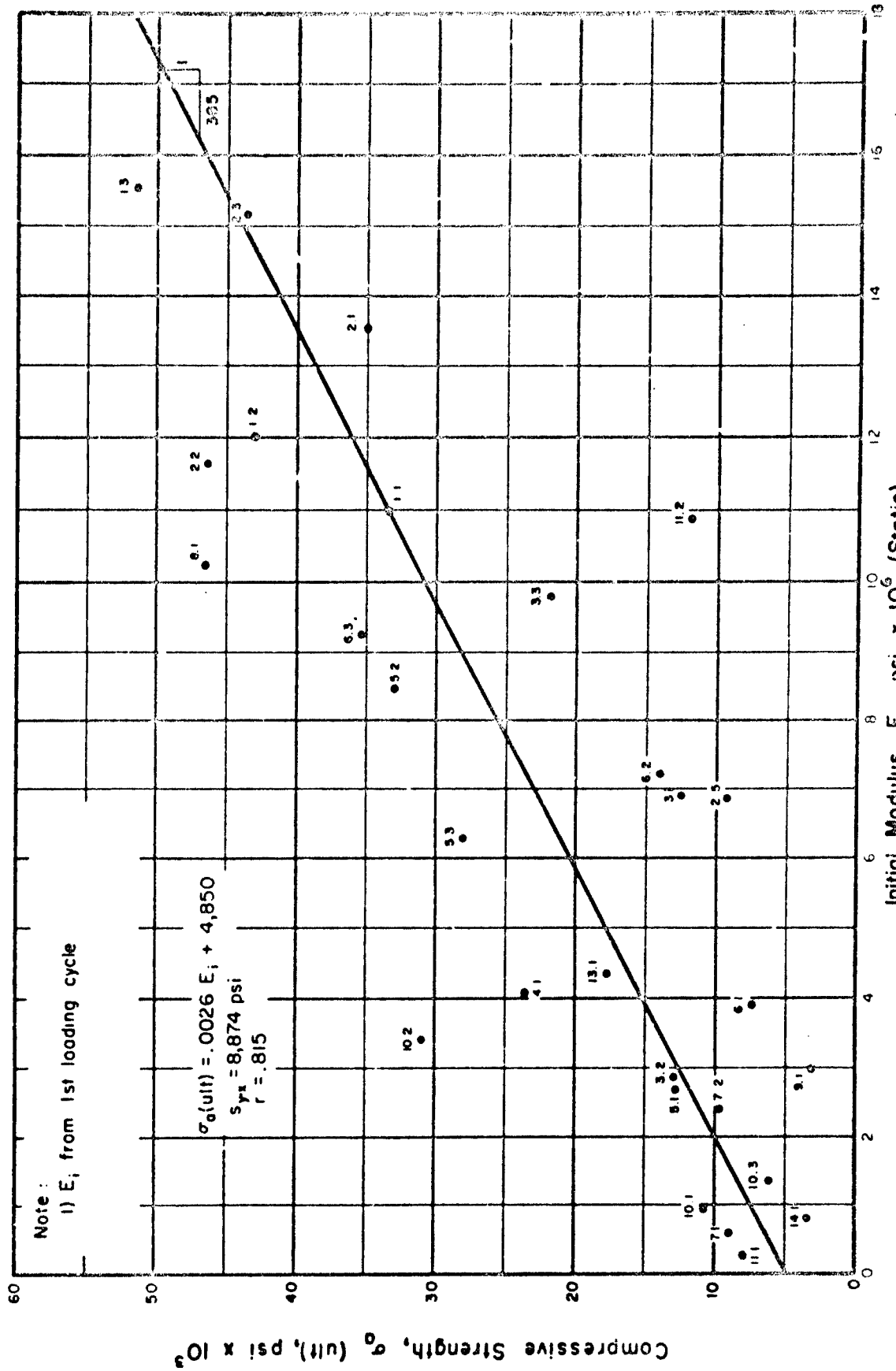


FIGURE 5.11 RELATIONSHIP BETWEEN AVERAGE VALUES OF ULTIMATE COMPRESSIVE STRENGTH AND INITIAL MODULUS OF DEFORMATION FOR ROCK IN UNIAXIAL COMPRESSION



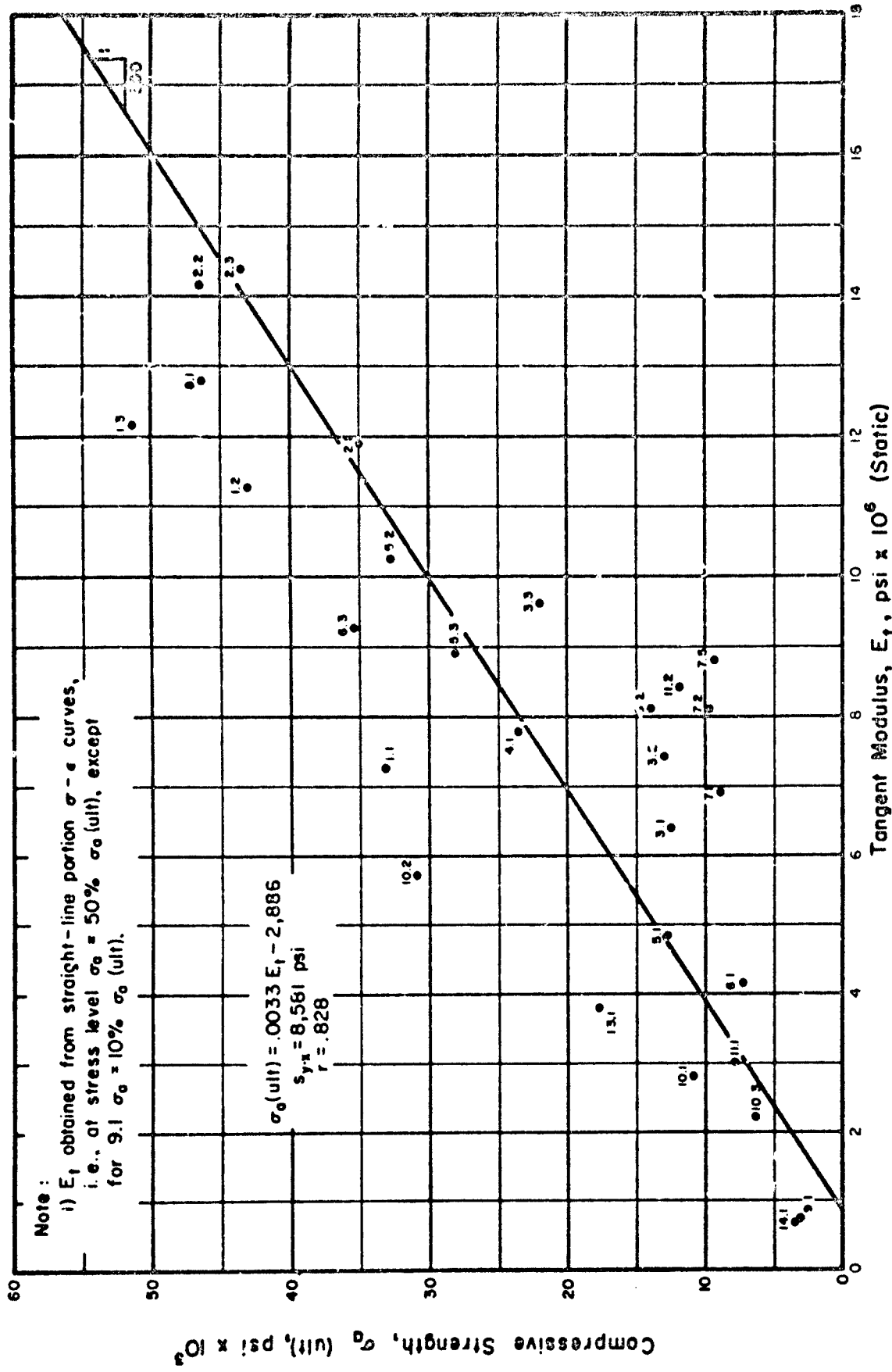


FIGURE 5.12 RELATIONSHIP BETWEEN AVERAGE VALUES OF ULTIMATE COMPRESSIVE STRENGTH AND TANGENT MODULUS OF DEFORMATION AT STRESS LEVEL OF ONE-HALF ULTIMATE STRENGTH FOR ROCK IN UNIAXIAL COMPRESSION.

are reasonably close. The ratio of the initial modulus to the compressive strength, as shown in Figure 5.11, is 385 to 1. The ratio of the tangent modulus (at 50% ultimate) to the compressive strength is shown as 300 to 1, in Figure 5.12. Both of these plots show a higher degree of correlation than that reported by either Judd and Huber (1961) or D'Andrea et al. (1964) for the dynamic modulus and compressive strength. For these,  $r = .68$  and  $.72$ , respectively. The relationship between compressive strength and the tangent modulus of deformation is utilized in the development of an engineering classification system for rock. This system is presented in Section Six.

c. Shore hardness and tangent modulus of deformation

Both methods of rebound hardness (Shore and Schmidt) employed in this study demonstrate a reasonable degree of correlation with the tangent modulus at 50% ultimate strength. Correlation with Shore hardness (which has the higher correlation coefficient of the two relationships) is shown in Figure 5.13. In general, the tangent modulus increases proportionally with Shore hardness. There is a noticeably distinct, vacant zone which parallels and includes the least-squares regression line below  $S_h = 70$ . Up to this value, the data are at a distance approximately equal to  $s_{y,x}$  from the regression line. This relation is also more or less typical of the initial modulus for all values of Shore hardness, but this plot is not included.

M. M. Protodyakonov (1963) suggests an empirical formula relating Shore hardness,  $S_h$ , with the modulus of longitudinal compression,  $E$ , in  $\text{kg/cm}^2$  as follows:

$$E = 1.07 \times 10^6 \frac{S_h}{154 - S_h} \text{ kg/cm}^2 \quad (5.6)$$

This equation is plotted in Figure 5.13, and appears to represent all the data as well as or better than the least squares line up to  $S_h = 60-70$ . Above this value, the line diverges considerably upward, away from both the data obtained herein and the resulting regression line. The data from which Protodyakonov derived this equation was not presented. Therefore, it is difficult to arrive at a reasonable explanation for the apparent differences.

d. Schmidt hardness and tangent modulus of deformation

Figure 5.14 shows the relationship of tangent modulus with Schmidt hardness. This plot resembles the plot relating unit weight and modulus (Figure 5.10), however, the correlation coefficient ( $r = .731$ ) is slightly less for this relation, but the data are more evenly distributed. Most notable scatter occurs in the zone between  $R = 28$  to  $40$ , in which schist (11.2) and tuff (14.1) show the greatest deviations. The relationship between initial modulus and Schmidt hardness (not shown), for which  $r = .705$ , has a similar pattern, but the scatter is more pronounced. The relationship between Schmidt hardness and tangent modulus is discussed in greater detail in Section Six, in the development and formulation of index property designations.

e. Absorption and tangent modulus of deformation

The semilogarithmic plot in Figure 5.15 shows the relationship between absorption and tangent modulus at one-half ultimate strength. An inverse relation is indicated, as expected, in which the modulus decreases as the

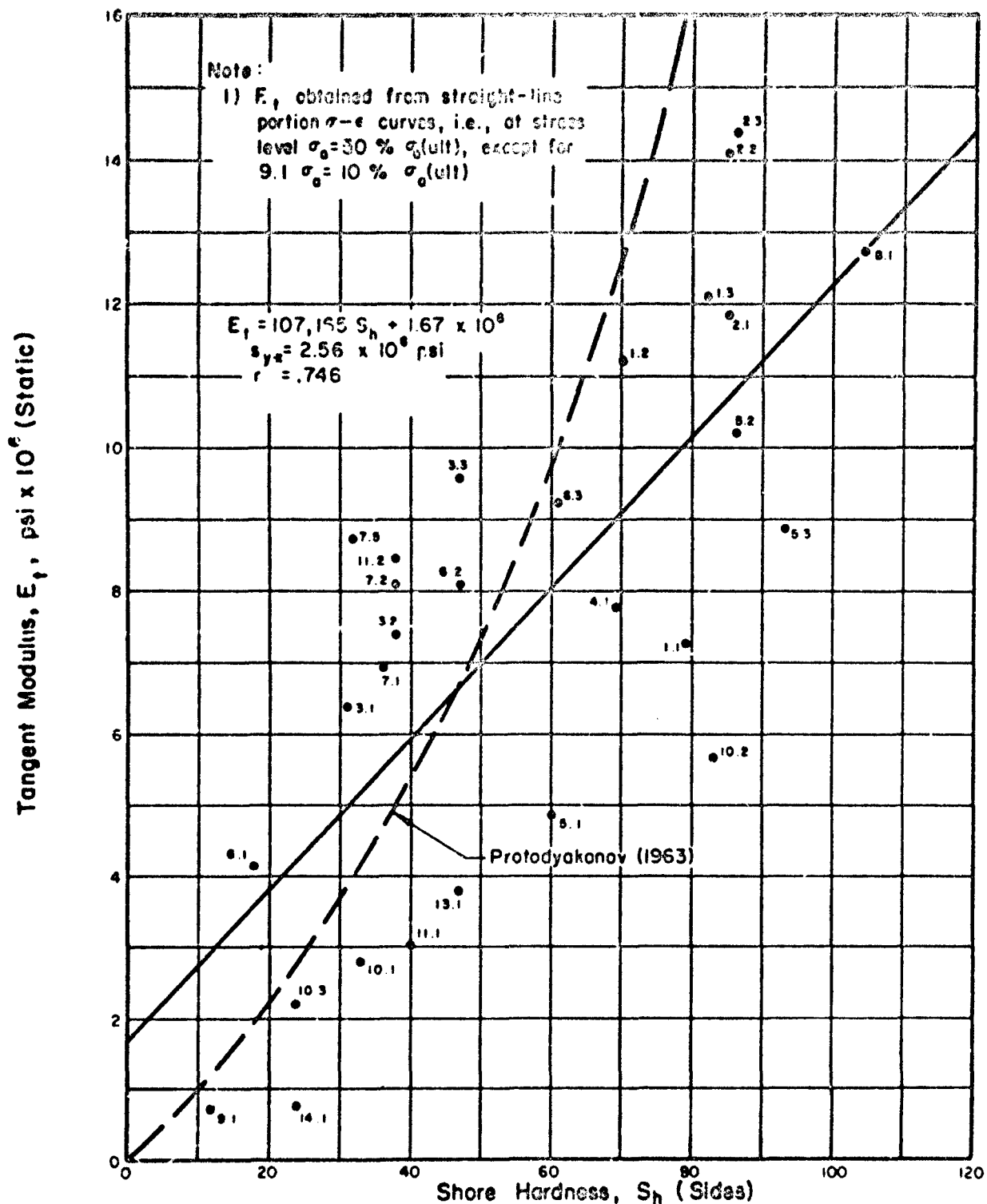


FIGURE 5.13 RELATIONSHIP BETWEEN AVERAGE VALUES OF SHORE HARDNESS AND TANGENT MODULUS OF DEFORMATION AT STRESS LEVEL OF ONE-HALF ULTIMATE STRENGTH FOR ROCK IN UNIAXIAL COMPRESSION

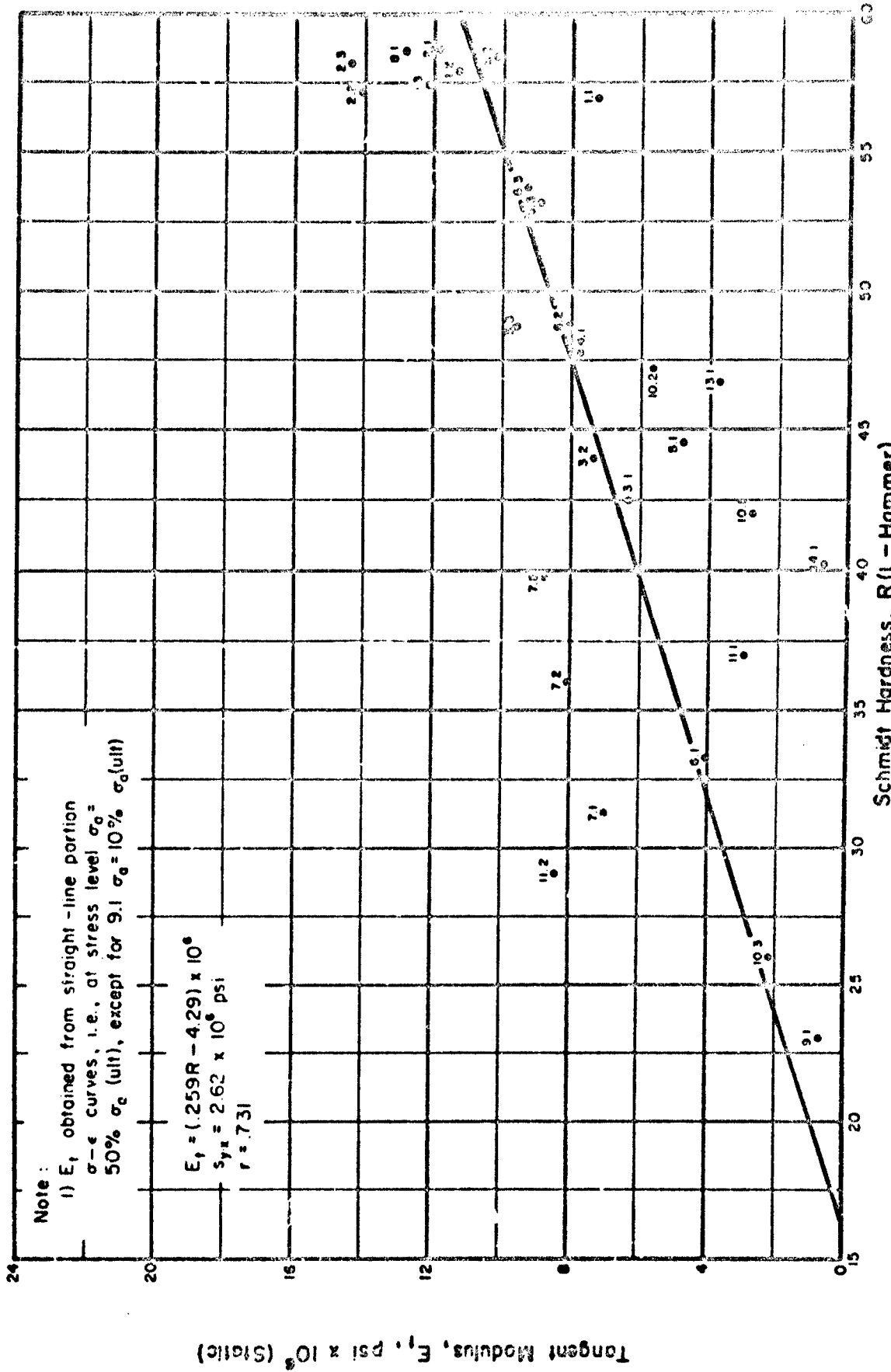


FIGURE 5.14 RELATIONSHIP BETWEEN AVERAGE VALUES OF SCHMIDT HARDNESS AND TANGENT MODULUS OF DEFORMATION AT STRESS LEVEL OF ONE-HALF ULTIMATE STRENGTH FOR ROCK IN UNIAXIAL COMPRESSION

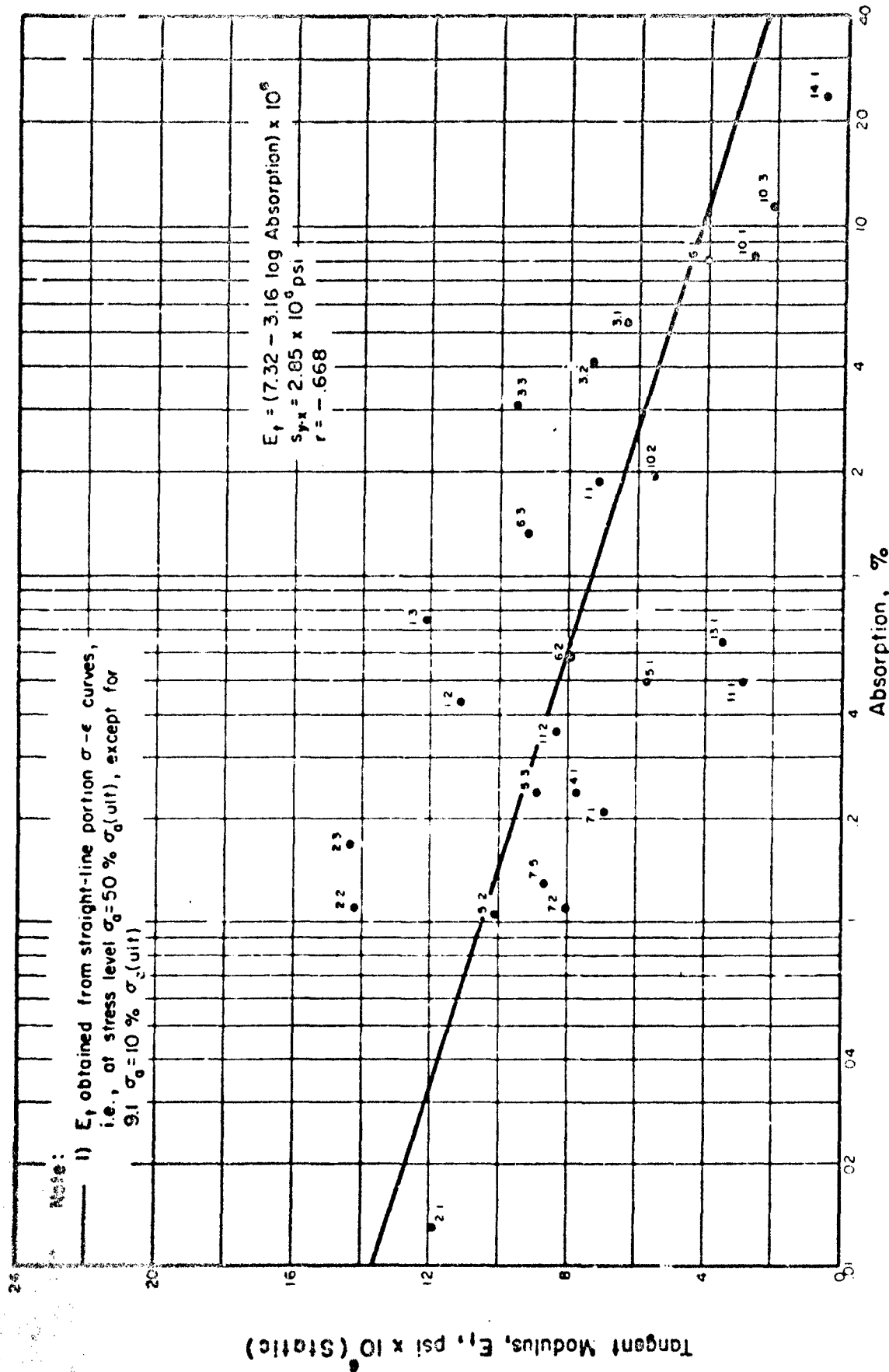


FIGURE 5.15 RELATIONSHIP BETWEEN ABSORPTION AND AVERAGE VALUES OF TANGENT MODULUS OF DEFORMATION AT STRESS LEVEL OF ONE-HALF ULTIMATE STRENGTH FOR ROCK IN UNIAXIAL COMP.

absorption (or porosity) increases. This relation is better than the one for the initial modulus values, for which scatter is so broad below 2% absorption as to obscure any consistent relationship.

Hamrol (1961) describes the use of absorption as a parameter for indicating the degree of alteration or weathering of rocks, which is termed the quality index, *i*. He presents data relating the modulus of elasticity and the quality index (or absorption) for extremely weathered granites. Because of this correlation and its simple determination, Rocha (1964) describes the usefulness of the quality index as a means for controlling the depth for foundation excavation in rock. Also, it can be used during the exploration of extensive areas for accurate zoning in rock surveys in order to reduce the number of in-situ tests.

The information given by Hamroi and Rocha impressively demonstrates the usefulness of absorption as an index of deformation quality at a particular site, for a given rock type, subjected to the same general conditions of alteration and weathering. The data, presented in Figure 5.15, seem to indicate that this relationship may not be so clearly defined when several rock types from different sources are all included on the same plot.

f. Unit weight and sonic velocity

Sonic velocity, at a stress of 5,000 psi, is shown in Figure 5.16 to be higher for rocks with higher unit weights as expected. This is not the case at low stress levels, in the vicinity of 100-150 psi. Whereas there is no detectable difference in unit weight at low stresses, the sonic velocity is strongly influenced by open micro-cracks, as previously discussed. Therefore, rocks with unit weights in the general range of 160 to 180 pcf may have velocities from 6,000-20,000 fps at low stress levels. As the pressure is increased to 5,000 psi the velocities increase and shift to the right, resulting in the relation as shown.

g. Sonic velocity and moduli of deformation

Figures 5.17 and 5.18 show the relationships between sonic velocity and the static moduli of deformation for two different stress levels. The least-squares regression lines defined in these plots have remarkable parallel slopes. However, the regression line in Figure 5.18 is shifted to the right and downward from that of Figure 5.17 because of increasing the stress level.

The combined changes in velocity and modulus, resulting from increased stress, are more clearly shown in Figure 5.19. In general, rocks in the lower half of this plot show relatively large increases in both modulus and sonic velocities when the stress is raised from 100 psi to 5,000 psi. These have stress-strain curves (Types III, IV, and V) which are initially concave upward, and have initial modulus values which are lower than the tangent modulus at 50% ultimate. Exceptions to this are shown by 3.1, 9.1, 13.1, and 14.1.

Rocks in the upper half of the plot show very little increase in velocity, but, in general, show a decrease in modulus when the stress is raised. These have stress-strain curves (Types I and II) which are initially convex

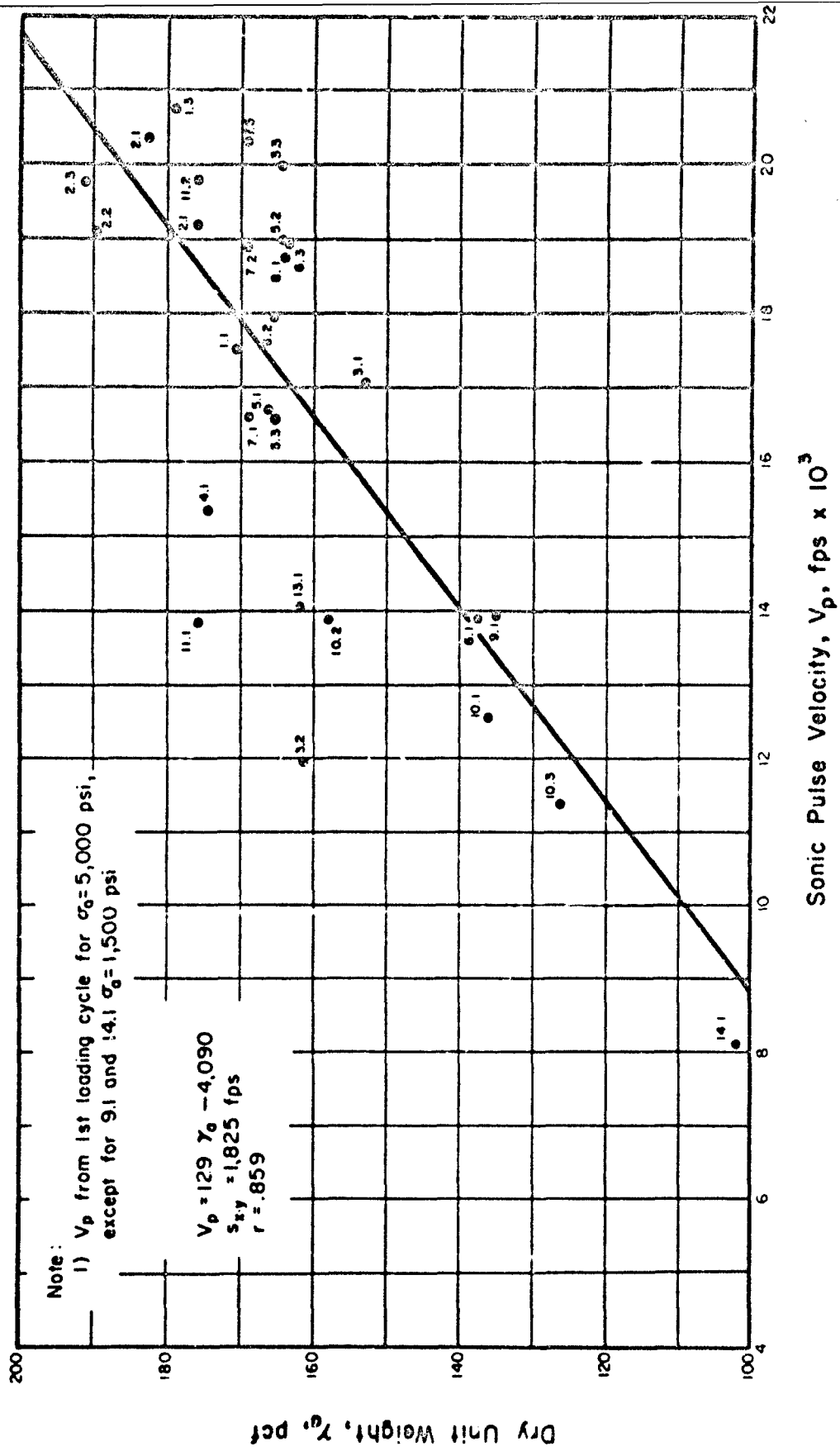


**FIGURE 5.16 RELATIONSHIP BETWEEN AVERAGE VALUES OF DRY UNIT WEIGHT AND DILATATIONAL WAVE VELOCITY FOR ROCK UNDER UNIAXIAL COMPRESSIVE STRESS OF 5,000 psi**

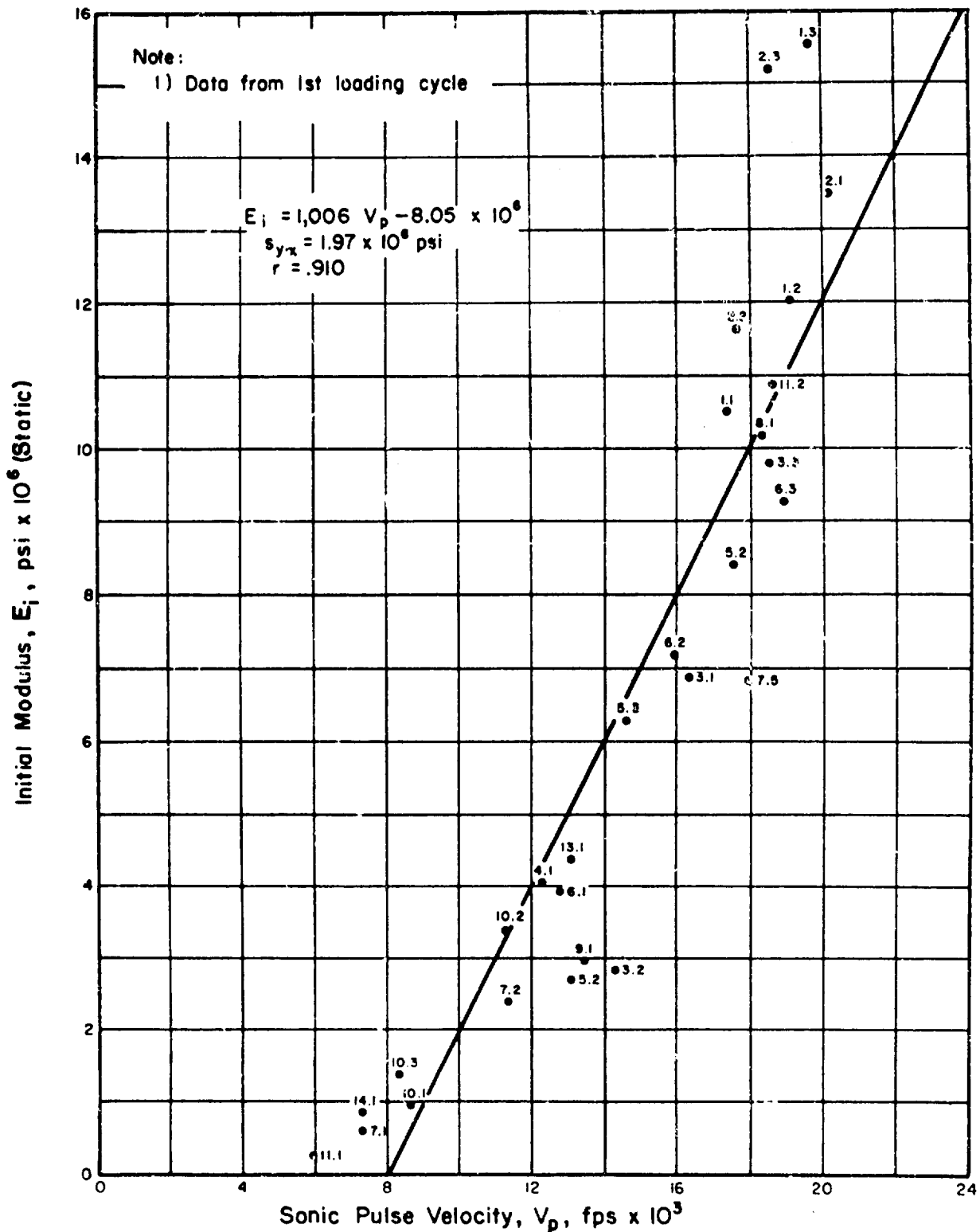


FIGURE 5.17 RELATIONSHIP BETWEEN AVERAGE VALUES OF INITIAL MODULUS OF DEFORMATION AND DILATATIONAL WAVE VELOCITY FOR ROCK UNDER UNIAXIAL COMPRESSIVE STRESS OF 100 -150 psi



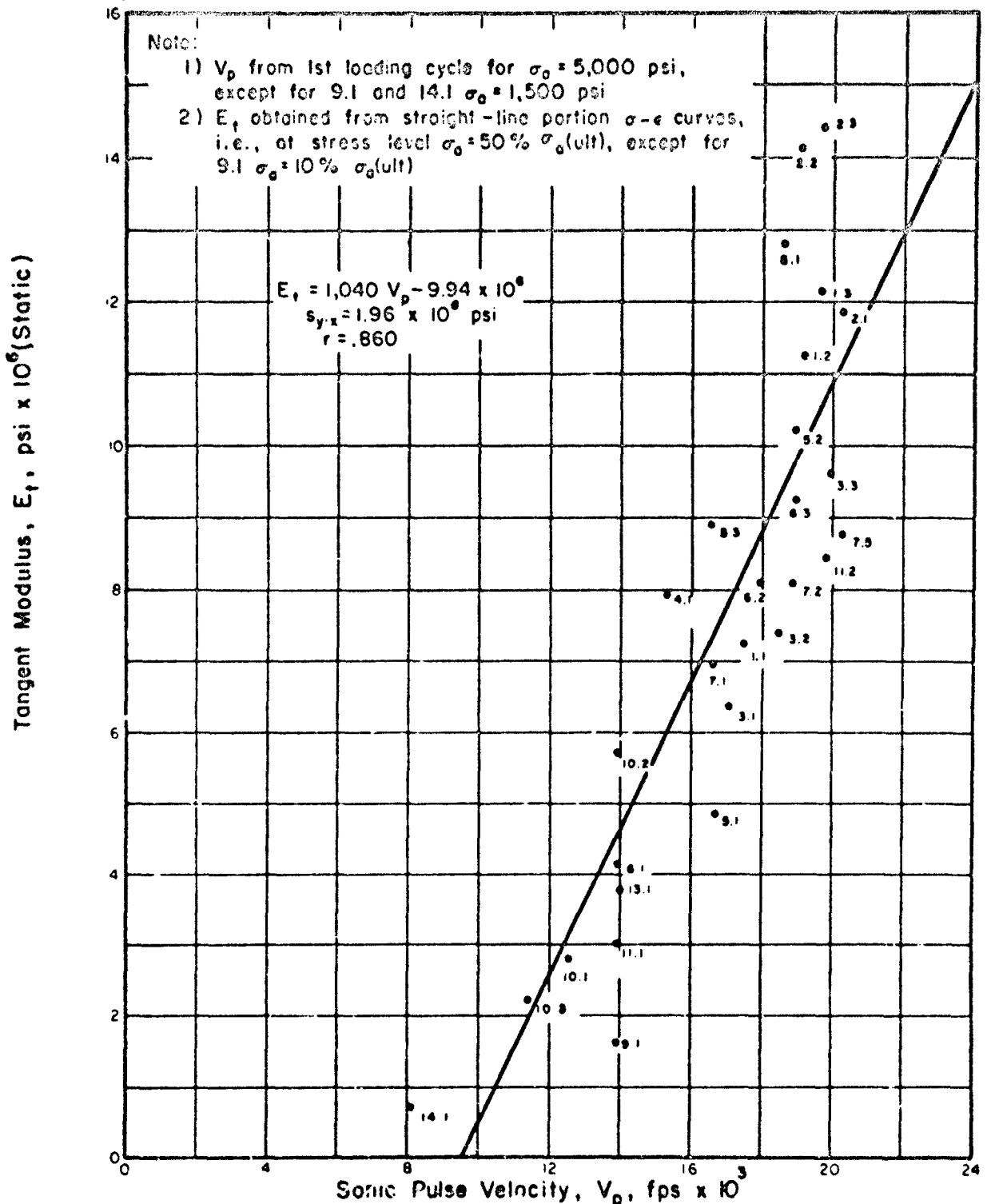


FIGURE 5.18 RELATIONSHIP BETWEEN AVERAGE VALUES OF TANGENT MODULUS OF DEFORMATION AT STRESS LEVEL OF ONE-HALF ULTIMATE STRENGTH AND DILATATIONAL WAVE VELOCITY FOR ROCK UNDER UNIAXIAL COMPRESSIVE STRESS OF 5,000 psi

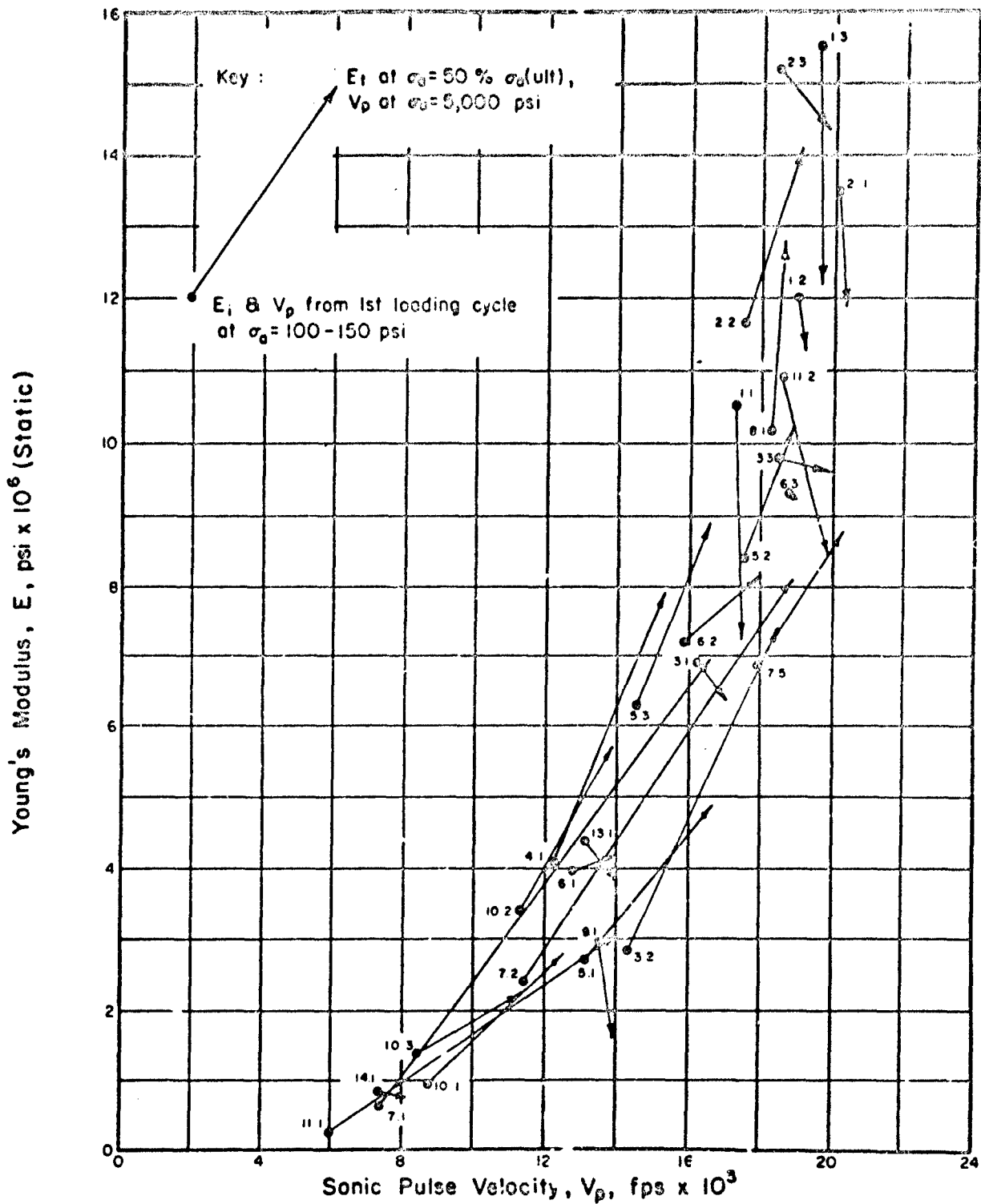


FIGURE 5.19 VELOCITY—MODULUS VECTORS FOR ROCK UNDER INCREASING UNIAXIAL COMPRESSIVE STRESS

upward and, therefore, have higher initial modulus values than the tangent modulus at 50% ultimate. Exceptions to this are shown by 2.2 and 8.1.

The dividing lines, for the behaviors described above, appear to be in the vicinity of  $E = 9 \times 10^6$  psi and  $V_p = 16,000$  fps. Rocks having initial moduli and velocities below these values are in the "lower half" of the plot, and rocks for which initial values are greater than these limits are in the "upper half." Apparently, 3.1, 5.2 and 7.5 are borderline exceptions to these generalizations.

In accord with theory, the data in Figures 5.17 and 5.18 indicate that a curvilinear relationship would provide a better fit. Even so, the coefficients of correlation for the linear regression lines shown are both fairly high,  $r = .910$  and  $.860$ , respectively. The possible reasons for a lower coefficient for sonic velocities at a stress of 5,000 psi, as plotted in Figure 5.18, are as follows:

- i) The sonic velocities for rocks of which the strengths at 50% ultimate are less than 5,000 psi, are higher (as plotted hereon) than they would be at a stress level equal to 50% of their ultimate strength. Therefore, these rocks plot further to the right of the regression line than they "should."
- ii) The sonic velocities plotted for rocks, of which the strengths at 50% ultimate are greater than 5,000 psi, are lower than they would be at a stress level equal to 50% of their ultimate strength. Therefore, these rocks plot further to the left of the regression line than they "should."

It is apparent from Figure 5.19 and the discussion in paragraph 4.c. that the errors, resulting from the above sources, in the procedure used herein for comparing data at the higher stress levels (5,000 psi), are probably less than 5%. This seems reasonable because the percentage increase in  $V_p$ , for the majority of the rocks, is less than 10% for the entire stress change from 100 to 5,000 psi.

## 7. COMPARISON OF STATIC AND DYNAMIC PROPERTIES

Application of the theory of elasticity to problems relating the propagation of elastic waves through rock with the static deformation characteristics is a subject of long and continued discussion. Elastic theory has been used for derivation of the following well-known equations:

$$E = \rho V_p^2 \frac{(1+\nu)(1-2\nu)}{(1-\nu)} \quad (5.7)$$

$$= 2\rho V_s^2 (1+\nu) \quad (5.8)$$

$$G = \rho V_s^2 \quad (5.9)$$

$$\nu = \frac{1/2 \left( \frac{V_p}{V_s} \right)^2 - 1}{\left( \frac{V_p}{V_s} \right)^2 - 1} \quad (5.10)$$

in which  $E$  = Young's modulus of elasticity of the material  
 $V_p$  = dilatational wave velocity for an unbounded medium  
 $V_s$  = distortional or shear wave velocity  
 $\nu$  = Poisson's ratio  
 $\rho$  = mass density  $\left( \frac{\gamma}{g} \right)$   
 $G$  = modulus of rigidity

Hence,  $E$  may be calculated from the above equations by measuring both  $V_p$  and  $V_s$  during dynamic sonic-velocity tests.  $E$  may also be computed from static stress-strain tests by use of the procedures described in paragraph 4.a. Unfortunately these two methods do not always yield the same results.

During static load application to a rock specimen, the micro-cracks and crevices become compacted. Even though the amount of compaction is very small,  $E_d$ , determined from wave velocity measurements, increases as the compressive load is increased.  $E_t$ , determined statically as the ratio of incremental stress to incremental strain at various mean stress levels, also increases with the compressive load. Both  $E_d$  and  $E_t$  will approach a constant value for the particular rock specimen (for reasons previously discussed); and this value should be the same, regardless of whether or not it is determined statically or dynamically, provided the rock is truly elastic (Onodera, 1963).

Statically obtained values of  $E$  for rock are almost always lower than dynamically obtained values. According to Rinehart et al. (1961), these differences may vary from 0 to 300%. Zisman (1933) and Ide (1936) found with few exceptions that the dynamically determined values of the modulus are from 4 to 20% higher than those statically obtained. They conclude that the cause of these differences is the liability of static measurements to uncertainties from (i) the presence in the rock of minute cracks and cavities, and (ii) the rock's nonlinear elastic response to static stress. The more compact the rock, the more nearly do the static and dynamic constants agree. The two methods give the most divergent results for rocks possessing low moduli of elasticity.

Dvorak (1957) found for a medium under pressure that the differences between dynamic and static modulus do not exceed 50% because the fractures are closed by pressure. Data given by the U. S. Bureau of Reclamation (1953) show that the ratio of dynamically to statically measured Young's modulus varies between 0.85 to 2.9. Sutherland (1963) reports the percentage difference between the sonically and statically determined values of  $E$  to vary from 4 to 25%, with the sonic value greater than the static in all but two cases. He states that the large percentage difference obtained by some investigators may be due to the use of total stress/total strain (secant modulus) to calculate  $E$ , instead of incremental stress/incremental strain (tangent modulus). Thus, the effect of the initial high strain is present throughout the test, resulting in low values of  $E$ .

Gregory (1963) and Walsh (1965) explain in a qualitative way the lack of agreement between static and dynamic values of Young's modulus, even though measurements are made at the same level of applied stress. The passage of a sound wave corresponds to the superposition of a small alternating stress on the existing, applied compressive stress, as shown schematically in Figure 5.20. The static value of E is taken as the slope of the stress-strain curve at the selected stress-level, P. On the other hand, the dynamic modulus calculated from the sonic velocity corresponds to the average slope of the unloading and rebound loop created by the superimposed sound wave. As shown, the static value would be expected to be somewhat lower than the dynamic value, which is comparable to line b in Figure 5.1.

Ide (1936) concludes that the discrepancies found between static and dynamic values of E are real, and that most rocks are, therefore, imperfectly elastic media. They are not sufficiently homogeneous and isotropic to meet exactly the conditions for which the formulas from elastic theory were derived.

In order to compute dynamic values of Young's modulus, E, from equation (5.7), it is necessary to determine  $\nu$ , as given by equation (5.10). Dynamic values of Poisson's ratio,  $\nu$ , require measurement of the shear wave velocity. In the present investigation, a technique for producing and measuring shear wave velocities under axial load conditions was not satisfactorily developed. Some of the problems encountered in measuring S-waves are discussed by Gregory (1963).

A comparison of static and dynamic properties, however, may be conducted on the basis of the "constrained" modulus of deformation, which is defined as the rate of change of vertical stress with respect to vertical strain, under conditions of zero lateral strain ( $\epsilon_x = \epsilon_y = 0$ ). The constrained modulus,  $M_c$ , requires only the measurement of the dilatational wave velocity,  $V_p$ , and the mass-density,  $\rho$ , given in equation (4.3), and restated here as follows:

$$M_c = \rho V_p^2 \quad \text{Dynamic} \quad (4.3)$$

This modulus is related to Young's modulus and other elastic properties by the following equations:

$$M_c = E \left[ \frac{1-\nu}{(1+\nu)(1-2\nu)} \right] \quad \text{Static} \quad (5.11)$$

$$= K + 4/3 G \quad (5.12)$$

in which K = bulk modulus of elasticity.

The theoretical relationship for the ratio  $M_c/E$  for all values of Poisson's ratio is given by the curve in Figure 5.21. The average values for Poisson's ratio, as determined by the tangent method, for all rocks in this investigation are also given thereon. For the first and third loading cycles, the average  $\nu = .125$ . At a stress level equal to 50% ultimate, the average  $\nu = .341$ .

In Figures 5.22 and 5.23, data are plotted relating the constrained modulus, computed from velocity measurements by equation (4.3), and Young's modulus from static stress-strain measurements. These are given for the stress

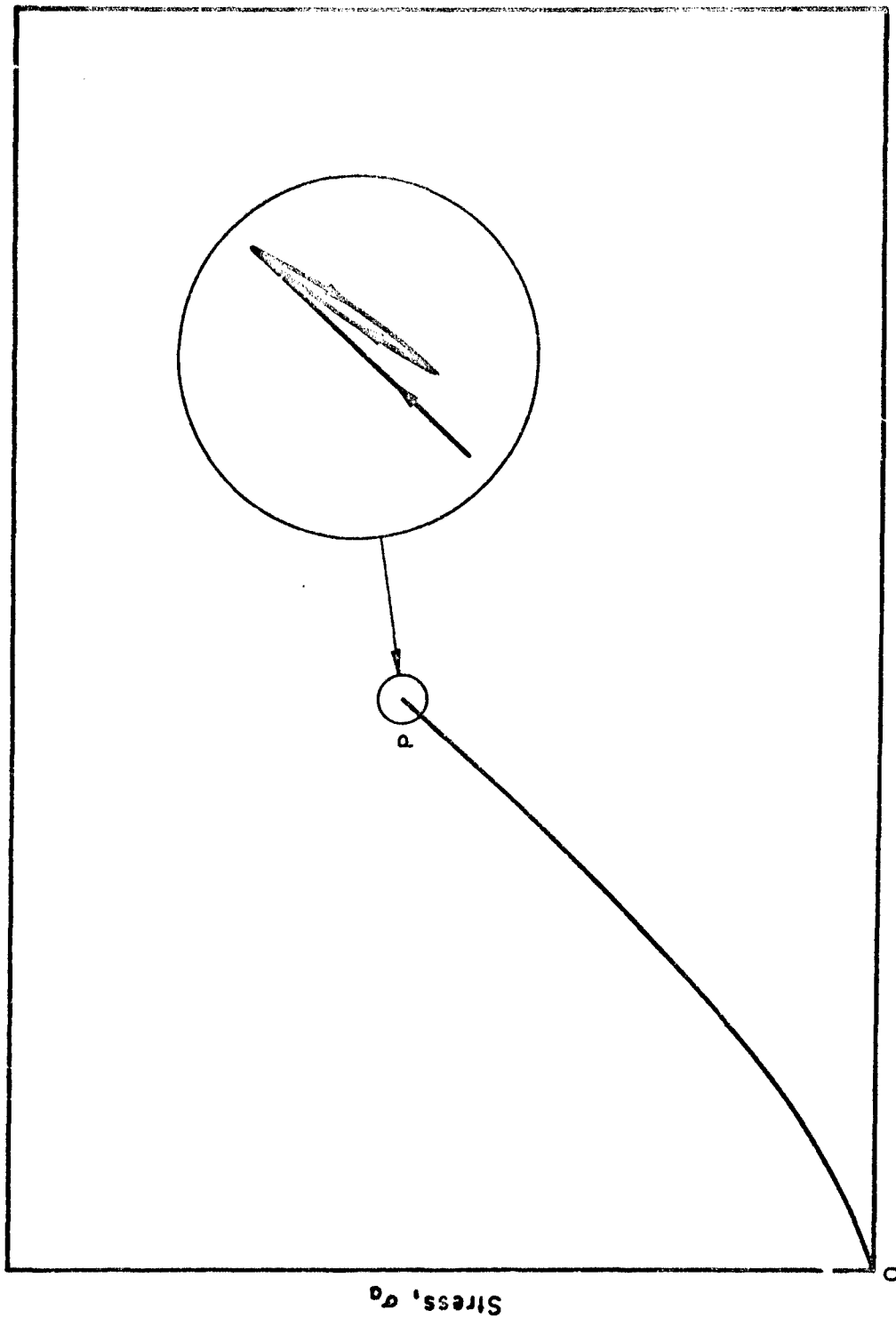


FIGURE 5.20 SONIC STRESS WAVE SUPERIMPOSED UPON A STATICALLY APPLIED STRESS (After Walsh, 1965)

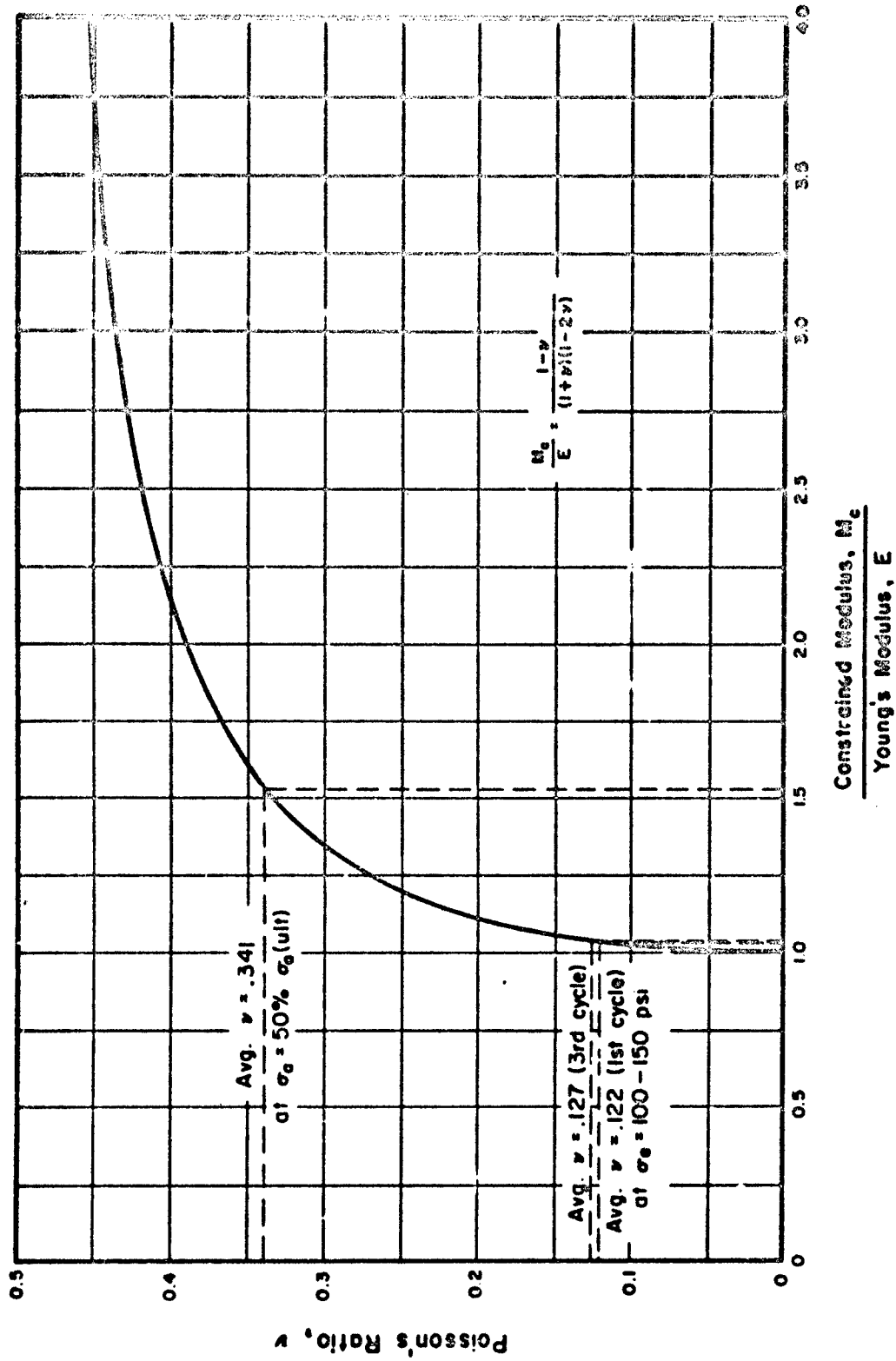


FIGURE 5.21 THEORETICAL CURVE RELATING CONSTRAINED MODULUS OF DEFORMATION AND YOUNG'S MODULUS OF ELASTICITY FOR DIFFERENT VALUES OF POISSON'S RATIO.

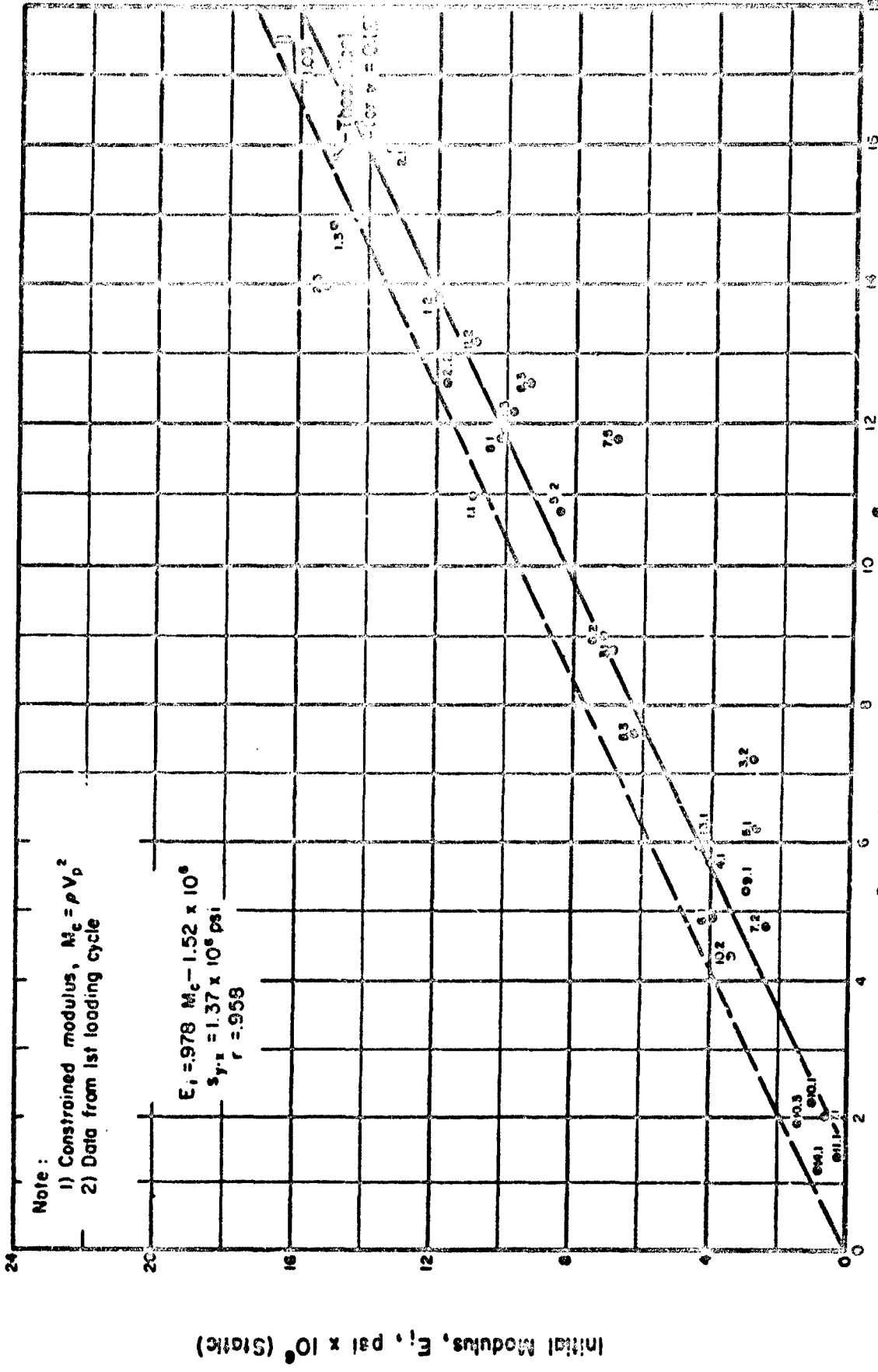


FIGURE 5.22 RELATIONSHIP BETWEEN AVERAGE VALUES OF INITIAL AND CONSTRAINED MODULI OF DEFORMATION FOR ROCK UNDER UNIAXIAL COMPRESSIVE STRESS OF 100-150 PSI



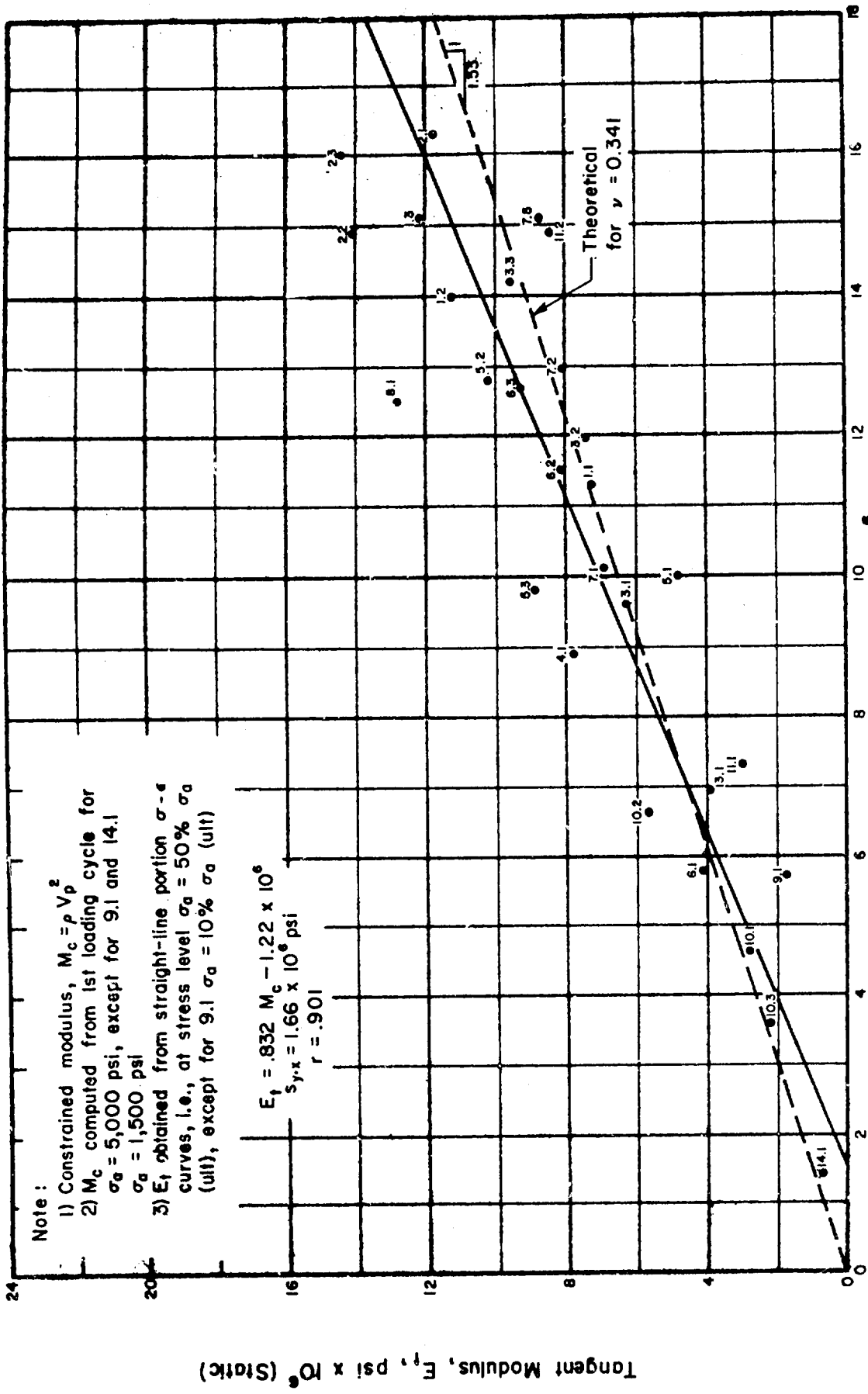


FIGURE 5.23 RELATIONSHIP BETWEEN AVERAGE VALUES OF TANGENT MODULUS AT STRESS LEVEL OF ONE-HALF ULTIMATE STRENGTH AND CONSTRAINED MODULUS OF DEFORMATION FOR ROCK UNDER UNIAXIAL COMPRESSIVE STRESS OF 5,000 PSI

ranges of 100-150 psi and 5,000 psi, respectively. The theoretical relationship between  $M_c$  and  $E$  for the average Poisson's ratio,  $\nu$ , obtained at each stress level, is shown by the dashed line in each figure. These are taken from the theoretical curve in Figure 5.21. It is interesting to note that the two regression lines, defined in Figures 5.22 and 5.23, converge at an  $M_c$ -intercept of approximately  $1.6 \times 10^6$  psi. Since  $M_c$  is a function of  $V_p$ , it would appear that the propagation velocity of P-waves in rock tend to approach a lower, limiting value, regardless of the stress level (within the range investigated herein). This is probably a function of the structure of rock, the degree of cementation, grain contact, et cetera. The lowest limiting value approximately equal to 1,130 fps should occur if there were no grain contact or cementation; this is the velocity of sound in air at 1 atmosphere. Logically, such rocks would have no coherence. The lower limiting velocity from these two figures is approximately 6,570 fps, computed for the average density of 162.3 pcf for all rocks in this investigation.

By plotting the dynamic measurements for  $M_c$ , computed from equation (4.3) as abscissas, and the static measurements for  $M_c$ , from equation (5.11) as ordinates, a more "normalized" comparison between static and dynamic properties is obtained. These data are given in Figures 5.24 and 5.25. Static data computed for initial values,  $E_i$  and,  $\nu$ , at stress levels of 100-150 psi are shown in Figure 5.24. Dynamic values of  $M_c$  also are shown for the same stress levels. The correlation coefficient,  $r = .949$ , suggests this relation to be quite good. It is noted that the ratio of dynamic and static values of  $M_c$ , as defined by the regression line, decreases with increasing modulus values (this was the same observation made by Ide). The more compact rocks approach a ratio of 1:1, whereas the lower modulus rocks diverge to a dynamic/static ratio of 2:1 for  $M_c$  (dynamic) =  $3 \times 10^6$  psi.

Onodera (1963, Fig. 3) presents data relating static,  $E$ , and dynamic,  $E_d$ , for rock pieces under no-load conditions. A line drawn through the center of gravity of his data points, parallel to his Line A, is defined approximately as follows:

$$E \cong 1.0 E_d - 1.422 \times 10^6 \text{ psi} \quad (5.13)$$

This equation is remarkably similar to the regression equation given in Figure 5.24 as follows:

$$M_c \text{ (static)} = 1.11 M_c \text{ (dynamic)} - 1.92 \times 10^6 \text{ psi} \quad (5.14)$$

In Figure 5.25 the dynamic  $M_c$  was computed at the maximum stress level of 5,000 psi for all rocks except 9.1 and 14.1, which were at 1,500 psi. However, since this stress level was approaching failure for rocks with strengths less than 10,000 psi, the static  $M_c$  was computed from  $E_t$  and  $\nu$  values at stresses equal to 50% ultimate strengths for these rocks. For all others,  $E_t$  and  $\nu$  were computed at 5,000 psi. This manipulation is probably a partial explanation of the lower correlation coefficient than that shown in Figure 5.24. In Figure 5.25, the ratio between dynamic and static values is more constant for all rocks. This varies from 1.5:1, for  $M_c$  (dynamic) =  $3 \times 10^6$  psi, to about 1.2:1, for  $M_c$  (dynamic) =  $16 \times 10^6$  psi.

For a dry rock, saturated with air, the dilatational wave velocity may be calculated from the static elastic constants by means of equation (5.4).

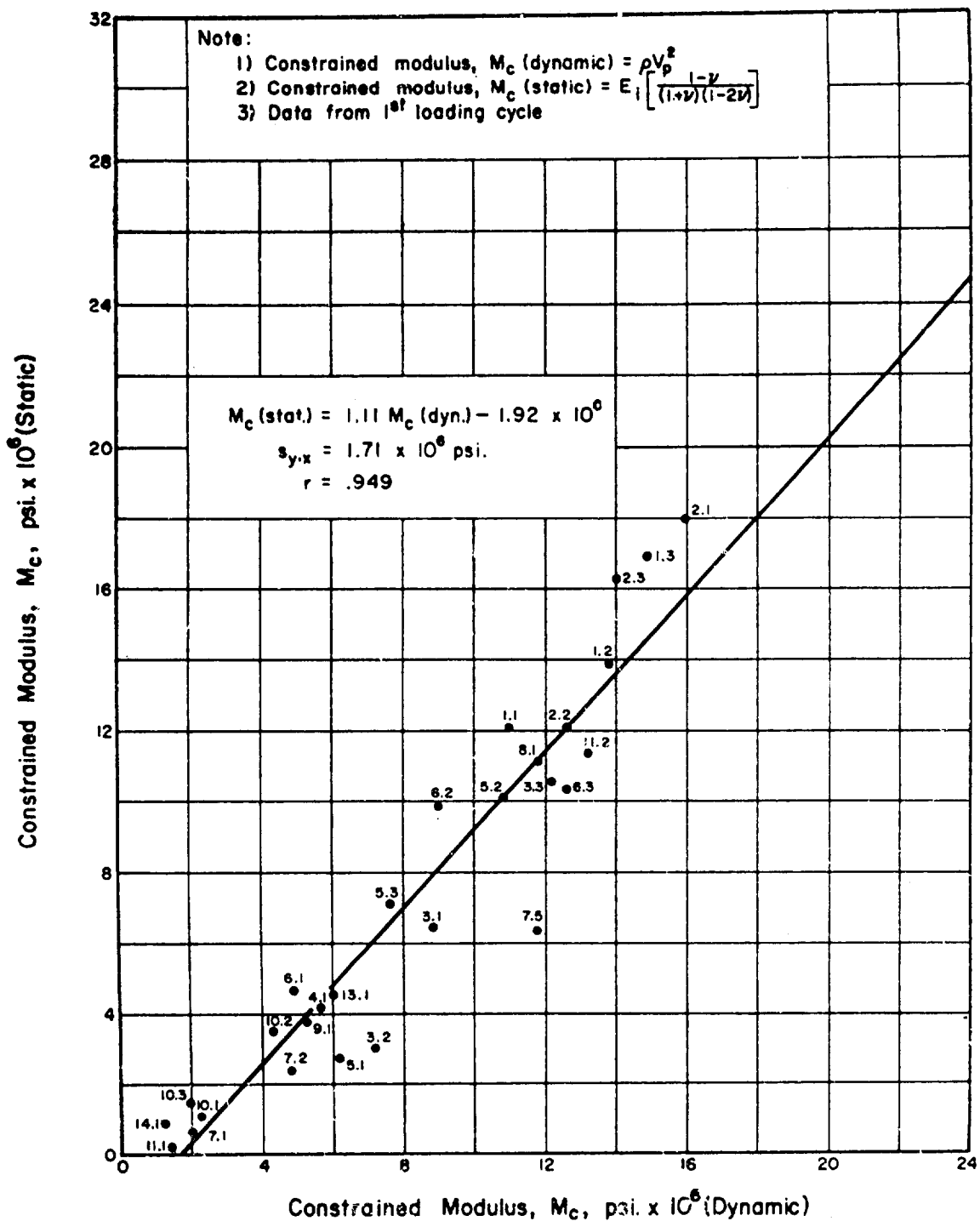


FIGURE 5.24 RELATIONSHIP BETWEEN AVERAGE VALUES OF CONSTRAINED MODULI OF DEFORMATION COMPUTED FROM STATIC AND DYNAMIC MEASUREMENTS FOR ROCK UNDER UNIAXIAL COMPRESSIVE STRESS OF 100-150 psi.

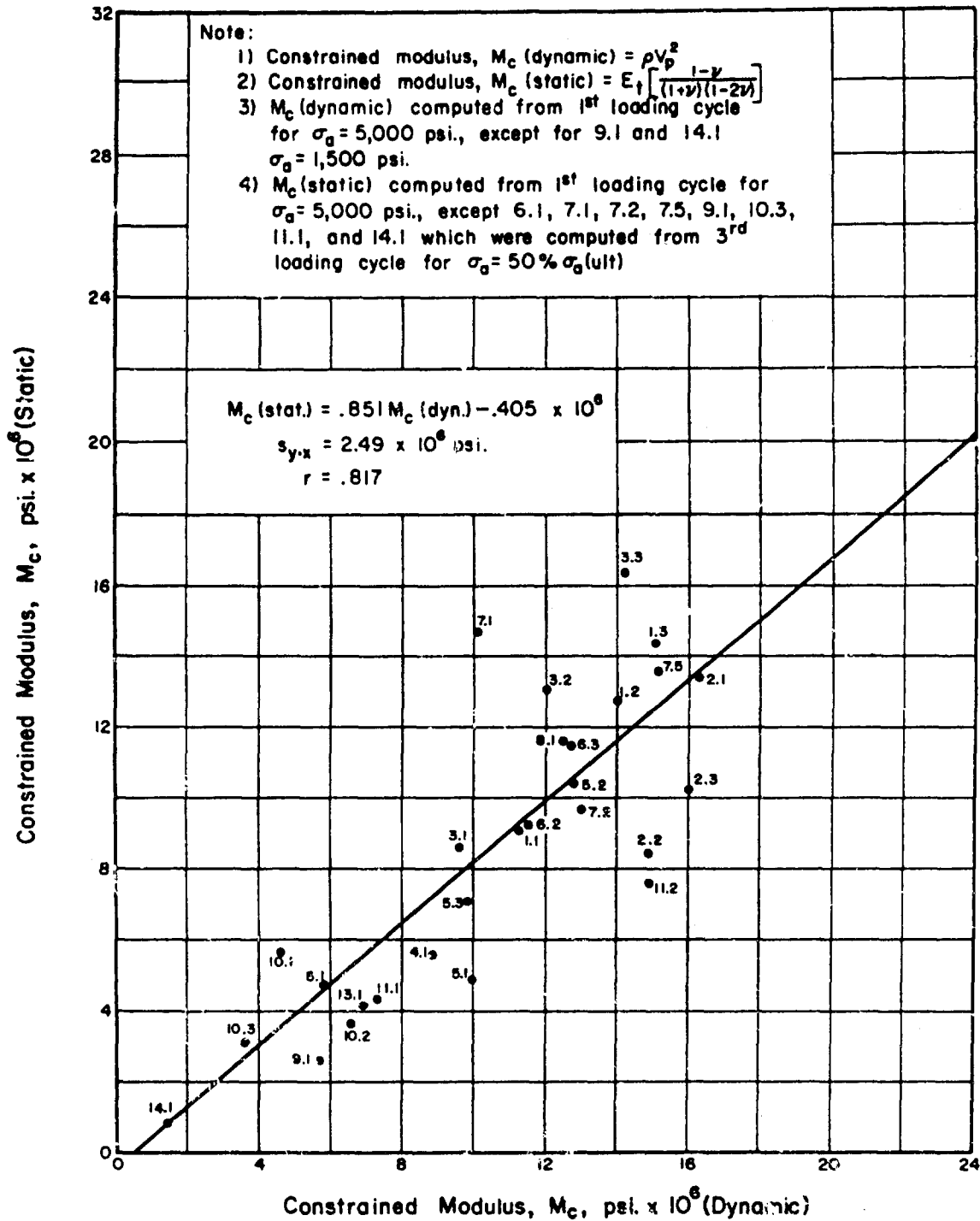


FIGURE 5.25 RELATIONSHIP BETWEEN AVERAGE VALUES OF CONSTRAINED MODULI OF DEFORMATION COMPUTED FROM STATIC AND DYNAMIC MEASUREMENTS FOR ROCK UNDER UNIAXIAL COMPRESSIVE STRESS UP TO 5,000 psi.

Wyllie et al. (1958) computed the velocity for Berea sandstone from the values of E and  $\nu$  obtained statically at different stress levels; these were compared to the measured values of  $V_p$  at the same stress levels. Similarly, the average velocities computed by equation (5.4), for all rocks in the present investigation, are plotted as ordinates in Figures 5.26 and 5.27. The measured velocities are plotted as abscissas for comparison.

A high degree of correlation ( $r = .96$ ) for the "static" and dynamic velocities, obtained by these two methods, is shown in Figure 5.26 at the lower stress level of 100-150 psi. Note that a high degree of correlation ( $r$  approaching 1.0) does not mean that there is a 1:1 relation between static and dynamic values. It means that the data plotted in this figure are well-defined by the least-squares regression line shown thereon. Again it is seen that the more compact rocks approach a dynamic/static ratio of 1:1 whereas the less compact (hence lower velocity) rocks approach a ratio of 2:1.

The degree of correlation in Figure 5.27 is somewhat lower, probably for the same reasons as given for Figures 5.18 and 5.25. For the high levels of stress, in Figure 5.27, the dynamic/static ratio for all rocks is more constant than for low stress levels as previously noted. This ratio varies from 1.3:1 for the lower velocity rocks (8,000 fps) to approximately 1.1:1 for the higher velocity rocks (20,000 fps).

Wyllie (noted above) plotted the data for both measured and computed values of  $V_p$  versus stress level up to 5,000 psi. He found that the dynamic/static ratio for the Berea sandstone, at 2,000 psi, is approximately 1.3:1. At 5,000 psi, the ratio was about 0.9:1. Both of these values are in close agreement with the Berea sandstone (10.1) in the present study.

A summary of the observations made in Figures 5.24 through 5.27 is given in the following table:

TABLE 5.3  
PERCENT BY WHICH DYNAMIC PROPERTIES ARE GREATER THAN  
STATIC PROPERTIES FOR ROCKS

	$\frac{\text{Dynamic-Static}}{\text{Static}} \times 100\%$	
	Less compact	More compact
Low stress (100 psi)	100%	0-3%
High stress (5,000 psi)	30-50%	10-20%

On the basis of these data, the following conclusions are made:

- i) The magnitudes of dynamic and static properties of rocks are equal only for compact rocks at low stresses.
- ii) Since compact rocks in general have slightly convex (Type I or II) stress-strain curves, the initial modulus may be somewhat higher than the tangent modulus at 50% ultimate strength.



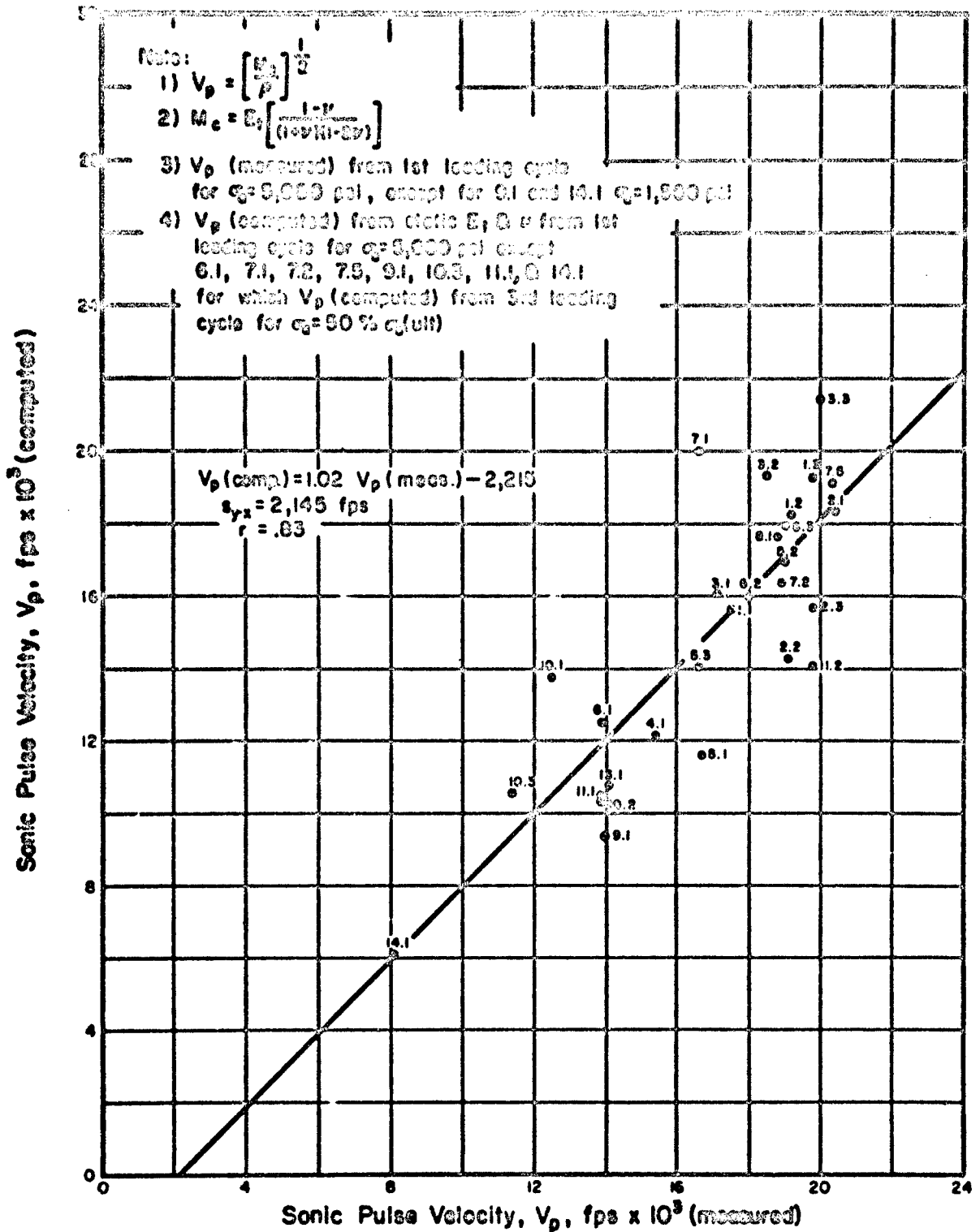


**FIGURE 5.27 RELATIONSHIP BETWEEN AVERAGE VALUES OF DILATATIONAL WAVE VELOCITY COMPUTED FROM STATIC AND DYNAMIC MEASUREMENTS FOR ROCK UNDER UNIAxIAL COMPRESSIVE STRESS UP TO 5,000 psi**

Therefore, at high stress levels, the magnitudes of the dynamic properties are greater than those of the static properties by 10-20%.

- iii) The difference between the values of dynamic and static properties of less compact rocks decreases with increasing stress.
- iv) Less compact rocks do not appear to meet the basic assumptions for which the theoretical equations relating velocity and Young's modulus were derived.

In this section the experimental data obtained in the current investigation have been presented in graphical form. Predominantly, data plots were given for those properties of rock which indicated a relatively high degree of correlation in simple regression analysis, and thus showed a reasonable potential for use in the development of index properties. In the section which follows, a system is presented for classifying rock in terms of its strength and deformation characteristics. Also, certain index properties are proposed which are formulated from the relationships developed herein.



## SECTION 6

### ENGINEERING CLASSIFICATION AND INDEX PROPERTIES FOR INTACT ROCK

#### 1. GENERAL

Classification of in-situ rock for engineering purposes takes into account both the physical properties of the intact blocks of rock within the rock mass, and the number and physical characteristics of the geological discontinuities which bound the blocks. The combined effect determines the engineering behavior of the rock mass in terms of strength, deformability, and permeability.

The present study is concerned only with the properties of the intact rock material as determined by tests of representative rock cores drilled from the joint blocks. It is advisable to develop a classification system based upon the physical properties of the intact rock before attempting to consider the adverse effects of geological discontinuities.

In this section a system for classifying intact rock is introduced which has as its basis the strength and deformation characteristics of the rock. Certain index properties are also proposed which are developed from the relationships given in Section Five and which can be used to estimate the uniaxial compressive strength and the modulus of deformation. The index properties may also be used for assigning a rock to the proper engineering classification. Statistical methods of analysis are utilized for determining least-square regression relationships between the suggested indices and corresponding strength or modulus properties, along with the confidence limits for dispersion.

#### 2. PROPOSED ENGINEERING CLASSIFICATION

In classifying rock for engineering purposes it is desirable to have a relatively simple system of classification with a small number of categories. The classification should be based on significant physical properties so that the system has wide application and is not limited to a specific problem. An optimum classification system should also provide good reproducibility, and the classification should not be a function of the background and experience of the person making the classification.

The system of engineering classification proposed herein provides qualitative descriptions in terms of two engineering characteristics, strength and deformation. The rocks may be classified by using the actual laboratory-determined values of the uniaxial compressive strength and modulus of elasticity, or by using the approximate values obtained from the index property correlations. A summary of the proposed classification is given in Table 6.1. For a complete description it is necessary to use both the strength class (A, B, C, D, or E) and the modulus ratio (H for High Modulus Ratio, L for Low Modulus Ratio, and no suffix for an Average Modulus Ratio, as described below). Thus, a rock may be classified as B, BH, BL, et cetera.

TABLE 6.1

## ENGINEERING CLASSIFICATION FOR INTACT ROCK

I. On Basis of Strength

<u>Class</u>	<u>Description</u>	<u>Uniaxial Compressive Strength,</u> <u>lb/in<sup>2</sup></u>
A	Very High Strength	Over 32,000
B	High Strength	16,000-32,000
C	Medium Strength	8,000-16,000
D	Low Strength	4,000-8,000
E	Very Low Strength	Less than 4,000

II. On Basis of Modulus Ratio

<u>Class</u>	<u>Description</u>	<u>Modulus Ratio</u> <sup>1</sup>
H	High Modulus Ratio	Over 500
-	Average Modulus Ratio	200-500
L	Low Modulus Ratio	Less than 200

Classify rock as B, BH, BL, etc.

$$1) \text{ Modulus Ratio} = E_t / \sigma_a (\text{ult.})$$

where  $E_t$  = tangent modulus at 50% ultimate strength;

$\sigma_a$  = uniaxial compressive strength

The strength classification is similar to the one given by Coates (1964), shown as Table 2.2 in this report, except that five categories of strength are proposed rather than three. The proposed Class E - Very Low Strength, for compressive strengths less than 4,000 psi, corresponds approximately to Coates' Weak Category (less than 5,000 psi). His Strong and Very Strong categories (with the dividing line at 25,000 psi) are replaced in the present system by four categories: Class D - Low Strength (4,000-8,000 psi); Class C - Medium Strength (8,000-16,000 psi); Class B - High Strength (16,000-32,000 psi); and Class A - Very High Strength (greater than 32,000 psi). It will be noted that the limiting values in the strength categories increase in geometric progression.

The division between the High Strength rocks and Very High Strength rocks at a compressive strength of 32,000 psi has been selected on the basis of three considerations. First, the relationships between the compressive

strength and the Shore hardness, (Figure 5.4), and the Schmidt hardness (Figure 5.5), show changes in slope in the vicinity of 32,000 psi. The data points above this value are "stacked" almost vertically. This relationship may be interpreted as indicating the rocks with compressive strengths in excess of about 32,000 psi have an intergranular coherence which cannot be measured by hardness tests, but which accounts for very high compressive strengths.

A second consideration concerns the shapes of the stress-strain curves; for almost all rocks with compressive strengths greater than 32,000 psi, the curves are essentially linear (Figure 5.2, Type I), and show brittle-failure characteristics as given in Coates' classification. A third and purely practical consideration is that the Very High Strength igneous rocks -- diabase and dense basalt -- are separated by the 32,000-psi line from other fine-grained igneous rocks such as dacite, rhyolite, and andesite, as well as from most rocks of the granite family. In addition, almost all foliated, metamorphic rocks (i.e., gneisses, schists, some phyllites, and slates), and the common sedimentary rocks fall below the 32,000-psi line.

It was originally believed that the classification on the basis of modulus could use various sub-divisions of the actual modulus values, e.g., less than  $1 \times 10^6$  psi,  $1-2 \times 10^6$  psi, et cetera. However, as the system was developed it became apparent that each strength category would have three or four modulus categories and that fifteen to twenty classifications would result. Of even greater concern was the fact that on the classification plot of modulus versus strength the categories plotted as rectangles with any given corner common to four rectangles and therefore to four classifications. This situation resulted in as many as four classifications for a suite of samples from a particular sample site even though the actual variations in strength and modulus values were quite minor.

In order to circumvent the above difficulty, the proposed classification system makes use of the modulus ratio which is defined as the modulus of elasticity (tangent modulus at 50% ultimate strength) divided by the uniaxial compressive strength. The relationship between average values of the compressive strength and tangent modulus of the rocks tested for this report is shown in Figure 5.12 as an arithmetic plot. The plot indicates that the data may be fitted approximately by a straight line, the equation of which is  $E_t = 300 \sigma_a(\text{ult.})$ . The slope of this line is the modulus ratio, whose value in this case is 300.

The proposed classification chart, entitled Engineering Classification for Intact Rock, is shown in Figure 6.1. Both the modulus and strength axes are logarithmic, in order to provide for a wide range of value. The strength categories A through E are indicated. Although the 300:1 modulus-ratio line is shown in this figure, the classification system makes use of a zone (shown by stippling) which extends on either side of this average line and which is bounded by lines representing modulus ratios of 200 and 500. These limiting values were chosen so as to encompass the majority of the rocks with interlocking texture, e.g., diabase, granite, basalt, quartzite, rock salt, and some limestones, dolomites, and sandstones. Rocks included within this zone are considered to have average modulus ratios, and their classification

Note:

- 1)  $E_t$  = tangent modulus at 50% ultimate strength
- 2) Classify rock as B, BH, BL, etc.

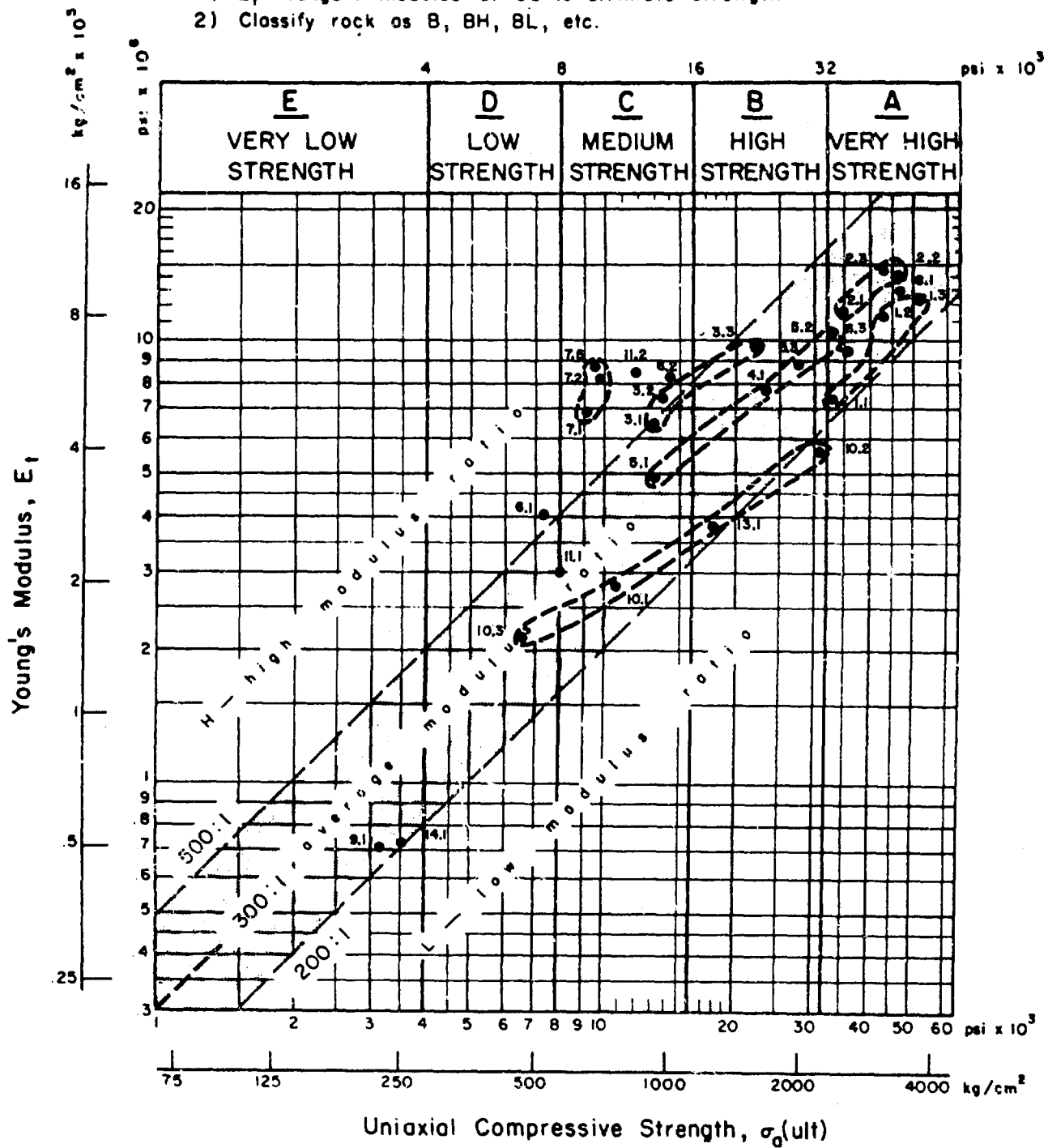


FIGURE 6.1 ENGINEERING CLASSIFICATION FOR INTACT ROCK— AVERAGE VALUES FOR 13 ROCK TYPES (28 Locations)

consists only of a strength category, i.e., A, B, C, et cetera, without reference to the modulus ratio. Rocks with modulus ratios greater than 500, as noted in the figure, are of high modulus ratio and their classification would consist of a strength category followed by the letter H as, for instance, BH. Similarly, rocks with modulus ratios less than 200 are designated low modulus ratio and their classification includes the letter L as, for instance, CL.

The plotted positions of the data points in Figure 6.1 give a strong indication that the classification system may be a very workable one, and one that will take into account both mineralogy and textural fabric. To illustrate these aspects broken lines have been placed around the data points representing given rock types in Figure 6.1. The lowermost envelope around points 10.1, 10.2, 10.3, and 13.1 encloses all the sandstones and siltstones (13.1) tested in the present study. Several trends are apparent. The envelope is unique in position with respect to the other rock types. Although the envelope follows the general trend of the stippled zone (average modulus ratio), it is closer to the 200:1 limiting line. The position indicates that the sandstones are more compressible with respect to their strength than most rock types. This is considered to be a result of the closing of small micro-cracks parallel to the bedding planes. The bedding was near horizontal in most of the specimens and the axial load was applied normal to the bedding direction.

The envelope around points 5.1, 5.2, 5.3, and 4.1 encloses all the granites and granite gneiss (4.1) tested in the present study. Again, a rather unique position is indicated. The granite textures are essentially equigranular and interlocking and the plotted positions are parallel to, and in the center of, the zone of average modulus ratio. Anisotropy of fabric is not indicated. The position of point 5.1 in the C-strength category is anomalous but these samples were of a slightly weathered granite.

The envelope for diabase (2.1, 2.2, and 2.3) is essentially an extension of the granite plot, but in a higher strength category. The basalt envelope (1.1, 1.2 and 1.3) is in the A strength category but it is located in the lower portion of the average modulus-ratio zone. The dolomite envelope (3.1, 3.2, and 3.3) plots parallel to and near the boundary between the zones of average modulus ratio and high modulus ratio. Two of the limestones (6.1 and 6.2) plot similarly but the third (6.3 - Solenhofen limestone) plots well away from the trend. The marbles (7.1, 7.2, and 7.5) plot in a restricted area in the zone of high modulus ratio. The majority of the carbonates, then, have a trend toward a high modulus ratio. This fact is felt to be a result of an interlocking texture and low porosity as well as the particular stress-strain characteristics of calcite and dolomite.

Attention is also called to the schist samples (11.1 and 11.2). Sample 11.1 was tested with the axial load applied normal to the schistosity; it plots in the zone of average modulus ratio. Sample 11.2 was tested with the axial load applied parallel to the schistosity; it plots in the zone of high modulus ratio. The effect of textural anisotropy is dealt with further in the discussion of Figure 6.3.

The data points in Figure 6.1 are the averages of given rock types from specific locations. Each point is the average of from 3 to 8 individual tests. In Figure 6.2 all test results are shown although the individual points are not identified. Thirteen rock types and 128 specimens are represented. The plotted points further emphasize the validity of the concept of a zone of average modulus ratio.

To investigate further the effect of anisotropy a series of tests were run on samples of a sandstone, which showed pronounced bedding, and on a slate. These samples, referred to as Indiana sandstone and Virginia slate were not part of the systematic study, and the only tests conducted on them were strength and modulus determinations. The test results are shown in Figure 6.3. The number beside each point represents the angle between the specimen axis (direction of loading) and the plane of anisotropy. The effect of the anisotropy created by the bedding planes is not great for the sandstone although both the strength and modulus are affected to some extent. The classification designation changes from C for the 90° loading to D for all other angles.

The anisotropy caused by the slaty cleavage has a very pronounced effect on the classification of the slate. The designation ranges from B to C, CH, and DH as the angle between the specimen axis and plane of anisotropy changes from 90° to 30°. At angles less than 30° both the strength and the modulus increase; designations of CH and BH result at angles of 15° and 0°, respectively. It is apparent that samples tested perpendicular to the direction of anisotropy, or within 45° or so of that orientation, show a lower modulus ratio than those obtained for samples in which the anisotropy is steeply inclined (small angle between the specimen axis and plane of anisotropy). The strength classification is also a function of the angle of anisotropy. Minimum strengths are found in the 30° range although random low strengths are often obtained whenever the anisotropic feature is steeper than about 45°.

A summary plot showing the classification of various igneous rocks is given in Figure 6.4. Three rock groups are shown: diabase, granite family, and basalt and other flow rocks. The granite family includes syenites, monzonites, granodiorites, quartz diorites, et cetera. The flow rocks included with basalt are dacite, andesite, and rhyolite. The envelopes shown are those that include 75% of the points for the rock type in question. A total of 176 test results were used in preparing the plot. These included the results of the present study as well as values obtained from private reports and from the literature.

The individual points for the diabase plot are shown in Figure 6.5, those for the granite in Figure 6.6, and those for the basalt and other flow rocks in Figure 6.7. The envelope enclosing 75% of the points is shown in each case. The envelopes have been drawn so as to omit about the same number of points on each side and yet maintain a parallel or sub-parallel alignment with the trend of the average modulus ratio zone, wherever this could be done without undue bias.

The tight grouping of the 26 specimens of diabase from 8 different locations (Figure 6.5) is quite striking. The samples have modulus values greater than  $10 \times 10^6$  psi and the majority have compressive strengths greater

Note:

- 1)  $E_t$  = tangent modulus at 50 % ultimate strength
- 2) Classify rock as B, BH, BL, etc.

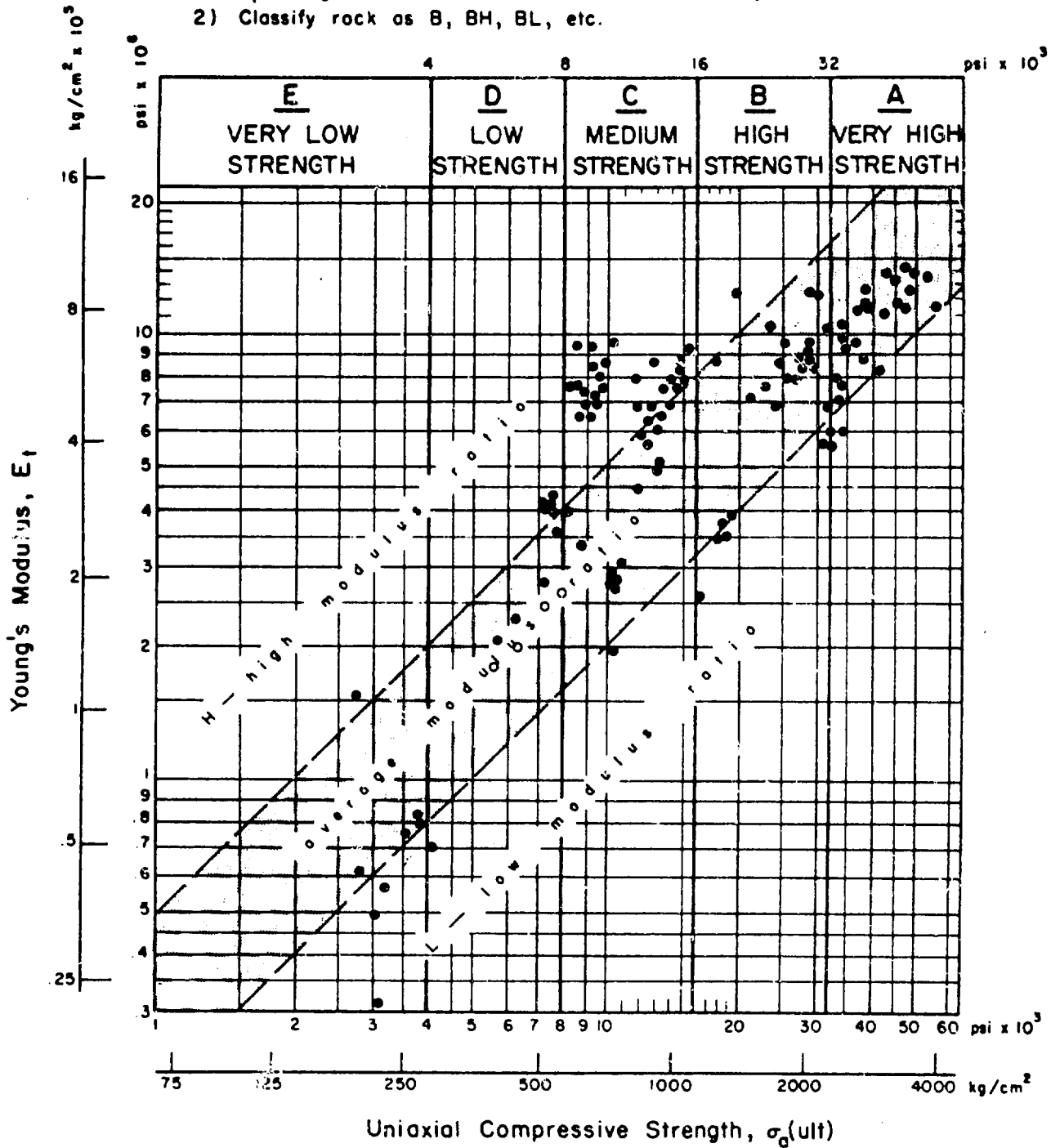


FIGURE 6.2 ENGINEERING CLASSIFICATION FOR INTACT ROCK—INDIVIDUAL TEST RESULTS (124 Specimens, 13 Rock Types)

2) Classify rock as D, CH, BL, etc.

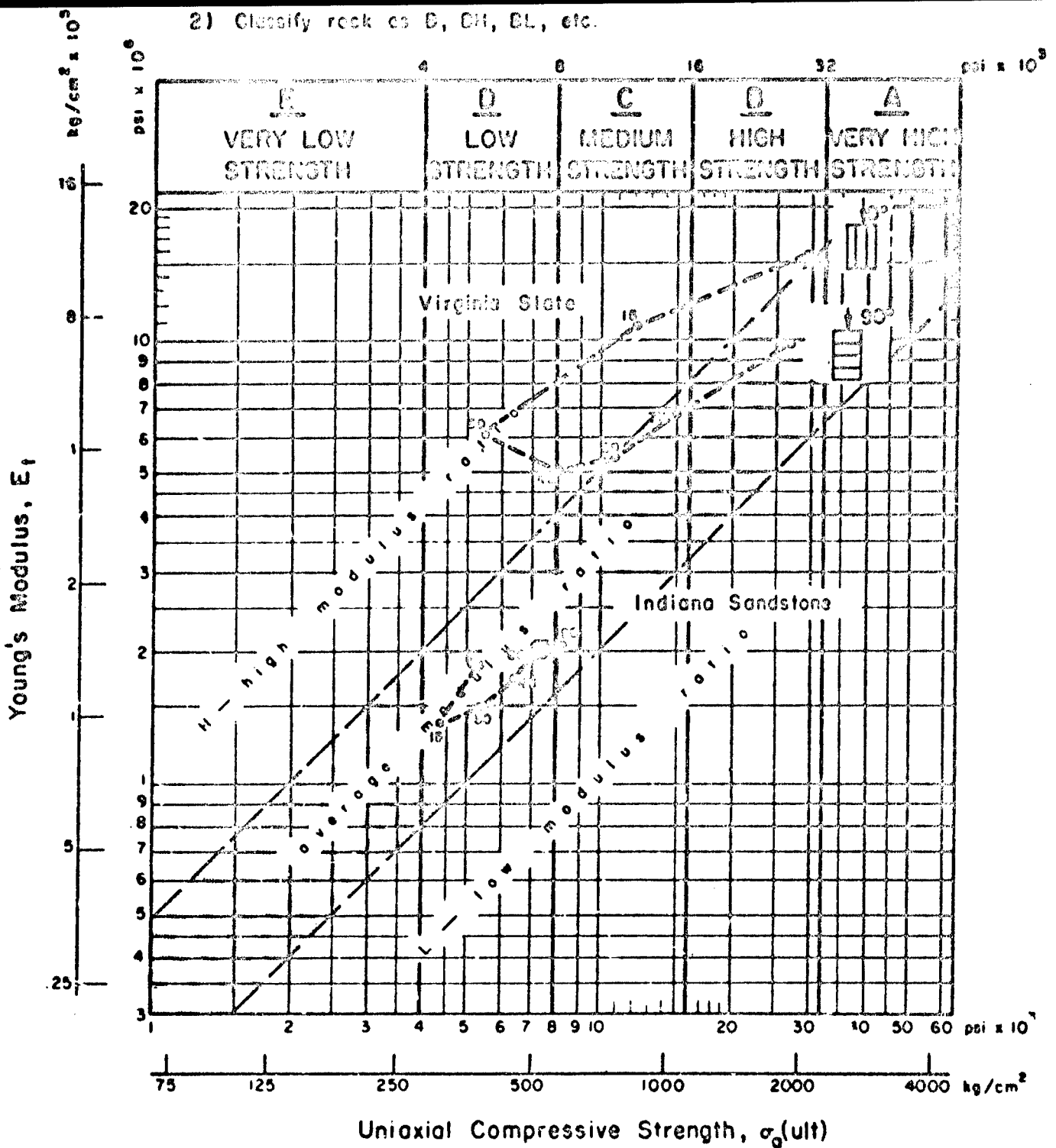


FIGURE 6.3 ENGINEERING CLASSIFICATION FOR INTACT ROCK—EFFECT OF ANGLE OF BEDDING AND FOLIATION



Note:

- 1)  $E_t$  = tangent modulus at 50% ultimate strength
- 2) Classify rock as D, DI, DL, etc.

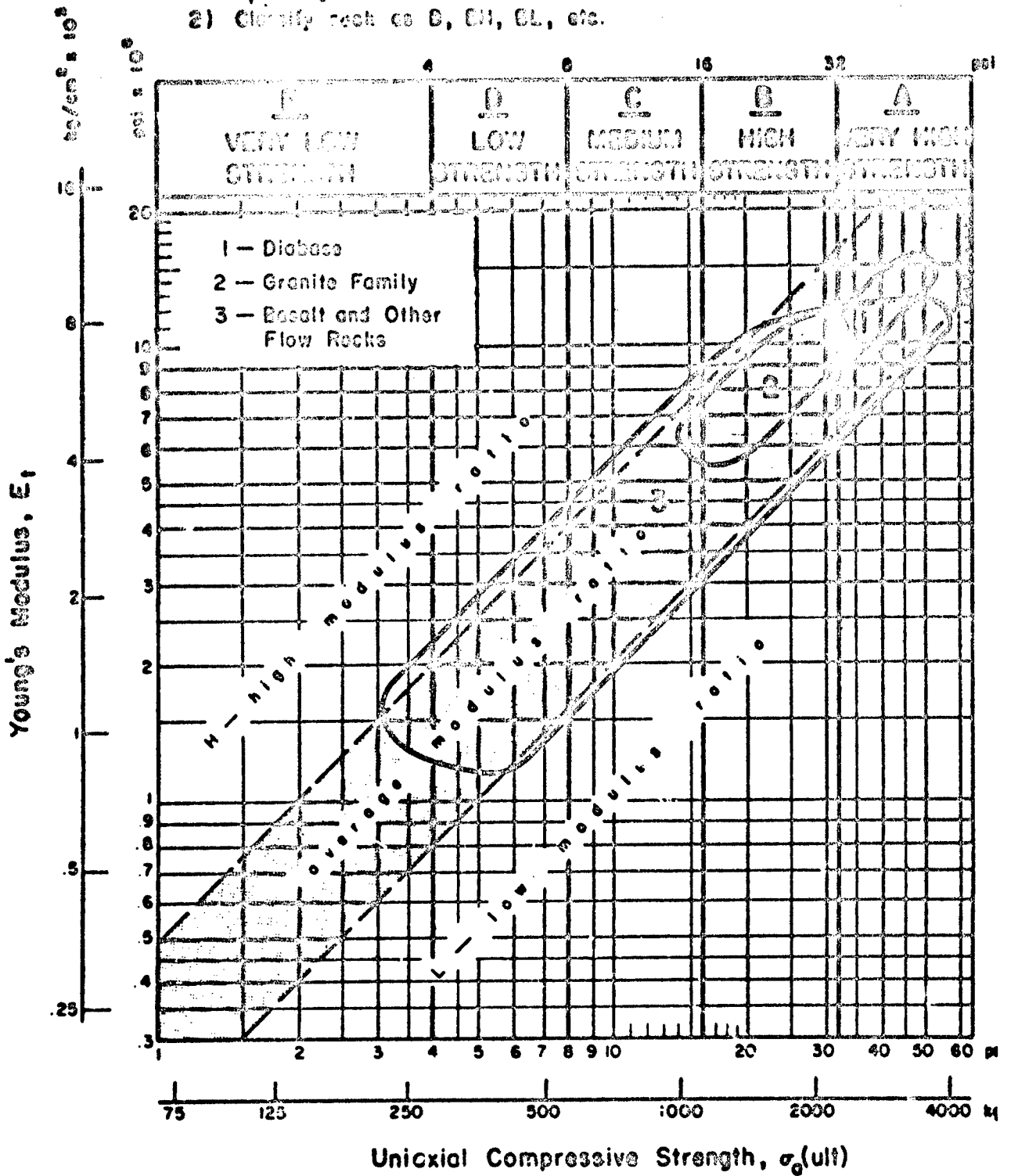


FIGURE 6.4 ENGINEERING CLASSIFICATION FOR INTACT ROCK SUMMARY PLOT IGNEOUS ROCKS (176 Specimens, 75% of Points)

Note:

- 1)  $E_t$  = tangent modulus at 50 % ultimate strength
- 2) Classify rock as D, CM, BL, etc.

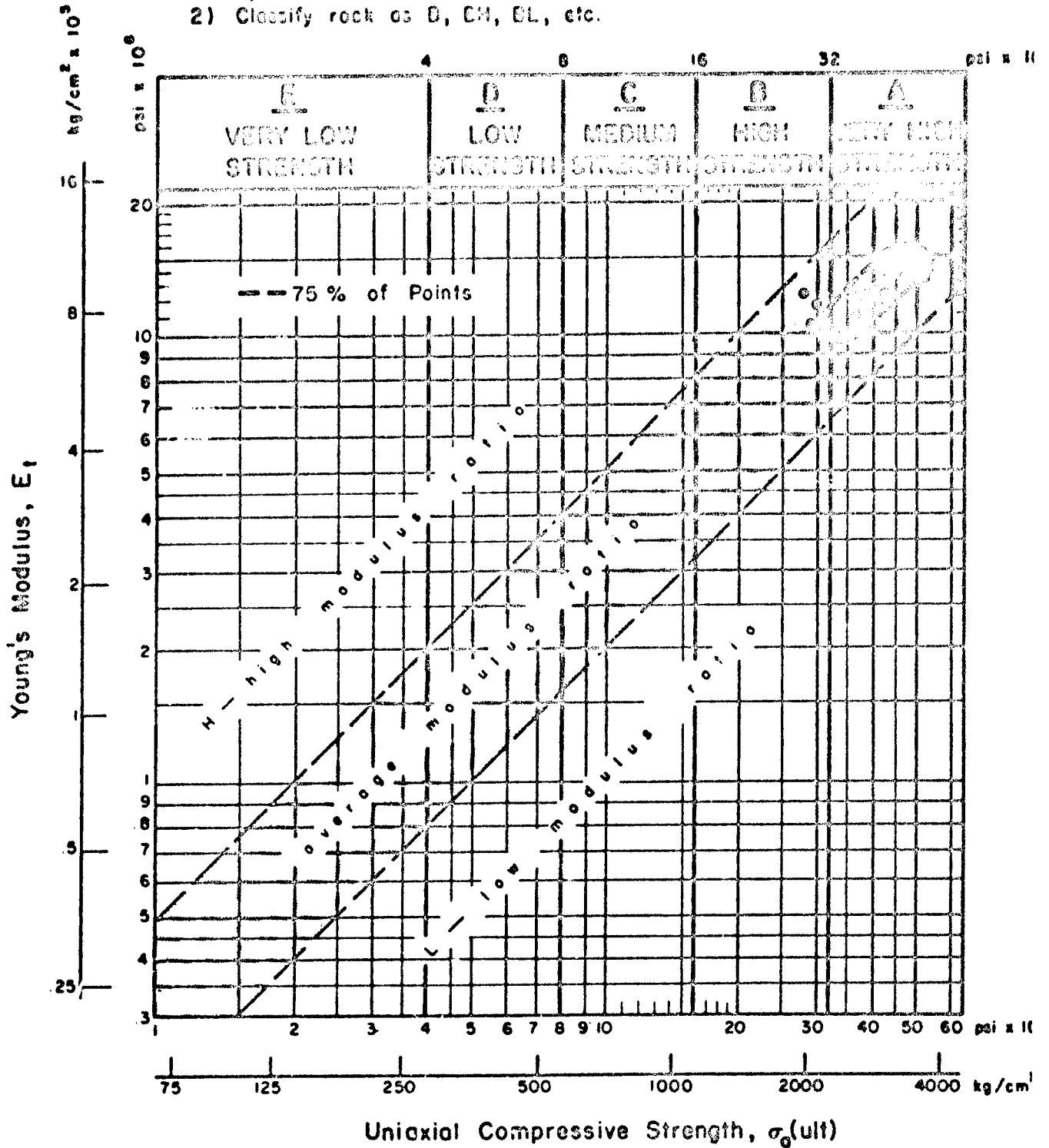
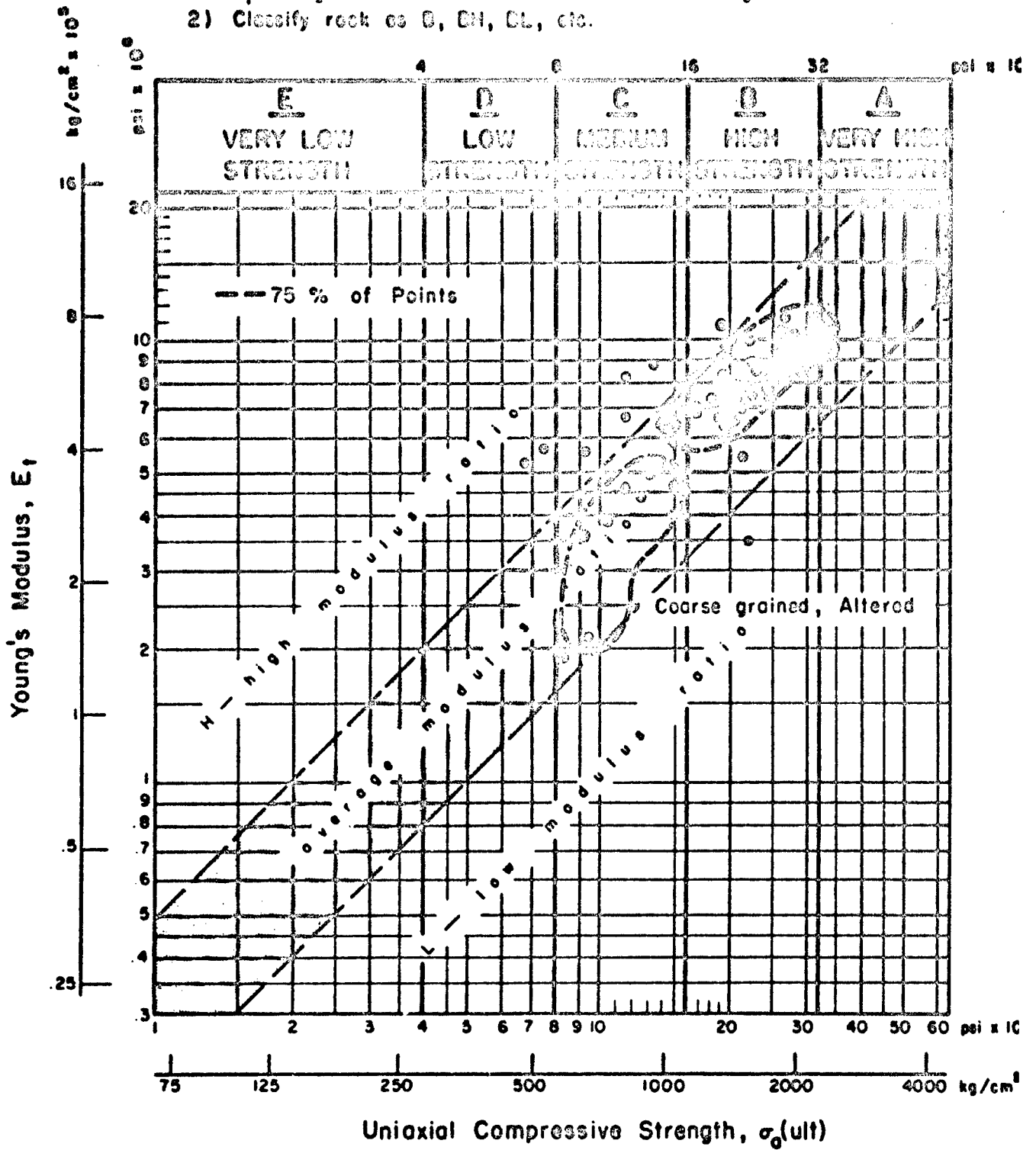


FIGURE 6.5 ENGINEERING CLASSIFICATION FOR INTACT ROCK—  
DIABASE (26 Specimens, 8 Locations, Various Sources)

Note:

- 1)  $E_t$  = tangent modulus at 50% ultimate strength
- 2) Classify rock as E, D, C, B, A, etc.



**FIGURE 6.6 ENGINEERING CLASSIFICATION FOR INTACT ROCK—GRANITE FAMILY (80 Specimens, 16 Locations, Various Sources)**

Note:

- 1)  $E_t$  = tangent modulus of 50 % ultimate strength
- 2) Classify rock as D, DL, DL, etc.

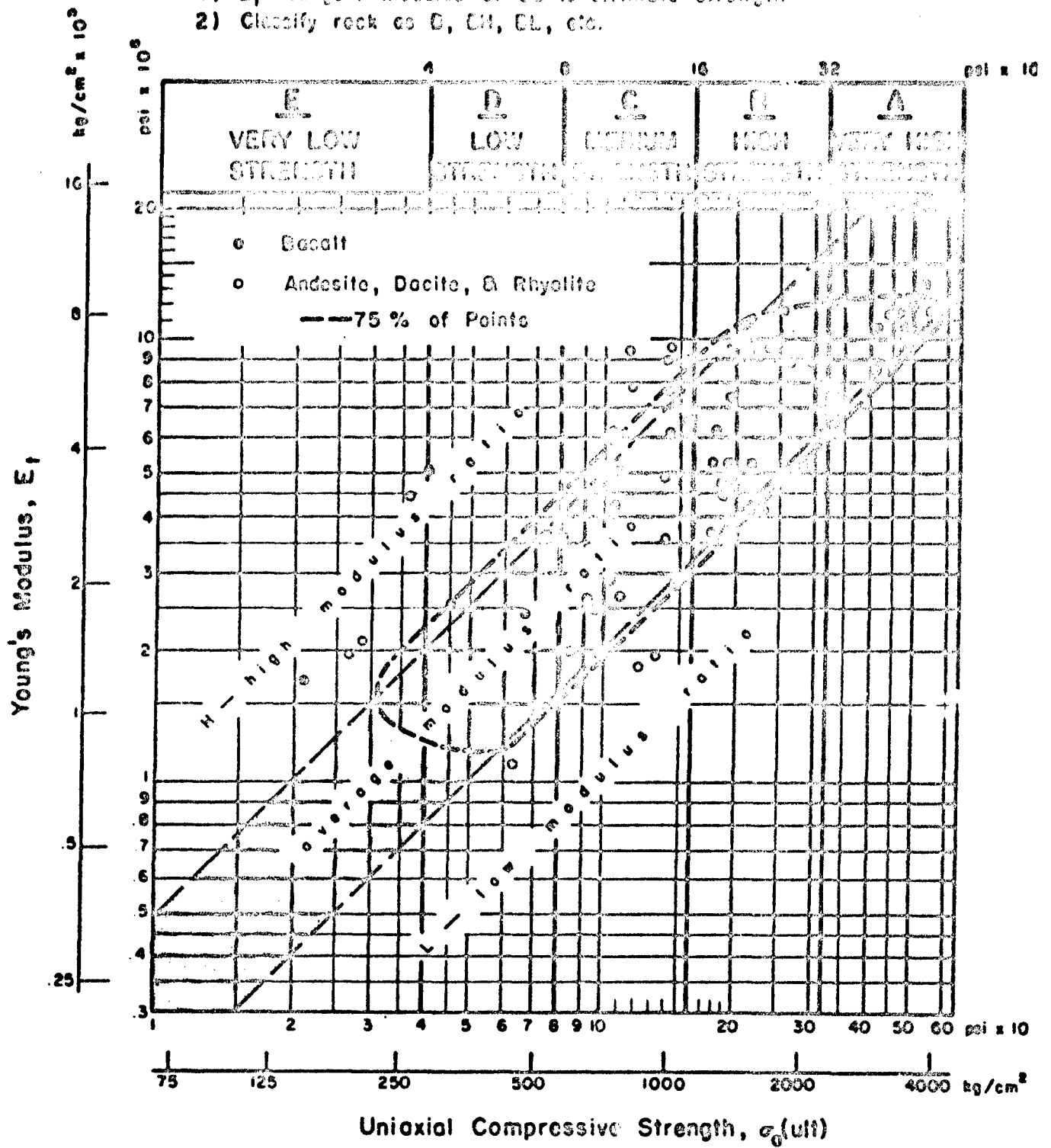


**FIGURE 6.7 ENGINEERING CLASSIFICATION FOR INTACT ROCK—  
BASALT AND OTHER FLOW ROCKS (70 Specimens;  
20 Locations, Various Sources)**

than 35,000 psi. Diabase plots as Very High Strength rock with an average modulus ratio -- or category A. The granite family rocks (Figure 6.6) plot chiefly as B-category rocks although several coarse-grained or altered specimens plot in the C grouping. The basalt and other flow rocks (Figure 6.7) show the greatest range in values as would be expected because of the wide range in mineralogy, texture, and homogeneity. The strength classification ranges from A - Very High Strength for the densest basalts to E - Very Low Strength for the weakest samples. The majority of the flow rocks, however, fall in the B and C strength categories. The 75% envelope coincides reasonably well with the zone of average modulus ratio.

The sedimentary rock summary plot is given in Figure 6.8. The rock types included are limestone and dolomite, sandstone, and shale. The envelopes for sandstone and shale are not closed at their lower ends because a great number of test results indicated strengths less than 1,000 psi and modulus values below  $0.3 \times 10^6$  psi and could not be shown on the present plot.

The positions of the envelopes of the sedimentary rocks are quite distinct from those for the igneous rocks. The limestone-dolomite envelope extends well into the zone of high modulus ratio. This position seems to be a response to both the texture (interlocking) and to the particular mineralogy (calcite and dolomite). The detailed plot of Figure 6.9 shows that the majority of the specimens fall in the B and C strength ranges as B, BH, C, or CH. A few points extend into the A and D (or E) categories.

The sandstone envelope (Figures 6.8 and 6.10) extends into the low modulus ratio range. This position is considered to be the result of a cemented, porous texture and the anisotropy created by the bedding. The modulus values are low because almost all the samples were tested with the core axis perpendicular to the bedding. This orientation gives low modulus values because of deformation caused by closure across bedding planes. As may be noted, most of the samples plot in the C and D strength ranges although points are present in all strength ranges.

The detailed plot for shales is shown in Figure 6.11. The shales that plot on this graph are referred to as hard shales to distinguish them from soft shales (clay-shales and poorly cemented silty or sandy shales) that plot well below the limits of the present diagram. The dividing line has been taken as the tangent modulus value (at 50% ultimate strength) of  $0.3 \times 10^6$  psi. The corresponding strength value is approximately 4,000 psi. Thus, hard shales may plot as B, C, or D strength rocks, usually with the suffix L to indicate their low modulus ratio, while the soft shales all plot as E - Very Low Strength rocks, and usually as EL because of the low modulus ratio. In the figure it may be desirable to show more of the Very Low Strength range and to further subdivide the E-rocks. Test data, which would plot to the lower left of the present classification, show that the soft shales extend into the soil groups (stiff glacial clayey till, loess, residual soils, et cetera). An interesting point to note is that the soils and soft shales both follow the trend of low modulus ratio, i.e., from 300 to values as low as 100 or so. There is evidence which indicates that some of the lower values may be the result of sample disturbance. However, the lower modulus ratio is considered in general to be a result of anisotropy caused by the orientation

Note:

- 1)  $E_t$  = tangent modulus at 50 % ultimate strength
- 2) Classify rock as E, D, C, B, A, etc.

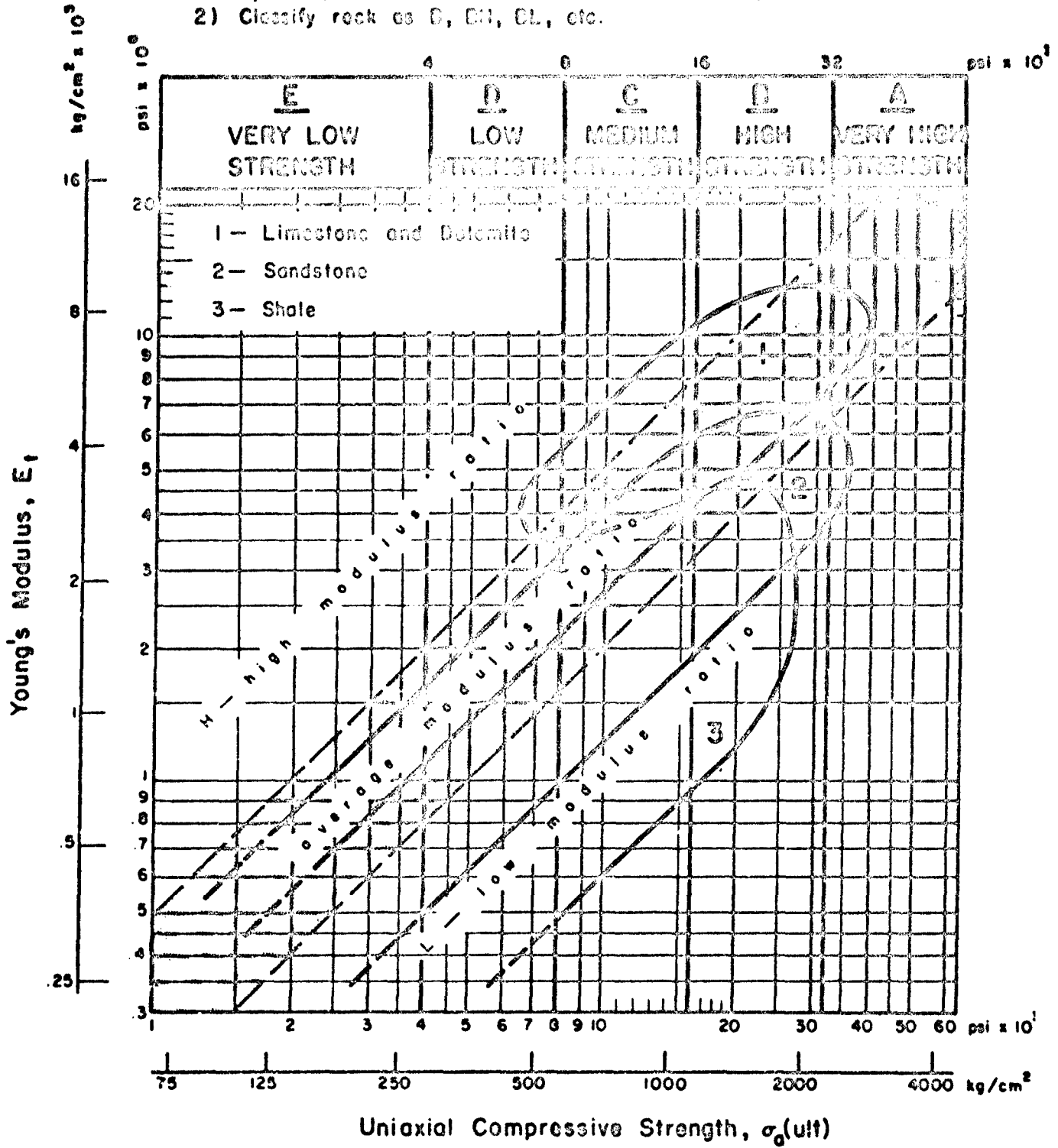
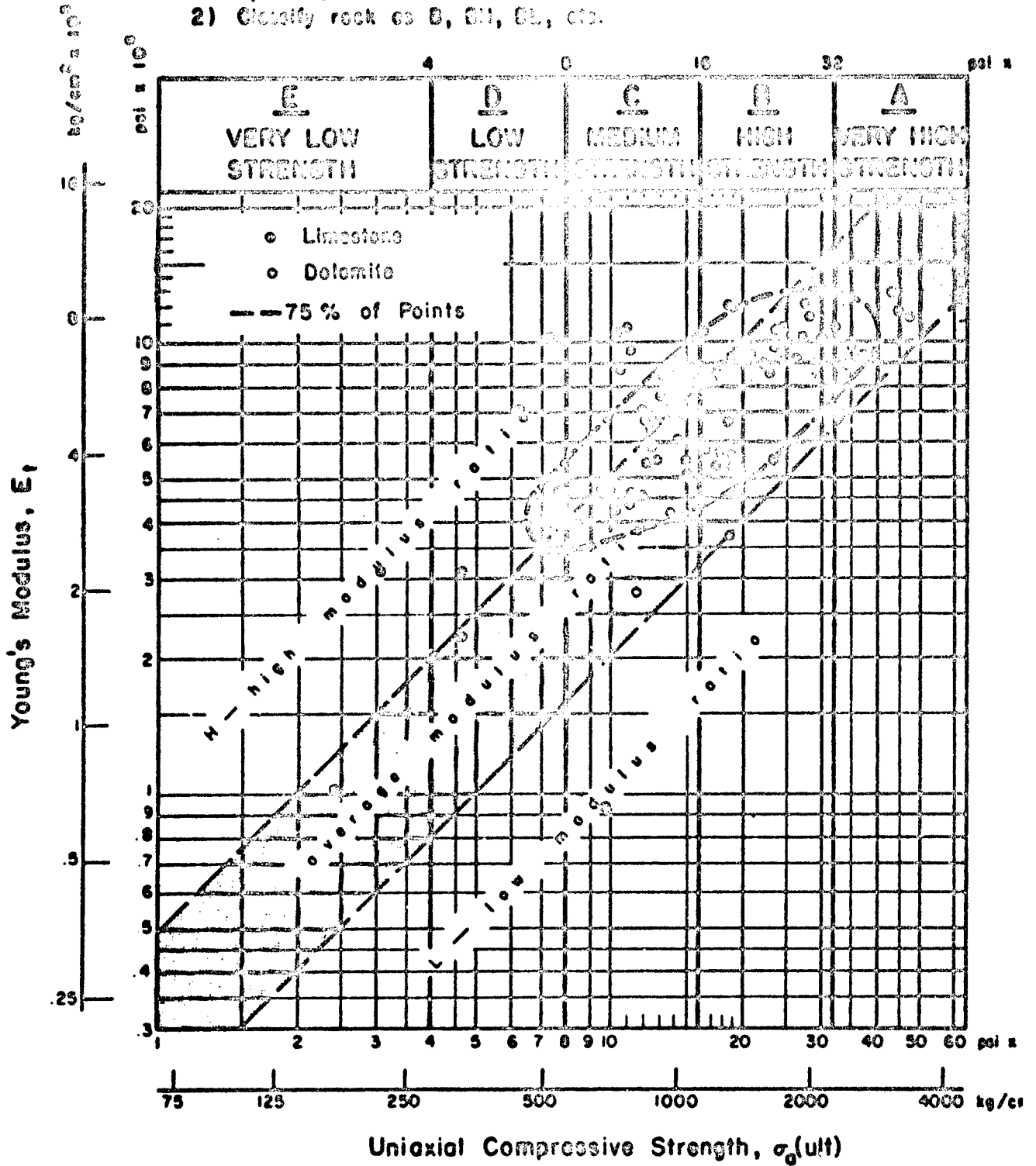


FIGURE 6.8 ENGINEERING CLASSIFICATION FOR INTACT ROCK — SUMMARY PLOT SEDIMENTARY ROCKS (193 Specimens, 75 % of Points)

Note:

- 1)  $E_t$  = tangent modulus at 60% ultimate strength
- 2) Classify rock as B, BH, BL, etc.



**FIGURE 6.9 ENGINEERING CLASSIFICATION FOR INTACT ROCK - LIMESTONE AND DOLOMITE (77 Specimens, 22 Locations, Various Sources)**

Note:

- 1)  $E_t$  = tangent modulus of 50 % ultimate strength
- 2) Classify rock as D, GII, GL, etc.

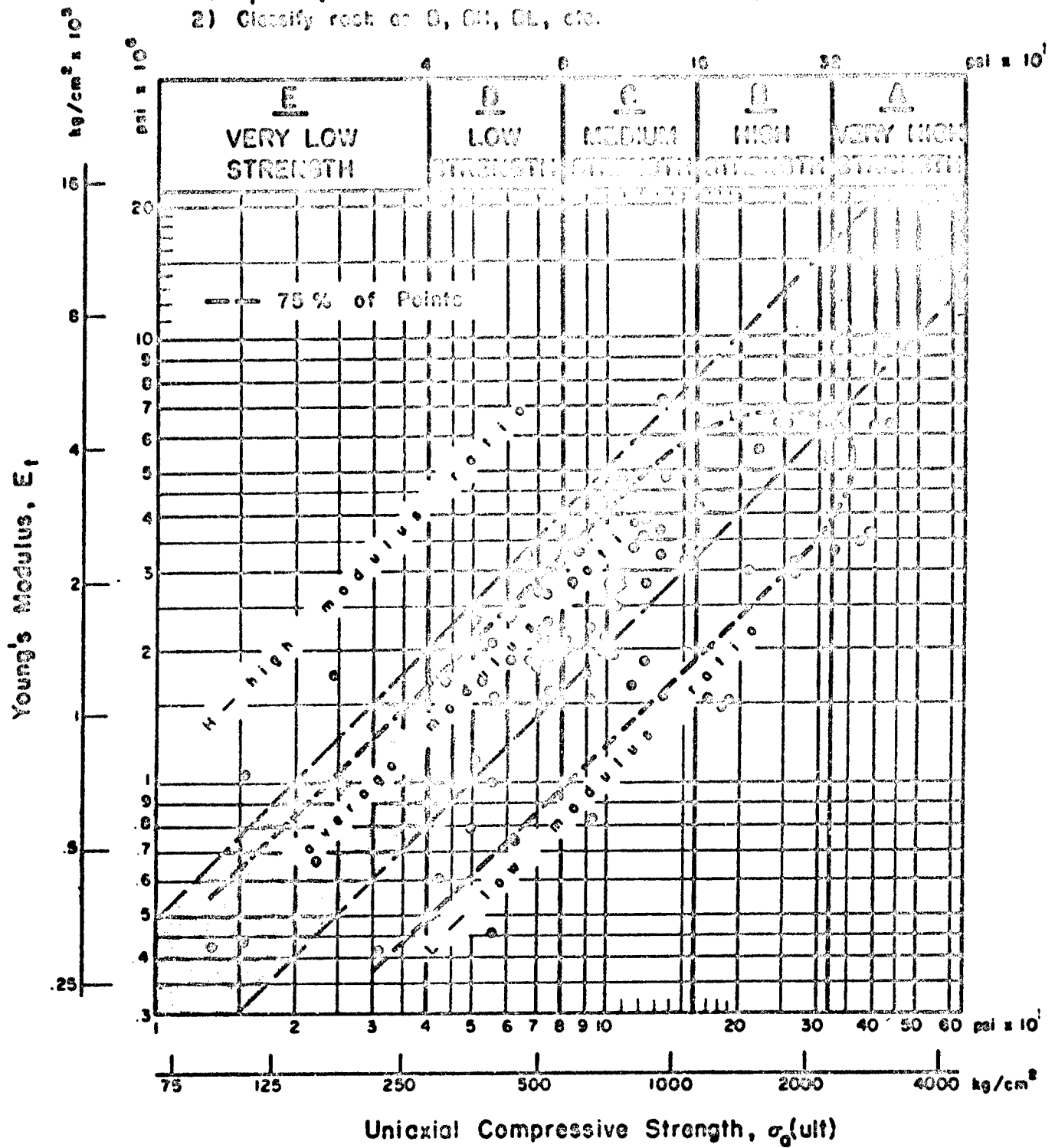


**FIGURE 6.10 ENGINEERING CLASSIFICATION FOR INTACT ROCK - SANDSTONE (82 Specimens, 18 Location, Various. Sources)**



Note:

- 1)  $E_t$  = tangent modulus at 50% ultimate strength
- 2) Classify rock as D, DH, BL, etc.

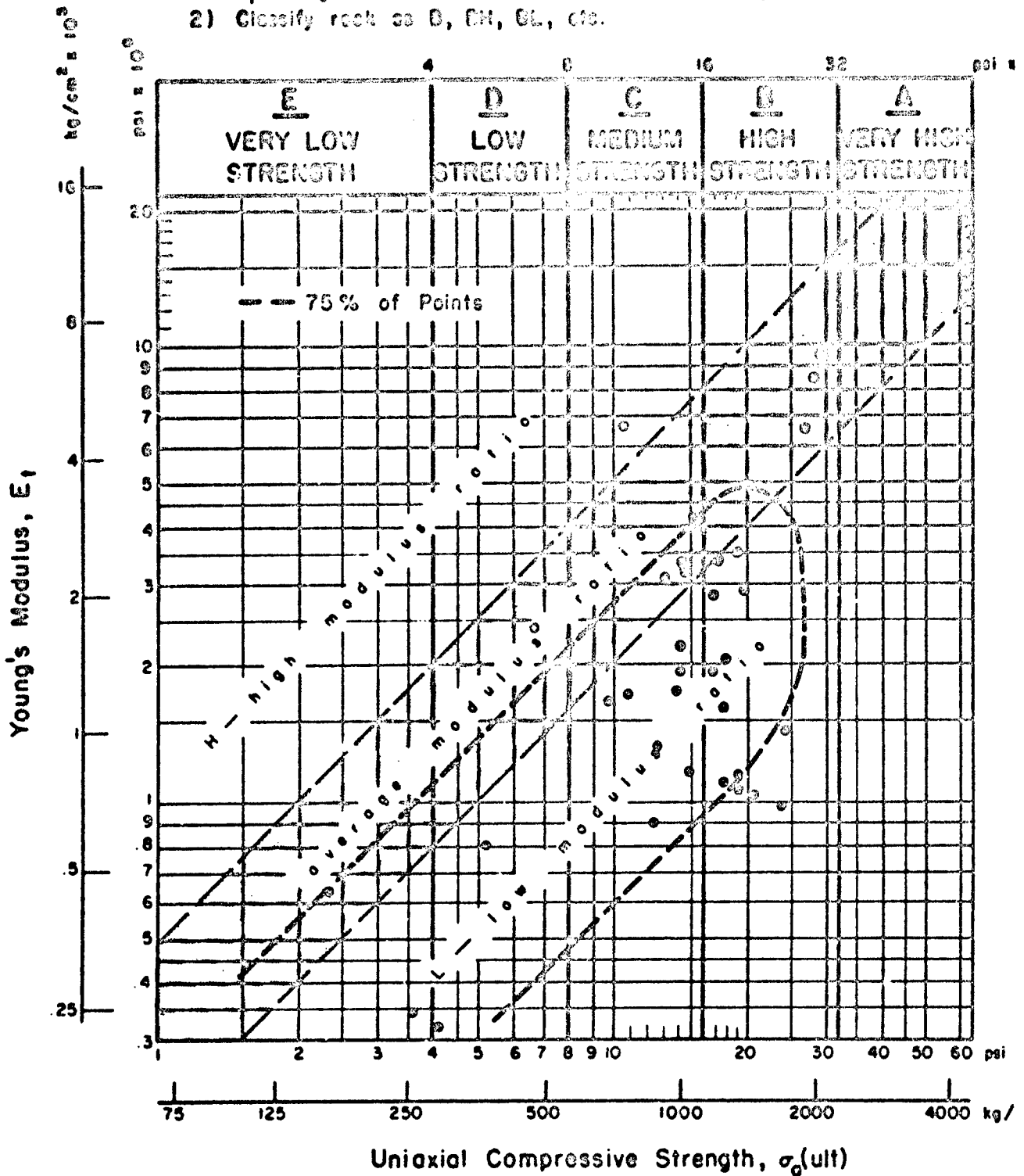


FIGURE 6.II ENGINEERING CLASSIFICATION FOR INTACT ROCK-HARD SHALE (34 Specimens, 14 Locations, Various Sources)

of particles parallel to the bedding during deposition and diagenesis. The bedding is normally horizontal and the samples usually have a vertical orientation. Thus the axial loading is perpendicular to the laminar structure and a low modulus results.

The results of 44 specimens of porous tuff are given in Figure 6.12. The natural water content of the samples is in the general range of 20-30%. The average strength is shown to be about 1,500 psi with an average modulus ratio. Upon air-drying the tuff to approximately 5% water content, the strength is increased to values of 2500-5500 psi. Although the tuff is bedded, it is cemented by secondary clay minerals and zeolites and behaves more like a uniform material of interlocking texture than an anisotropic one and, consequently, plots in the zone of average modulus ratio.

The metamorphic rock summary plot is given in Figure 6.13. The scatter in results is greater than noted for the other rock types because of the great range in both mineralogy and degree of anisotropy. The rock types summarized are quartzite, gneiss, marble, and schist. Figure 6.14 indicates the quartzite data. As would be expected, the modulus values are high -- uniformly above  $7 \times 10^6$  psi, and with more than half exceeding  $10 \times 10^6$  psi. The strength values range from High to Very High and the samples plot as A, B, or BH. It is interesting to note that the dense, compact rocks with equigranular and interlocking texture -- such as dense basalt, diabase, and quartzite -- plot in the A category in essentially the same position.

The gneiss plot is given in Figure 6.15. The gneisses are predominately granite gneisses and they plot in about the granite position but with a somewhat lower average strength and more scatter in the modulus ratio. The additional scattering is in response to both a greater variation in mineralogy than is the case for granite and of anisotropy in the form of lineation or foliation. The several points which appear above the average modulus ratio zone as BH and CH probably represent premature failures along schistose bands of samples with steep foliation (low angle between the specimen axis and plane of anisotropy).

The plot of the marble specimens is given in Figure 6.16. The envelope includes all the samples of the 3 marbles tested for this report (15 specimens). These samples were all of building-stone variety but they were from three different states; the fact that they all fall in such a tight grouping is surprising. The other 7 samples were from either construction sites or mines and the scatter in results is apparent. A greater number of test results from several localities are needed before a meaningful plot can be obtained. It does appear that the high modulus ratio shown by many of the samples is consistent with the trend of limestone and dolomite which contain the same minerals.

Perhaps the most interesting plot is that for schist, shown in Figure 6.17. The mineralogy of schist is extremely variable with both the kind and percentage of platy minerals such as muscovite, biotite, chlorite, and talc varying widely. Also, the degree of development of the highly schistose bands may range from slight to high. When one considers the other important variable that enters into the test results, i.e., the angle of the

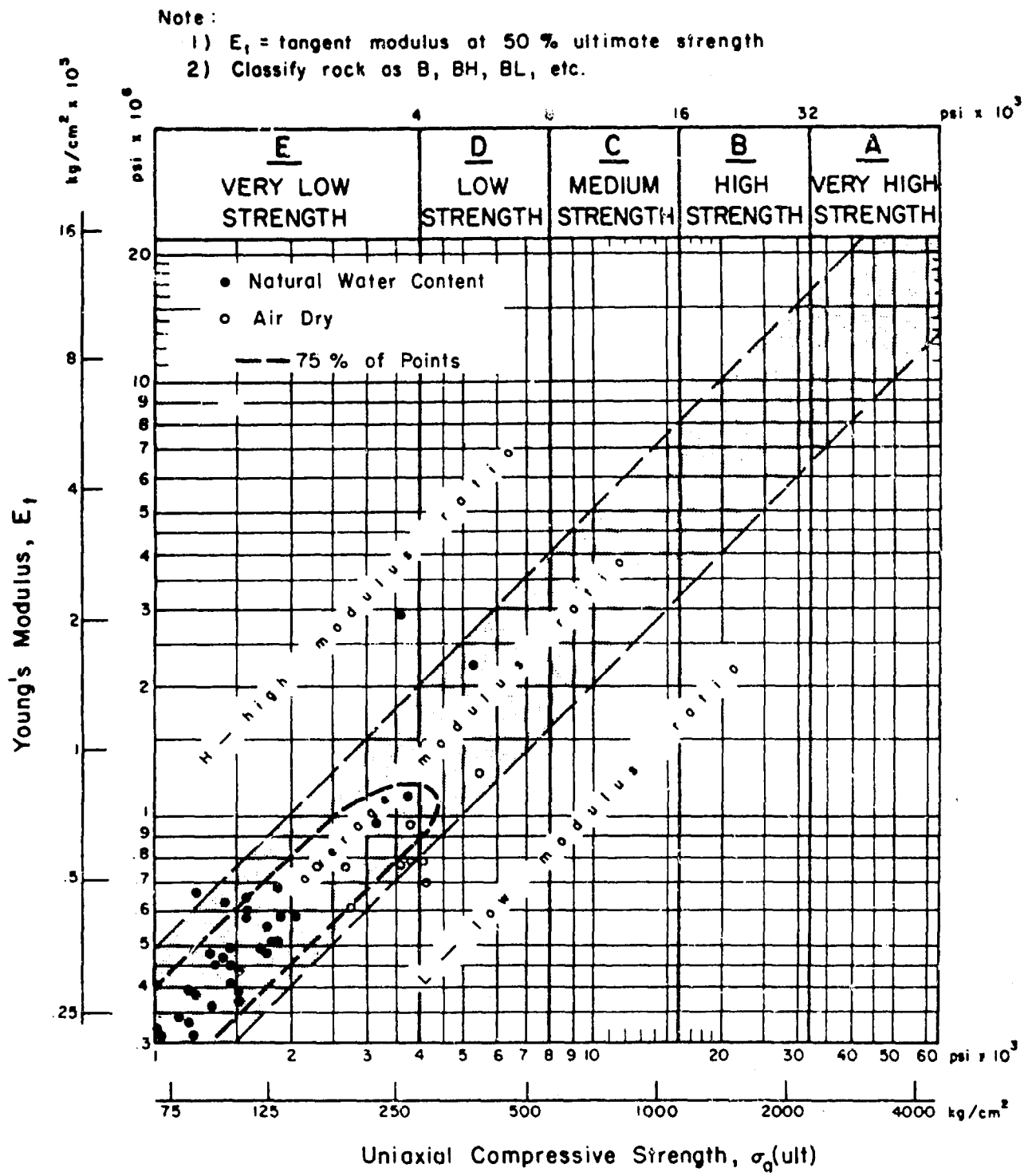


FIGURE 6.12 ENGINEERING CLASSIFICATION FOR INTACT ROCK—POROUS TUFF (44 Specimens, 2 Locations, Various Sources)

Note:

- 1)  $E_t$  = tangent modulus at 50% ultimate strength
- 2) Classify rock as B, BH, BL, etc.

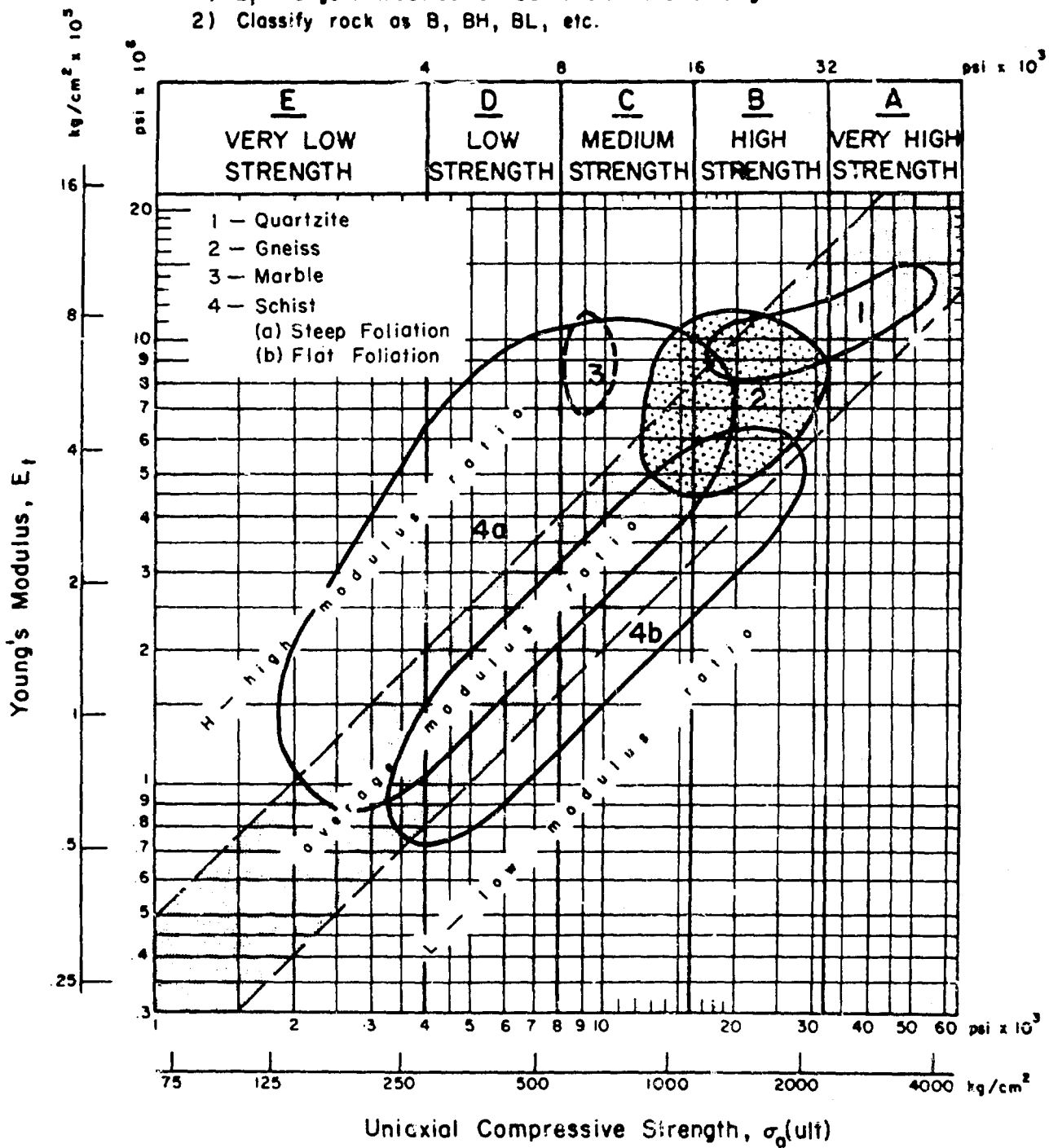


FIGURE 6.13 ENGINEERING CLASSIFICATION FOR INTACT ROCK--  
SUMMARY PLOT METAMORPHIC ROCKS (167  
Specimens, 75% of Points)

Note:

- 1)  $E_t$  = tangent modulus at 50% ultimate strength
- 2) Classify rock as D, DM, DL, etc.

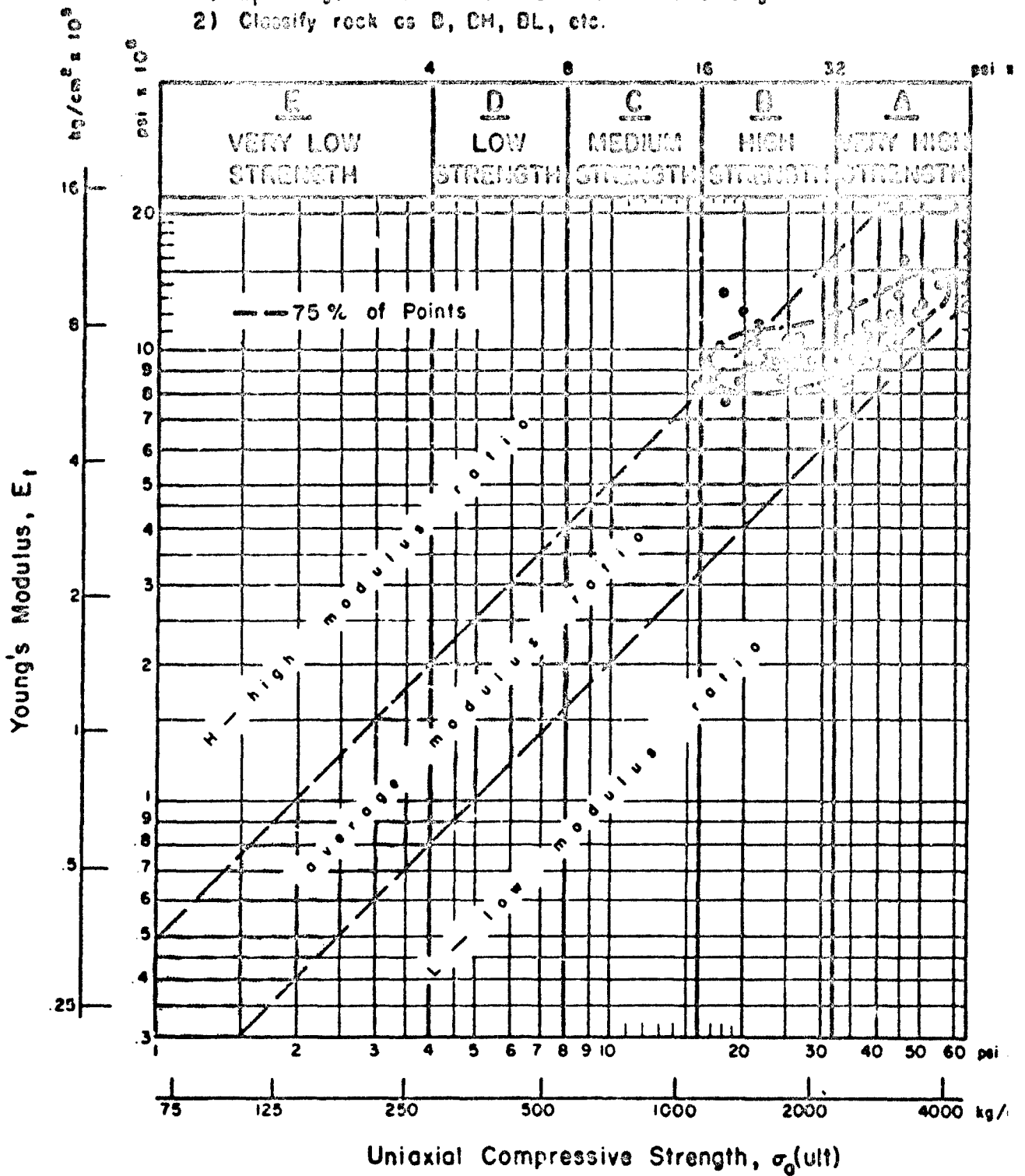


FIGURE 6.14 ENGINEERING CLASSIFICATION FOR INTACT ROCK-QUARTZITE (41 Specimens, 11 Locations, Various Sources)

Note:

- 1)  $E_t$  = tangent modulus at 50 % ultimate strength
- 2) Classify rock as B, BH, BL, etc.

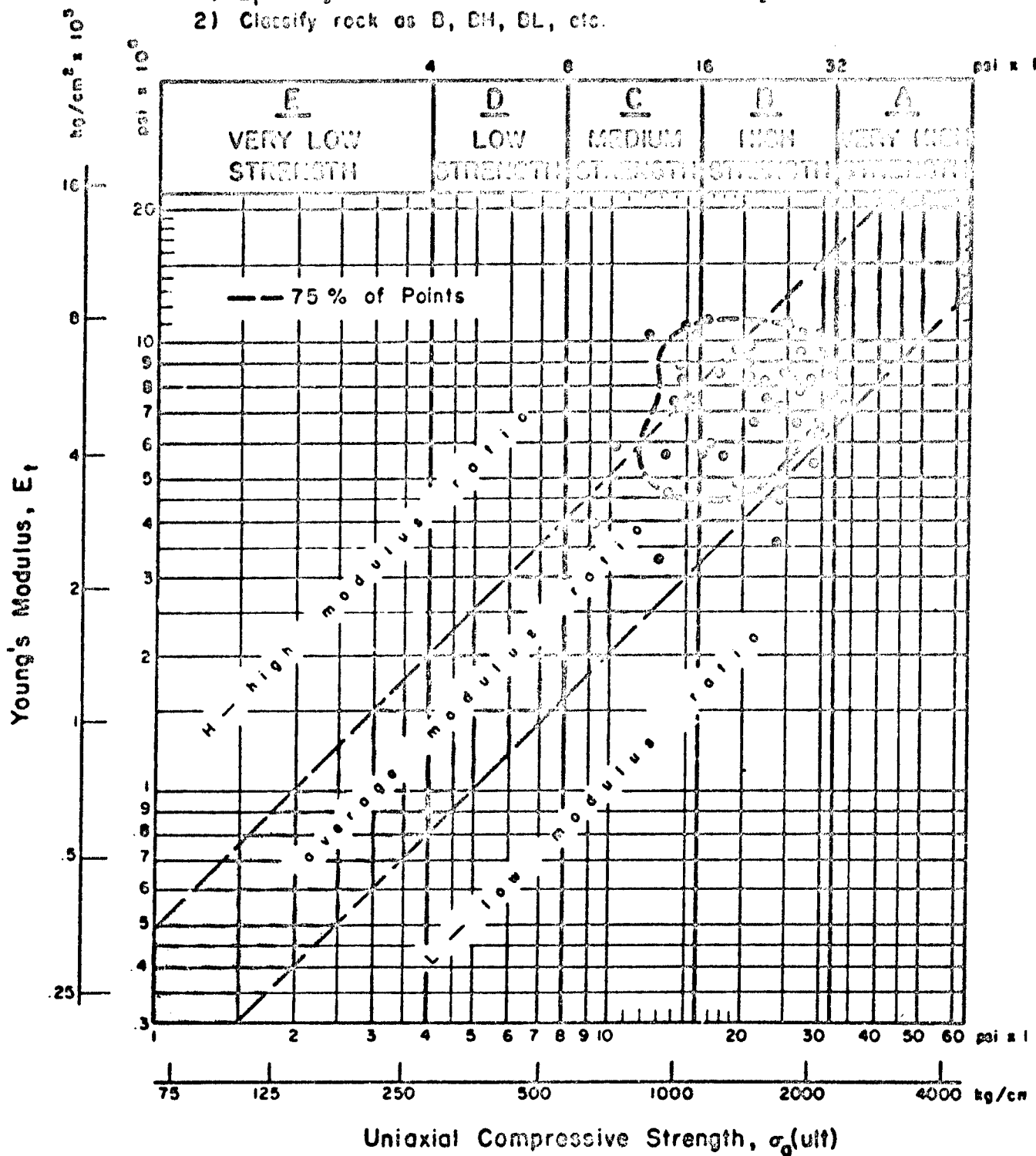


FIGURE 6.15 ENGINEERING CLASSIFICATION FOR INTACT ROCK—  
GNEISS (43 Specimens, 14 Locations, Various Sources)

Note:

- 1)  $E_t$  = tangent modulus at 50% ultimate strength
- 2) Classify rock as B, BH, BL, etc.

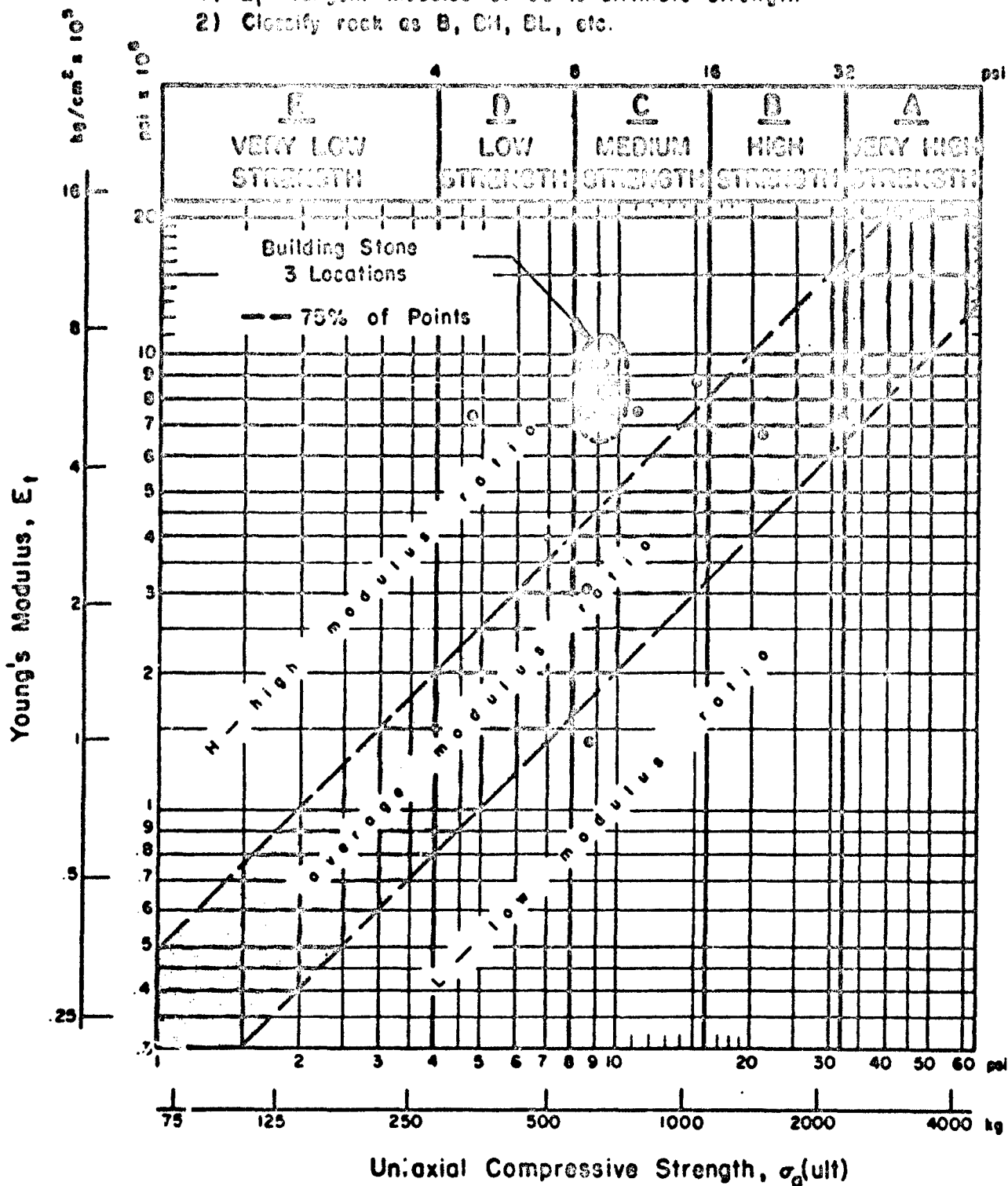


FIGURE 6.16 ENGINEERING CLASSIFICATION FOR INTACT ROCK MARBLE (22 Specimens, 7 Locations)

Note:

- 1)  $E_t$  = tangent modulus at 50% ultimate strength
- 2) Classify rock as D, B1, B2, etc.

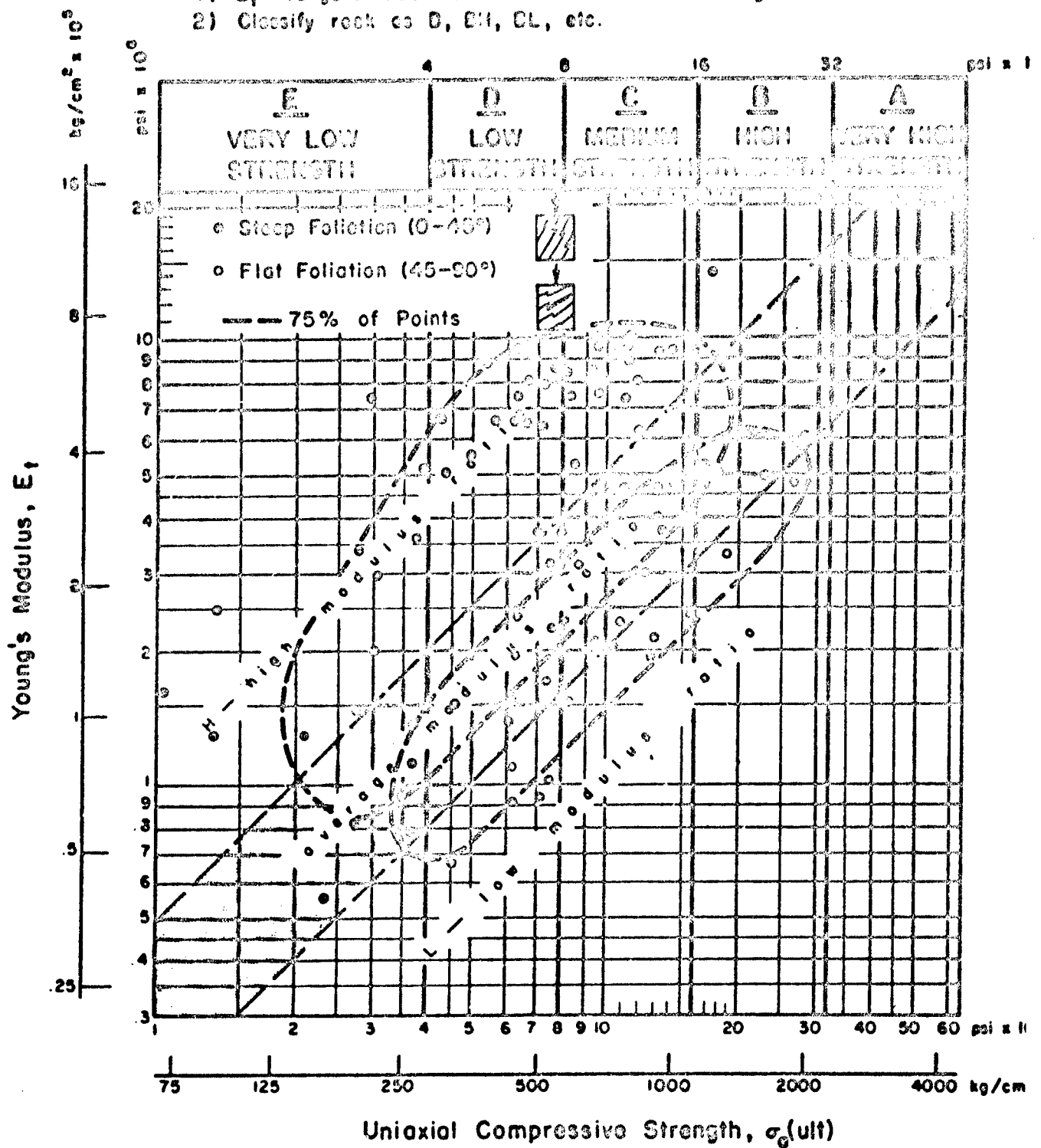


FIGURE 6.17 ENGINEERING CLASSIFICATION FOR INTACT ROCK-SCHIST (61 Specimens, 11 Locations, Various Sources)



schistosity with respect to the specimen axis, it is not surprising that the schist classification includes 11 of the 15 categories (no schist plotted in the three A-categories or in the EL category). The effect of the angle of schistosity on the test results becomes apparent when the samples with steep foliation are separated from those with flat foliation. The latter grouping extends into the low modulus ratio zone because of the effect of closure of the micro-cracks parallel to the foliation. The steep-foliation grouping extends up into the zone of high modulus ratio indicating that some fairly hard, high-modulus rocks ( $5-10 \times 10^6$  psi) failed along a schistose band at relatively lower stresses.

Referring again to Figure 6.13, which summarizes the metamorphic rock classifications, it is significant to note that the gneiss envelope overlaps the quartzite plot and the two schist plots. This transition position indicates an increasing complexity in both mineralogy and texture fabric as one goes from quartzite to gneiss and then to schist. The summary plots for the igneous rocks and the sedimentary rocks (Figures 6.4 and 6.8) show similar responses to differences in mineralogy and textural fabric.

The proposed engineering classification for intact rock is considered a workable and useful system. The classification is based on the compressive strength and modulus of elasticity -- two important physical properties of rock that enter into many engineering problems. The classification is also sensitive to the mineralogy, textural fabric, and direction of anisotropy of the rock so that specific rock types fall within certain areas on the classification plot. These areas as shown on the present summary plots will no doubt be subject to some modification as additional test results become available.

### 3. INDEX PROPERTIES

Index properties provide a quantitative method for assigning a rock to a particular classification, independently of the background and experience of the person making the classification. Usefulness of index properties to engineering classification is generally indicated by (a) their relationship to a material property used in solving a design problem, (b) their simplicity, low cost, and rapidity of determination, and (c) their reproducibility.

Of the various properties considered, the Schmidt hammer hardness, Shore scleroscope hardness, sonic velocity, and unit weight show greatest promise for serving as indices of the engineering behavior for intact rock. The relationships between Schmidt hammer hardness and the strength and deformation characteristics of the rocks investigated herein clearly show the Schmidt hardness,  $R$ , to be in accord with the requirements for index properties as stated above. The Shore hardness is also presented as a possible index property for strength and deformation, but has a slightly lower degree of correlation than that shown by the recommended Schmidt hardness; it is also more restricted to laboratory usage. Another index of rock deformation is the sonic pulse velocity, which has a high degree of correlation with static modulus. However, the sonic velocity does not satisfactorily meet all of the requirements specified for index properties because of the more costly, specialized nature of the laboratory equipment needed for its determination. A fourth index property, unit weight, is used

in conjunction with each of the first three indices, in order to provide a means for differentiating rocks with the same hardnesses or sonic velocity, but which have different values of strength or modulus.

Five charts are presented in this section which have as their bases the numerical values given either by the Schmidt hammer, the Shore scleroscope, or the sonic pulse velocity, each in conjunction with the unit weight of the rock. The suggested index properties are utilized for estimating the compressive strength or static modulus of deformation of intact rock samples. These values may then be used in obtaining an approximate classification for the rock.

Statistical methods of analysis, as described in Appendix C, are used for obtaining the functional relationships, standard errors of estimate, and correlation coefficients between the indices and the strength or deformation characteristics of the rocks. The confidence interval (and corresponding dispersion limits) for prediction purposes with respect to rocks is also discussed in this section.

#### 4. UNIT WEIGHT AS AN INDEX OF STRENGTH AND DEFORMATION

The unit weight of a material is one of the most basic properties obtainable in engineering materials testing. Whereas the total weight may be relatively easily determined with an accurate balance or scale, the unit weight requires also the determination of the dimensions, or volume of the material. For a specimen which has a regular, geometrical shape, the volume is easily determined. For irregular specimens, a procedure similar to that used with the Jolly balance may be employed. This involves weighing the specimen in air and then again while immersed in a liquid of known density such as water. For a cylindrical core specimen which has irregular broken ends, but which also has a known or easily measured diameter, the unit weight can be accurately estimated by measuring its total weight and closely approximating its length. Obviously, as familiarity with weights of rock and rock core is established, the unit weight itself may be estimated with sufficient accuracy. Thus, it is clearly seen that the determination of the unit weight is a simple, economical, and relatively rapid test procedure. The reproducibility of the test results in the laboratory is excellent, as shown by the average coefficient of variation,  $V\% = .5$ , given in Table 5.1. The reproducibility under field conditions will depend upon the methods used for its determination.

##### a. Relationship between unit weight and compressive strength

An arithmetic plot relating dry unit weight and uniaxial compressive strength is given in Figure 5.3. As indicated by the regression line in this figure, the more compact and denser rocks generally have a higher strength than those of less density. This relationship is, however, not well-defined in the range of 160-180 pcf, as these rocks are noted to vary in strength from approximately 8,000-45,000 psi.

The data in Figure 5.3 suggest a more curvilinear relationship than given by the least-squares regression line. Below 140 pcf, the data indicate a flatter, and more asymptotic relation to the X-axis. Above 160 pcf, the

data curve upward and tend to indicate a steeper relation than shown by the regression line. Thus, although the coefficient of correlation might be improved for curvilinear regression, it is seen that the unit weight by itself is not, for all values, a sensitive index of compressive strength. However, its use in conjunction with other index properties for differentiating strength values is shown to be quite significant in the following paragraphs.

b. Relationship between unit weight and modulus of deformation

The relationship between unit weight and tangent modulus of deformation, at a stress level of 50% ultimate strength, shows a higher degree of correlation ( $r = .784$ ) in simple linear regression than unit weight and compressive strength ( $r = .604$ ). Just as for strength, the modulus increases with increasing unit weight as shown in Figure 5.10. Some samples, however, appear to be anomalous, i.e., 8.1, 9.1, 11.1, and 14.1. In multiple regression, in which the unit weight is used as a coefficient for other index properties, the correlation with modulus of deformation is considerably higher. This is discussed in detail in the paragraphs which follow.

5. SCHMIDT HARDNESS AS AN INDEX OF STRENGTH AND DEFORMATION

The Schmidt test hammer provides a simple method for determining relative rebound-hardness values for rock. Test data can be rapidly obtained from either NX-size exploratory drill core, or block samples, without special preparation. The cost of determining the Schmidt hardness is quite low because of the rapidity and ease of test performance. The initial cost of the instrument is approximately \$135.00 (including metal sheath and leather carrying case). Reproducibility of the test data is excellent, as indicated by the low coefficient of variation (approximately 5%) given in Table 5.1. The relationship of Schmidt hardness to the material properties of strength and deformation is discussed in the following paragraphs.

a. Relationship between Schmidt hardness and compressive strength

An arithmetic plot relating Schmidt hardness and uniaxial compressive strength is given in Figure 5.5. The correlation coefficient for these data in linear regression is .880. Figure 5.5 indicates that a curvilinear relationship might provide a better fit of the data. Further, the higher strength rocks tend to "stack up," indicating that above  $R = 55$  the impact hammer is somewhat insensitive to variation in compressive strength. It is also noted that some lower-strength rocks, such as tuff (14.1) can have a relatively high R-value, suggesting that the magnitude of rebound is influenced to a considerable degree by some variable other than compressive strength.

In attempting to provide a better distribution of the data, the R-values are multiplied by dry unit weight,  $\gamma_a$ , and plotted in Figure 6.18. This plot clearly shows better discrimination of strength at all values of  $\gamma_a R$ , in which the functional relationship between the X and Y variables closely approximates a logarithmic curve. The equation of the curve is obtained by least-square regression analysis, in which the compressive strengths are transformed to their corresponding logarithms.

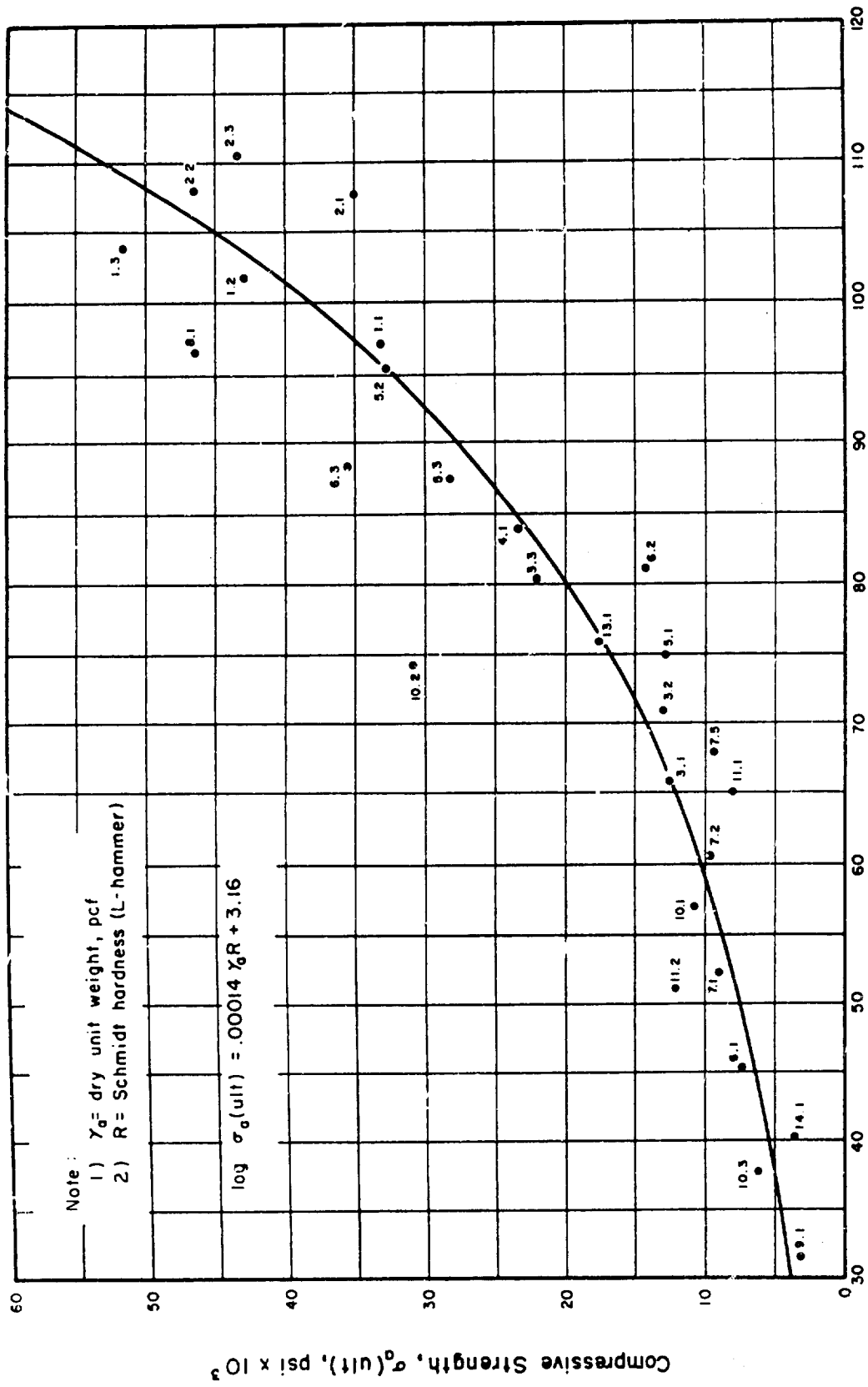


FIGURE 6.18 RELATIONSHIP BETWEEN AVERAGE VALUES OF  $\gamma_0 R$  AND ULTIMATE COMPRESSIVE STRENGTH FOR ROCK IN UNIAXIAL COMPRESSION

Figure 6.19 shows a semi-logarithmic plot of the same data given in Figure 6.18. Here, the correlation coefficient  $r = .943$ , which is considerably higher than  $r = .880$ , as given by Figure 5.5. One standard error of estimate for the experimental data is shown by the two short-dashed lines, parallel to the regression line. On the basis of the characteristics of the normal curve, Figure C.1, approximately 68% of the observations fall within this interval, if we assume that the sampling distributions of the means (given by the average group values shown hereon) are normal in shape, and that the population means for all the rocks are defined by the regression line.

In order to set a confidence interval on the estimate of the means for a fixed set of X-data (i.e., the data shown in Figure 6.19), equation (C.18), Appendix C, is used for any desired level of significance. The generalized confidence belt is defined by branches of a hyperbola, as shown in Figure C.3. However, for predictions of individual events to be made on the basis of a given set of data, a random element must be included as an additional source of uncertainty, modifying equation (C.18) to that of equation (C.19). Further, because of the great variability of rocks and their properties, it is not considered to be within practical engineering interests to expect as high a level of significance for rock data as frequently used in other statistical studies (i.e., 95% confidence). Thus, for prediction purposes, the 75% confidence limits have been selected and are shown by the outer, curved-dashed lines in Figure 6.19. The 75% confidence limits are branches of a hyperbola, defined by equation (C.19) modified as follows:

$$CL(Y) = \bar{y} + b(X-\bar{x}) \pm t_{.25} s_{y \cdot x} \sqrt{1 + \frac{1}{n} + \frac{(X-\bar{x})^2}{\sum(X-\bar{x})^2}} \quad (6.1)$$

where  $t_{.25}$  is for  $n-2$  degrees of freedom. Therefore, it is inferred that on the average 75% of all rocks to be encountered will have properties which lie within the confidence belt shown in Figure 6.19.

It is interesting to note that the only two rocks which have strengths falling outside the 75% confidence belt (10.2 and 11.2) were both loaded in a direction parallel to the direction of bedding or foliation. Thus, a higher strength was measured than that which is indicated by the Schmidt hardness in the relationship defined in Figure 6.19. The other 26 rocks were all loaded in a direction perpendicular to bedding or fabric, where such was present.

It is recognized that a requirement of regression is that the X's, or independent variables, be measured without error. Actually, there are errors in X as well as in Y. However, in the present study it is reasonable to assume that the errors in X (i.e.,  $\gamma_a R$ ) are insignificant for two reasons:

- i) the average coefficient of variation for each of the properties in X is quite small (i.e., for  $\gamma_a$ ,  $V\% = .5$ ; for R,  $V\% = 4.7$ ).
- ii) the unit weights given herein are in agreement with unit weights obtained by others, for those rocks which are reported in the literature (i.e., 2.3, 3.3, 4.1, 5.3, 6.1, 8.1, et cetera);

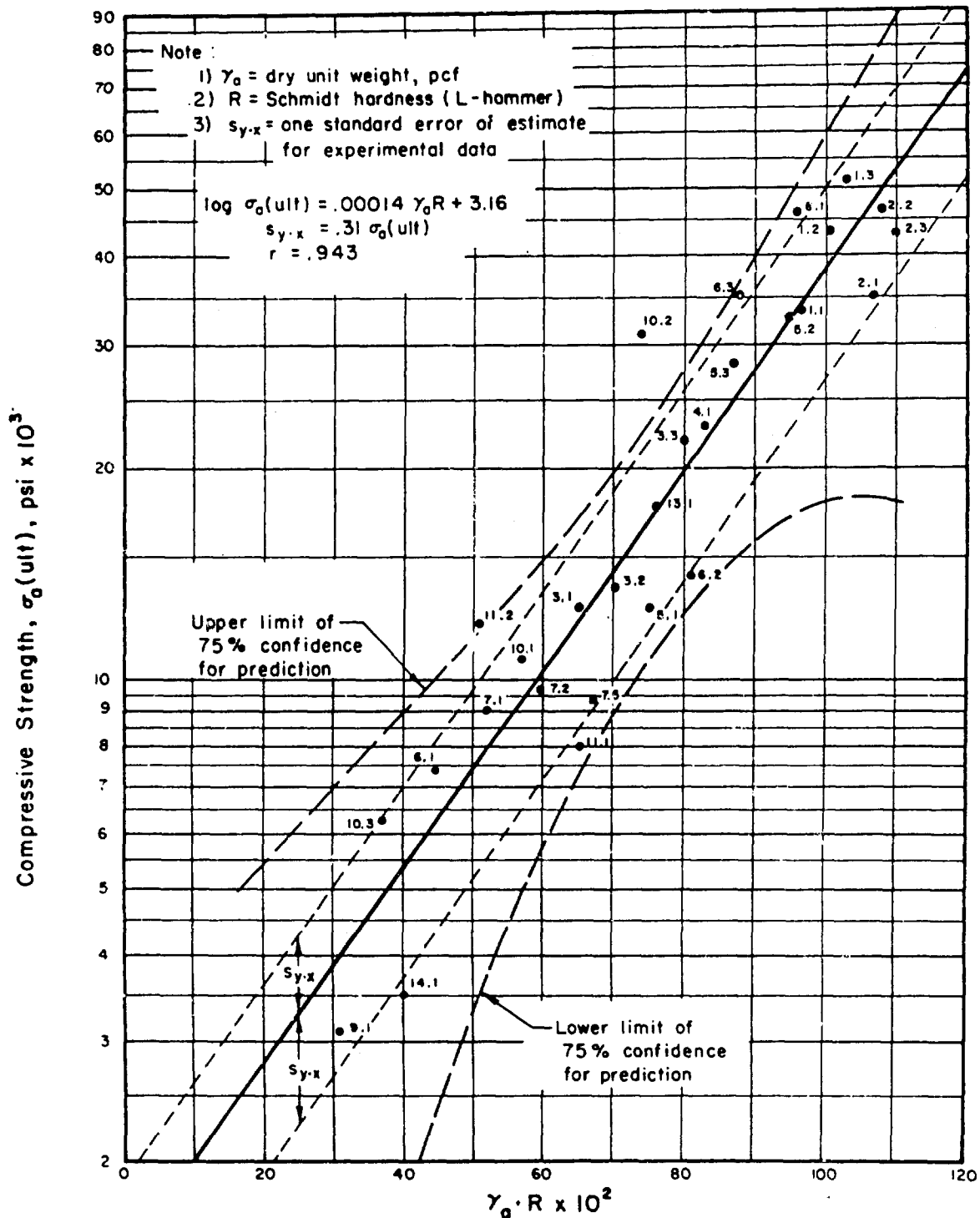


FIGURE 6.19 RELATIONSHIP BETWEEN AVERAGE VALUES OF  $\gamma_0 \cdot R$  AND ULTIMATE COMPRESSIVE STRENGTH FOR ROCK IN UNIAXIAL COMPRESSION (SEMI-LOG PLOT)

also, the R-values were regularly checked against a standard, and were found to give identical hardness readings throughout the test program.

Therefore, all relationships and corresponding charts, presented in this section, are based on the assumption that there are no measurement errors in X, or that they are so small they can be neglected. (Reasoning similar to i and ii, above, is used in the cases of  $S_h$  and  $V_p$  as well.)

By means of the functional relationship presented in Figure 6.19, uniaxial compressive strengths can be approximated for various combinations of Schmidt hardness and unit weight. By use of this procedure, a rock strength chart has been developed and is shown in Figure 6.20. By obtaining the Schmidt hardness, R, and the unit weight,  $\gamma_a$ , an estimate of the strength can be made. The statistical dispersion, or possible deviation from the correct value of strength (defined by the 75% confidence limits in Figure 6.19), is shown by the curved line at the left side of the chart. For example, the Dworshak gneiss (4.1) has an R-value of 48, and a unit weight of 175 pcf. By entering the chart at  $R = 48$ , and following the short-dashed line up to  $\gamma_a = 175$ , the strength is estimated by then proceeding horizontally left to the value of  $\sigma_a(\text{ult}) = 21,500$  psi. Statistical dispersion from the estimated value of strength may be as much as  $\pm 8,500$  psi, which is shown by the horizontal distance of the dispersion line from the left border. The actual measured strength of the Dworshak gneiss is 23,500 psi, as given in Table 4.2.

Unfortunately, a strict adherence to a purely statistical dispersion results in an unreasonably wide variation in predicted values for the higher strength rocks. Such a variation was not actually observed in the experimental data in the present study. Therefore, in the realistic application of this chart to engineering projects, use of the statistical dispersion limits may not be warranted.

#### b. Relationship between Schmidt hardness and modulus of deformation

Just as for strength, the correlation between Schmidt hardness and tangent modulus of deformation at 50% ultimate strength is considerably improved when R is multiplied by unit weight. This relationship and the corresponding linear regression line are shown in Figure 6.21 for which the correlation coefficient  $r = .847$ . (Figure 5.14 shows the relation between  $E_t$  and R alone, for which  $r = .731$ .) A still higher correlation is obtained by squaring the unit weight and multiplying by R, for the independent (X) variable. This relationship is shown in Figure 6.22 in which  $r = .876$ . Again, one standard error of estimate for the experimental data is shown by the short-dashed, parallel lines. The 75% confidence interval for prediction, as determined by equation (6.1), is given by the heavier-dashed, hyperbolic lines.

The regression equation in Figure 6.22 is used for computing the tangent modulus of deformation for various combinations of Schmidt hardness and unit weight. From these computations, a rock modulus chart has been developed and is shown in Figure 6.23. Just as for strength, by determining the Schmidt hardness, R, and the unit weight,  $\gamma_a$ , an estimate of the tangent modulus at 50% ultimate strength can be made. The statistical dispersion of the data, as defined by the 75% confidence limits from Figure 6.22, is shown

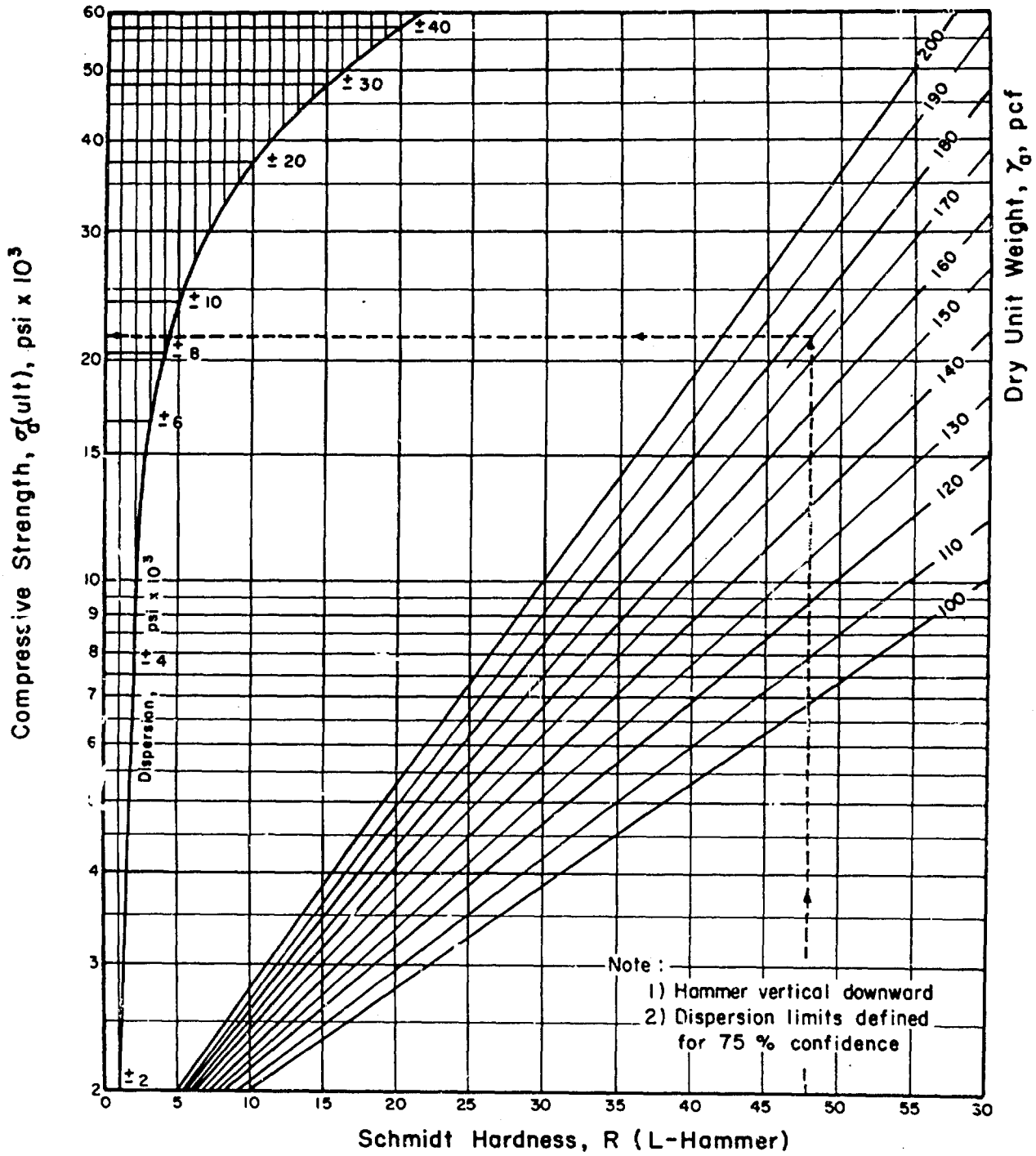


FIGURE 6.20 ROCK STRENGTH CHART BASED ON SCHMIDT HARDNESS



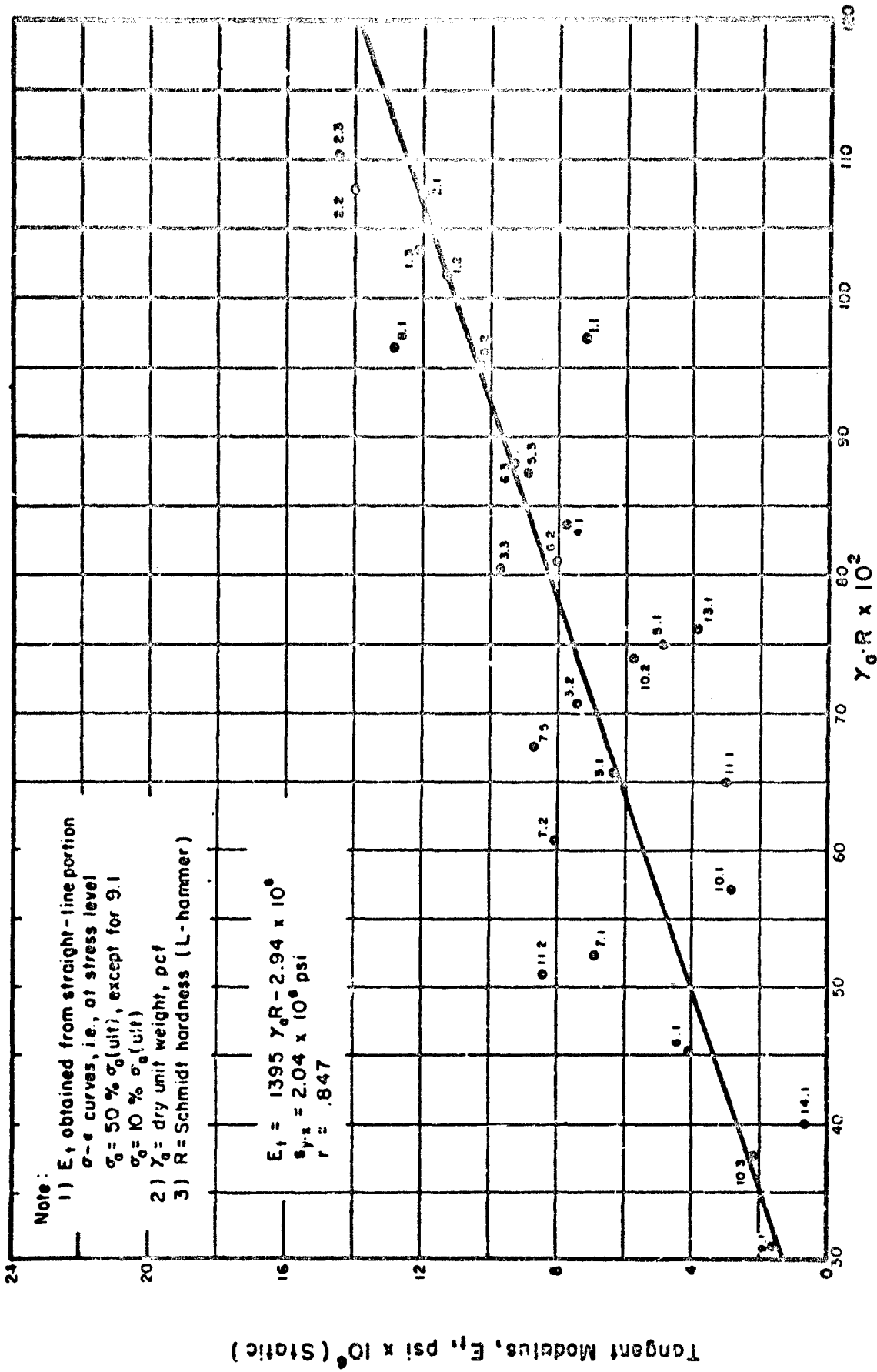


FIGURE 6.21 RELATIONSHIP BETWEEN AVERAGE VALUES OF  $\gamma_0.2 R$  AND TANGENT MODULUS OF REFORMATION AT STRESS 1 FIVE OF ONE-HALF ULTIMATE STRENGTH FOR ROCK IN

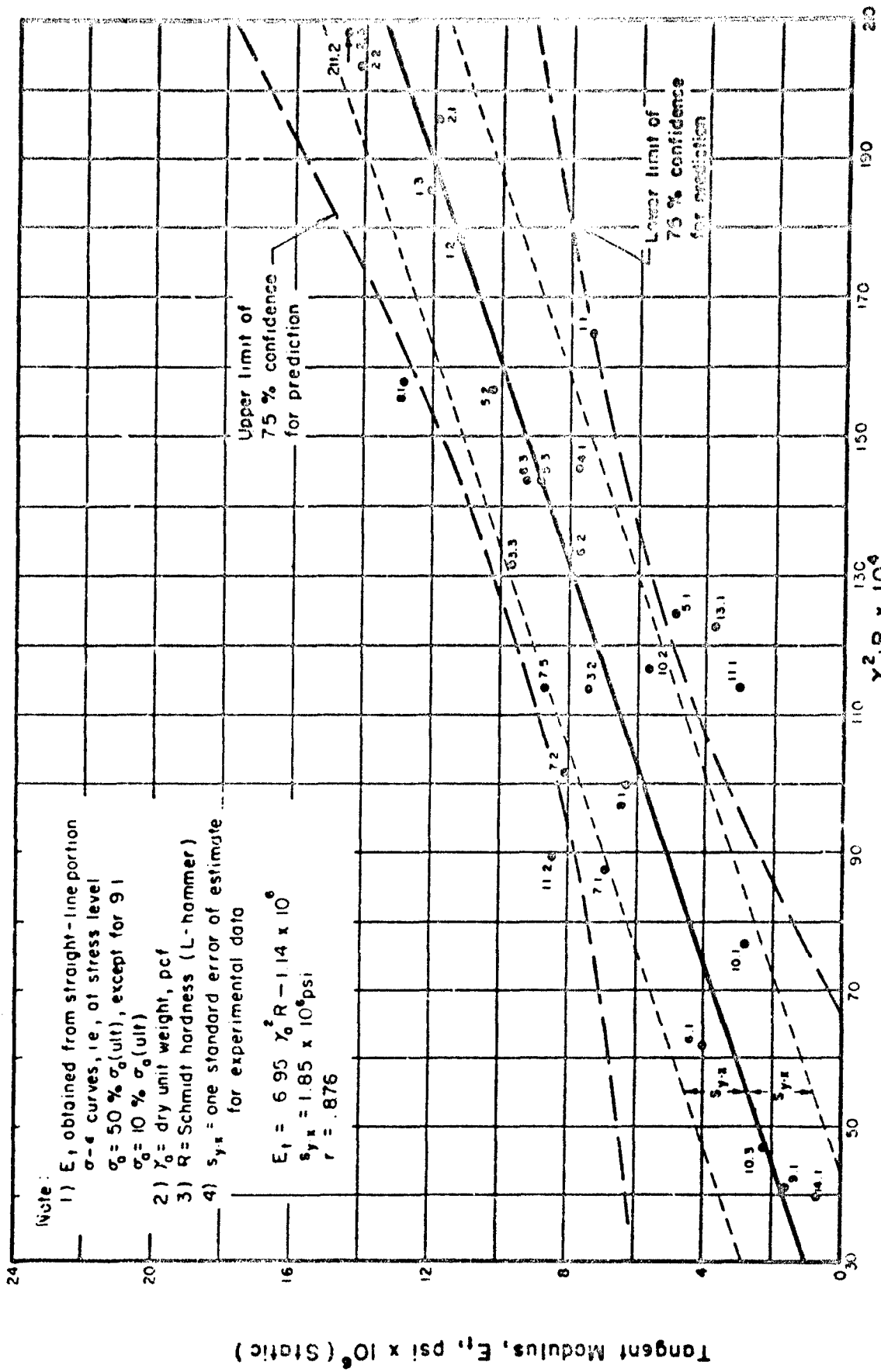


FIGURE 6.22 RELATIONSHIP BETWEEN AVERAGE VALUES OF  $\gamma_a^2 R$  AND TANGENT MODULUS OF DEFORMATION AT STRESS LEVEL OF ONE-HALF ULTIMATE STRENGTH FOR ROCK IN UNIAXIAL COMPRESSION

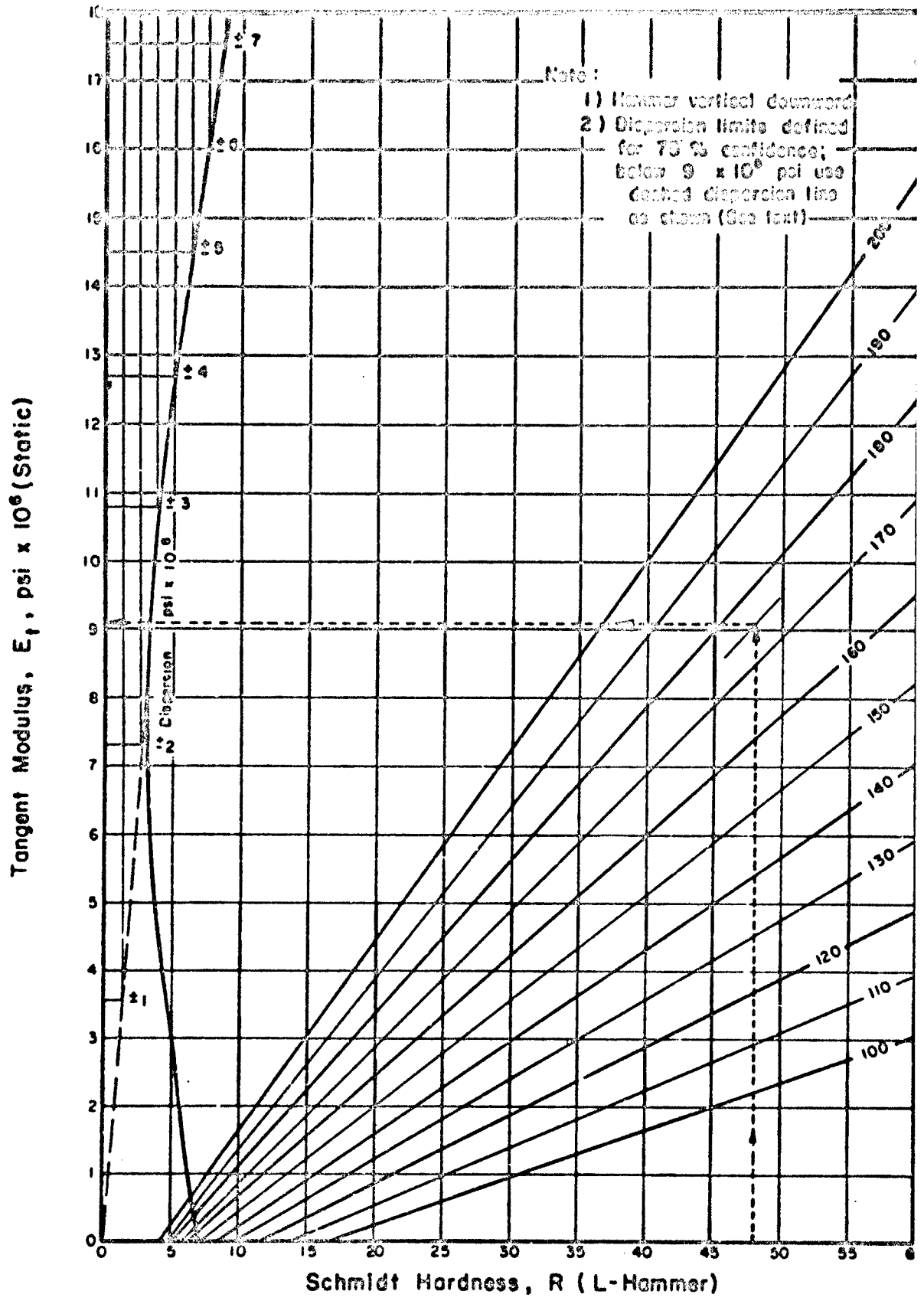


FIGURE 6.23 ROCK MODULUS CHART BASED ON SCHMIDT HARDNESS

by the curved, solid line at the left side of the chart. Thus, for example, by entering the chart at  $R = 48$  (again for Doorshok gneiss) and following the short-dashed line to  $\gamma_a = 175$ , then horizontally left,  $E_t$  is estimated to be  $9.1 \times 10^6$  psi ( $\pm 2.4 \times 10^6$ ). This is comparable to the measured modulus value of  $7.8 \times 10^6$  psi, as given in Table 4.3.

A strict statistical dispersion, as determined from the confidence limits in the arithmetic plot of Figure 6.22 increases with decreasing modulus below the data mean. This is shown by the curving, dispersion line below  $E_t = 7.5 \times 10^6$  psi. If this dispersion is used for the lower-modulus rocks, the predicted moduli values would lose their meaning; for example, at  $E_t = 1 \times 10^6$  psi, the statistical dispersion is shown to be  $\pm 5 \times 10^6$  psi. Such a dispersion is not reasonable in engineering usage, since negative moduli values do not exist. Further, the experimental data in the present study are, in reality, closer to the regression line than the statistical dispersion would infer. Therefore, for estimating tangent moduli values below  $E_t = 9 \times 10^6$  psi, it is suggested that the dispersion be obtained from the dashed line extending through the origin or, perhaps even more realistically, ignored altogether for actual engineering usage.

## 6. SHORE HARDNESS AS AN INDEX OF STRENGTH AND DEFORMATION

The Shore scleroscope has proven itself over the years to be a very useful laboratory instrument for measuring relative dynamic-hardness properties of metals. The scleroscope has, in recent years, been frequently utilized for laboratory-hardness measurements of rock, as described in Section Three; it has also been used in the present investigation for this purpose.

The relationship of the Schmidt rebound-hardness values to those determined by the Shore scleroscope is plotted in Figure 6.24. Two least-squares regression lines are shown, together with their corresponding equations. Line R is the regression line of Y on X, for which Shore hardness is the independent variable; and line  $S_h$  is the regression line of X on Y, for which Schmidt hardness is the independent variable. A reasonably high degree of correlation between the two methods for measuring hardness is indicated by the correlation coefficient,  $r = .872$ . The Shore hardness measures a very fine-pointed, surface property, whereas the Schmidt hardness appears to measure a broader, more macroscopic, mass-hardness property of the specimen.

Because of the obvious relationship between Shore and Schmidt hardness, and because the scleroscope is a standard piece of equipment in many testing laboratories, the same procedures as presented for the Schmidt hammer are utilized in developing rock property charts based upon Shore hardness. The relationships between Shore hardness and the strength and deformation characteristics for rock, together with the corresponding charts, are discussed only briefly in the following paragraphs because of the similarity to the discussion presented for Schmidt hardness.

### a. Relationship between Shore hardness and compressive strength

The relationship between Shore hardness and compressive strength was previously given in Figure 5.4, in which  $r = .897$  for linear regression. By

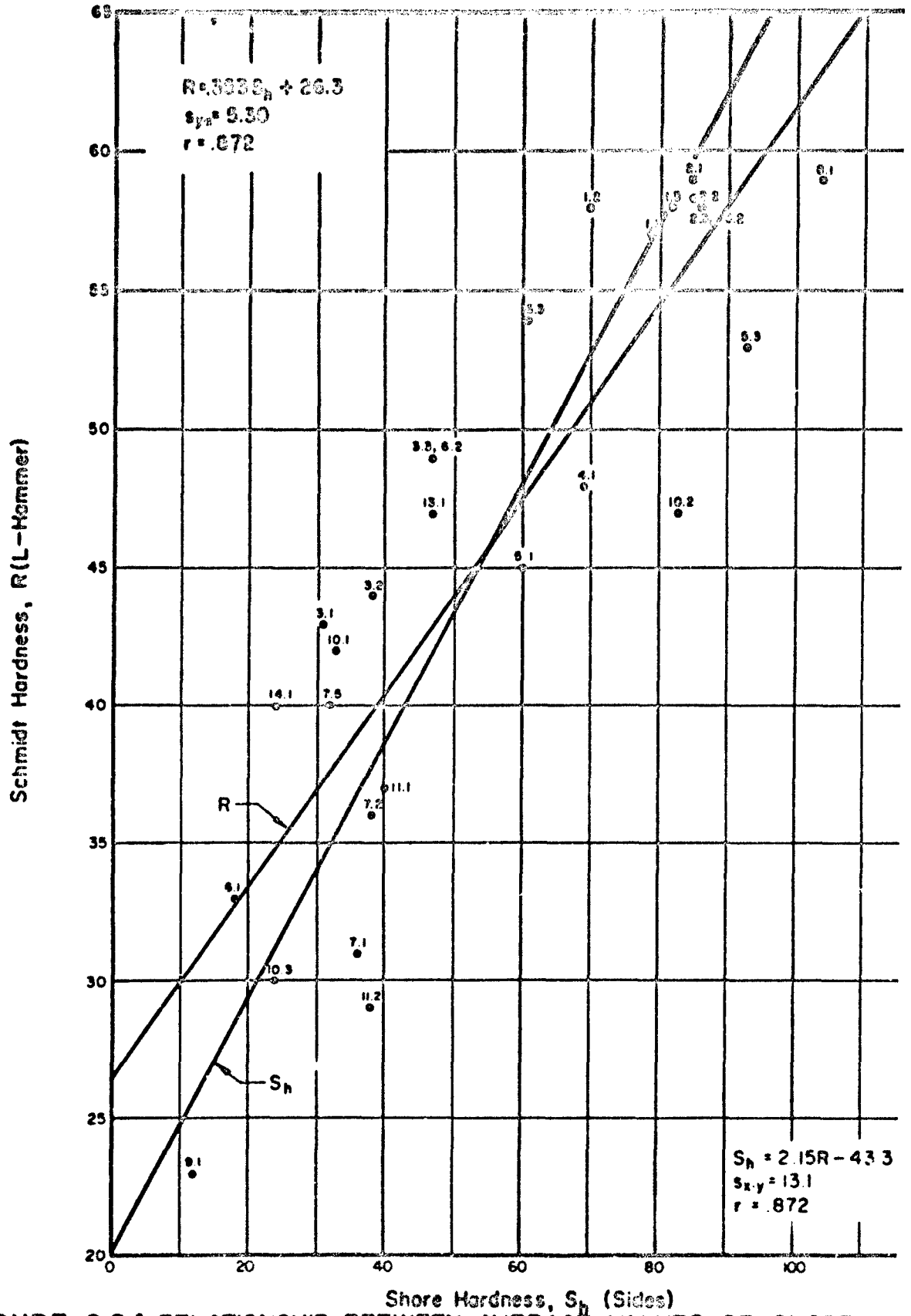


**FIGURE 6.24 RELATIONSHIP BETWEEN AVERAGE VALUES OF SHORE HARDNESS AND SCHMIDT HARDNESS FOR ROCK**

multiplying the Shore hardness by the unit weight of each rock, the curvilinear plot in Figure 6.25 is obtained.

A semi-logarithmic plot of the data shown in Figure 6.25 is given in Figure 6.26, for which  $r = .921$ . The regression equation in both figures is obtained from the linear regression line given in Figure 6.26. One standard error of estimate,  $s_{y,x}$ , is shown to be  $.37\sigma_a(\text{ult})$  in this plot, as compared to  $.31\sigma_a(\text{ult})$  based on Schmidt hardness. The 75% confidence belt for prediction is, thus, somewhat wider than that for Schmidt hardness; therefore, the statistical dispersion at any estimated strength level is correspondingly greater.

On the basis of the functional relationship in Figure 6.26, a rock strength chart has been developed and is shown in Figure 6.27. This chart is identical in form with the chart based on Schmidt hardness in Figure 6.20. Thus, again using the Dworshak gneiss (4.1) as an example, the chart is entered at  $S_h = 69$ . Following the short-dashed line up to  $\gamma_a = 175$ , then proceeding horizontally to the left, the strength is estimated to be 26,000 psi ( $\pm 13,500$ ). This is comparable to the measured strength of 23,500 psi, and to the strength predicted by the Schmidt hardness equal to 21,500 psi. Note that the statistical dispersion approaches 50% of the estimated value, whereas the estimated value is actually only 10.5% greater than the measured strength. Further, the strength predicted by the Schmidt hardness is only about 8.5% lower than the measured strength.

The rock strength chart based on Shore hardness, as shown in Figure 6.27 appears to be limited to rocks with strengths greater than 5,000 psi. This is due to the emphasis given to regression analyses in the development of the chart, and the consequent regression line defined in Figure 6.26 for all 28 rock groups. The two, lowest strength rocks, rock salt (9.1) and tuff (14.1), are probably not correctly represented by the suggested functional relationship. Indeed, the correct relationship may, more properly, curve downward toward the origin. Additional investigation and separate analysis of the lower-strength rocks would likely result in better definition for rocks having low Shore-hardness values (i.e., less than 30).

#### b. Relationship between Shore hardness and modulus of deformation

As in the case of Schmidt hardness, the correlation between Shore hardness and tangent modulus of deformation at 50% ultimate strength is considerably improved when  $S_h$  is multiplied by  $\gamma_a$ , and even more improved when  $\gamma_a^2$  is used instead of  $\gamma_a$ . The relationship between  $S_h$  and  $E_t$  has been given in Figure 5.13, in which  $r = .746$ . Figure 6.28 shows the relation between  $\gamma_a S_h$  and  $E_t$ , for which  $r = .800$ . The best correlation is shown in Figure 6.29 between  $\gamma_a^2 S_h$  and  $E_t$ , for which  $r = .831$ .

Figure 6.29 shows the limits for one standard error of estimate, and the 75% confidence belt for prediction, as determined by equation (6.1). When compared with the similar relationship for Schmidt hardness, Figure 6.22, the confidence interval in Figure 6.29 is seen to be somewhat broader.

A rock modulus chart based on Shore hardness and unit weight is shown in Figure 6.30. This chart is identical in form and use as the chart based on Schmidt hardness and unit weight of Figure 6.23. The regression

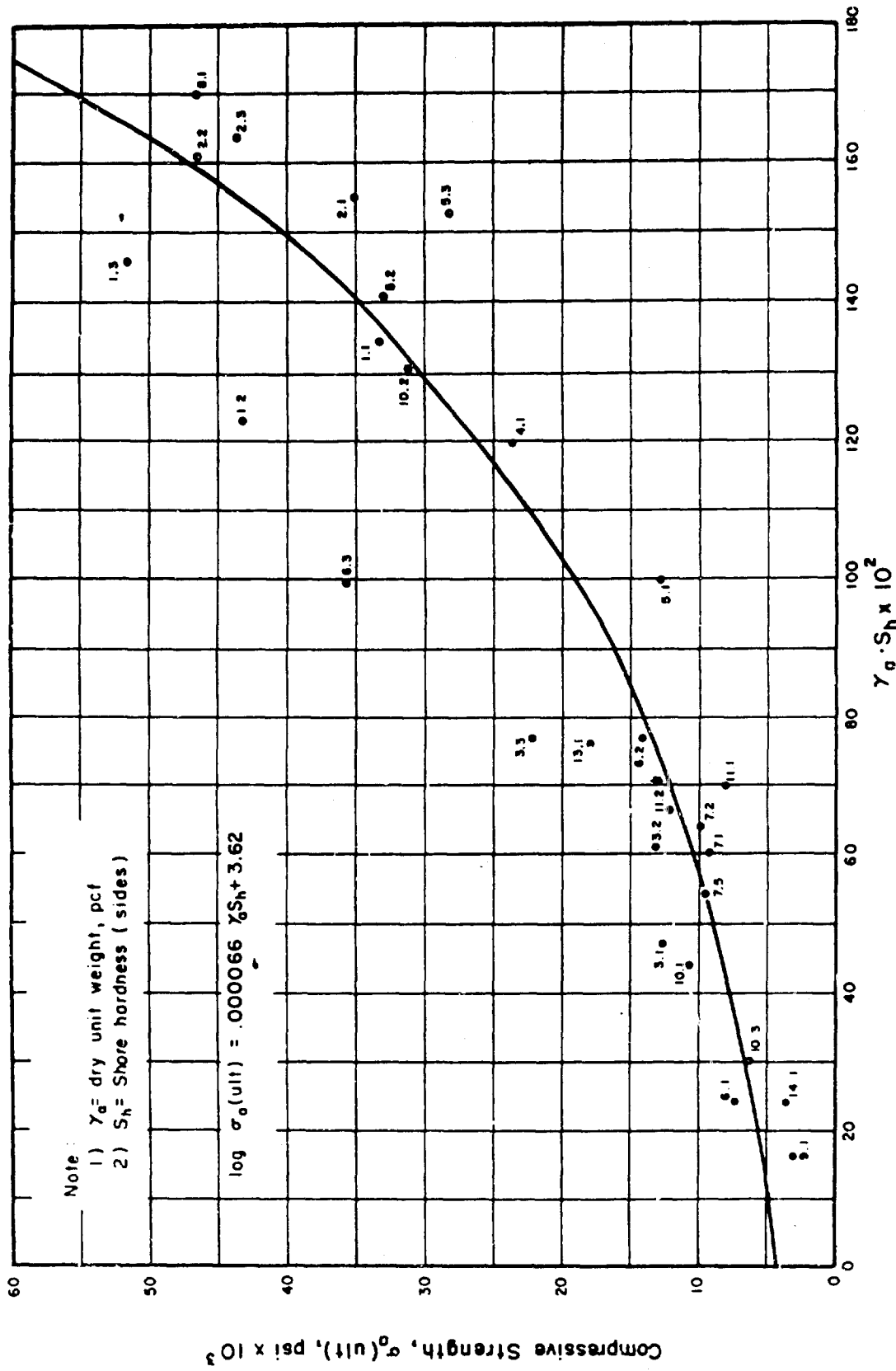


FIGURE 6.25 RELATIONSHIP BETWEEN AVERAGE VALUES OF  $\gamma_a \cdot S_h$  AND ULTIMATE COMPRESSIVE STRENGTH FOR ROCK IN UNIAXIAL COMPRESSION

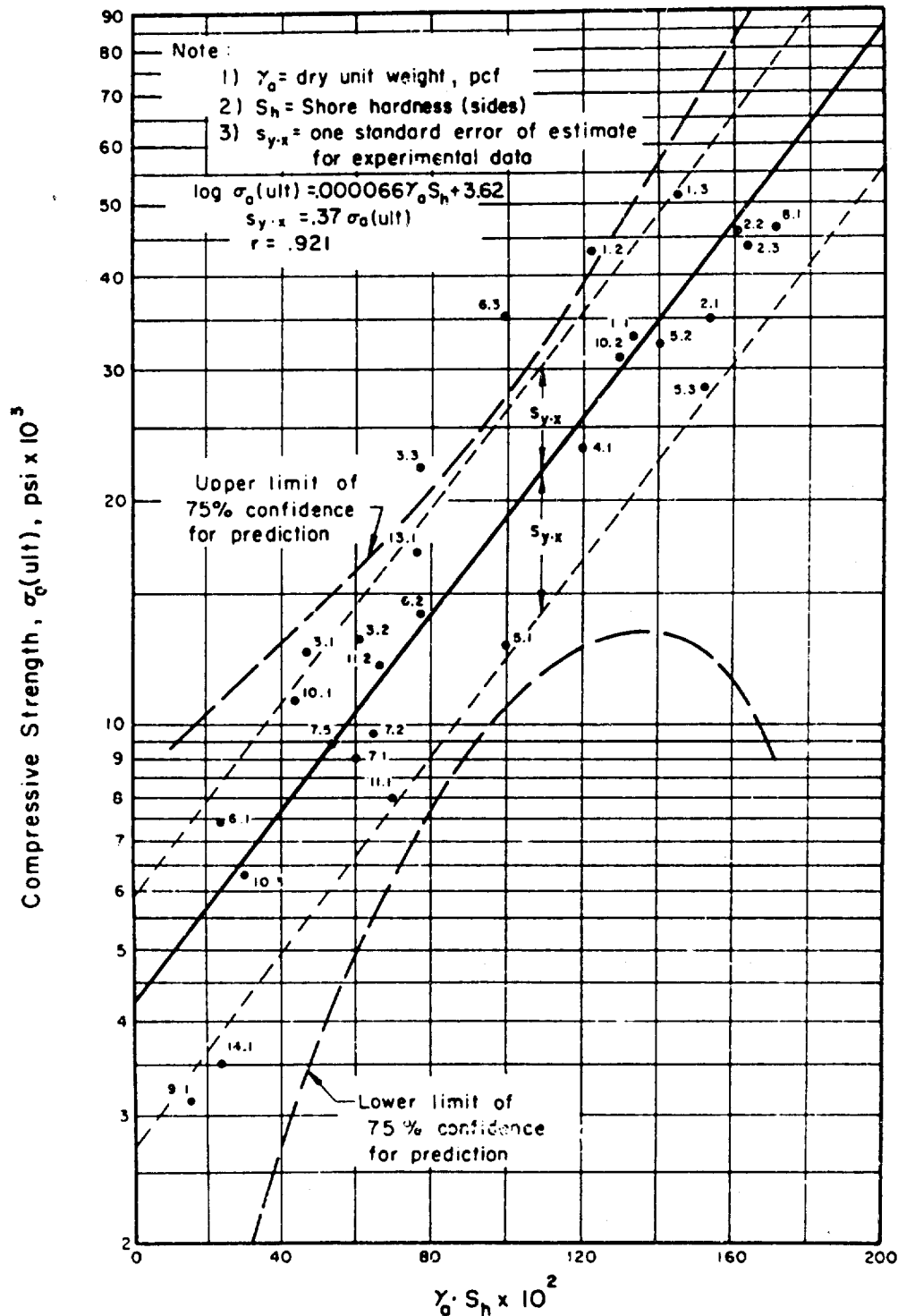


FIGURE 6.26 RELATIONSHIP BETWEEN AVERAGE VALUES OF  $\gamma_0 \cdot S_h$  AND ULTIMATE COMPRESSIVE STRENGTH FOR ROCK IN UNIAXIAL COMPRESSION (SEMI-LOG PLOT)



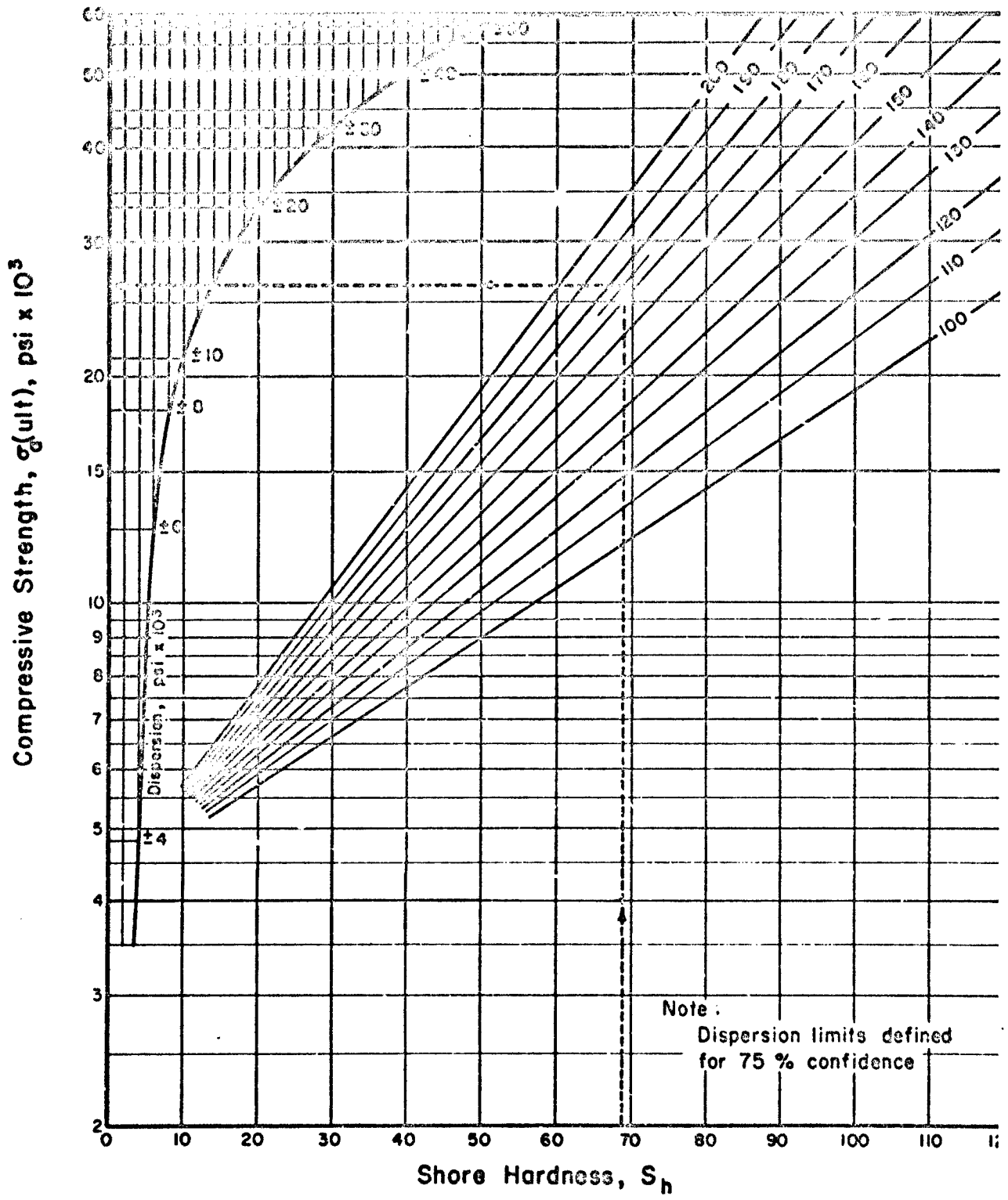


FIGURE 6.27 ROCK STRENGTH CHART BASED ON SHORE HARDNESS

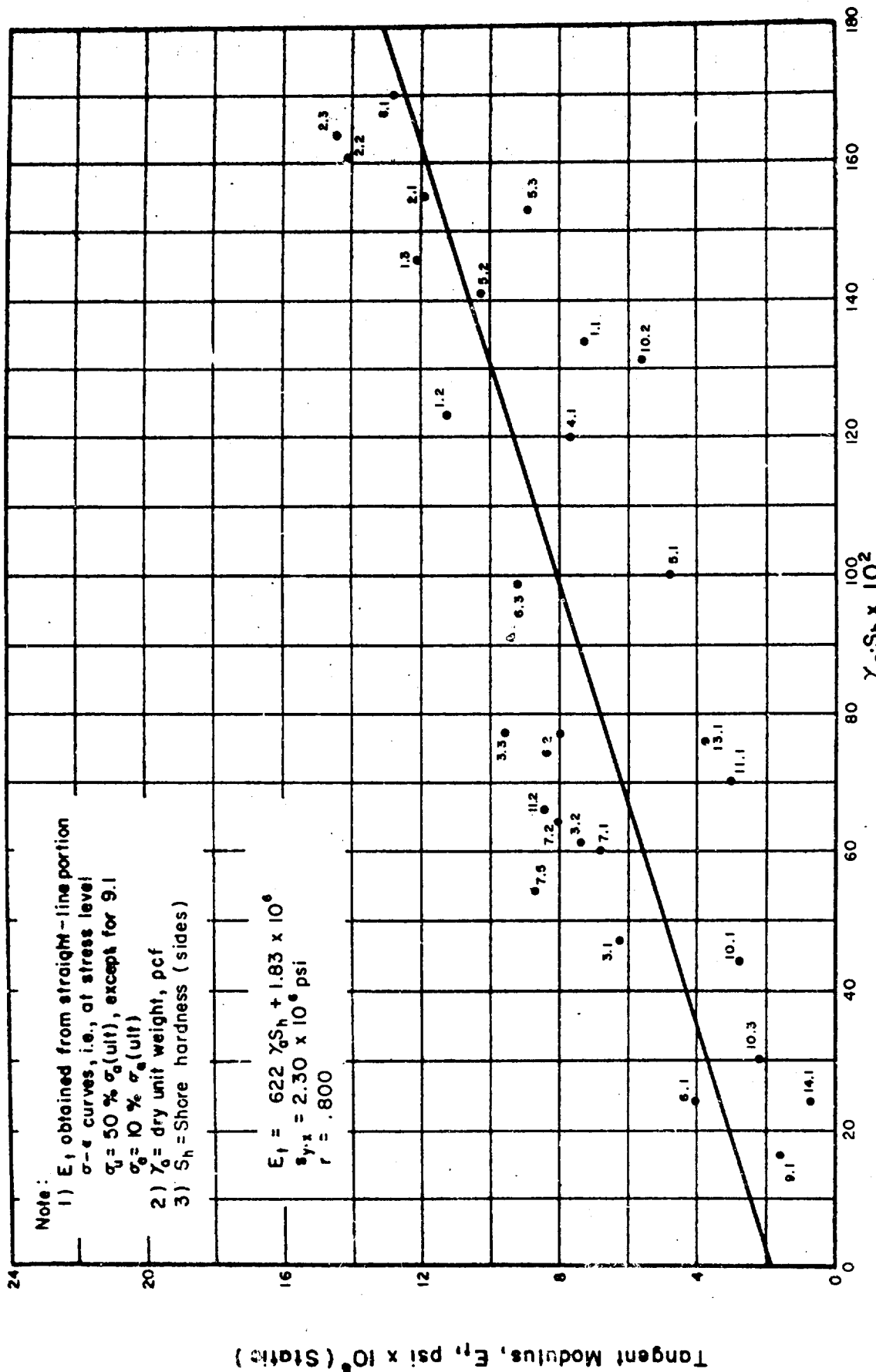


FIGURE 6.28 RELATIONSHIP BETWEEN AVERAGE VALUES OF  $\gamma_0 \cdot S_h$  AND TANGENT MODULUS OF DEFORMATION AT STRESS LEVEL OF ONE-HALF ULTIMATE STRENGTH FOR ROCK IN UNIAXIAL COMPRESSION

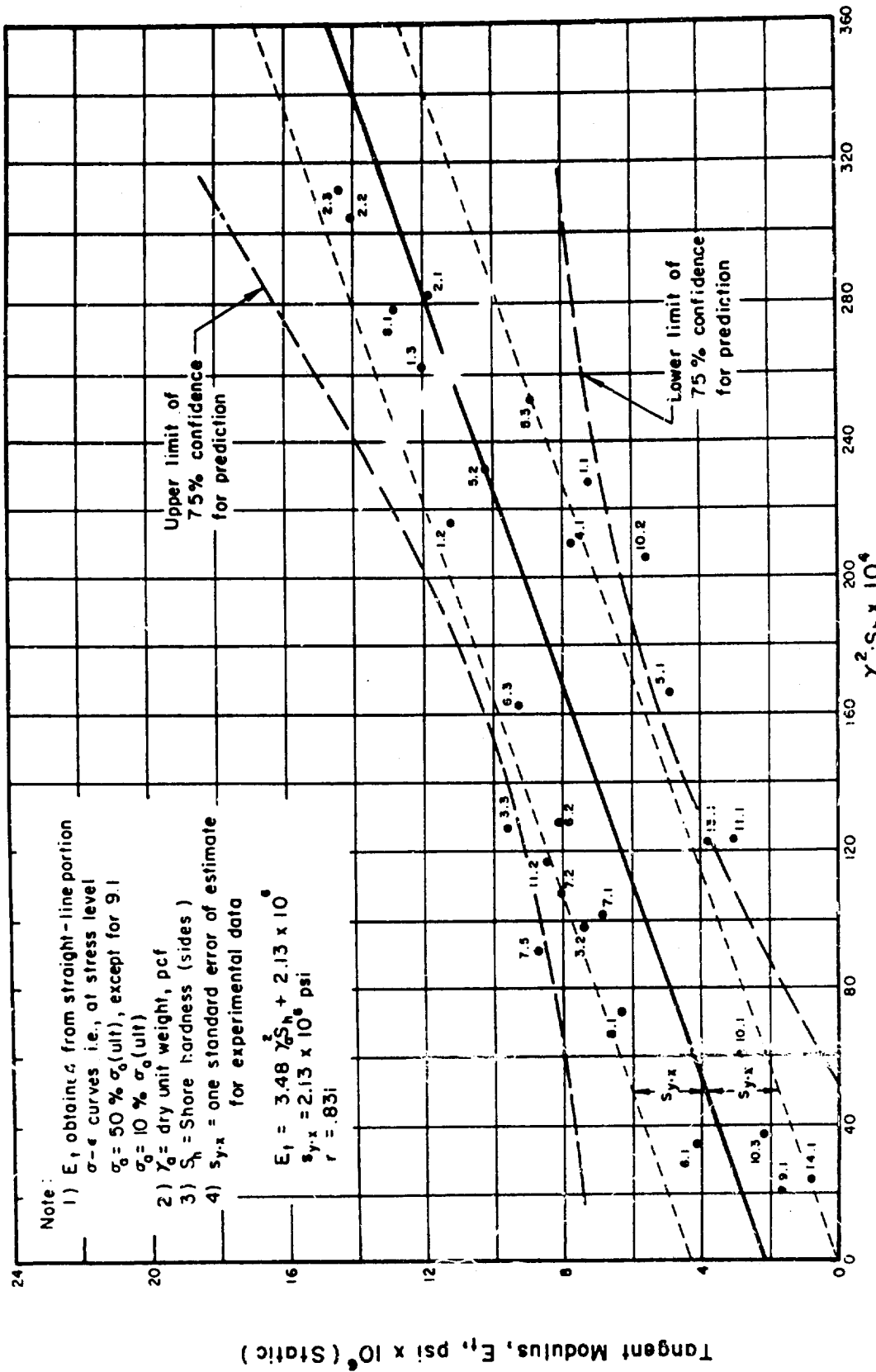


FIGURE 6.29 RELATIONSHIP BETWEEN AVERAGE VALUES OF  $\gamma_c^2 S_h$  AND TANGENT MODULUS OF DEFORMATION AT STRESS LEVEL OF ONE-HALF ULTIMATE STRENGTH FOR ROCK IN UNIAXIAL COMPRESSION

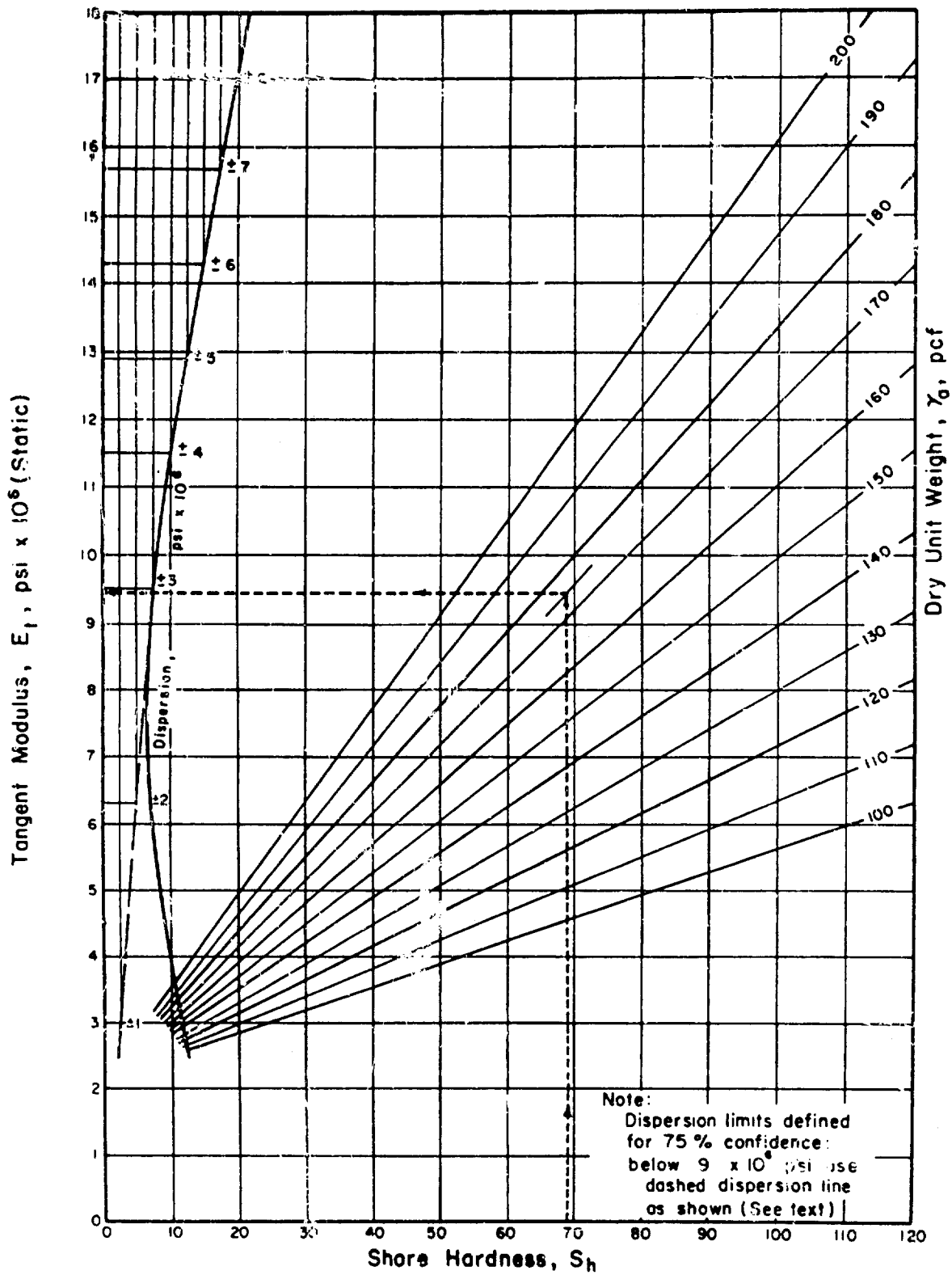


FIGURE 6.30 ROCK MODULUS CHART BASED ON SHORE HARDNESS

equation, given in Figure 6.29, provides the mathematical basis of the chart. In estimating the tangent modulus for Dworshak gneiss (4.1), the chart is entered at  $S_h = 69$ . By following the short-dashed line up to  $\gamma_a = 175$ , then left horizontally,  $E_t$  equals approximately  $9.4 \times 10^6$  psi ( $\pm 3 \times 10^6$ ). This is comparable to the measured modulus of  $7.8 \times 10^6$  psi and to the modulus predicted by the Schmidt hardness of  $9.1 \times 10^6$  psi ( $\pm 2.4 \times 10^6$ ).

Just as for the chart based on Schmidt hardness, the statistical dispersion is shown by the curved line on the left of the chart for Shore hardness, Figure 6.30. Again, for this chart, below  $E_t = 9 \times 10^6$  psi, it is suggested that the dispersion be estimated from the dashed line extending down toward the origin, rather than from the statistical, curving line.

The rock modulus chart, as shown in Figure 6.30 implies that the tangent modulus for rocks having low modulus values may not be evaluated by the Shore hardness. This is apparent for tuff (14.1) and rock salt (9.1). Again, this is due to a strict adherence to the statistical, regression line of Figure 6.29, which apparently does not properly represent the lower-modulus rocks. Such rocks may need to be separately analyzed in order to obtain a more representative correlation among the engineering properties of the rocks and the Shore scleroscope.

## 7. SONIC VELOCITY AS AN INDEX OF DEFORMATION

A comparison of the static and dynamic properties for rock has been presented in Section Five. Figures 5.22 through 5.27 show various relationships between dynamic properties based on some function of sonic velocity, and static deformation properties of rock. In all cases, the correlation is quite good and the relationships are fairly well defined. Thus, it appears to be logical to utilize the sonic pulse velocity as an index for static modulus of deformation.

The sonic velocity has excellent reproducibility as indicated by the small coefficient of variation in Table 5.1 ( $V\% = 1.9$ ). Because of the necessary preparation of the specimen, and the specialized nature and cost of the laboratory equipment, the sonic velocity at the present time does not fully meet the criteria for an index property, as given previously. However, because numerous rock laboratories are equipped to measure sonic pulse velocity, and because of its relationship with static modulus, a rock modulus chart based upon sonic velocity is included herein.

The relationship between sonic pulse velocity and tangent modulus at 50% ultimate strength was given in Figure 5.18, in which  $r = .860$  for the linear regression line shown therein. The data, in accord with theory, indicate that a curvilinear relationship would provide a better fit. Again, a linear relationship was shown in Figure 5.23 between the constrained modulus (a function of  $\gamma_a v_p^2$ ) and  $E_t$ , for which the correlation coefficient,  $r = .901$ . Finally, in Figure 6.31 a plot of  $\gamma_a v_p$  in relation with  $E_t$  is shown, in which a curvilinear relationship provides the best fit of the data.

The data shown in Figure 6.31 are given in the semi-logarithmic plot of Figure 6.32, in which  $r = .929$  for the linear regression line shown. One standard error of estimate is equal to  $.31 E_t$ , and is shown by the lighter,

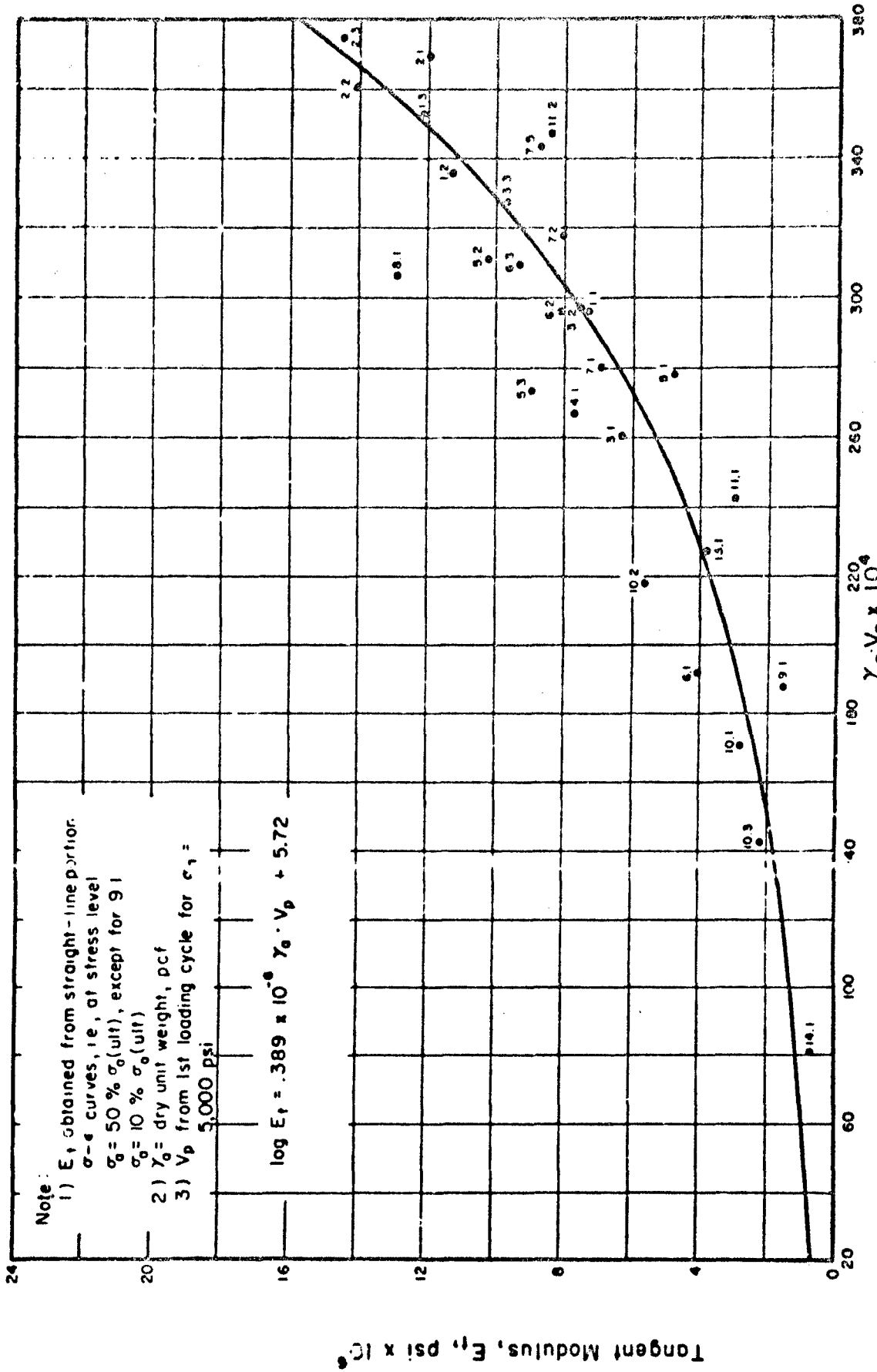


FIGURE 6.31 RELATIONSHIP BETWEEN AVERAGE VALUES OF  $\gamma_0 \cdot V_p$  AND TANGENT MODULUS OF DEFORMATION AT STRESS LEVEL OF ONE-HALF ULTIMATE STRENGTH FOR ROCK IN UNIAXIAL COMPRESSION

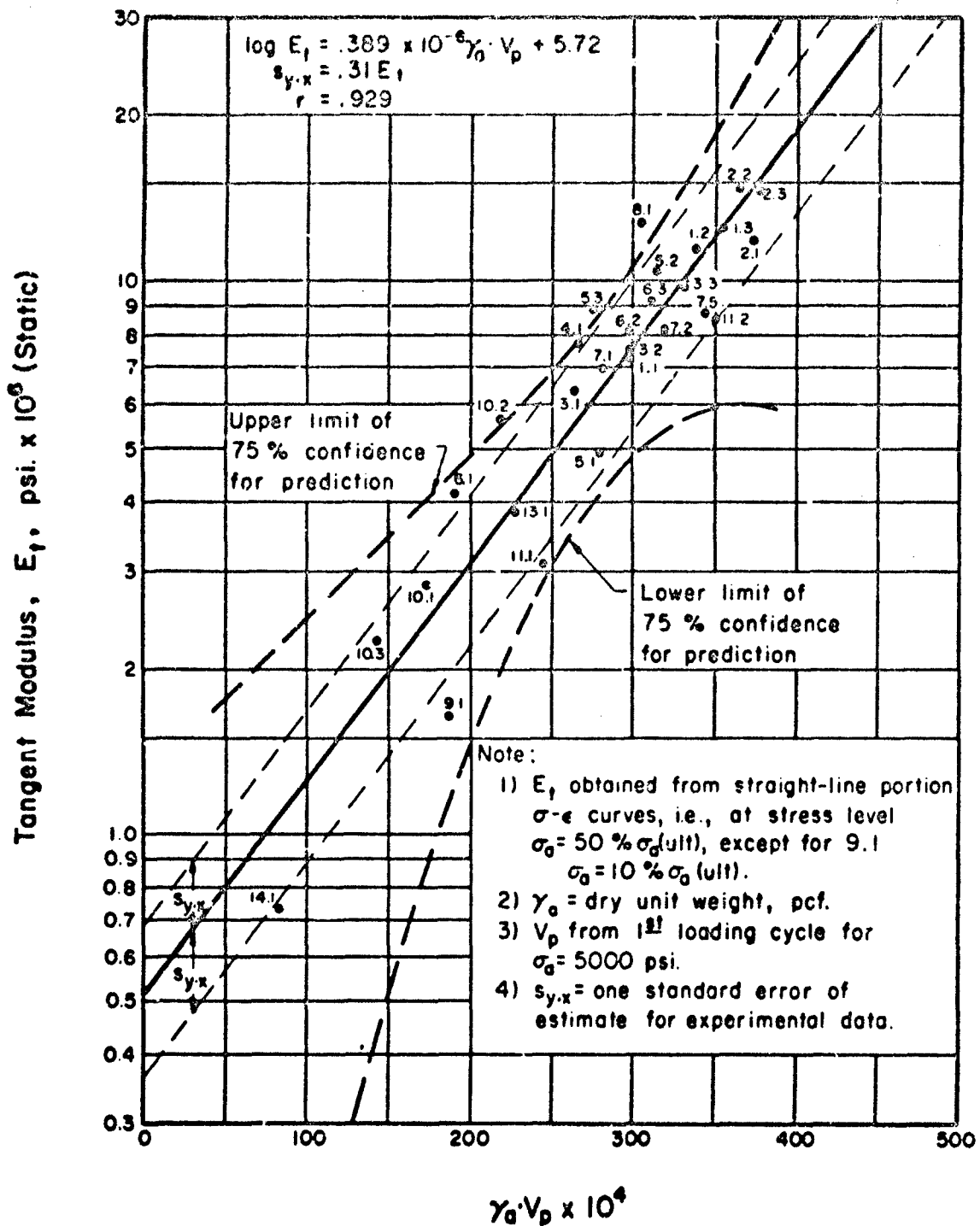


FIGURE 6.32 RELATIONSHIP BETWEEN AVERAGE VALUES OF  $\gamma_d \cdot V_p$  AND TANGENT MODULUS OF DEFORMATION AT STRESS LEVEL OF ONE-HALF ULTIMATE STRENGTH FOR ROCK IN UNIAXIAL COMPRESSION (SEMI-LOG PLOT)

short-dashed lines, parallel to the line of regression. The 75% confidence belt for prediction, as determined by equation (6.1), is also shown, and is noted to be similar in form to the semi-logarithmic plots for strength given in Figures 6.19 and 6.26.

A rock modulus chart based on dilatational wave (sonic pulse) velocity and unit weight is shown in Figure 6.33. This chart is used in the same manner as those for Schmidt and Shore hardness presented in Figures 6.23 and 6.30, respectively. It is based on the functional relation given in Figure 6.32, and requires only the dry unit weight and the sonic pulse velocity of the rock.

In estimating the tangent modulus at 50% ultimate strength for Dworshak gneiss (4.1), the chart is entered at  $V_p = 15,350$  fps (i.e., the velocity measured at a stress level of 5,000 psi). By following the short-dashed line up to  $\gamma_a = 175$ , then horizontally left,  $E_t$  is estimated to be  $5.8 \times 10^6$  psi ( $\pm 2 \times 10^6$ ). This is comparable to the measured  $E_t$  of  $7.8 \times 10^6$  psi at 50% ultimate strength.  $E_t$  predicted by Schmidt hardness is  $9.1 \times 10^6$  psi ( $\pm 2.4 \times 10^6$ ), and  $E_t$  predicted by Shore hardness is  $9.4 \times 10^6$  psi ( $\pm 3 \times 10^6$ ). It is interesting to note that the tangent modulus for Dworshak gneiss, when measured at the same stress level as the velocity (i.e., 5,000 psi instead of 50% ultimate), is  $5.2 \times 10^6$  psi, as given in Table 4.3.

Although the above discussion pertains to intact rock specimens tested in the laboratory, it is pertinent to observe that the seismic (dilatational wave) velocity measured in the field is one of the most economical procedures used in subsurface exploration. The relationships and charts, presented herein, for intact rock cannot presently be utilized for field evaluation in connection with seismic exploration. However, at such time as the influence of geological discontinuities on rock-mass behavior can be properly evaluated, the seismic velocity (which is related to the sonic pulse velocity) will then likely prove to be an important, economical index of rock-deformation characteristics.



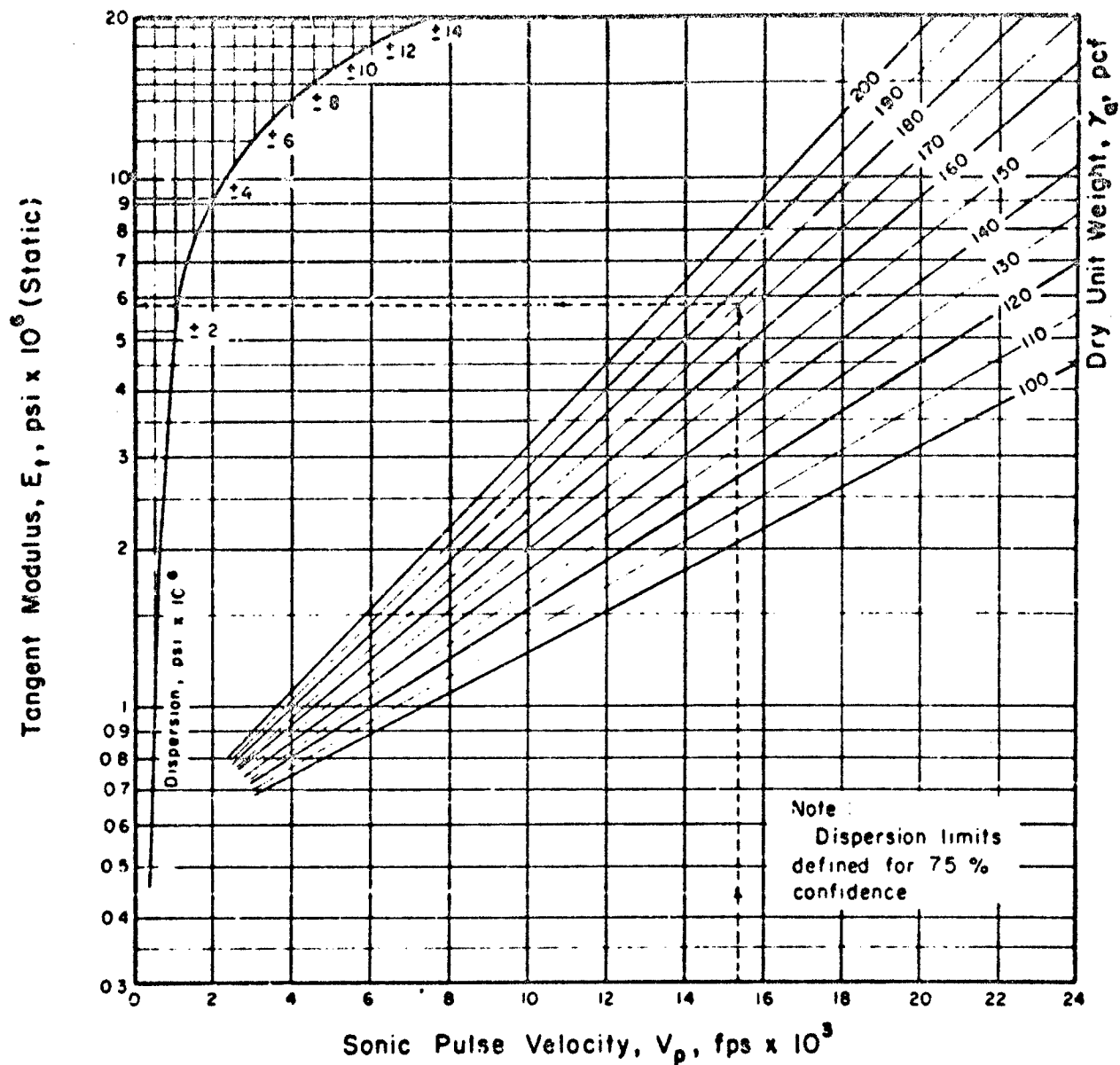


FIGURE 6.33 ROCK MODULUS CHART BASED ON DILATATIONAL WAVE VELOCITY

## SECTION 7

### SUMMARY AND CONCLUSIONS

An experimental investigation has been conducted with the objective of developing an engineering classification system for intact rock and a related set of index properties. This study has not dealt with the characteristics of the in-situ rock mass with its inherent discontinuities. Rocks from 27 localities, representing the following 13 geological rock types were studied: basalt, diabase, dolomite, gneiss, granite, limestone, marble, quartzite, rock salt, sandstone, schist, siltstone, and tuff. Laboratory tests were conducted on NX-size cylindrical core specimens of these rocks in order to determine the following ten physical and elastic properties: unit weight, uniaxial compressive strength, Shore scleroscope hardness, Schmidt hammer hardness, abrasion hardness, absorption, point-load tensile strength, Young's modulus, Poisson's ratio, and sonic pulse (dilatational wave) velocity. A total of 257 rock specimens, all having L/D ratios of 2:1 were tested in this investigation.

All tests were conducted on specimens which were initially oven-dried, then allowed to remain in the ambient air of the laboratory for at least two weeks prior to testing. The following nondestructive tests were performed on all specimens: dry unit weight, Shore hardness, and sonic pulse velocity under a uniaxial seating load of 100-150 psi. Approximately one-half of the specimens from each rock group were subjected to sonic velocity and stress-strain measurements while undergoing two complete static-loading cycles up to 5,000 psi uniaxial compression. These specimens were then loaded to failure on the third cycle, during which stress and strain measurements only were obtained. The other one-half of the specimens were subjected to Schmidt-hardness tests, and then were tested for determination of abrasion hardness, absorption, and point-load tensile strength.

The test results for each group of specimens were subjected to statistical analyses in order to obtain average values and coefficients of variation, and to determine the number of replications required for every property of each rock group included in the investigation. The average data for each rock-group property were subjected to statistical correlation and regression analyses from which the least-squares regression lines, simple correlation coefficients, standard errors of estimate, and functional relationships were determined for selected pairs of variables. These relationships were presented graphically for visual comparison with the corresponding test data. All data reduction and statistical analyses were performed with the aid of the IBM 7094 electronic computer.

Static and dynamic properties for the rocks in this investigation were compared on the basis of the theoretical equations for the constrained modulus of deformation. The constrained moduli values were computed dynamically as a function of the sonic pulse velocity, and statically as a function of Young's modulus and Poisson's ratio from static stress-strain measurements.

A system of engineering classification has been proposed in which intact rock may be classified in terms of its strength and deformation characteristics. With this system rocks can be classified by either determining the strength and modulus of elasticity in actual laboratory tests or by using the approximate values from the index property charts. Five charts have been presented from which the strength and modulus values may be estimated. The charts have as their bases the numerical indices obtained by either the Schmidt hammer, the Shore scleroscope, or the sonic pulse velocity, each used in conjunction with a fourth index property, the unit weight of the rock. The charts also provide an indication of dispersion of the strength and modulus values, based on the 75% confidence interval determined by statistical analysis.

## 2. CONCLUSIONS

The more important conclusions and pertinent observations drawn as a result of this research study are summarized in the following paragraphs:

- i) An engineering classification for intact rock has been developed which is based on the compressive strength and modulus of elasticity -- two important physical properties of rock that enter into many engineering problems. The classification is considered a workable and useful system. It is sensitive to the mineralogy, textural fabric, and direction of anisotropy of the rock so that specific rock types fall within certain areas on the classification plot. (See summary plots for igneous rocks, sedimentary rocks, and metamorphic rocks in Figures 6.4, 6.8 and 6.13, respectively.) In the proposed system a rock is classified on the basis of its unconfined compressive strengths into one of 5 categories: Class A - Very High Strength (greater than 32,000 psi); Class B - High Strength (16,000-32,000 psi); Class C - Medium Strength (8,000-16,000 psi); Class D - Low Strength (4,000-8,000 psi); and Class E - Very Low Strength (less than 4,000 psi). The rock is further classified on the basis of its modulus ratio (defined as the tangent modulus at 50% ultimate strength divided by the uniaxial compressive strength) into one of three categories: Class H - High Modulus Ratio (greater than 500); Class L - Low Modulus Ratio (less than 200); and Average Modulus Ratio (between 200 and 500) which carries no letter designation. Thus, a rock may be classified as BH, BL, B, et cetera.
- ii) The results of this investigation verify that meaningful index properties may be determined for rocks. Usefulness of these properties to engineering classification is indicated by (a) their relationship to material properties which are used in design (modulus of elasticity and unconfined compressive strength), (b) their simplicity, low cost, and rapidity of determination, and (c) their reproducibility. The Schmidt hammer hardness together with the unit weight show the greatest promise for use as indices of the strength and modulus properties for intact rock. Again, when used together with the unit

weight, the Shore hardness is an index for the strength and modulus properties, but it has a lower degree of correlation with either of these properties and is more limited to laboratory usage than the Schmidt hardness. The sonic velocity, also in conjunction with unit weight, is an index of static modulus. However, the sonic velocity apparently is not as good an index property as Schmidt and Shore hardness because it has higher statistical dispersion values. Further, it does not fully meet the requirements for an index property because of the more costly, specialized nature of the laboratory equipment needed for its determination. It is more restricted in that it cannot be used directly as an index of compressive strength.

Several, interesting subsidiary observations have been noted during this investigation. Some of these observations have also been made previously by other investigators. These observations are briefly summarized as follows:

- i) In general, crystalline rocks have nonlinear stress-strain curves that are S-shaped. The curves are concave upward at low stresses, approximately linear at 50% ultimate strength, and concave downward as failure is approached. This behavior is more pronounced for the lower-strength, lower-modulus rocks, and is not so apparent for the higher-strength, higher-modulus rocks for which the stress-strain relation is nearly linear. The nonlinear elastic behavior of rocks under uniaxial compression is attributable to minute cracks which are open at low stresses and become closed as the stress is increased.
- ii) Most rocks under uniaxial compression exhibit an elastic hysteresis in their stress-strain curves during unloading. Because of friction, it has been suggested that cracks which have undergone sliding during compression do not immediately slide in the opposite sense when the load is reduced; thus, a clockwise loop is formed in the stress-strain curve as the stress is raised and then reduced to zero.
- iii) Sonic pulse velocity for rocks increases with increasing stress. This effect was noted to be most pronounced on those rocks which exhibited well-defined, S-shaped stress-strain curves. Both the increase in sonic velocity and the shape of the stress-strain curves are apparently due to closing of minute cracks under increasing stress. The greatest effect of stress increase was observed in schist (11.1). When the axial stress was increased from 115 psi to 5,000 psi,  $V_p$  increased by 132%. The smallest effect, for the same stress increase, was exhibited by Solenhofen limestone (6.3), for which  $V_p$  increased by less than 1/4%. When there is no pressure on the rock, open cracks (which are most predominant in schist) impede the progress of the sonic wave which must then travel around the cracks. The percentage increase in  $V_p$  for the majority of the rocks in the present investigation, was found to be less than 10% for a stress increase from 100 psi to 5,000 psi.

- iv) In order to obtain meaningful sonic velocity data from rocks, a relatively large stress must be applied in the direction of the wave propagation so that a terminal velocity is approached. For most rocks in this investigation the greatest increase in velocity took place within the first 1,000 psi axial stress. In nearly all cases, a terminal velocity appeared to be approached at 5,000 psi. However, no measurements were made above 5,000 psi.
- v) In general, rocks which have initial modulus values  $E_i$  of less than  $9 \times 10^6$  psi and sonic velocities  $V_p$  of less than 16,000 fps have stress-strain curves which are initially concave upward. Also, such rocks exhibit relatively large increases in both modulus and sonic velocity when the stress is raised from 100 psi to 5,000 psi. In such cases the initial modulus is lower than the tangent modulus at 50% ultimate strength. On the other hand, rocks for which  $E_i$  is greater than  $9 \times 10^6$  psi and  $V_p$  is greater than 16,000 fps show very little increase in velocity and, in general, show a decrease in modulus as the stress is increased to 5,000 psi. The latter have stress-strain curves which are initially linear, or slightly convex upward and, therefore, may have somewhat higher initial modulus values than the tangent modulus at 50% ultimate strength.
- vi) The values of dynamic and static properties of rocks are equal only for compact rocks at low stresses. At high stress levels (i.e., 5,000 psi) the values of dynamic properties are 10-20% greater than static properties for compact rocks. For less compact rocks, the magnitude of the dynamic properties may be 100% greater than the static properties at low stress levels, but the difference between them decreases with increasing stress. However, it has been suggested that these lower-modulus rocks apparently are not sufficiently homogeneous and isotropic to meet the conditions for which the formulas from elastic theory were derived.
- vii) The propagation velocity of dilatational waves in rock tends to approach a lower limiting value regardless of the stress level to which the rock is subjected (within the range of stress investigated herein). This observation is probably a function of the structure of rock, the degree of cementation, grain contact, et cetera. The lower limiting velocity observed herein is approximately 6,600 fps for the average density of 162 pcf for all rocks in this investigation.
- viii) The influence of anisotropy on sonic velocity decreases with increasing stress level for the Luther Falls schist (11.1 and 11.2). The ratio of  $V_p$  in the direction of foliation to  $V_p$  perpendicular to foliation is 3.1:1 at a stress level of 110 psi, but only 1.4:1 at a stress level of 5,000 psi. Since this effect was not studied for any of the other rocks in this investigation, no general statement regarding the effects of anisotropy can be made.

- ix) In general, oven-drying rock at 100°C., causes a decrease in sonic velocity of less than 2%. Two exceptions which were noted are dolomite (3.2), for which the magnitude of the velocity decreased by 8.5%, and marble (7.2), for which the velocity decreased by 21.6%. The latter is probably related to the very large grain size, and corresponding nonuniform expansion and contraction.
- x) Negative values of Poisson's ratio were consistently observed for two marbles (7.1 and 7.2) and schist (11.1) at low-stress levels (i.e., approximately 1,000 psi). The physical concept of this is not completely understood although it appears to be related to the closing of microcracks in the axial direction without an attendant lateral expansion of the sample. Only those samples with pronounced S-shaped stress-strain curves exhibited this phenomenon.

### 3. SUGGESTIONS FOR FURTHER RESEARCH

Several areas of additional research are suggested. Some of these are the natural outgrowth and continuation of the present investigation; others are the result of miscellaneous observations made during the course of the investigation. These are commented on in the following paragraphs:

- i) Additional tests should be made on almost all rock types to obtain more data points (tangent modulus and compressive strength) for the rock classification charts of Figures 6.4 to 6.17. With more points it will be possible to draw more meaningful envelopes for each rock type (i.e., the bounding envelope which includes 75% of the points).
- ii) Additional testing of numerous samples of all rock types should be carried out in which the index properties (Schmidt hammer hardness, Shore hardness, sonic pulse velocity, and dry unit weight) are determined as well as the unconfined compressive strengths and tangent moduli at 50% ultimate strength. The new data points when plotted on the corresponding index property charts of Figures 6.19, 6.22, 6.26, 6.29, and 6.32 would aid in verifying or modifying the regression curves and may increase the level of significance.
- iii) As more data points for a particular rock type become available it would appear worthwhile to construct individual index property charts for that rock type. The regression curves and significance level should prove to be enhanced when working with a plot of only one rock type versus a plot which contains all rock types as is currently being presented. It is recognized that a considerable amount of testing will have to be done before enough data become available for constructing these individual plots.
- iv) Detailed investigation of the index property relationships of the Class D and Class E rocks is desirable as the data for these

lower strength rocks are sparse. The shales in particular warrant more study.

- v) The data obtained in the present study did not permit final conclusions to be drawn with respect to the textural classification suggested by Deere (1963b). As additional test data become available, his proposed textural grouping, i.e., interlocking, cemented, laminated-foliated, may allow for more consistent interrelationships among the physical rock properties than when the rocks are undifferentiated.
- vi) Because of the qualitative use presently made of the abrasive properties of rock in classifying exploration drill core (i.e., its response to scratching with a knife), and because of the quantitative relationships between abrasive and strength properties as shown in the present study, special investigations directed toward the development of a portable, abrasive-hardness indicator should prove to be worthwhile.
- vii) The development of a re-usable crystal transducer which will provide for measurement of shear-wave velocities under variable stress conditions continues to be a requirement for better understanding of the relationship between static and dynamic properties of rocks.
- viii) The effects of moisture and of anisotropy on the behavior of the intact rock materials should be studied further. Both unconfined and triaxial compression tests should be conducted at various rates of loading and different conditions of drainage.
- ix) As frequently reiterated, a universal engineering classification system for rock in-situ must include an indication of the influence of the geological discontinuities. Thus, in order to extend the system as developed herein to the in-situ rock mass, a method of classifying the rock in accordance with the number and type of geological discontinuities must be developed. Such a continuing study would be a natural outgrowth of the present investigation. Its successful completion would allow realistic estimates to be made of the expected engineering behavior of an in-situ rock mass solely on the basis of the rock quality classification.

APPENDIX A  
PETROGRAPHIC DESCRIPTIONS  
AND  
THIN-SECTION PHOTOMICROGRAPHS



1.1 Basalt (Lower Granite), Pullman, Washington

This rock consists of 48% plagioclase ( $An_{41}$ ), 16% olivine, 18% augite, 11% glass, 6% magnetite, and 1% apatite and sphene. Corroded olivine granules (0.003 to 0.02 mm.) rimmed with dusty magnetite particles are contained within an intergranular matrix of plagioclase laths, (up to 0.07 mm. in length) intersertal glass, and augite. Some zoned plagioclase crystals have grown to lengths of 0.5 mm. thus imparting a porphyritic texture to the rock. Euhedral to corroded subhedral crystals of magnetite are scattered throughout the section. The glass, brown with upper nicols out, is in places partially devitrified to radial growths of acicular crystals.



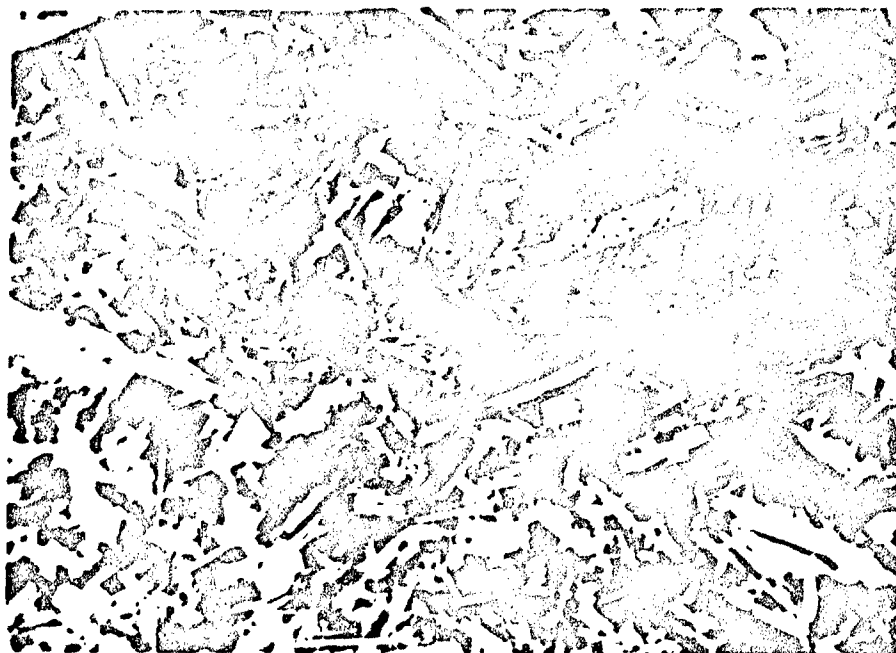
25X - Nicols crossed

1 mm.

Black crystals of magnetite and laths of plagioclase (white) with intergranular olivine and augite.

## 1.2 Basalt (Little Goose), Walla Walla, Washington

This basalt shows a hyalophitic texture in which olivine (26%), augite (5%), laths of plagioclase (41%), and euhedral to subhedral grains of titaniferous magnetite (4%) lie in a matrix of dark green, probably iron-rich, glass (25%). The average crystal size for augite and plagioclase is 0.2 mm., although several grains are as much as 2 mm. long imparting a porphyritic texture to the whole. The rock is essentially free of alteration products.



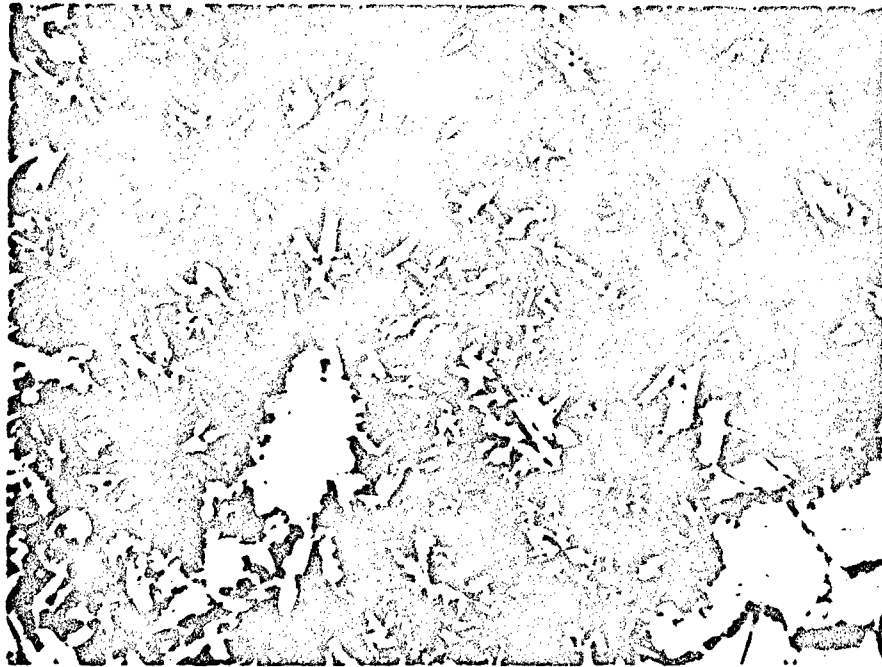
25X - Nicols crossed

1 mm.

Twinned plagioclase laths and augite crystals in a matrix of glass (black).

### 1.3 Basalt (John Day), Arlington, Oregon

This rock contains subhedral phenocrysts of normal zoned plagioclase (up to 0.8 mm. long) in a groundmass of olivine (33%), glass (20%), titaniferous magnetite (7%), and laths of plagioclase  $An_{46}$  (total plagioclase is 40%). The groundmass minerals are from 0.2 mm. to 0.3 mm. long. Olivine is intersertal to the laths of randomly oriented plagioclase. All minerals are free of alteration products.



25X - Nicols crossed

1 mm.

Corroded phenocrysts of plagioclase lie in a fine groundmass of plagioclase, olivine, and glass (black).

## 2.1 Diabase (Palisades), West Nyack, New York

This rock contains 52% plagioclase ( $An_{51}$ ), 30% diopside, and 6% accessory magnetite and apatite (1%). Secondary minerals are epidote - sericite (3%) and chlorite (8%). The plagioclase laths have been altered to sericite which, in places, covers large patches of the section. Secondary chlorite borders many of the diopside grains or replaces them along cleavage directions. Small patches of micro-pegmatite are intersertal to the plagioclase laths.



25X - Nicols crossed



Randomly oriented laths of twinned plagioclase (heavily sericitized - left central portion) intersertal to diopside anhedra. Black patches are magnetite.

## 2.2 Diabase (Coggins), Culpeper, Virginia

A very fresh rock containing 47% plagioclase ( $An_{55}$ ), 51% diopside, 1% accessory biotite and less than 1% apatite and magnetite. Diopside crystals (0.5 to 4.0 mm.) are either intersertal to plagioclase laths or optically enclose them. Exsolution of orthopyroxene on the (001) planes can be seen on a few diopside grains. Widely scattered irregular blebs of magnetite and biotite are closely associated with diopside. Plagioclase exhibits multiple twinning and normal zoning.



25X - Nicols crossed

1 mm.

Twinned crystals of plagioclase intersertal to diopside.

### 2.3 Diabase (French Creek), St. Peters, Pennsylvania

The main constituents of this rock are plagioclase ( $An_{59}$ , 49%) and diopsidic-augite (40%). The only minor constituent is biotite (2%), in places altered to chlorite. Accessory magnetite (1%) is scattered throughout the section in grain sizes ranging from 0.2 to 0.8 mm, and is closely associated with the magnetite. The pyroxene grains (0.5 mm. to 7 mm. long) optically enclose plagioclase laths (up to 4 mm. long). The plagioclase laths have a random orientation.



25X - Nicols crossed

1 mm.

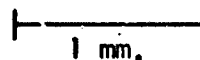
Twinned plagioclase laths optically enclosed by pyroxene (bottom right). Irregular patches of magnetite (black) are interstitial to pyroxene crystals.

### 3.1 Dolomite (Onago), Kasota, Minnesota

A mosaic of dolomite anhedral and rhombs ranging in size from 0.05 to 0.15 mm. The dolomite is clouded with opaque dust which, in some grains, has migrated to the boundaries.



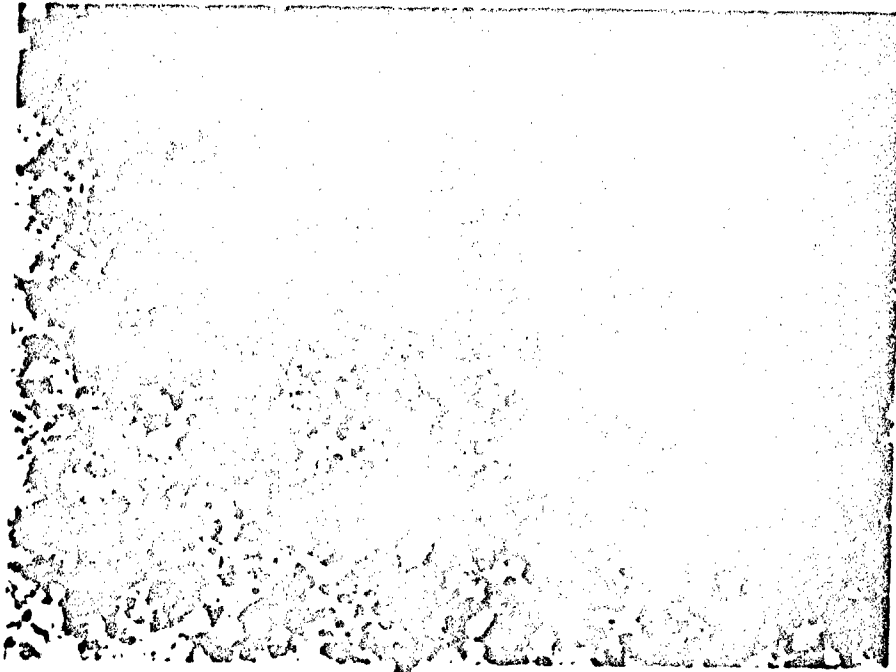
25X - Nicols crossed



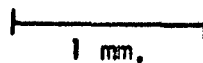
Mosaic intergrowth of dolomite grains.  
Small calcite vein at lower right corner.

3.2 Dolomite (Lockport), Niagara Falls, New York

An equigranular, non-porous rock in which rhombs and anhedral grains of dolomite (0.06 mm.) form an interlocking network. Fine opaque dust borders some grains.



25X - Nicols crossed



Interlocking mosaic of dolomite grains -- low porosity.  
(Large black areas are void spaces caused by grinding the thin-section)

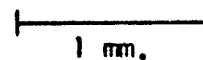


### 3.3 Dolomite (Bonne Terre), Bonne Terre, Missouri

An interlocking mosaic of dolomite fragments and rhombs ranging in size from 0.05 to 0.14 mm. A few rounded grains of quartz and microcline of equivalent size are scattered throughout. The section shows a continuous fracture filled with calcite.



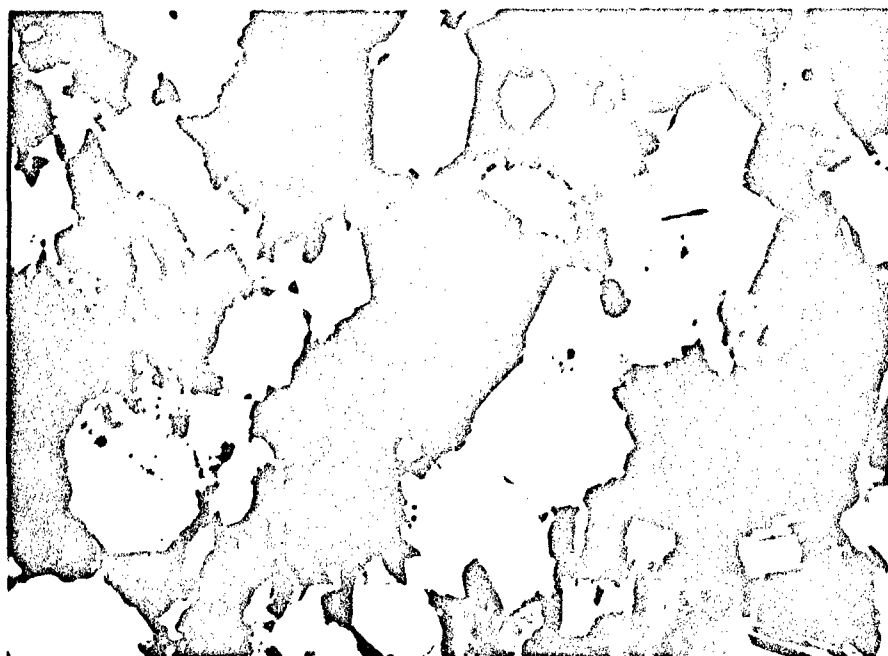
25X - Nicols crossed



Dolomite with narrow vein of calcite cutting across  
from top center towards bottom left.

#### 4.1 Gneiss (Dworshak), Orofino, Idaho

This rock is essentially composed of quartz, plagioclase, hornblende, and biotite, with minor amounts of accessory sphene, magnetite, apatite, and secondary white mica and epidote. The sphene, hornblende, and biotite are concentrated in discontinuous elongate patches. A few of the hornblende crystals have attained a length of 3 mm. Anhedral quartz and plagioclase grains (1.5 mm. in size) form an interlocking network between the dark minerals. Wispy patches of secondary white mica weave and flow through the quartzo-feldspathic layers and parallel the foliation.



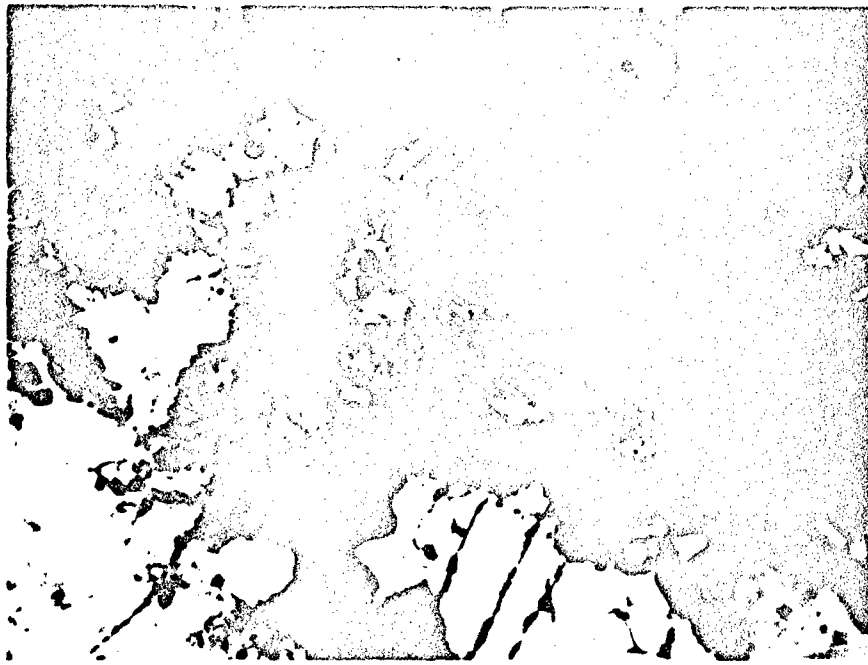
25X - Nicols crossed

1 mm.

Anhedral grains of quartz (white) and twinned plagioclase surrounding biotite flakes with their cleavage planes in the plane of foliation (top to bottom).

5.1 Granite (Pikes Peak), Colorado Springs, Colorado

A coarse-grained allotriomorphic-granular granite composed of albite microcline, quartz, and biotite. Myrmekitic intergrowths of quartz and plagioclase are common. Apatite, sphene (altering to leucoxene), magnetite, and zircon are accessory. Most of the feldspars show patches of secondary white mica. Some intergranular areas are filled with fine, angular quartzo-feldspathic material. These areas of possible recrystallization occur roughly along two different fracture planes which are characterized by discontinuous veinlets of quartz and small displacements in the minerals cut by the fractures.



25X - Nicols crossed

1 mm.

Sericitized microcline (upper right), fractured quartz (bottom center), and biotite (center). Note the two intersecting veinlets of quartz.

## 5.2 Granite (Pikes Peak), Colorado Springs, Colorado

This section shows large areas of recrystallization and is cut by patches and veinlets of calcite. Plagioclase feldspar ( $An_9$ , 11%), is much more altered to sericite than microcline (35%). Perthite grains (12%) are essentially free of alteration. Quartz (27%) is present as large grains (up to 3 mm.), or in patches where it has been recrystallized into grains of 0.5 mm. Dark brown biotite is intersertal to the quartz and feldspar. Some flakes have been bent during stress and others are altered in part to chlorite along cleavages. Large crystals of sphene (2.7 mm. long), titaniferous magnetite (1%), and apatite are accessory.



25X - Nicols crossed

1 mm.

Twinned sericitized plagioclase crystals (left side),  
quartz, and sericitized microcline (bottom right).

### 5.3 Granite (Barre), Barre, Vermont

The section shows the typical hypidiomorphic granular texture of granite. Brown biotite (7%), altering in places to penninite, contains small crystals of zircon. Quartz (29%) exhibits undulatory extinction and is interstitial to the subhedral grains of plagioclase ( $An_7$ , 15%), orthoclase, and microcline (36% combined). Perthitic intergrowths of microcline and plagioclase make up 9% of the rock. Muscovite (4%) has developed in cleavage planes, or as irregular masses on the orthoclase. Accessory apatite, zircon, and magnetite, make up less than 1% of the total.



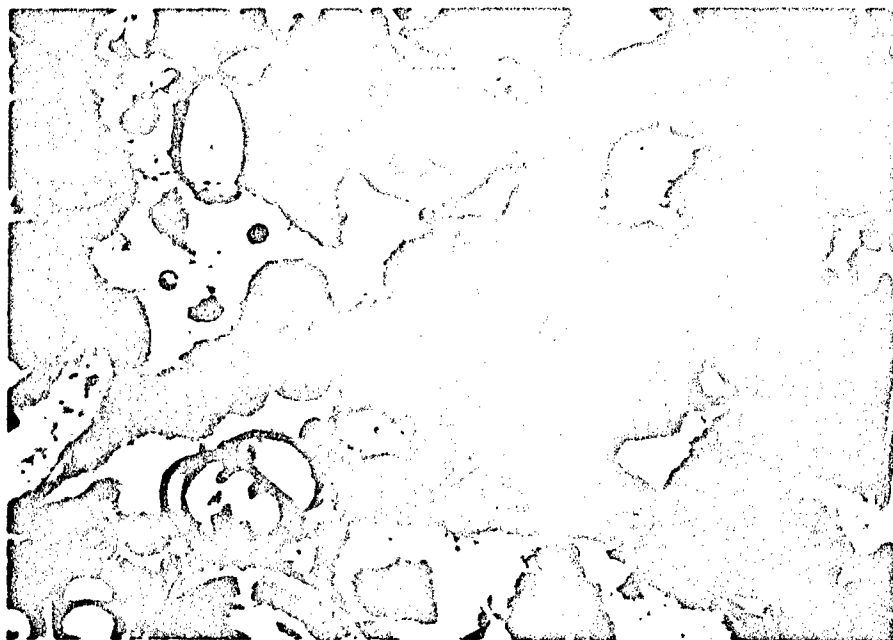
25X - Nicols crossed

1 mm.

Microcline (cross-hatched twinning - central portion of photo), biotite (center top), quartz (extreme left), and orthoclase with secondary white mica (right) in a hypidiomorphic granular granite.

## 6.1 Limestone (Bedford), Bedford, Indiana

A fossiliferous limestone in which foram tests (up to 0.86 mm. in diam.), brachiopod shells, fragments of bryozoans, ostracods, and oolites of carbonate material (1 mm. in diam.) lie in a cement of optically continuous calcite.



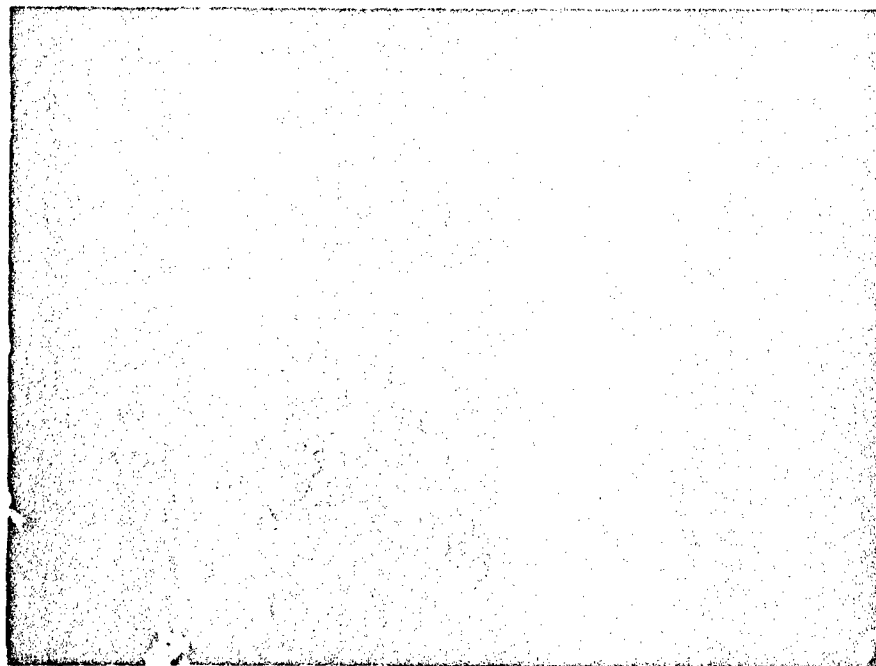
25X - Upper Nicol out



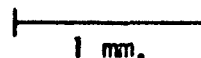
Fossiliferous limestone. Clear patches represent areas where calcite cement was worn away during grinding. Small dark circles are bubbles in the mounting media.

6.2 Limestone (Ozark Tavernelle), Carthage, Missouri

An oolitic limestone with oolites, up to 0.6 mm. in diameter, of microcrystalline calcite with small subangular detrital quartz grains, or shell fragments at the centers. Other shell fragments and fossiliferous matter, varying in size from 0.14 to 1.2 cm, are firmly cemented by a matrix of fine-grained calcite having a somewhat variable grain size.



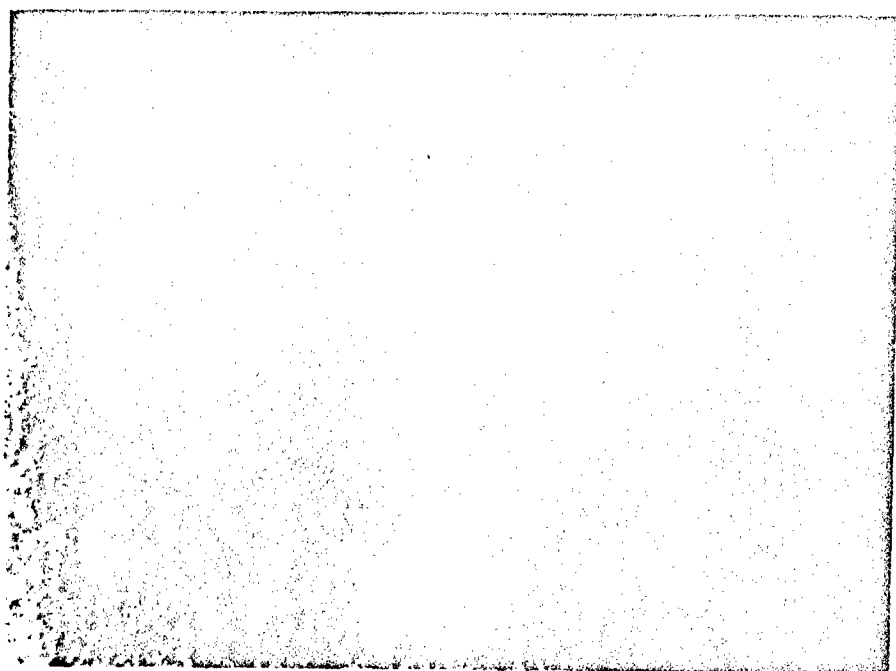
25X - Upper Nicol out



Oolites (center) and shell fragments in  
a fine calcite cement.

### 6.3 Limestone (Solenhofen), Solenhofen, Bavaria

An extremely fine-grained rock consisting of minute carbonate crystals which impart a turbid appearance to the section. The only discernable variations are lighter, more coarse-grained, slightly elongate patches of calcite (up to 0.4 mm. long). Faint bedding traces are evident (see photo).



25X - Upper Nicol out



Extremely fine-grained calcite groundmass in which lie larger calcite grains and opaque minerals. Faint bedding planes (top to bottom) are evident.

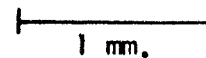


7.1 Marble (Tascenic White), West Rutland, Vermont

An extremely pure calcite marble having a tightly interlocking mosaic texture. Grain size varies from 0.02 mm. to 0.1 mm.



25X - Nicols crossed



Calcite anhedral of variable grain size in a tightly interlocking mosaic. Cleavage and twinning (bottom center) evident on some grains. Dark circles are air bubbles trapped in mounting media.

7.2 Marble (Cherokee), Tate, Georgia

A coarse-grained calcite marble with interlocking calcite grains (2 mm.), some containing round quartz crystals.



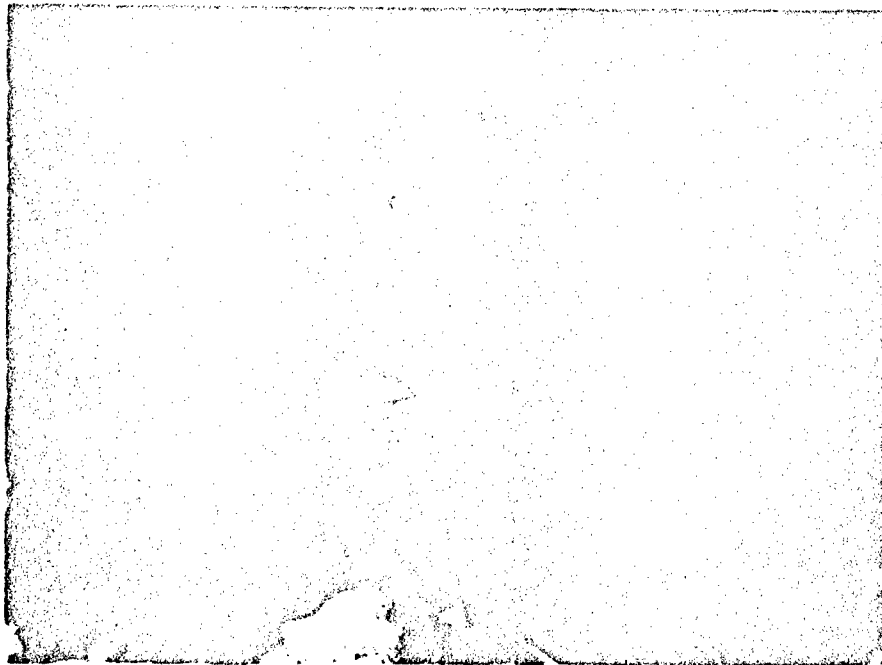
25X - Nicols crossed

1 mm.

Interlocking twinned calcite grains. Small quartz inclusions (black) "float" within the calcite (upper left).

**7.5 Marble (Imperial Quarry), West Rutland, Vermont**

An inequigranular mosaic of calcite anheda in which "float" small (0.07 mm.) rounded grains of quartz and plagioclase.



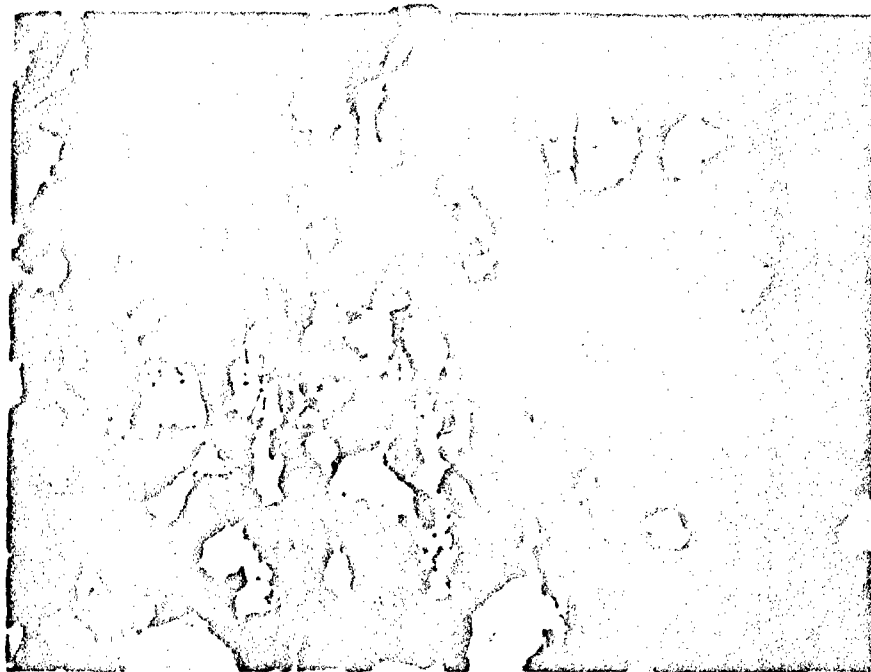
25X - Nicols crossed



Calcite grains showing rhombohedral  
cleavage and twinning.

## 8.1 Quartzite (Paraboo), Paraboo, Wisconsin

A highly pure quartzose rock in which quartz grains ranging in size from 0.15 to 0.85 mm. show parallel elongation. The grains have been pressure welded together in a tightly interlocking mosaic pattern. Most grains show undulatory extinction. Small wisps and patches of white mica lie between some grain boundaries. Small particles of iron oxide are distributed throughout.



25X - Nicols crossed

1 mm.

Elongate grains of quartz welded together to form a mosaic pattern. A few shreds of mica are seen in the top left section of the photograph. Grains are elongated in a direction from top to bottom.

9.1 Rock Salt (Diamond Crystal), Jefferson Island, Louisiana

A very coarse-grained mosaic intergrowth of halite crystals varying from 1/4 in. to 1/2 in. long. All grains contain inclusions of anhydrite ranging in size from 0.05 to 0.8 mm. These are the only two minerals present in this section.



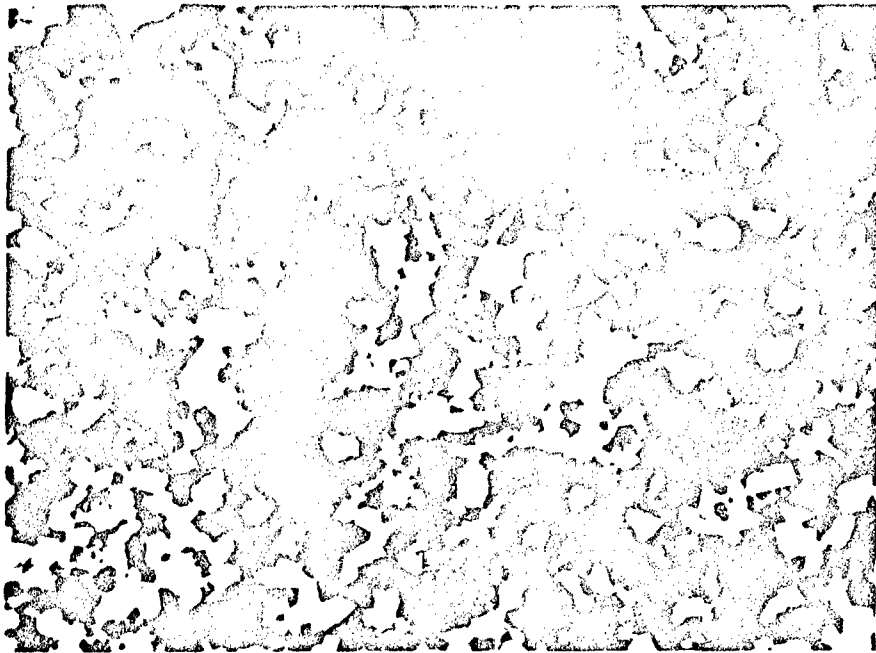
3X

H  
1 mm.

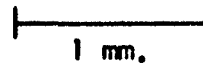
Above is close-up photography of core specimen. Photomicrograph of thin section was essentially "blank" because of very large crystals.

10.1 Sandstone (Dove), Ashurst, Ohio

This rock consists of tightly packed subangular grains of quartz, and small amounts of plagioclase and microcline all having a well sorted average grain size of 0.15 to 0.2 mm. Secondary quartz growth serves as the predominant cementing material; however, in places, a fine-grained calcite cement holds the detrital quartz grains in place.



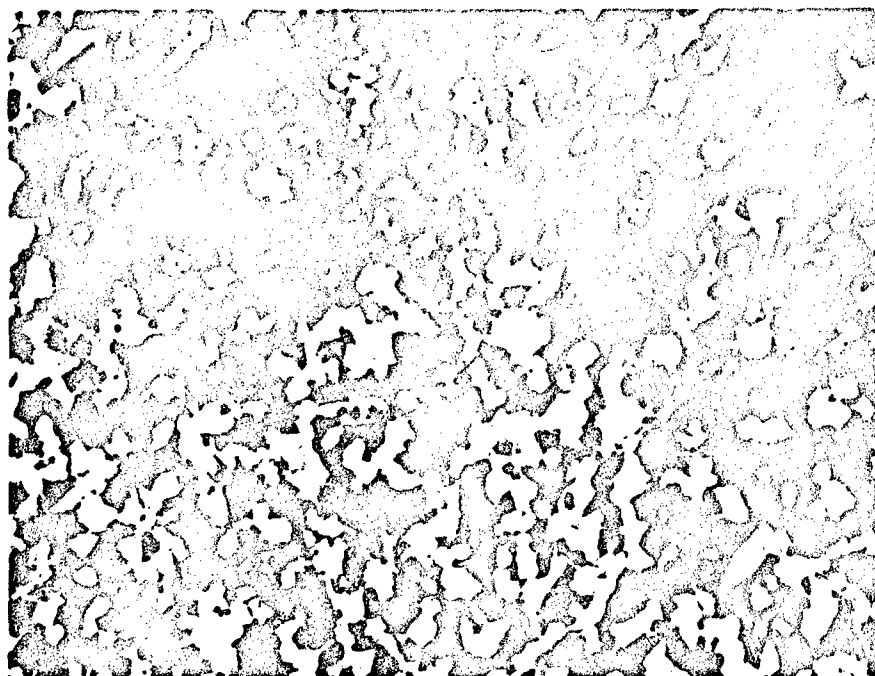
25X - Nicols crossed



Even-grained quartz fragments in  
fine-grained calcite cement.

10.2 Sandstone (Crab Orchard), Crossville, Tennessee

This section shows a tightly interlocking, welded mosaic of detrital quartz grains (0.1 mm). There is no authigenic cement, but a concentration of carbonate or opaque material along some grain boundaries. The grains tend to lie with their long axis parallel to the bedding planes. Flakes of muscovite are scattered throughout the section.



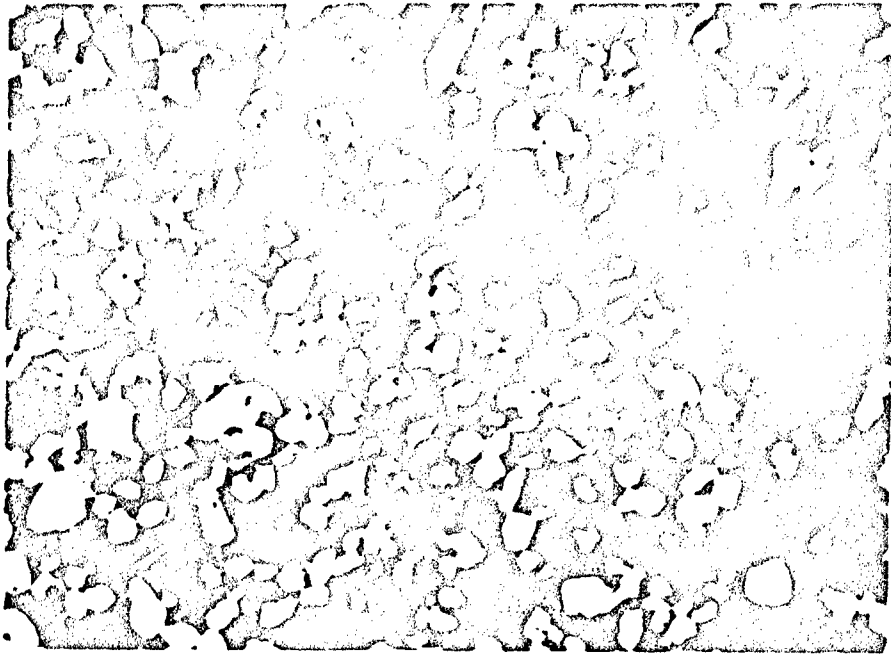
25X - Nicols crossed



Mosaic intergrowth of quartz grains  
in a low porosity sandstone.

10.3 Sandstone (Navajo), Glen Canyon, Arizona

This rock is composed of well-sorted, subrounded quartz grains and minor amounts of microcline and plagioclase. The grains vary in size from 0.07 to 0.26 mm. There is very little authigenic cement except for some hematite and silica and, as a consequence, the rock has much open pore space.



25X - Nicols crossed



Quartz grains of varying size, some with inclusions of opaque iron oxides, loosely packed together in a porous aggregate



### 11.1 & 11.2 Schist (Luther Falls), Unknown Origin

An extremely crenulated quartz-mica-garnet schist with minor amounts of tourmaline, staurolite, sillimanite, zircon, and magnetite. The major constituent, quartz, is present as an even-grained (0.4 mm.) interlocking matrix in which folia of biotite and muscovite are scattered. The biotite contains small crystals of zircon. Tourmaline, present as small euhedral grains (0.07 mm.), has a preferred orientation within the plane of schistosity. Small amounts of staurolite and sillimanite are scattered throughout the section. Euhedral garnet crystals, some up to 0.7 mm. in diameter, enclose small quartz grains, or have been partially replaced by magnetite along irregular fractures.



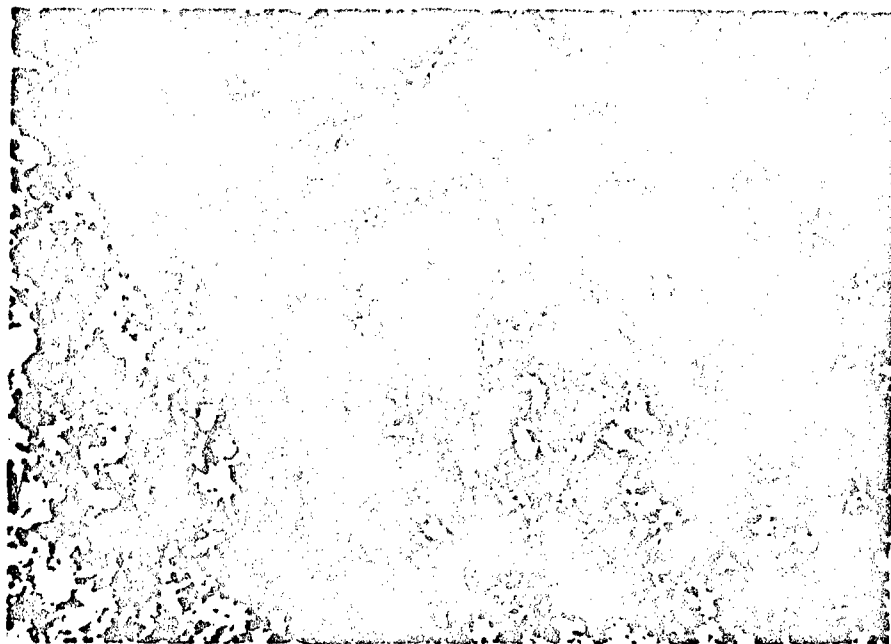
25X - Nicols crossed

1 mm.

Quartz (gray, black, and white) enclosing blades of mica and garnet (large nearly black crystals, upper left).

13.1 Siltstone (Hackensack), Hackensack, New Jersey

Angular detrital quartz and plagioclase grains (0.01 to 0.1 mm.) lie in a red, hematite-rich matrix, speckled with tiny flakes of clay minerals (?). Thin cleavage flakes of muscovite lie with their  $c$ -axis roughly perpendicular to the bedding planes. Irregular narrow veinlets of calcite traverse the section.



25X - Upper Nicol out



Dark to black areas are hematite which mark irregular bedding planes. Light patches are quartz. Elongate shred at top center of photo is muscovite.

#### 14.1 Tuff (NTS-E Tunnel), Mercury, Nevada

This tuff contains numerous fragments of welded pyroclastic material (up to 4 mm. in length) with elongate vesicles and partially devitrified spherulites. Some fragments of very fine-grained recrystallized quartz are laced with secondary white mica. Euhedral crystals and crystal chips of zoned plagioclase and quartz are scattered throughout. All are inclosed in a fine-grained dark, dusty, red matrix of devitrified glass and shards which are rimmed with black iron dust and small amounts of chlorite.

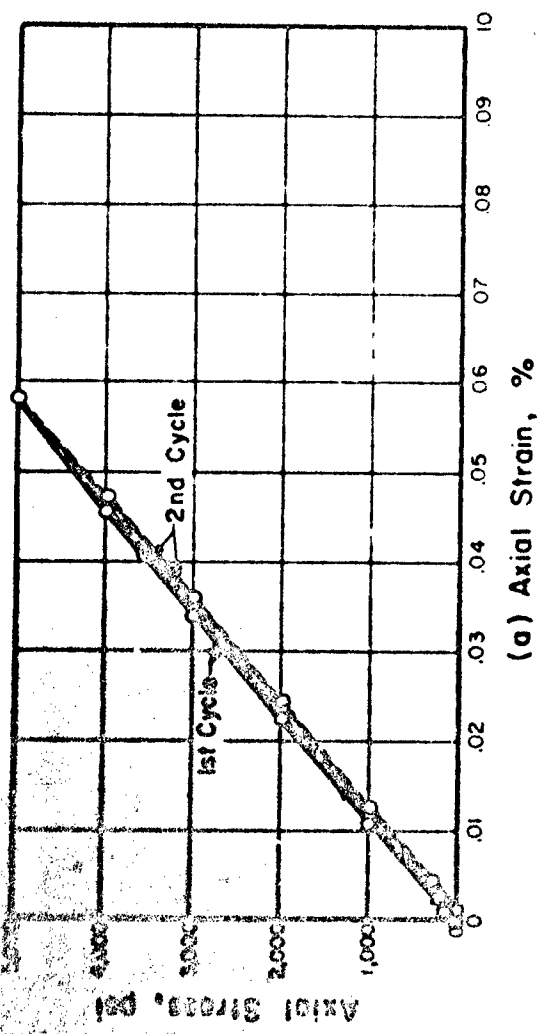


25X - Nicols crossed

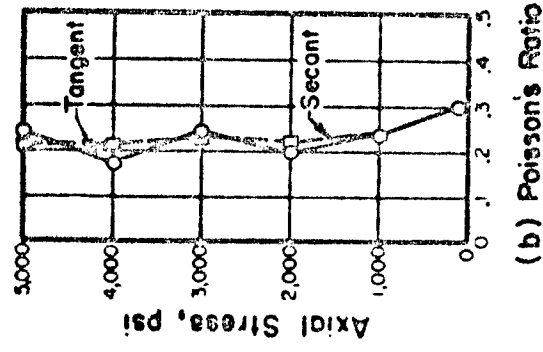
1 mm.

Chips of quartz (white), dark orbicular materials, and shards exemplify the vitroclastic character of this rock.

APPENDIX B  
TYPICAL TEST RESULTS



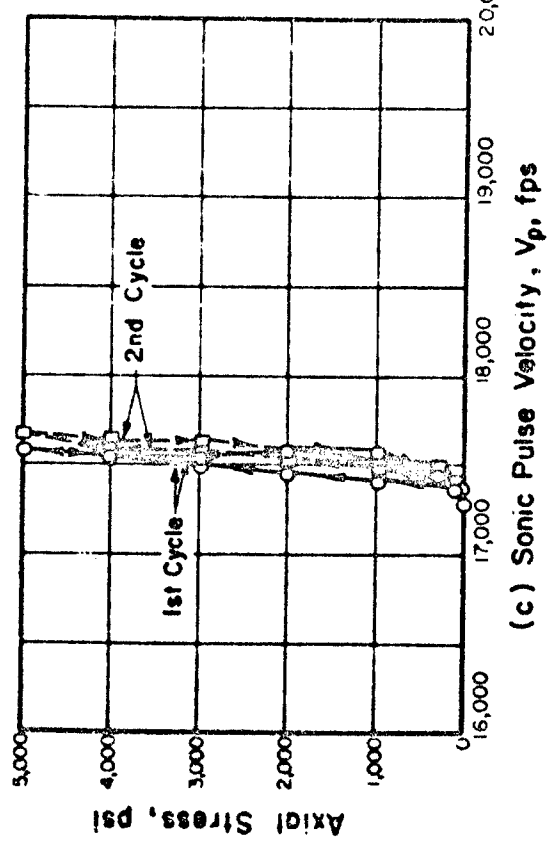
(a) Axial Strain, %



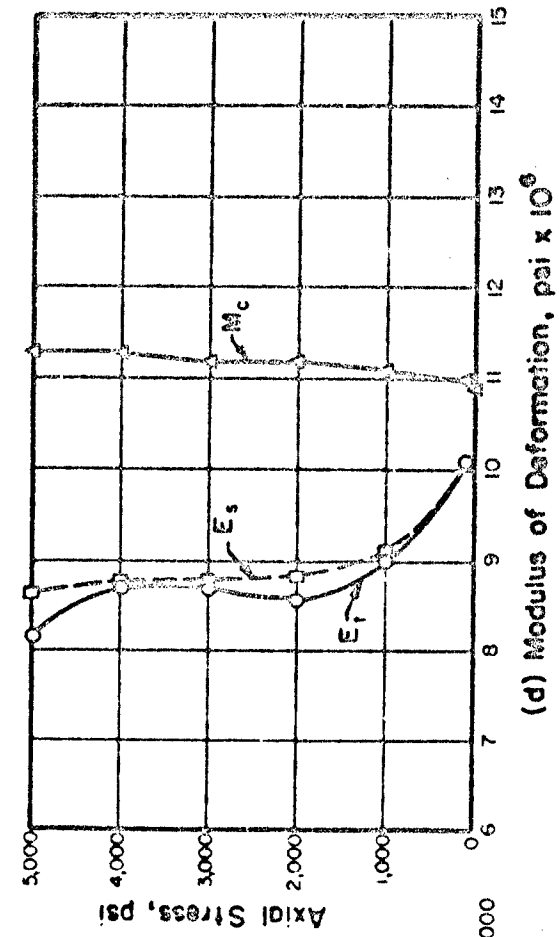
(b) Poisson's Ratio

Rock Type	Basalt
Specimen No.	II-(DH-14,19)
L/D	2.070
$\gamma_0$	170.0
$S_n$	95.4
$\sigma_0$ (ult)	32.4
Texture	Interlocking

Note:  
 1)  $V_p$  = Dilatational wave velocity  
 2)  $E_t$  = Tangent modulus (static)  
 3)  $E_s$  = Secant modulus (static)  
 4)  $M_c = \rho V_p^2$  (dynamic)



(c) Sonic Pulse Velocity,  $V_p$ , fps



(d) Modulus of Deformation,  $\text{psi} \times 10^6$

FIGURE B.1A STRESS-STRAIN BEHAVIOR AND SONIC PULSE VELOCITY FOR ROCK IN UNIAXIAL COMPRESSION

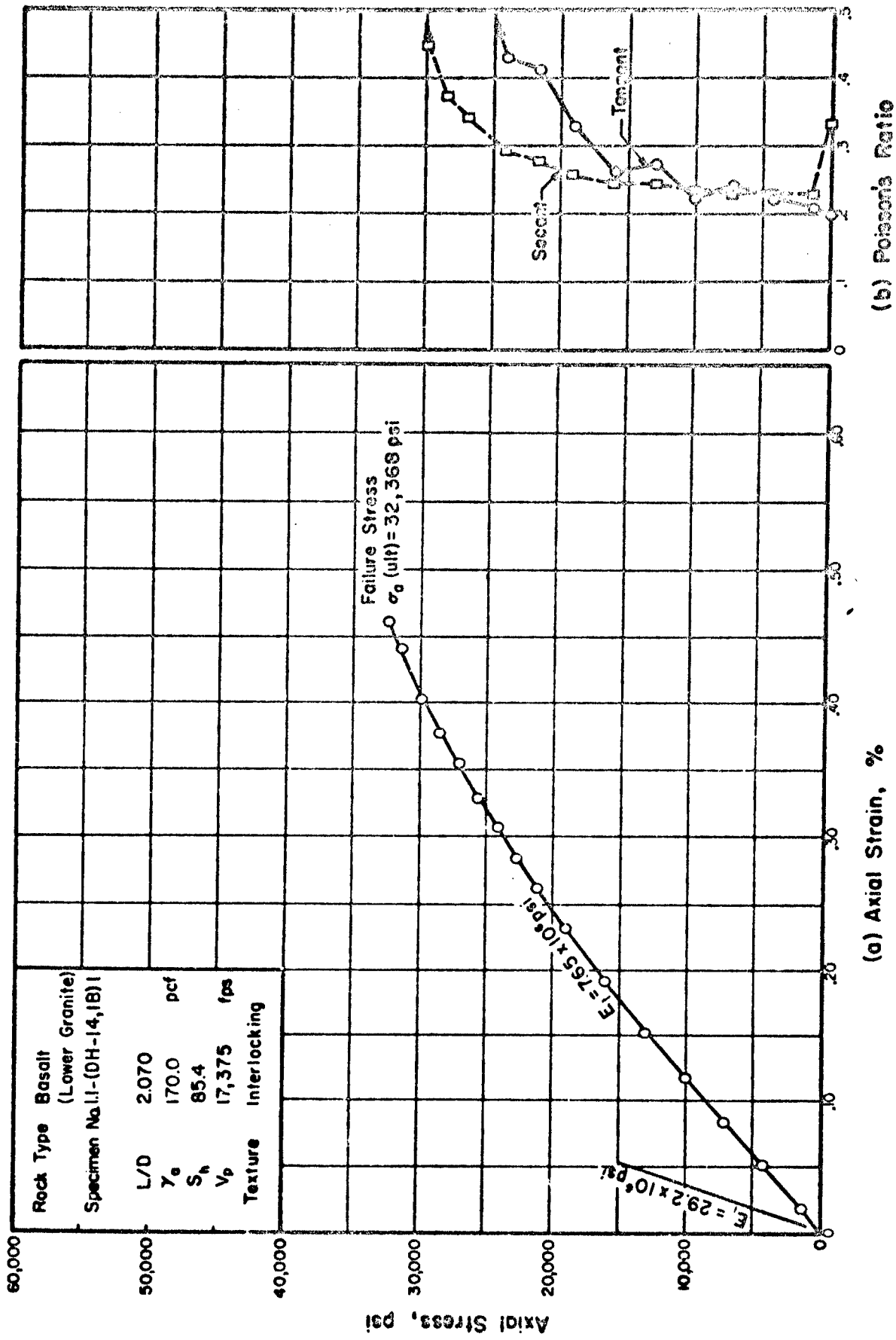
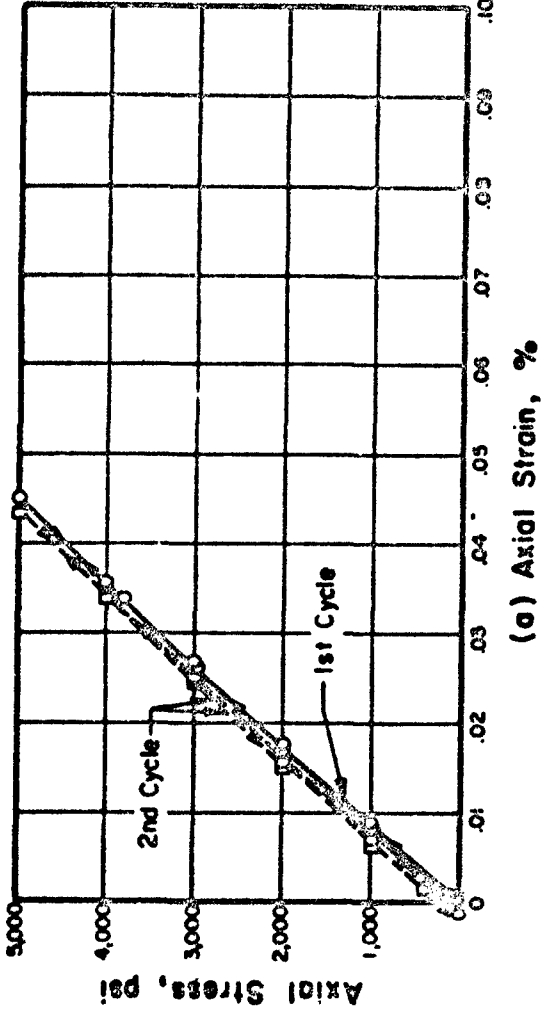
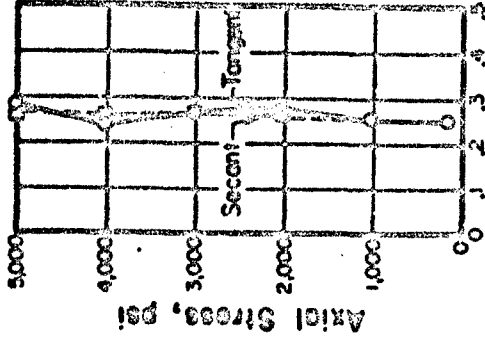


FIGURE B.1B STRESS-STRAIN CURVE AND POISSON'S RATIO FOR ROCK IN UNIAXIAL COMPRESSION TO FAILURE



(a) Axial Strain, %

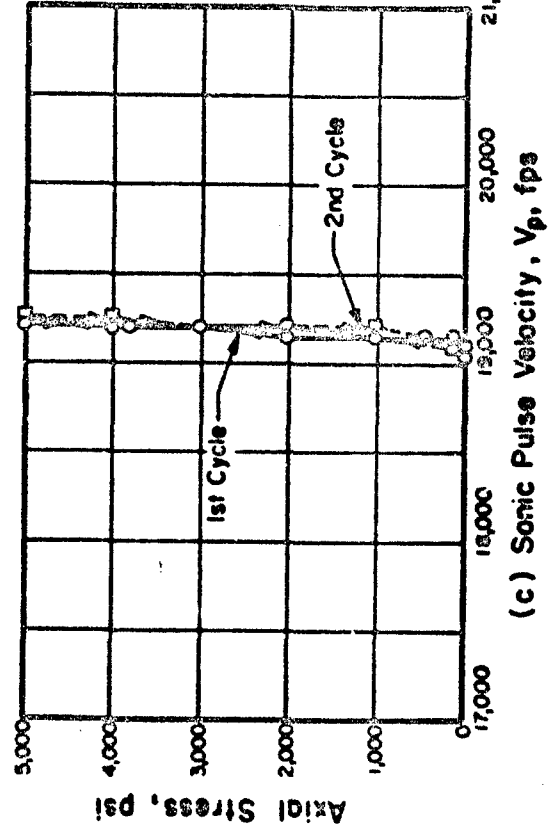


(b) Poisson's Ratio

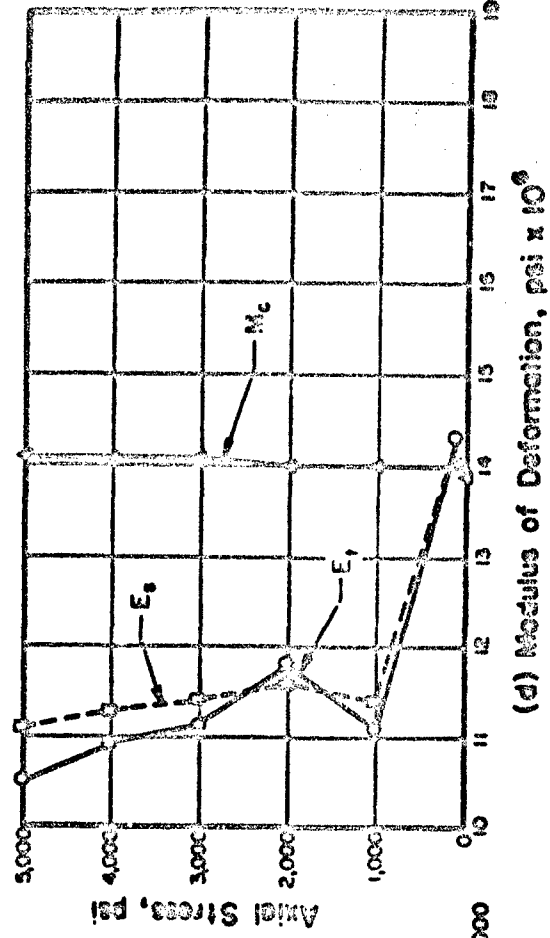
Rock Type	Basalt
(Little Gorge)	
Specimen No.	L2-104-14, 1C, Or 595
L/D	2.115
$\gamma_0$	176.9
$S_h$	68.7
$c_0$ (psi)	45.4
Texture	Interlocking

Note:

- 1)  $V_p$  = Distorted wave velocity
- 2)  $E_1$  = Tangent modulus (static)
- 3)  $E_2$  = Secant modulus (static)
- 4)  $M_c = \rho V_p^2$  (Dynamic)

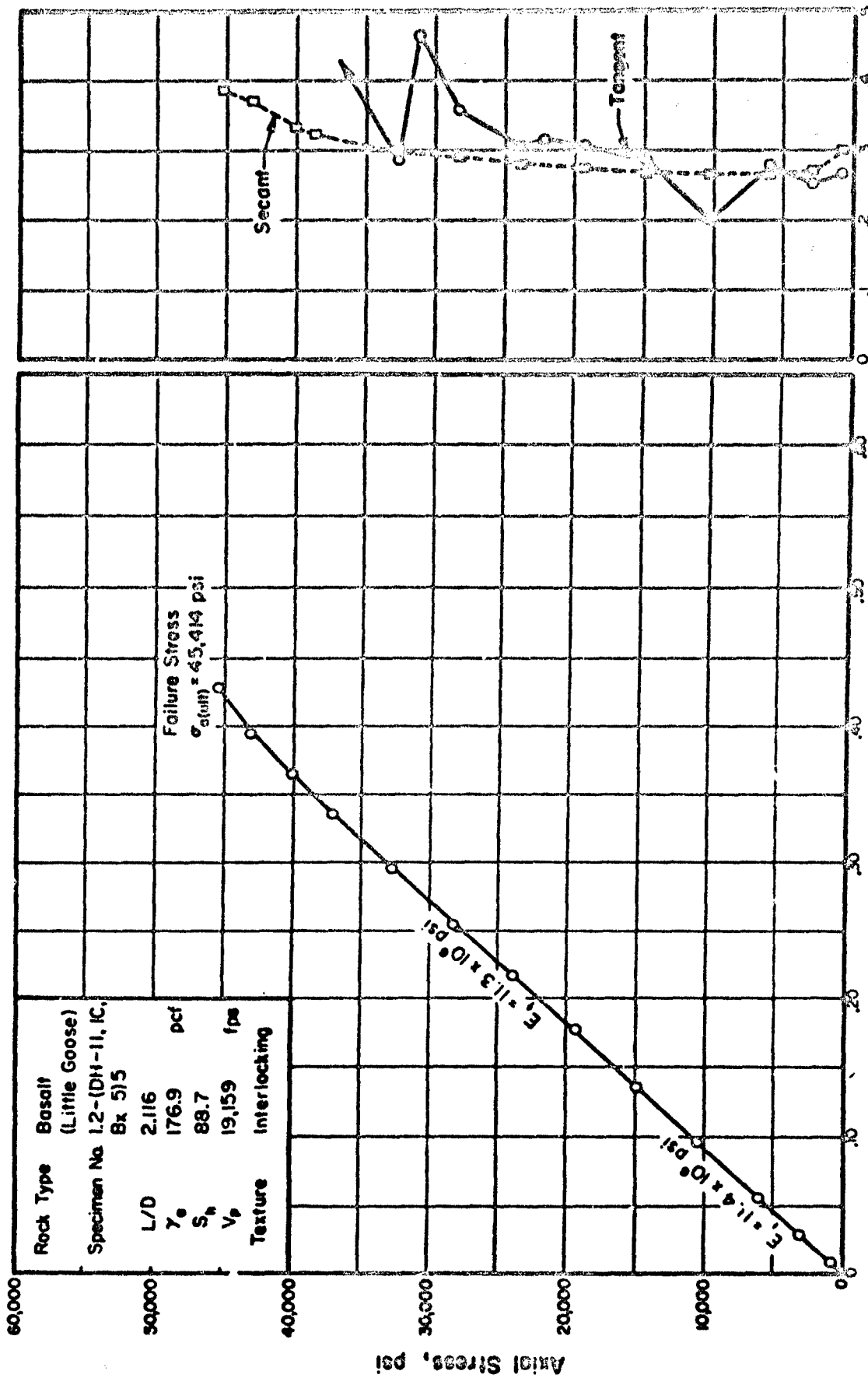


(c) Sonic Pulse Velocity,  $V_p$ , fps



(d) Modulus of Deformation,  $\text{psi} \times 10^6$

FIGURE B.2.A STRESS-STRAIN BEHAVIOR AND SONIC PULSE VELOCITY FOR ROCK IN UNIAXIAL COMPRESSION

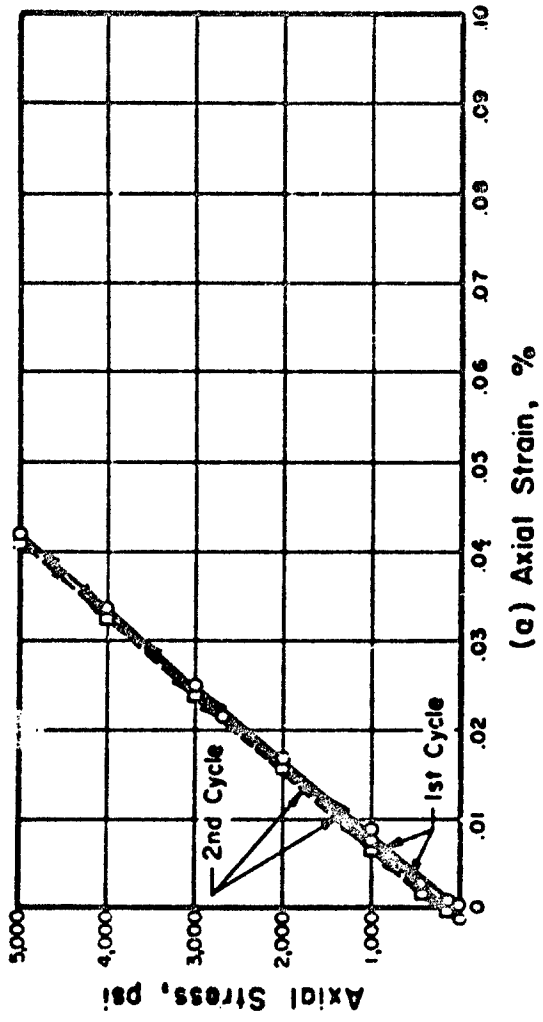


(a) Axial Strain, %

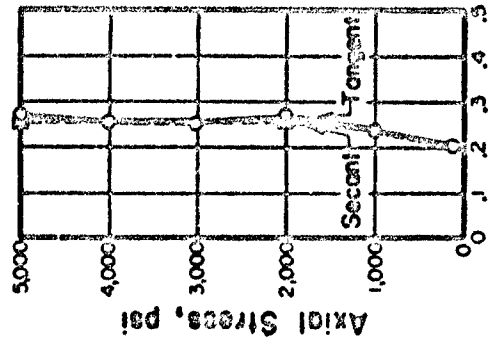
(b) Poisson's Ratio

FIGURE D.2B STRESS-STRAIN CURVE AND POISSON'S RATIO FOR ROCK IN UNIAxIAL COMPRESSION TO FAILURE





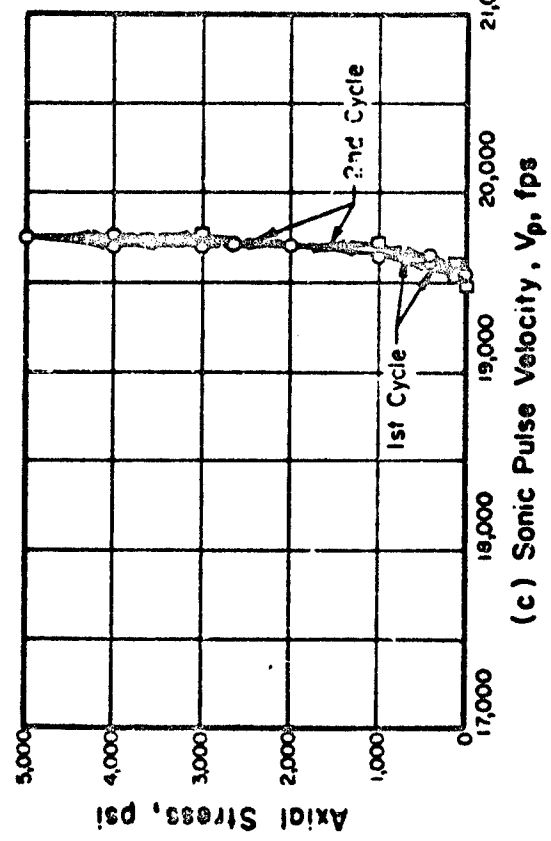
(a) Axial Strain, %



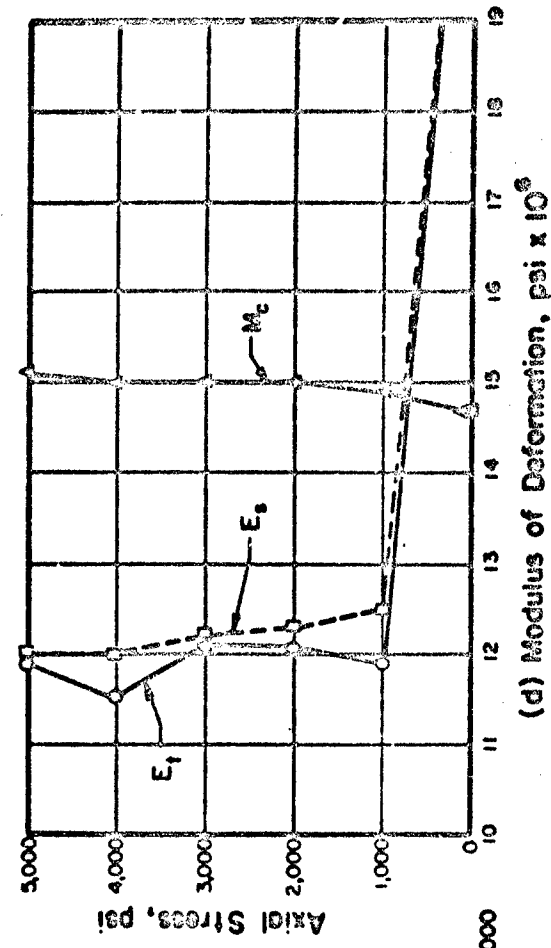
(b) Poisson's Ratio

Rock Type	Basalt
Specimen No.	13-15N-75, 2A, Ex 412
$L/D$	2.004
$\gamma_e$	1790
$S_n$	93.3
$\sigma_o$ (ult)	51.6
Texture	Interlocking

Note:  
 1)  $V_p$  = Dilatational wave velocity  
 2)  $E_t$  = Tangent modulus (static)  
 3)  $E_s$  = Secant modulus (static)  
 4)  $M_c$  = Constrained modulus  
 =  $\rho V_p^2$  (dynamic)



(c) Sonic Pulse Velocity,  $V_p$ , fps



(d) Modulus of Deformation,  $\text{psi} \times 10^6$

FIGURE B.3A STRESS-STRAIN BEHAVIOR AND SONIC PULSE VELOCITY FOR ROCK IN UNIAXIAL COMPRESSION

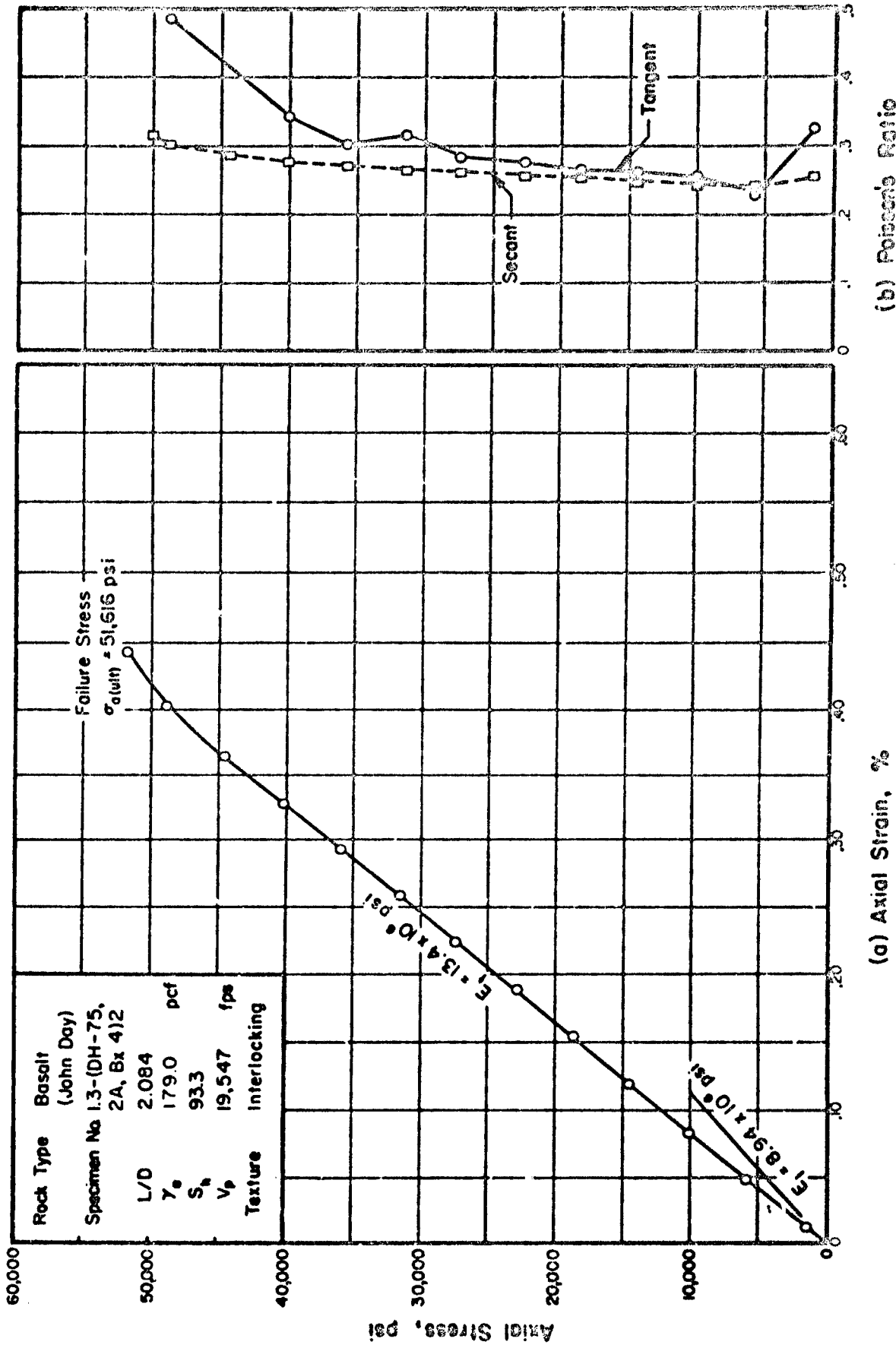
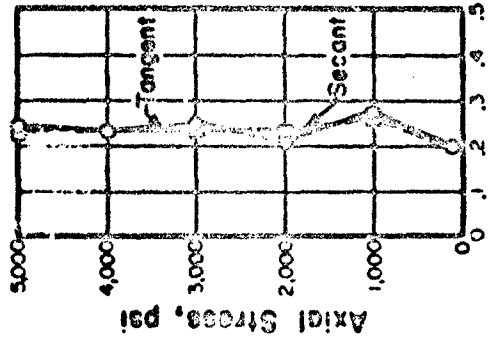
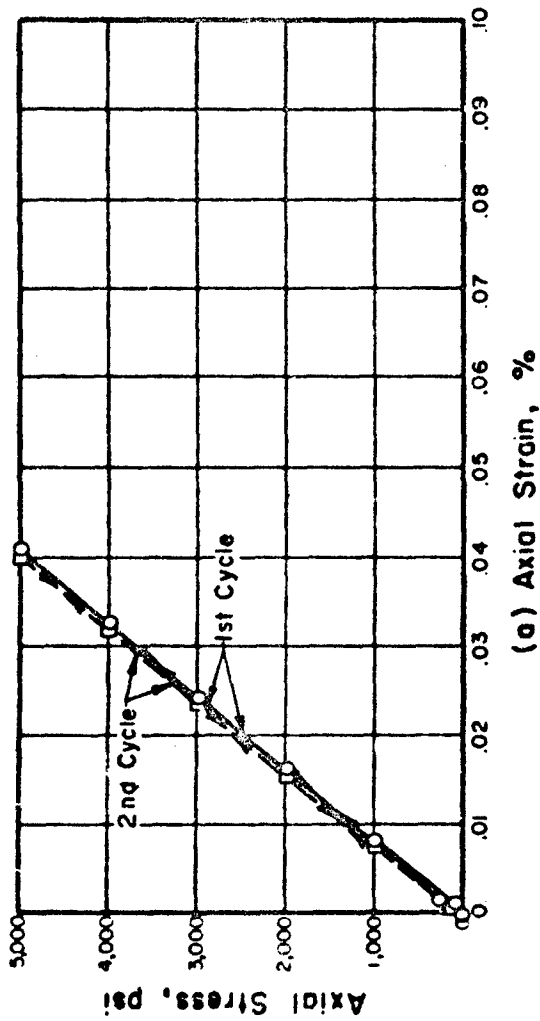


FIGURE B.3B STRESS-STRAIN CURVE AND POISSON'S RATIO FOR ROCK IN UNIAxIAL COMPRESSION TO FAILURE



Rock Type	Diabase (Pallasdes)
Specimen No.	2.1-(1)12
L/D	2.012
$\gamma_0$	102.0
$S_b$	90.6
$\sigma_0$ (ult)	375
Texture	Interlocking

Note:  
 1)  $V_0$  = Dilatational wave velocity  
 2)  $E_t$  = Tangent modulus (static)  
 3)  $E_s$  = Secant modulus (static)  
 4)  $M_c = \rho V_p^2$  (dynamic)

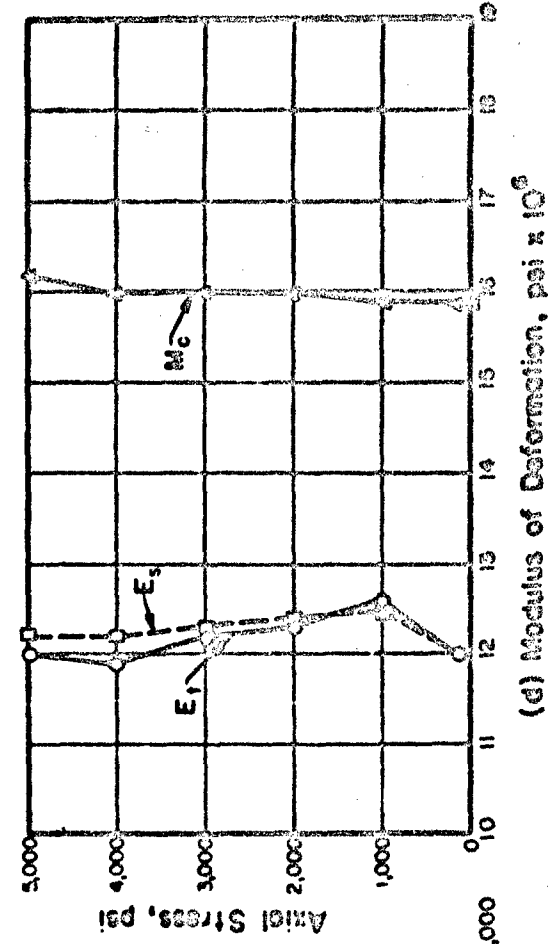
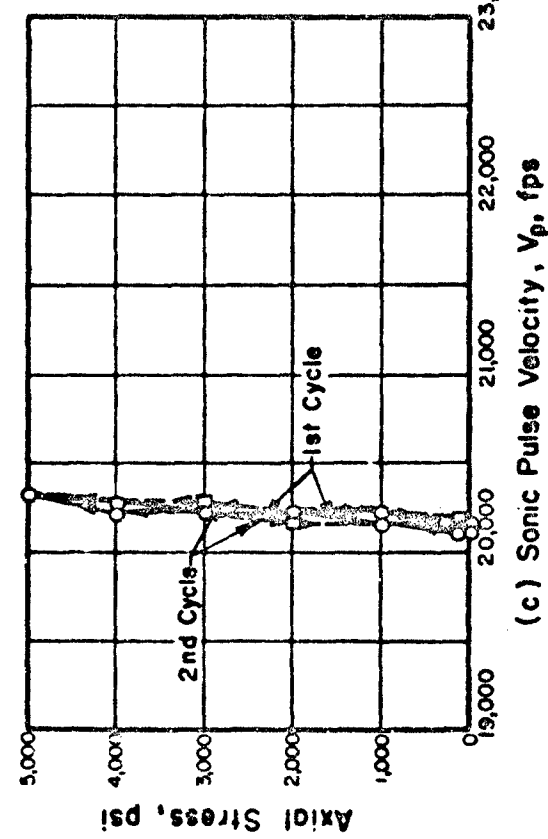
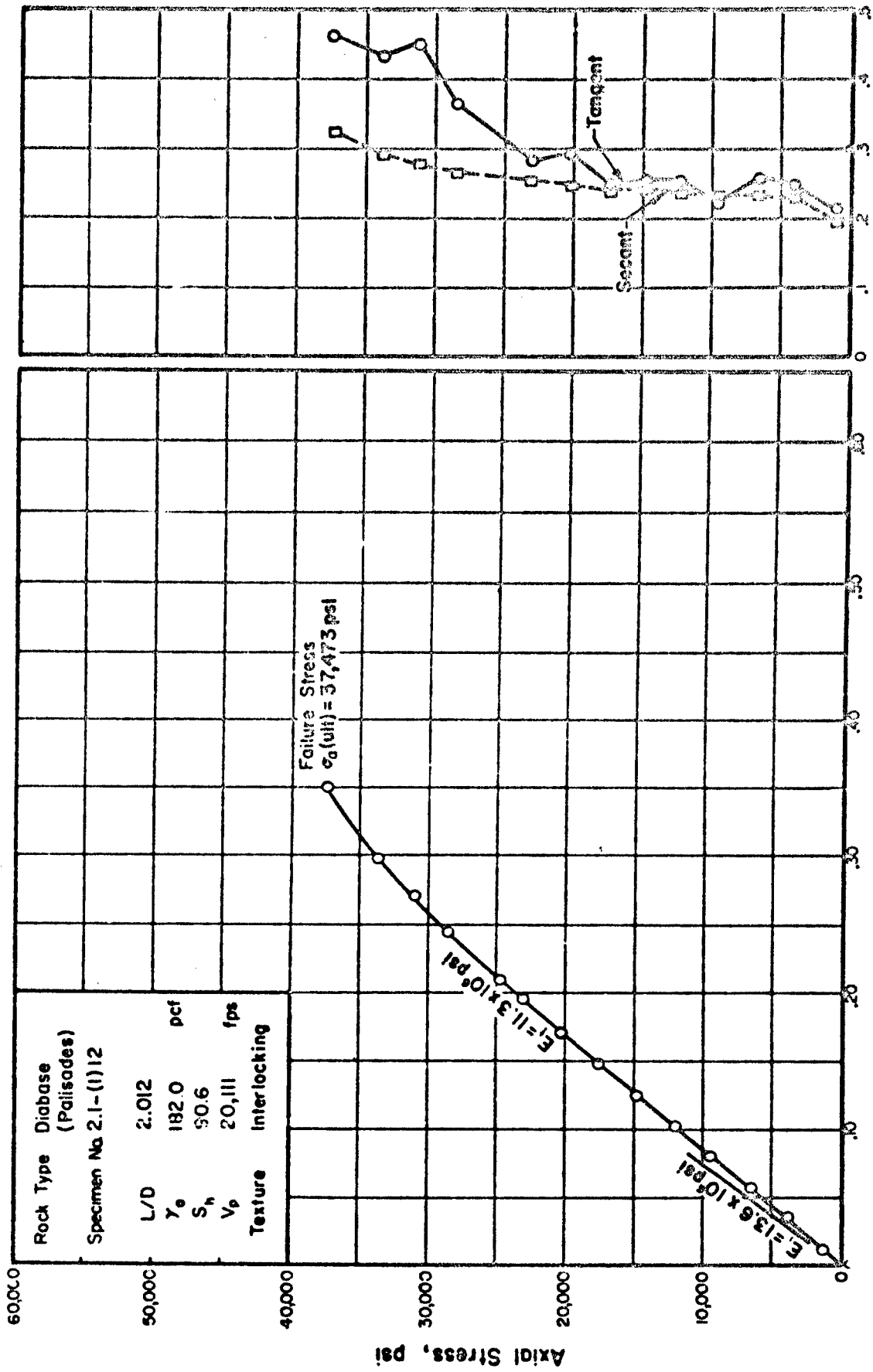
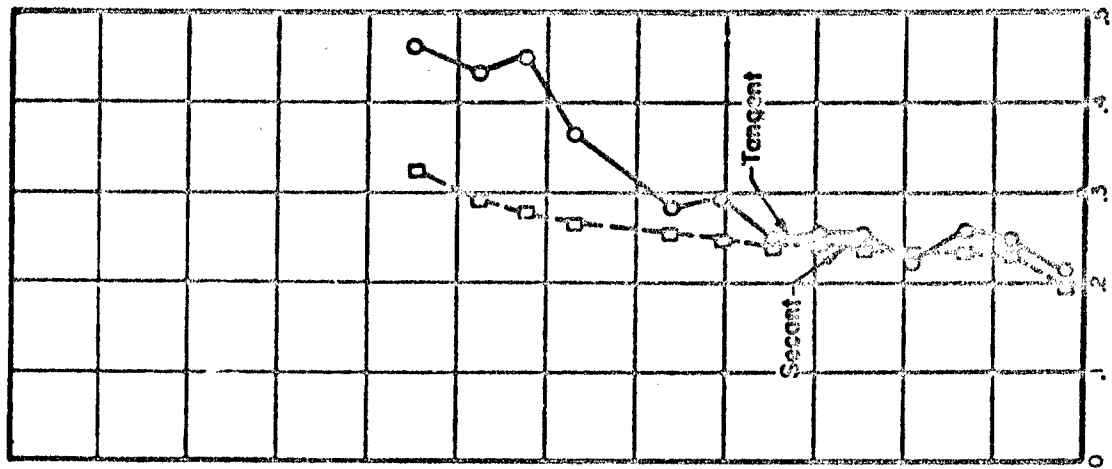


FIGURE B.4A STRESS-STRAIN BEHAVIOR AND SONIC PULSE VELOCITY FOR ROCK IN UNIAXIAL COMPRESSION

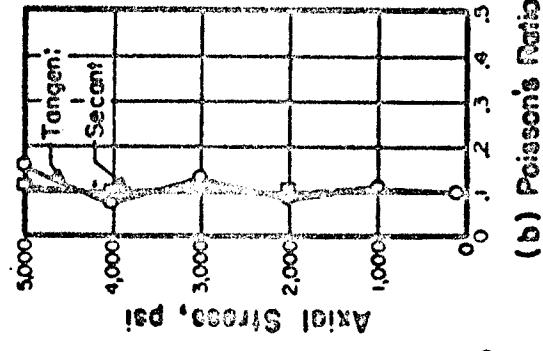
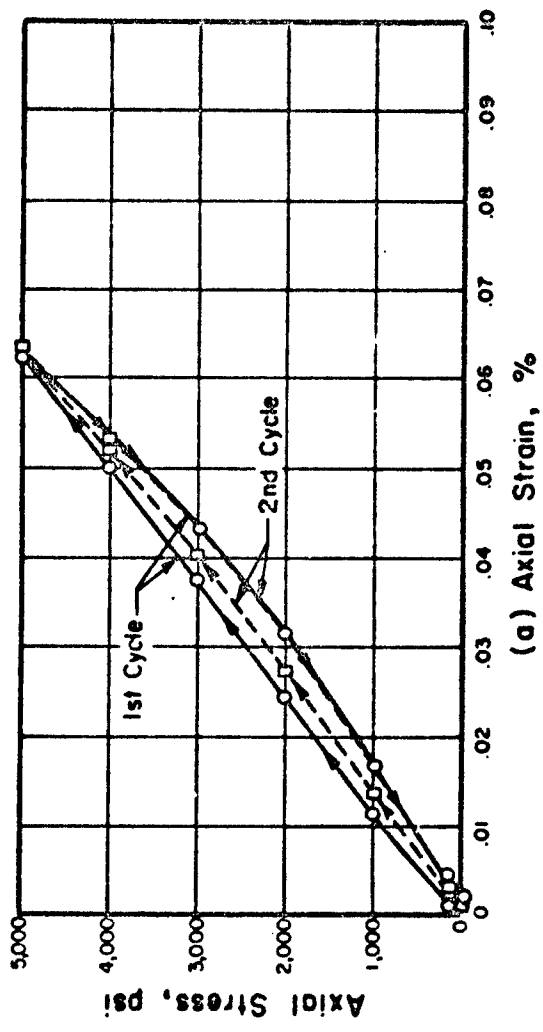


(a) Axial Strain, %



(b) Poisson's Ratio

FIGURE B.4B STRESS-STRAIN CURVE AND POISSON'S RATIO FOR ROCK IN UNIAxIAL COMPRESSION TO FAILURE



Rock Type	Diabase (Coggins)
Specimen No.	2.2-112
L/D	2.002
$\gamma_0$	199.2
$S_h$	91.3
$\sigma_0$ (ult)	49.6
Texture	Interlocking

Note:  
 1)  $V_p$  = Dilational wave velocity  
 2)  $E_t$  = Tangent modulus (static)  
 3)  $E_s$  = Secant modulus (static)  
 4)  $M_c = \rho V_p^2$  (Dynamic)

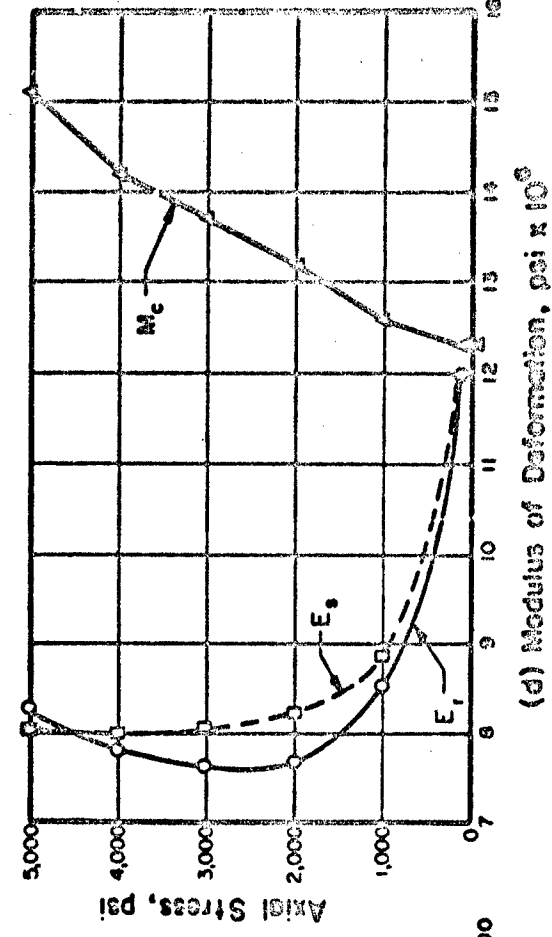
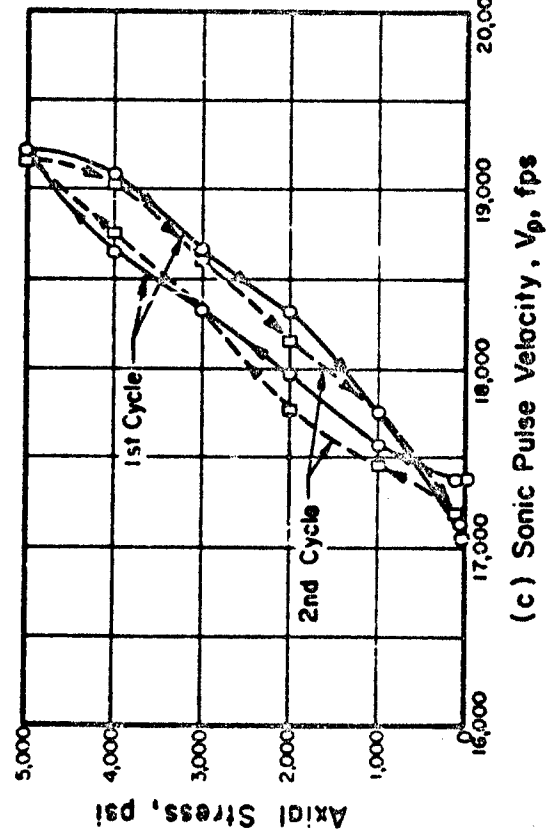
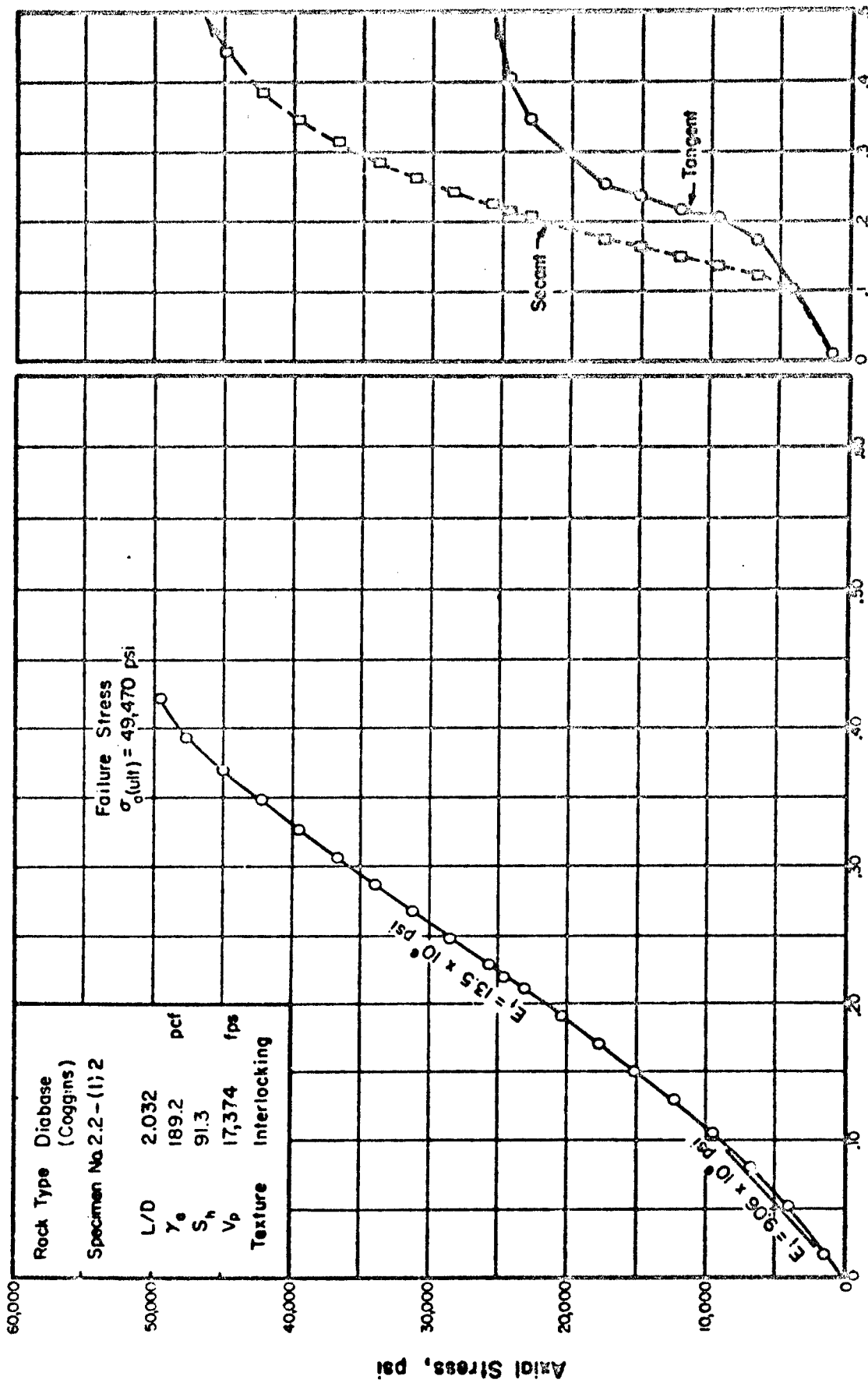


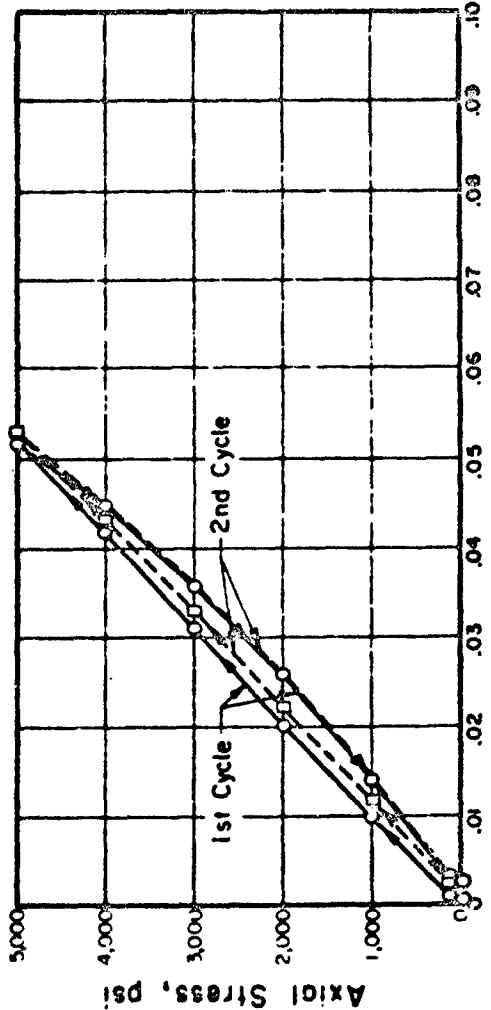
FIGURE B.5A STRESS-STRAIN BEHAVIOR AND SONIC PULSE VELOCITY FOR ROCK IN UNIAXIAL COMPRESSION



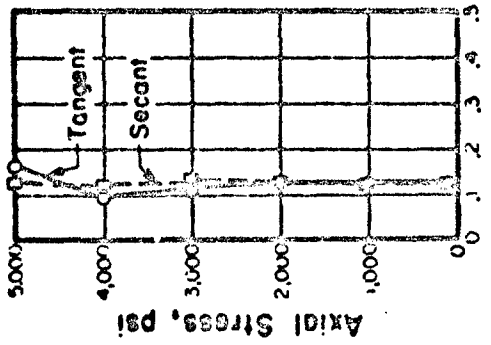
(b) Poisson's Ratio

(a) Axial Strain, %

FIGURE B.5B STRESS-STRAIN CURVE AND POISSON'S RATIO FOR ROCK IN UNIAXIAL COMPRESSION TO FAILURE



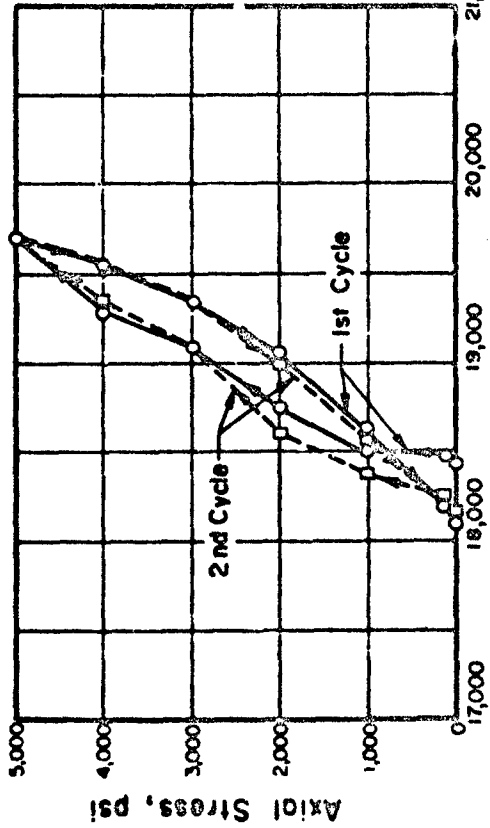
(a) Axial Strain, %



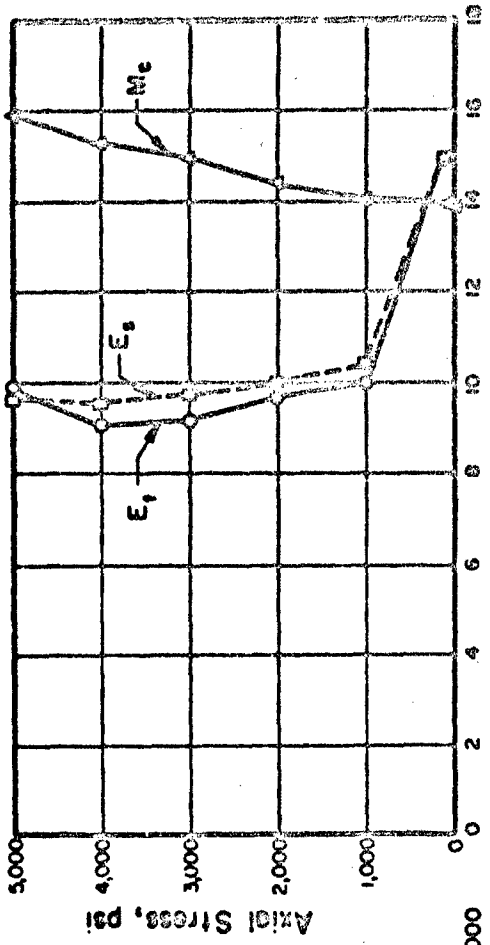
(b) Poisson's Ratio

Rock Type	Diabase (French Creek)
Specimen No	2.3-(112)
L/D	2.031
$\gamma_e$	190.6
$S_n$	95.6
$\sigma_e$ (ult)	40.4
Texture	Interlocking

Note:  
 1)  $V_p$  = Dilatational wave velocity  
 2)  $E_t$  = Tangent modulus (static)  
 3)  $E_s$  = Secant modulus (static)  
 4)  $M_c = \rho V_p^2$  (dynamic)



(c) Sonic Pulse Velocity,  $V_p$ , fps



(d) Modulus of Deformation,  $\text{psi} \times 10^6$

FIGURE B.6A STRESS-STRAIN BEHAVIOR AND SONIC PULSE VELOCITY FOR ROCK IN UNIAXIAL COMPRESSION

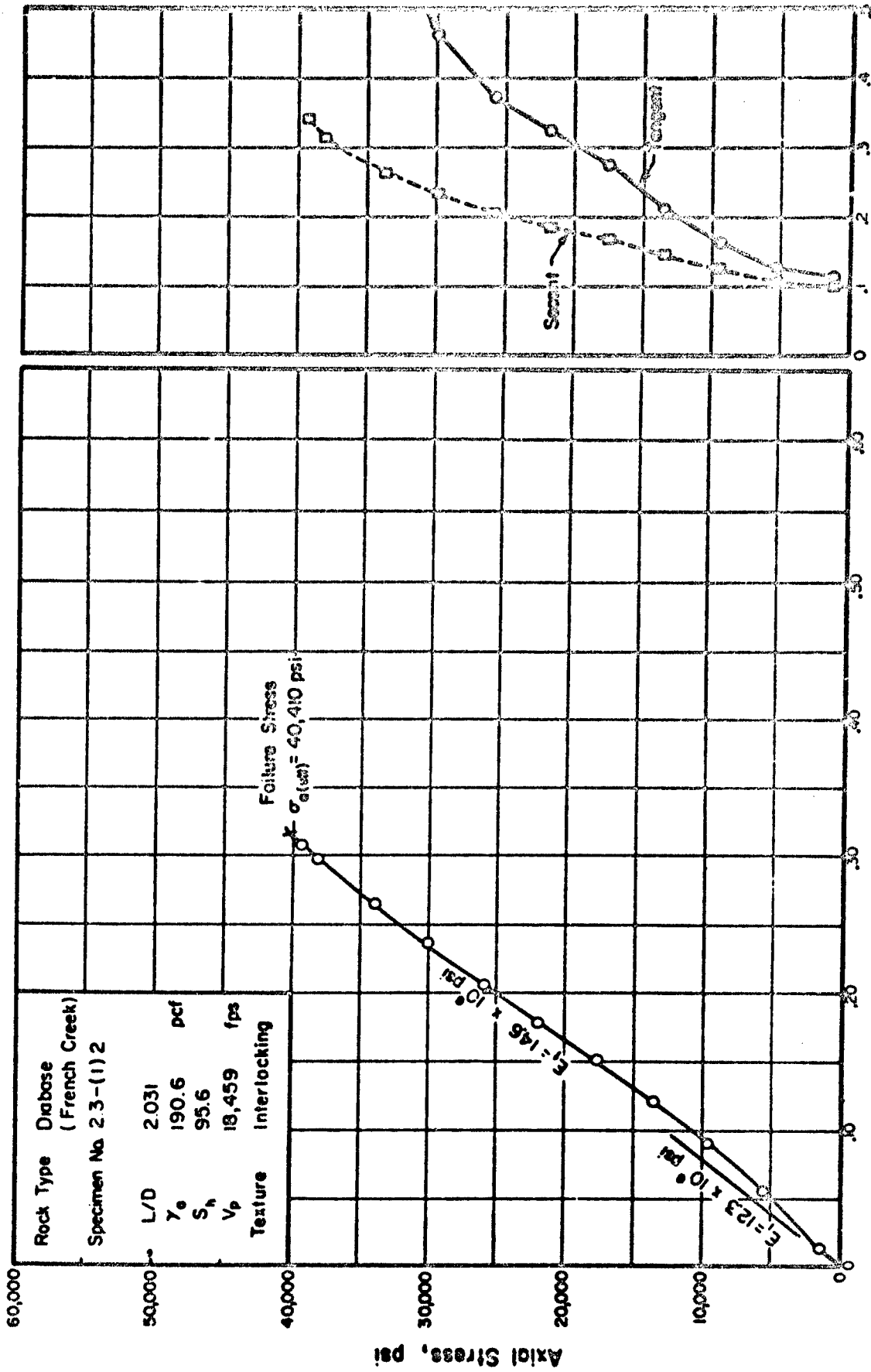
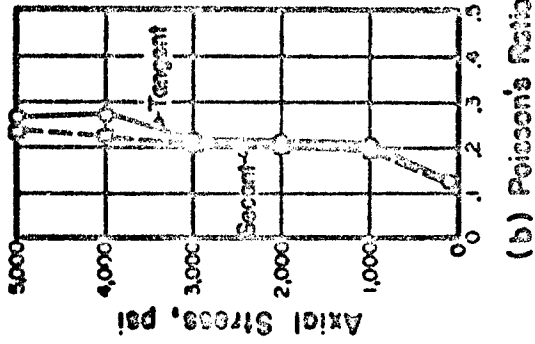
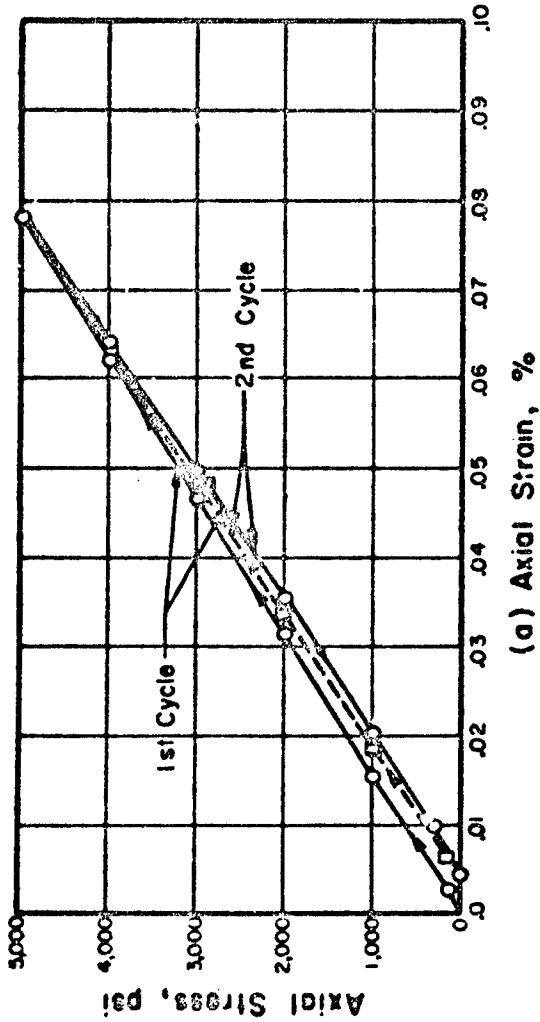


FIGURE B.6B STRESS-STRAIN CURVE AND POISSON'S RATIO FOR ROCK IN UNIAXIAL COMPRESSION TO FAILURE





Rock Type	Delemite (Oncoite)
Specimen No.	3.1-(1)12
L/D	1.000
$\gamma_0$	153.4
$S_n$	33.9
$\sigma_a$ (ult)	12.2
Texture	Interlocking

Note:  
 1)  $V_p$  = Dilational wave velocity  
 2)  $E_1$  = Tangent modulus (static)  
 3)  $E_2$  = Secant modulus (static)  
 4)  $M_c$  = Controlled modulus  
    =  $\rho V_p^2$  (dynamic)

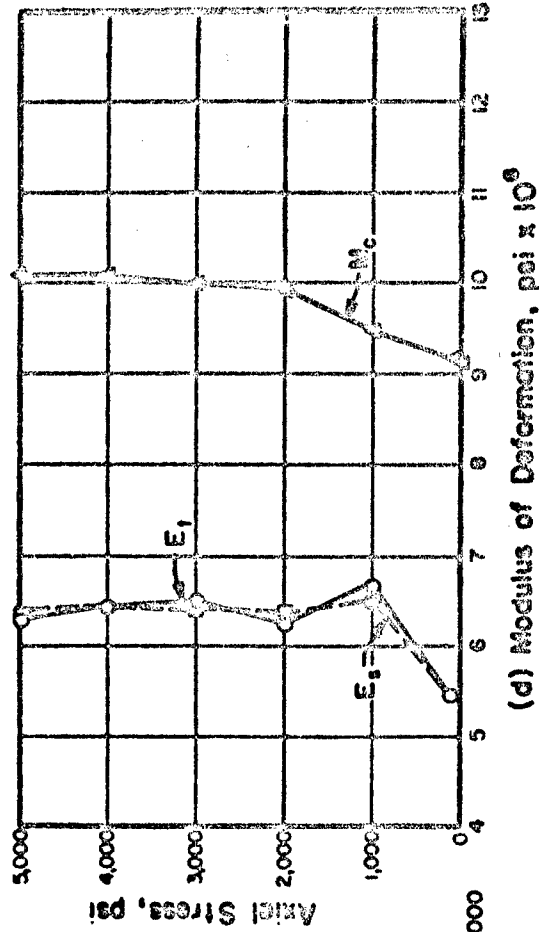
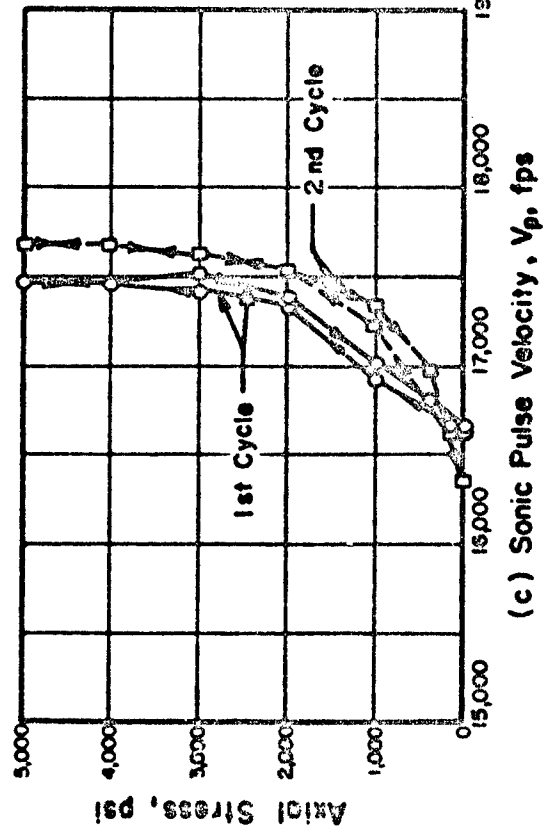
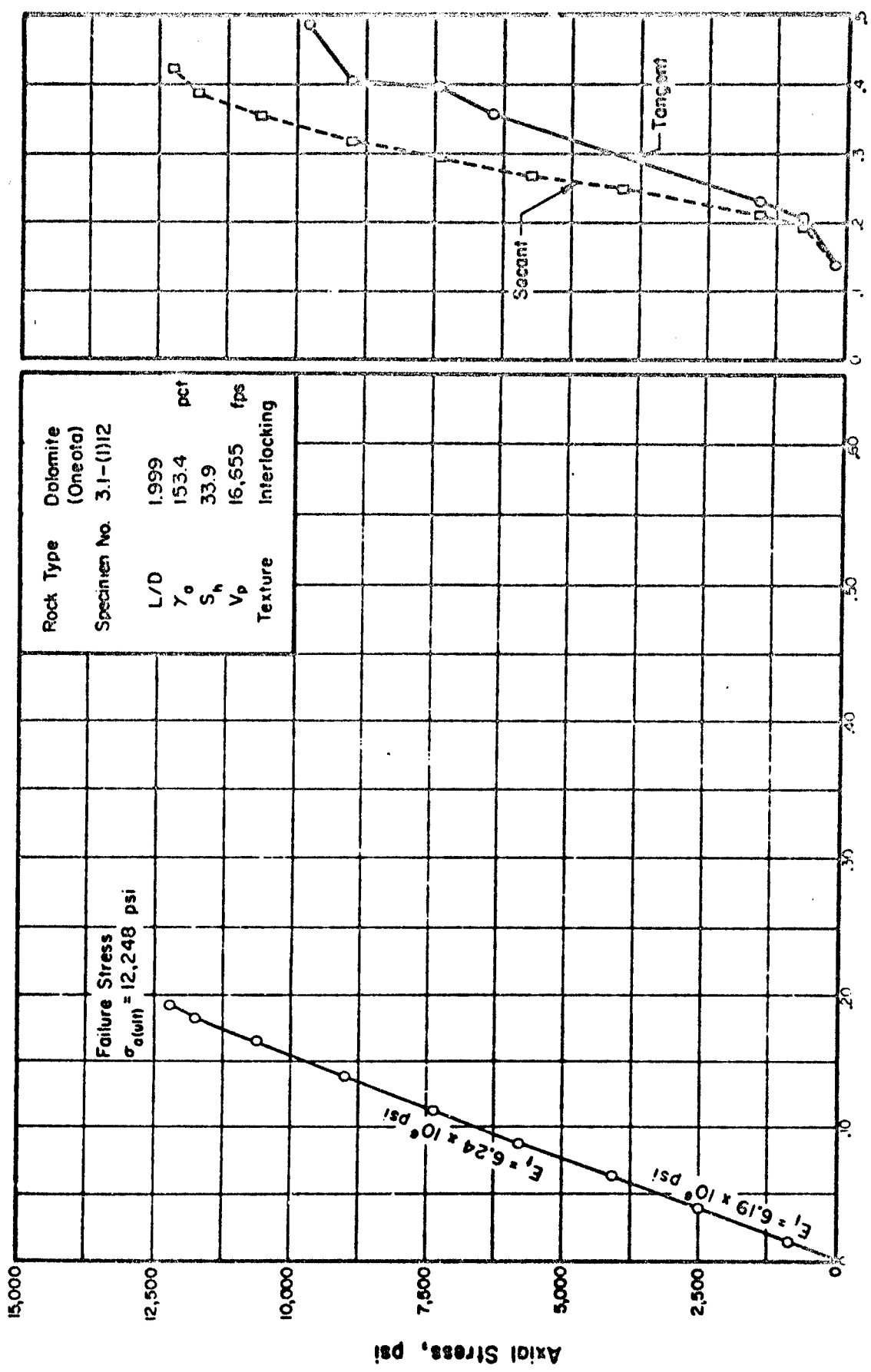
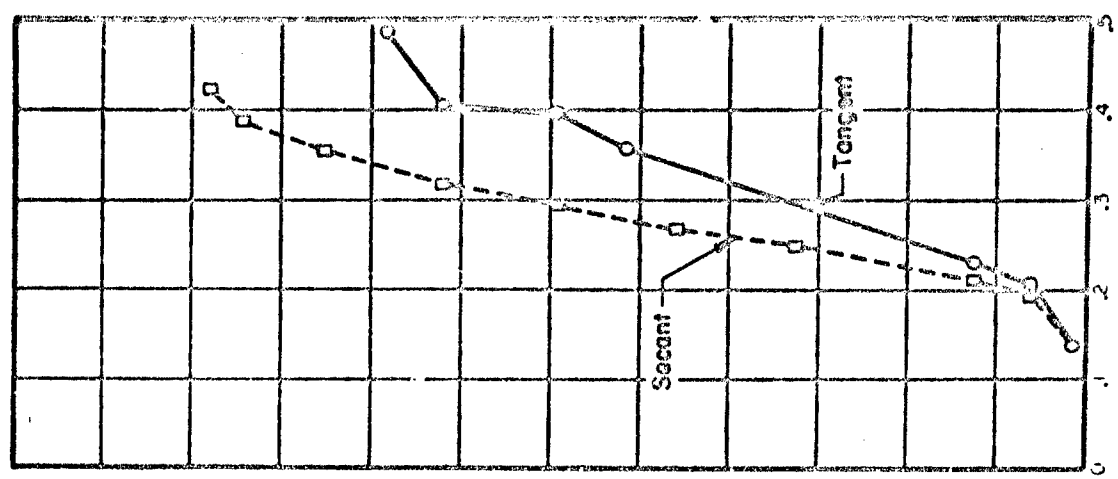


FIGURE B. 7A STRESS-STRAIN BEHAVIOR AND SONIC PULSE VELOCITY FOR ROCK IN UNIAXIAL COMPRESSION

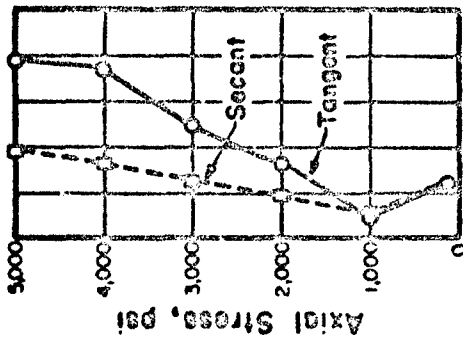
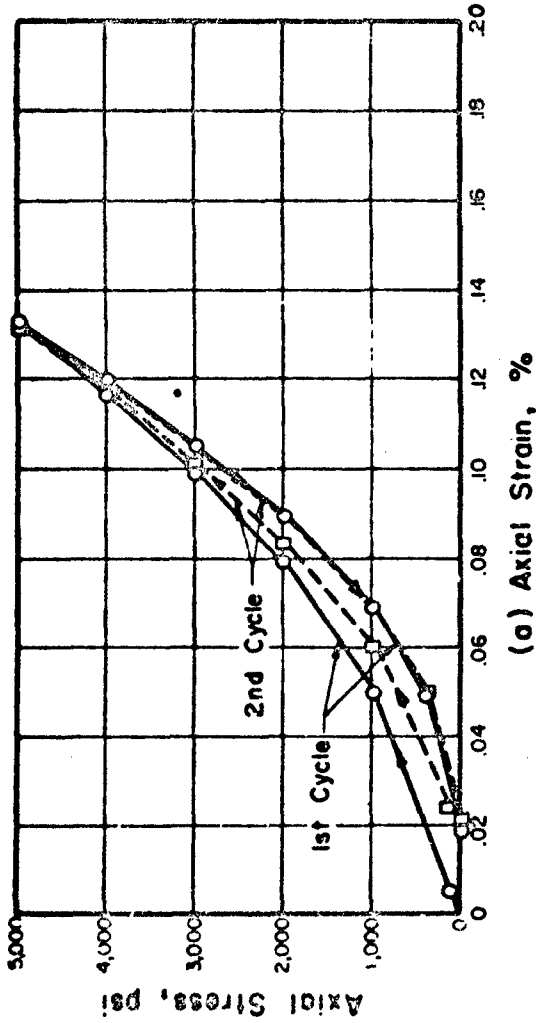


(a) Axial Strain, %



(b) Poisson's Ratio

FIGURE B.1 B STRESS-STRAIN CURVE AND POISSON'S RATIO FOR ROCK IN UNIAXIAL COMPRESSION TO FAILURE



Rock Type	Dolomite (Leitchport)
Specimen No.	3.2-(1)5
L/D	2.025
$\gamma_0$	162.0
$S_n$	45.0
$\sigma_0$ (psi)	13.9
Texture	Interlocking

Note:  
 1)  $V_p$  = Dilational wave velocity  
 2)  $E_t$  = Tangent modulus (static)  
 3)  $E_s$  = Secant modulus (static)  
 4)  $M_c = \rho V_p^2$  (dynamic)

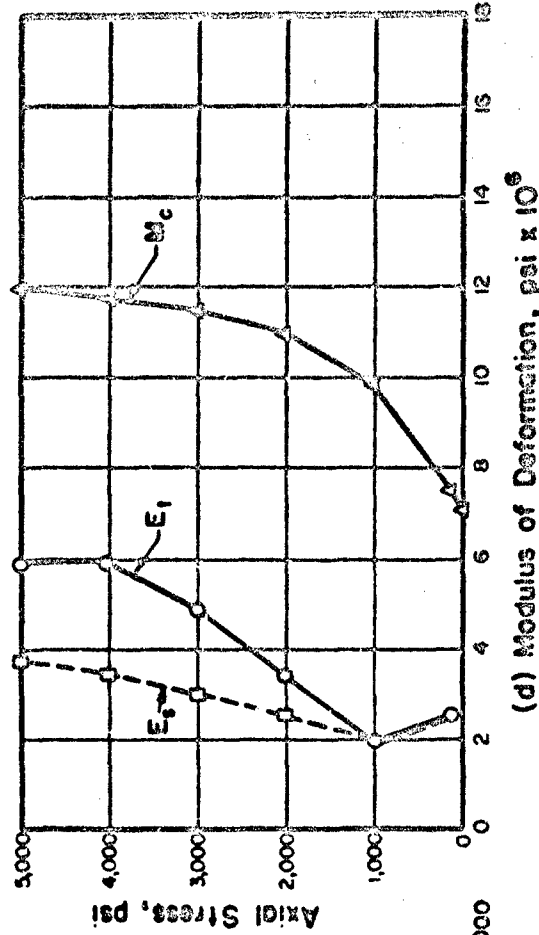
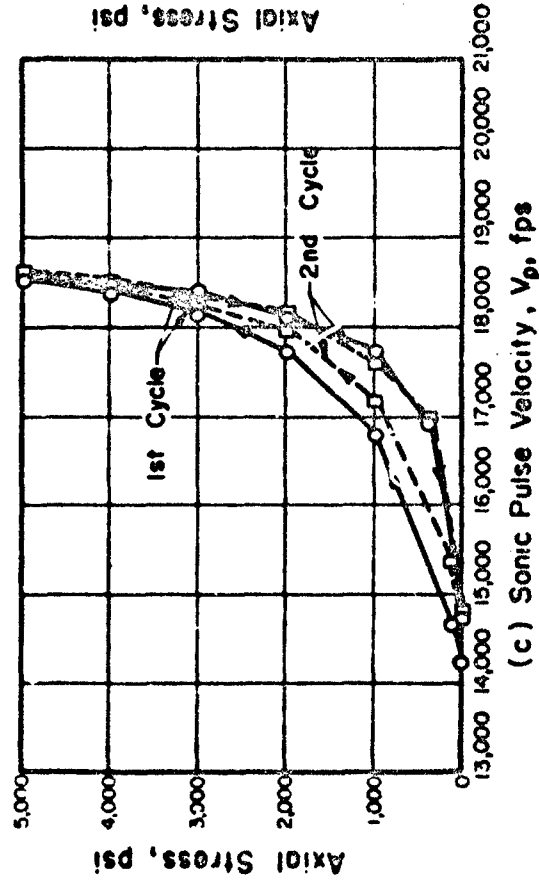
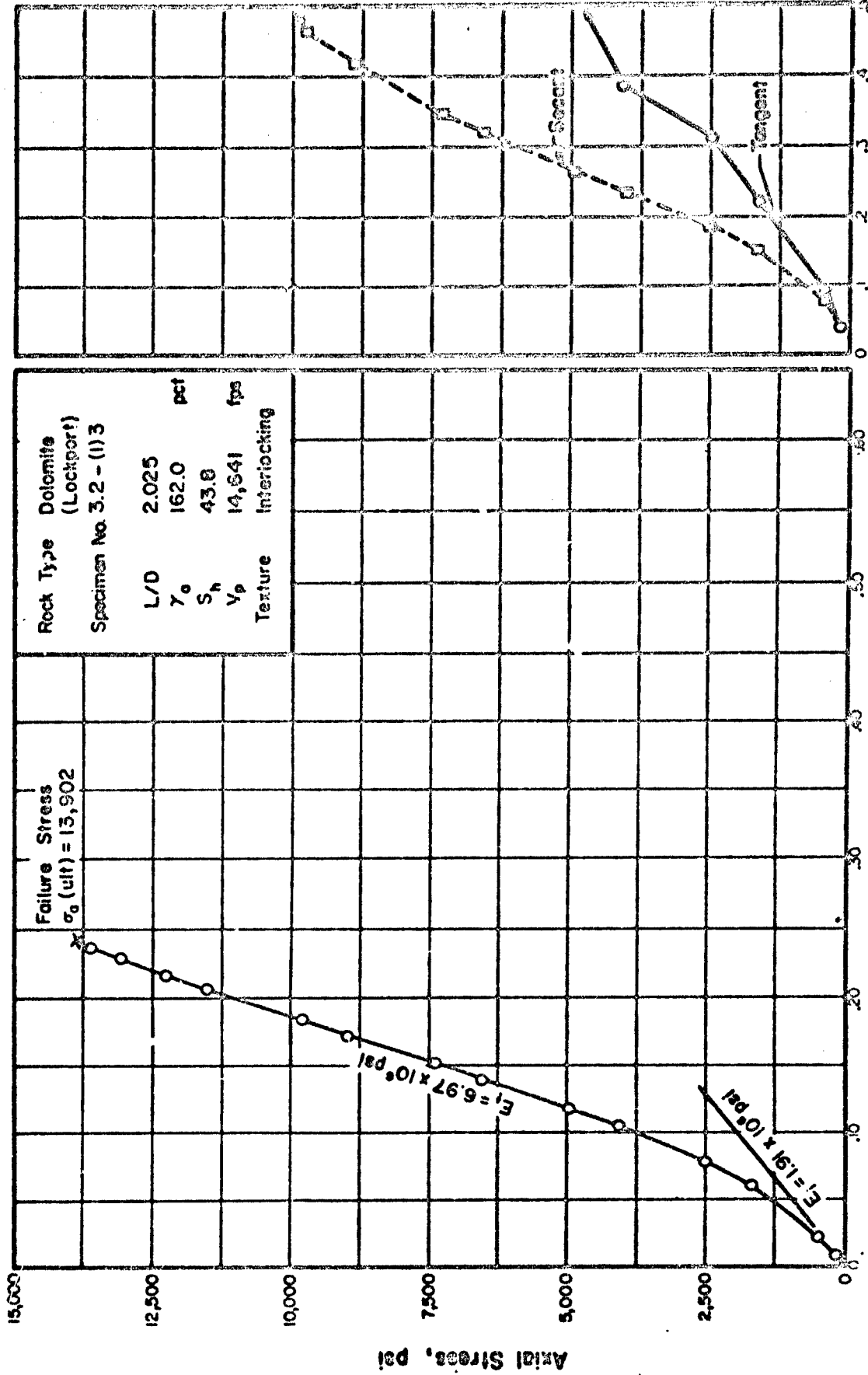


FIGURE B.8A STRESS-STRAIN BEHAVIOR AND SONIC PULSE VELOCITY FOR ROCK IN UNIAXIAL COMPRESSION

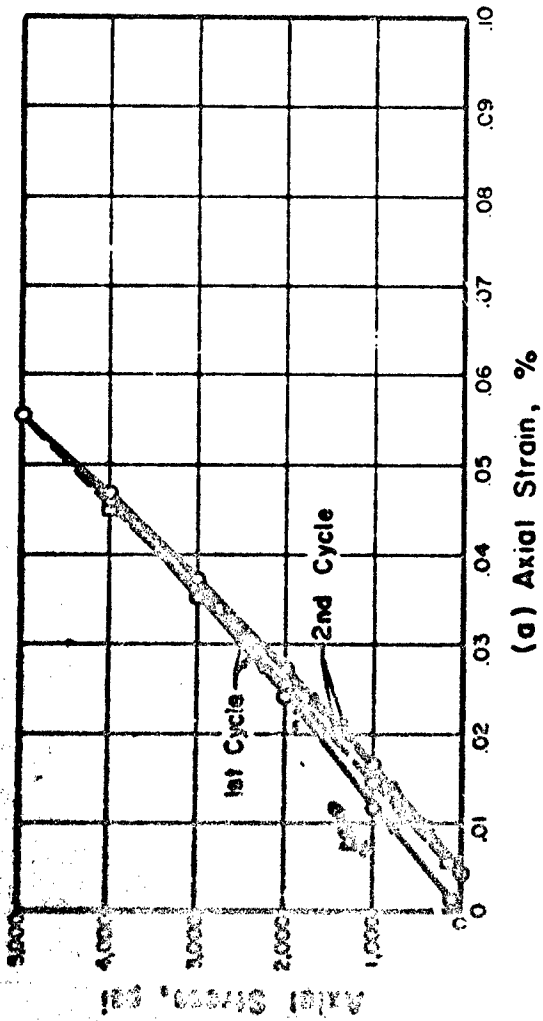


Rock Type Dolomite (Lockport)  
 Specimen No. 3.2 - (1) 3

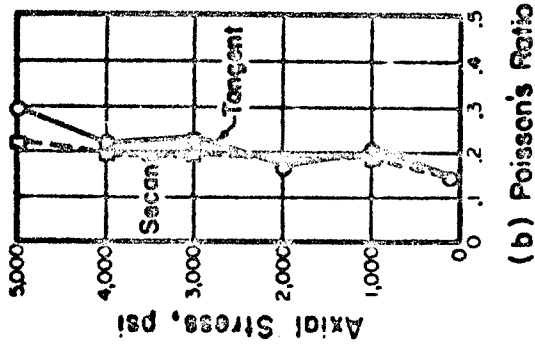
L/D 2.025  
 $\gamma_c$  162.0 pct  
 $S_h$  43.6  
 $V_p$  14,641 fps  
 Texture Interlocking

(a) Axial Strain, % (b) Poisson's Ratio

FIGURE 9.8B STRESS-STRAIN CURVE AND POISSON'S RATIO FOR ROCK IN UNIAxIAL COMPRESSION TO FAILURE



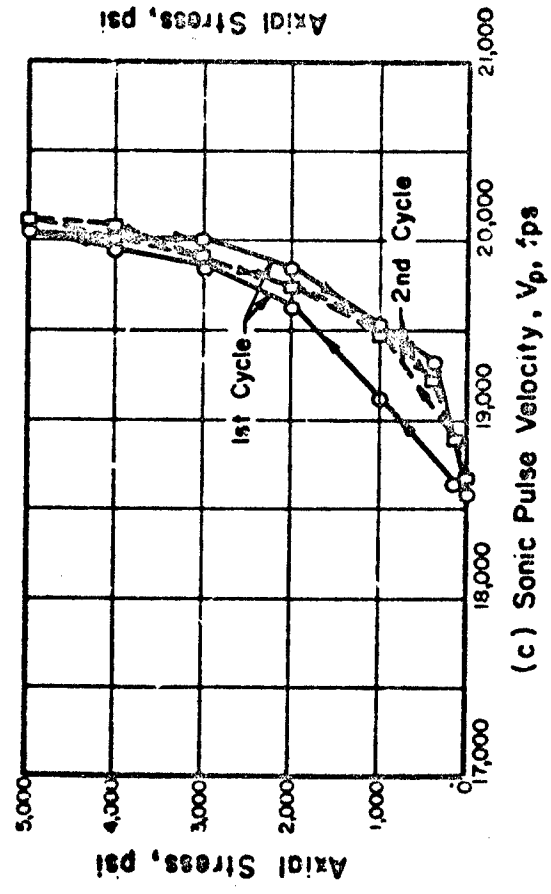
(a) Axial Strain, %



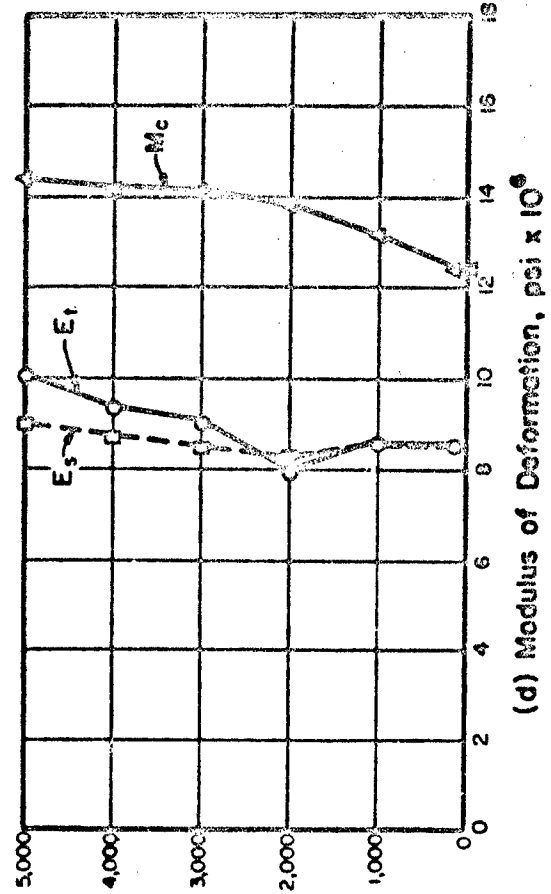
(b) Poisson's Ratio

Rock Type	Dolomite (Bonne Terre)		
Specimen No	3.3 - (I) 5		
L/D	2.025		
$\gamma_0$	165.9	pcf	
$S_n$	50.0		
$\sigma_0$ (ult)	23.1	ksi	
Texture	Interlocking		

Note:  
 1)  $V_p$  = Dilatational wave velocity  
 2)  $E_t$  = Tangent modulus (static)  
 3)  $E_s$  = Secant modulus (static)  
 4)  $M_c$  = Constrained modulus  
 $= \rho V_p^2$  (dynamic)

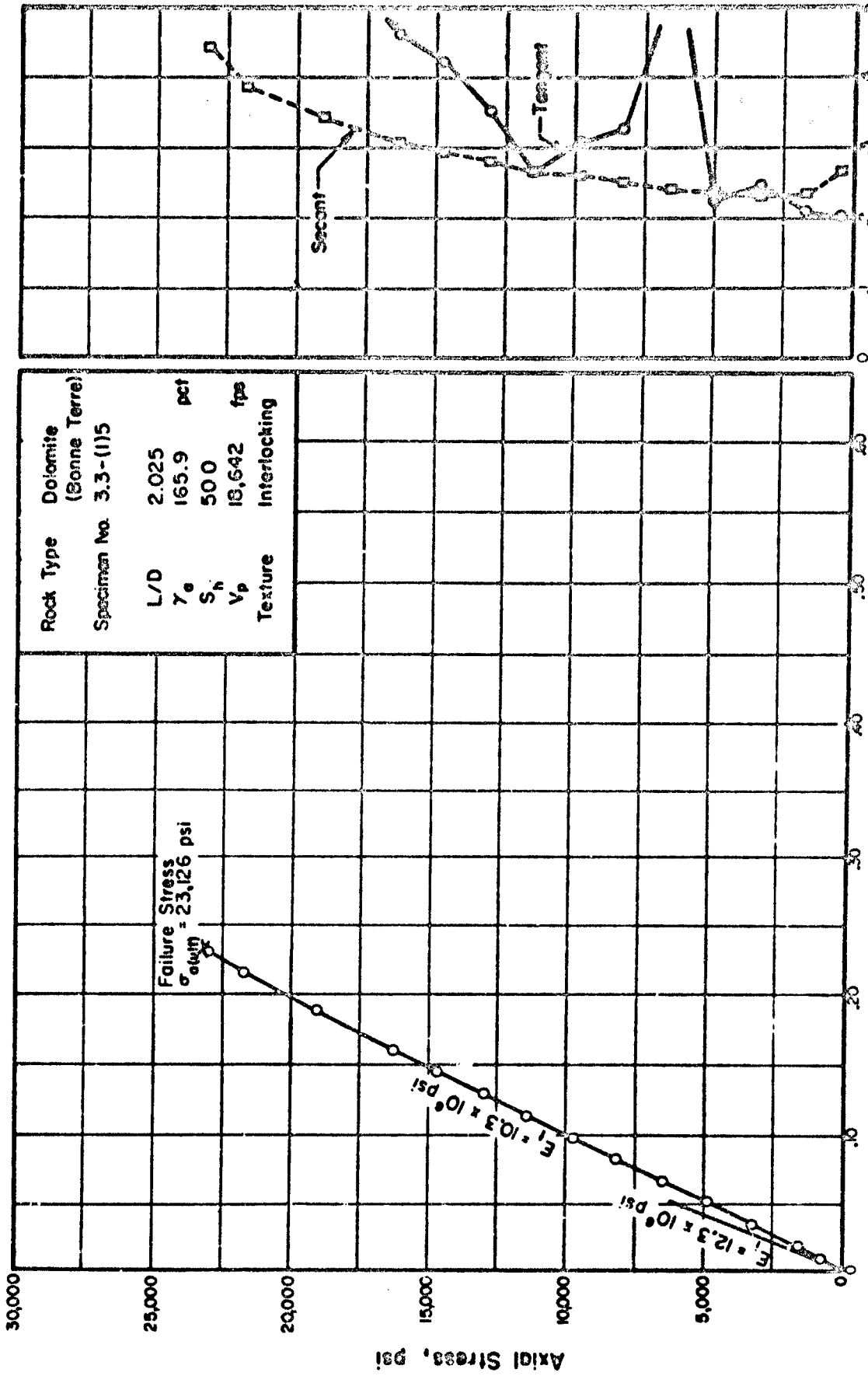


(c) Sonic Pulse Velocity,  $V_p$ , fps



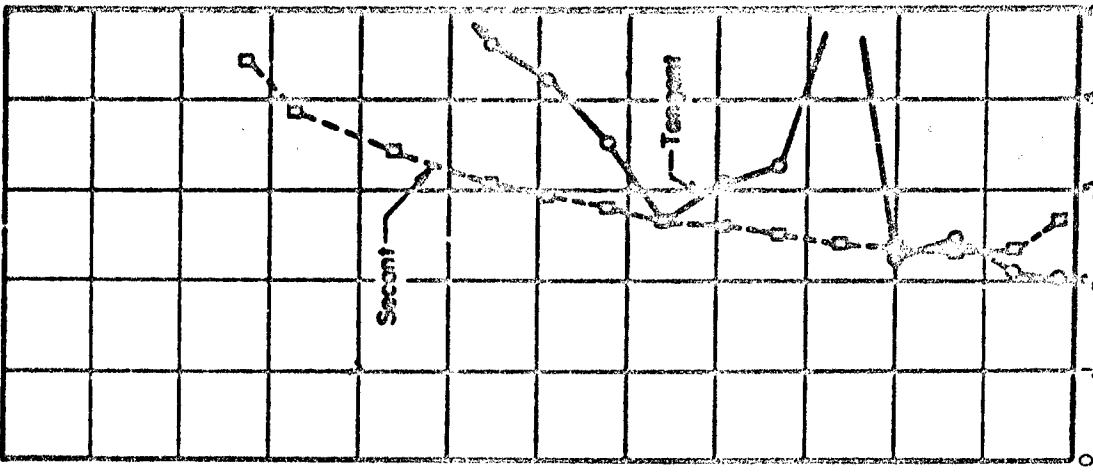
(d) Modulus of Deformation,  $\text{psi} \times 10^6$

FIGURE B.9A STRESS-STRAIN BEHAVIOR AND SONIC PULSE VELOCITY FOR ROCK IN UNIAXIAL COMPRESSION



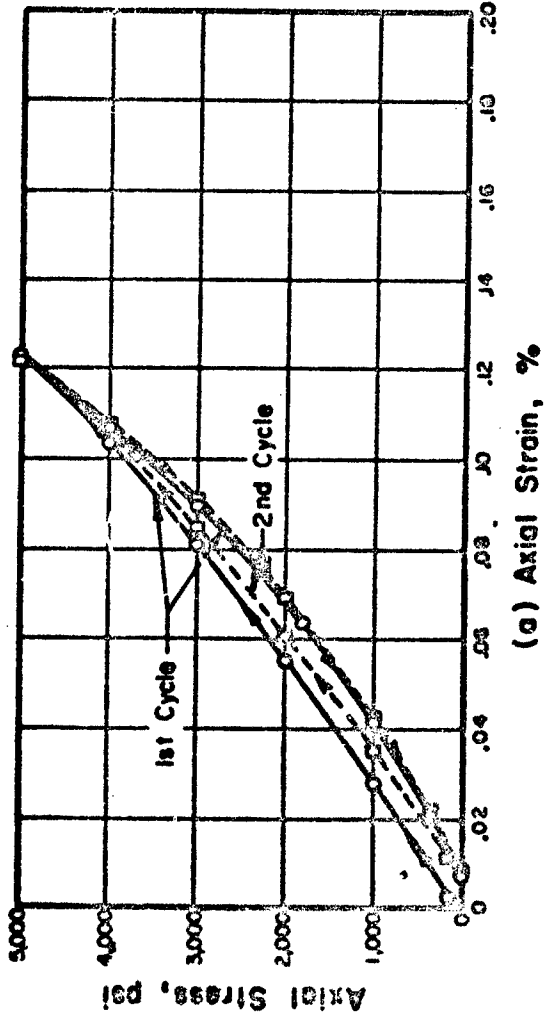
Rock Type	Dolomite (Bonne Terre)
Specimen No.	3.3-(115)
L/D	2.025
$\gamma_e$	165.9 pct
$S_h$	500
$V_p$	18,642 fps
Texture	Interlocking

(a) Axial Strain, %

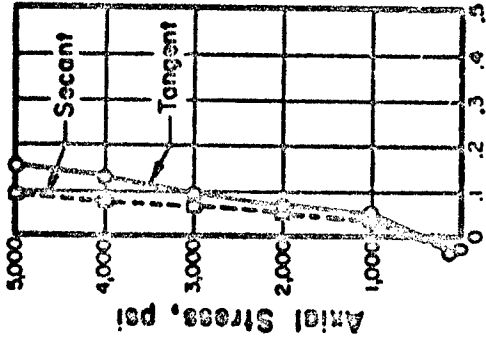


(b) Poisson's Ratio

FIGURE 3.9B STRESS-STRAIN CURVE AND POISSON'S RATIO FOR ROCK IN UNIAXIAL COMPRESSION TO FAILURE



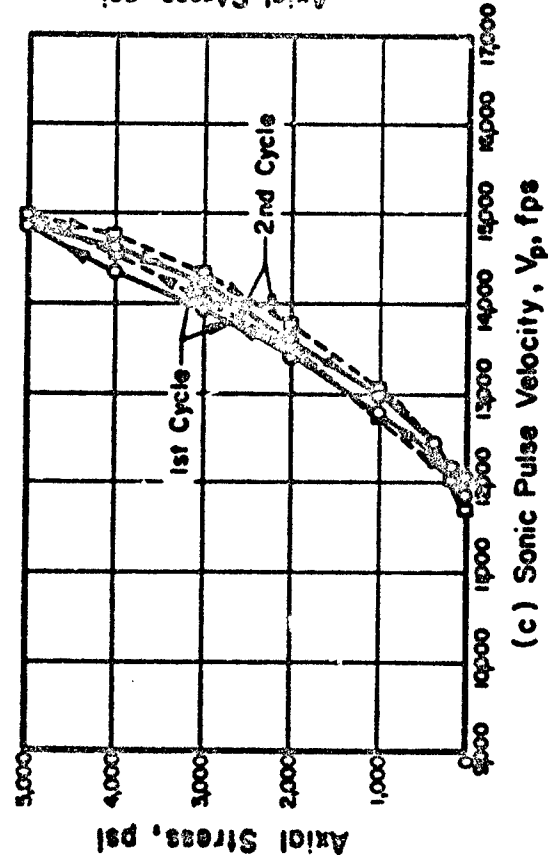
(a) Axial Strain, %



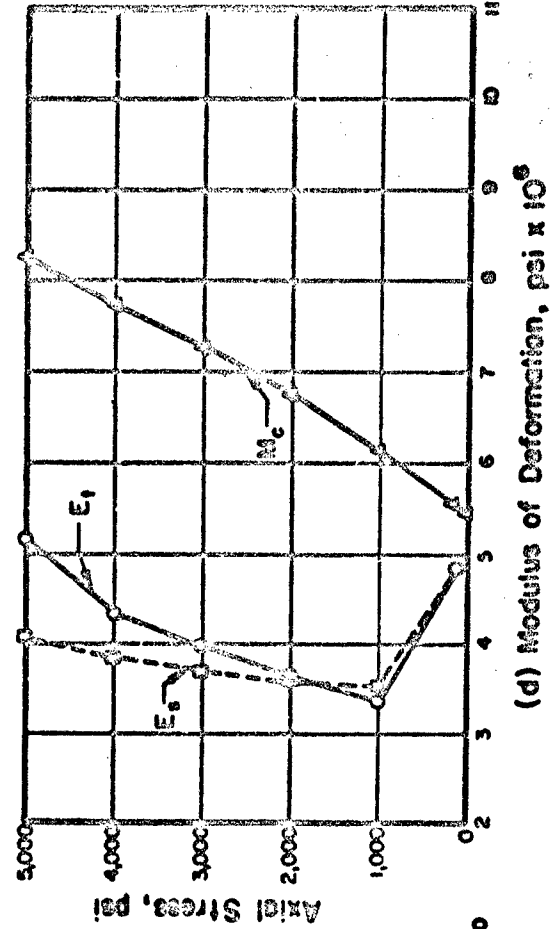
(b) Poisson's Ratio

Rock Type	Gneiss (Dumortierite)
Specimen No.	4.12X157.2-50
L/D	2.105
$\gamma_0$	173.6 pcf
$S_n$	87.9
$\sigma_0$ (ult)	25.7 ksi
Texture	Foliated

Note:  
 1)  $V_p$  = Dilatational wave velocity  
 2)  $E_t$  = Tangent modulus (static)  
 3)  $E_s$  = Secant modulus (static)  
 4)  $M_c$  = Consolidated modulus  
       =  $\rho V_p^2$  (dynamic)



(c) Sonic Pulse Velocity,  $V_p$ , fps



(d) Modulus of Deformation,  $\text{psi} \times 10^6$

FIGURE B.10A STRESS-STRAIN BEHAVIOR AND SONIC PULSE VELOCITY FOR ROCK IN UNIAXIAL COMPRESSION

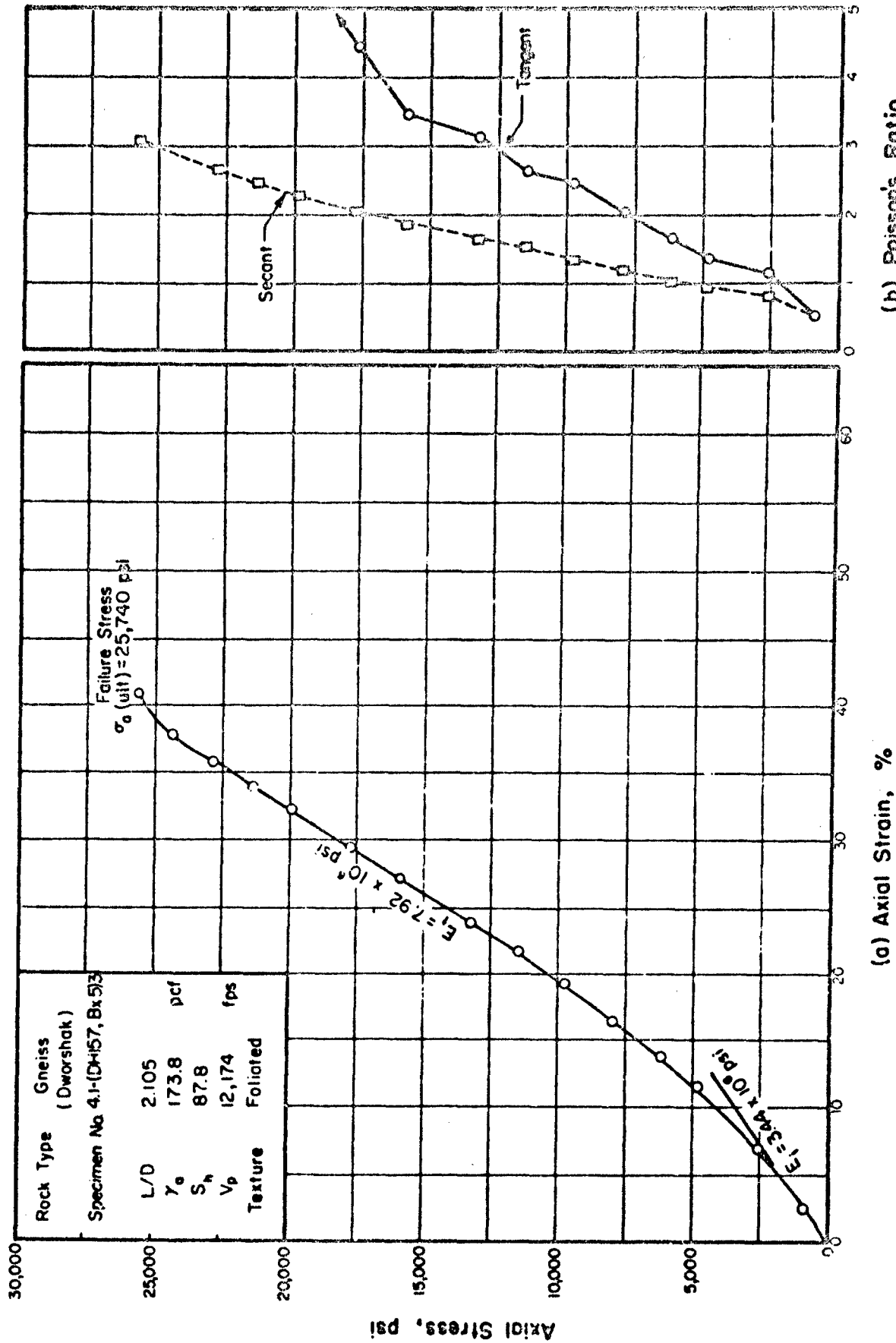
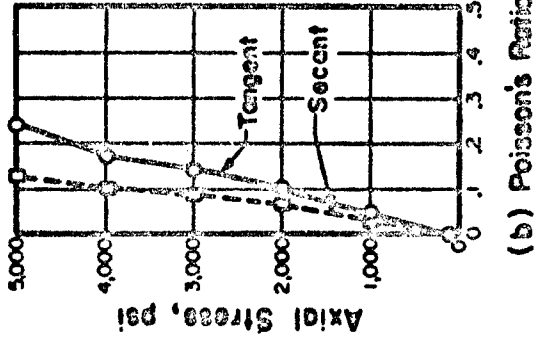
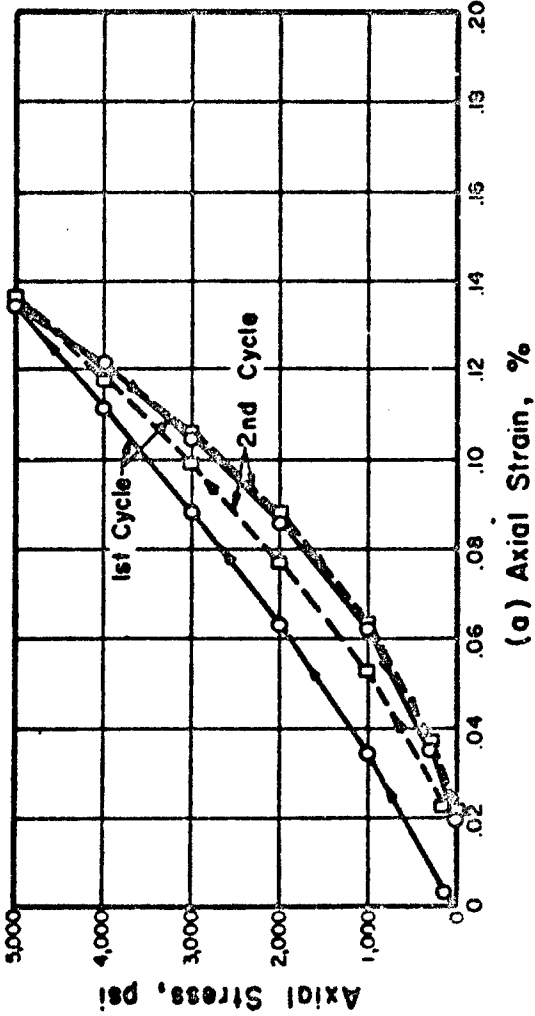


FIGURE B.10B STRESS-STRAIN CURVE AND POISSON'S RATIO FOR ROCK IN UNIAxIAL COMPRESSION TO FAILURE





Rock Type	Granite
(Photo Rock)	
Specimen No.	51 - (R1, R2, R-3)3
L/D	2.003
$\gamma_0$	156.9
$S_h$	70.5
$\sigma_0$ (ult)	13.6
Texture	Interlocking

Note:  
 1)  $V_p$  = Dilational wave velocity  
 2)  $E_t$  = Tangent modulus (static)  
 3)  $E_s$  = Secant modulus (static)  
 4)  $M_c$  = Constrained modulus  
 $= \rho V_p^2$  (dynamic)

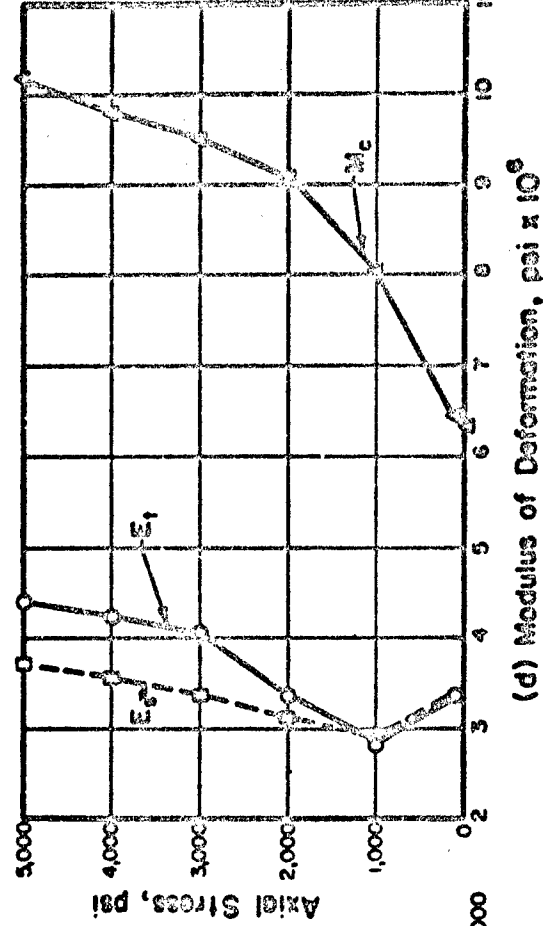
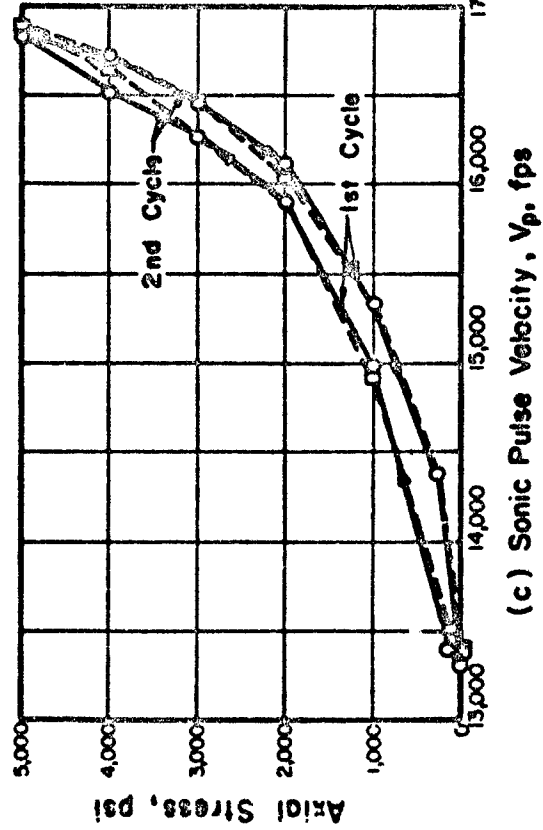
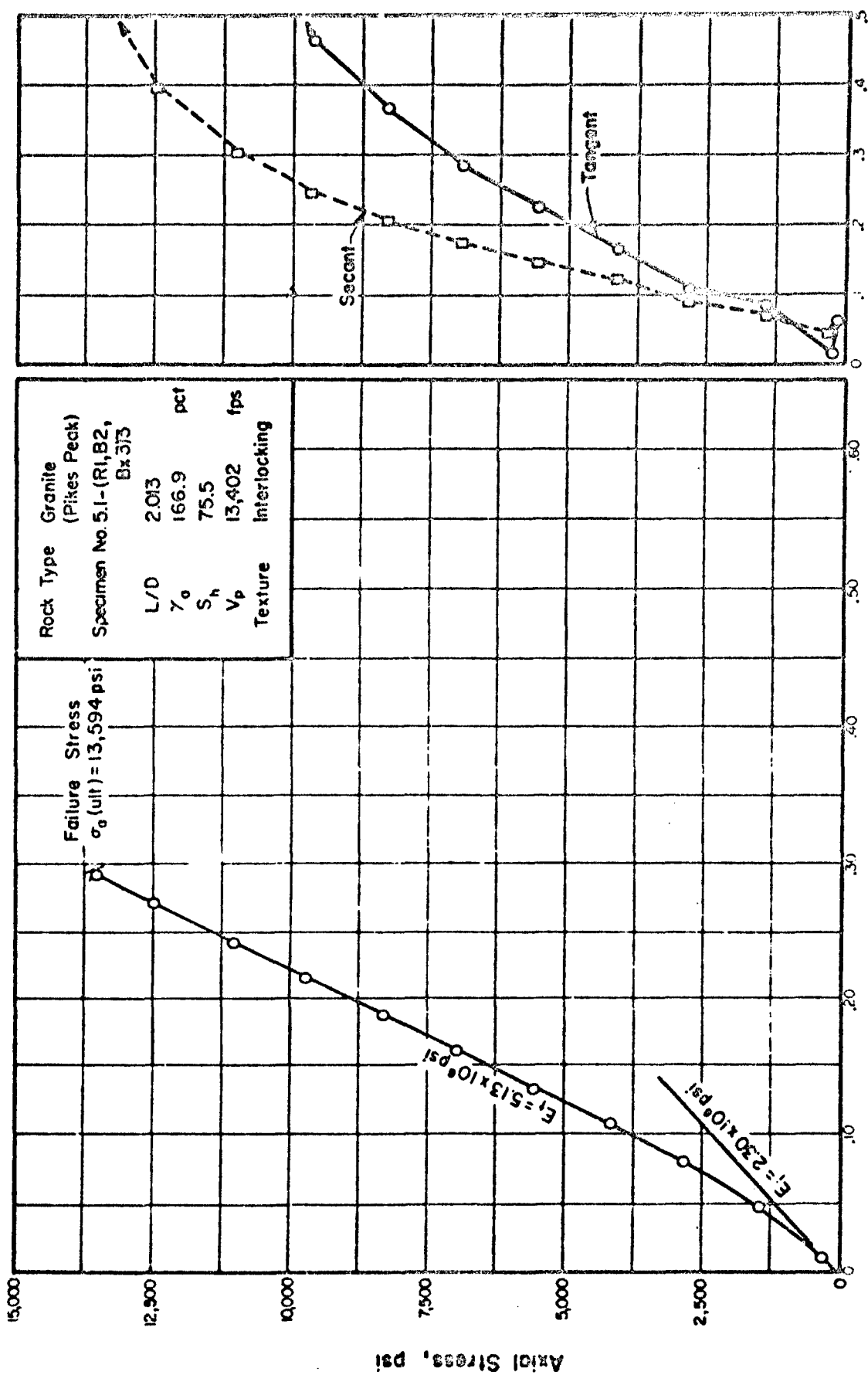
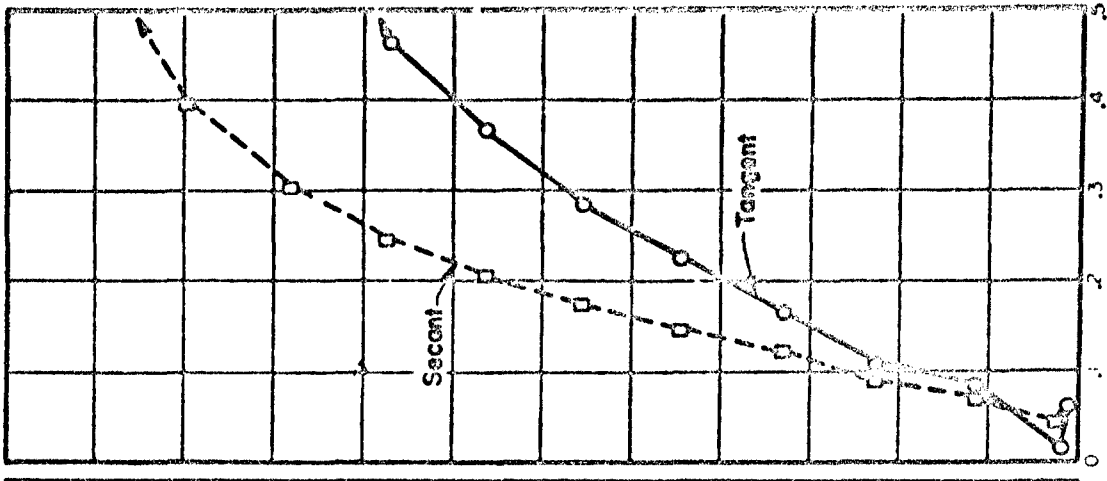


FIGURE B.11A STRESS-STRAIN BEHAVIOR AND SONIC PULSE VELOCITY FOR ROCK IN UNIAXIAL COMPRESSION



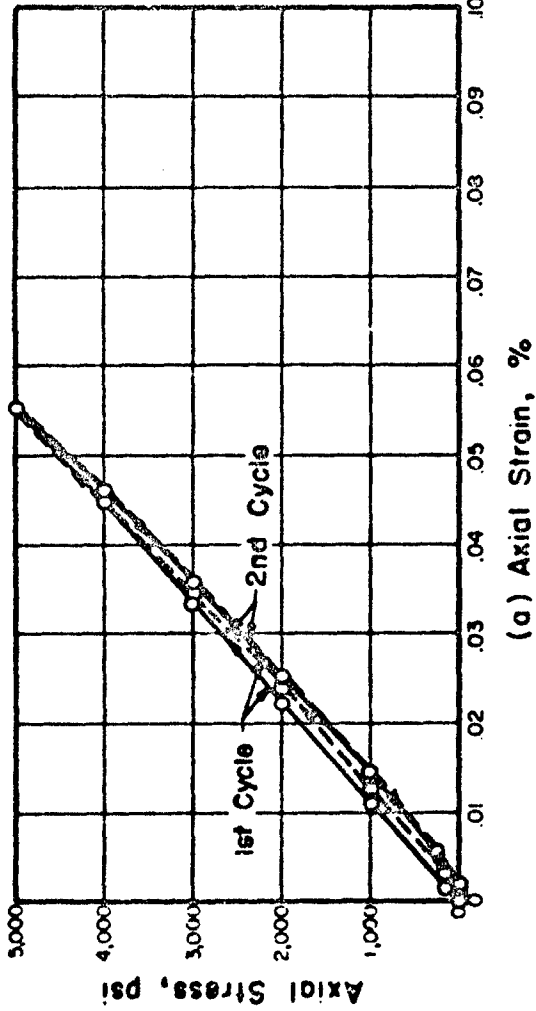
Rock Type	Granite (Pikes Peak)
Specimen No.	5.1-(R1,B2, Bx3)3
L/D	2.013
$\gamma_a$	166.9 pct
$S_h$	75.5
$V_p$	13,402 fps
Texture	Interlocking

(a) Axial Strain, %

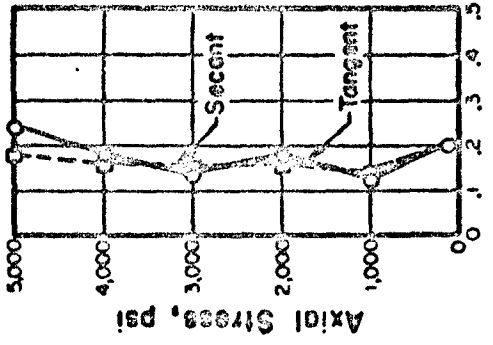


(b) Poisson's Ratio

FIGURE B.11B STRESS-STRAIN CURVE AND POISSON'S RATIO FOR ROCK IN UNIAXIAL COMPRESSION TO FAILURE



(a) Axial Strain, %

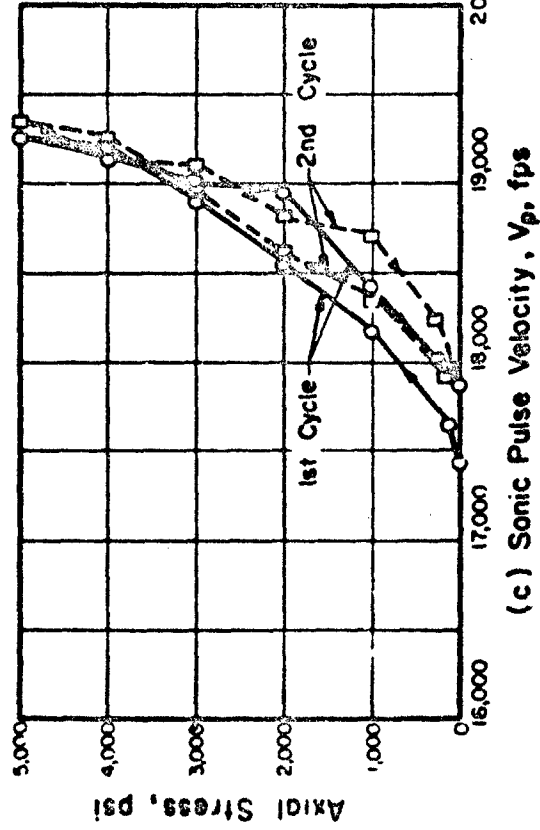


(b) Poisson's Ratio

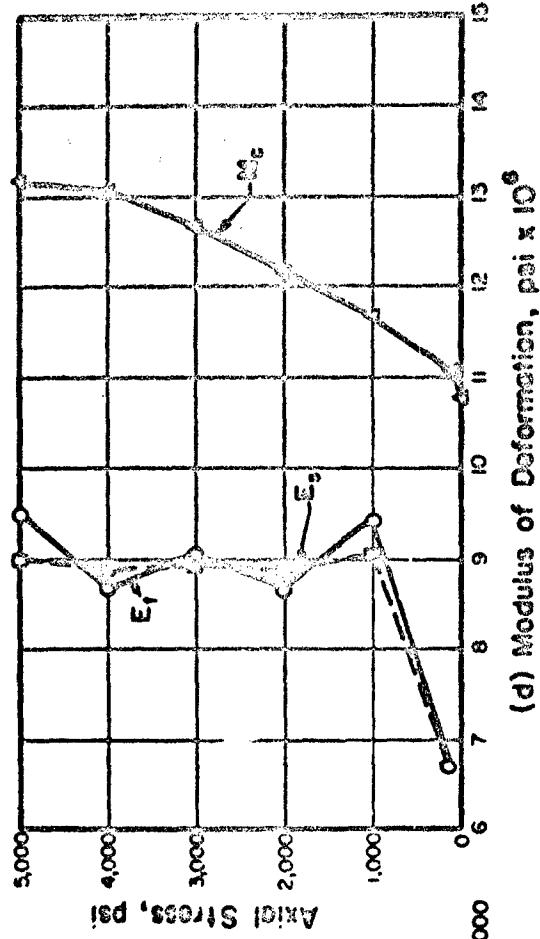
Rock Type	Granite (Plus Peak)
Specimen No	5.2 - (73,530)
L/D	2.015
$\gamma_0$	164.6
$S_h$	103.7
$\sigma_0$ (ult)	33.1
Texture	Interlocking

Note:

- 1)  $V_p$  = Dilatational wave velocity
- 2)  $E_t$  = Tangent modulus (static)
- 3)  $E_s$  = Secant modulus (static)
- 4)  $M_c$  = Constrained modulus  
=  $\rho V_p^2$  (dynamic)



(c) Sonic Pulse Velocity,  $V_p$ , fps



(d) Modulus of Deformation,  $\text{psi} \times 10^6$

FIGURE B.12A STRESS-STRAIN BEHAVIOR AND SONIC PULSE VELOCITY FOR ROCK IN UNIAXIAL COMPRESSION

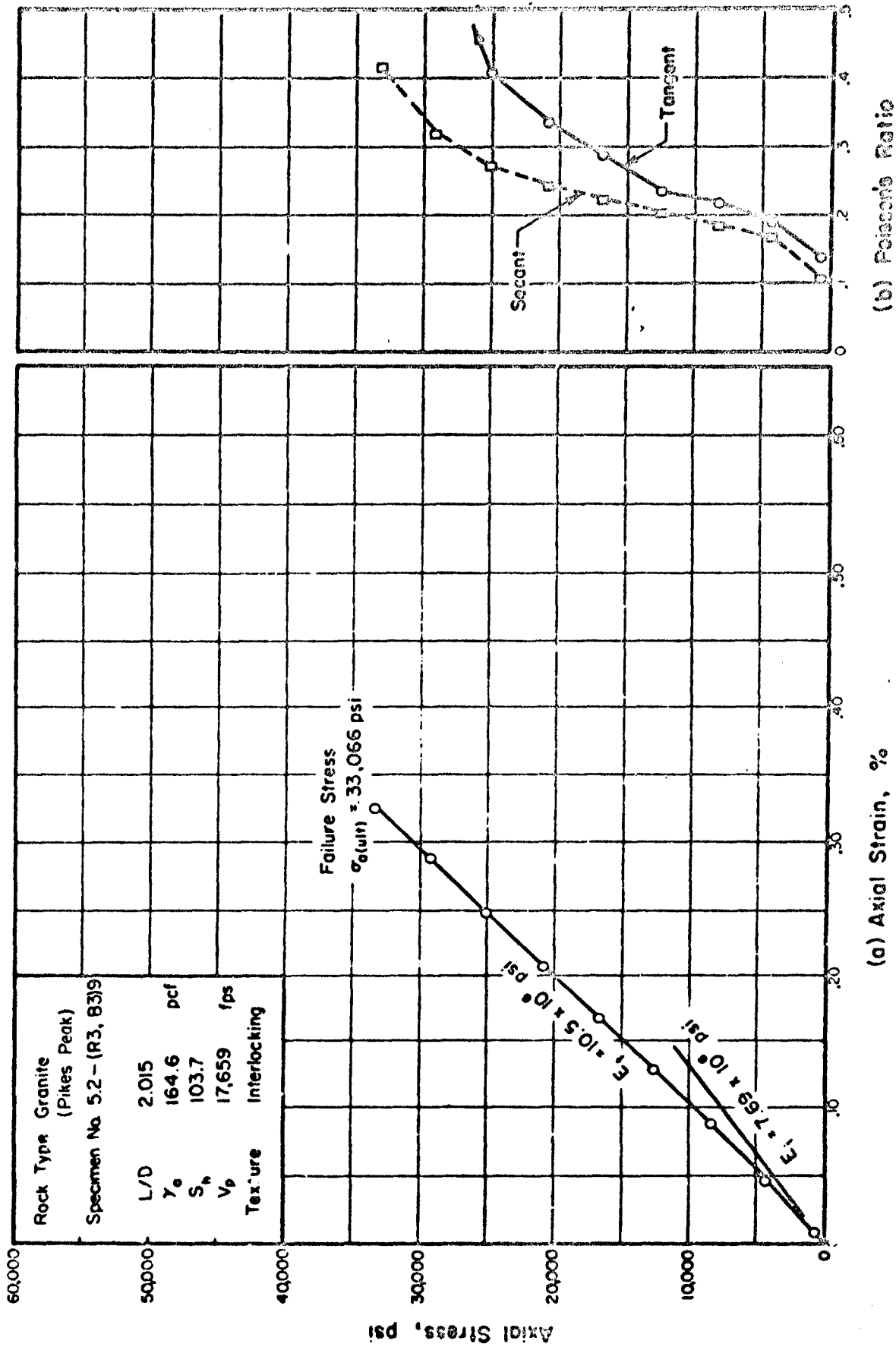
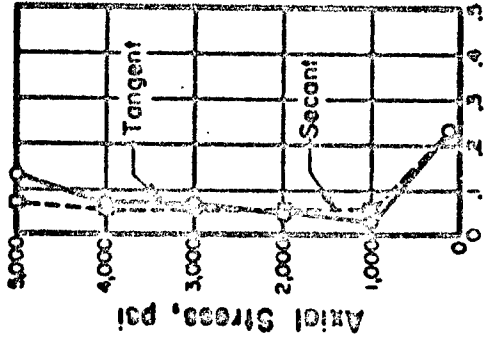
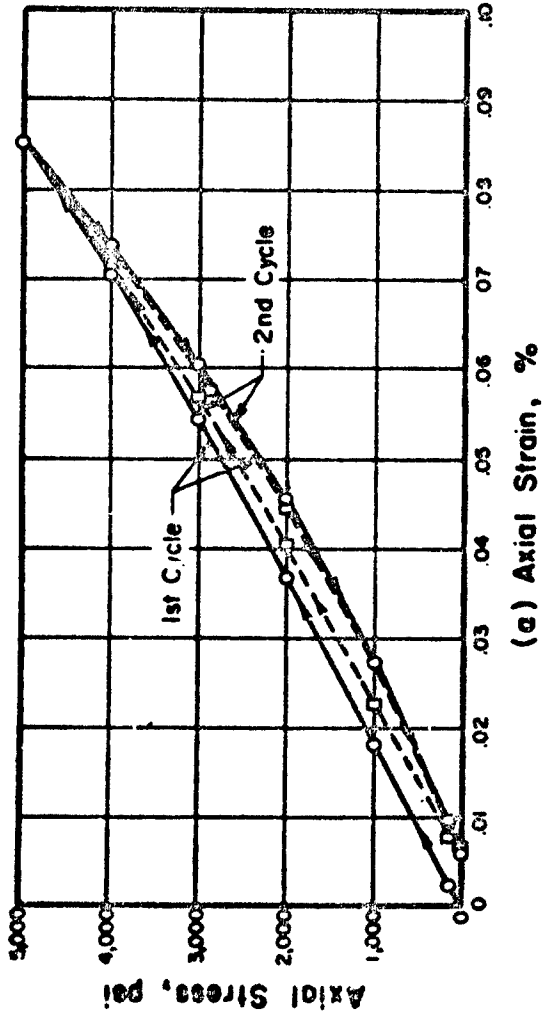


FIGURE B.12B STRESS-STRAIN CURVE AND POISSON'S RATIO FOR ROCK IN UNIAXIAL COMPRESSION TO FAILURE



Rock Type	Granite (Barre)
Specimen No.	5.3-(1)2
L/D	2.034
$\gamma_0$	165.3
$S_h$	1010
$\sigma_0$ (ult)	29.6
Texture	interlocking

Note:  
 1)  $V_p$  = Dilatational wave velocity  
 2)  $E_t$  = Tangent modulus (static)  
 3)  $E_s$  = Secant modulus (static)  
 4)  $M_c = \rho V_p^2$  = Constrained modulus (dynamic)

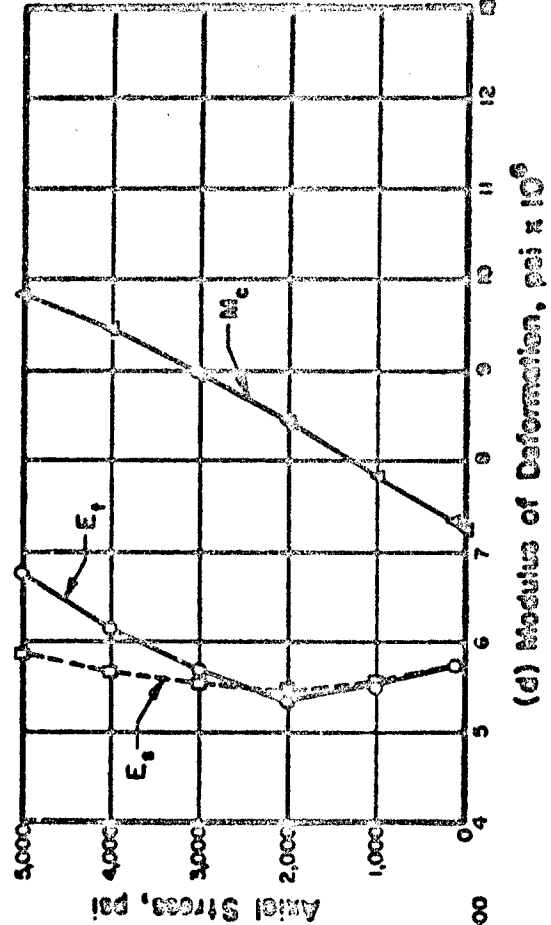
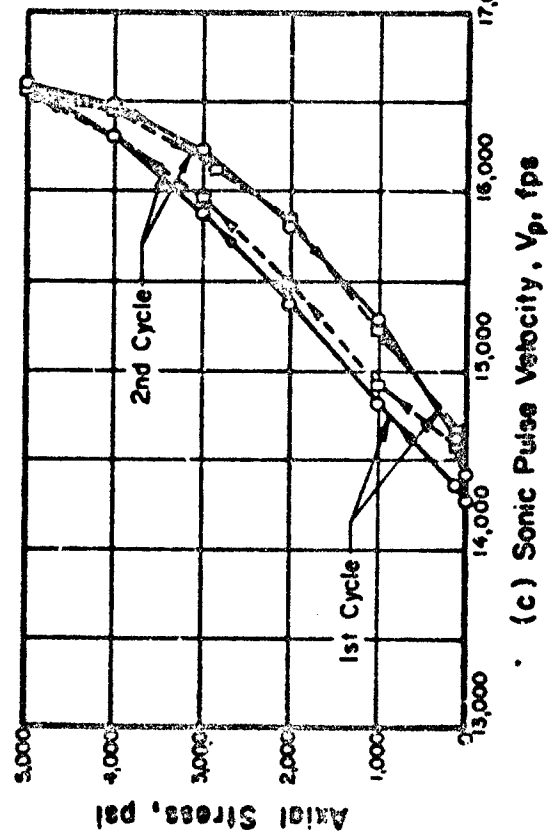


FIGURE B.13A STRESS-STRAIN BEHAVIOR AND SONIC PULSE VELOCITY FOR ROCK IN UNIAXIAL COMPRESSION

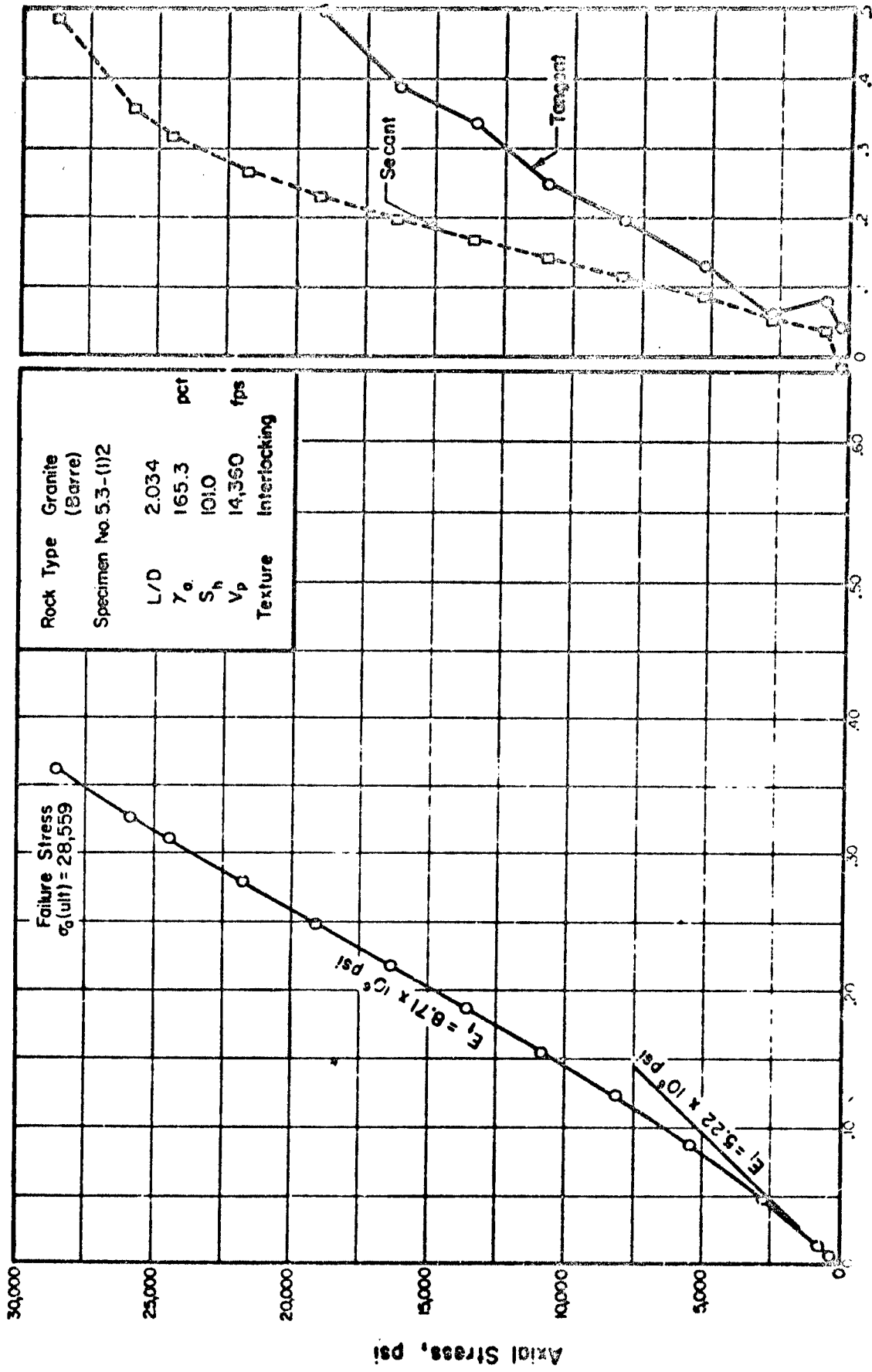
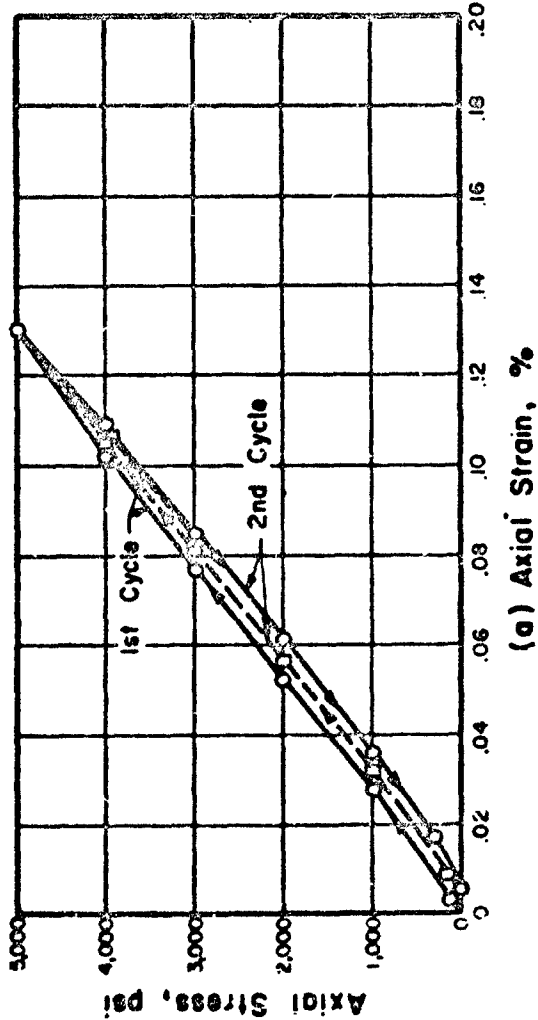
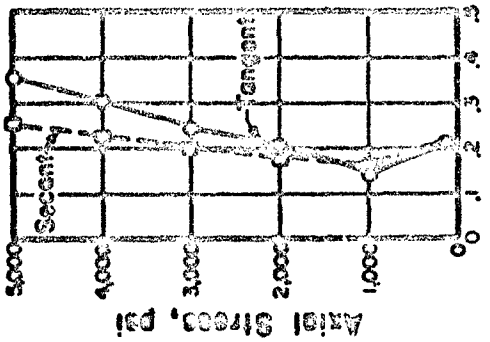


FIGURE B13B STRESS-STRAIN CURVE AND POISSON'S RATIO FOR ROCK IN UNIAXIAL COMPRESSION TO FAILURE



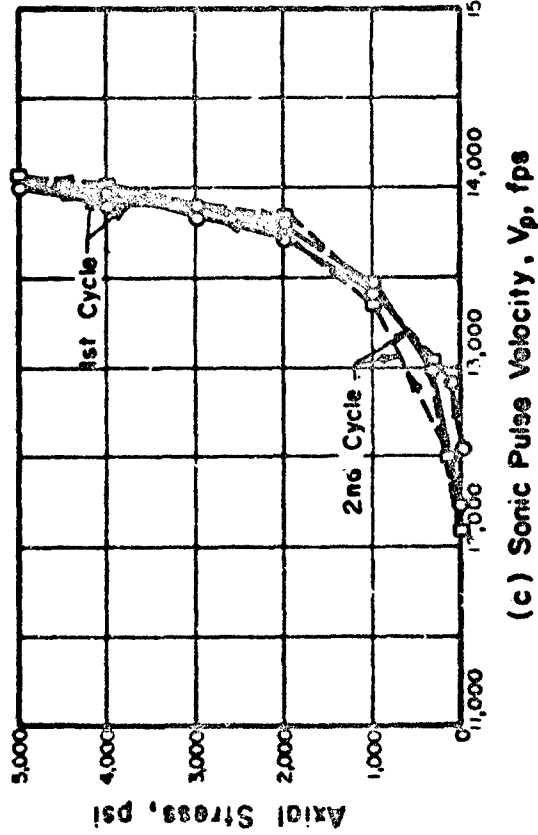
(a) Axial Strain, %



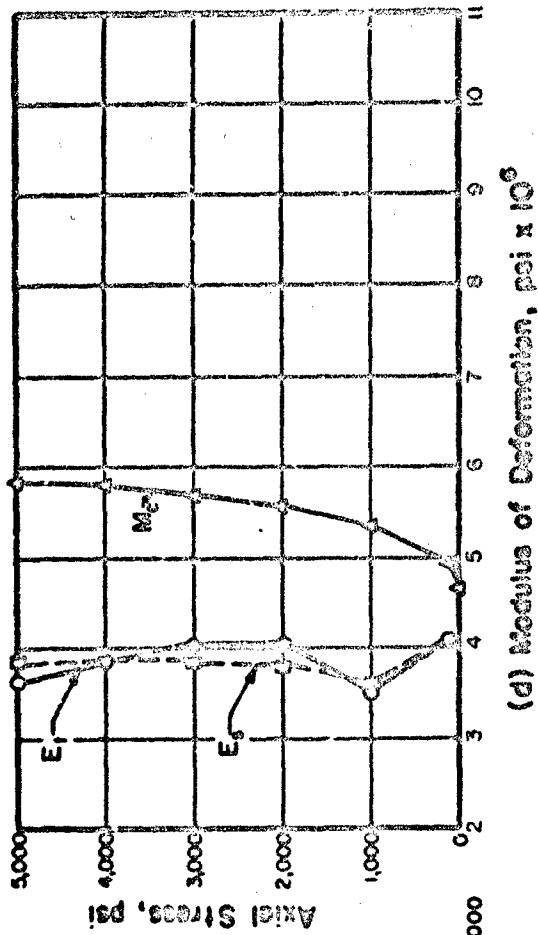
(b) Poisson's Ratio

Rock Type	Limestone (Bedford)
Specimen No.	G.1-(1) 4
L/D	2.000
$\gamma_c$	138.0
$S_h$	18.9
$\sigma_c$ (ult.)	7.50
Texture	Cemented

Note:  
 1)  $V_p$  = Dilatational wave velocity  
 2)  $E_1$  = Tangent modulus (static)  
 3)  $E_s$  = Secant modulus (static)  
 4)  $M_c$  = Constrained modulus  
 $= \rho V_p^2$  (dynamic)

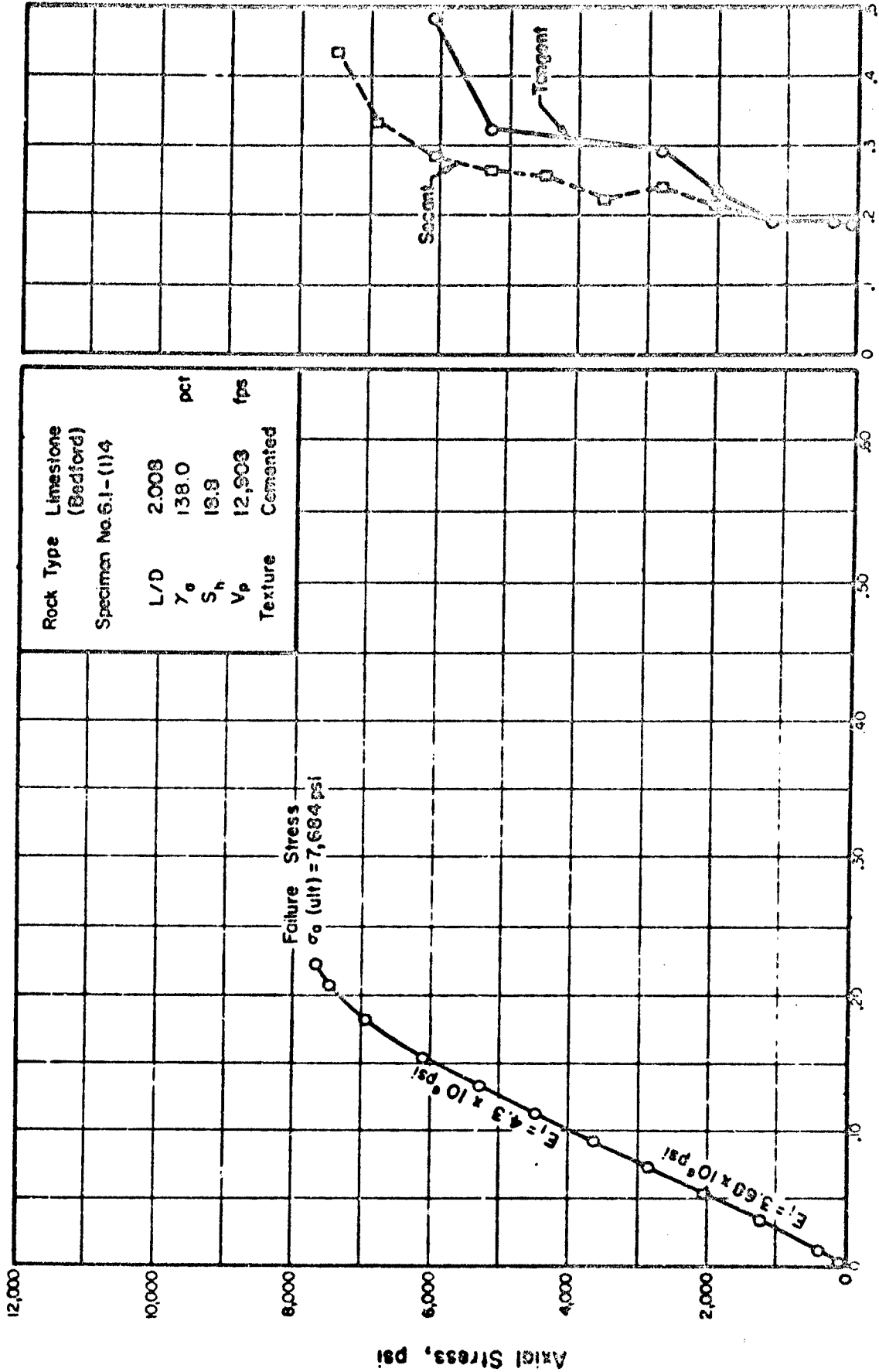


(c) Sonic Pulse Velocity,  $V_p$ , fps



(d) Modulus of Deformation,  $\text{psi} \times 10^6$

FIGURE B.14A STRESS-STRAIN BEHAVIOR AND SONIC PULSE VELOCITY FOR ROCK IN UNIAxIAL COMPRESSION

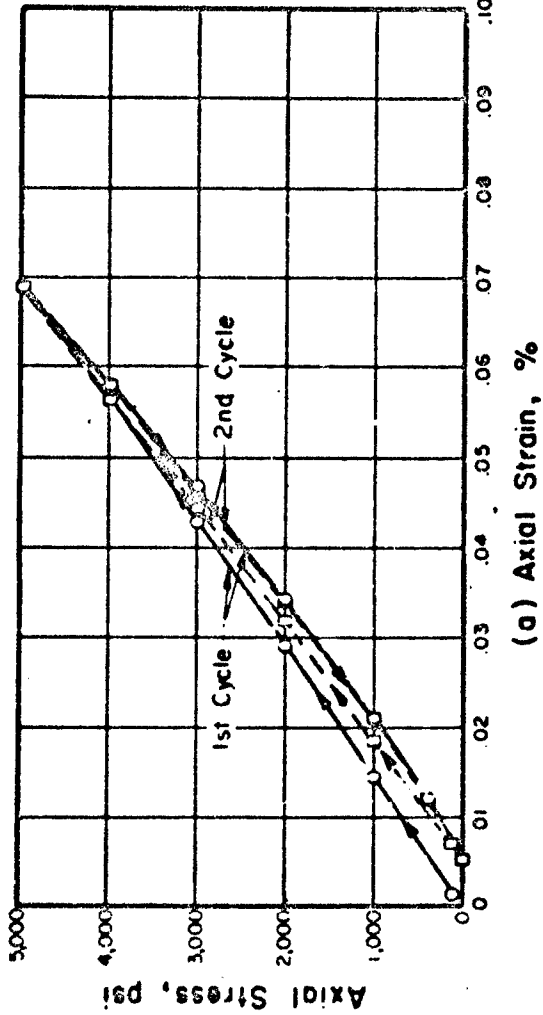


(a) Axial Stress, %

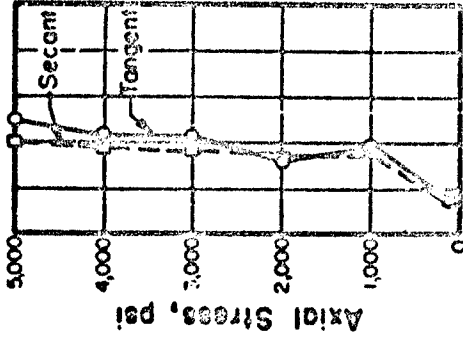
(b) Poisson's Ratio

FIGURE B.14B STRESS-STRAIN CURVE AND POISSON'S RATIO FOR ROCK IN UNIAxIAL COMPRESSION TO FAILURE





(a) Axial Strain, %

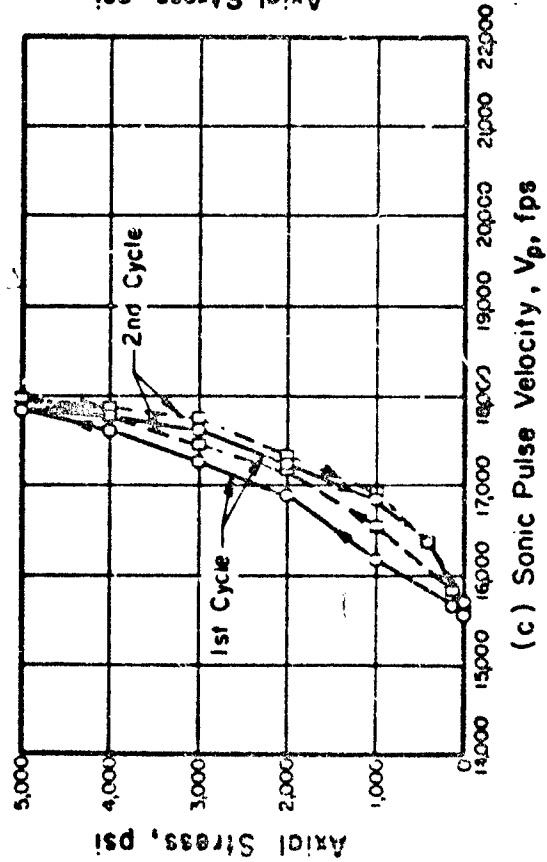


(b) Poisson's Ratio

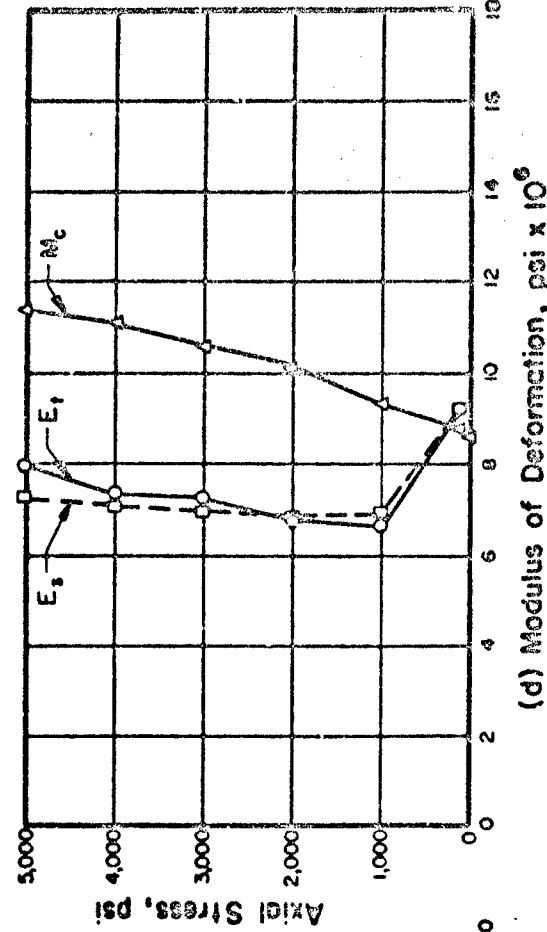
Rock Type	Limestone
(Ozark Tovernalto)	
Specimen No.	6.2 - (1)B
L/D	2.003
$\gamma_0$	165.7 pcf
$S_h$	50.5
$\sigma_0$ (ult)	14.0 ksi
Texture	Cemented

Note:

- 1)  $V_p$  = Stational wave velocity
- 2)  $E_t$  = Tangent modulus (static)
- 3)  $E_s$  = Secant modulus (static)
- 4)  $M_c = \rho V_p^2$  (dynamic)

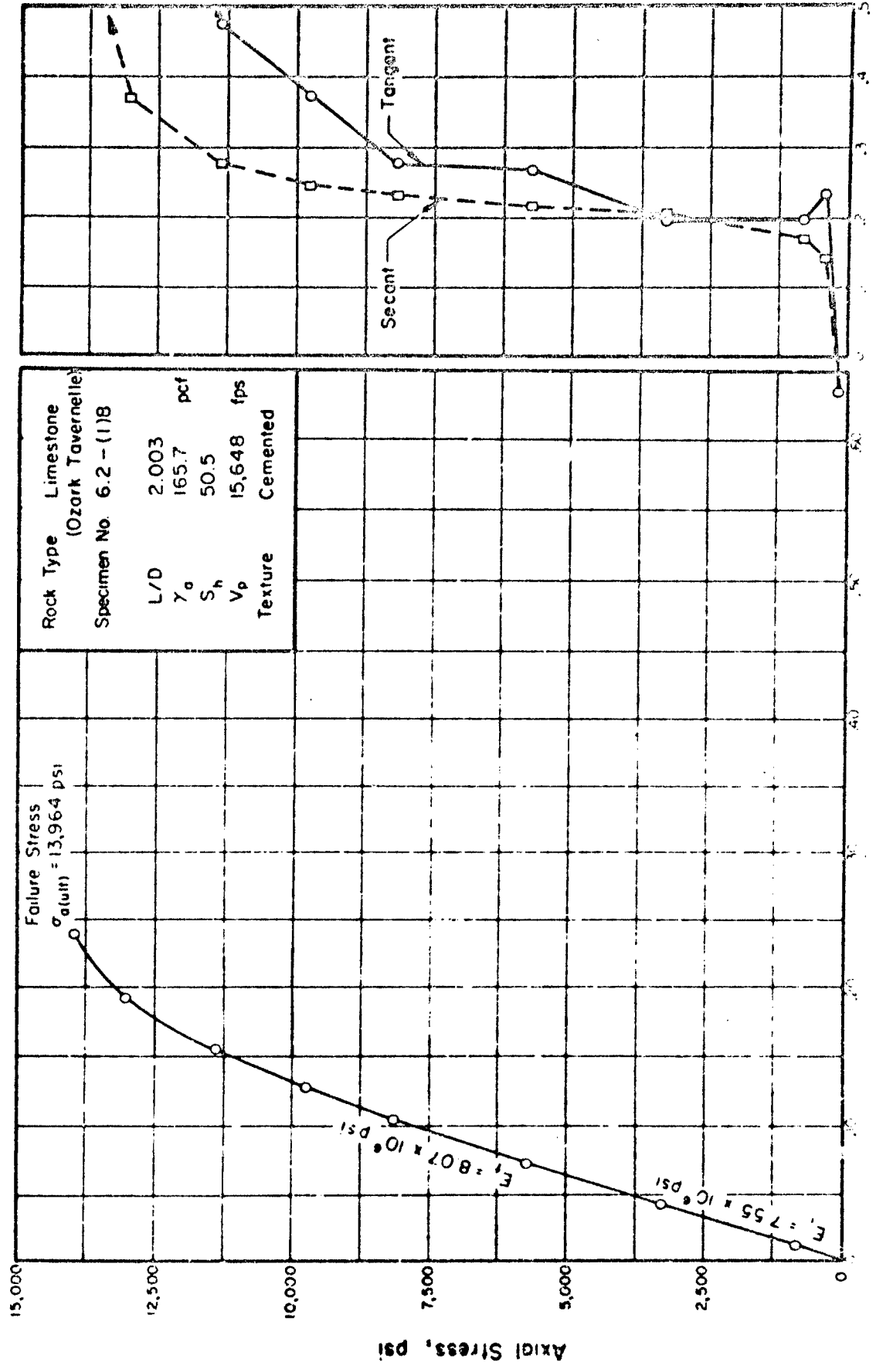


(c) Sonic Pulse Velocity,  $V_p$ , fps

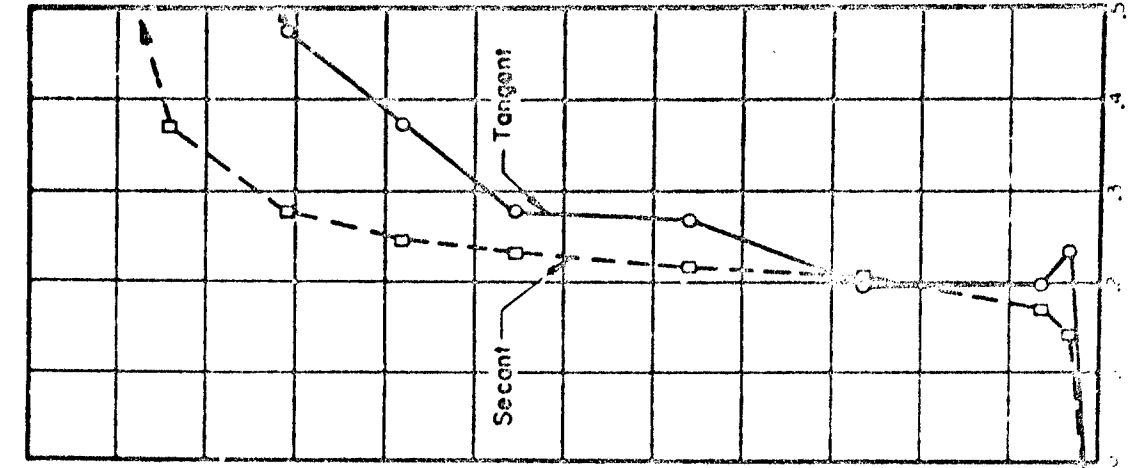


(d) Modulus of Deformation,  $\text{psi} \times 10^6$

FIGURE B.15A STRESS-STRAIN BEHAVIOR AND SONIC PULSE VELOCITY FOR ROCK IN UNIAXIAL COMPRESSION

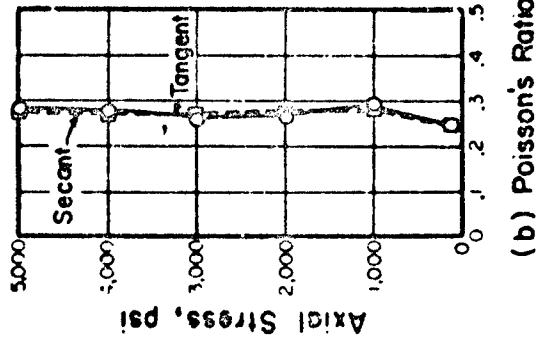
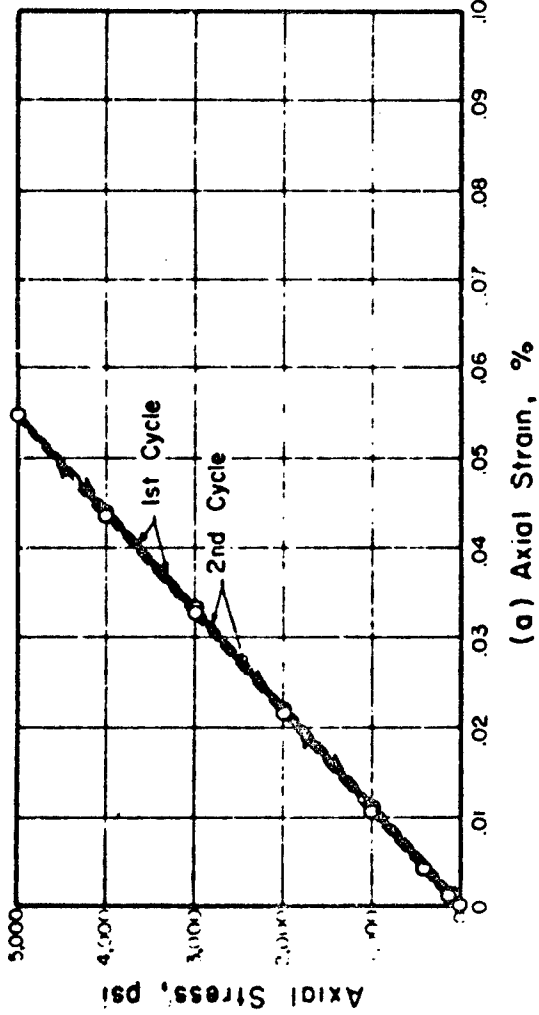


(a) Axial Strain, %



(b) Poisson's Ratio

FIGURE B.15B STRESS-STRAIN CURVE AND POISSON'S RATIO FOR ROCK IN UNIAXIAL COMPRESSION TO FAILURE



Rock Type	Limestone (Selenhofen)
Specimen No	6.3-(1)5
L/D	2.033
$\gamma_0$	163.3 pcf
$S_h$	64.0
$\sigma_0$ (ult)	35.0 ksi
Texture	Interlocking

Note:  
 1)  $V_p$  = Dilatational wave velocity  
 2)  $E_t$  = Tangent modulus (static)  
 3)  $E_s$  = Secant modulus (static)  
 4)  $M_c = \rho V_p^2$  (dynamic)

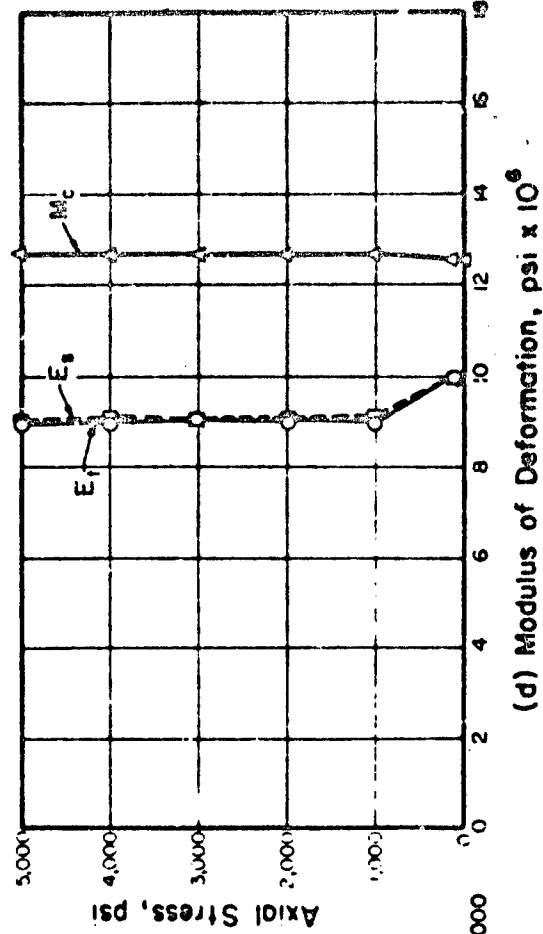
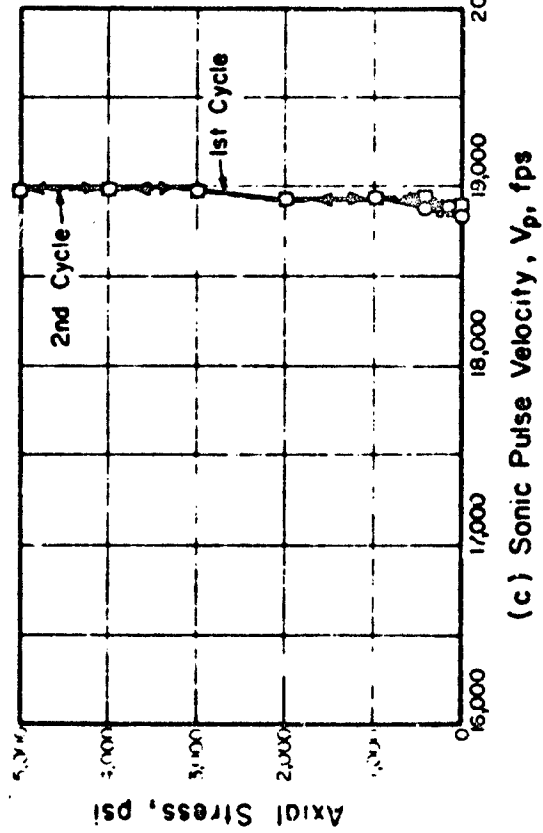
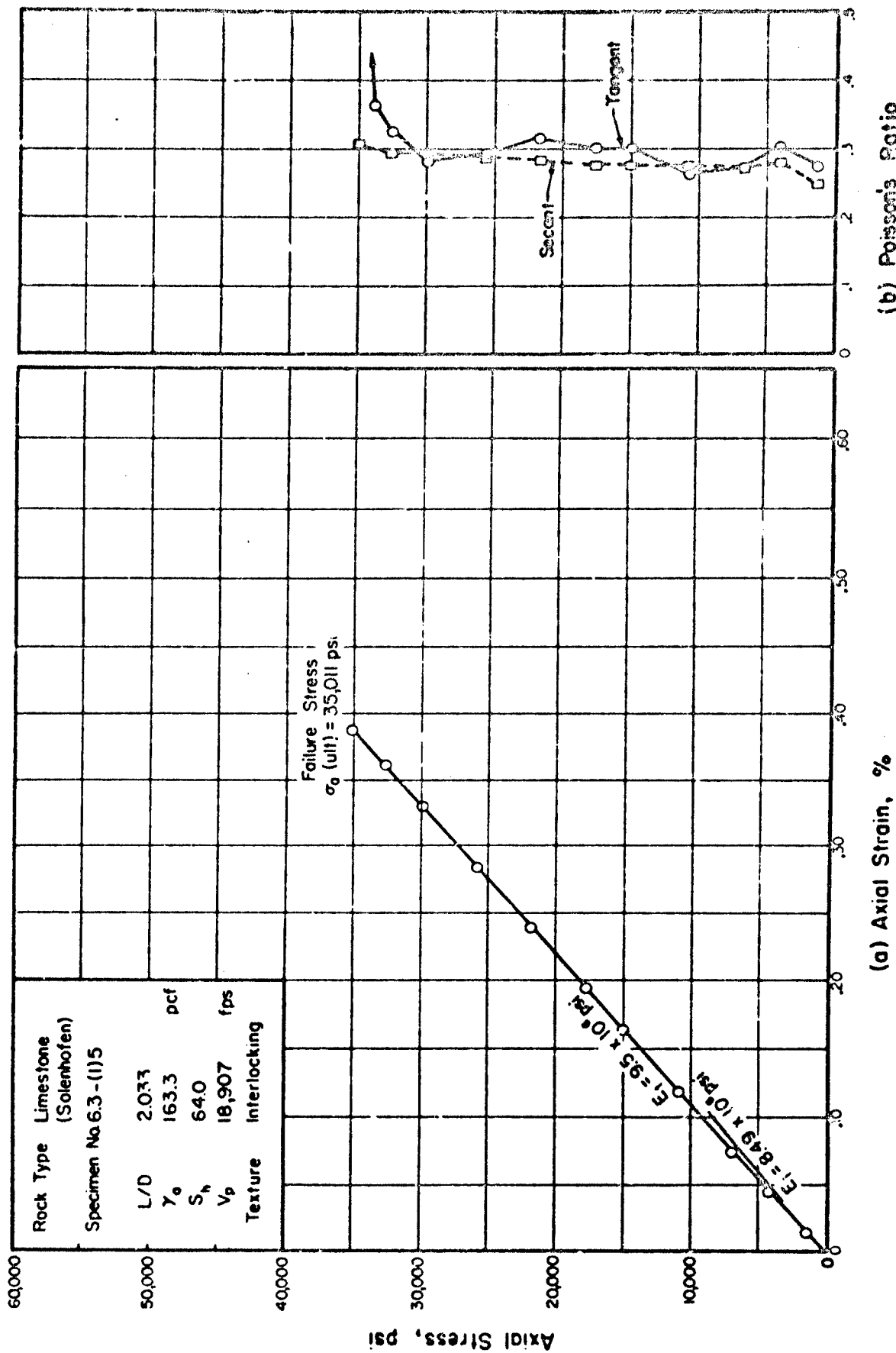


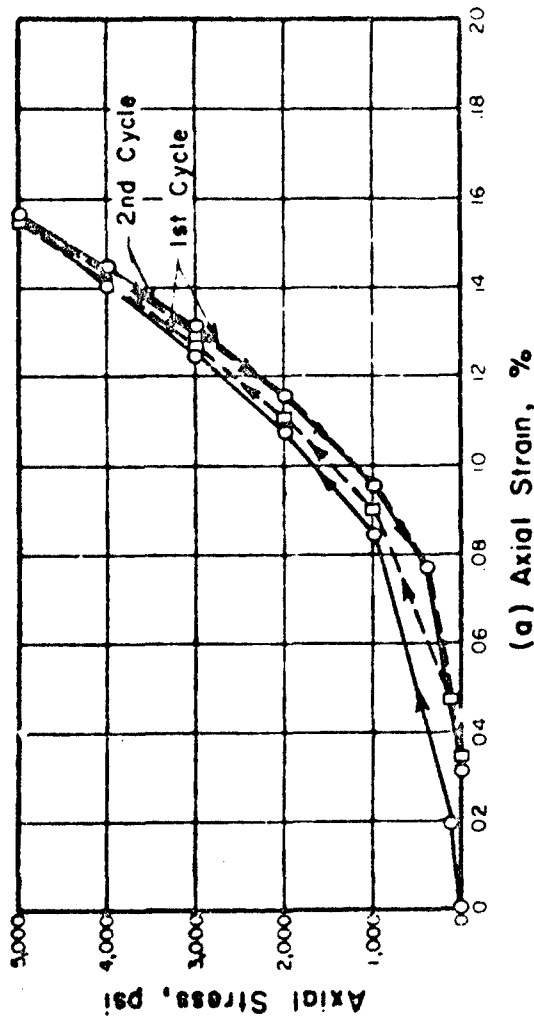
FIGURE B.16A STRESS-STRAIN BEHAVIOR AND SONIC PULSE VELOCITY FOR ROCK IN UNIAXIAL COMPRESSION



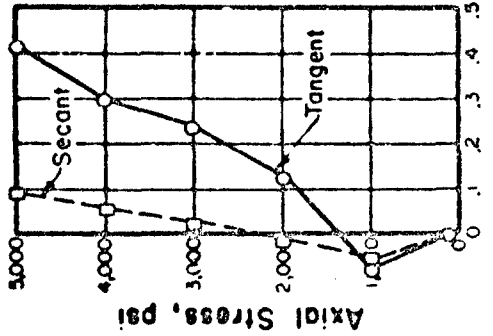
(a) Axial Strain, %

(b) Poisson's Ratio

FIGURE B.108 STRESS-STRAIN CURVE AND POISSON'S RATIO FOR ROCK IN UNIAXIAL COMPRESSION TO FAILURE



(a) Axial Strain, %

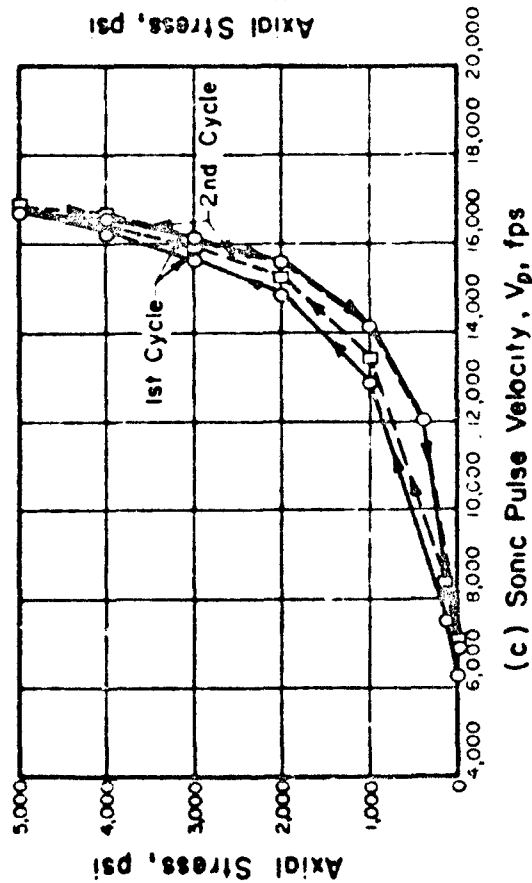


(b) Poisson's Ratio

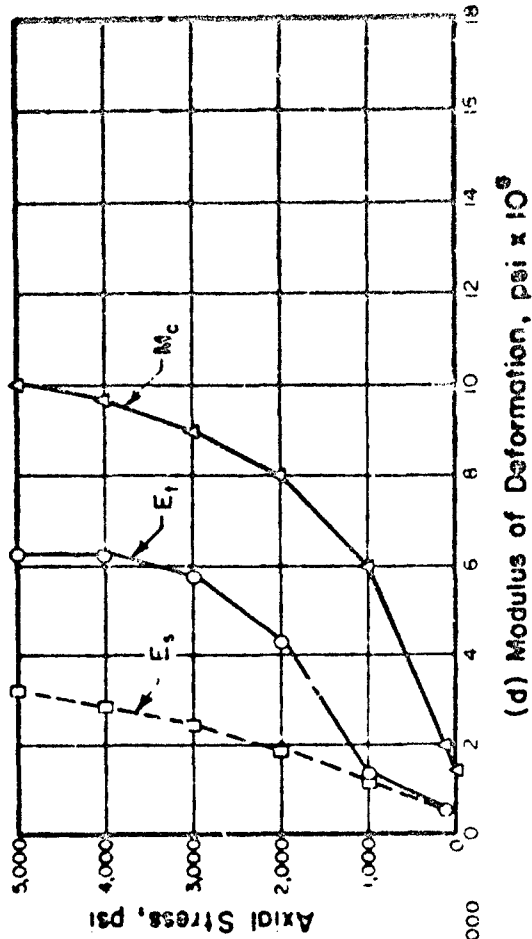
Rock Type	Marble (Taconic White)	
Specimen No.	7.1-(1)4	
L/D	2.006	
$\gamma_0$	169.0	pcf
$S_n$	36.9	
$\sigma_a$ (ult)	9.01	ksi
Texture	Interlocking	

Note:

- 1)  $V_p$  = Dilatational wave velocity
- 2)  $E_t$  = Tangent modulus (static)
- 3)  $E_s$  = Secant modulus (static)
- 4)  $M_c$  = Constrained modulus  
=  $\rho V_p^2$  (dynamic)

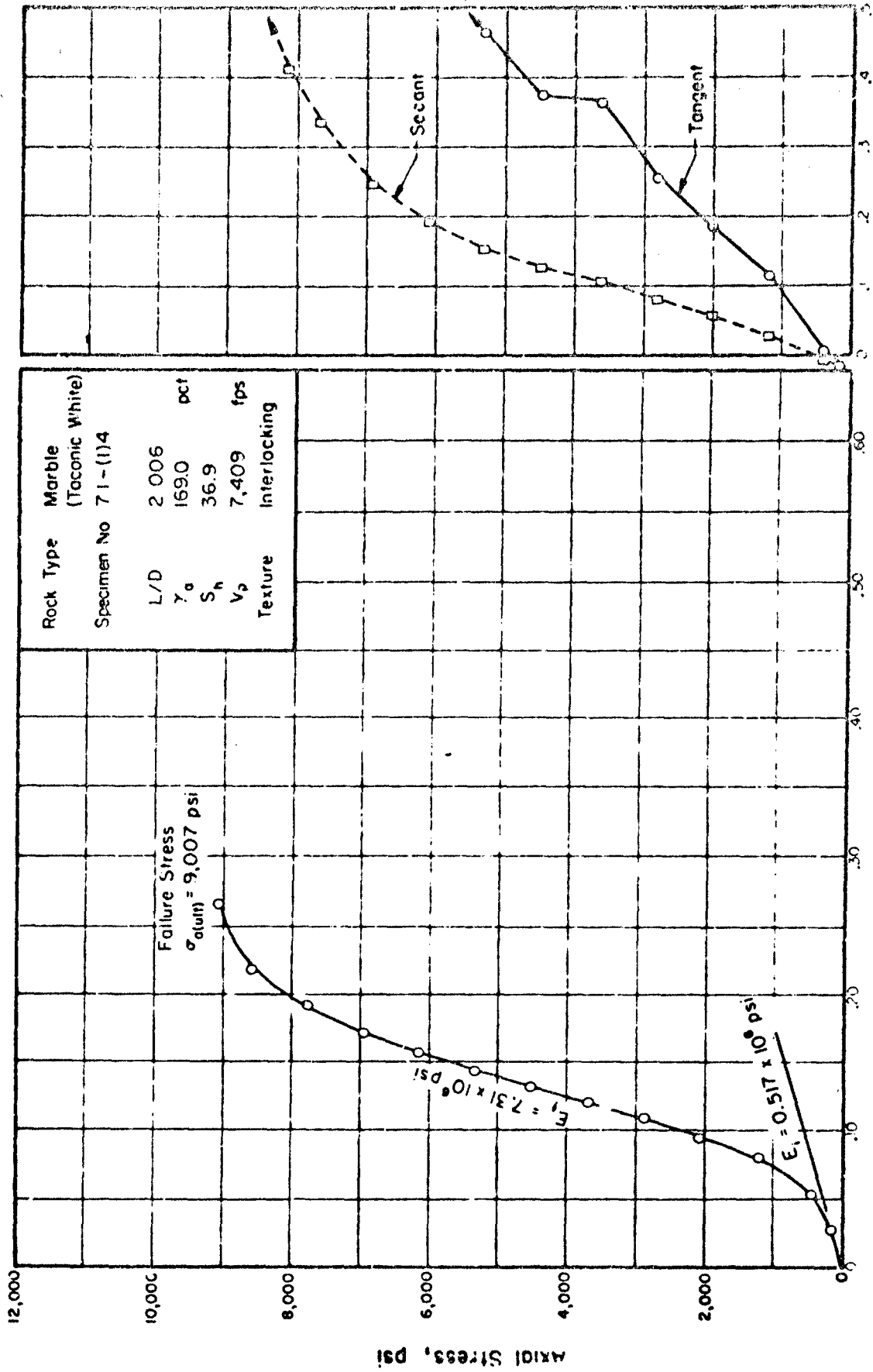


(c) Sonic Pulse Velocity,  $V_p$ , fps



(d) Modulus of Deformation,  $\text{psi} \times 10^6$

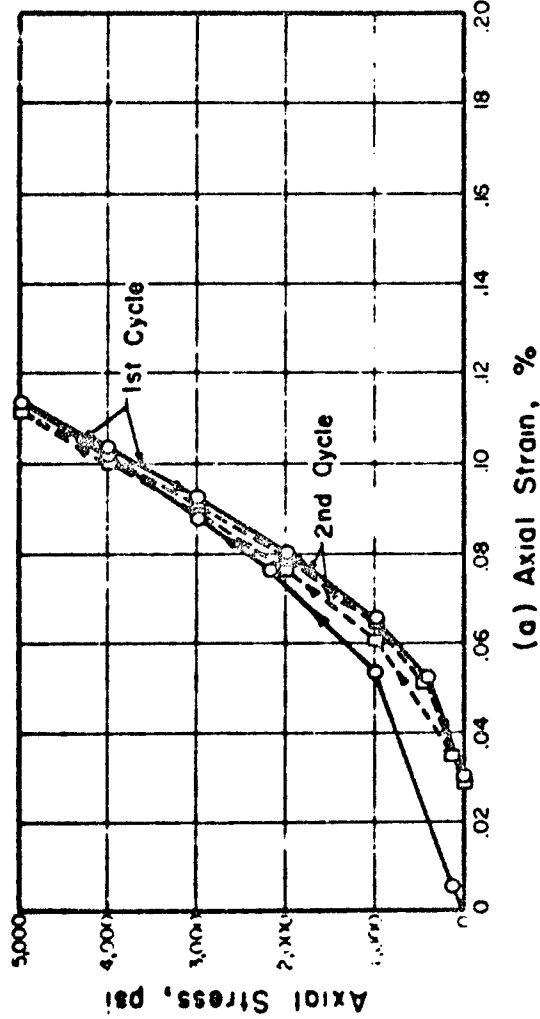
FIGURE B.1.7A STRESS-STRAIN BEHAVIOR AND SONIC PULSE VELOCITY FOR ROCK IN UNIAXIAL COMPRESSION



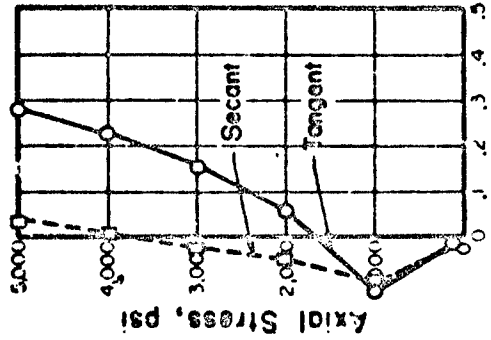
(a) Axial Strain, %

(b) Poisson's Ratio

FIGURE B.17B STRESS-STRAIN CURVE AND POISSON'S RATIO FOR ROCK IN UNIAXIAL COMPRESSION TO FAILURE



(a) Axial Strain, %

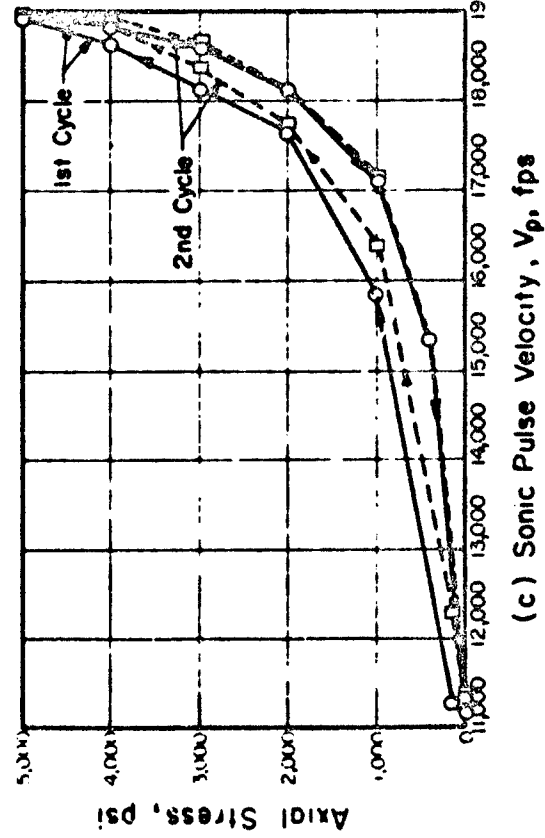


(b) Poisson's Ratio

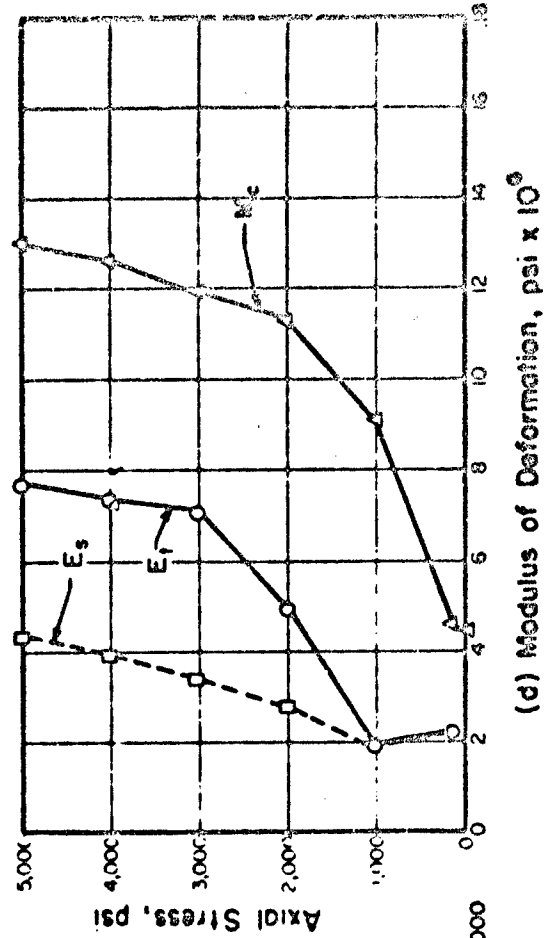
Rock Type	Marble (Chertisee)	
Specimen No	7.2 - (116)	
L/D	2.033	
$\gamma_0$	169.1	pcf
$S_h$	42.4	
$\sigma_0$ (ult)	983	ksi
Texture	Interlocking	

Note:

- 1)  $V_p$  = Dilatational wave velocity
- 2)  $E_t$  = Tangent modulus (static)
- 3)  $E_s$  = Secant modulus (static)
- 4)  $M_c = \rho V_p^2$  (dynamic)

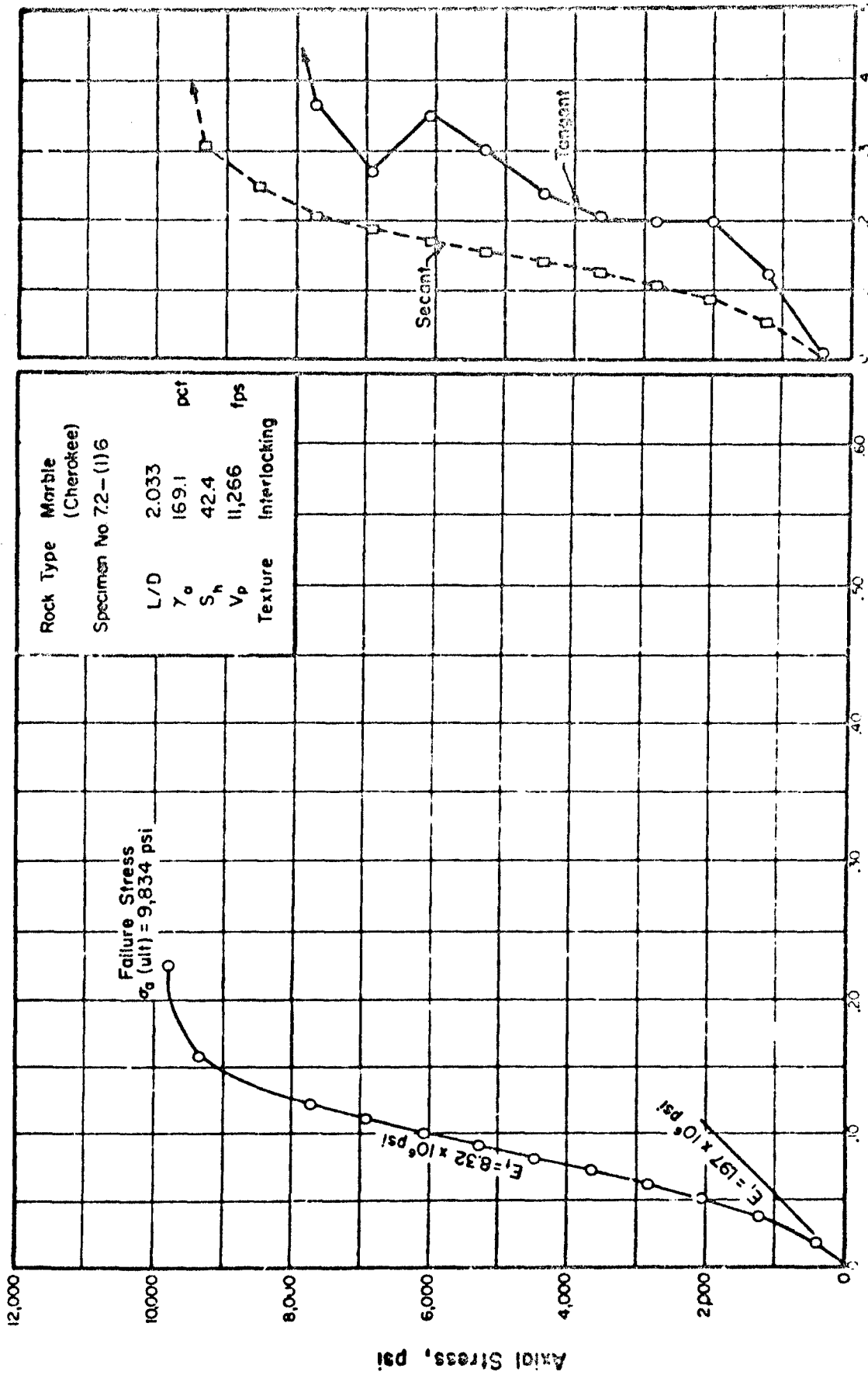


(c) Sonic Pulse Velocity,  $V_p$ , fps



(d) Modulus of Deformation,  $\text{psi} \times 10^9$

FIGURE B.18A STRESS-STRAIN BEHAVIOR AND SONIC PULSE VELOCITY FOR ROCK IN UNIAXIAL COMPRESSION

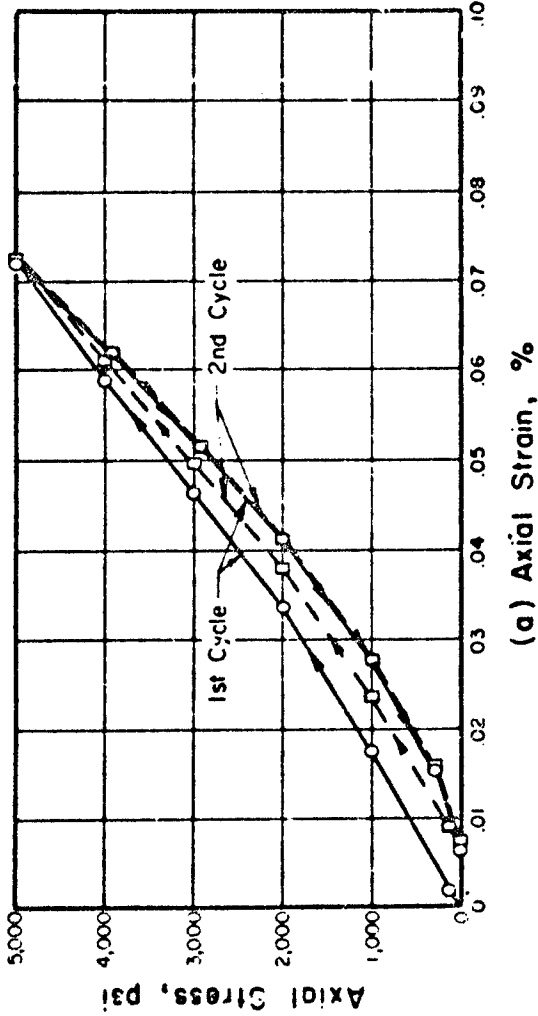


(a) Axial Strain, %

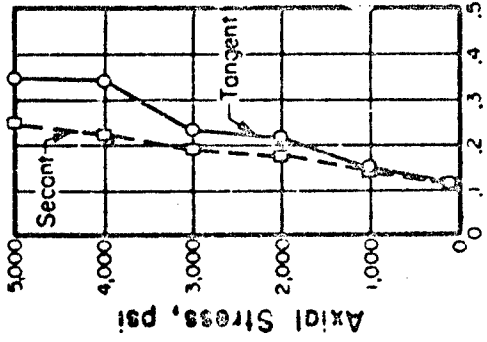
(b) Poisson's Ratio

FIGURE B.18B STRESS-STRAIN CURVE AND POISSON'S RATIO FOR ROCK IN UNIAXIAL COMPRESSION TO FAILURE





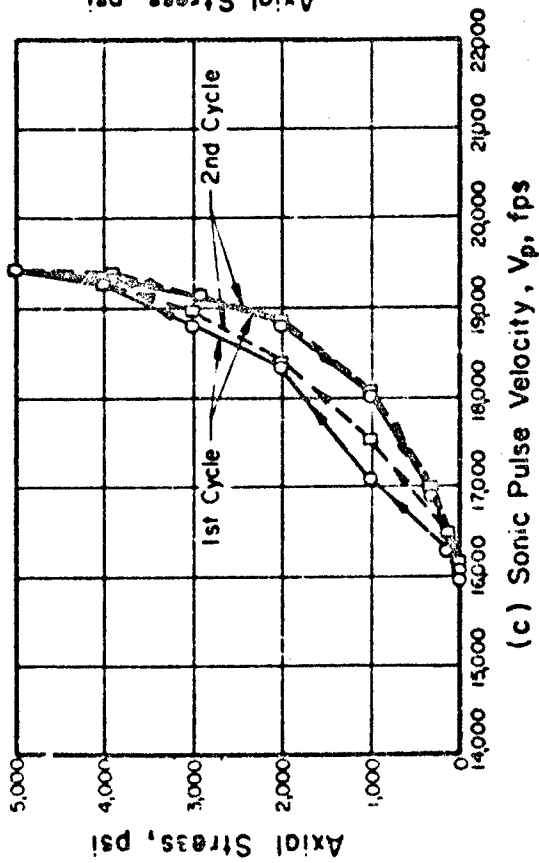
(a) Axial Strain, %



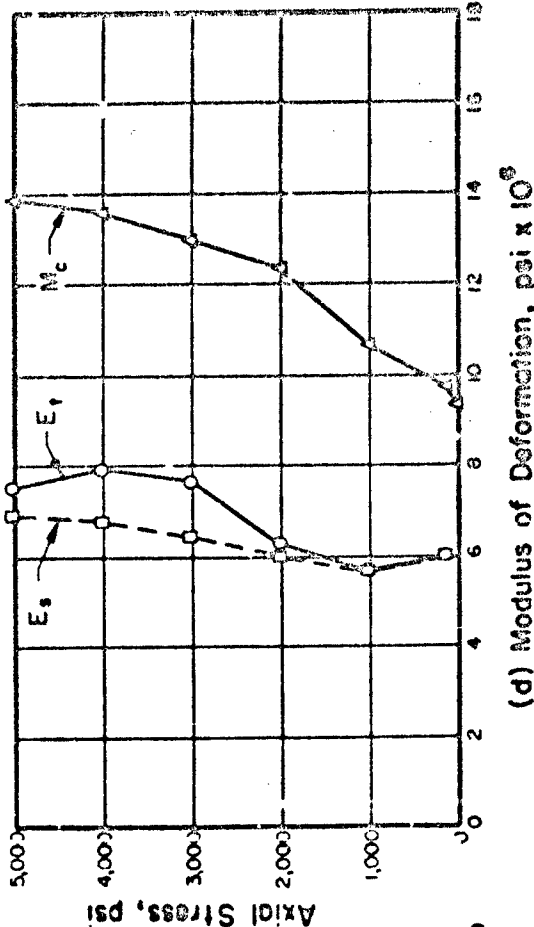
(b) Poisson's Ratio

Rock Type	Marble
(Imperial Density)	
Specimen No.	7.5 - (1110)
L/D	2.025
$\gamma_0$	169.9
$S_n$	39.0
$\sigma_0$ (ult)	9.37
Texture	Interlocking

Note:  
 1)  $V_p$  = Dilatational wave velocity  
 2)  $E_t$  = Tangent modulus (static)  
 3)  $E_s$  = Secant modulus (static)  
 4)  $M_c = \rho V_p^2$  (dynamic)

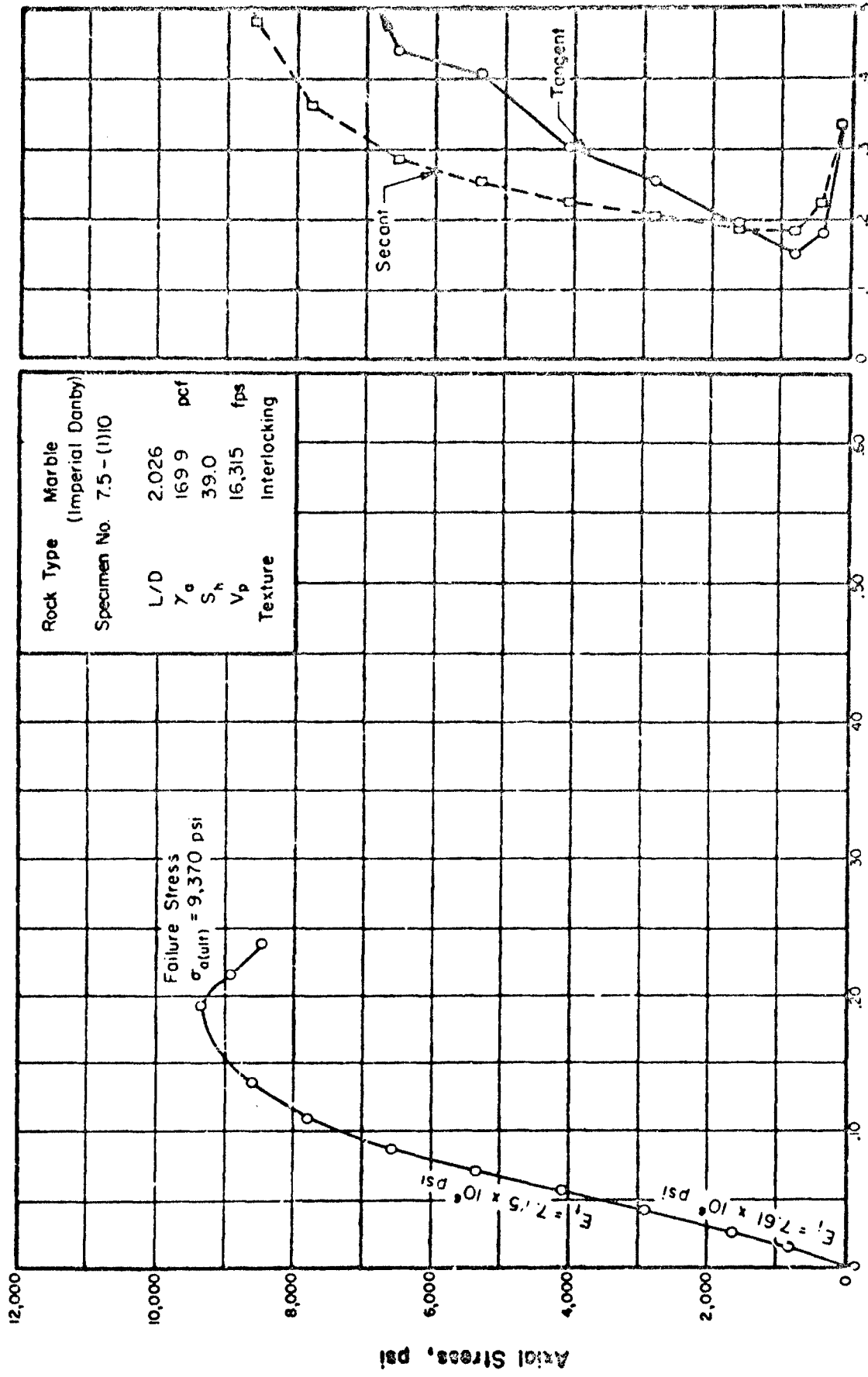


(c) Sonic Pulse Velocity,  $V_p$ , fps

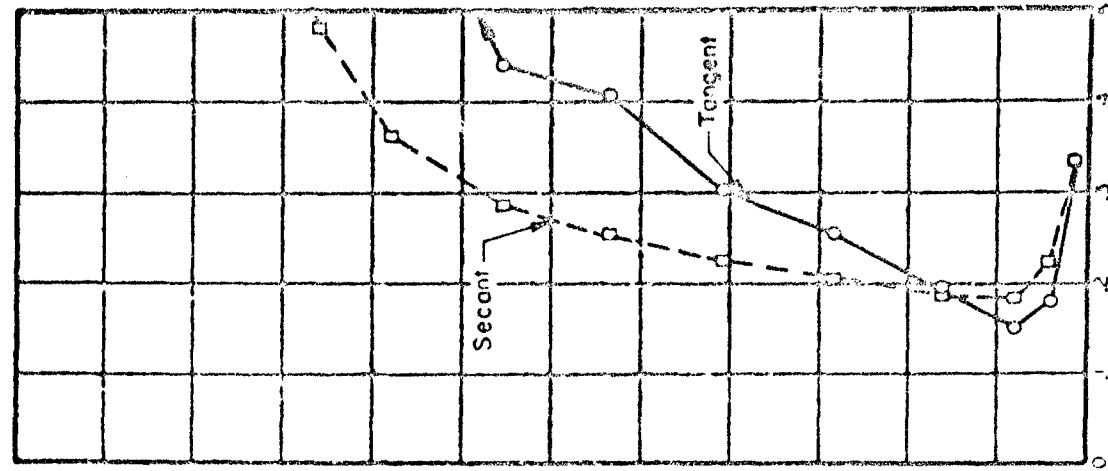


(d) Modulus of Deformation,  $\text{psi} \times 10^6$

FIGURE B.19A STRESS-STRAIN BEHAVIOR AND SONIC PULSE VELOCITY FOR ROCK IN UNIAXIAL COMPRESSION

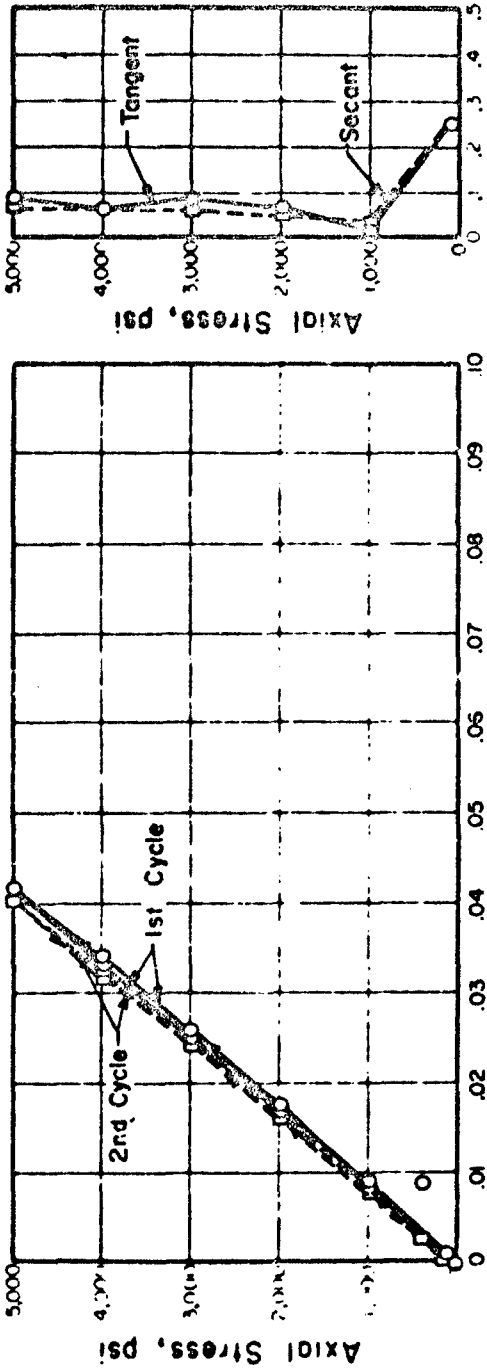


(a) Axial Strain, %

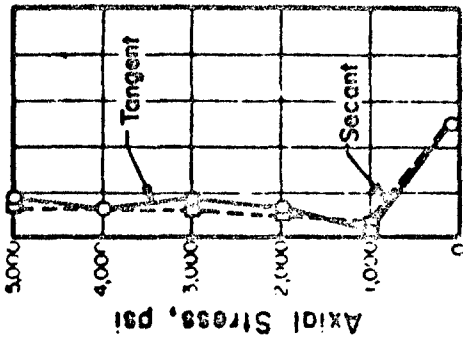


(b) Poisson's Ratio

FIGURE B.19B STRESS-STRAIN CURVE AND POISSON'S RATIO FOR ROCK IN UNIAXIAL COMPRESSION TO FAILURE



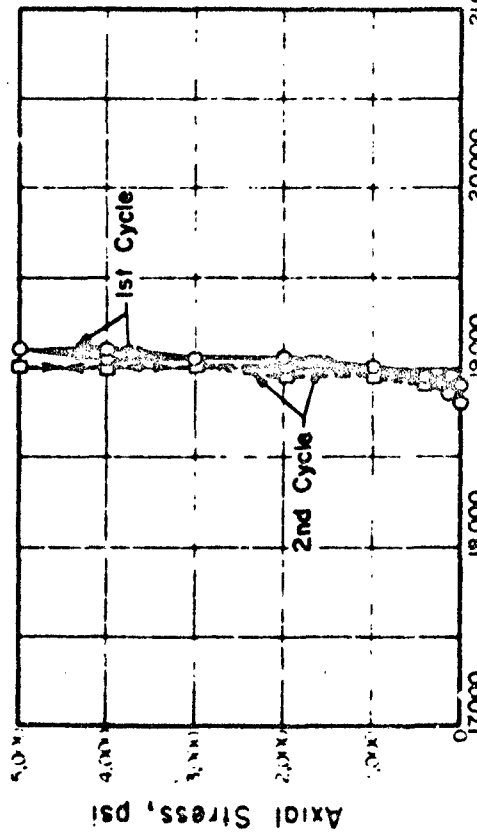
(a) Axial Strain, %



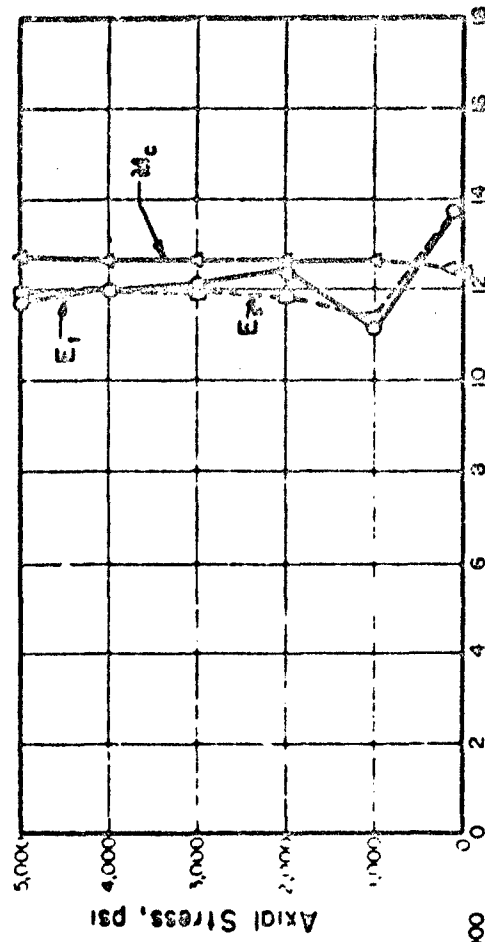
(b) Poisson's Ratio

Rock Type	Quartzite (Essexboro)
Specimen No	B.1- (1) 3
L/D	2.017
$\gamma_0$	162.9
$S_h$	111.5
$\sigma_0$ (ult)	48.0
Texture	Interlocking

Note:  
 1)  $V_p$  = Dilatational wave velocity  
 2)  $E_t$  = Tangent modulus (static)  
 3)  $E_s$  = Secant modulus (static)  
 4)  $M_c = \rho V_p^2$  (dynamic)



(c) Sonic Pulse Velocity,  $V_p$ , fps



(d) Modulus of Deformation,  $\text{psi} \times 10^6$

FIGURE B.20A STRESS-STRAIN BEHAVIOR AND SONIC PULSE VELOCITY FOR ROCK IN UNIAXIAL COMPRESSION

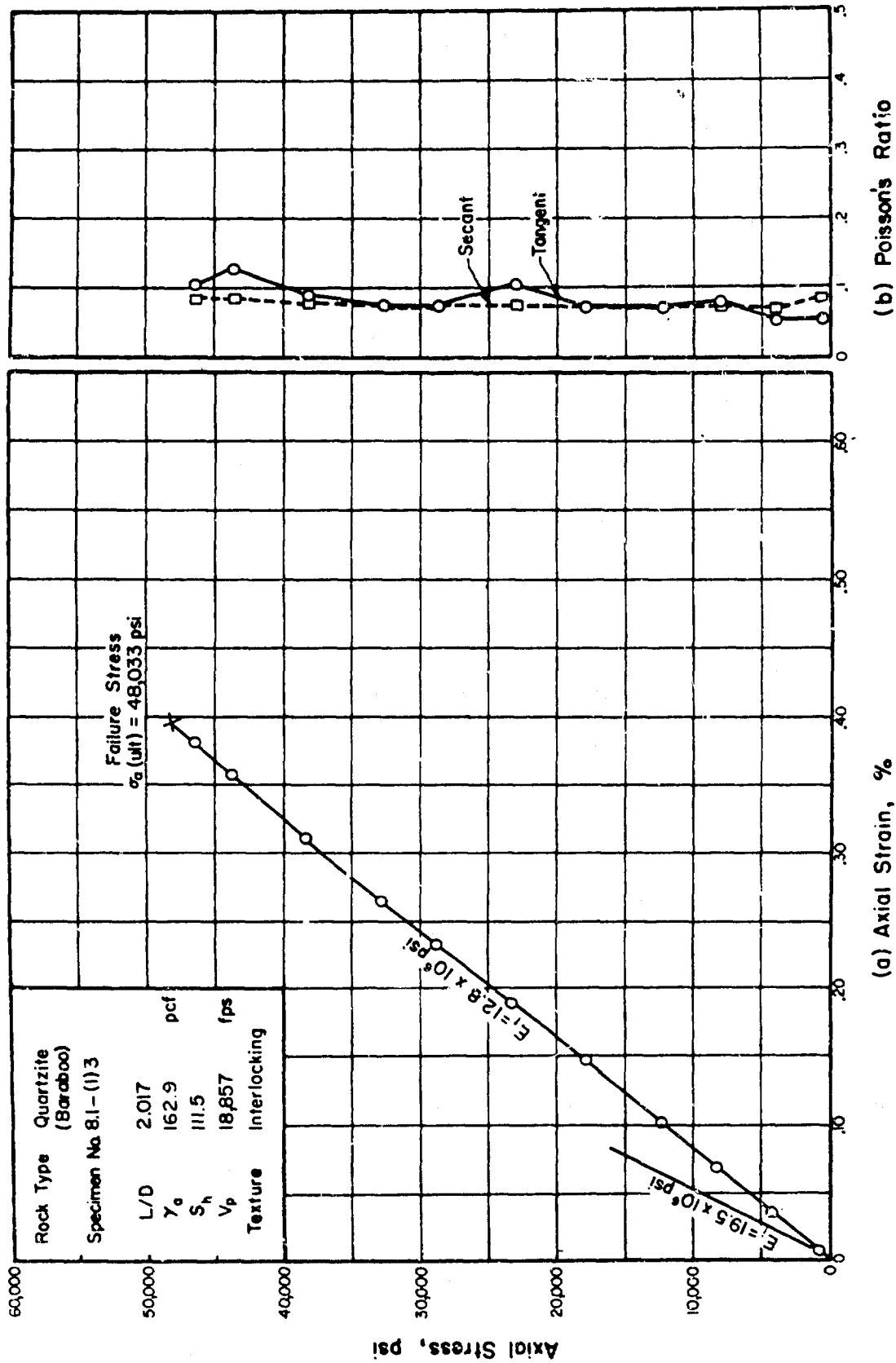
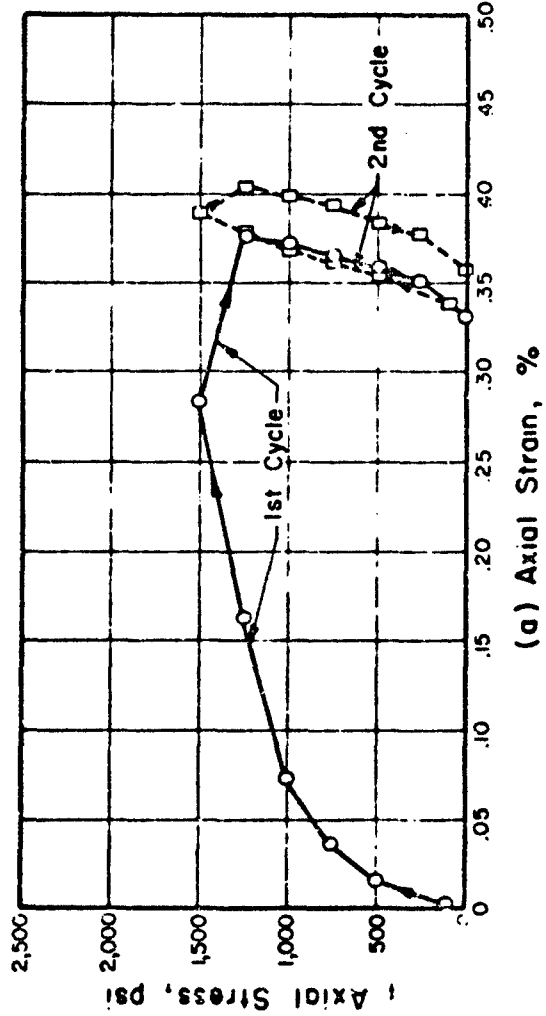
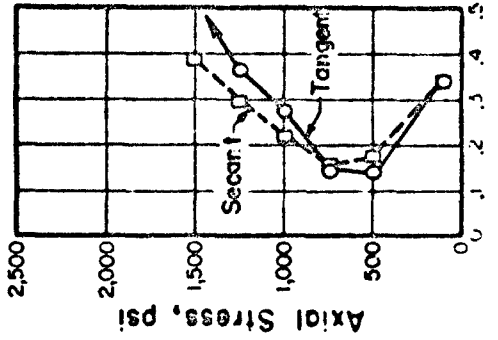


FIGURE B.20B STRESS-STRAIN CURVE AND POISSON'S RATIO FOR ROCK IN UNIAxIAL COMPRESSION TO FAILURE



(a) Axial Strain, %

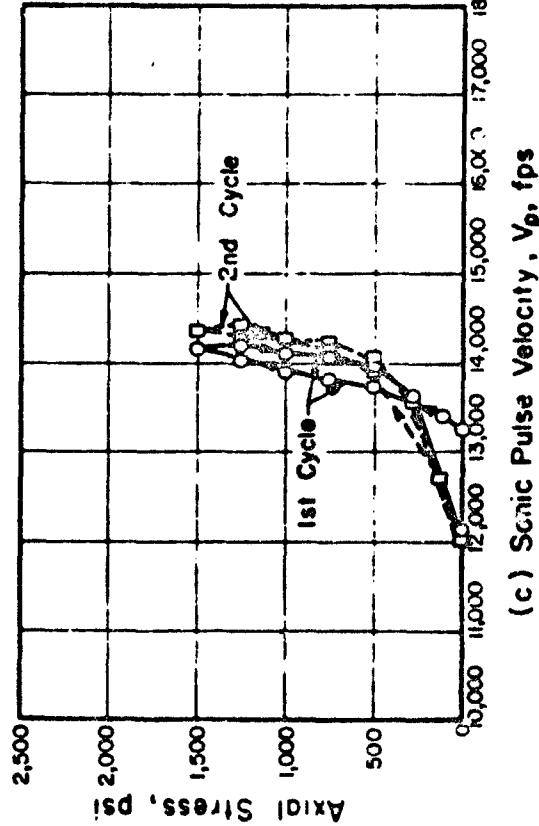


(b) Poisson's Ratio

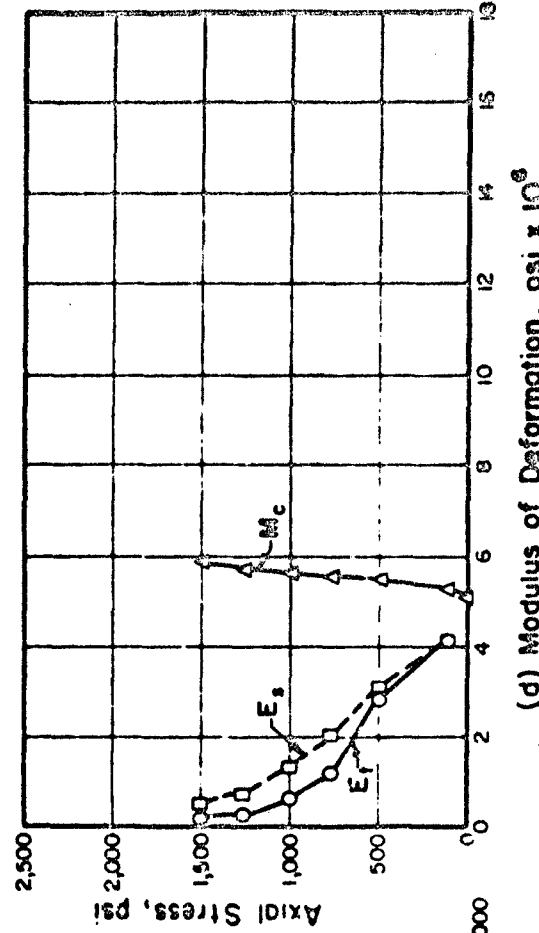
Rock Type	Rock Salt (Diamond Crystal)	
Specimen No	9.1-(1)5	
L/D	2.003	
$\gamma_0$	135.0	pcf
$S_h$	12.0	
$\sigma_0$ (ult)	3.3	ksi
Texture	Interlocking	

Note:

- 1)  $V_p$  = Dilatational wave velocity
- 2)  $E_t$  = Tangent modulus (static)
- 3)  $E_s$  = Secant modulus (static)
- 4)  $M_c$  = Constrained modulus  
=  $\rho V_p^2$  (dynamic)



(c) Sonic Pulse Velocity,  $V_p$ , fps



(d) Modulus of Deformation,  $\text{psi} \times 10^6$

FIGURE B.2.1A STRESS-STRAIN BEHAVIOR AND SONIC PULSE VELOCITY FOR ROCK IN UNIAXIAL COMPRESSION

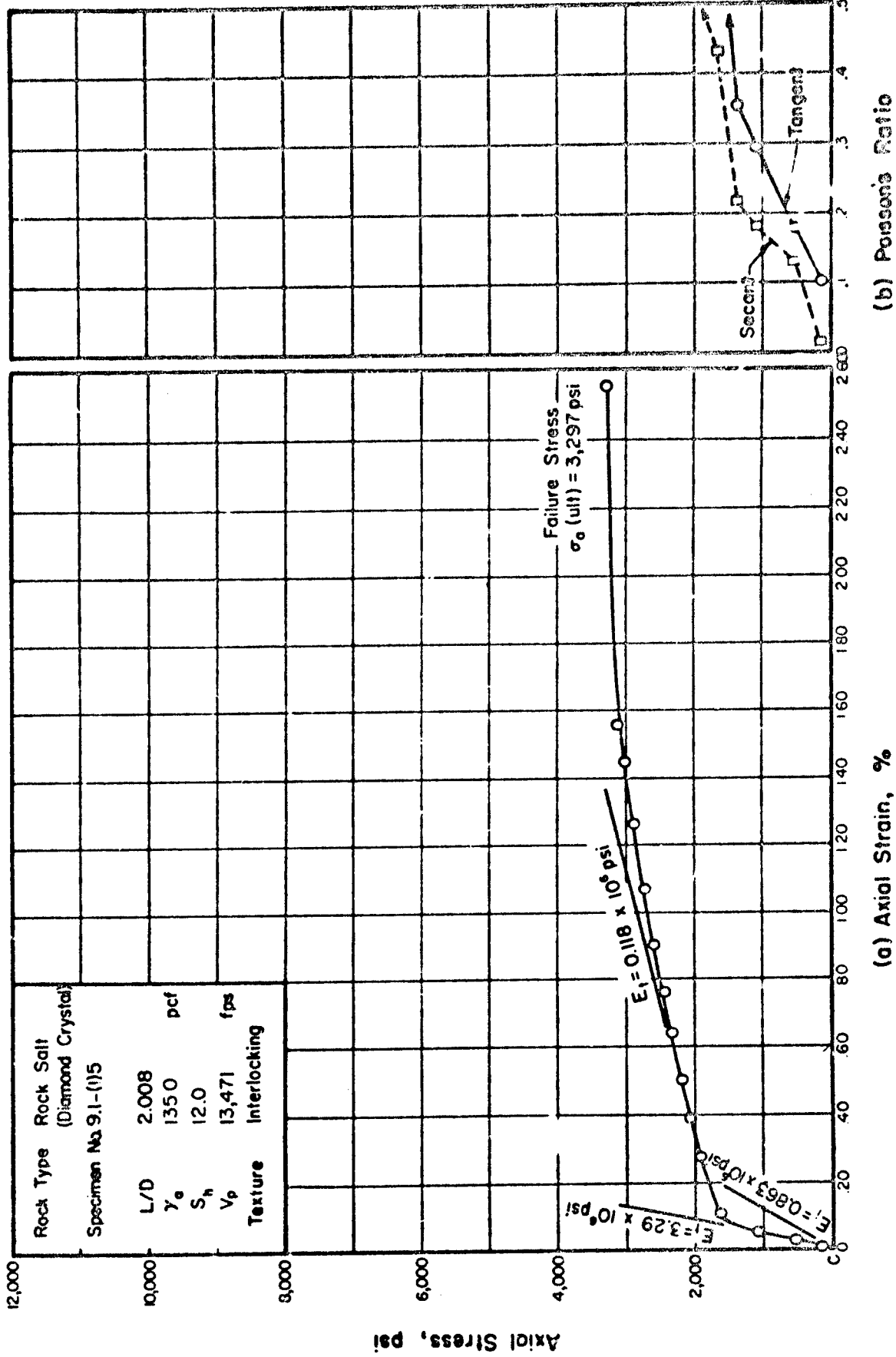
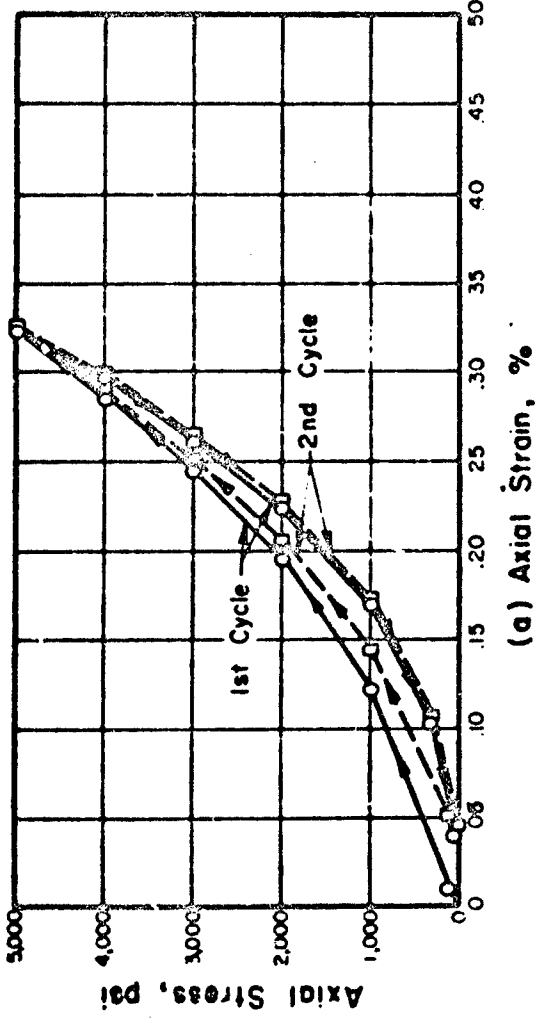
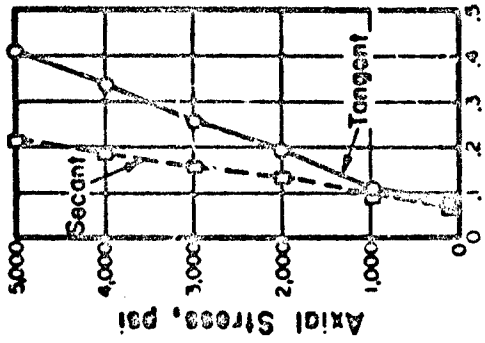


FIGURE B.2.1B STRESS-STRAIN CURVE AND POISSON'S RATIO FOR ROCK IN UNIAXIAL COMPRESSION TO FAILURE



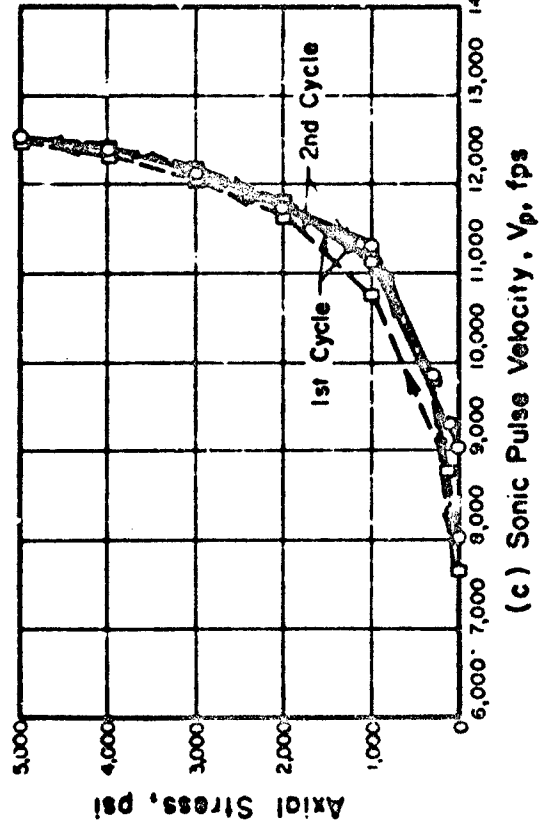
(a) Axial Strain, %



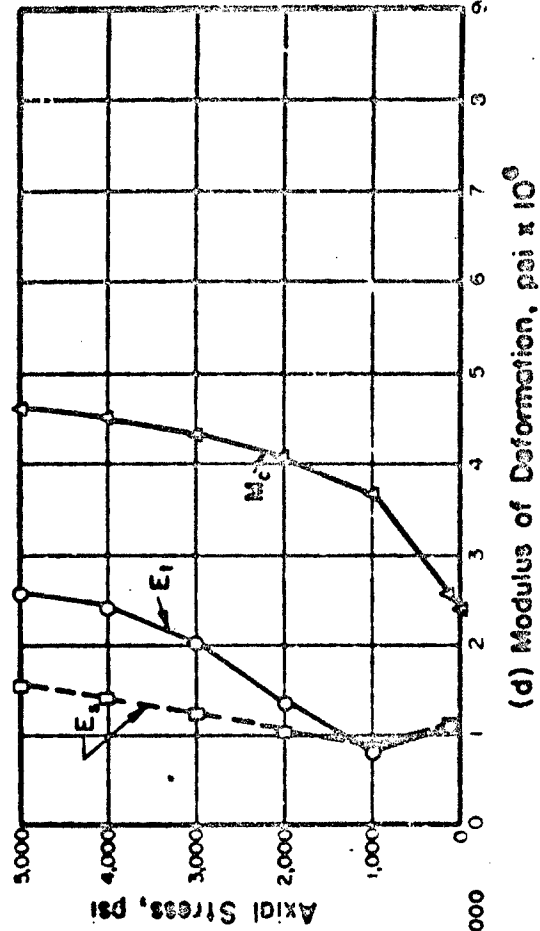
(b) Poisson's Ratio

Rock Type	Sandstone (Sareo)
Specimen No	10.1-(1)7
L/D	2.007
$\gamma_0$	136.3
$S_n$	44.4
$\sigma_0$ (ult)	10.9
Texture	Cemented

Note:  
 1)  $V_p$  = Dilational wave velocity  
 2)  $E_t$  = Tangent modulus (static)  
 3)  $E_s$  = Secant modulus (static)  
 4)  $M_c = \rho V_p^2$  (dynamic)

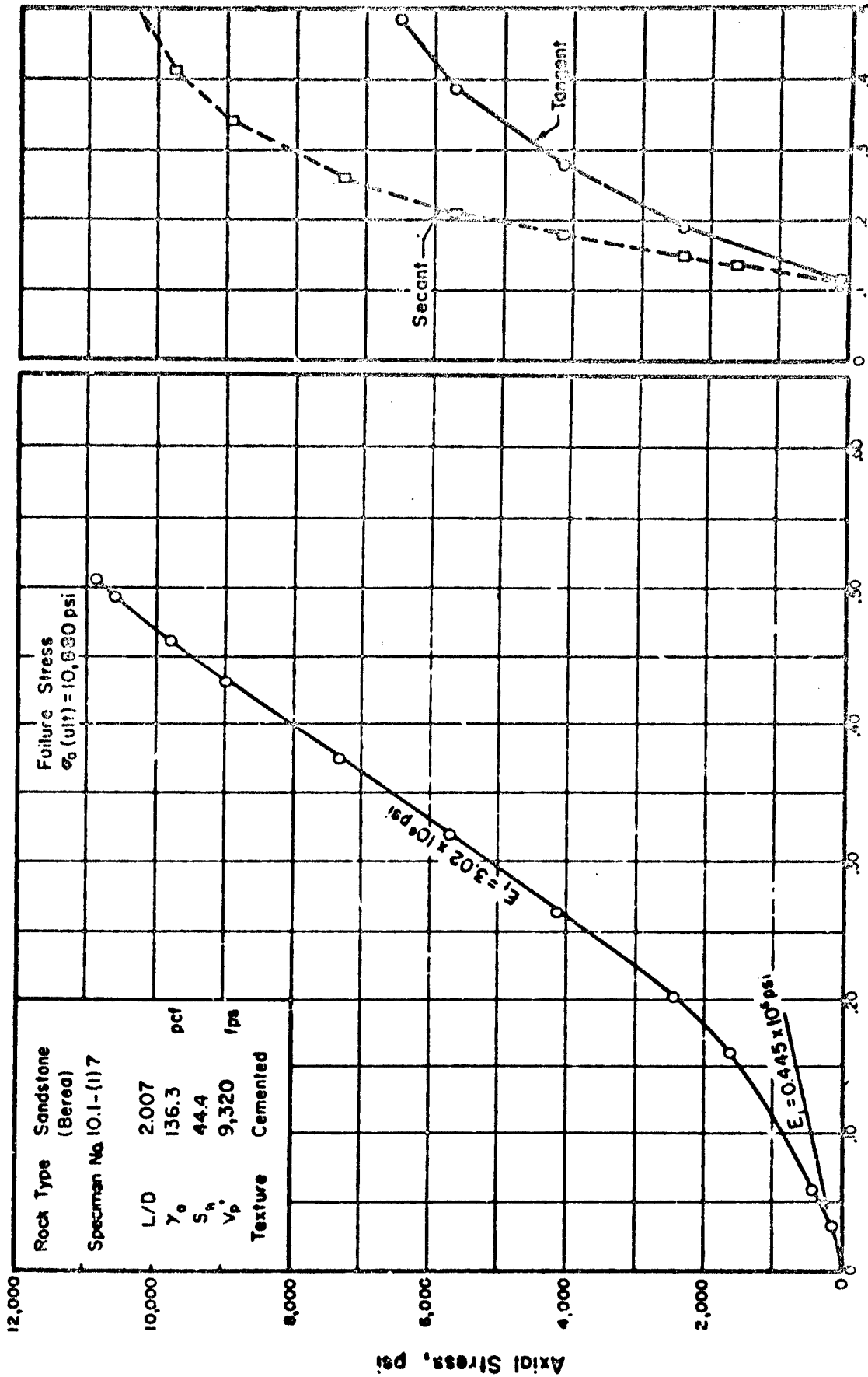


(c) Sonic Pulse Velocity,  $V_p$ , fps



(d) Modulus of Deformation,  $\text{psi} \times 10^6$

FIGURE B.2.2A STRESS-STRAIN BEHAVIOR AND SONIC PULSE VELOCITY FOR ROCK IN UNIAXIAL COMPRESSION

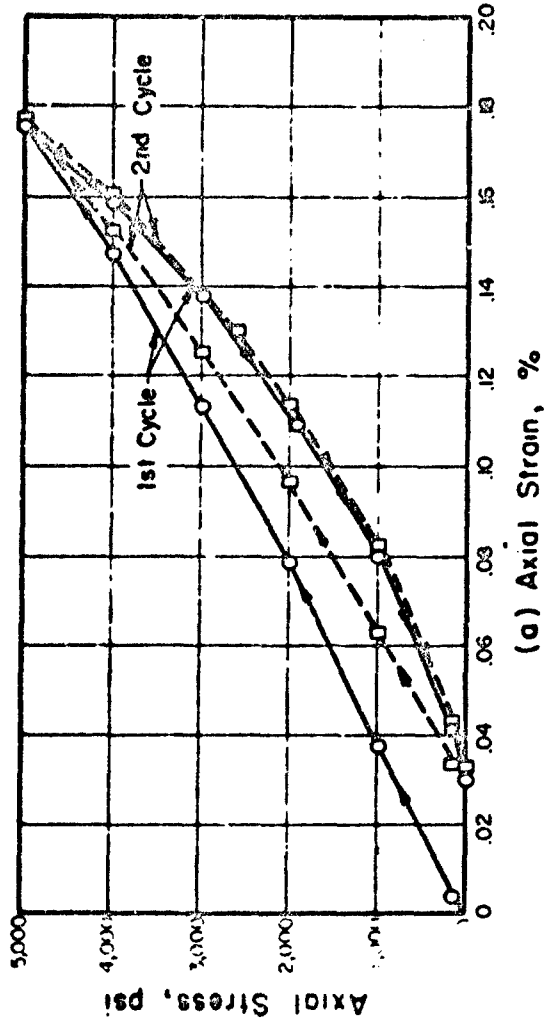


(a) Axial Strain, %

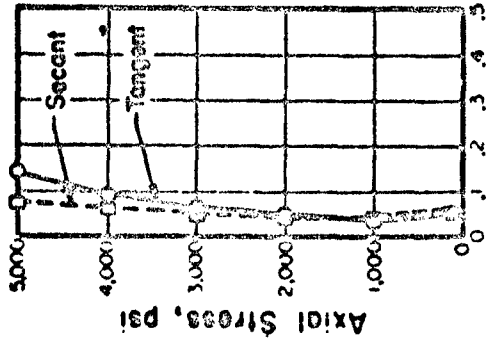
(b) Poisson's Ratio

FIGURE B.22B STRESS-STRAIN CURVE AND POISSON'S RATIO FOR ROCK IN UNIAXIAL COMPRESSION TO FAILURE





(a) Axial Strain, %

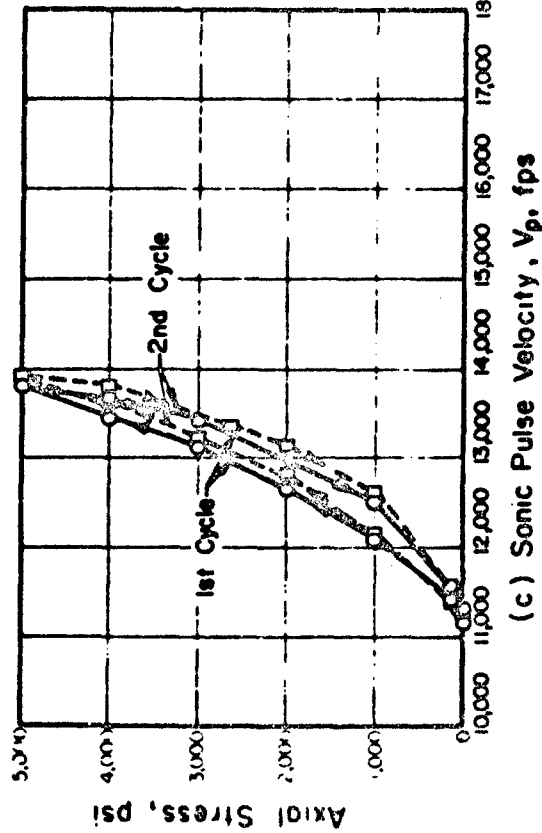


(b) Poisson's Ratio

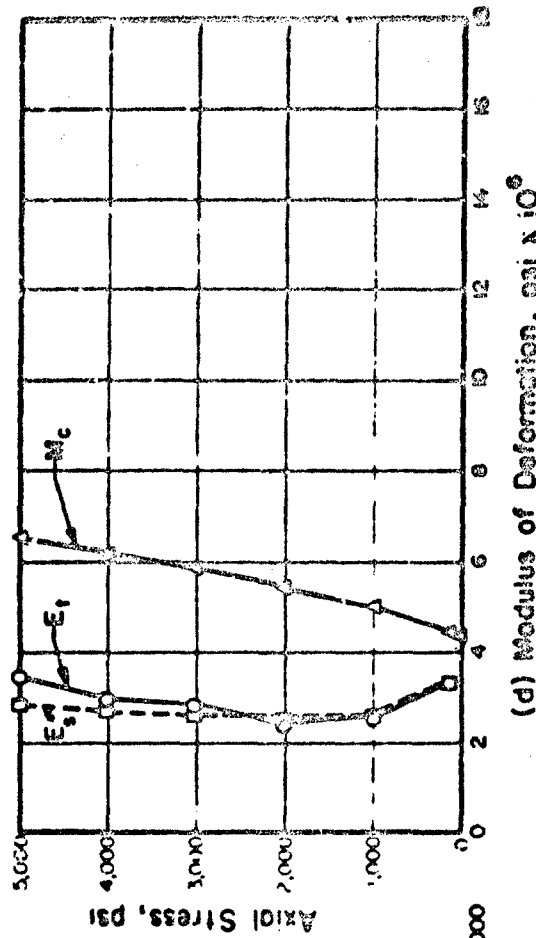
Rock Type	Sandstone (Crab Orchard)
Specimen No	10.2 - (1)
L/D	2.024
$\gamma_0$	157.9
$S_h$	0.01
$\sigma_0$ (ult)	31.2
Texture	Interlocking

Note:

- 1)  $V_p$  = Dilational wave velocity
- 2)  $E_t$  = Tangent modulus (static)
- 3)  $E_s$  = Secant modulus (static)
- 4)  $M_c = \rho V_p^2$  (dynamic)

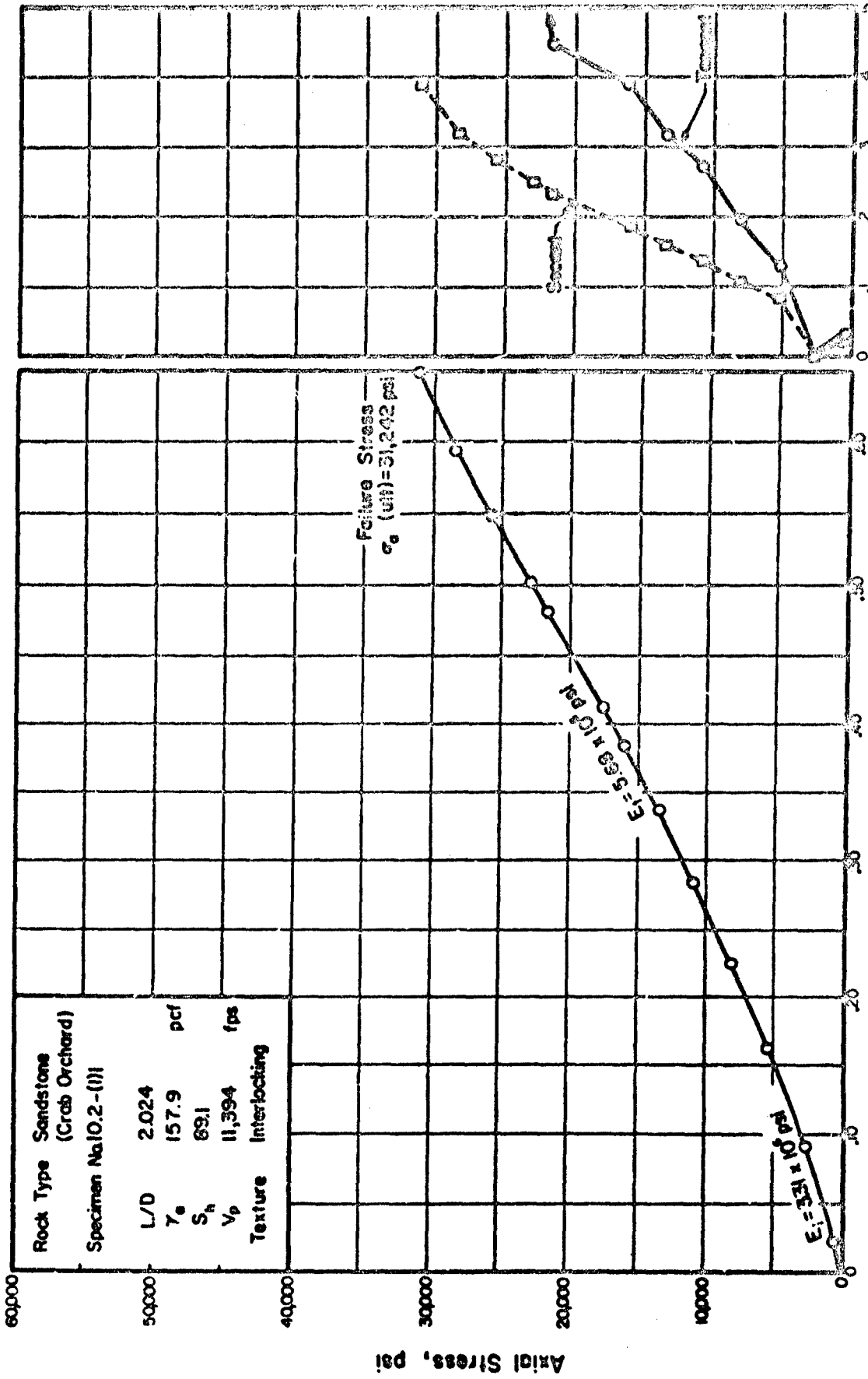


(c) Sonic Pulse Velocity,  $V_p$ , fps



(d) Modulus of Deformation,  $\text{psi} \times 10^6$

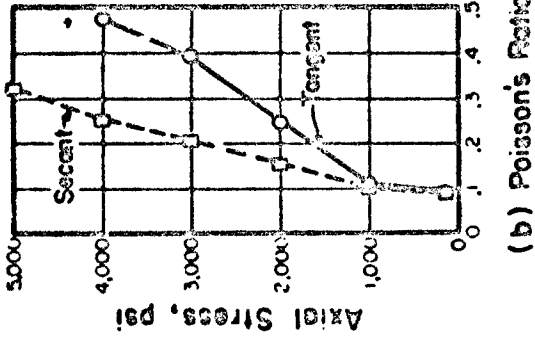
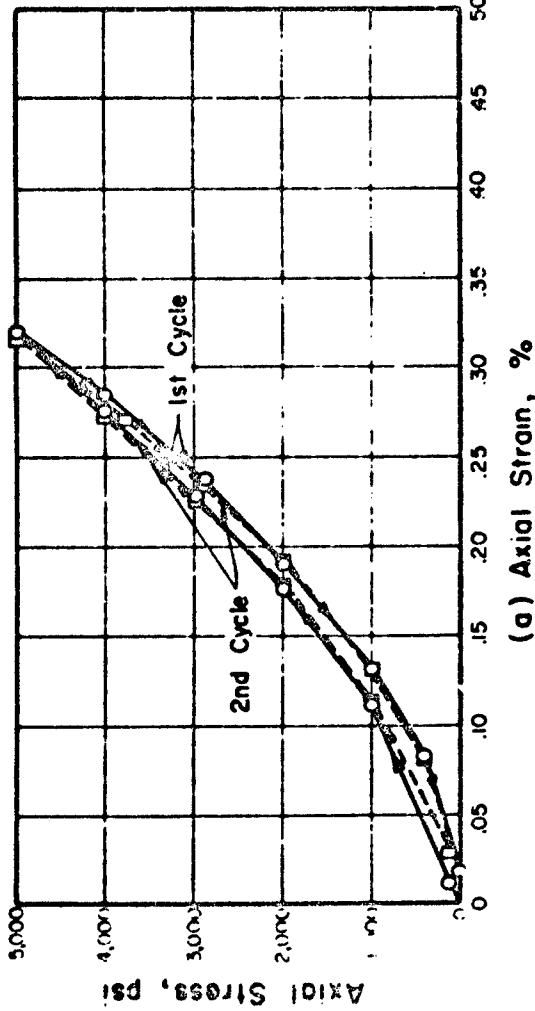
FIGURE B.23A STRESS-STRAIN BEHAVIOR AND SONIC PULSE VELOCITY FOR ROCK IN UNIAXIAL COMPRESSION



(a) Axial Strain, %

(b) Poisson's Ratio

FIGURE B.23B STRESS-STRAIN CURVE AND POISSON'S RATIO FOR ROCK IN UNIAXIAL COMPRESSION TO FAILURE



Rock Type	Sandstone (Navajo)
Specimen No	10.3-(62-9)6
L/D	2.073
$\gamma_0$	124.1
$S_n$	21.6
$\sigma_0$ (ult)	6.1
Texture	Combed
	ksi

Note:  
 1)  $V_p$  = Dilational wave velocity  
 2)  $E_t$  = Tangent modulus (static)  
 3)  $E_s$  = Secant modulus (static)  
 4)  $M_c = \rho V_p^2$  (dynamic)

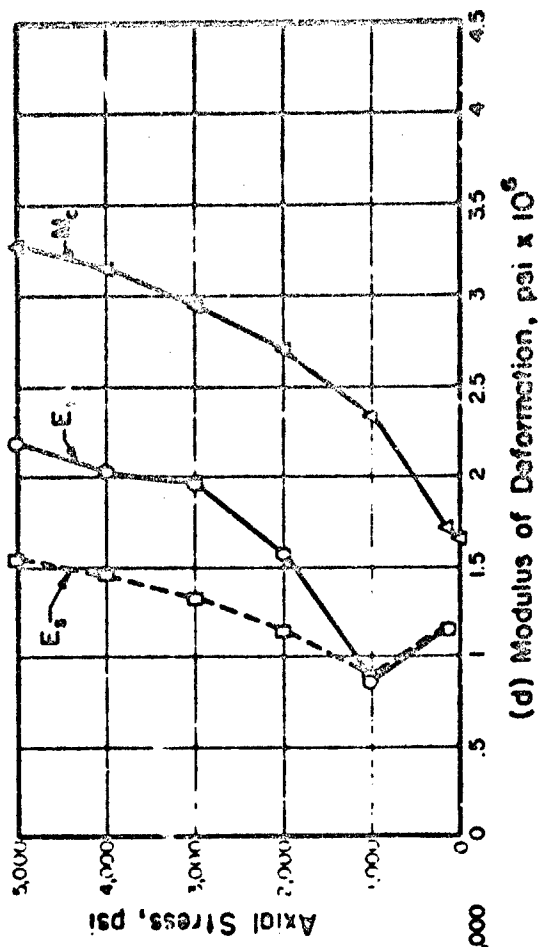
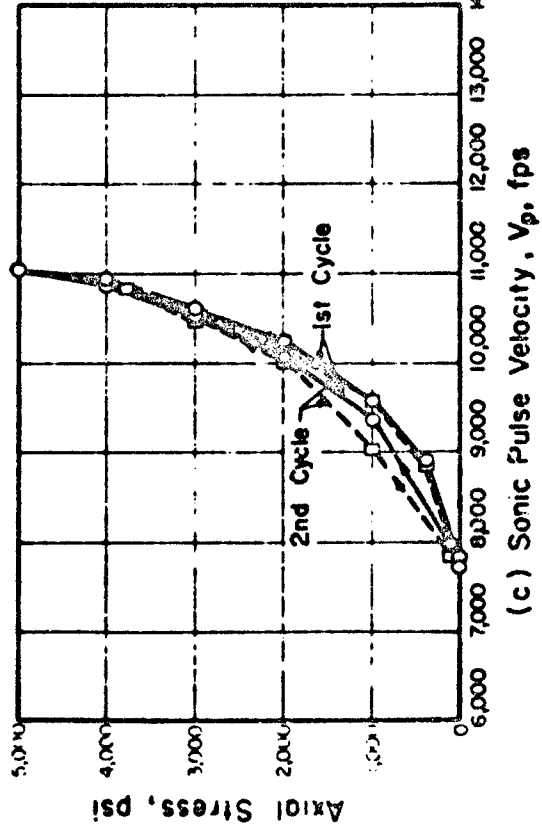


FIGURE B.24A STRESS-STRAIN BEHAVIOR AND SONIC PULSE VELOCITY FOR ROCK IN UNIAXIAL COMPRESSION

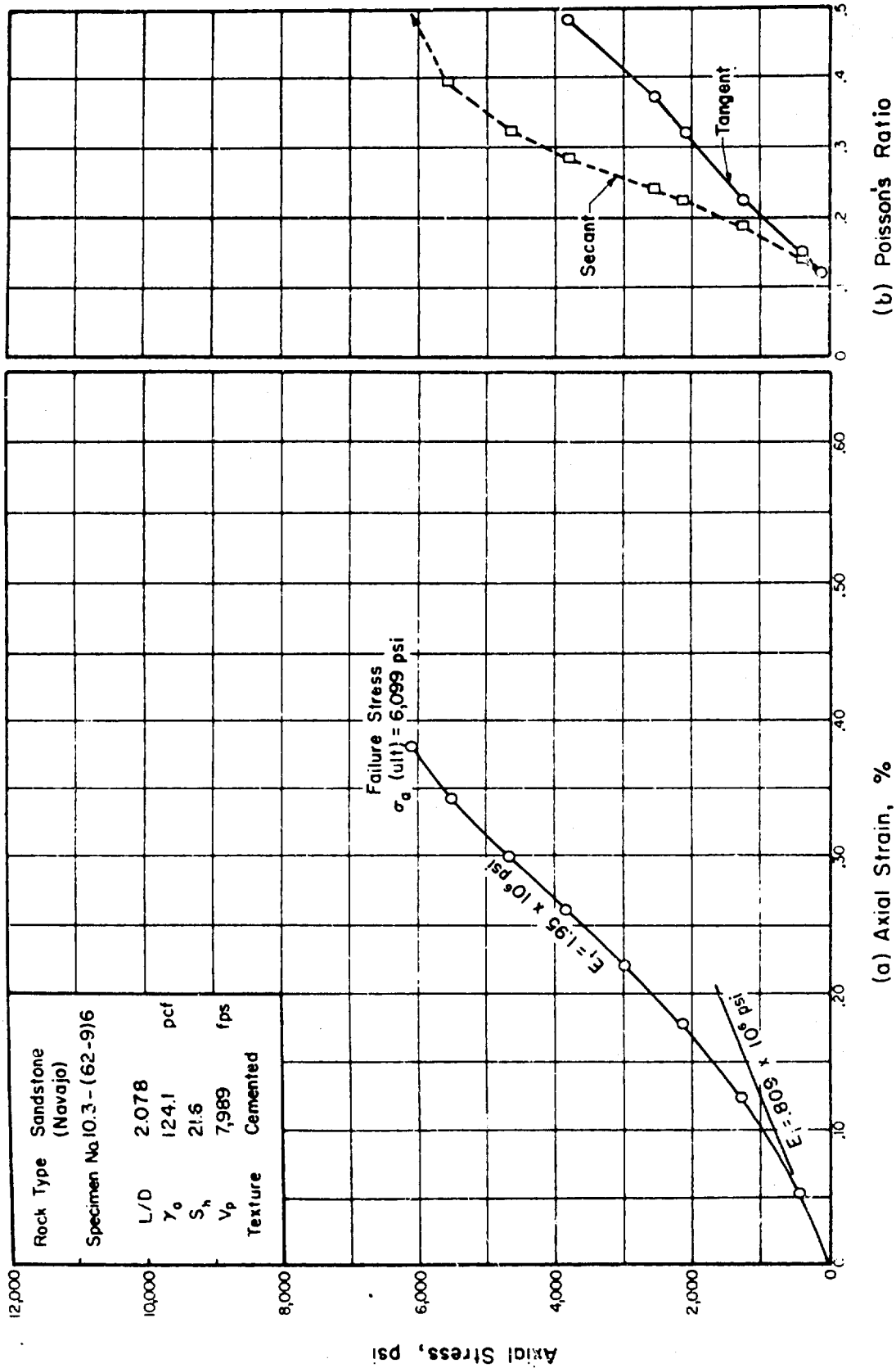
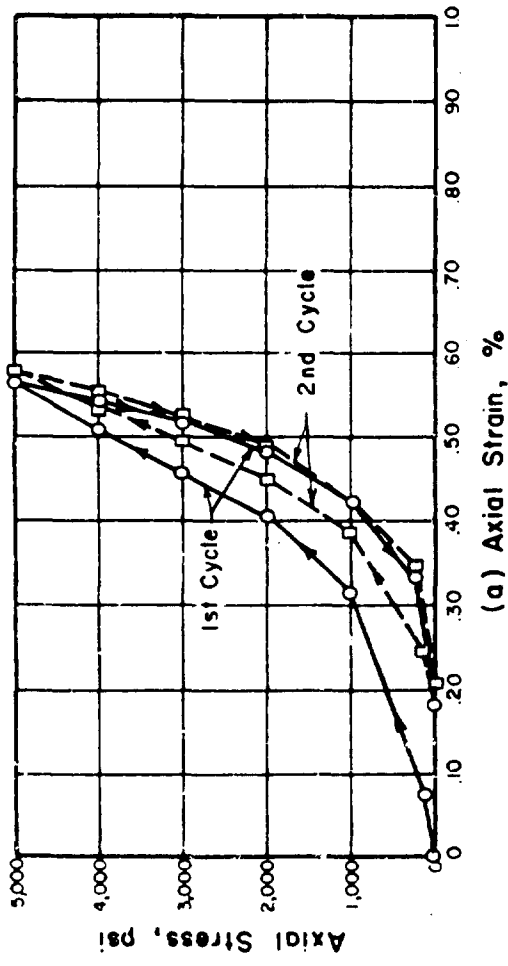
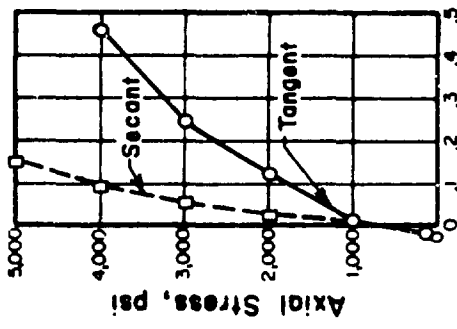


FIGURE B.24B STRESS-STRAIN CURVE AND POISSON'S RATIO FOR ROCK IN UNIAXIAL COMPRESSION TO FAILURE



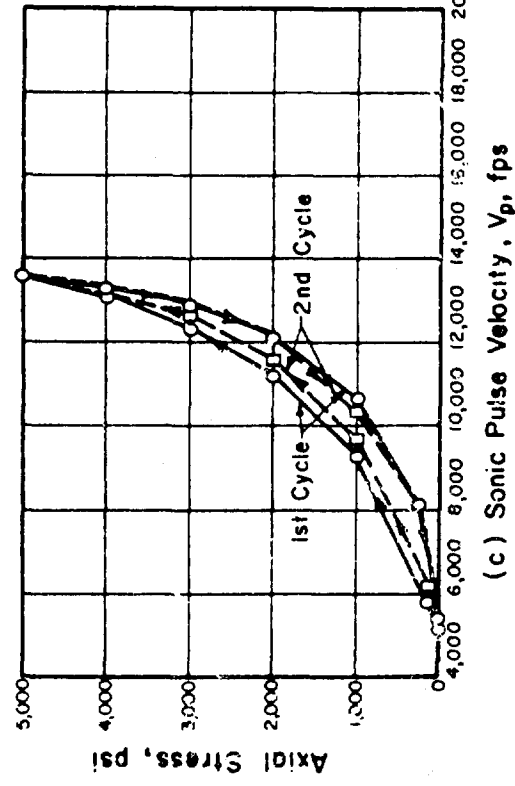
(a) Axial Strain, %



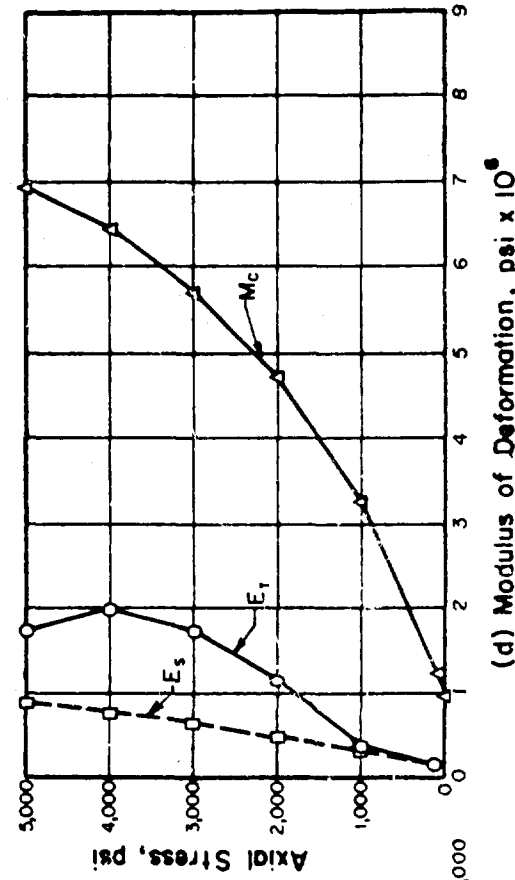
(b) Poisson's Ratio

Rock Type	Schist (Luther Falls) II
Specimen No.	II.1 - (I) II
L/D	2.014
$\gamma_0$	175.4 pcf
$S_h$	51.7
$\sigma_a$ (ult.)	8.00 ksi
Texture	Laminated-Foliated

Note:  
 1)  $V_p$  = Dilatational wave velocity  
 2)  $E_t$  = Tangent modulus (static)  
 3)  $E_s$  = Secant modulus (static)  
 4)  $M_c = \rho V_p^2$  (dynamic)



(c) Sonic Pulse Velocity,  $V_p$ , fps



(d) Modulus of Deformation,  $\text{psi} \times 10^6$

FIGURE B.25A STRESS-STRAIN BEHAVIOR AND SONIC PULSE VELOCITY FOR ROCK IN UNIAXIAL COMPRESSION

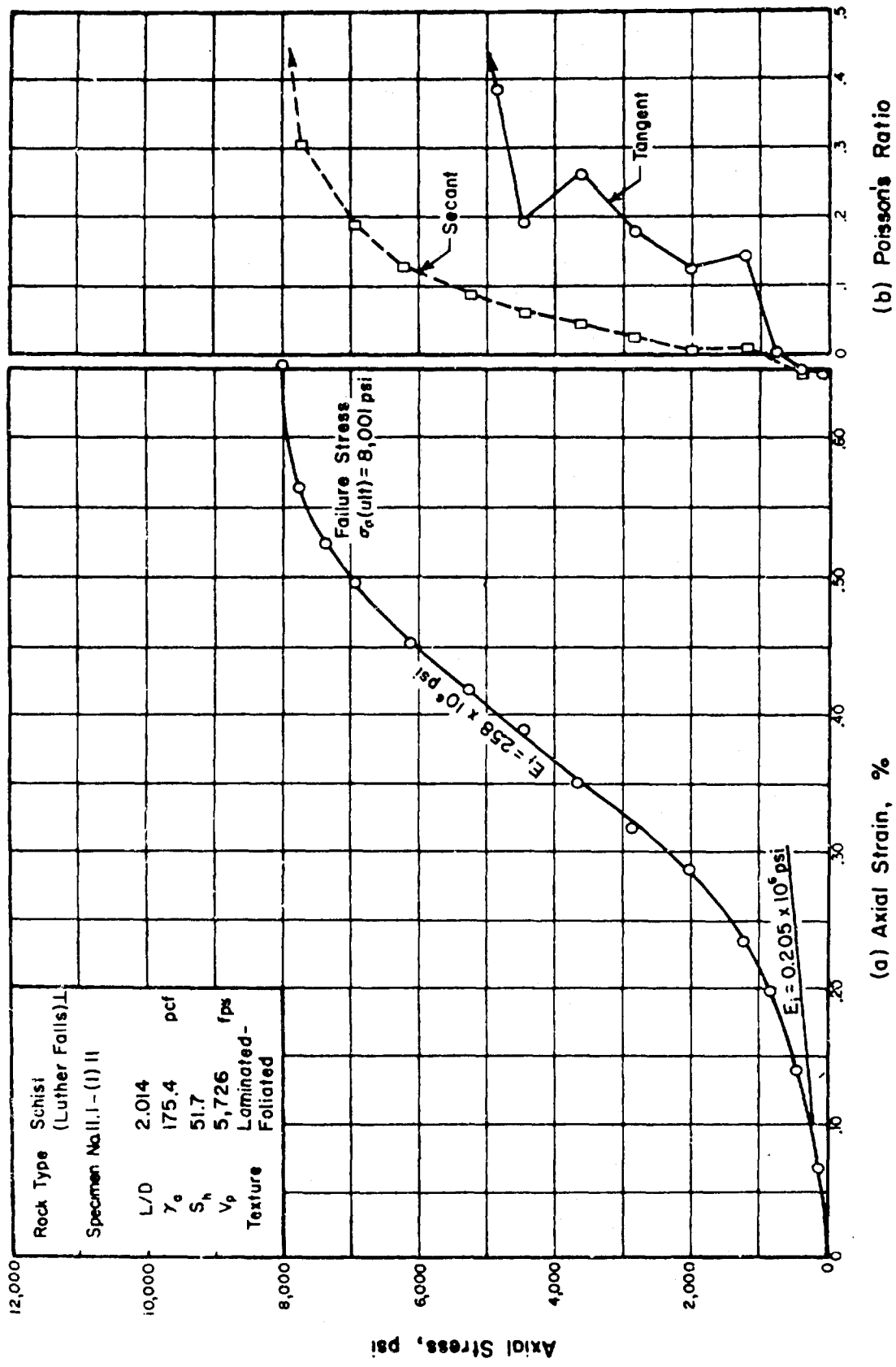
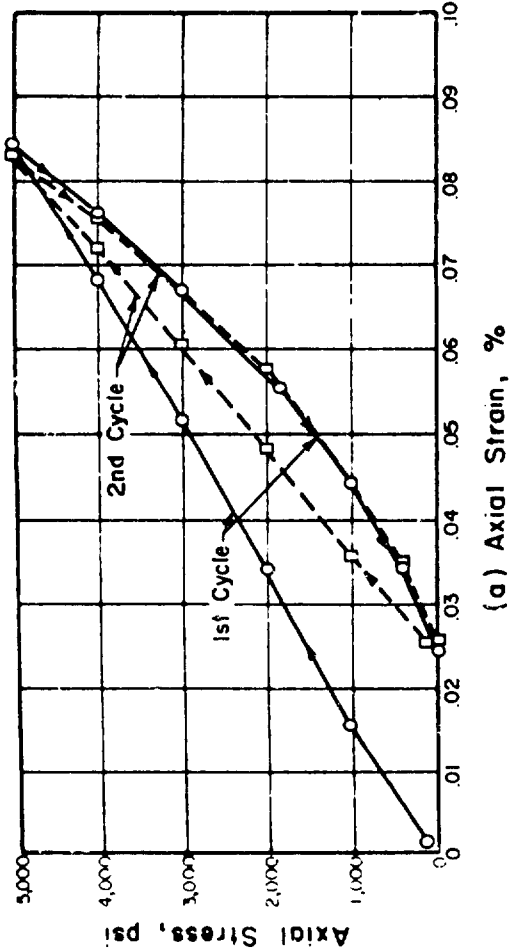
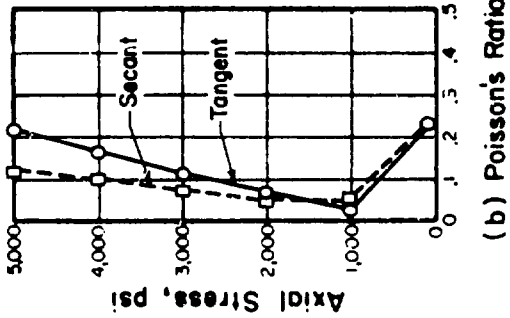


FIGURE B.25B STRESS-STRAIN CURVE AND POISSON'S RATIO FOR ROCK IN UNIAxIAL COMPRESSION TO FAILURE



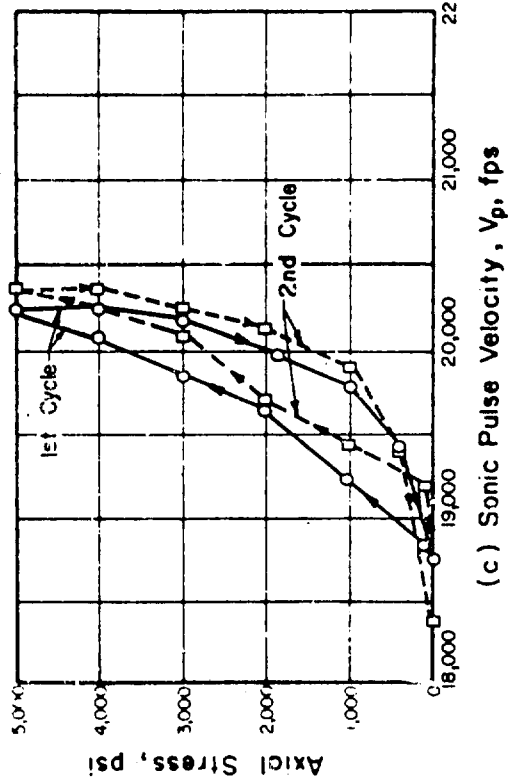
(a) Axial Strain, %



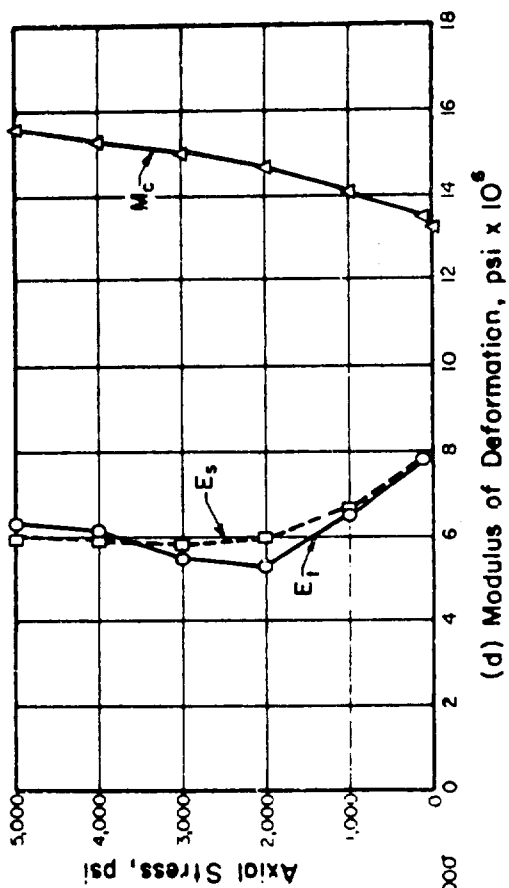
(b) Poisson's Ratio

Rock Type	Schist (Luther Falls) II
Specimen No.	II.2-(1)6
L/D	2.035
$\gamma_c$	176.7
$S_h$	49.1
$\sigma_c$ (ult)	9.20
Texture	Laminated Fatigued
	pcf
	ksi

Note:  
 1)  $V_p$  = Dilatational wave velocity  
 2)  $E_t$  = Tangent modulus (static)  
 3)  $E_s$  = Secant modulus (static)  
 4)  $M_c$  = Constrained modulus  
 $= \rho V_p^2$  (dynamic)

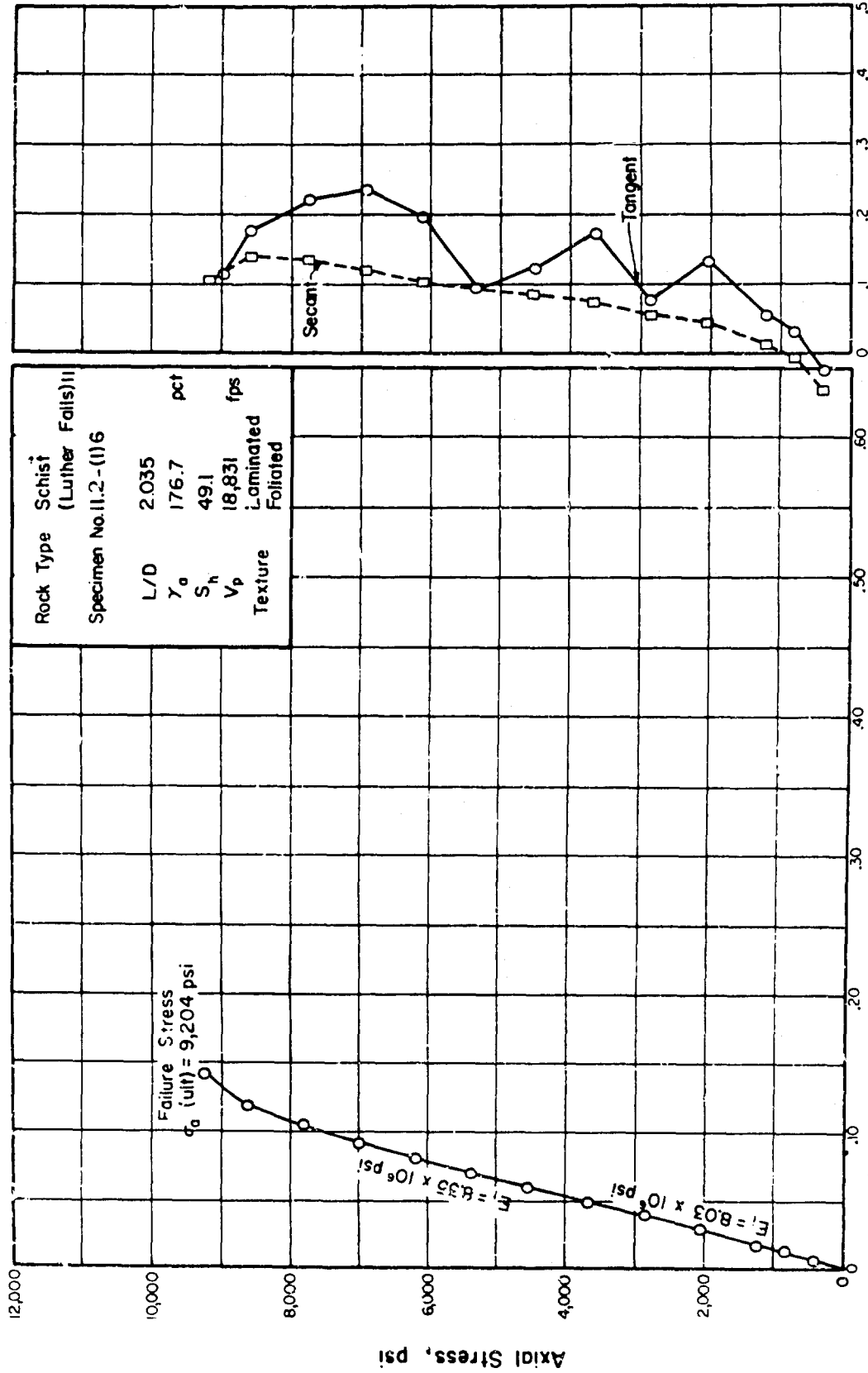


(c) Sonic Pulse Velocity,  $V_p$ , fps



(d) Modulus of Deformation,  $\text{psi} \times 10^6$

FIGURE B.26A STRESS-STRAIN BEHAVIOR AND SONIC PULSE VELOCITY FOR ROCK IN UNIAXIAL COMPRESSION

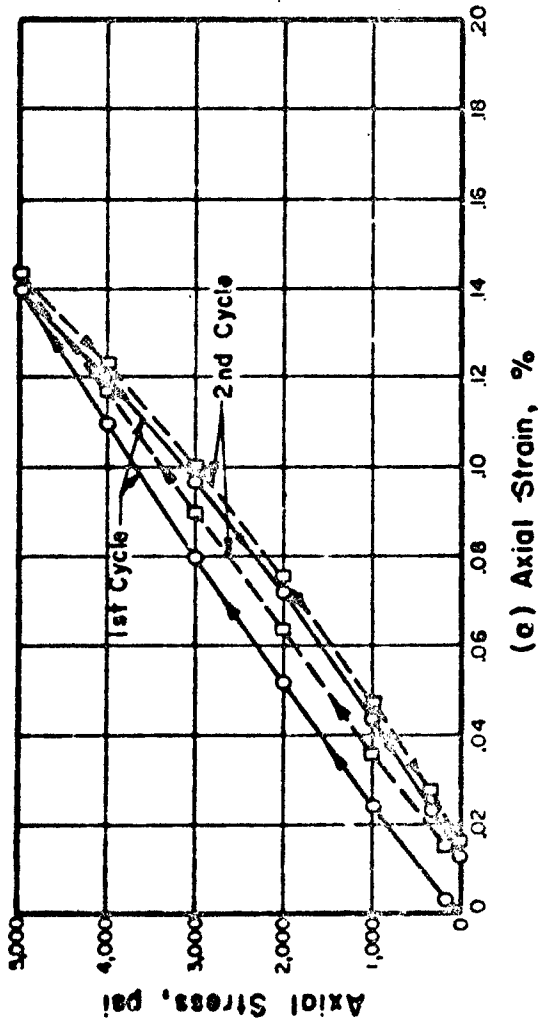


(a) Axial Strain, %

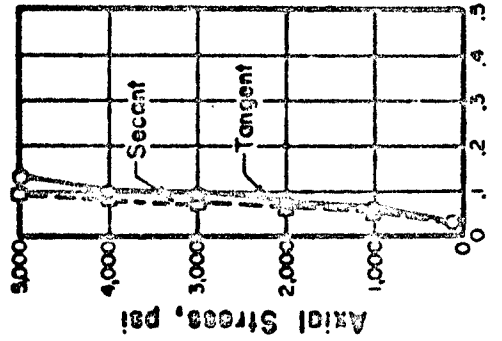
(b) Poisson's Ratio

FIGURE B.26B STRESS-STRAIN CURVE AND POISSON'S RATIO FOR ROCK IN UNIAXIAL COMPRESSION TO FAILURE





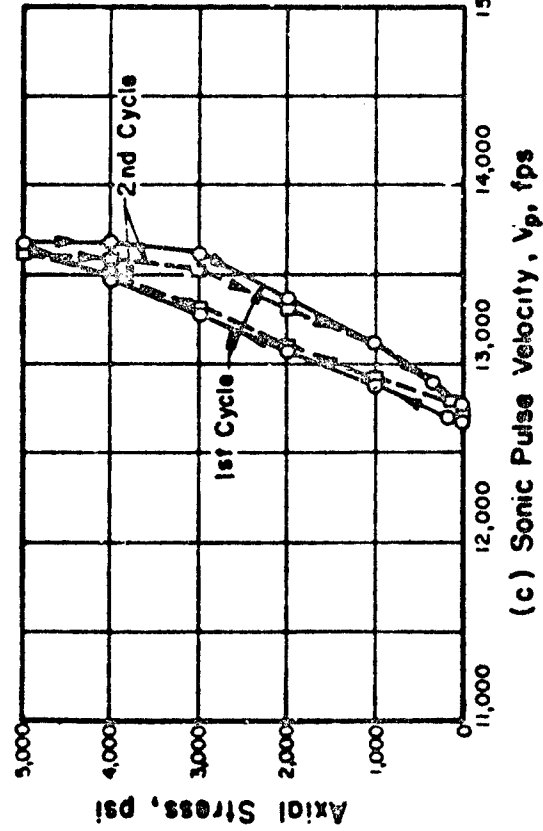
(e) Axial Strain, %



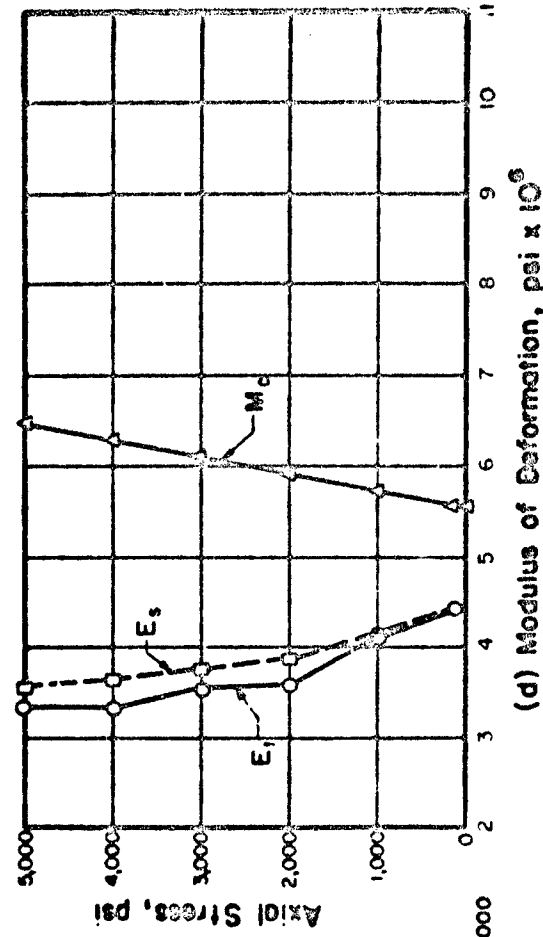
(b) Poisson's Ratio

Rock Type	Siltstone (Mackenzack)
Specimen No.	B.1-(DB-1)II
L/D	2.029
$\gamma_0$	151.0
$S_h$	62.2
$\sigma_0$ (ult)	10.4
Texture	Combed

Note:  
 1)  $V_p$  = Dilational wave velocity  
 2)  $E_t$  = Tangent modulus (static)  
 3)  $E_s$  = Secant modulus (static)  
 4)  $M_c = \rho V_p^2$  (dynamic)



(c) Sonic Pulse Velocity,  $V_p$ , fps



(d) Modulus of Deformation,  $\text{psi} \times 10^6$

FIGURE B.27A STRESS-STRAIN BEHAVIOR AND SONIC PULSE VELOCITY FOR ROCK IN UNIAXIAL COMPRESSION

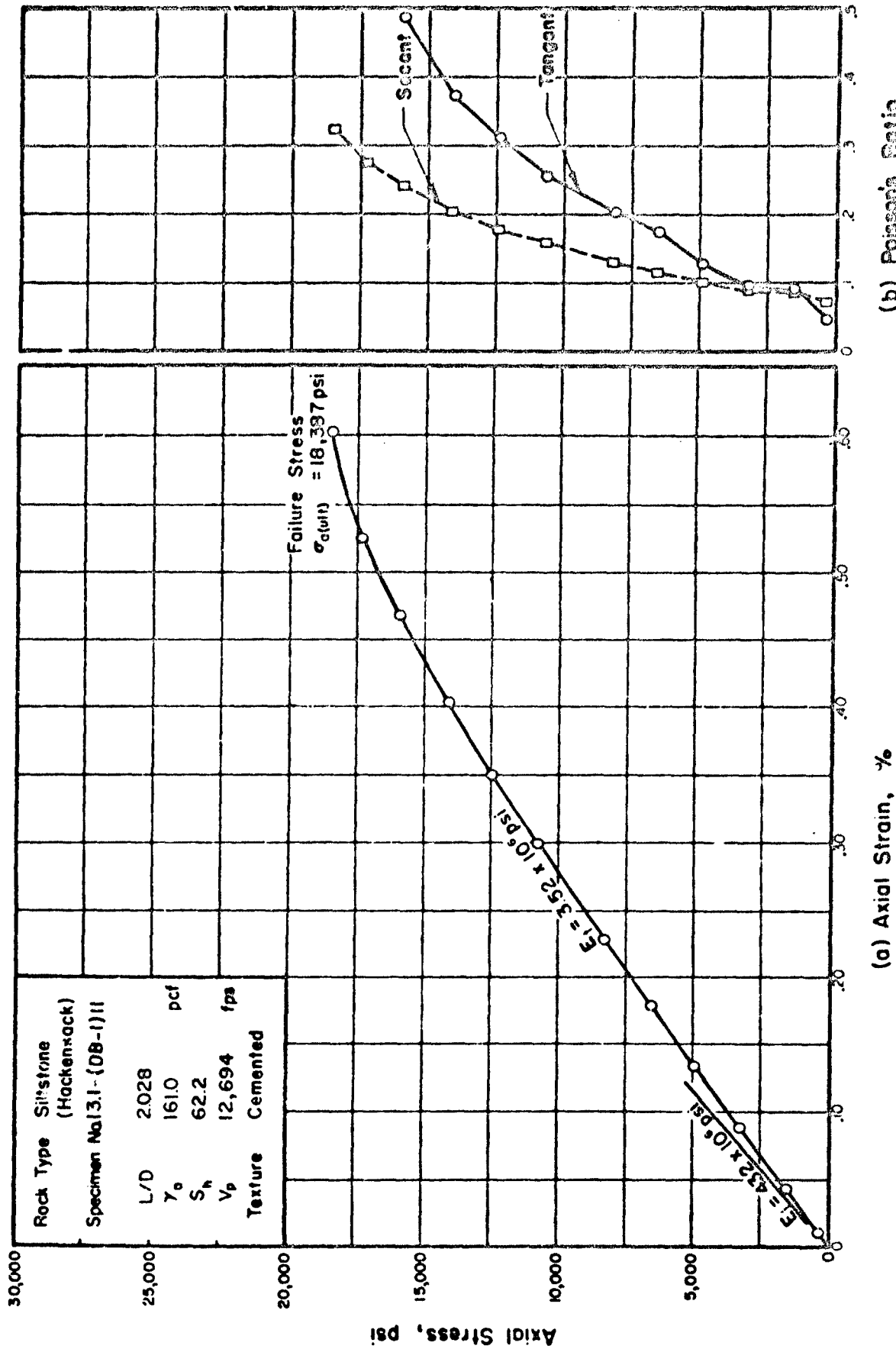
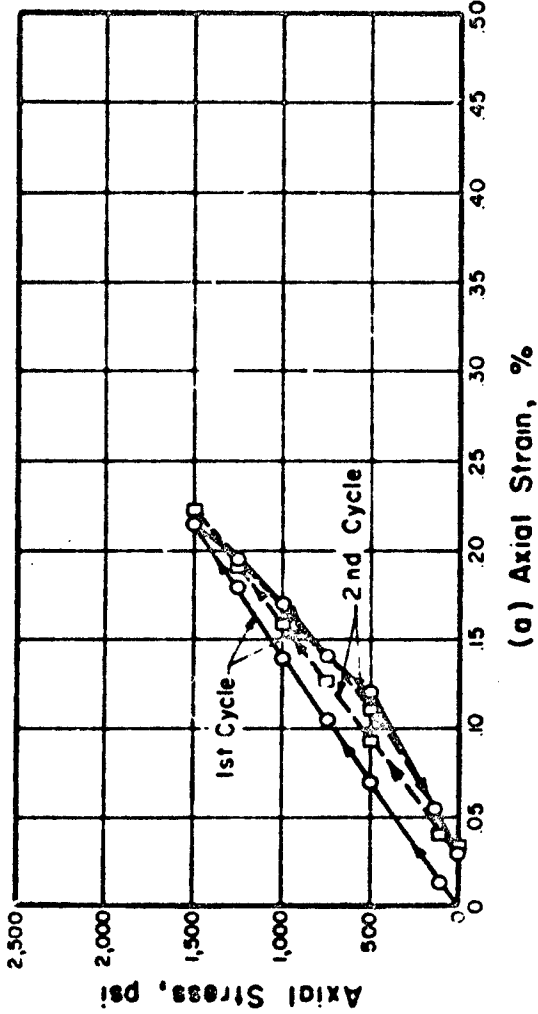
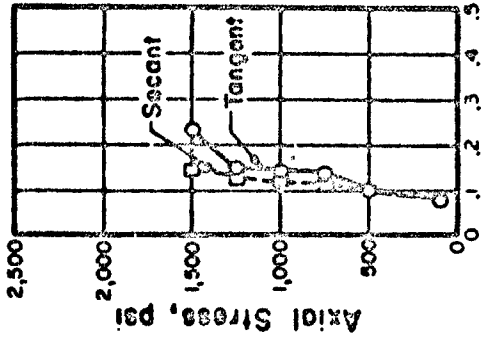


FIGURE B.27B STRESS-STRAIN CURVE AND POISSON'S RATIO FOR ROCK IN UNIAXIAL COMPRESSION TO FAILURE



(a) Axial Strain, %

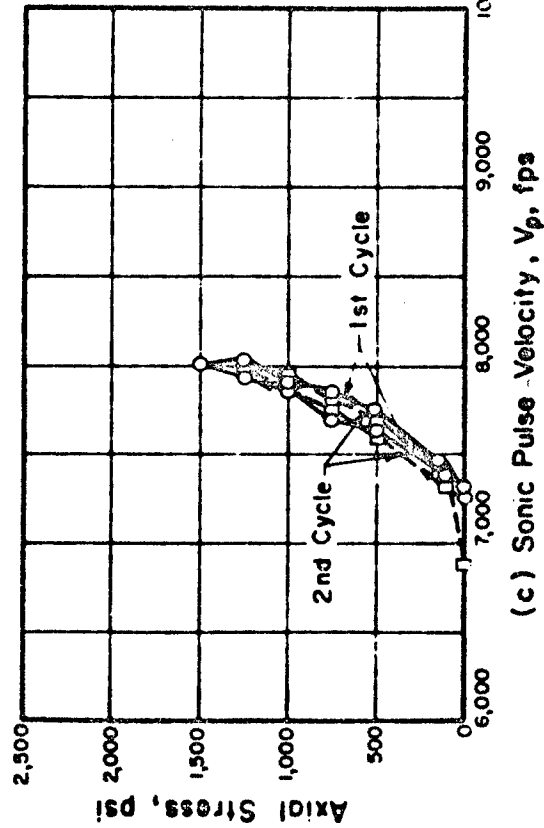


(b) Poisson's Ratio

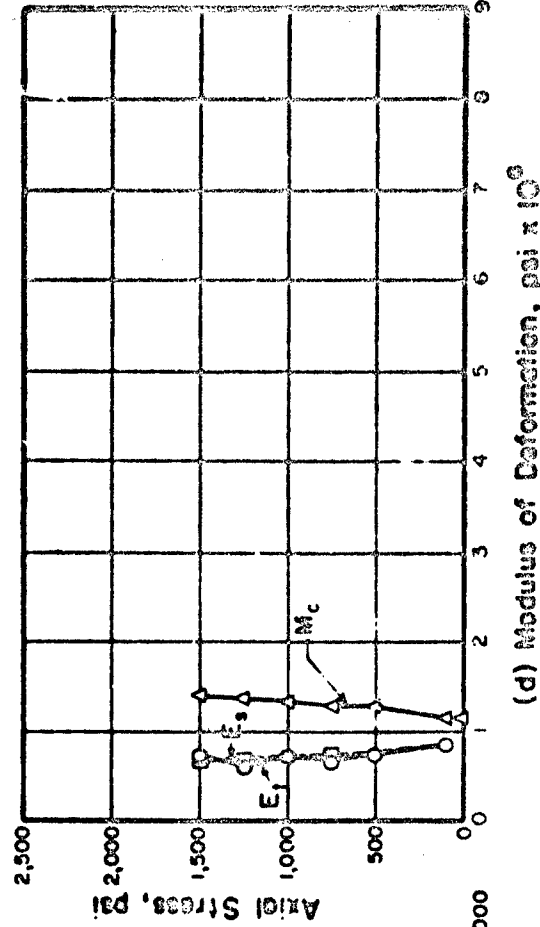
Rock Type	Tuff
NTS (E Tunnel)	
Specimen No. 14.1- (1) S	
L/D	2.000
$\gamma$	100.9
$S_n$	30.2
$\sigma_0$ (ult)	3.55
Texture	Cemented

Note:

- 1)  $V_p$  = Dilational wave velocity
- 2)  $E_t$  = Tangent modulus (static)
- 3)  $E_s$  = Secant modulus (static)
- 4)  $M_c$  = Constrained modulus  
=  $\rho V_p^2$  (dynamic)

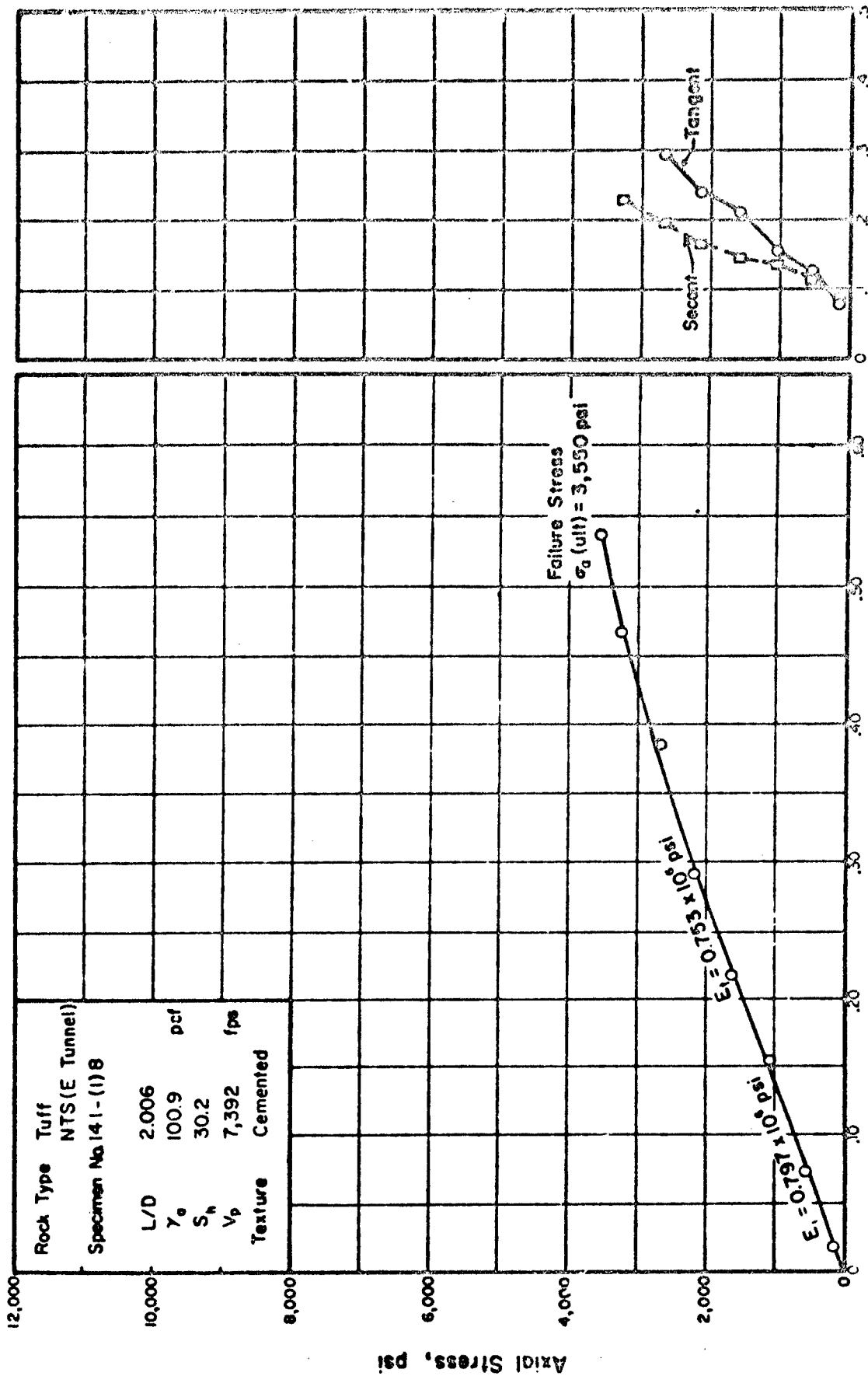


(c) Sonic Pulse Velocity,  $V_p$ , fps

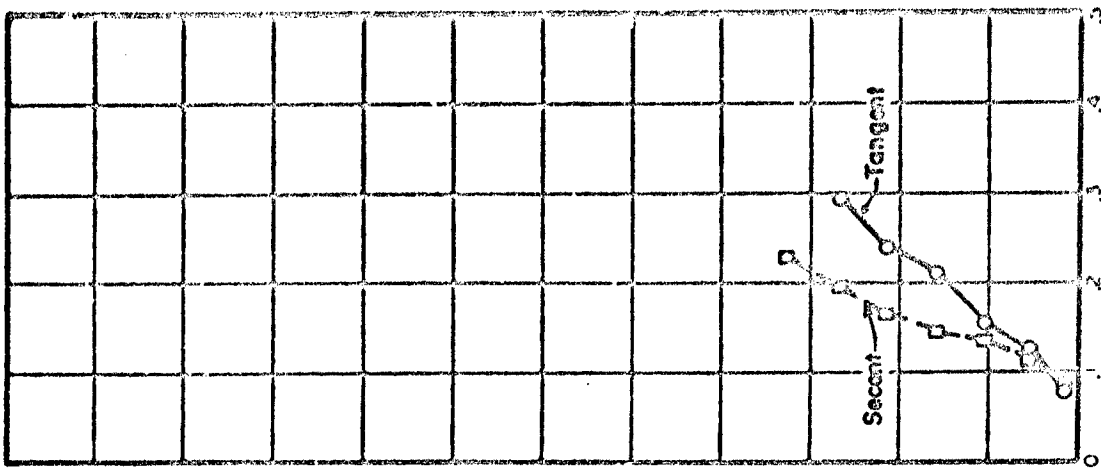


(d) Modulus of Deformation,  $\text{psi} \times 10^6$

FIGURE B.28A STRESS-STRAIN BEHAVIOR AND SONIC PULSE VELOCITY FOR ROCK IN UNIAXIAL COMPRESSION



(a) Axial Strain, %



(b) Poisson's Ratio

FIGURE B.28B STRESS-STRAIN CURVE AND POISSON'S RATIO FOR ROCK IN UNIAxIAL COMPRESSION TO FAILURE

APPENDIX C  
STATISTICAL METHODS OF ANALYSIS

## APPENDIX C

### STATISTICAL METHODS OF ANALYSIS

#### 1. GENERAL

"Statistics is concerned with scientific methods for collecting, organizing, summarizing, presenting and analyzing data, as well as drawing valid conclusions and making reasonable decisions on the basis of such analysis." (Spiegel, 1961)

In a narrower sense the term is used to denote the data themselves or numbers derived from the data as, for example, the averages. In physical tests on rock the average of a series of readings is said to be representative of the whole. This average characteristic is influenced by three important factors which introduce uncertainties in the result:

- i) Instrumental errors.
- ii) Variations in the sample being tested.
- iii) Variations between the sample and the other samples that might be drawn from the same source.

In collecting data on the properties of rocks it is impossible to observe even one type from all its numerous sources, let alone all rock types. Instead of examining all sources called the universe or population only a small part of one source, called a sample, is examined. A sample may consist of one single observation, or a million observations. A population can be finite or infinite.

If a sample is representative of a population, important conclusions about the population can often be inferred from analysis of the sample. The phase of statistics dealing with conditions under which such inference is valid is called statistical inference. Because such inference cannot be absolutely certain, a statement of probability is often used in stating conclusions.

If a number of identical specimens from a homogeneous sample were available for testing, or if the test were nondestructive and could be repeated a number of times on the same specimen, determination of instrumental errors (or errors of observation) would be relatively simple because the variations could be observed independently of the specimen. Since

"perfect" specimens are not available, the variations encountered in testing include variations inherent within and among the specimens and those caused by the test apparatus. Some of the tests used in determining the physical properties of rock are destructive (completely or in part). For these, it is particularly difficult to distinguish between instrumental variations and those caused by changes in composition or structure of the rock because the test cannot be repeated with the identical specimen (or part thereof). This problem is further complicated in the comparison of the results of two or more different tests, all of which are destructive.

The usual method of recording the highest, lowest, and average readings fails to give an adequate conception of the rock property under study. For example, in determining the average Shore (scleroscope) hardness, one sample may be essentially uniform with occasional stray inclusions or impurities that account for the low and high readings. Another, with the same average hardness, may be a heterogeneous mixture in which the hardness ranges gradually from the same low to high value. It is important to know not only the size of the deviations from the average, but also their frequency of occurrence (Obert, et al., 1946).

## 2. MEASURES OF CENTRAL TENDENCY

An average is a value which is typical or representative of a set of data. Since such typical values tend to lie centrally within a set of data arranged according to magnitude, averages are also called measures of central tendency. One of the most common averages is the arithmetic mean or mean which is denoted by the symbol  $\bar{x}$  and computed as follows:

$$\bar{x} = \frac{X_1 + X_2 + X_3 + \dots + X_n}{n} = \frac{\sum_{i=1}^n X_i}{n} = \frac{\Sigma X}{n} \quad (C.1)$$

This is the sum of all the observations in the sample divided by the number of observations.

## 3. MEASURES OF DISPERSION

The degree to which numerical data tend to spread about an average value is called the variation or dispersion of the data. A commonly used measure of dispersion is the variance.

a. Variance

The variance is the sum of the squares of deviations of individual observations from the mean, divided by one less than the total number of observations. The sample variance,  $s^2$ , is computed thus:

$$s^2 = \frac{\sum_{i=1}^n (X_i - \bar{x})^2}{n-1} \quad (C.2)$$

The divisor is known as the number of degrees of freedom in the sample, which has the same meaning in statistics as in geometry and mechanics (Liu and Thornburn, 1965). The result obtained by use of  $(n-1)$  in the denominator instead of  $(n)$  is said to represent a better and unbiased estimate of the variance of a population from which the sample was taken. For large values of  $(n)$ , say  $(n) > 30$ , there is practically no difference between values of  $s^2$  determined by using  $(n)$  or  $(n-1)$ .

b. Standard deviation

The dispersion of the observations about the mean is usually measured by the standard deviation, which is defined as the positive square root of the variance,  $s^2$ . It is thus denoted by the equation:

$$s = \sqrt{\frac{\sum_{i=1}^n (X_i - \bar{x})^2}{n-1}} \quad (C.3)$$

The standard deviation can also be calculated without first calculating the sample mean by using the equivalent equation of the form:

$$s = \sqrt{\frac{\sum_{i=1}^n X_i^2 - \frac{\left(\sum_{i=1}^n X_i\right)^2}{n}}{n-1}} \quad (C.4)$$

The sample mean and deviations therefrom are related to the mathematical statistical principle of least squares in the following manner: If deviations of the observations are measured from the sample mean, then the sum of their squares is a minimum (i.e., the sum of the squares of the deviations of a set of numbers,  $X_i$ , from any number,  $a$ , is a minimum if and only if  $a = \bar{x}$ ).



### c. Coefficient of variation

The actual variation as determined from the standard deviation or other measure of dispersion is called the absolute dispersion. However, for the purpose of comparing the degree of variation within the sample or between samples with respect to different properties, it is more convenient to express the standard deviation,  $s$ , as a percentage of the mean  $\bar{x}$ . This provides a measure of the relative dispersion, called the coefficient of variation,  $V$ . This coefficient is usually expressed as a percentage, and is given by the equation:

$$V\% = \frac{s}{\bar{x}} (100) \quad (c.5)$$

Since it is a ratio of two quantities having the same unit of measurement, the coefficient of variation is independent of the units used. A disadvantage of the coefficient of variation is that it fails to be useful when  $\bar{x}$  is close to zero. This is particularly exemplified by the initial values of Poisson's ratio as reported in Table 4.3.

## 4. NORMAL DISTRIBUTION, SAMPLING AND CONFIDENCE INTERVALS

### a. Normal Distribution

Observations that differ by little from the mean occur more frequently than observations which differ considerably from the mean. Experimental evidence in many fields of science, in conjunction with theory, has led to a general distribution relating the frequency of occurrence of an observation to the amount by which it differs from the population mean. This is known as the normal distribution and is one of the most important examples of a continuous probability distribution in statistics. The curve representing this distribution has the physical appearance of a symmetrical bell-shape, extending infinitely far at both ends as shown in Figure C.1. The equation of the normal curve is:

$$Y = \frac{1}{\sigma \sqrt{2\pi}} e^{-\frac{1}{2} \left(\frac{X - \mu}{\sigma}\right)^2} \quad (c.6)$$

in which  $X$  = abscissa

$Y$  = ordinate

$\pi$  = 3.14159

$e$  = 2.71828

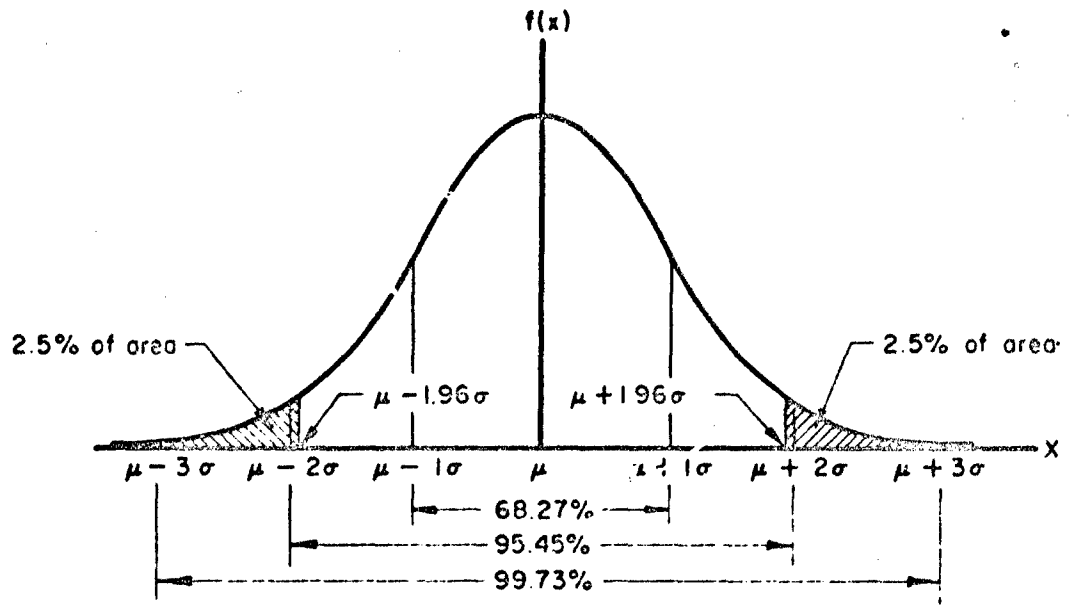


FIGURE C.1 CHARACTERISTICS OF NORMAL DISTRIBUTION

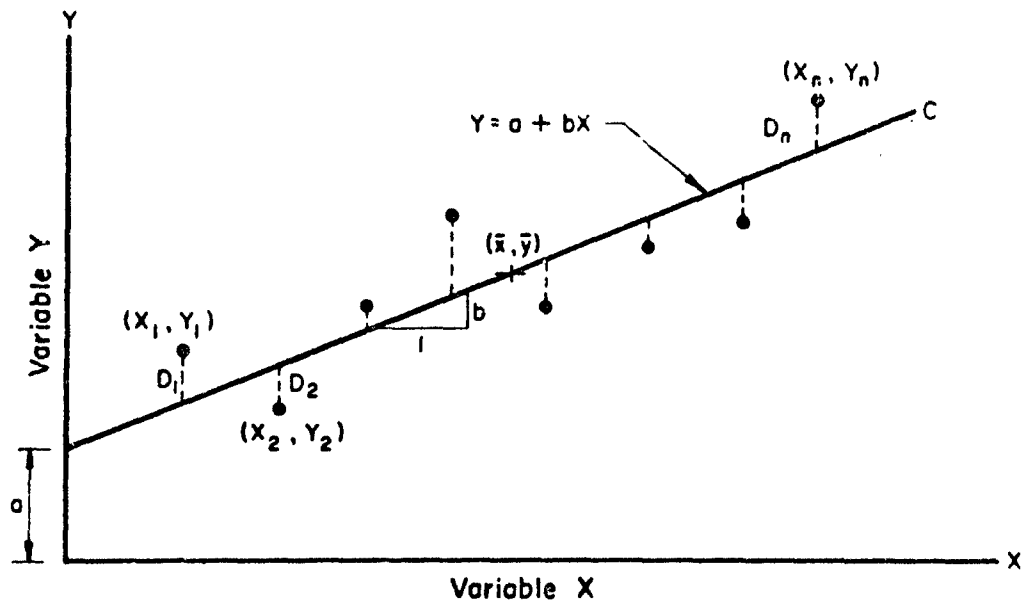


FIGURE C.2 RELATIONSHIP BETWEEN VARIABLES X AND Y

$\mu$  = mean of the distribution or population

$\sigma$  = standard deviation of the distribution or population

If the total area between the curve and X-axis is one (100%), then the portion of the area under the curve between any two values of X is completely determined by  $\mu$  and  $\sigma$ . By integration, it is found that 68.27% of the total area lies in the interval  $\mu \pm 1\sigma$ , while 95.45% of the observations are in the interval  $\mu \pm 2\sigma$ . Only 0.27% of the total frequency lie beyond  $\mu \pm 3\sigma$ . Figure C.1 also indicates that 5% of the total area lies beyond  $\mu \pm 1.96\sigma$  (Liu and Thornburn, 1965).

If large samples of a specified size,  $n$ , from any distribution with finite variance are taken and the mean values calculated, these sample means would also form a distribution which is called sampling distribution of the means and would approximate a normal distribution. In most experimental work it is safe to assume a normal distribution. In a sampling distribution of the means, the standard deviation of the means,  $s_{\bar{x}}$ , is related to the population standard deviation,  $\sigma$ , as follows:

$$s_{\bar{x}} = \frac{\sigma}{\sqrt{n}} \quad (C.7)$$

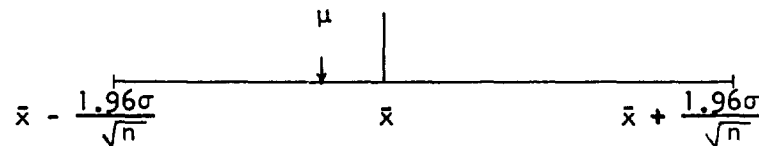
This is referred to statistically as the standard error. On the basis of the characteristics of the sampling distributions of the means and the variances, it is possible to conclude that  $s^2$  can be used as an estimate of  $\sigma^2$  and  $\bar{x}$  of  $\mu$  (Liu and Thornburn, 1965).

#### b. Sampling and confidence intervals

In order that conclusions of sampling theory and statistical inference be valid, samples must be chosen so as to be representative of the population. One way in which a representative sample may be obtained is by a process called random sampling according to which each member of a population has an equal chance of being included in the sample.

Since the sampling distribution of the means has a mean of  $\mu$  and a standard deviation of  $\frac{\sigma}{\sqrt{n}}$  and is normal in shape, it is possible to determine the probability that a sample mean,  $\bar{x}$ , might be found within a specified distance of the population mean,  $\mu$ , based on the characteristics of the normal curve.

Assuming that  $\mu$  and  $\sigma$  are known, the chances are 68.27 in 100 that the sample mean,  $\bar{x}$ , will be found within the distance  $\pm \frac{1.0\sigma}{\sqrt{n}}$  from  $\mu$ . Similarly, the probability is 95.45 in 100 that  $\bar{x}$  will be found within  $\pm \frac{2.0\sigma}{\sqrt{n}}$ . This distance can be designated to cover any specified probability as  $\pm \frac{Z\sigma}{\sqrt{n}}$ . If  $\bar{x}$  is added to any of these distances, an interval is formed which includes  $\mu$  at a specified probability, depending on what value is chosen for  $Z$ . (The Z-distribution is a standard normal distribution obtained from the equation  $Z = \frac{X - \mu}{\sigma}$ .) If the probability is chosen at 95 in 100, the Z-value will be 1.96. In other words,  $\mu$  will fall within the range of  $(\bar{x} - \frac{1.96\sigma}{\sqrt{n}})$  to  $(\bar{x} + \frac{1.96\sigma}{\sqrt{n}})$ . This can be expressed geometrically as follows:



An interval is set up around  $\bar{x}$ , and then the probability is 95 in 100 that  $\mu$  will be found someplace in this interval. This is called the confidence interval. That is, there is a 95% confidence of finding the population mean,  $\mu$ , within this interval.

Usually, both the population parameters  $\mu$  and  $\sigma$  are unknown; however, the sample statistics  $\bar{x}$  and  $s$  are known. As previously noted,  $\bar{x}$  is an estimate of  $\mu$ , and  $s$  of  $\sigma$ . When statistics are used instead of parameters, the confidence interval inequality is:

$$\bar{x} - \frac{ts}{\sqrt{n}} < \mu < \bar{x} + \frac{ts}{\sqrt{n}} \quad (C.8)$$

The t-distribution is similar to a normal Z-distribution and closely approaches it, provided that the sample size is large. Generally,  $t$  is larger than  $Z$  for a specified probability. The  $t$ -values may be found in most statistical texts.

The values of  $\bar{x} \pm \frac{ts}{\sqrt{n}}$  or  $\bar{x} \pm ts_{\bar{x}}$  are referred to statistically as confidence limits and  $\frac{ts}{\sqrt{n}}$  or  $ts_{\bar{x}}$  as the limit of accuracy. The larger the value of  $s$ , the wider the confidence interval will be because the confidence interval is directly proportional to the size of the standard deviation.

The shaded areas in Figure C.1 are each composed of 2.5% of the total area. These are the areas of the distribution of the statistics in which a

hypothesis will be rejected, and are known as the critical regions or regions of significance. The chance of rejecting the hypothesis that  $\mu$  falls within these critical regions (when in reality it does) is 5% because the critical regions are determined by the t-value at the 95% point. Thus, there are about five chances in 100 that we would reject the hypothesis when it should be accepted, i.e., we are 95% confident that we have made the right decision. This chance is called the level of significance and is denoted by the Greek letter,  $\alpha$ . It is usually stated that a result is significant if the hypothesis is rejected with  $\alpha = .05$  and highly significant if it is rejected with  $\alpha = .01$ . These are designated conventionally as significant at the 5% level and significant at the 1% level respectively. It can be seen that when the level of significance is raised, the confidence interval will be widened, because the chances of rejecting a true hypothesis are decreased (Liu and Thornburn, 1965).

## 5. CURVE FITTING AND THE METHOD OF LEAST SQUARES

### a. Curve fitting

It is frequently desirable to express a relationship existing between two (or more) variables in mathematical form by determining an equation containing the variables. When a series of concomitant observations  $(X_1, Y_1)$ ,  $(X_2, Y_2)$ , ---  $(X_n, Y_n)$  is plotted on a rectangular coordinate system, the resulting set of points is sometimes called a scatter diagram. If the data appear to be well-approximated by a straight line, a linear relationship is said to exist between the variables. If a curved line is a better approximation, a non-linear relationship is said to exist. The general problem of finding equations for approximating curves which fit given sets of data is called curve fitting.

### b. The method of least squares

In order to avoid individual judgment in constructing lines, parabolas, or other approximating curves to fit sets of data, it is necessary to agree on a definition of a "best-fitting line," "best-fitting parabola," et cetera. Figure C.2 shows a scatter diagram obtained from a series of observations. For a given value of  $X$ , say  $X_1$ , there is a difference between the value  $Y_1$  and the corresponding value as determined from the "curve" or line C. As

indicated in the figure, this difference is denoted by  $D_1$ , which is referred to as a deviation, error, or residual and may be positive, negative, or zero. Similarly, corresponding to the values  $X_2, \dots, X_n$ , we obtain  $D_2, \dots, D_n$ . Of all curves approximating a given set of data points, the curve having the property that  $D_1^2 + D_2^2 + \dots + D_n^2$  is a minimum, is called a best-fitting curve. A curve having this property is said to fit the data in the least-square sense and is called a least-square curve. Thus, the line C in Figure C.2, is a least-square line if it has this property.

The above definition applies when X is the independent variable, and Y the dependent variable. If X is dependent, the definition is modified by considering horizontal instead of vertical deviations, which amounts to an interchange of the X and Y axes. These two definitions, in general, lead to different least-square lines. Thus, when these two lines approach coincidence, there is an indication that the data are very well described by a linear relationship.

Non-linear relationships can usually be reduced to linear relationships by appropriate transformation of variables, such as logarithmic functions. In such cases, the same methods for curve fitting may be applied as used for the linear relationships.

## 6. CORRELATION AND REGRESSION

The degree of relationship between variables, or correlation, seeks to determine how well a linear or other equation describes the relationship. If all values of the variables satisfy an equation exactly, we say that the variables are perfectly correlated, or that there is a perfect correlation between them.

On the basis of sample data, we can estimate the value of a variable Y, corresponding to a given value of a variable X, from a least-square line (or curve) which fits the sample data. The resulting line is called a regression line of Y on X, since Y is estimated from X. Conversely, the value of X may be estimated from the regression line of X on Y, in which case X is the dependent and Y the independent variable. In general, the regression line or curve of Y on X is not the same as the regression line or curve of X on Y. When only two variables are involved, we are concerned with

simple correlation and simple regression. When more than two variables are involved, we are concerned with multiple correlation and multiple regression.

a. Linear correlation

If all points in a scatter diagram appear to lie near a line, as in Figure C.2, the correlation is called linear. If Y tends to increase as X increases, the correlation is a positive or a direct correlation. If Y tends to decrease as X increases, the correlation is a negative or an inverse correlation. If there is no relationship indicated between the variables, they are uncorrelated. The correlation is non-linear if all points appear to lie near some curve.

b. Least-square regression

The least-square regression line of Y on X has the equation:

$$Y = a + bX \quad (C.9)$$

in which Y = dependent variable

X = independent variable

a = Y-intercept of regression line

b = slope of regression line, also

called the coefficient of regression

By means of the calculus, the so-called normal equations are obtained, and expressed as follows:

$$\begin{aligned} \Sigma Y &= an + b\Sigma X \\ \Sigma XY &= a\Sigma X + b\Sigma X^2 \end{aligned} \quad (C.10)$$

These two equations are solved simultaneously to obtain a and b:

$$\begin{aligned} a &= \frac{(\Sigma Y)(\Sigma X^2) - (\Sigma X)(\Sigma XY)}{n\Sigma X^2 - (\Sigma X)^2} \\ b &= \frac{n\Sigma XY - (\Sigma X)(\Sigma Y)}{n\Sigma X^2 - (\Sigma X)^2} \end{aligned} \quad (C.11)$$

The regression line of X on Y is similarly obtained. However, the resulting least-square line is, in general, not the same as noted previously.

The two least-square regression lines thus obtained both pass through the point  $(\bar{x}, \bar{y})$ , which is the centroid or center of gravity of the data. These regression equations are identical only if all points of the

scatter diagram lie on a line. In such case there is a perfect correlation between X and Y (Spiegel, 1961).

c. Coefficient of correlation

A correlation coefficient is a measure of intensity of association or relationship between variables. A regression coefficient describes the change in the dependent variable as a result of changing the independent variable. Unlike a variance or a regression coefficient, the correlation coefficient is independent of the units of measurement; it is an absolute or dimensionless quantity. The use of X and Y is no longer intended to imply an independent and a dependent variable.

The total variation of Y is defined as  $\Sigma(Y-\bar{y})^2$ , i.e., the sum of the squares of the deviations of the values of Y from the mean  $\bar{y}$ . This can be written by the equation:

$$\Sigma(Y-\bar{y})^2 = \Sigma(Y-Y_{\text{est.}})^2 + \Sigma(Y_{\text{est.}} - \bar{y})^2 \quad (\text{C.12})$$

in which  $Y_{\text{est.}}$  = value of Y for given values of X as estimated from (C.9)

$$\Sigma(Y-Y_{\text{est.}})^2 = \text{unexplained variation}$$

$$\Sigma(Y_{\text{est.}} - \bar{y})^2 = \text{explained variation}$$

The deviations  $Y_{\text{est.}} - \bar{y}$  have a definite pattern while the deviations  $Y - Y_{\text{est.}}$  behave in an unpredictable manner.

The ratio of the explained variation to the total variation is called the coefficient of determination denoted by  $r^2$ , hence is always positive. The square root of the coefficient of determination is called the coefficient of correlation, r, which is given by:

$$r = \pm \sqrt{\frac{\text{explained variation}}{\text{total variation}}} = \pm \sqrt{\frac{\Sigma(Y_{\text{est.}} - \bar{y})^2}{\Sigma(Y-\bar{y})^2}} \quad (\text{C.13})$$

The quantity, r, varies between -1 and +1, which are the values for a perfect correlation. The signs  $\pm$  denote positive or negative linear correlation, respectively. The practical range of r varies with opinion from one field of research to another. In some studies, investigators will look upon  $r = 0.90$  as small, while in others  $r = 0.20$  may be considered as unusually large.



d. Standard error of estimate

As previously indicated, no relationship is perfect; therefore, the actual values will not coincide with the theoretical values estimated from the regression line. If the scatter is definitely measured, the variation is determined and a range is established within which a given percentage of values will fall. The standard error of estimate,  $s_{y \cdot x}$ , is a measure of the scatter about the regression line of Y on X and is given by the equation:

$$s_{y \cdot x} = \sqrt{\frac{\Sigma(Y - Y_{est.})^2}{n - 2}} \quad (C.14)$$

Similarly, the standard error of estimate of X on Y is obtained by interchanging Y with X in this equation.

The standard error of estimate has properties analogous to those of the standard deviation. If lines are constructed parallel to the regression line of Y on X at respective vertical distances  $\pm s_{y \cdot x}$ ,  $\pm 2s_{y \cdot x}$  and  $\pm 3s_{y \cdot x}$  from it, approximately 68%, 95% and 99.7% of the sample points would be included between these lines.

e. Confidence limits

An unbiased estimate of the true variance about regression is given by the residual mean square with  $n-2$  degrees of freedom. It is defined by the square of equation (C.14) as follows:

$$s_{y \cdot x}^2 = \frac{\Sigma(Y - Y_{est.})^2}{n - 2} \quad (C.15)$$

Figure C.3 shows that a single standard deviation of Y for a fixed X (i.e., standard error of estimate) does not apply to all  $Y_{est.}$ 's but must depend upon the X-value that determines the Y-population. For a fixed set of X-values,  $\bar{x}$  is a constant, while  $\bar{y}$  and  $b$  are variables. Variation in  $\bar{y}$  raises or lowers the regression line parallel to itself (thus increasing or decreasing all estimates of means by a fixed value). Variation in  $b$  rotates the regression line about the point  $\bar{x}, \bar{y}$ , but has no effect upon the estimate of the mean if  $X = \bar{x}$ . Otherwise, it increases the estimate of the mean in proportion to the size of  $(X - \bar{x})$ . This is readily seen from the equation that estimates the population mean,  $Y_{est.} = \bar{y} + b(X - \bar{x})$ .

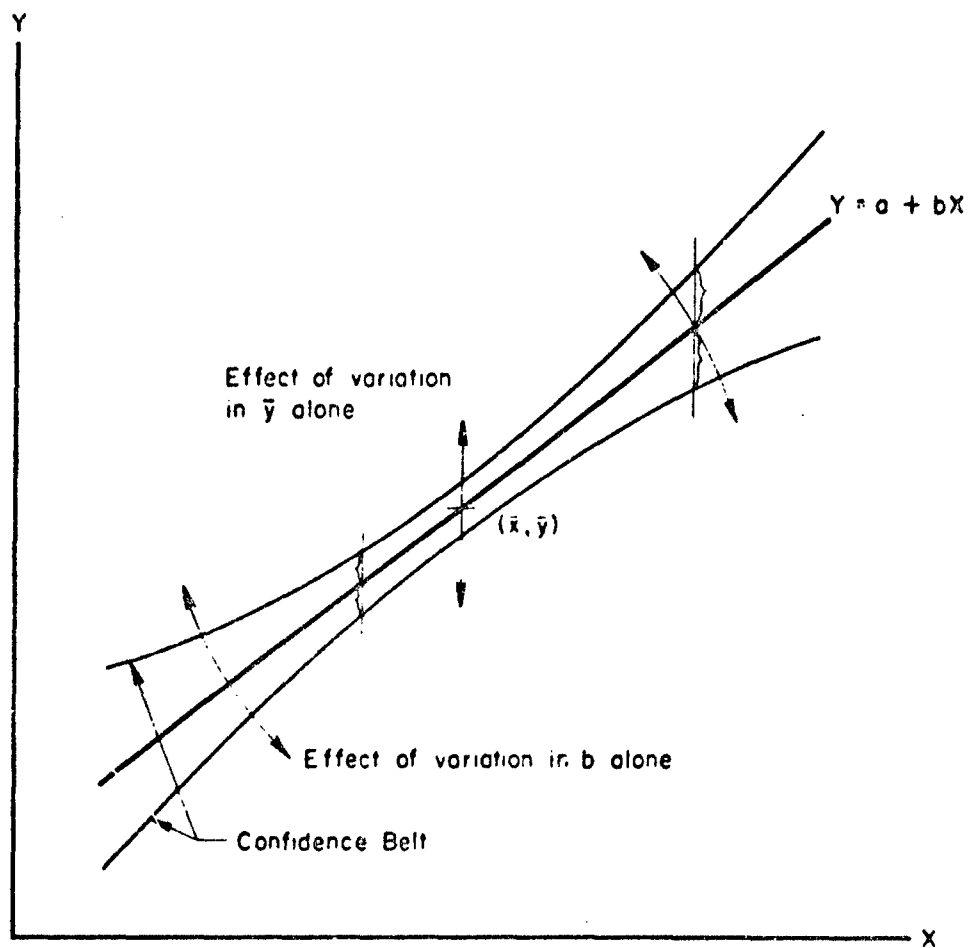


FIGURE C.3 EFFECT OF SAMPLING VARIATION ON REGRESSION ESTIMATES OF POPULATION MEANS (After Steel & Torrie, 1960)

A standard deviation applicable to an estimate of a mean must allow for variation in both  $\bar{y}$  and  $b$ , and for the distance  $(X-\bar{x})$ . The variance of  $\bar{y}$  is an estimate of  $\frac{\sigma^2_{y \cdot x}}{n}$ , namely  $\frac{s^2_{y \cdot x}}{n}$ . An estimate of the variance of  $b$  is given by the equation:

$$s_b^2 = \frac{s^2_{y \cdot x}}{\Sigma(X-\bar{x})^2} \quad (C.16)$$

The required variance of an estimate,  $Y_{est.} = \bar{y} + b(X-\bar{x})$ , of a population mean is given by the sum of the variances of  $\bar{y}$  and  $b(X-\bar{x})$  as follows:

$$s^2_{y \cdot x} \left[ \frac{1}{n} + \frac{(X-\bar{x})^2}{\Sigma(X-\bar{x})^2} \right] \quad (C.17)$$

This variance increases as  $(X-\bar{x})$  increases. If  $t$  times the standard deviation were plotted in conjunction with the regression line, the confidence belt shown in Figure C.3 would be formed.

To set a confidence interval on the estimate of the mean, the variance in equation (C.17) is added to the regression equation. The 95% confidence limits are then defined as follows:

$$CL(Y_{est.}) = \bar{y} + b(X-\bar{x}) \pm t_{.05} s_{y \cdot x} \sqrt{\frac{1}{n} + \frac{(X-\bar{x})^2}{\Sigma(X-\bar{x})^2}} \quad (C.18)$$

where  $t$  is for  $n-2$  degrees of freedom.

If a prediction is to be made, it is usually a prediction of individual events rather than for the population. Thus, the random element is an additional source of uncertainty and equation (C.18) is modified as follows:

$$CL(Y) = \bar{y} + b(X-\bar{x}) \pm t_{.05} s_{y \cdot x} \sqrt{1 + \frac{1}{n} + \frac{(X-\bar{x})^2}{\Sigma(X-\bar{x})^2}} \quad (C.19)$$

Using this procedure, a confidence belt for  $Y$  may be plotted which is somewhat broader than that defined by (C.18). In general, about 5% of the sample points are expected to fall outside the belt given by (C.19), (Snedecor, 1956).

## BIBLIOGRAPHY

- American Geological Institute, (1962), Glossary of Geology and Related Sciences, The American Geological Institute, Washington, D. C.
- American Society for Testing and Materials, (1964), "Resistance to Abrasion of Small Size Coarse Aggregate by use of the Los Angeles Machine," Tentative Method ASTM Designation: C 131-64T, ASTM Standards, part 10, p. 80.
- American Society for Testing and Materials, (1964), "Abrasion Resistance of Concrete," Tentative Method ASTM Designation: C 418-64T, ASTM Standards, part 10, p. 309.
- American Society for Testing and Materials, (1964), "Relative Resistance to Wear of Unglazed Ceramic Tile by the Taber Abraser," Tentative Method ASTM Designation: C 501-62T, ASTM Standards, part 13, p. 455.
- American Society for Testing and Materials, (1964), "Resistance to Abrasion of Large Size Coarse Aggregate by use of the Los Angeles Machine," Tentative Method ASTM Designation: C 535-64T, ASTM Standards, part 10, p. 361.
- American Society for Testing and Materials, (1964), "Standard Method of Test for Abrasion of Rock by use of the Deval Machine," Standard Method ASTM Designation: D 2-33, ASTM Standards, part 10, p. 363.
- American Society for Testing and Materials, (1964), "Standard Method of Test for Toughness of Rock," Standard Method ASTM Designation: D 3-18, ASTM Standards, part 10, p. 365.
- American Society for Testing and Materials, (1964), "Resistance of Transparent Plastics to Surface Abrasion," Standard Method ASTM Designation: D 1044-56, ASTM Standards, part 27, p. 442.
- American Society for Testing and Materials, (1964), "Resistance to Abrasion of Plastic Materials," Standard Method ASTM Designation: D 1242-56, ASTM Standards, part 27, p. 472.
- American Society for Testing and Materials, (1964), "Bierbaum Scratch Hardness of Plastic Materials," Tentative Method ASTM Designation: D 1526-58T, ASTM Standards, part 27, p. 527.
- American Society for Testing and Materials, (1964), "Identification Hardness of Plastics by Means of a Durometer," Standard Method ASTM Designation: D 1706-61, ASTM Standards, part 27, p. 570.
- American Society for Testing and Materials, (1965), "Compressive Strength of Natural Building Stone," Standard Method ASTM Designation: C 170-50, ASTM Standards, part 12, p. 144.

- American Society for Testing and Materials, (1965), "Brinnell Hardness of Metallic Materials," Standard Method ASTM Designation: E 10-65, ASTM Standards, part 30, p. 158.
- American Society for Testing and Materials, (1965), "Rockwell Hardness and Rockwell Superficial Hardness of Metallic Materials," Standard Methods ASTM Designation: E 18-65, ASTM Standards, part 30, p. 187.
- American Society for Testing and Materials, (1965), "Diamond Pyramid Hardness of Metallic Materials," Standard Method ASTM Designation: E 92-65, ASTM Standards, part 30, p. 317.
- Appl, F. C., and Gatley, W. S., (1961), "Rate of Loading Effects in Chisel Impact," Proceedings of the Fourth Symposium on Rock Mechanics, Bulletin of the Mineral Industries Experiment Station, The Pennsylvania State University, p. 229.
- Blair, B. E., (1955), Physical Properties of Mine Rock, Part III, U. S. Bureau of Mines, R. I. 5130.
- Blair, B. E., (1956), Physical Properties of Mine Rock, Part IV, U. S. Bureau of Mines, R. I. 5244.
- Bond, F. C., (1946), "Crushing Tests by Pressure and Impact," Trans. AIME, Mining Technology, Vol. 169, p. 58.
- Bond, F. C., (1961), Crushing and Grinding Calculations, Allis-Chalmers Manufacturing Company, Milwaukee, Wisconsin.
- Bowker, A. H., and Lieberman, G. J., (1959), Engineering Statistics, Prentice-Hall, Inc., Englewood Cliffs, N. J.
- Brace, W. F., (1960), "Behavior of Rock Salt, Limestone and Anhydrite During Indentation," Journal of Geophysical Research, Vol. 65, No. 6, p. 1773.
- Brace, W. F., (1963), "Brittle Fracture of Rocks," International Conference on the State of Stress in the Earth's Crust, Santa Monica, June.
- Brown, P. D., and Robertshaw, J., (1953), "The In Situ Measurement of Young's Modulus for Rock by a Dynamic Method," Geotechnique, Vol. III, No. 7, p. 283.
- Burbank, B. B., (1955), "Measuring the Relative Abrasiveness of Rocks, Minerals and Ores," Pit and Quarry, August, p. 114.
- Cheatham, J. B., Jr., (1958), "An Analytical Study of Rock Penetration by a Single Bit Tooth," Proceedings of the Eighth Drilling and Blasting Symposium, University of Minnesota, October, p. 1A-25A.
- Christensen, C. J., (1947), "Diamond Coring in Rangely," Presented at Regional Meeting of AIME, Denver, Colorado, September.
- Coates, D. F., (1964), "Classification of Rocks for Rock Mechanics," International Journal of Rock Mechanics and Mining Sciences, Vol. 1, No. 3, p. 421.

- Colback, P. S. B., and Wiid, B. L., (1965), "The Influence of Moisture Content on the Compressive Strength of Rock," Third Canadian Symposium on Rock Mechanics, University of Toronto, January.
- Dana, E. S., (1932), A Textbook of Mineralogy, John Wiley & Sons, New York.
- D'Andrea, D. V., Fischer, R. L., and Fogelson, D. E., (1964), "Prediction of Compressive Strength from Other Rock Properties," Quarterly of the Colorado School of Mines, Vol. 59, No. 4-Part B, p. 623.
- Deere, D. U., (1963a), Class Notes from Advanced Graduate courses in Rock Mechanics.
- Deere, D. U., (1963b), "Technical Description of Rock Cores for Engineering Purposes," Felsmechanik und Ingenieurgeologie/Rock Mechanics and Engineering Geology, Journal of the International Society of Rock Mechanics, Vol. 1, No. 1, p. 16.
- Deere, D. U., (1964), Private communication.
- Devries, R. P., (1911), "Hardness in its Relation to Other Physical Properties," Proceedings ASTM, Vol. 11, p. 726.
- Dvorak, A., (1957), "Field Test of Rocks on Dam Sites," Proceedings of the Fourth International Conference on Soil Mechanics and Foundation Engineering, Butterworths Scientific Publications, London, Vol. 1, p. 221.
- Eshback, O. W., (1952), Handbook of Engineering Fundamentals, John Wiley & Sons, Inc., New York.
- Evison, F. F., (1956), "The Seismic Determination of Young's Modulus and Poisson's Ratio for Rocks In Situ," Geotechnique, Vol. VI, No. 3, p. 118.
- Fairhurst, C., and Lacabanne, W. P., (1957), "Hard Rock Drilling Techniques," Mine & Quarry Engineering, April, p. 157, May, p. 194.
- Fairhurst, C., (1961a), "Wave Mechanics of Percussive Drilling," Mine & Quarry Engineering, March, p. 122, April, p. 169.
- Fairhurst, C., (1961b), "Laboratory Measurement of Some Physical Properties of Rock," Proceedings of the Fourth Symposium on Rock Mechanics, Bulletin of the Mineral Industries Experiment Station, Pennsylvania State University, p. 105.
- Gilbert, B. W., (1954), Shore Scleroscope Hardness Tests Made on Mohs' Scale Minerals from Talc to Quartz, Inclusive, Department of Mining and Metallurgical Engineering, University of Illinois.
- Greaves, R. H., (1909), "The Physical Interpretation of Hardness as Measured by the Shore Scleroscope," Proceedings Institute of Civil Engineering, London, Vol. 181, p. 478.

- Gregory, A. R., (1963), "Shear Wave Velocity Measurements of Sedimentary Rock Samples under Compression," Proceedings of the Fifth Symposium on Rock Mechanics, The Macmillan Company, New York, p. 439.
- Griffith, J. H., (1937), Physical Properties of Typical American Rocks, Iowa Engineering Experiment Station Bulletin 131.
- Grout, F. F., (1940), Kemp's Handbook of Rocks, D. Van Nostrand Company, Inc., New York.
- Gyss, E. E., and Davis, H. E., (1927), "The Hardness and Toughness of Rocks," Mining and Metallurgy, Vol. 8, p. 261.
- Hamrol, A., (1961), "A Quantitative Classification of the Weathering and Weatherability of Rocks," Proceedings of the Fifth International Conference on Soil Mechanics and Foundation Engineering, Paris, Vol. II, p. 771.
- Hardy, H. R., Jr., (1959), Standardized Procedures for the Determination of the Physical Properties of Mine Rock under Short-Period Uniaxial Compression, Department of Mines and Technology Surveys, Ottawa, Canada, Mines Branch Technical Bulletin TB 8.
- Harley, G. T., (1926), "Proposed Ground Classification for Mining Purposes-- I and II," Engineering and Mining Journal, Vol. 122, No. 10 and 11, pp. 368 and 413.
- Hartman, H. L., (1959), "Basic Studies of Percussion Drilling," Mining Engineering, Vol. 11, p. 68.
- Harvey, R. D., (1963), Impact Resistance of Illinois Limestones and Dolomites, Illinois State Geological Survey Circular 345.
- Head, A. L., Jr., (1951), "A Drillability Classification of Geological Formations," World Oil, October, p. 125.
- Huang, W. T., (1962), Petrology, McGraw-Hill Book Company, Inc., New York.
- Hucka, V., (1965), "A Rapid Method of Determining the Strength of Rocks In Situ," International Journal of Rock Mechanics and Mining Sciences, Vol. 2, No. 2, p. 127.
- Ide, J. M., (1936), "Comparison of Statically and Dynamically Determined Young's Modulus of Rocks," Proceedings of the National Academy of Science, Vol. 22, No. 2, p. 81.
- Jackson, F. H., (1916), Methods for the Determination of the Physical Properties of Road-Building Rock, U. S. Department of Agriculture, Department Bulletin 347.
- Jaeger, J. C., (1962), Elasticity, Fracture and Flow, John Wiley & Sons, Inc., New York.

- Jastrzebski, Z. D., (1959), Nature and Properties of Engineering Materials, John Wiley & Sons, Inc., New York.
- John, K. W., (1962), "An Approach to Rock Mechanics," Journal of the Soil Mechanics and Foundations Division, Proceedings of the American Society of Civil Engineers, Vol. 88, No. SM4, Part 1, p. 1.
- Judd, W. R., and Huber, C., (1961), "Correlation of Rock Properties by Statistical Methods," International Symposium on Mining Research, Rolla, Missouri, February.
- Kapadia, A. H., (1951), Correlation of Scleroscope Hardness with Physical and Elastic Properties of Rock, M. S. Thesis, Colorado School of Mines.
- King, R. F., and Tabor, D., (1954), "The Strength Properties and Frictional Behavior of Brittle Solids," Proceedings Royal Society, Ser. A, 223, p. 225.
- Klapka, K. J., (1948), "Drilling with Industrial Diamonds," World Oil, October, p. 101.
- Knill, J. L., and Jones, K. S., (1965), "The Recording and Interpretation of Geological Conditions in the Foundations of the Roseires, Kariba, and Latiyan Dams," Geotechnique, Vol. XV, No. 1, p. 94.
- Knoop, F., Peters, C. G., and Emerson, W. B., (1939), "A Sensitive Pyramidal-Diamond Tool for Indentation Measurements," RP 1220, Journal of Research of the National Bureau of Standards, Vol. 23, No. 1, p. 39.
- Kolsky, H., (1963), Stress Waves in Solids, Dover Publications, Inc., New York.
- Kraatz, P., (1964), Rockwell Hardness as an Index Property of Rocks, M. S. Thesis, University of Illinois.
- Krynine, D. P., and Judd, W. R., (1957), Principles of Engineering Geology and Geotechnics, McGraw-Hill Book Company, Inc., New York.
- Lea, F. C., (1936), Hardness of Metals, Charles Griffin & Co., Ltd., London.
- Liu, T. K., and Thornburn, T. H., (1965), Engineering Index Properties of Some Surficial Soils in Illinois, University of Illinois Engineering Experiment Station Bulletin 477.
- Mahin, E. G., and Foss, G. J., (1939), "Absolute Hardness," Trans. American Society for Metals, Vol. 27, p. 337.
- Mather, W. B., (1951), "Rock Hardness as a Factor in Drilling Problems," Trans. AIME, Vol. 190, p. 173.
- McCarthy, J. H., (1964), Electronic Methods for Determining Young's Modulus and Poisson's Ratio of Portland Cement, Technical Report R 295, U. S. Naval Civil Engineering Laboratory, Port Hueneme, California.



- McCray, A. W., (1948), "Diamond Coring of Chert, Limestone and Dolomite of West Texas Permian Basin," Petroleum Engineer, Vol. 19, No. 6, p. 76.
- Mielenz, R. C., (1961), Petrography and Engineering Properties of Igneous Rocks, U. S. Department of the Interior, Bureau of Reclamation, Denver, Engineering Monographs, No. 1.
- Mohs, F., (1824), Grundriss der Mineralogie, English translation by W. Haldinger, (1825), Treatise on Mineralogy, Constable and Co., Ltd., Edinburgh.
- Nicholis, H. R., (1961), In Situ Determination of the Dynamic Elastic Constants of Rock, U. S. Bureau of Mines R. I. 5088.
- Obert, L., Windes, S. L., and Duvall, W. I., (1946), Standardized Tests for Determining the Physical Properties of Mine Rock, U. S. Bureau of Mines, R. I. 3891.
- Onodera, T. F., (1963), "Dynamic Investigation of Foundation Rocks In Situ," Proceedings of the Fifth Symposium on Rock Mechanics, The Macmillan Company, New York, p. 517.
- Panama Canal Company, (1947), Isthmian Canal Studies Memo 210, Department of Operation and Maintenance, Special Engineering Division, April.
- Panama Canal Company, (1959), Geological Logs of Drill Holes for Construction of Balboa Bridge, Substructure, Canal Zone, Balboa Heights, April.
- Peck, R. B., Hanson, W. E., and Thornburn, T. H., (1953), Foundation Engineering, John Wiley & Sons, Inc., New York.
- Pennington, J. V., (1954), "Rock Failure in Percussion," The Petroleum Engineer, May, p. B-76.
- Pomeroy, C. D., (1957), "A Simple Method for the Assessment of Coal Strength," Journal of the Institute of Fuels, February, p. 50.
- Protodyakonov, M. M., (1960), "New Methods of Determining Mechanical Properties of Rocks," Proceedings Third International Conference on Strata Control, Paris, p. 187.
- Protodyakonov, M. M., (1963), "Mechanical Properties and Drillability of Rocks," Proceedings of the Fifth Symposium on Rock Mechanics, The Macmillan Company, New York, p. 103.
- Reich, H., (1930), "Geologische Unterlagen der Angewandten Geophysik," Handbuch der Experimentalphysik, Vol. 25, part 3.
- Reichmuth, D. R., (1963), "Correlations of Force-Displacement Data with Physical Properties of Rock for Percussive Drilling Systems," Proceedings of the Fifth Symposium on Rock Mechanics, The Macmillan Company, New York, p. 33.

- Richards, C. W., (1961), Engineering Materials Science, Wadsworth Publishing Company, Inc., Belmont, California.
- Ridgway, R. R., Ballard, A. H., and Bailey, B. L., (1933), "Hardness Values for Electrochemical Products," Trans. The Electrochemical Society, Vol. 63, p. 369.
- Rinehart, J. S., Fortin, J. P., and Burgin, L., (1961), "Propagation Velocity of Longitudinal Waves in Rocks," Proceedings of the Fourth Symposium on Rock Mechanics, Bulletin of the Mineral Industries Experiment Station, Pennsylvania State University, p. 119.
- Rocha, M., (1964), "Mechanical Behaviour of Rock Foundations in Concrete Dams," Eighth International Conference on Large Dams, Edinburgh, R. 44, Q. 28, p. 785.
- Rollow, A. G., (1963), "Estimating Drillability in the Laboratory," Proceedings of the Fifth Symposium on Rock Mechanics, The Macmillan Company, New York, p. 93.
- Roxborough, F. F., and Whittaker, B. N., (1964), "Roof Control and Coal Hardness," Colliery Engineering, December, p. 511.
- Roxborough, F. F., and Whittaker, B. N., (1965), "Roof Control and Coal Hardness," Colliery Engineering, January, p. 19.
- Scott, F. L., (1946), "Hard-Rock Rotary Drilling," The Oil and Gas Journal, October, p. 74.
- Seely, F. B., and Smith, J. O., (1956), Resistance of Materials, John Wiley & Sons, Inc., New York.
- Seely, F. B., and Smith, J. O., (1959), Advanced Mechanics of Materials, John Wiley & Sons, Inc., New York.
- Shepherd, R., (1950), "Physical Properties and Drillability of Mine Rock," Colliery Engineering, December, p. 48.
- Shepherd, R., (1951), "Physical Properties and Drillability of Mine Rock," Colliery Engineering, January, p. 28, February, p. 61, March, p. 121.
- Shepherd, R., (1953), "Drillability of Rock in Rotary Drilling," Manual of Rock Blasting, AB Atlas Diesel, Stockholm.
- Singh, M. M., and Hartman, H. L., (1961), "Hypothesis for the Mechanism of Rock Failure Under Impact," Proceedings of the Fourth Symposium on Rock Mechanics, Bulletin of the Mineral Industries Experiment Station, Pennsylvania State University, p. 221.
- Snedecor, G. W., (1956), Statistical Methods, The Iowa State University Press, Ames, Iowa.
- Sosman, R. B., (1927), Properties of Silica, American Chemical Society, Monograph No. 37, Chemical Catalog Co., Inc., New York.

- Spiegel, M. R., (1961), Theory and Problems of Statistics, Schaum Publishing Company, New York.
- Spock, L. E., (1953), Guide to the Study of Rocks, Harper & Brothers, Publishers, New York.
- Statistical Service Unit, (1964), SSUPAC, Manual of Computer Programs for Statistical Analysis University of Illinois, Urbana, Illinois.
- Steel, R. G. D., and Torrie, J. H., (1960), Principles and Procedures of Statistics, McGraw-Hill Book Company, Inc., New York.
- Stokes, W. L., and Varnes, D. J., (1955), "Glossary of Selected Geologic Terms," Colorado Scientific Society Proceedings, Vol. 16, Denver.
- Sutherland, R. B., (1963), "Some Dynamic and Static Properties of Rock," Proceedings of the Fifth Symposium on Rock Mechanics, The Macmillan Company, New York, p. 473.
- Tabor, D., (1947), "A Simple Theory of Static and Dynamic Hardness," Proceedings Royal Society of London, Ser. A., Vol. 192, p. 247.
- Tabor, D., (1951), The Hardness of Metals, Oxford at the Clarendon Press.
- Tabor, D., (1954), "Mohs' Hardness Scale -- A Physical Interpretation," Proceedings Physical Society of London, Sect. B, Vol. 67, p. 249.
- Tabor, D., (1956), "The Physical Meaning of Indentation and Scratch Hardness," British Journal of Applied Physics, Vol. 7, p. 159.
- Talobre, J., (1957), La Mecanique des Roches, Dunod, Paris.
- Terzaghi, K., (1946), "Rock Defects and Loads on Tunnel Supports," Section I, Rock Tunneling with Steel Supports, The Commercial Shearing & Stamping Co., Youngstown, Ohio.
- Terzaghi, K., and Peck, R. B., (1948), Soil Mechanics in Engineering Practice, John Wiley & Sons, New York.
- Tocher, D., (1957), "Anisotropy in Rocks Under Simple Compression," Trans. American Geophysical Union, Vol. 38, No. 1, p. 89.
- Travis, R. B., (1955), "Classification of Rocks," Quarterly of the Colorado School of Mines, Vol. 50, No. 1.
- U. S. Army Corps of Engineers, (1961), "Presenting Subsurface Information in Contract Plans and Specifications," Engineering and Design Manual, EM 1110-1-1806, 24 January.
- U. S. Bureau of Mines, (1962), A Study of Mine Examination Techniques for Detecting and Identifying Underground Nuclear Explosions, Information Circular 8091.

- U. S. Bureau of Reclamation, (1948), Effect of Cracks in Concrete Upon Dynamic Measurements of Elastic Modulus, U. S. Bureau of Reclamation Materials Lab. Report No. C-383, Research and Geology Division.
- U. S. Bureau of Reclamation, (1953), Physical Properties of Some Typical Foundation Rocks, U. S. Bureau of Reclamation Concrete Lab Report No. SP-39.
- Von Moos, A., and De Quervain, F., (1948), Technische Gesteinskunde, Verlag Birkhauser, Basel.
- Walsh, J. B., (1965), "The Effect of Cracks on the Uniaxial Elastic Compression of Rocks," Journal of Geophysical Research, Vol. 70, No. 2, p. 399.
- Watstein, D., (1953), "Effect of Straining Rate on the Comprehensive Strength and Elastic Properties of Concrete," American Concrete Institute Journal, Vol. 24, No. 8, p. 729.
- White, R. E., (1963), "Pretest Tiebacks and Drilled-In Caissons," Civil Engineering, April, p. 36.
- Williams, S. R., (1942), Hardness and Hardness Measurements, American Society for Metals, Cleveland, Ohio.
- Windes, S. L., (1949), Physical Properties of Mine Rock, Part I, U. S. Bureau of Mines R. I. 4459.
- Windes, S. L., (1950), Physical Properties of Mine Rock, Part II, U. S. Bureau of Mines R. I. 4727.
- Wolansky, D., (1949), "Zur Frage der Harteproofung der Karbongesteine nach dem Ruckprallverfahren," Glückauf, Vol. 85, January.
- Wooddell, C. E., (1935), "Methods of Comparing the Hardness of Electric Furnace Products and Natural Abrasives," Trans. The Electrochemical Society, Vol. 68, p. 111.
- Wolf, D. O., (1930), The Results of Physical Tests of Road-Building Rock, U. S. Department of Agriculture Misc. Publ. 76.
- Wuerker, R. G., (1953), "The Status of Testing Strength of Rocks," Trans. AIME, Mining Engineering, p. 1108.
- Wuerker, R. G., (1956), Annotated Tables of Strength and Elastic Properties of Rocks, Published by Petroleum Branch, AIME, December, Paper No. 663-G.
- Wuerker, R. G., (1959), "Influence of Stress Rate and Other Factors on Strength and Elastic Properties of Rocks," Quarterly of the Colorado School of Mines, Vol. 54, No. 3, p. 3.
- Wyllie, M. R. J., Gregory, A. R., and Gardner, G. H. F., (1958), "An Experimental Investigation of Factors Affecting Elastic Wave Velocities in Porous Media," Geophysics, Vol. 23, No. 3, p. 459.

Zismon, W. A., (1933), "Comparison of the Statically and Seismologically Determined Elastic Constants of Rocks," Proceedings of the National Academy of Science, Vol. 19, No. 7, p. 680.

Zwikker, C., (1954), Physical Properties of Solid Materials, Interscience Publishers, Inc., New York.

Unclassified

Security Classification

DOCUMENT CONTROL DATA - R&D

(Security classification of title, body of abstract and indexing classification must be entered when the overall report is classified)

1. ORIGINATING ACTIVITY (Corporate author) University of Illinois Department of Civil Engineering Urbana, Illinois		2a. REPORT SECURITY CLASSIFICATION Unclassified	
2b. GROUP			
3. REPORT TITLE ENGINEERING CLASSIFICATION AND INDEX PROPERTIES FOR INTACT ROCK			
4. DESCRIPTIVE NOTES (Type of report and inclusive dates) 1 February 1964 through 1 April 1966			
5. AUTHOR(S) (Last name, first name, initial) Deere, D. U.; Miller, R. P.			
6. REPORT DATE December 1966		7a. TOTAL NO. OF PAGES 324	7b. NO. OF REFS 140
8a. CONTRACT OR GRANT NO. AF29(601)-6319		9a. ORIGINATOR'S REPORT NUMBER(S) AFWL-TR-65-116	
b. PROJECT NO. 5710		9b. OTHER REPORT NO(S) (Any other numbers that may be assigned this report)	
c. Subtask 13.144			
d.			
10. AVAILABILITY/LIMITATION NOTICES Distribution of this document is unlimited.			
11. SUPPLEMENTARY NOTES		12. SPONSORING MILITARY ACTIVITY Air Force Weapons Laboratory (WLDC) Kirtland Air Force Base, New Mexico 87117	
13. ABSTRACT <p>Physical and elastic properties of NX-size rock core from 27 localities were investigated in order to develop an engineering classification system for intact rock, and also to develop index properties related to important physical and engineering characteristics. Thirteen rock types are represented. Laboratory tests were conducted on these rocks as follows: unit weight, Shore scleroscope hardness, Schmidt hammer hardness, abrasion hardness, absorption, sonic-velocity stress-strain under cyclic loading to 5,000 psi, uniaxial stress-strain to failure, and point-load tensile strength. A total of 257 specimens with L/D ratios of 2:1 were tested. Statistical studies were conducted with the IBM 7094 computer to determine correlation and regression relationships for selected pairs of variables. A system of engineering classification is proposed in which rocks are classified on the basis of their strength and modulus properties either obtained directly from laboratory tests, or approximately from index properties recommended herein. Application of the proposed engineering classification system to data obtained by others is shown by individual charts for each of several different rock types. Five charts are presented for estimating the strength or modulus properties for intact rock from the numerical indices obtained by either the Schmidt hammer, the Shore scleroscope, or the sonic pulse velocity, all used in conjunction with the unit weight of the rock.</p>			

DD FORM 1473  
1 JAN 64

Unclassified

Security Classification

14 KEY WORDS	LINK A		LINK B		LINK
	ROLE	WT	ROLE	WT	ROLE
Rock Mechanics Intact Rock Cores Various Rock Types Engineering Classification System Index Properties Elastic Properties Physical Properties Static Tests Dynamic Tests Strength Deformation Statistical Analysis					

**INSTRUCTIONS**

1. **ORIGINATING ACTIVITY:** Enter the name and address of the contractor, subcontractor, grantee, Department of Defense activity or other organization (*corporate author*) issuing the report.
- 2a. **REPORT SECURITY CLASSIFICATION:** Enter the overall security classification of the report. Indicate whether "Restricted Data" is included. Marking is to be in accordance with appropriate security regulations.
- 2b. **GROUP:** Automatic downgrading is specified in DoD Directive 5200.10 and Armed Forces Industrial Manual. Enter the group number. Also, when applicable, show that optional markings have been used for Group 3 and Group 4 as authorized.
3. **REPORT TITLE:** Enter the complete report title in all capital letters. Titles in all cases should be unclassified. If a meaningful title cannot be selected without classification, show title classification in all capitals in parenthesis immediately following the title.
4. **DESCRIPTIVE NOTES:** If appropriate, enter the type of report, e.g., interim, progress, summary, annual, or final. Give the inclusive dates when a specific reporting period is covered.
5. **AUTHOR(S):** Enter the name(s) of author(s) as shown on or in the report. Enter last name, first name, middle initial. If military, show rank and branch of service. The name of the principal author is an absolute minimum requirement.
6. **REPORT DATE:** Enter the date of the report as day, month, year; or month, year. If more than one date appears on the report, use date of publication.
- 7a. **TOTAL NUMBER OF PAGES:** The total page count should follow normal pagination procedures, i.e., enter the number of pages containing information.
- 7b. **NUMBER OF REFERENCES:** Enter the total number of references cited in the report.
- 8a. **CONTRACT OR GRANT NUMBER:** If appropriate, enter the applicable number of the contract or grant under which the report was written.
- 8b, &c, & 8d. **PROJECT NUMBER:** Enter the appropriate military department identification, such as project number, subproject number, system numbers, task number, etc.
- 9a. **ORIGINATOR'S REPORT NUMBER(S):** Enter the official report number by which the document will be identified and controlled by the originating activity. This number must be unique to this report.
- 9b. **OTHER REPORT NUMBER(S):** If the report has been assigned any other report numbers (*either by the originator or by the sponsor*), also enter this number(s).
10. **AVAILABILITY/LIMITATION NOTICES:** Enter any limitations on further dissemination of the report, other than those

imposed by security classification, using standard statement such as:

- (1) "Qualified requesters may obtain copies of this report from DDC."
- (2) "Foreign announcement and dissemination of this report by DDC is not authorized."
- (3) "U. S. Government agencies may obtain copies of this report directly from DDC. Other qualified DDC users shall request through \_\_\_\_\_"
- (4) "U. S. military agencies may obtain copies of this report directly from DDC. Other qualified users shall request through \_\_\_\_\_"
- (5) "All distribution of this report is controlled. Qualified DDC users shall request through \_\_\_\_\_"

If the report has been furnished to the Office of Technical Services, Department of Commerce, for sale to the public, cite this fact and enter the price, if known.

11. **SUPPLEMENTARY NOTES:** Use for additional explanatory notes.
12. **SPONSORING MILITARY ACTIVITY:** Enter the name of the departmental project office or laboratory sponsoring (*performing for*) the research and development. Include address.
13. **ABSTRACT:** Enter an abstract giving a brief and factual summary of the document indicative of the report, even though it may also appear elsewhere in the body of the technical report. If additional space is required, a continuation sheet be attached.

It is highly desirable that the abstract of classified reports be unclassified. Each paragraph of the abstract shall end with an indication of the military security classification of the information in the paragraph, represented as (TS), (S), (C), or (U).

There is no limitation on the length of the abstract. However, the suggested length is from 150 to 225 words.

14. **KEY WORDS:** Key words are technically meaningful terms or short phrases that characterize a report and may be used in index entries for cataloging the report. Key words must be selected so that no security classification is required. Identifiers, such as equipment model designation, trade name, project code name, geographic location, may be used as key words but will be followed by an indication of technical content. The assignment of links, rules, and weights is optional.